

Electronic Thesis and Dissertation Repository

10-4-2016 12:00 AM

The Character and Distribution of Cu-PGE Mineralization at the Geordie Lake Deposit Within the Coldwell Complex, Ontario

Imran Meghji, *The University of Western Ontario*

Supervisor: Dr. Robert Linnen, *The University of Western Ontario*

A thesis submitted in partial fulfillment of the requirements for the Master of Science degree in
Geology

© Imran Meghji 2016

Follow this and additional works at: <https://ir.lib.uwo.ca/etd>



Part of the [Geochemistry Commons](#), and the [Geology Commons](#)

Recommended Citation

Meghji, Imran, "The Character and Distribution of Cu-PGE Mineralization at the Geordie Lake Deposit Within the Coldwell Complex, Ontario" (2016). *Electronic Thesis and Dissertation Repository*. 4321.
<https://ir.lib.uwo.ca/etd/4321>

This Dissertation/Thesis is brought to you for free and open access by Scholarship@Western. It has been accepted for inclusion in Electronic Thesis and Dissertation Repository by an authorized administrator of Scholarship@Western. For more information, please contact wlsadmin@uwo.ca.

Abstract

Cu-PGE mineralization at the Geordie Lake Deposit (GLD) is spatially associated with weak to intense actinolite and albite alteration within gabbro and troctolite. Previous studies have determined a magmatic and magmatic-hydrothermal origin of the deposit. The most significant Cu-PGE occurrence in the GLD is dominantly stratiform, and in contact with a basal syenite. Similar patterns of REE with progressive enrichment from troctolite, to gabbro, and basal syenite indicate that these lithologies are genetically linked. Major element geochemistry shows no discernable variation between the altered and unaltered samples. Whole rock $\delta^{18}\text{O}$ analyses were conducted in equal intervals down the stratigraphy of the GLD revealing a steady depletion in $\delta^{18}\text{O}$ from 5.1‰ at the surface of the deposit, to 1.3 ‰ at the basal contact with cross-cutting syenite. The results show that sulfide deposition is magmatic, though interaction with late stage magmatic fluid redistributed some sulfide components.

Keywords

Geordie Lake, gabbro, sulfides, PGEs, mafic intrusion, Coldwell Alkaline Complex

Acknowledgments

First and foremost, I would like to thank my supervisor Dr. Bob Linnen for his guidance and encouragement through the years. There were many trying moments during the course of this dissertation, and as a result of his patience and understanding, I was able to finish something that was started long ago. I must also like to express my gratitude to Dr. David Good, who not only employed me at Stillwater Canada for two summers, but acted as a mentor and was always available for discussion and guidance along the way. Much thanks to Dr. Iain Samson and Dr. Doreen Ames for all the various discussion and suggestions. And special thanks to Dr. Neil Banerjee and Dr. Elizabeth Webb for all their assistance with oxygen isotopes; a subject that quickly became a part of my life for a good few years. Funding for this project was graciously provided by the Natural Sciences and Engineering Research Council of Canada (NSERC), and through the Research Affiliate Program (RAP) which was an initiative sponsored by the Geological Survey of Canada (GSC) and Stillwater Canada Inc.

I am also very grateful for all the friends and acquaintances I made during my time at Western University. It was undoubtedly a period in my life that shaped who I am today, and I am forever thankful for their friendships and influences. If any of you are reading this, then I'm sure you're disappointed that I didn't mention you by name. But then again, you probably aren't reading this.

Table of Contents

Abstract	i
Acknowledgments	ii
Table of Contents	iii
List of Tables	vii
List of Figures	ix
List of Abbreviations, Symbols and Nomenclature	xv
List of Appendices	xvii
Chapter 1	1
1 Introduction	1
1.1 Thesis Objectives	1
1.2 History of the Geordie Lake Deposit	2
1.3 Summary of Previous Work at the GLD.....	4
1.4 Why Platinum-Group Elements?	5
1.4.1 What Exactly Are PGE?	6
1.5 Ni-Cu-PGE Deposits Worldwide.....	6
1.6 Global Distribution and Classification of PGE Deposits.....	7
1.6.1 Classification of the GLD	9
1.7 Formation of a Ni-Cu-PGE Deposit	9
1.8 Notable Sulfide Rich, PGE-Poor Deposits	11
1.8.1 Noril'sk Deposit Russia	11
1.8.2 Jinchuan Deposit, China	12
1.8.3 Voisey's Bay, Canada.....	13
1.9 Notable Sulfide Poor, PGE-Rich Deposits	14

1.9.1	Bushveld Complex	14
1.9.2	Stillwater Complex	15
1.9.3	Other Sulfide-Poor PGE-Rich Deposits Within North America	16
1.10	Stable $\delta^{18}\text{O}$ Isotopes.....	16
Chapter 2	19
2	Geology	19
2.1	Archean Superior Province	19
2.1.1	Wawa-Abitibi Subprovince	20
2.1.2	Quetico Subprovince.....	21
2.1.3	Winnipeg River Terrane	22
2.2	Mid-Continent Rift System of North America (MCR).....	23
2.2.1	Geology of Mineral Occurrences Related to the MCR	25
2.3	Coldwell Alkaline Complex	28
2.3.1	Emplacement of the Coldwell Alkaline Complex	30
2.3.2	Mafic Units Within the Coldwell Alkaline Complex	30
2.4	Geordie Lake Intrusion	35
2.4.1	Plagioclase Aligned Gabbro (Unit 2a).....	39
2.4.2	Fine to Medium-Grained Homogeneous Gabbro (Unit 2b).....	39
2.4.3	Medium-Grained Homogeneous Troctolite (Unit 2c)	39
2.4.4	Heterogeneous Gabbro (Unit 3a)	40
2.4.5	Skeletal Troctolite (Unit 3b)	40
2.4.6	Basal Fine-Grained Gabbro (Unit 3c).....	42
2.4.7	Stratigraphy of the GLD	42
2.4.8	Basal Syenite.....	44
2.4.9	Infilled Fractures at the GLD.....	45

2.4.10 Mineralization at the Geordie Lake Deposit	46
2.4.11 Sulfide Zonation at the Geordie Lake Deposit	52
Chapter 3	54
3 Methodology	54
3.1 Sample Collection.....	54
3.1.1 Diamond Drill Hole Selection Criteria	54
3.1.2 Albite Pod Selection Criteria	56
3.2 Analytical Techniques	61
3.2.1 Major and Trace Element Geochemistry	62
3.2.2 Oxygen Isotope Chemistry	64
3.2.3 Scanning Electron Microscopy	65
Chapter 4	66
4 Petrography	66
4.1 Umineralized Lithologies at the GLD.....	66
4.1.1 Plagioclase Aligned Gabbro (Unit 2a).....	66
4.1.2 Fine to Medium-Grained Homogeneous Gabbro (Unit 2b).....	74
4.1.3 Medium-Grained Homogeneous Troctolite (Unit 2c)	78
4.2 Mineralized Lithologies at the GLD.....	82
4.2.1 Heterogeneous Gabbro (Unit 3a).....	83
4.2.2 Skeletal Troctolite (Unit 3b).....	92
4.2.3 Basal Fine-Grained Gabbro (Unit 3c).....	105
4.3 Syenite.....	109
4.3.1 Mineralization.....	110
4.4 Albite Pods at the GLD.....	113
Chapter 5	119

5	Geochemistry	119
5.1	Results of Major and Trace Element Geochemistry	119
5.1.1	Down-hole Whole Rock Geochemistry	134
5.1.2	Albite Pod Transect Geochemistry	146
5.1.3	Major and Trace Element Geochemistry	156
5.1.4	Cu-PGE Diagrams and Down Hole Metal Ratios.....	173
Chapter 6	186
6	Stable $\delta^{18}\text{O}$ Isotopes	186
6.1	Down-hole Whole Rock Oxygen Isotopes	186
6.2	Albite Pod Whole Rock Oxygen Isotopes	196
6.2.1	Discovery Outcrop Albite Pod.....	196
6.2.2	Albite Pod #3	198
6.2.3	Relationship Between Albite Pod Oxygen Isotopes and Geochemistry .	200
Chapter 7	205
7	Discussion and Conclusion	205
7.1	Discussion of Geochemical Data	205
7.2	Discussion of Geology	206
7.2.1	Significance of Alteration at the GLD	207
7.3	Mineralization and Metal Ratios.....	209
7.3.1	Upper Zone Mineralization.....	210
7.3.2	Main Zone Mineralization	211
7.4	Discussion of Whole Rock Oxygen Isotopes.....	211
7.4.1	Discussion of Down-hole Whole Rock Oxygen Isotopes.....	212
7.4.2	Discussion of Whole Rock Oxygen Isotopes in Albite Pods.....	213
7.5	Conclusion	214

References	215
Appendix	225
Curriculum Vitae	336

List of Tables

Table 3.1 – Collar information for all four drill-holes used in this study	55
Table 3.2 – The detection limits of trace elements analyzed in this study	64
Table 3.3 – The detection limits for PGE	64
Table 4.1 – Average mineral abundances for plagioclase aligned gabbro	67
Table 4.2 – Average mineral abundances for homogeneous gabbro	75
Table 4.3 – Average mineral abundances for homogeneous troctolite	80
Table 4.4 – Average mineral abundances for heterogeneous gabbro	84
Table 4.5 – Average mineral abundances for skeletal troctolite	94
Table 4.6 – Average mineral abundances for basal fine grained gabbro	106
Table 5.1 – Major element chemistry of plagioclase aligned gabbro	122
Table 5.2 – Major element chemistry of homogeneous gabbro	123
Table 5.3 – Major element chemistry of heterogeneous gabbro	123
Table 5.4 – Major element chemistry of weakly albitized heterogeneous gabbro	124
Table 5.5 – Major element chemistry of skeletal troctolite samples	124
Table 5.6 – Major element chemistry of altered skeletal troctolite samples	125
Table 5.7 – Major element chemistry of Albite Pods #3 and #5	125
Table 5.8 – Major element chemistry of the Discovery Outcrop Albite Pod	126
Table 5.9 – Trace element chemistry of plagioclase aligned gabbro	126
Table 5.10 – Trace element chemistry of homogeneous gabbro	127
Table 5.11 – Trace element chemistry of heterogeneous gabbro	128

Table 5.12 – Trace element chemistry of weakly albitized heterogeneous gabbro	129
Table 5.13 – Trace element chemistry of skeletal troctolite samples	130
Table 5.14 – Trace element chemistry of altered skeletal troctolite samples	131
Table 5.15 – Trace element chemistry of Albite Pods #3 and #5	132
Table 5.16 – Trace element chemistry of the Discovery Outcrop Albite Pod	133
Table 5.17 – PGE data for a sample suite chosen based on high Pd values	133

List of Figures

Figure 1.1 – The global distribution of platinum production.....	8
Figure 1.2 – The global distribution of palladium production.....	8
Figure 2.1 – General map of Ontario, Canada	21
Figure 2.2 - Cartoon map of the North American basement rocks	24
Figure 2.3 - A bouger gravity map outlining the high gravity anomaly of the MRS	25
Figure 2.4 – The location of MRS-related Ni-Cu-PGE deposits	26
Figure 2.5 – Geological map of the Coldwell Alkaline Complex	31
Figure 2.6 – Typical features of the Coubran Lake basalt	33
Figure 2.7 – Geological map of the Geordie Lake Deposit	36
Figure 2.8 – Close up on the black outline within Figure 2.7.....	37
Figure 2.9 – North facing, east-west cross section of the GLD	38
Figure 2.10 – A summary of the main lithologies that comprise the GLD	41
Figure 2.11 – Xenoliths of basal fine grained gabbro enclosed by syenite	46
Figure 2.12 – Two different textures of basal syenite	47
Figure 2.13 – Different examples of cross-cutting veins present at the GLD	48
Figure 2.14 – Mineralization within fracture slip-surfaces.....	49
Figure 2.15 – Disseminated chalcopyrite occurring within an actinolite bleb	50
Figure 2.16 – Pyrrhotite mineralization occurring in close contact with acinolite.....	51
Figure 2.17 – An intergrowth of chalcopyrite and bornite	51
Figure 2.18 – Chalcopyrite mineralization near skeletal magnetite	52
Figure 2.19 – North-facing East-West cross section of GLD with sulfides logged	53
Figure 3.1 – Location of samples taken for geochemical analysis	56
Figure 3.2 – Transect of Albite Pod #3.....	58
Figure 3.3 – Transect of Albite Pod #3 with cut blocks	59

Figure 3.4 – Transect of Albite Pod #5.....	60
Figure 3.5 – Transect of the Discovery Outcrop Albite Pod	61
Figure 4.1 – Overall texture of the plagioclase aligned gabbro	68
Figure 4.2 – Stubby irregular magnetite crystals in plagioclase aligned gabbro	69
Figure 4.3 – Patchy chlorite alteration of clinopyroxene.....	70
Figure 4.4 – Radially extending chlorite grains intergrown with actinolite	72
Figure 4.5 – Close up image of Figure 4.4c showing prominence of albite	73
Figure 4.6 – General texture of homogeneous gabbro.....	76
Figure 4.7 – Relatively minor patchy actinolite alteration of clinopyroxene	77
Figure 4.8 – An opaque mineral occurring as an inclusion in a plagioclase grain.....	78
Figure 4.9 – General texture of homogeneous troctolite	81
Figure 4.10 – Stubby grains of olivine within plagioclase strongly rimmed by biotite .	81
Figure 4.11 – Albite alteration within homogeneous troctolite	82
Figure 4.12 – General texture of heterogeneous gabbro.....	85
Figure 4.13 – A PPL image showing a thin section that has fresh gabbro on right.....	86
Figure 4.14 – A predominantly fresh clinopyroxene grain with actinolite alteration.....	87
Figure 4.15 – Chalcopyrite mineralization occurring interstitial to actinolite.....	89
Figure 4.16 – Sulfide mineralization spatially associated with actinolite	90
Figure 4.17 – Chalcopyrite containing lamellae of pyrrhotite.....	91
Figure 4.18 – Opaque mineral completely enveloped by actinolite and biotite	92
Figure 4.19 – General texture of skeletal troctolite	95
Figure 4.20 – PPL image showing the bimodal variation in grainsize in troctolite	96
Figure 4.21 – General texture of weakly altered skeletal troctolite.....	97
Figure 4.22 – PPL image of skeletal troctolite thin section sample.....	98
Figure 4.23 – Typical unaltered sulfide mineralization within skeletal troctolite	100

Figure 4.24 – Opaque mineral fully enveloped by albite and actinolite	100
Figure 4.25 – Opaque mineral occurs at the boundary between olivine grains	101
Figure 4.26 – BSE image of an edge of a skeletal magnetite grain	102
Figure 4.27 – BSE image of a subhedral magnetite grain	103
Figure 4.28 – A BSE image of a magmatic magnetite grain	104
Figure 4.29 – The occurrences of PGM within skeletal troctolite	105
Figure 4.30 – General texture of the basal fine grained gabbro.....	107
Figure 4.31 – Opaque mineral occurring interstitial to albitized plagioclase laths	109
Figure 4.32 – BSE image of chalcopyrite being resorbed by hydrothermal magnetite ..	110
Figure 4.33 – Photomicrograph in PPL showing general texture of syenite	111
Figure 4.34 – Amphibole syenite beginning to envelop basal fine grained gabbro	112
Figure 4.35 – A photomicrograph in PPL showing irregular bleb of opaque mineral ...	113
Figure 4.36 – Photomicrographs in PPL showing general texture of Albite Pod #3.....	115
Figure 4.37 – Photomicrographs in PPL showing general texture of Albite Pod #5	116
Figure 4.38 – Unaltered texture in Albite Pod #5	117
Figure 4.39 – General texture of Block 1-7 in Discovery Outcrop Albite Pod	118
Figure 4.40 – Reflected light images of mineralization in Discovery Outcrop	119
Figure 5.1 – A plot of Fe_2O_3 vs TiO_2	134
Figure 5.2 – Down-hole plot of major elements in drill hole G-10-04.....	137
Figure 5.3 – Down-hole plot of major elements in drill hole G-10-16.....	138
Figure 5.4 – Down-hole plot of major elements in drill hole G-10-17.....	139
Figure 5.5 – Down-hole plot of trace elements in drill hole G-10-04	140
Figure 5.6 – Down-hole plot of trace elements in drill hole G-10-16	141
Figure 5.7 – Down-hole plot of trace elements in drill hole G-10-17	143
Figure 5.8 – CIPW normalized values for drill hole G-10-04	144

Figure 5.9 – CIPW normalized values for drill hole G-10-16	144
Figure 5.10 – CIPW normalized values for drill hole G-10-07	145
Figure 5.11 – A transect of Albite Pod #3 with major element chemistry shown	148
Figure 5.12 – A transect of Albite Pod #5 with major element chemistry shown	149
Figure 5.13 – A transect of the Discovery Outcrop Albite Pod with major elements	150
Figure 5.14 – A transect of Albite Pod #3 with trace element chemistry shown	151
Figure 5.15 – A transect of Albite Pod #5 with trace element chemistry shown	152
Figure 5.16 – A transect of the Discovery Outcrop Albite Pod with trace elements.....	153
Figure 5.17 – CIPW normalized values for Albite Pod #3	154
Figure 5.18 – CIPW normalized values for Albite Pod #5	155
Figure 5.19 – CIPW normalized values for the Discovery Outcrop Albite Pod.....	156
Figure 5.20 – Harker diagram with the least altered samples plotted	158
Figure 5.21 – Harker diagram with all samples plotted.....	159
Figure 5.22 – Mg # plotted against major elements with least altered samples	160
Figure 5.23 – Mg # plotted against major elements with all samples.....	161
Figure 5.24 – Chondrite normalized spider diagram arranged by lithology.....	162
Figure 5.25 – Zr vs. Y with unaltered samples plotted.....	164
Figure 5.26 – Zr vs. Y with all samples plotted.....	164
Figure 5.27 – Ya vs. Yb with unaltered samples plotted.....	165
Figure 5.28 – Ya vs. Yb with all samples plotted.....	166
Figure 5.29 – La/Yb vs. Zr/Y with unaltered samples plotted.....	167
Figure 5.30 – La/Yb vs. Zr/Y with all samples plotted	168
Figure 5.31 – Zr vs. Na ₂ O with unaltered samples plotted.....	169
Figure 5.32 – Zr vs. Na ₂ O with all samples plotted.....	169

Figure 5.33 – Zr vs. Rb with unaltered samples plotted	170
Figure 5.34 – Zr vs. Rb with all samples plotted	170
Figure 5.35 – Rb vs. K ₂ O with unaltered samples plotted.....	170
Figure 5.36 – Rb vs. K ₂ O with all samples plotted.....	171
Figure 5.37 – K ₂ O vs. Zr with unaltered samples plotted.....	172
Figure 5.38 – K ₂ O vs. Zr with all samples plotted.....	172
Figure 5.39 – Cu vs. Pd with unaltered samples plotted.....	174
Figure 5.40 – Cu vs. Pd with all samples plotted.....	175
Figure 5.41 – Pd vs. Cu/Pd with unaltered samples plotted	176
Figure 5.42 – Pd vs. Cu/Pd with all samples plotted	178
Figure 5.43 – A plot of PGE and Au normalized to mantle values	178
Figure 5.44 – Down-hole metal summary of drill hole G-10-17	179
Figure 5.45 – Down-hole metal summary of drill hole G-10-16.....	180
Figure 5.46 – Down-hole metal summary of drill hole G-10-04.....	180
Figure 5.47 – Down-hole metal summary of drill hole G-10-02.....	182
Figure 6.1 – Down-hole $\delta^{18}\text{O}$ plots of drill holes G-10-17 and G-10-17.....	187
Figure 6.2 – Comparison of $\delta^{18}\text{O}$ values within plagioclase aligned gabbro	188
Figure 6.3 – Comparison $\delta^{18}\text{O}$ values within heterogeneous gabbro	188
Figure 6.4 - Comparison $\delta^{18}\text{O}$ values within skeletal troctolite.....	189
Figure 6.5 – Whole rock $\delta^{18}\text{O}$ values vs. major elements.....	190
Figure 6.6 - Whole rock $\delta^{18}\text{O}$ values vs. Mg #	191
Figure 6.7 – Whole rock $\delta^{18}\text{O}$ values vs. Na+Ca in moles	192
Figure 6.8 – Whole rock $\delta^{18}\text{O}$ values vs. CIPW normative mineral modal percents	193
Figure 6.9 – Whole rock $\delta^{18}\text{O}$ values vs. Cu and Pd	195
Figure 6.10 – Whole rock $\delta^{18}\text{O}$ values in Discovery Outcrop Albite Pod transect	197

Figure 6.11 – Whole rock $\delta^{18}\text{O}$ values in Albite Pod #3 transect.....	199
Figure 6.12 – Whole rock $\delta^{18}\text{O}$ values vs. Mg # for albite pods	201
Figure 6.13 – Whole rock $\delta^{18}\text{O}$ values vs. Na+Ca in molar for albite pods	202
Figure 6.14 – Whole rock $\delta^{18}\text{O}$ values vs. CIPW normalized values for albite pods.....	203
Figure 6.15 – Whole rock $\delta^{18}\text{O}$ values vs. Cu and Pd for albite pods	204

List of Abbreviations, Symbols and Nomenclature

Ab	Albite
Act	Actinolite
Ap	Apatite
Bn	Bornite
Bt	Biotite
Ccp	Chalcopyrite
Cct	Chalcocite
Chl	Chlorite
Cpx	Clinopyroxene
EDS	Energy-dispersive X-ray spectroscopy
GLD	Geordie Lake Deposit
GLI	Geordie Lake Intrusion
IPGE	Iridium-group platinum-group elements
Kfs	K-feldspar
LMI	Large mafic intrusion
Mag	Magnetite
MCR	Mid-continent rift system of North America
Mil	Millerite
MORB	Mid-ocean ridge basalt
MSS	Monosulfide solid solution
Ol	Olivine
PGE	Platinum-group element
PGM	Platinum-group mineral
Pl	Plagioclase

Pn	Pentlandite
Po	Pyrrhotite
PPGE	Palladium-group platinum-group elements
PPL	Plane-polarized light
Py	Pyrite
REFL	Reflected light
SCSS	Sulfur content at sulfide saturation
SEM	Scanning electron microscopy
Sp	Sphalerite
TDLG	Two Duck Lake Gabbro
TDLI	Two Duck Lake Intrusion
VSMOW	Vienna Standard Mean Ocean Water
XPL	Cross-polarized light

List of Appendices

Appendix 1 – SEM-EDS data	227
Appendix 2 – Petrographic reports	228

Chapter 1

1 Introduction

The Geordie Lake Deposit (GLD) is hosted by a weakly layered, elongate mafic intrusion located within the Coldwell Alkaline Complex, which is the largest alkaline igneous intrusion in North America (Heaman and Machado, 1992). Generally, layered mafic intrusions (LMIs) tend to occur in tectonic environments where basaltic magma is generated, such as mid-ocean ridges and mid-continent rift systems (Young, 2003). However, the largest and best preserved intrusions are those where a substantial volume of magma is generated in a short period of time, and where they can be exposed at surface by erosion, i.e., within the continental crust (Young, 2003). An ideal environment for vast magma production in a continental setting are continental flood basalts where rifting is associated with mantle hotspots. LMIs tend to be coeval with such flood basalts (Mahoney and Coffin, 1997). Unfortunately, for the most part, layered ultramafic to mafic intrusions are quite uncommon within the geologic record (Zientek, 2012). However, where present, they are known to host magmatic ore deposits containing some of the world's most economic concentration of platinum-group elements (PGE) (Figure 1.1).

1.1 Thesis Objectives

The GLD provides an excellent opportunity to study the behaviour of Cu-PGE mineralization within a mafic intrusion in a region that has not undergone metamorphism. One of the main concerns at the GLD is fundamental lack of understanding of how the present-day distribution of sulfides and associated PGE-mineralization originated. While Mulja and Mitchell (1991) concluded that the PGE-Cu mineralization was magmatically emplaced due to rapid quenching of tholeiitic magma, it fails to address the absence of pyrrhotite in the mineralized horizons, in addition to the lack of primary magmatic sulfide textures. Conversely, Good and Crocket (1994) maintained that the sulfides formed from post-magmatic fluids, and that sulfide deposition took place gradually as the interstitial fluid evolved and reacted with a crystalline mush which resulted in the spatial associations between sulfides and secondary silicate minerals including actinolite, and

albite. Additionally, to the immediate north of the GLD, there have been numerous occurrences of Cu-mineralization in the Coubran Lake basaltic flows of similar Keweenawan age (Cundari, 2012), which may indicate remobilization of Cu and precious metals from the underlying gabbros. However, the bulk of mineralization at the GLD is found proximal to the basal contact of the deposit, which is reminiscent of a magmatic model that includes the gravitational settling of dense sulfide liquid (Naldrett, 2004). The geologic setting of the mineralization at the GLD needs to be extensively defined in order to characterize the paragenesis Cu-PGE mineralization relative to lithology, and secondary alteration.

The primary objective of this study is determine what the structure and control of Cu-PGE mineralization at the GLD is, and to explore how the distribution of Cu-PGE mineralization varies by host lithology, and by various degrees of secondary alteration. This will be attained by: 1) Fully characterizing the lithologies present at the GLD using drill core logging, silicate and sulfide mineral petrography combined with scanning electron microscopy, and whole rock geochemistry, 2) Characterizing the host rocks to the mineralization, the secondary alteration, and the spatial and temporal relationships among these features, 3) Determining the distribution of, and controls on Cu-PGE in the GLD relative to its host rocks, and albite-actinolite alteration, and 4) Determining the distribution of PGE ratios in the Geordie Lake Deposit and the controls of metal ratio values, and to evaluate whether these can be used as vectors towards additional resources. A study of whole rock oxygen isotopes will also be utilized in order to determine the origin and evolution of the magmas, and potentially the nature of fluids that were involved in geological processes. Addressing these research goals will allow for the development of a model for the formation of the Geordie Lake deposit.

1.2 History of the Geordie Lake Deposit

The Cu-mineralization at the Geordie Lake Deposit was discovered in 1963, during field work which was related to a copper exploration project funded by Ameranium Mines Limited (Patterson et al., 1987). At the time, Ameranium Mines Ltd. had staked thirty adjoining claims centered on Latvian Lake. Many years later, in 1986, the presence of PGM within Cu-sulfides was documented by a group of prospectors from Marathon,

Ontario, who ultimately rediscovered an exploratory trench of Ameranium Mines Limited. This trench was originally known as the Ameranium showing (later renamed the MacRae showing) (Drennan and Fell, 2010).

In 1987, the property was acquired by St. Joe Canada Inc. from Fleck Resources Ltd. St. Joe Canada Inc. subsequently began a detailed field mapping in conjunction with a drill program that targeted the mineralized area. The detailed mapping and sampling was conducted along the eastern contact of the Geordie Lake Intrusion. Analysis of roughly 300 grab, panel and channel samples indicated above average grades of base and precious metals along the eastern contact of the intrusion. In October 1987, through a joint venture agreement with Giant Bay Resources Ltd., a helicopter-assisted diamond drill program was conducted, and a total of eight diamond drill holes were completed in order to test the continuity of mineralization at the eastern contact of the GLD. A total of 773 m was drilled. This exploration project was short lived, however, as Giant Bay terminated the joint venture in 1988 (Drennan & Fell, 2010).

In 1995, three prospectors named Melvin Joa, Brian Fowler and Michael Shurman staked a six claim block totaling 64 units centered on the Geordie Lake property. They initiated a program consisting of line cutting, trenching, and a beep mat survey. This work led to the discovery of three sub-parallel mineralized zones slightly west of the eastern contact which correlated to mineralization that was intersected in the 1987 diamond drill holes. In 1998, Gryphon Metals Corporation optioned the property from Joa, Fowler and Shurman. The following year, Discovery PGM Exploration Ltd. entered into an option agreement with Gryphon Metals Corporation. Roughly 80% of the drill core from the 1987 drill program by St. Joe Canada Inc. was assayed for palladium, copper, platinum, gold, silver, nickel and cobalt. An additional diamond drill hole was attempted, but never completed (Drennan & Fell, 2010).

In 2000, Discovery PGM (formerly L.E.H. Ventures Ltd.) completed a three phase drill program which consisted of 23 diamond drill holes, which totaled 3,928 m. The program continued into 2001, when an additional 2552 m of core was drilled. In 2002, four more diamond drill holes were completed, totaling another 673 m. Subsequently, Discovery

PGM published the first resource estimate for the Geordie Lake Deposit (at a C\$10/tonne NSR cut-off the indicated resource is 24.4 million tonnes averaging 0.326 % Cu, 0.537 g/t Pd, 0.007 % Co, 0.011 % Ni, 0.030 g/t Pt, 2.52 g/t Ag and 0.04 g/t Au. An additional 5.4 million tonnes are considered inferred at an average grade of 0.36%Cu, 0.626 g/t Pd, 0.007% Co, 0.012% Ni, 0.04 g/t Pt, 3.04 g/t Ag and 0.05 g/t Au. In 2006, Discovery PGM expanded the drill program in order to determine the continuity of mineralized lithologies at depth. Three more drill holes were completed, with each of them intersecting mineralization; however no syenite was encountered at depth despite reaching the limit of the drill (Drennan & Fell, 2010).

In 2010, a winter drill program was initiated by Marathon PGM. A total of 21 holes were drilled for a total of 2998 m of core. Drilling was conducted perpendicular to the strike of the target mineralization (at an average dip of 45 degrees), with all holes being drilled close to a 90 degree azimuth. The vast majority of samples obtained for this thesis were obtained as a result of this particular drill program.

1.3 Summary of Previous Work at the GLD

Two previous studies have been conducted on the Geordie Lake gabbro: one by Mulja and Mitchell (1990, 1991), and the other by Good and Crocket (1994). While the scope of each study was slightly different, the overall emplacement model established by each study also differed. Mulja and Mitchell (1991) supported a magmatic origin for the Cu-PGE mineralization at the GLD. They suggested that rapid cooling of the magma and crystallization of olivine and magnetite induced the early separation of an immiscible sulfide melt. This melt remained liquid until surrounding silicate rocks had cooled to subsolidus temperatures. During the final stages of crystallization of the silicate magma, the sulfide melt and residual water-rich fluids were trapped together within pore spaces. They concluded that, due to the predominance of Pd, Cu, sulfides and tellurides, coupled with low Pt/(Pt+Pd) and high Cu/(Cu+Ni) ratios, suggests that the PGE-sulfide mineral assemblage at the GLD crystallized from a relatively evolved sulfide melt associated with an evolved tholeiitic magma.

On the other hand, Good and Crocket (1994) argued that disseminated sulfides and PGM are spatially associated with sporadic, patchy albite alteration at the GLD. The albite alteration manifested itself as albite pods, ranging from less than a centimeter to meters across and consisted predominantly of albite (Ab95-99) with minor hornblende, biotite, and actinolite. The abundances of Zr, Hf, Nb, Th, U and the REE within the albite pods are high relative to surrounding Geordie Lake gabbro, while inter-element ratios between albite pods and surrounding Geordie Lake gabbro are similar. They believed that this data indicated that the albite pods are representative of pockets of fluid-enriched residual magma, whereby the albite formed in two steps: 1) Hornblende and plagioclase crystallized from the residual magma, and 2) a hydrous fluid separated from the residual magma and interacted with the plagioclase to form albite. Hence, the close spatial association of biotite, actinolite, sulfides, PGM and albite implies that they originated from the same fluid, though deposition took place at different times as the temperature decreased and as fluid composition continually evolved. The fluid itself was likely sourced from the highly evolved magma which formed the albite pods.

1.4 Why Platinum-Group Elements?

PGE are of increasing economic value due to their numerous industrial applications. Their value is a direct result of their stable electrical properties, chemical resistivity, and high melting point (Hunt & Lever, 1969). Their durability and resistance to tarnish also make them ideal for, and quite valuable as jewelry. These unique physical and chemical properties make them critical to many emerging technologies. Hence, PGE are regarded as strategic metals due to their specialized applications in a broad range of industries. Platinum and palladium in particular are important metals in automobiles as they are key components of catalytic converters, which convert noxious car exhaust fumes into harmless non-toxic emissions. Platinum also plays a crucial role in the refining of petroleum and in the production of petrochemical feedstocks that are used in the manufacture of plastics, synthetic rubber and polyester fibers. Thus, as a consequence of rapid global economic growth, both platinum and palladium are more than likely to be in extensive global demand. As a result, more efficient methods of locating and ultimately mining PGE deposits will be necessary to meet this rapid global demand.

1.4.1 What Exactly Are PGE?

PGE typically refer to a group of six metallic elements in the periodic table sharing similar physical-chemical properties: ruthenium, rhodium, palladium, osmium, iridium and platinum. They are transition metals that have a tendency to occur together in deposits (Harris & Cabri, 1991). However, they can be further subdivided into two sub-categories: the iridium-group platinum group elements (IPGE) which include Os, Ir, and Ru, and the palladium-group platinum group elements (PPGE) which include Rh, Pt, and Pd (Barnes et al., 1985). This subdivision was made as a result of their distinct behaviour in geological systems. However in this thesis, for the purpose of simplicity, I will henceforth refer to all platinum-group elements simply as PGE and all platinum-group minerals as PGM.

1.5 Ni-Cu-PGE Deposits Worldwide

Globally, deposits which contain Ni, Cu and PGE are distinctly associated with mafic and ultramafic rocks. At the GLD, there is a notable depletion in Ni-sulfides relative to Cu-sulfides; however, virtually all magmatic sulfide deposits are Ni-Cu-bearing, and collectively these deposits account for roughly 90 percent of the world's Ni production (Naldrett, 2004). These deposit types have two further subdivisions: 1) Ores that contain Ni and Cu as primary products, and where PGE and other precious metals are byproducts, and 2) Deposits which contain PGE as the principal products, and Ni-Cu are the byproducts. Magmatic ores that are principally mined for Ni and Cu usually contain more than 10% sulfide minerals and tend to occur as irregular ore bodies within relatively small intrusions (Maier, 2005). Some world class examples of these deposit types include: the Noril'sk and Pechenga deposits in Russia, the Jinchuan deposit in China, Voisey's Bay in Newfoundland and Labrador, the Kabanga mine in Tanzania, and the Nkomati mine in South Africa. More comprehensive descriptions of these, and other magmatic Ni-Cu±PGE sulfide deposit types are given in Naldrett (2004), Barnes and Lightfoot (2005), and in Eckstrand and Hulbert (2007). These deposit types are, however, generally difficult to locate owing to their small sizes (one notable exception is the massive sulfide mineralization in Sudbury, Ontario, that is derived from a large impact-related melt sheet). Ores that are primarily mined for their PGE content typically contain

less than 1-2% sulfide minerals, and commonly form laterally continuous, stratiform horizons within larger layered mafic intrusions that are relatively easy to trace once they have been intersected (Maier, 2005).

1.6 Global Distribution and Classification of PGE Deposits

The vast majority of global PGE production originates from South Africa, and Russia. Although PGE deposits are quite widespread worldwide, deposits with economically recoverable PGE-grades are limited. PGE recovery is currently constrained to three main sources: 1) primary PGE deposits, 2) from secondary (recycled) resources, and 3) as byproducts of Ni and Cu recovery. Collectively, South Africa, Russia, Canada and the United States account for approximately 97.6 percent of the global platinum production, and 96 percent of the global palladium production (Figures 1.1 and 1.2; Hilliard, 2003). The majority of the world's PGE are sourced from magmatic ore deposits found within mafic and ultramafic portions of large tholeiitic intrusions of late Archean to early Proterozoic age (Maier, 2005). Five widely recognized categories of PGE deposit were established by Sutphin and Page (1986), but this classification scheme has since been modified and added to (Keays and Lightfoot, 2002; Eckstrand and Hulbert, 2007) and now includes seven different classification types: 1) "Merensky type" deposits in which PGE occur within large Precambrian mafic to ultramafic layered intrusions, such as the Merensky Reef of the Bushveld Complex in South Africa, the Great Dyke in Zimbabwe, and the J-M Reef within the Stillwater Complex in the United States, 2) "Chromitite type" deposits that are enriched in PGE and contain very sparse base metal sulfide minerals, including the Upper Group 2 (UG2) reef of the Bushveld Complex, and the Lower Chromitites of the Stillwater Complex, United States, 3) "Contact type" deposits which contain disseminated sulfides that are enriched in PGE, and associated with the contact zones of mafic to ultramafic intrusions such as the Platreef deposit in South Africa or composite plutons at the Lac des Iles deposit in Canada, 4) "Rift related" deposits, which are nickel and copper bearing sills found in association with rift-related structures. Examples include the Noril'sk Talnakh District in Russia, and the Jinchuan deposit in China, 5) "Meteor impact related", and in particular, a norite intrusion such as the Sudbury Irruptive Complex in Sudbury, Canada where a meteoritic impact is believed

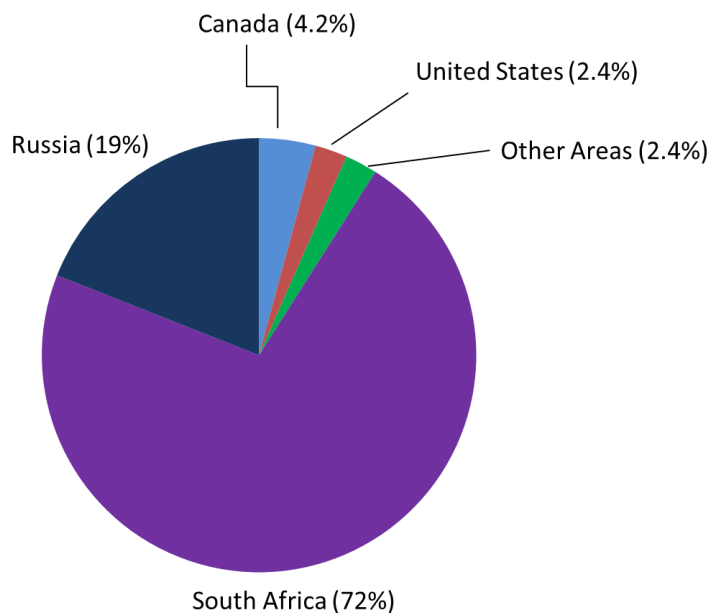


Figure 1.1 – The global distribution of platinum production. Data sourced from Hilliard, 2003

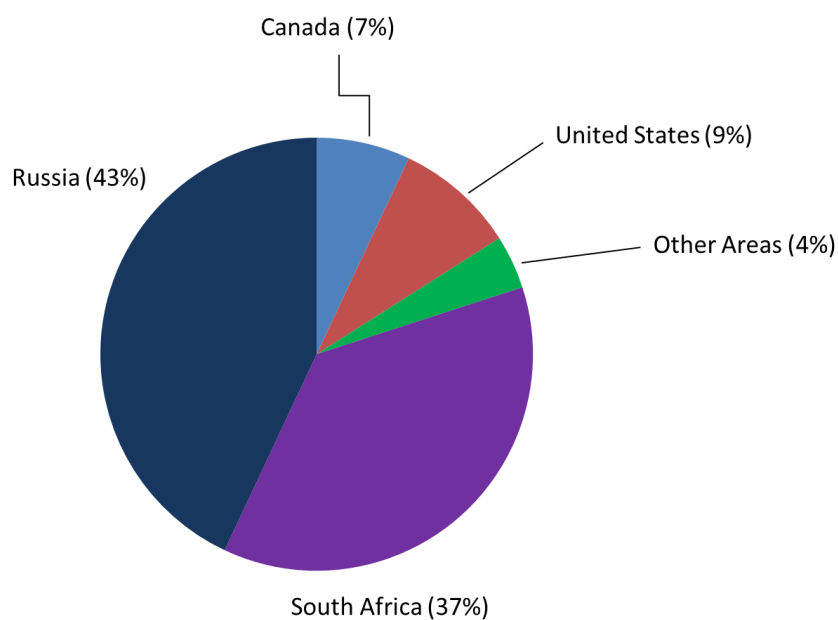


Figure 1.2 – The global distribution of palladium production. Data sourced from Hilliard, 2003

to have triggered significant quantities of magma emplacement, 6) “Dunite pipe type” in which high grade platinum mineralization occurs within discordant dunite pipes which may be up to 1 km in diameter, and 7) “Komatiite related”, which encompass all Ni-Cu-

PGE deposits related to komatiitic volcanic and intrusive rocks of Archean and Paleoproterozoic age.

1.6.1 Classification of the GLD

The mineralization style at the GLD consists primarily of disseminated PGE-hosting sulfides, namely chalcopyrite and bornite, which are most prominent at the basal contact margin of the intrusion. Mulja and Mitchell (1991) classified the GLD as a magmatic sulfide deposit that was derived from an evolved tholeiitic magma, while Good and Crocket (1994) classified the GLD as a late-stage magmatic-hydrothermal deposit. Before attempting to reconcile these different classifications of the GLD, the most current knowledge on Cu-PGE deposits will be summarized in the subsequent sections. Because Cu-PGE deposits are invariably associated with Ni, the following summaries will include Ni-Cu-PGE deposits.

1.7 Formation of a Ni-Cu-PGE Deposit

Most Ni-Cu-PGE deposits are the result of high temperature magmatic processes, and are commonly found within mafic and ultramafic hosts (Gunn and Benham, 2009). The abundance of PGE within basalts is low, but nevertheless enriched relative to most other igneous rocks. Average continental basaltic magmas contain 1-10 ppb Pt and Pd, whereas mid-ocean ridge basalts (MORB) are depleted in PGE containing < 1 ppb Pt and Pd due to multiple extended melting events (Naldrett, 2004). Relatively high PGE values of non-MORB melts indicate that these magmas did not attain sulfide saturation during their ascent from the mantle (Naldrett, 2004). Because the sulfur content within the mantle is low, these melts are generally sulfur under-saturated prior to interaction with crustal rocks.

The formation of a magmatic Ni-Cu-PGE deposit first requires that the magma is fertile in terms of PGE (Maier, 2005), followed by the equilibration of an immiscible sulfide melt within a silicate magma (Naldrett, 2004). Prior to equilibration, however, the magma must contain enough sulfur in order for a sulfide droplet to occur. The amount of sulfur required for a silicate melt to become saturated in sulfide is described as the sulfur

content at sulfide saturation (SCSS). Factors which control the SCSS within a silicate melt include: 1) changes in the bulk composition of the magma, particularly the addition of FeO, MgO, and CaO to the melt would require additional S in order to achieve sulfide saturation, whereas the addition of SiO₂ and Al₂O₃ would require less S in the melt to attain sulfide saturation, 2) the fugacity of oxygen and sulfur (fO_2 and fS_2 respectively), in that increasing fO_2 (while decreasing fS_2) at conditions where sulfur is sulfide results in less dissolved S within the silicate melt, since S is able to dissolve by displacing oxygen that is bonded to Fe²⁺, and consequently, a higher fO_2 results in an increase in Fe³⁺, thereby limiting the amount of S that is able to dissolve (Naldrett, 2004), 3) temperature, whereby an increase in temperature results in more readily dissolved sulfur, and consequently, more sulfur would be required in the silicate melt to reach sulfide saturation (Ripley and Li, 2013), 4) pressure, in that solubility of a sulfide within a mafic magma increases with decreasing pressure. Mavrogenes and O'Neill (1999) demonstrated that sulfur solubility in a mafic magma increases with decreasing pressure thus deducing that the emplacement of mafic magmas at shallow depths is not conducive with attaining sulfur saturation. Furthermore, they noted that if sulfur saturation were to be attained in a low-pressure environment, it would have to occur either through extensive fractional crystallization, or via the introduction of an external source of sulfur. In the case of fractional crystallization, the crystallization of olivine, pyroxene and feldspar may result in the separation of cotectic proportions of sulfide liquid (Ripley and Li, 2013). In such a sulfide-bearing system, the subsequent concentrations of Ni, Cu, and PGE within these sulfide phases is not only a measure of the composition of the parental magma, but also a function of the chemical and physical processes that take place during equilibration of the two immiscible melts (Naldrett, 2004).

Once sulfide saturation has been reached, the behaviour of the newly exsolved sulfide melt is quite complicated, particularly during its crystallization, and the products of its crystallization are affected by the proportions of Cu-Ni-Fe-S within the system (Barnes et al., 1996). Once the sulfide droplets segregate from the silicate magma, these droplets act as 'collectors' of chalcophile metals, owing to the high partition coefficients that chalcophile elements have into sulfide liquid (Barnes et al., 1996). Due to relatively high

density of sulfide liquid compared to silicate liquid, sulfide melt droplets are able to settle towards the base of an intrusion where they may coalesce to form a homogeneous or massive sulfide. In addition to collecting metals during gravitational settling, the sulfide melt may accumulate in a depression or area of lower flow in a conduit (owing to the very low viscosity of the sulfide liquid) after which subsequent pulses of PGE-bearing silicate magma may pass over, thereby furthering the upgrading process. The sulfide melt droplets can either crystallize in situ, or may also be injected into underlying or adjacent faults or breccia zones (or any structural trap). During crystallization of the sulfide liquid, the first mineral to form is monosulfide solid solution (MSS) (Naldrett et al., 1994; 1999). Fractional crystallization of the sulfide liquid, however, can produce an MSS-rich cumulate enriched in Os, Ir, Ru, and Rh, and consequently, a fractionated sulfide liquid enriched in Cu, Pt, Pd and Au (Figure 1.3) (Barnes et al., 1996; Mungall, 2007; Holwell and McDonald, 2010).

1.8 Notable Sulfide Rich, PGE-Poor Deposits

Keays and Lightfoot (1994) commented on several distinguishing features that are commonly used when evaluating exploration opportunities of newly discovered magmatic Ni-Cu-PGE deposits. Some of these features include: 1) the availability of source metals within mafic and ultramafic magmas, 2) a source of sulfur which could help the magma reach sulfur saturation (for example, sulfidic black shales), 3) the potential for gravitational segregation of dense immiscible sulfide liquid, and 4) the concentration of these sulfides into physical traps. These features, coupled with distinct geochemical characteristics and geophysical signatures (such as magnetic high signatures) have been crucial in distinguishing a variety of Ni-Cu-PGE deposits (Lightfoot, 2007). Some of the most notable Ni-Cu-PGE deposits will be briefly reviewed in this chapter, with particular attention to ore genesis.

1.8.1 Noril'sk Deposit Russia

At the Noril'sk deposit in Russia, the mineralized mafic to ultramafic intrusions intersect Devonian and Permian sedimentary formations, as well as basal trachybasaltic and tholeiitic members of Siberian Trap continental flood basalt (Fedorenko, 1991). There are

four mineralization types associated with the intrusions of the Noril'sk deposit: 1) Massive Ni-rich ores that occur the basal contact, and extend into underlying sedimentary rocks, 2) Brecciated ores at the upper contact of the Kharaelakh Intrusion, or the lower contact of the Talnakh Intrusion, 3) Disseminated sulfides within picritic gabbrodolerites and a group of variably-textured rocks with inclusions and vesicles, named "taxitic gabbrodolerites", and 4) PGE-mineralization associated with low sulfidic, pegmatoidal rocks that typically develop near the roof of economically mineralized intrusions (Sluzhenikin et al., 1994) (Lightfoot, 2007).

The Noril'sk intrusions are believed to have formed through a series of magma pulses, each of which produced lithologies of distinct petrological and chemical compositions. The variety in magma types is attributed to the mixing of mantle-derived magmas with crustal rock that was assimilated during passage to the surface (Arndt et al., 2003). Most commonly, the ore-bearing intrusions at the Noril'sk deposit are spatially associated with sulfate-rich Devonian sedimentary rocks, which Naldrett (1992) determined to be the source of sulfur within the mineralized intrusions. The magmas which fed the ore-bearing intrusions have trace element and isotopic compositions similar to overlying basalts, which occupy two-thirds of the volcanic sequence (Arndt et al., 2003). These magmas are believed to have experienced a very low degree of contamination prior to their passage to the surface. During their ascent, Arndt et al. (2003) believed that they encountered anhydrite-rich sediments during passage to the surface. However, physical evidence of magma assimilation during the intrusion of Noril'sk feeder pipes is not easily found, as angular xenoclasts of anhydrite show no signs of partial melting or assimilation (Lightfoot, 2007).

1.8.2 Jinchuan Deposit, China

The most well-known Chinese nickel sulfide deposits are commonly small intrusions that possess high R-factors (the ratio of sulfide melt to silicate melt), and they commonly contain multiple structurally-controlled ore zones (Chai and Naldrett, 1992). The Jinchuan deposit is associated with a structural zone which runs parallel to the Proterozoic Longshushan Belt (Lightfoot, 2007). The intrusion consists primarily of five

different lithologies, including (in decreasing abundance): lherzolite, dunite, plagioclase lherzolite, olivine websterite, and websterite (Chai and Naldrett, 1992). Mineralization is primarily represented by disseminated sulfides within plagioclase lherzolite. Sulfide mineralization commonly occurs lower in the stratigraphy of the intrusion, and are represented by lesser amounts of net-textured sulfide, in addition to small amounts of massive sulfide ore (Chai and Naldrett, 1992).

The disseminated and net-textured sulfides are distinguished by generally low concentrations of PGE, while massive sulfides are characterized by exceptionally low values of Pt, but high Cu/Pd ratios. These low PGE values suggest that the sulfides most likely formed from silicate magmas that had already undergone prior sulfide segregation (Song et al., 2009). Hence, the Jinchuan sulfides are thought to have developed through a second stage of sulfide segregation from a PGE-depleted magma. Ultimately, the Jinchuan intrusion and associated ore bodies were formed by injections of sulfide-free and sulfide-bearing olivine mushes from a deep-seated staging chamber (Song et al., 2009).

1.8.3 Voisey's Bay, Canada

The Voisey's Bay deposit is located within the 1.334 Ga (Amelin et al., 1997) Voisey's Bay complex, which in turn is associated with the larger anorthosite-granite-troctolite-ferrodioritic Nain Plutonic Suite (1.35-1.29 Ga) (Naldrett, 1998). The Voisey's Bay Ni-Cu-Co deposit lies partly within a 30-100 m sheet of troctolite, and partly within the base of the intrusion. The troctolitic sheet is interpreted to be a feeder for the Voisey's Bay intrusion (Naldrett, 1998).

The genesis of ore at Voisey's Bay is recognized in two stages. First, troctolitic magma rose to form what is now the Reid Brook intrusion within the Tasiuyak gneiss. This magma intrusion is believed to represent a magma chamber which fractionated, and hence, formed ultramafic cumulates. The melt then reacted with the Tasiuyak gneiss, and consequently attained sulfur saturation. Then, in the second stage, this magma migrated upwards the upper (Eastern Deeps) chamber. Simultaneously, fresh magma entered the

lower chamber, disrupting the cumulate phase and mixing with residual magma and sulfides within it, resulting in stronger metal tenors within the sulfides. The sulfides concentrated in the widened zones within the linking sheet, and at the mouth of the feeder where the rate of magma flow was notably slower as magma entered the chamber (Naldrett, 1998).

1.9 Notable Sulfide Poor, PGE-Rich Deposits

The majority of global PGE reserves are contained within sulfide poor, stratabound deposits. These low sulfide, PGE-rich systems are synonymous with mafic to ultramafic layered intrusions that contain PGE-enriched lode mineralization (Zientak, 2012). The term “PGE-reef” is commonly used to describe such a deposit style, and in the literature, refers to either: 1) a rock layer with a distinct texture and mineralogy that contains mineralization, or 2) only the PGE-mineralization that is present within a rock layer (Naldrett, 2004). Reef-type mineralization tends to be laterally continuous along strike for tens to hundreds of kilometers (Zientak, 2012). Some of the most notable reef-type PGE deposits are briefly reviewed in this section.

1.9.1 Bushveld Complex

Formation of the world-class PGE mineralization at the Bushveld Complex is undoubtedly one that is hotly debated (Lee and Perry, 1988; Scoon and Teigler, 1994; Naldrett et al., 2009). One of the most prominent models is that of Maier et al. (2012), who describes how an incompletely solidified magma chamber can undergo subsidence in response to crustal loading. This results in slumping of semi-consolidated slurries of cumulate-laden magma towards the center of the intrusions, where they are hydrodynamically separated, resulting in the formation of dense layers that are enriched in sulfides, oxides, olivine, pyroxene and less dense layers enriched in plagioclase. The emplacement depth of the Bushveld Complex had to have been relatively shallow, as deeper, more ductile crust would not collapse as readily and trigger subsidence (Maier et al., 2012).

The Bushveld complex comprises three very different ore bodies, including the Merensky Reef, the Upper Group 2 (UG2) chromitite, and the Platreef. Both the Merensky Reef and the UG2 chromitite are traceable on surface for over 300 km in two separate arcs, while the Platreef extends for over 30 km (Cawthorn, 1999). Due to the enormous volume of magma involved during formation of the Bushveld Complex, cooling and crystallization were very slow processes (Cawthorn, 1999). As cooling progressed, phase relations dictated the sequence and rate at which different minerals precipitated. Eventually, accumulation of these minerals occurred in sub-horizontal layers, building upwards from the base of the chamber. Erratic magma replenishment led to repetition of this crystal sequence, producing pronounced repetitions in mineral layering. While most of these mineral layers are economically insignificant, some of the monomineralic layers are benefitted by the constant replenishment of magma which allows for the potential enrichment in precious metal constituents that otherwise would be insufficiently concentrated. An example of such favourable enrichment is noted by the presence of chromite and vanadium-bearing magnetite layers that are enriched by factors up to 300 relative to the composition of the parent magma (Cawthorn, 1999). Further studies have also demonstrated that chloride-carbonate rich fluids may have played a factor in the distribution of ore around the deposit (Kanitpanyachoen and Boudreau, 2013).

1.9.2 Stillwater Complex

Located in southern Montana, the Stillwater Complex has been defined as a layered ultramafic to gabbroic intrusion dated at 2,700 Ma (Todd et al., 1982), and has drawn many comparisons to the Bushveld Complex (Maier et al., 1996). Exposure of the Stillwater Complex occurs for over 44 km along a WNW strike adjacent to a northern boundary with the Beartooth Mountains. The intrusion is underlain by Archean metasedimentary rocks, and overlain by Phanerozoic sedimentary assemblages (Keays et al., 2012). Exposed metasedimentary rocks include metagraywacke, iron-formation, blue quartzite, diamictite, and metashale. Sulfide minerals within the metagraywackes, metashales and iron-formation consist of pyrrhotite, pentlandite and chalcopyrite, all of which are spatially associated with a pyroxene-hornfels facies zone (Zientek and Ripley, 1990). The Stillwater Complex is comprised of five subdivisions, known as: the Basal,

Ultramafic, Lower Banded, Middle Banded, and the Upper Banded Series (Keays et al., 2012).

Sulfide mineralization within the intrusion occurs throughout the stratigraphic succession, but is most concentrated towards the basal contact, occurring within chromitite layers, podiform pegmatoids, discontinuous discordant pods or pipes, and within thin stratiform layers (Zientek and Ripley, 1990). Common sulfide minerals include pyrrhotite, pentlandite and chalcopyrite, all of which exhibit textures that are consistent with formation as a result of crystallization from an immiscible sulfide liquid (Zientek and Ripley, 1990). Sulfide saturation appears to have been attained due to contamination from iron-formation. Pd enrichment within the sulfides is believed to have occurred in PGE in two stages (Godel and Barnes, 2008): 1) first the sulfide liquid interacted with a large volume of magma with PGE composition similar to that of a high-Mg basalt, and ultimately crystallized at a level where the porosity of the crystal mush could not facilitate further migration. Post crystallization, a fluid deposited Pd while altering base metal sulfides to magnetite (Godel and Barnes, 2008).

1.9.3 Other Sulfide-Poor PGE-Rich Deposits Within North America

Other PGE-rich and sulfide poor deposits within North America include the Duluth Complex in Minnesota, the Eagle Deposit in Michigan, the Lac des Iles Deposit in Thunder Bay, Ontario, and the Marathon Deposit in Marathon, Ontario. Some of these occurrences are summarized in further detail in Chapter 2, under “Geology of Mineral Occurrences Related to the MCR” in Section 2.2.1 as they are associated with the mid-continent rift system (MCR) of North America, which provided an ideal tectonic setting for the heavy magmatism that is required to produce such deposits (Naldrett, 2004), including the GLD.

1.10 Stable $\delta^{18}\text{O}$ Isotopes

Isotopes are atoms that contain the same amount of protons and electrons, but a different amount of neutrons. Stable isotopes are those which contain stable nuclides that are not

radioactive, meaning that they do not undergo spontaneous radioactive decay. Naturally, oxygen is comprised of three stable isotopes (with their abundances in parentheses): ^{16}O (99.758%), ^{17}O (0.039%) and ^{18}O (0.205%) (Hoefs, 2004). The mass of the heavy oxygen isotope ^{18}O differs from that of the lightest isotope ^{16}O by 12.5 %. The difference in the mass of an isotope of any element affects the strength of covalent bonds that these isotopes form with atoms of other elements (Faure and Mensing, 2005). Due to the high abundances of ^{16}O and ^{18}O , the ratio of $^{18}\text{O}/^{16}\text{O}$ is typically used in determining the oxygen isotopic composition of a rock. However, this data is reported relative to their deviation from a standard material known as Vienna Standard Mean Ocean Water (VSMOW). This can be summarized as:

$$\delta = \left(\frac{R_{\text{sample}}}{R_{\text{standard}}} - 1 \right) \times 1000 \quad \text{Eq. 1.1}$$

where R_{sample} is the $^{18}\text{O}/^{16}\text{O}$ ratio in the sample, and R_{standard} is the $^{18}\text{O}/^{16}\text{O}$ ratio for the standard VSMOW, reported in a ‘per mil’ notation (‰). For instance, if a rock sample had a whole rock $\delta^{18}\text{O}$ value of +10‰, this would mean that the sample is 10 per mil (or 10 parts per thousand) richer in ^{18}O than that of VSMOW. Notice that the oxygen isotope value of a whole rock sample is dependent upon the $\delta^{18}\text{O}$ -values of the constituent minerals, and the proportions of these minerals. Additionally, the $\delta^{18}\text{O}$ -value of each mineral is dependent upon the bond strength, and bond type within each respective crystal structure (Hoefs, 2004). Additional factors that affect $\delta^{18}\text{O}$ values of rock include temperature of formation, and the $\delta^{18}\text{O}$ of magma and waters that have been in exchange with the rock.

Equilibrating effects can result in various ratios of oxygen isotopes. These processes, which affect the relative abundances of isotopes, are collectively described by equilibrium fractionation (Hoefs, 2004). The fractionation factor, or α , represents the isotopic partition coefficient for two minerals or chemical compounds in equilibrium (species A and species B) and is summarized in Taylor (1979) as:

$$\alpha_{AB} = \frac{R_A}{R_B} \quad \text{Eq. 1.2}$$

And thus, from the definition of δ in Eqn. 1.1, the following can be derived:

$$\ln \alpha_{AB} = \ln \left(1 + \frac{\delta_A}{1000} \right) - \ln \left(1 + \frac{\delta_B}{1000} \right) \quad \text{Eq. 1.3}$$

Temperature dependence of oxygen isotope fractionation between minerals in rock and fluid is also a variable that should be considered. Since oxygen is a primary constituent in most rocks, and H₂O tends to be the dominant constituent of ore-forming fluids, the interaction between rock and circulating fluids can be documented by using $\delta^{18}\text{O}$ values (Taylor, 1979). Typically, this interaction between rock and circulating fluids results in either the re-equilibration of primary minerals, or the precipitation of new minerals (Hoefs, 2004). The outcome of this interaction is dependent on the $\delta^{18}\text{O}$ content of the original minerals, the proportions of these minerals within the rock, and the extent of the interaction between the rock and fluids (Hoefs, 2004). In general, when silicate rocks come in contact with meteoric water, the water becomes enriched in ^{18}O while the rocks become depleted in ^{18}O (Criss et al., 1987). The effect that such isotope exchange reactions have on the oxygen isotopic composition of the rocks and water depends on both the temperature of the system, and the water-rock ratio. As the temperature of the system increases, the effective solid-liquid fractionation factor (α) approaches unity, and consequently the difference between the $\delta^{18}\text{O}$ content of the rocks and the water also approaches zero. However, in situations where water percolates through permeable rocks at moderate temperatures, the water-rock ratio is large and the isotope composition of the rocks approaches that of the water. Conversely, if the system is dominated by rock (which yields a small water rock ratio) then the isotope composition of the water will approach that of the rocks. In most cases, water dominates and the isotopic composition of affected rocks is permanently altered by being depleted in ^{18}O (Faure and Mensing, 2005).

Chapter 2

2 Geology

The Geordie Lake Deposit (GLD) is contained within an elongate, mafic intrusion known as the Geordie Lake Intrusion (GLI) that is associated with the Proterozoic Coldwell alkaline complex in north-western Ontario, roughly 14 km north-west of the Town of Marathon, Ontario (Figure 2.1). The Coldwell alkaline complex was emplaced at 1108 ± 1 Ma, resulting from the failed mid-continent rift system (MCR) in North America (Heaman and Machado, 1992). The entire rift system stretches for over 2000 km from Kansas, USA, to the Lake Superior Region (Van Schmus and Hinze, 1985). The Coldwell alkaline complex is located between the Pic River and Dead Horse Creek, on the north shore of Lake Superior. The southern part of the complex is accessible via Highway 17 (the Trans-Canada highway). A wide range of mineral occurrences exist within the complex, including: base metals (primarily Cu, Ni), PGE and associated metals (V, Ti), rare metals (Nb, Y, Zr and various rare-earth elements), industrial minerals (nepheline), semi-gemstones (spectrolite), as well as building stone (Van Schmus and Hinze, 1985). The regional geology of the Lake Superior region is dominated by rocks of Proterozoic age, which overlie or cross cut Archean basement rocks.

2.1 Archean Superior Province

Rocks related to the MCR are underlain by Archean basement rocks of the Superior Province, which individually comprises 23 percent of Earth's exposed Archean crust (Thurston, 1991). The majority of the Superior Province is believed to have accreted as a result of east-west trending belts during the Kenoran Orogeny, between 3.0 to 2.7 Ga. At its margins, the Superior Province is bounded by Proterozoic orogenic belts including the New Quebec orogeny to the north-east, the Grenville Orogeny to the southeast, the Penokean Orogeny to the south, and finally, the Trans-Hudson Orogeny to west and north-west (Hoffman, 1989). The Superior Province has classically been subdivided into smaller provinces on the basis of lithological variations, degree of metamorphism, and geophysical characteristics (Stockwell, 1964, Card and Ciesielski, 1986). Four distinct

subprovinces within the Superior Province are currently recognized: 1) metasedimentary subprovinces that are accumulations of mainly clastic metasedimentary rocks with low-grade metamorphosed margins, and amphibolite to granulite facies interiors, 2) volcanoplutonic subprovinces that are distinguished by low metamorphic grade greenstone belts, 3) gneissic or plutonic subprovinces distinguished by tonalitic gneiss, and a variety of extrusive and intrusive mafic enclaves, and 4) high-grade gneissic subprovinces consisting of amphibolite to granulite facies gneisses cut by tonalitic, granodioritic and syenitic intrusions (Card and Ciesielski, 1986, Thurston, 1991, Williams et al., 1992, Card and Poulson, 1998). The boundaries of these subprovinces are distinguished by contrasts in metamorphic and structural geology, highlighted by a series of east-west trending faults. Only the subprovinces proximal to the intrusive Coldwell alkaline complex will be summarized any further in this chapter.

2.1.1 Wawa-Abitibi Subprovince

The Wawa-Abitibi subprovince is characterized as an aggregation of granitoid plutons, with lesser greenstone belts (Percival et al., 2006). To the north, the boundary is structurally defined by overlying metasedimentary rocks of the Quetico subprovince. To the south it shares a boundary with the Great Lakes Tectonic Zone, which marks a contact with the Minnesota River Valley gneiss terrane and the Marquette greenstone belt (Stott, 2011). Within the Wawa-Abitibi subprovince, there are two concentrations of greenstone belts; one being at its northern boundary with the Quetico subprovince, and the other within the Mishibishu-Michipicoten-Gamitagama area.

Initially, both the Wawa and Abitibi subprovinces were divided into their own separate classifications (Williams et al., 1991). However, it is now widely accepted that there is a correlation across the Kapuskasing uplift structure between the Wawa and Abitibi terranes (Percival and West, 1994; Percival, 2006). Volcanism within the Wawa terrane appears to have begun between 2.89-2.88 Ga with what formed the Hawk assemblage (Turek et al., 1992). The Wawa (2.745 Ga), Greenwater and Manitouwadge (2.72 Ga) assemblages formed a large back arc-system that is known to host massive sulfide deposits in the Shebandowan, Winston Lake, and Manitouwadge greenstone belts

(Williams et al., 1991, Sage et al., 1996, Corfu and Stott, 1998). Studies on the Schreiber belt have shown that it is composed of a variety of oceanic magma types, and hence, it is interpreted to be a tectonic mélangé (Polat and Kerrich, 1999). Deformation occurred at 2.689, and was synchronous with sanukitoid magmatism between 2.68 to 2.65 Ga (Percival, 2006). The Wawa subprovince amalgamated with the Quetico accretionary prism to the north due to continued plate convergence and transpressive interaction post-subprovince amalgamation (Williams et al., 1991).



Figure 2.1 – General map of Ontario, Canada, with the location of the Geordie Lake Deposit indicated by a red star

2.1.2 Quetico Subprovince

The Quetico subprovince, also referred to as the Quetico basin, is a predominantly linear metasedimentary terrane measuring more than 1000 km from Minnesota in the southwest, extending all the way through Ontario, and into Quebec (Stott et al., 2010). The Quetico subprovince is bounded to the south by the Wawa-Abitibi subprovince, and to the north by the Wabigoon subprovince. Lithologies consist primarily of supracrustal sedimentary

sequences, particularly turbiditic greywacke and pelites that are metamorphosed to schists, paragneisses, and migmatites. Anatexis of these sedimentary sequences have resulted in the intrusion of abundant S-type granites and pegmatites. The greywackes and pelites that comprise the Quetico subprovince were formed as an accretionary prism that developed south of the Wabigoon terrane before collision of the Wawa terrane from the south (Williams, 1991; Valli et al., 2004).

The sedimentary environment during the deposition of Quetico wackes and pelites is believed to have been a submarine basin of great lateral extent, since the wackes and pelites show very little compositional variation and exhibit sedimentary features that are reflective of unstructured turbidite fans (Fralick et al., 2006). These sedimentary lithologies were subjected to intense shearing and subsequent layer-thickening. One of the most notable features within the Quetico terrane is the Dog Lake Granite chain, which is comprised of six ovoid, magnetite-bearing granitic intrusions (Kuzmich, 2012). These intrusions are believed to have been derived from mafic melts that evolved into granitic melts through crystal fractionation (Kuzmich, 2012). Deformation of the Quetico terrane occurred prominently between 2.70 to 2.66 Ga, as a response to a variety of tectonic stresses (Williams, 1991).

2.1.3 Winnipeg River Terrane

The Winnipeg River terrane describes the plutonic domain bounded to the east and west by the Eastern and Western Wabigoon domains, respectively, the English River Basin to the north, and the Marmion terrane to the south. It is comprised of two elements: 1) An over 500 km long terrane of Neoproterozoic plutonic rocks, and 2) a Neoproterozoic plutonic domain that was formerly referred to as the central Wabigoon subprovince.

Tonalites are the oldest units at 3.32-3.04 Ga, followed by Neoproterozoic tonalite-granodiorites at around 2.72-2.71 Ga, and the emplacement of granites at 2.70-2.69 Ga (Beakhouse, 1991; Corfu and Stott, 1996). There was a noted lack of magmatism in a particular section of the Winnipeg River terrane just north of the Wabigoon subprovince during the time period 2.75-2.71 Ga, which happened to be a time of major activity in

nearby Wabigoon and Uchi subprovinces. The reasoning for this is that this particular part of the Winnipeg River terrane remained tectonically isolated until around 2.71 Ga, at which point it began to interact with neighbouring arc terranes (Percival, 2006).

2.2 Mid-Continent Rift System of North America (MCR)

The mid-continent rift system (MCR), or also referred to as the Keweenaw Rift, is one of the largest known continental rifts in the world (Heaman and Machado, 1992). The MCR is hosted by the Archean Superior Province within the Canadian Shield, the Early Proterozoic Southern Province (1.9 Ga), and extends south-west into the Yavapai-Mazatzal suture (1.65-1.68 Ga) (Figure 2.2). Lake Superior occupies a basin that was created by the rift, and near the lake, rift-rocks are found on surface in the Keweenaw Peninsula of Upper Michigan, northwest Wisconsin, and on the north shore of Lake Superior in Minnesota and Ontario (Van Schmus and Hinze, 1985). Rift-related rocks are seen as far south as Interstate Park near Saint Paul, Minnesota, but a large portion of the rift remains buried beneath sedimentary rocks up to 9 km thick (Palacas, 1995). The full extent of the MCR is more easily observed through gravity anomalies (Figure 2.3), where dense basaltic rock of the early rift increases gravity locally.

Rifting began consequently after the development of a mantle plume beneath modern day Lake Superior and the upper peninsula of Lake Michigan, which caused thermal doming of proto North America (Laurentia), eventual thinning of the crust, and subsequent rifting. Stresses generated by the deep heat and pressure differences generated by a mantle plume pulled at the continent and opened fissures through its crust. As the rift continued to grow and the valley floor sank, more and more volcanic rocks were deposited, eventually reaching tens of thousands of metres in thickness. Ultimately, for reasons still not quite yet known, the rift failed to develop but not before intrusions of gabbro, syenite, and the eruption of mafic volcanics filled much of the rift. This Keweenaw volcanism took place between 1108 and 1087 Ma (Palmer and Davis, 1987). Studies conducted on Keweenaw volcanism suggest that this period was marked by substantial plutonism, with one study estimating that approximately 300,000 km³ of magma was intruded (Green & Fitz, 1993), while another study estimated that 850,000

km³ (Hutchinson, et al. 1990) of magma was intruded into the Archean Superior and Early Proterozoic Southern Provinces. Deposition of siliciclastic sediment filled the remainder of the rift prior to uplift and erosion towards the end of the Precambrian.

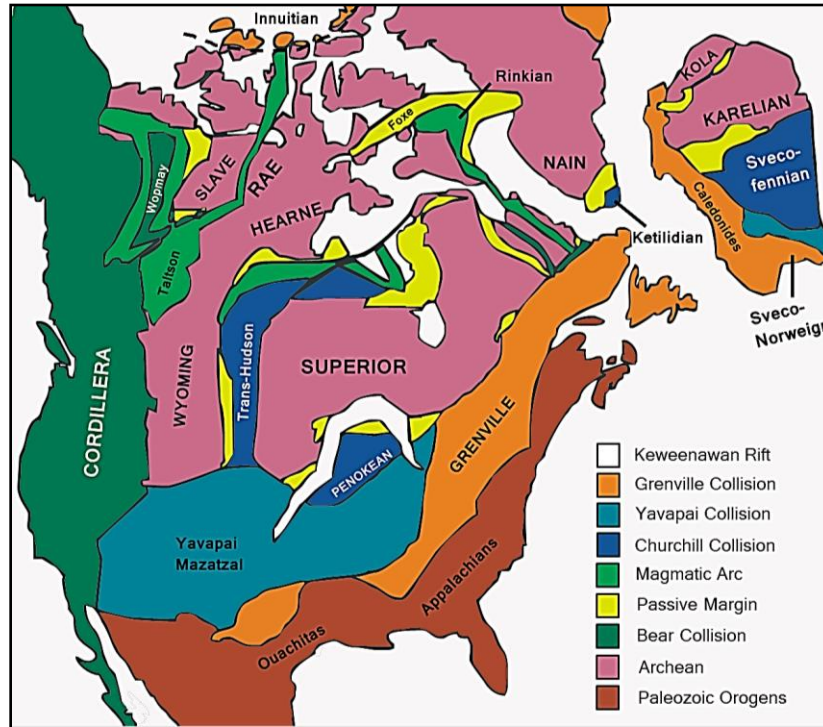


Figure 2.2 – Cartoon map of the North-American, and some Scandinavian basement rocks. The Keweenawan Rift, also known as the mid-continent rift system (MRS) is shown in the roughly the middle of the continent in white. Modified after USGS Open File Report (1995)

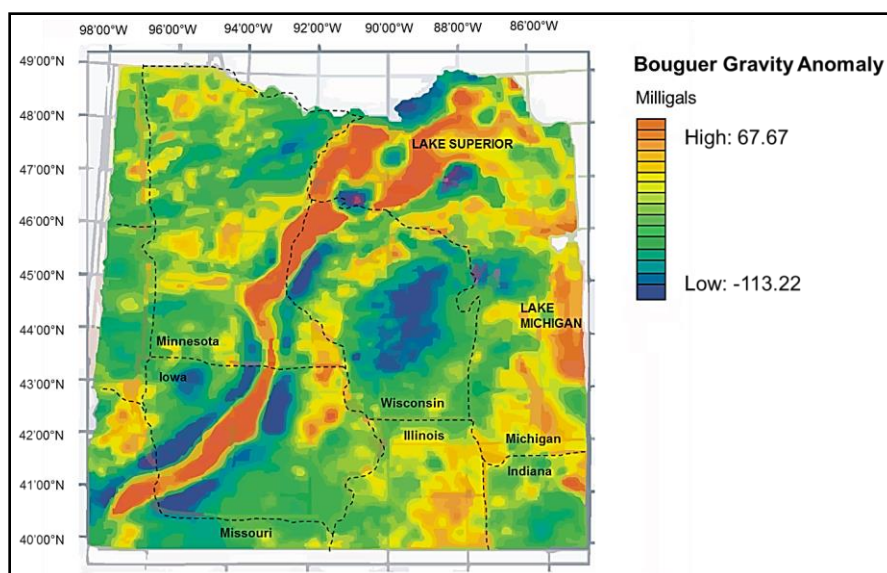


Figure 2.3 – A bouguer gravity map, outlining the high gravity anomaly caused by the Mid-continent rift system (MRS) in orange. Figure modified from Farrow and Johnson, 2012

2.2.1 Geology of Mineral Occurrences Related to the MCR

Naldrett (1992) pointed out that the Lake Superior region possesses an ideal geologic situation to justify such rigorous exploration, noting the presence of a triple junction with associated rifting and subsequent basalt formation (with some basalts even showing evidence of chalcophile element depletion). Economic to near-economic concentrations of mineralization within the MCR are commonly hosted within mafic to ultramafic intrusions. Mineralization style ranges from disseminated, net-textured, semi-massive, to even massive sulfide mineralization (Miller et al., 2010). Notable deposits associated with the MCR include the Duluth Complex (high-tonnage, low-grade), Eagle deposit (high grade, low tonnage), Marathon deposit (low-to-medium grade, mid-range tonnage), and the Geordie Lake Deposit (low-to-medium grade, low tonnage) (Figure 2.4).



Figure 2.4 – The location of MRS-related Ni-Cu-PGE deposits in and around the Lake Superior region, indicating grade and tonnage. Data obtained from Magma Metals Thunder Bay North 43-101 (Thomas et al., 2011), Marathon PGM Marathon Deposit 43-101 (Puritch et al., 2009), Listerud and Meineke (1977) (Duluth Complex), Ware (2007) (Eagle Deposit), and Rio Tinto conceptual estimate (2008) (Tamarack Deposit)

2.2.1.1 Duluth Complex

The Duluth Complex is a product of voluminous magmatism caused by the MCR of North America, and is composed of an extensive sequence of mainly anorthosites and troctolites. The complex extends roughly 240 km northeast from Duluth, Minnesota. The western margin of complex dips at approximately 50 degrees, while the north-western margin of the complex dips shallower at roughly 20-30 degrees.

At least 26 different intrusions have been distinguished; however the Partridge River intrusion and the South Kawishiwi intrusion contain most of the Cu-Ni-PGE mineralization (Gal et al., 2011). Mineralization is broadly defined as being hosted by a layered gabbro; however continuous layering is often difficult to distinguish (Miller, 2002). Four broadly grouped rock series characterize the Duluth Complex based on age, dominant lithology, internal structure, and structural position relative to the complex: 1)

The Felsic Series (~1108 Ma) consisting of massive granophyric granite with lesser amounts of intermediate rock, 2) the Early Gabbro Series (~1107 Ma) which is a predominantly gabbroic, layered sequence of cumulates that were emplaced early during initial magmatism at the northeastern contact of the complex, 3) the Anorthositic Series (~1099 Ma) consisting of complicated plagioclase-rich gabbroic cumulates that are foliated, but rarely layered, and 4) the Layered Series (~1099 Ma) which is a suite of stratiform ferro-gabbroic to troctolitic cumulates emplaced mainly at the base of the complex, which include at least 11 variably differentiated mafic layered intrusions (Miller et al., 2002). Sulfide mineralization is discontinuous and heterogeneous, and not constrained to any one of these rock series.

The Duluth Complex hosts a significant reserve of mineralization, with more than 4×10^9 tonnes averaging 0.66 wt.% Cu and 0.20 wt.% Ni (Listerud and Meineke, 1977). The bulk of this mineralization occurs near the base of the Partridge River and South Kawishiwi intrusions, although local zones of sulfide containing high concentrations of PGE occur stratigraphically higher than the main zone of Cu-Ni mineralization within the South Kawishiwi intrusion (Miller and Ripley, 1996). Mineralization comprises pyrrhotite, chalcopyrite, pentlandite, and cubanite that is weakly disseminated (termed 'cloud sulfides') and hosted by troctolite and norite. Different mechanisms have been proposed to explain the heterogeneous nature of the Duluth Complex, but the main factors include: 1) The turbulent nature of the magma, 2) The path through which it was emplaced, 3) The size of magma pulses, 4) The sulfur content in the magma before it was emplaced and 5) The amount of sulfur present in the footwall rocks (Miller et al., 2002).

The vast reserves of sulfide mineralization at the Duluth Complex are best explained to have originated magmatically via external sulfur being added to the parent magma essentially in-situ by surrounding country rock, including the adjacent Virginia slates and Biwabic Iron Formation (Ripley, 1986). Sulfur isotopes indicate positive $\delta^{34}\text{S}$ along the sulfide mineralized footwall contact, indicating secondary sulfur enrichment through metapelitic crustal contamination. A comparison of MgO, FeO and SiO₂ reveal that different intrusions within the Duluth Complex are genetically related, but are

differentiated from one another due to fractional crystallization. The Duluth Complex may be an example of a reaction chamber from which sulfide-bearing magma ascends to a higher level. It is within this rise through a magma conduit that the sulfides become concentrated to their current economic levels (Naldrett, 2004).

2.2.1.2 Eagle Deposit

The Eagle intrusion, which hosts the Eagle deposit, is irregularly shaped and is associated with the Mesoproterozoic Marquette-Baraga dyke swarm (Ripley, 2014). Sulfide mineralization developed in a dynamic magma conduit setting during the early stages of the MCR (Ding et al., 2012). There are four widely recognized zones of sulfide mineralization at the Eagle deposit: 1) disseminated sulfides hosted within olivine-rich rocks, 2) massive sulfides, 3) semi-massive sulfides both above and below the zone of massive sulfides, and 4) sulfide veins along sedimentary country rock. All of these sulfide-bearing zones contain pyrrhotite, pentlandite and chalcopyrite, except that the upper semi-massive sulfide zone (which lies above the massive sulfide zone) contains more cubanite (Ding et al., 2012).

The host magma is picritic to ferro-picritic in composition, and sulfide saturation of the magma was attained due to country rock-derived sulfur (Ding et al., 2012). The accumulation of suspended olivine crystals and sulfide droplets from ascending magmas as they passed through wide parts of the conduits played a critical role in the formation of olivine-rich rocks and sulfide ores within the Eagle intrusion. The distribution of PGE, however, is variable among the different zones of sulfide mineralization. Such variability is explained through the fractional crystallization of mss from sulfide liquids (Ding et al., 2012).

2.3 Coldwell Alkaline Complex

The Coldwell alkaline complex is one of a number of regionally scattered plutonic suites that are believed to have formed from the aborted MCR in the Proterozoic. It is the largest recognized alkaline intrusion in North America, measuring roughly 28 km in diameter (Walker et al., 1993). It is widely considered to be a composite intrusion (Jago,

1980; Nicol, 1990) that measures 580 km² and was intruded into Archean metavolcanic and metasedimentary rocks of the Schreiber-White River greenstone belt, which forms part of the Wawa-Abitibi subprovince (Mitchell and Platt, 1978; Polat et al., 1998). On the eastern edge of the complex, the contact with the Archean rocks of the Wawa-Abitibi subprovince has a regular, arcuate shape whereas on the western edge, the contact is irregular and faulted. Within 50 m of these contacts, the rocks are contact metamorphosed to pyroxene hornfels grade (Shaw, 1997). The complex is unusual in that it contains a wide variety of rock types including those which are silica oversaturated, silica saturated and silica undersaturated. However, the genetic relationship between the various magma types remains unclear (Heaman and Machado, 1992). It is likely that a number of processes, including fractional crystallization, liquid immiscibility, co-mingling of magmas, post-crystallization alteration, and crustal contamination had at some point played a role in the complicated geochemical and isotopic evolution of the Coldwell complex. Mafic rocks of the Coldwell Alkaline Complex are mainly tholeiitic and sub-alkaline, whereas felsic rocks, specifically syenites, are most commonly alkaline. The overall configuration of shallow-dipping units within the complex shows that it was emplaced as sheet-like bodies during cauldron subsidence (Mitchell and Platt, 1977). Some of the earliest work by Lilley (1964) interpreted the Coldwell alkaline complex as a funnel shaped body of gabbro which fractionally crystallized, and was later intruded by nepheline syenites. Later work by Puskas (1967) reinterpreted the complex as a large lopolith. Detailed field and petrographic studies conducted by Puskas (1970), Mitchell and Platt (1977, 1982), Mitchell et al. (1993), and Shaw (1997) show that the complex in fact consists of three overlapping ring intrusions. These ring centers, later termed intrusive centers I, II, and III are each believed to represent a different pulse of magmatism (Figure 2.5).

Center I is the oldest magmatic center and hosts the eastern gabbro. The eastern gabbro contains significant Cu-PGE mineralization within the Two Duck Lake Intrusion (TDLI) (Watkinson et al., 1973; Wilkinson and Colvine, 1978; Watkinson et al., 1983; Good and Crockett, 1990, 1994; Ruthart et al., 2012). Center II consists mainly of nepheline-bearing alkali gabbros and syenites, and center III is primarily comprised of syenites and

quartz syenites exhibiting various degrees of crustal contamination (McLaughlin & Mitchell, 1989).

2.3.1 Emplacement of the Coldwell Alkaline Complex

Results from a U-Pb study of zircon and baddeleyite within a broad spectrum of Coldwell Complex lithologies, conducted by Heaman and Machado (1992), demonstrate that the majority of rock types were emplaced around 1108 ± 1 Ma. During this brief window of emplacement, a diverse suite of magma types were intruded including those of magmatic centers I, II, and III. This data, in addition to detailed U-Pb chronostratigraphy available for MCR volcanism (Davis and Sutcliffe, 1985; Palmer and Davis, 1987; Davis and Paces, 1990), clearly shows that Coldwell Complex igneous activity occurred during the early stages of rifting. This is in stark contrast to some previous works that have reported that Coldwell magmatism occurred relatively late in the magmatic evolution of the rift, with a gradual progression from tholeiitic to alkaline magmas over time (Mitchell et al., 1983). The age date of 1108 ± 1 Ma obtained for the Coldwell Complex is in excellent agreement with U-Pb age dates obtained for multiple igneous suites within the Lake Superior region, including the Logan sills ($1109^{+4/-2}$ Ma; Davis and Sutcliffe, 1985), and a rhyolite porphyry from the base of the Keweenawan Osler Group Volcanics ($1108^{+4/-2}$ Ma; Davis and Sutcliffe, 1985). These age dates document the contemporaneous production of tholeiitic and alkaline magmatism during the early developmental stages of the MCR.

2.3.2 Mafic Units Within the Coldwell Alkaline Complex

Mafic intrusives associated with the Coldwell Alkaline Complex have historically been an active exploration target for Ni-Cu-PGE deposits. Gabbroic bodies within the Coldwell Complex include the TDLI and the GLI, the Eastern Gabbro series, as well as a Fine-Grained series which pre-dates the Eastern Gabbro (Good, 2014). The Coubran

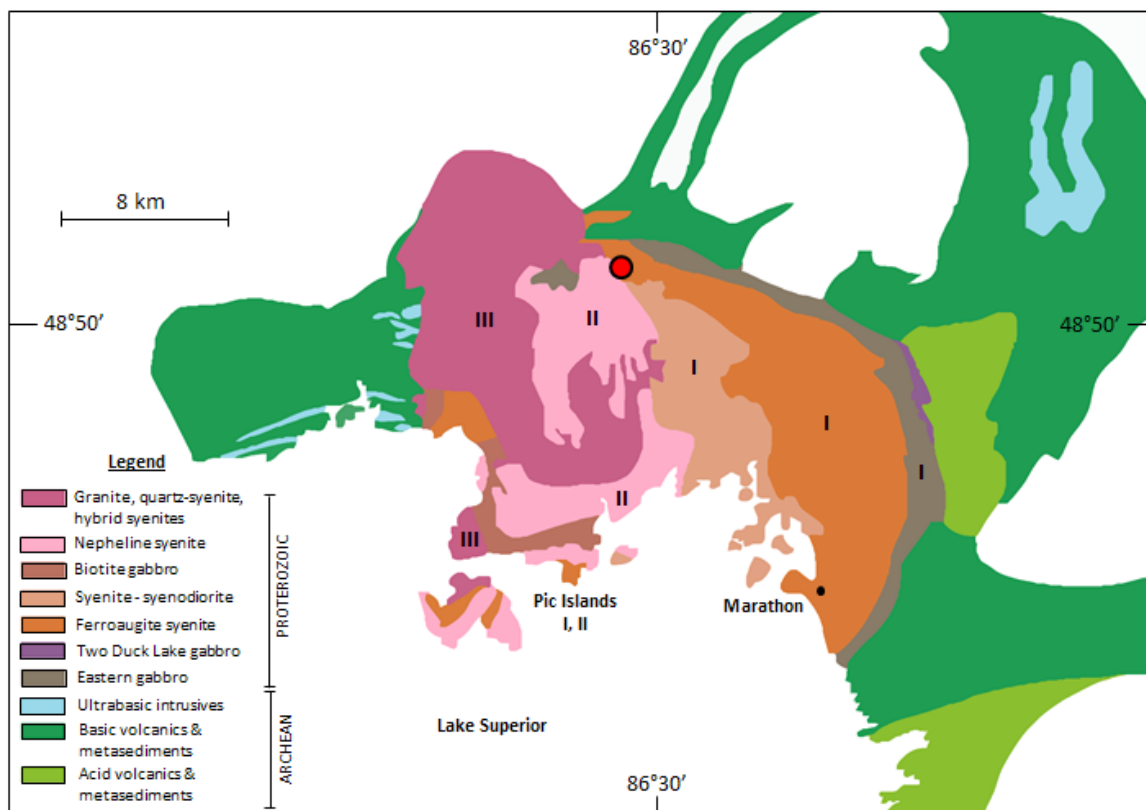


Figure 2.5 – Geological map of the Coldwell Alkaline Complex. Modified from Mulja and Mitchell (1991). The location of the GLD is denoted by the red dot.

Lake basalt lies roughly 2-3 km north of the Geordie Lake gabbro and has been shown by Cundari (2012) to be geochemically similar to the Two Duck Lake gabbro. Gravity modelling of the complex has indicated that there is a large body of mafic rock deep below the surface (Mitchell et al., 1983), which signifies its strong exploration potential. In the following section, the mafic units within and contemporaneous within the Coldwell Alkaline Complex will be summarized and briefly discussed.

2.3.2.1 Coubran Lake Basalt

The Coubran Lake basalt was first observed as kilometer-scale basaltic xenoliths within Center II syenites by Puskas (1967), then again by Walker et al. (1993). However, in 2011, a thin body of basalt (only 3 to 5 m in width) and up to 350 m long was exposed during overburden stripping by Stillwater Canada Inc. This thin occurrence of basalt trends roughly to the west. The lower contact of the Coubran Lake basalt has not been defined. The basaltic exposure covers the side of a local topographic high, and is believed

to represent the downslope-flow of material (Cundari, 2012). Amygdules are a common feature within the basalt and are infilled by variations of quartz, calcite, and chalcopyrite (Figures 2.6a and 2.6b). These amygdules exhibit round to ovoid morphologies, ranging from 0.2 to 0.4 cm. Several ropy flow tops are also observed, which indicate subaerial emplacement (Cundari, 2012).

2.3.2.2 Marathon Deposit, Canada

The Marathon Cu-PGE deposit is hosted by the mid-continent rift-related Coldwell alkaline complex, and was emplaced contemporaneously with the mid-continent rift system of North America as part of the Center I intrusives (Heaman and Machado, 1992). Disseminated sulfide mineralization, namely that of pyrrhotite, chalcopyrite, and bornite with minor pentlandite, cobaltite and pyrite is hosted by a fresh olivine-bearing gabbro known as the Two Duck Lake Gabbro (TDLG) which comprises the majority of the Marathon Series rocks (Good, 2014). The TDLG is a coarse-grained to pegmatitic intrusion that exhibits a fresh, predominantly unaltered ophitic texture that distinguishes it from the nearby Fine-Grained Series and Layered Series rocks (Good, 2014). The sulfide mineral assemblage is believed to represent a typical magmatic sulfide assemblage that crystallized from sulfide droplets trapped within the interstices of primary silicate minerals (Miller et al., 2010). Surface exposure of the TDLG ranges between 50 m and 250 m thick and traceable over 6 km.

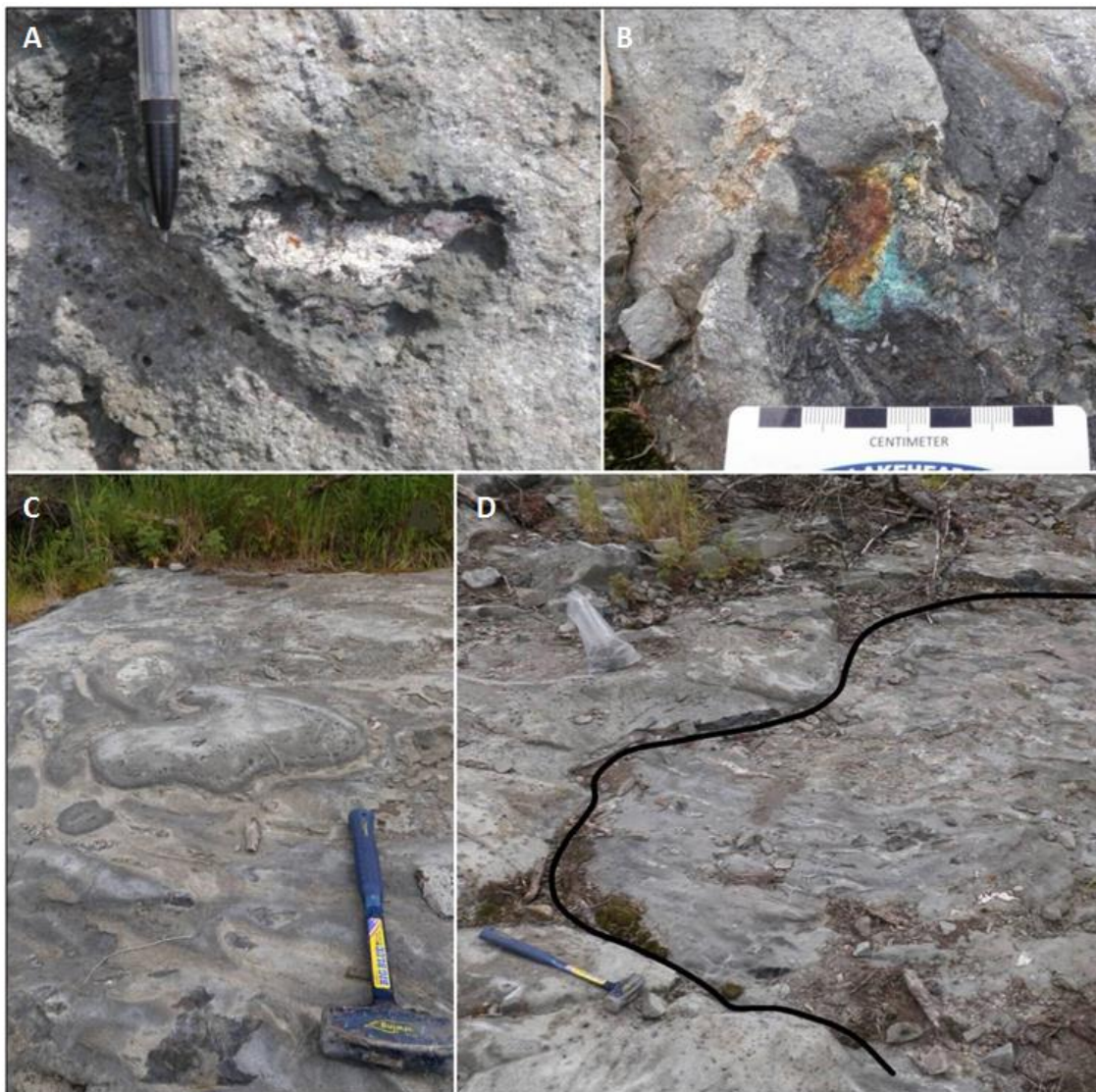


Figure 2.6 – Typical features of the Coubran Lake basalt; **a)** An ovoid-shaped amygdale, infilled by quartz and calcite, **b)** Another ovoid amygdale, and this time infilled by chalcopyrite. Malachite staining is seen to the bottom of the amygdale due to surface weathering, **c)** A very well-exposed ropy flow-top, **d)** A contact between a ropy-flow surface (to the right), and an overlying flow (to the left) marked with a black line. Rock hammer for scale is 1' long. Modified from Cundari (2012)

The Marathon deposit has previously been described as a contact-type deposit (Barrie et al., 2002; Miller and Nicholson, 2013), given that the deposit characteristics are similar to those which define contact-type deposits as described by Zientek (2012). More recently, however, the TDLG is interpreted to have intruded as a series of sills that, collectively, represented a dynamic conduit environment (Ruthart, 2013; Good et al., 2015). High sulfide metal tenors within the W-horizon of the Marathon deposit in particular are

explained by multistage dissolution upgrading in an open system, where sulfides are exposed to significant quantities of silicate magma (high R-factor). Sulfide saturation was likely attained via contamination of the magma chamber by surrounding Archean metasediments (Good and Crocket, 1994b). Sulfide droplets continually grew as they encountered new droplets during transport, but ultimately crystallized within a crystal mush of plagioclase and silicate melt. After crystallization, subsolidus reactions took place which involved local migration of components within deuteric fluid, resulting in features such as the replacement of pyrrhotite by chalcopyrite, and the deposition of PGM in spatial association with hydrous silicates (Good and Crocket, 1994b).

2.3.2.2.1 Magmatic Origin of the Deposit

The most favourable origin for the enrichment of Cu-PGE within sulfides at the Marathon deposit is that of a magmatic origin Good et al., 2015. Geochemical observations, particularly that of matching saw-toothed patterns for Cu and Pd within diamond drill-hole data, the association of enriched Cu and Pd grades within footwall troughs, as well as the behaviour of Pd-Ir, Pd-Rh, Pd-Pt, and Pd-Au pairs hint strongly towards the accumulation of sulfides within dynamic flow traps (Good et al., 2015).

2.3.2.2.2 Hydrothermal Origin of the Deposit

Another proposed mechanism of Cu-PGE enrichment within the sulfides of the Marathon deposit is rooted in a hydrothermal origin, and this is summarized through three key observations: 1) there is a common spatial association between PGE-bearing Cu-sulfides and hydrous silicates, alkali feldspar, and pegmatitic gabbro (Watkinson and Ohnenstetter, 1992; Dahl et al., 2001), 2) the trace element composition of hydrothermal sulfide differs from that of magmatic sulfide (Samson et al., 2008), and 3) PGM have been documented within saline inclusions (Watkinson and Jones, 1996). These observations, however, do not fully prove that hydrothermal mobilization played a role in concentrating Cu and PGE within sulfide (Good et al., 2015). There is no discernable spatial relationship between pegmatite and mineralization at a macroscopic scale, and there is no consistent correlation between alteration and mineralization. Furthermore, from a mass balance perspective, there is simply too much PGE and insufficient gabbro

for a zone refining mechanism to have played a role in the enrichment of sulfide at the Marathon deposit (Good et al., 2015).

2.4 Geordie Lake Intrusion

The GLI is a weakly layered, alternating intrusion of gabbro and troctolite associated with the magmatism of the Coldwell Alkaline Complex. The strike of the intrusion is roughly north-south, dipping approximately 45 degrees to the west. Along strike, the intrusion extends for at least 2.5 km with variable thickness, ranging from 50 to 100 m. The northern boundary of the deposit is covered by Coubran Lake, and hence, it has not been conclusively defined (Mulja and Mitchell, 1990; 1991).

The broadly defined lithologies that make up the GLD are shown on a geological map in Figure 2.8. They are (from west to east): 1) a plagioclase aligned gabbro, 2) homogeneous gabbro, 3) heterogeneous gabbro, and 4) mineralization, which consists of heterogeneous gabbro, skeletal troctolite, and basal fine-grained gabbro. The mineralization is in contact with syenite to the east. The undifferentiated gabbro was not examined during the course of this study. The mineralized unit consists of lenses of heterogeneous gabbro and skeletal troctolite and a basal fine-grained gabbro that is in contact with syenite. Mineralization consists of discontinuous stringers, disseminations, and blebs of chalcopyrite and bornite mineralization that contains PGE. The mineralization within these three units can contain more than 0.5 % Cu and 500 ppm Pd (Drennan & Fell, 2010).

The region denoted by a black box on Figure 2.7 is displayed on Figure 2.8, and shows the locations of drill holes used to create a north-facing east-west cross section of the GLD. All diamond drill holes are drilled at 90 degree azimuths. Diamond drill holes G-10-17, G-10-16, and G-10-04 are collared in plagioclase-aligned gabbro, whereas drill hole G-10-02 is collared in heterogeneous gabbro. These drill holes have various dip angles (G-10-17 at 63°, G-10-16 at 64.5°, G-10-04 at 63° and G-10-02 at 45°) but all dip to the east. A cross-section of the deposit is shown in Figure 2.9. The different lithologies that collectively make up the Geordie Lake intrusion are summarized in the following

subsections. The unit codes beside each lithology name were those used by Stillwater Canada Inc. for core logging purposes. The lithologies which contain trace

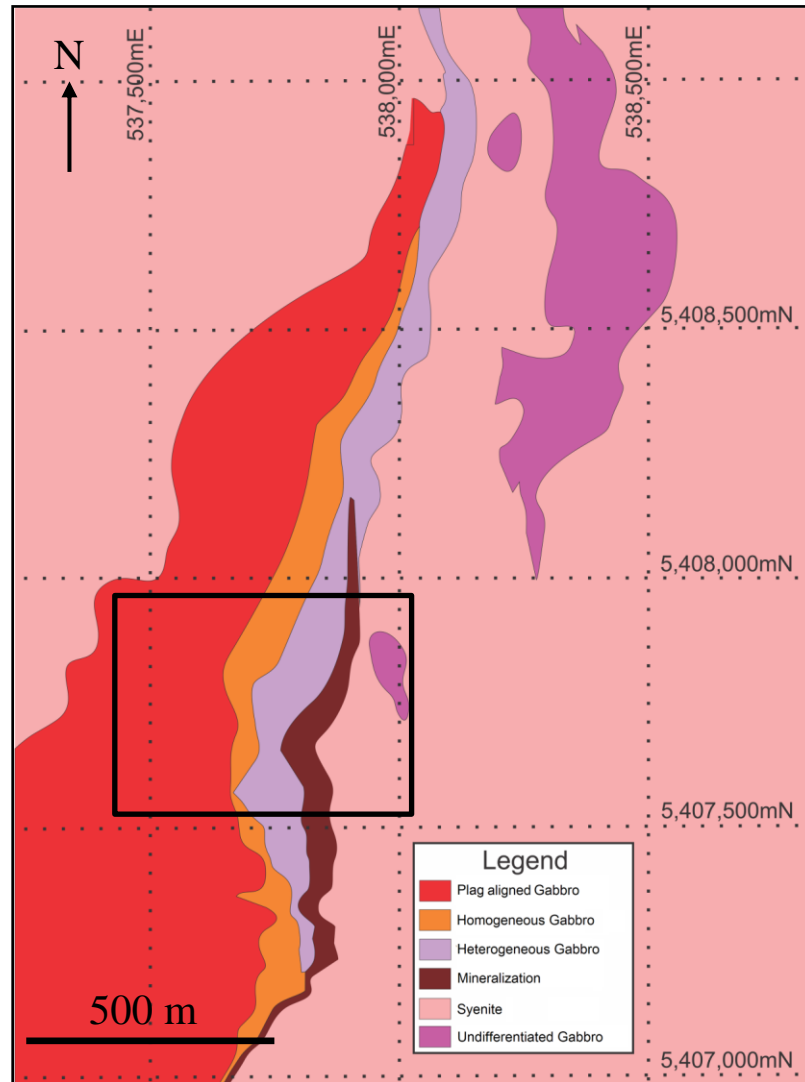


Figure 2.7 – Geological map of the Geordie Lake Deposit, showing the different lithologies relative to Cu-Pd mineralization. The mineralized units (in light purple and dark red) encompass alternations of both the heterogeneous gabbro, and skeletal troctolite. The weak mineralization consists of heterogeneous gabbro and skeletal troctolite with a Cu-grade under 0.5%, while strong mineralization consists of both heterogeneous gabbro and skeletal troctolite with a Cu-grade of over 0.5 %. Modified from Geordie Lake 43-101 (Drennan and Fell, 2010).

amounts of sulfides are the plagioclase aligned gabbro, homogeneous gabbro, and homogeneous troctolite. The lithologies which contain economic concentrations of sulfides are heterogeneous gabbro, skeletal troctolite, basal fine-grained gabbro, and the basal syenite (but only that which is within a few meters of the contact with the GLD). The unit codes that are used alongside each unit name are consistent with those utilized by Stillwater Canada Inc. (formerly Marathon PGM Corporation) when core logging. A more detailed description of each unit code is available in the Geordie Lake NI 43-101 (Drennan and Fell, 2010).

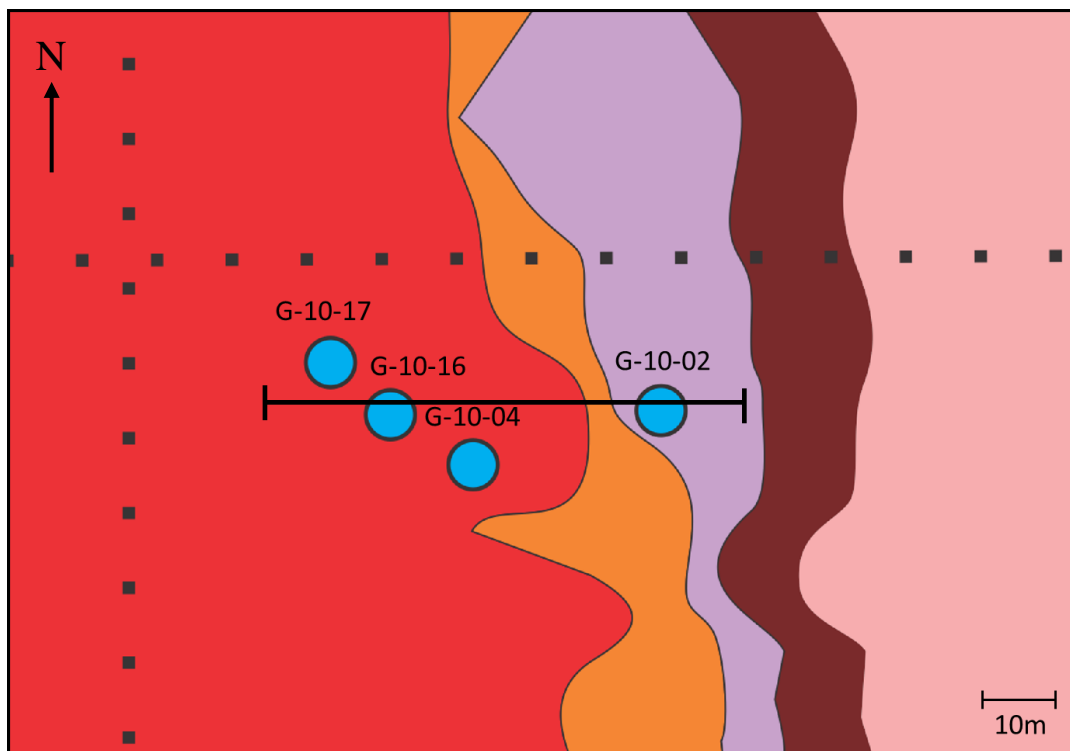


Figure 2.8 – Close up on the black outline within Figure 2.7, indicating the location of the drill holes used in this study to form a north-facing, east-west cross-section of the GLD. The cross-section is outlined by the black line, and is shown on Figure 2.9. Modified from Geordie Lake 43-101

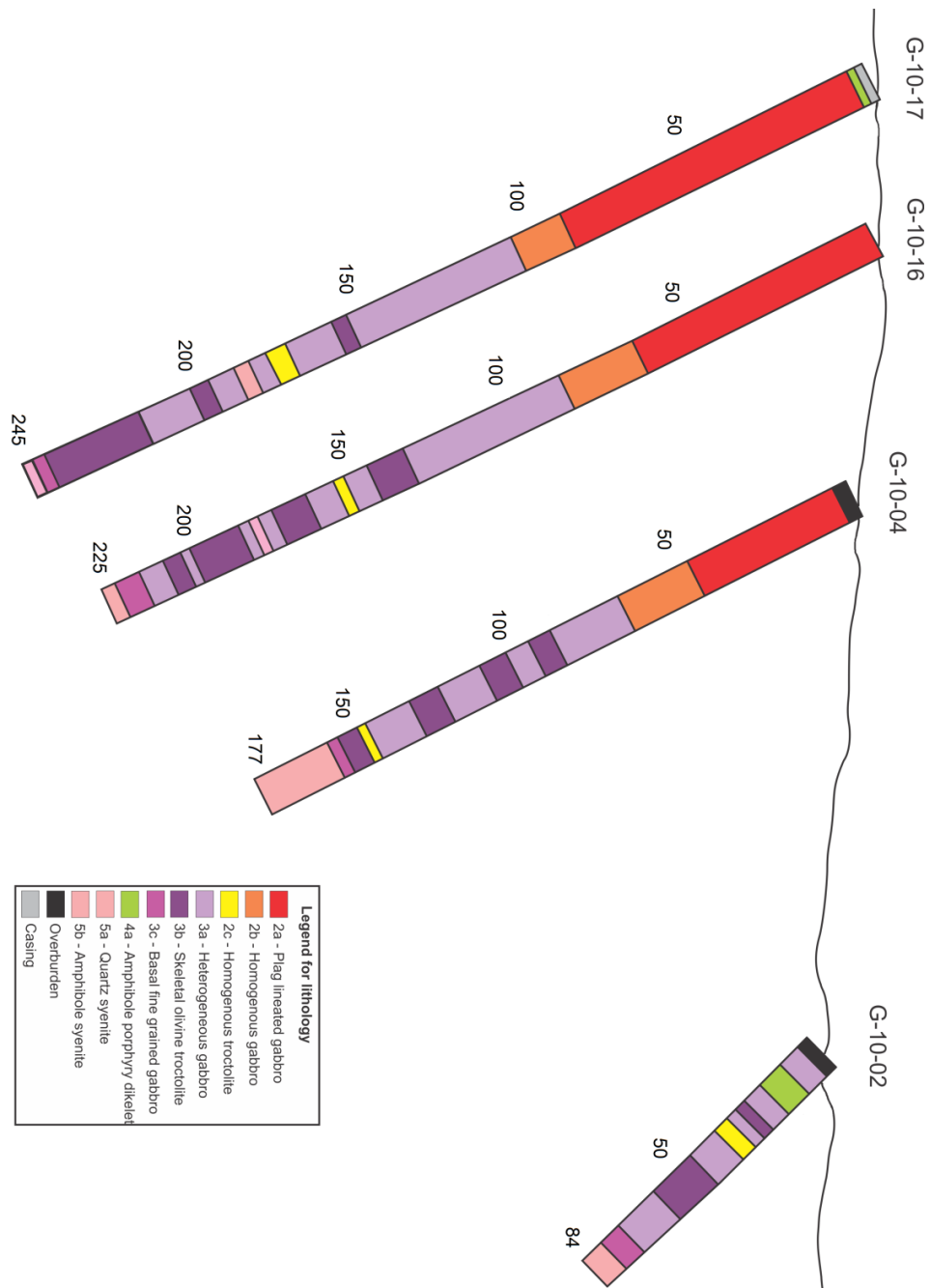


Figure 2.9 – North facing, east-west cross section of the GLD. Figure 2.8 indicates where on the GLD this cross-section occurs on the GLD. There are two aspects of this cross section: 1) The lithologies are shown in the center log of each drill hole, with a corresponding legend titled “Legend for lithology”, and 2) The presence of sulphides are shown on adjacent logs on either side of each drill hole. On the left side, is a log of where chalcopyrite mineralization is visible down-hole. On the right side, is a log of where pyrrhotite and bornite are visible down-hole. Pyrrhotite and bornite are not observed together in any drill hole, but their distribution at the GLD is well documented in this cross-section. A legend for the sulphides observed during core logging of all four drill holes is shown under the heading “Legend for sulphides”. The numbers along each drill hole are units in meters.

2.4.1 Plagioclase Aligned Gabbro (Unit 2a)

In the GLD stratigraphy, the uppermost gabbroic unit is characterized by plagioclase alignment with laths aligned parallel to primary gabbro contacts, dipping west roughly between 30 to 45 degrees. The overall appearance of the gabbro is bluish-green gray, faintly mottled with pink albite (which primarily occurs as rims on plagioclase) (Figure 2.10a). However, lath alignment is not always strongly pronounced, and the lower contact between plagioclase aligned gabbro and fine to medium-grained homogeneous gabbro is gradational for over two to five meters, and this contact is defined by the loss of plagioclase alignment. The plagioclase aligned gabbro has never been observed to be in contact with any of the ore-bearing lithologies. The dominant primary minerals are plagioclase (0.5-1.5 cm), clinopyroxene (<1 cm), magnetite (<0.5 cm), and minor apatite (<0.5 cm), while the dominant secondary minerals are fine-grained actinolite±biotite (pseudomorphic after clinopyroxene), and minor pink albite.

2.4.2 Fine to Medium-Grained Homogeneous Gabbro (Unit 2b)

The fine to medium-grained homogeneous gabbro is a bluish-green-gray to dark green-gray gabbro. Both primary and secondary mineralogy are similar to that of the plagioclase aligned gabbro, with only slight local variations in modal mineralogy and grain size (Figure 2.10b). The primary difference between the plagioclase aligned gabbro and the fine to medium-grained homogeneous gabbro is the lack of plagioclase alignment. The lower contact of the fine to medium-grained homogeneous gabbro is gradational with the underlying heterogeneous gabbro. This unit is never found in contact with skeletal olivine troctolite.

2.4.3 Medium-Grained Homogeneous Troctolite (Unit 2c)

The medium-grained homogeneous troctolite is characterized by a homogeneous texture consisting of subhedral plagioclase, olivine, and magnetite, with interstitial clinopyroxene, and is speckled with less than 1% euhedral apatite (Figure 2.10c). The unit varies in thickness from 10 cm, up to 20 m, and pinches out towards the north. It is commonly enclosed by heterogeneous gabbro and exhibits both gradational and well defined contacts. During the course of this study, it was not found in contact with skeletal

olivine troctolite. The dominant minerals include olivine (<0.5-1 cm and commonly skeletal), plagioclase (<0.5-1 cm), magnetite (<0.5 cm), and minor clinopyroxene (<0.5 cm). Homogeneous troctolite is found to cross-cut heterogeneous gabbro and skeletal troctolite.

2.4.4 Heterogeneous Gabbro (Unit 3a)

The heterogeneous gabbro is a medium to coarse-grained (<0.5 cm to 2 cm) gabbro that is defined by highly variable albite alteration that resembles small pink patches or pods (Figure 2.10d). The presence of patchy albite alteration and variable grain size is what defines the heterogeneity in this unit. The dominant minerals within the heterogeneous gabbro are plagioclase (commonly rimmed or fully replaced by pink albite), clinopyroxene, olivine, magnetite, and fine-grained apatite. The portions of the gabbro that are heavily albitized also contain strong actinolite, biotite, epidote and chlorite alteration that is mainly manifested as pseudomorphic alteration after clinopyroxene. Olivine is commonly altered to a fine-grained assemblage of serpentine and magnetite. The upper contact of the heterogeneous gabbro with the homogeneous gabbro is marked by a gradational change from a homogeneous gabbro with minor albite rims on plagioclase laths to variably textured gabbro with abundant, patchy pink zones. This contact is also marked by an increase in sulfide mineralization. Layers of heterogeneous gabbro alternate with skeletal olivine troctolite throughout the mineralized horizons.

2.4.5 Skeletal Troctolite (Unit 3b)

The skeletal olivine troctolite (hereafter referred to as “skeletal troctolite” for simplicity) is a coarse to very coarse-grained heterogeneous augite troctolite, characterized by abundant skeletal, or harrisitic olivine (up to 5 cm) and magnetite (Figure 2.10e). Plagioclase occurs as coarse subhedral laths (~1 cm) with albite rims and as anhedral intergrowths with skeletal olivine. Olivine occurs as medium to coarse-grained skeletal crystals up to 5 cm long inter-grown with plagioclase and clinopyroxene. Anhedral clinopyroxene (<0.5-1.5 cm) is ophitic, interstitial to olivine and plagioclase and is partly altered to actinolite. Fine to medium-grained (<0.5-1 cm) skeletal magnetite occurs proximal to skeletal olivine grains. Very fine-grained acicular apatite is commonly found

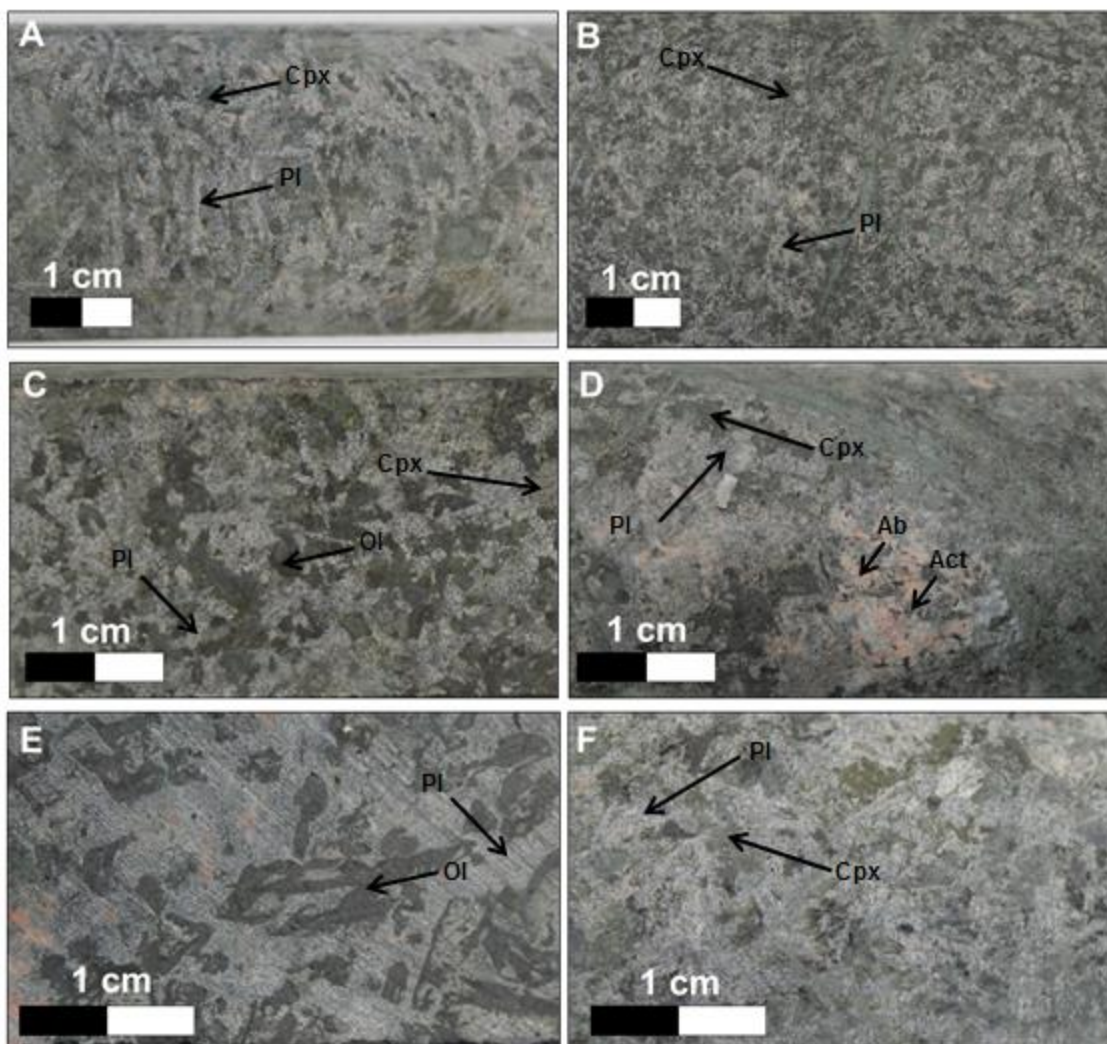


Figure 2.10 – A summary of the main lithologies that comprise the GLD; **a)** Plagioclase aligned gabbro with plagioclase laths are oriented north-south in the picture, but dip roughly 30–45 degrees on outcrop, **b)** Homogeneous gabbro defined by euhedral to subhedral plagioclase, subhedral clinopyroxene, olivine and magnetite, **c)** Homogeneous troctolite containing euhedral plagioclase with interstitial olivine that is strongly chloritized, and/or serpentinized, **d)** Heterogeneous gabbro characterized by the presence of patchy, pervasive to networked pink albite. Actinolite commonly forms within cores of intense albitization, **e)** Skeletal troctolite characterized by euhedral, skeletal to harrisitic olivine grains, and less commonly, magnetite, with interstitial frosty white plagioclase, and sporadic networks of pink, speckled albite, **f)** Basal, fine grained gabbro consisting mainly of euhedral plagioclase, with interstitial clinopyroxene, olivine and magnetite. Clinopyroxene is commonly altered to a suite of green, secondary minerals including actinolite, epidote, chlorite, or biotite.

within olivine, magnetite, plagioclase and clinopyroxene as inclusions. The skeletal troctolite unit has minor fine-grained albite which either rims plagioclase laths, or occurs as small (<1 cm) albite pods and bands. Local intense alteration zones of actinolite-biotite (after olivine and clinopyroxene) are common. The contact from heterogeneous gabbro to

skeletal troctolite exhibits a gradational to sharp increase in grain size (commonly becomes ~0.5 cm larger), skeletal olivine, and a decrease in pervasive albite alteration. Commonly, an albite pod or band occurs at the contact between heterogeneous gabbro, and skeletal troctolite.

2.4.6 Basal Fine-Grained Gabbro (Unit 3c)

The basal fine-grained gabbro occurs at the contact with the footwall syenite. The average grain size is 0.5 cm for all minerals. It is characterized by stubby plagioclase laths, that unlike plagioclase found in the rest of the intrusion, are not rimmed by albite alteration. Interstitial clinopyroxene is predominantly altered to actinolite and biotite. Olivine and apatite are not evident. The contact between the basal fine-grained gabbro and syenite is typically gradational with apparent assimilation of gabbro by syenite (Figure 2.11). The basal fine-grained gabbro tends to be 1 to 5 m thick and is overlain by skeletal troctolite.

2.4.7 Stratigraphy of the GLD

The four diamond drill holes utilized in this study intersect different thicknesses of each lithology, in addition to mineralization. The lithological contacts may either be well-defined or diffuse, and this varies among all drill holes. The style of mineralization, as well as the dominant sulfide mineralogy is varies from drill hole to drill hole.

2.4.7.1 G-10-17

G-10-17 is collared in plagioclase aligned gabbro which extends for 89.40 m, after which there is a gradational transition into medium-grained homogeneous gabbro until 104.65 m. At 104.65 m, there is a sharp contact between medium-grained homogeneous gabbro and heterogeneous gabbro. Heterogeneous gabbro dominates between 104.65-171.45 m, though within this interval there are multiple, thin intervals of skeletal troctolite. Skeletal troctolite within this interval contain pseudomorphs of skeletal olivine grains that are predominantly altered to actinolite±serpentine±biotite. At 171.45 m, there is a diffuse contact with a medium-grained homogeneous troctolite, which extends to 176.52 m. Between 176.52 and 181.80 m, there is a variably textured heterogeneous gabbro with

moderate fine-grained patches of albite. At 181.80 m, there is a sharp contact with quartz syenite. The syenite exhibits chill margins at both its upper and lower contact. The syenite extends up to 186.46 m, where it is in sharp contact with heterogeneous gabbro. From 186.46 to 241.86 m, there are alternating intervals of heterogeneous gabbro and skeletal troctolite. Alteration is patchy to pervasive, and mainly in the form of actinolite-biotite-chlorite that is pseudomorphic after clinopyroxene and olivine. Plagioclase in this interval tends to be albitized intermittently within the heterogeneous gabbro, but is predominantly rimmed by a thin mantle of pink albite. Plagioclase within the skeletal troctolite tends to be moderately sericitized, particularly within the interstices of skeletal olivine grains.

2.4.7.2 G-10-16

G-10-16 is also collared in plagioclase aligned gabbro, and intersects this unit for 70.30 m until a gradational contact with medium-grained homogeneous gabbro. The homogeneous gabbro extends until 91.96 m, where there is a well-defined lower contact with heterogeneous gabbro. The heterogeneous gabbro extends through to 148.47 m, where it is in gradational contact with skeletal troctolite. Skeletal troctolite and heterogeneous gabbro alternate until 155.40 m, where both lithologies are cross-cut by fine-grained medium homogeneous troctolite. This cross-cutting relationship has been established in the field. The homogeneous troctolite extends to 157.43 m, where it is in sharp contact with heterogeneous gabbro. The heterogeneous gabbro continues until 166.67 m, where it is in gradational contact with skeletal troctolite. From 166.67 m to 221.68 m, heterogeneous gabbro and skeletal troctolite alternate, and have a gradational contact with fine-grained gabbro at 221.68 m. From 221.68 m to 223.17 m, basal fine-grained gabbro extends until intersecting a fairly sharp contact at 223.17 m with medium-grained quartz syenite.

2.4.7.3 G-10-04

G-10-04 is collared in overburden, which extends for 4.20 m. Plagioclase aligned gabbro lies under the overburden at 4.20 m, and extends to 46.97 m where it is in gradational contact with medium-grained homogeneous gabbro. This interval extends until 68.07 m,

at which point it is in sharp contact with heterogeneous gabbro. The heterogeneous gabbro varies from ophitic textured, to sub-ophitic, to cumulate textured (dominated by clinopyroxene, magnetite, and less commonly olivine). Heterogeneous gabbro continues until 88.75 m, where it has a gradational contact with skeletal troctolite. This interval of skeletal troctolite contains minor patchy albite, and there is moderate to intense actinolite-biotite alteration of the skeletal olivine grains. At 94.54 m, there is another gradational contact with heterogeneous gabbro, which contains abundant fine-grained to pervasive networks of medium-grained albite. Between 100.68 m and 151.70 m, alternating layers of heterogeneous gabbro and skeletal troctolite dominate the interval, and at 151.70, there is a gradational contact towards basal fine-grained gabbro. The basal fine-grained gabbro terminates at 153.87 m, where there is a diffuse contact with the medium-grained quartz syenite.

2.4.7.4 G-10-02

G-10-02 is the only drill hole (from within the cross-section of drill holes) that is collared directly above mineralized, heterogeneous gabbro. The first 4 m of the drill hole are overburden, but between 4 m and 10.43 m, heterogeneous gabbro with a subophitic to cumulate texture is intersected. At 10.43 m, heterogeneous gabbro is cross-cut sharply by an amphibole porphyry dikelet. This unusual dikelet has an extremely well-defined sharp upper and lower contact at 18 m, and both contacts exhibit chill margins. Between 18 m and 29.40 m, heterogeneous gabbro alternates with skeletal troctolite and there are diffuse contacts between the two intermittent lithologies. At 29.40 m, there is a sharp contact with fine to medium-grained homogeneous troctolite. Homogeneous troctolite extends up to 34.85 m, where there is a sharp contact with heterogeneous gabbro once again. Heterogeneous gabbro and skeletal troctolite both alternate sporadically until 73.05 m, where there is a diffuse contact with basal fine-grained gabbro. Basal fine-grained gabbro terminates at 77.10 m, with a diffuse boundary into amphibole-rich syenite.

2.4.8 Basal Syenite

Mulja and Mitchell (1991) stated that the GLD intruded into the underlying syenite, which was disputed by Good and Crocket (1994). Mulja (1989) originally contended that

the presence of chalcopyrite mineralization extending from the GLD into surrounding syenites as stringers, combined with recrystallization in syenite adjacent to the gabbro, suggest that the GLD intruded into the syenites. Conversely, Good and Crocket (1989) interpreted these regions of recrystallization in the syenite as chilled margins, and thus, argued that the syenites intruded the gabbro. They noted that, at the contact between the GLD and the underlying syenite, the gabbro is medium-grained whereas the syenite is fine-grained (<0.5 mm). Two meters away from the contact, however, the syenite is medium to coarse-grained. Thus, the fine grained nature of the syenite is believed to be that of a chilled margin, which implies that the syenites cross cut the GLD. The observations made in this study are most consistent with the one made by Good and Crocket (1989). Figure 2.11 shows xenoliths of gabbro within syenite in a surface outcrop. Figure 2.12a shows the fine-grained syenitic stringers in drill-core near the contact between the syenite, and Geordie Lake gabbro. The syenite stringers are fine-grained and cross-cut mafic minerals of the Geordie Lake gabbro. Further down hole, the syenite is medium-grained and crystalline (Figure 2.12b). This observation is consistently made in drill-core at the contact between syenite and Geordie Lake gabbro.

2.4.9 Infilled Fractures at the GLD

It is common for infilled fractures (or veinlets) to cross-cut the various lithologies of the GLD. These are typically comprised of (in decreasing abundance): carbonate, chlorite, a mixture of chlorite and carbonate, and magnetite (Figure 2.13). Carbonate fractures are comprised of a combination of calcite, and pink carbonate (either rhodochrosite or Mn-bearing calcite). Carbonate-infilled fractures are common in all lithologies. Chlorite-infilled fractures are also observed in all GLD lithologies, as are both chlorite and carbonate infilled fractures. Magnetite-infilled fractures, however, are relatively uncommon and only observed within skeletal troctolite. Only chlorite-infilled fractures bear mineralization in the form of disseminated chalcopyrite and bornite, but more commonly, these fractures contain only disseminated to semi-massive chalcopyrite without any bornite (Figure 2.14a and 2.14b).

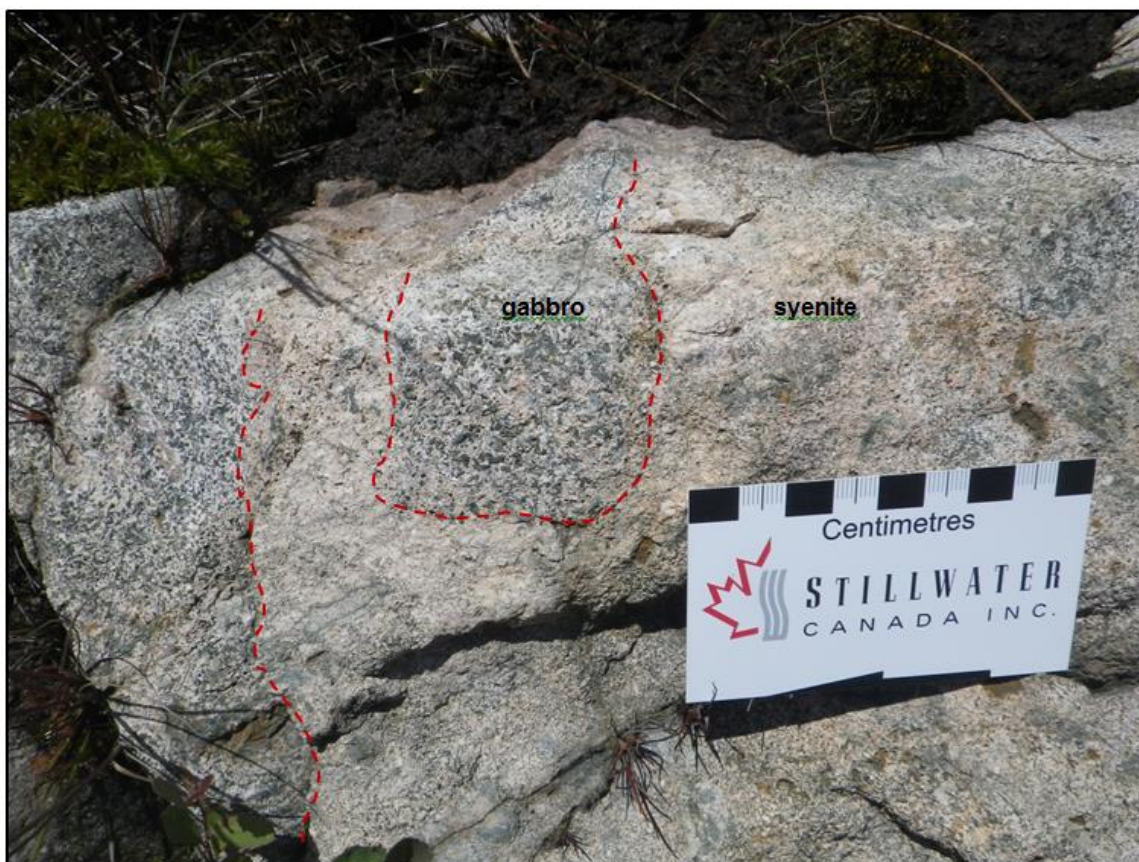


Figure 2.11 – Xenoliths of basal fine grained gabbro enclosed by syenite. This contact is highlighted by the dashed red line.

2.4.10 Mineralization at the Geordie Lake Deposit

The mineralization style at the GLD varies depending on the host rock lithology, and the association to alteration. A more comprehensive summary of how mineralization is related to these variable factors is presented in Chapter 4 (Petrography). In general, it consists of disseminations, blebs, and veins of sulfide minerals that are enriched in Cu, Ni, and Pd. The sulfides consist predominantly of the following associations: chalcopyrite and pyrrhotite (Figure 2.15 and 2.16), bornite and chalcopyrite (Figure 2.17), and only chalcopyrite (Figure 2.18). Accessory covellite, chalcocite, millerite, pentlandite, cobaltite, sphalerite, and galena are strongly associated with chalcopyrite and bornite. Pyrite is observed in association with chalcopyrite and pyrrhotite, and is not

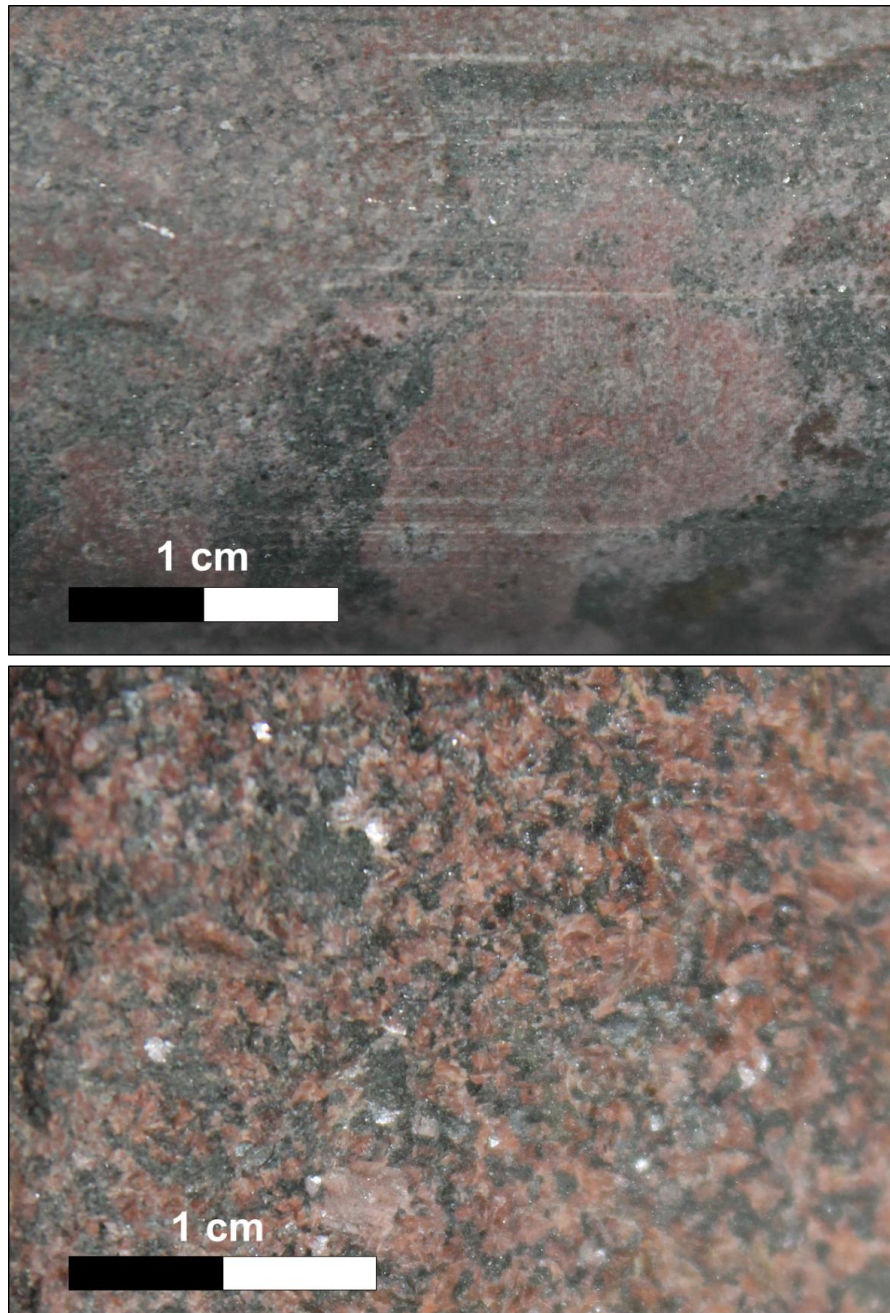


Figure 2.12 – Two different textures of basal syenite; **a)** Fine grained syenitic stringers which have intruded into the basal fine grained gabbro of the GLD. The contact between the basal fine grained gabbro and syenite is gradational, and features abundant irregularly shaped, fine grained syenite stringers which clearly cross-cut mafic minerals from the Geordie Lake gabbro, **b)** Medium grained syenite which occurs far from the contact between the syenite and Geordie Lake gabbro

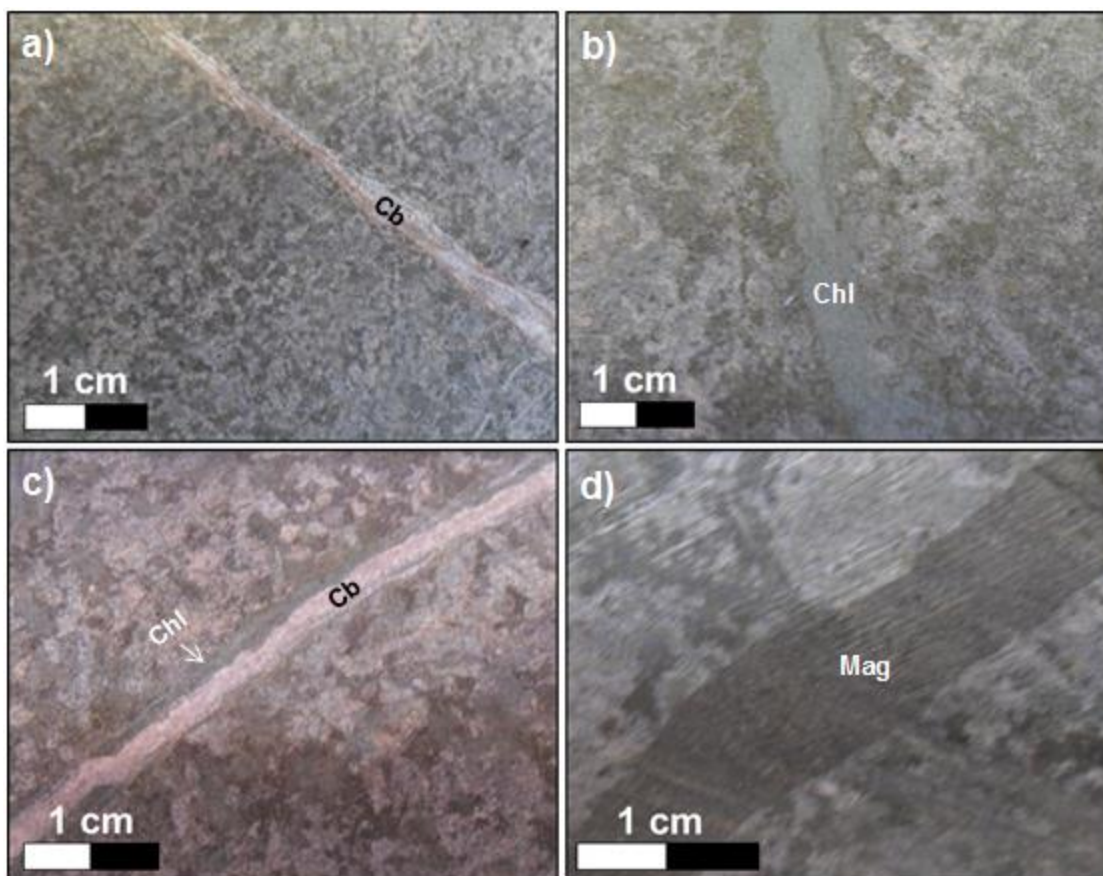


Figure 2.13 – Different examples of cross-cutting veins present at the GLD: a) A carbonate veinlet cross cutting homogeneous gabbro, b) A chlorite veinlet cross cutting heterogeneous gabbro, c) A chlorite and carbonate veinlet cross cutting heterogeneous gabbro that is interlayered with skeletal troctolite, and d) A magnetite veinlet cross cutting skeletal troctolite

associated with bornite. Platinum group minerals are strongly associated with chalcopyrite and bornite (Mulja and Mitchell, 1991). Chalcopyrite occurs as very fine disseminations, to coarse (up to 2.5 cm) blebby disseminations associated with actinolite alteration in the heterogeneous gabbro, skeletal troctolite, and basal fine-grained gabbro (Units 3a, 3b, and 3c). Very fine-grained chalcopyrite is also found within 1 to 3 mm wide actinolite veinlets, 1 to 2 cm wide magnetite veins, and smeared on chlorite fracture surfaces. Chalcopyrite is present within syenite near the contact with the GLD, and occurs as disseminated and stringer sulfides within actinolite stringers. Bornite is commonly associated with chalcopyrite as intergrowths or as rims around or cores within chalcopyrite. Bornite also occurs as fine-grained to very coarse-grained disseminated grains and as coarse-grained, irregularly shaped blebs. Pyrrhotite and pentlandite are minor components of the sulfide assemblage in the Geordie Lake intrusion. Pyrrhotite

occurs as fine to coarse-grained disseminated grains as well as coarse-grained local blebs. Pyrrhotite grains are often rimmed by chalcopyrite, actinolite, and/or magnetite.

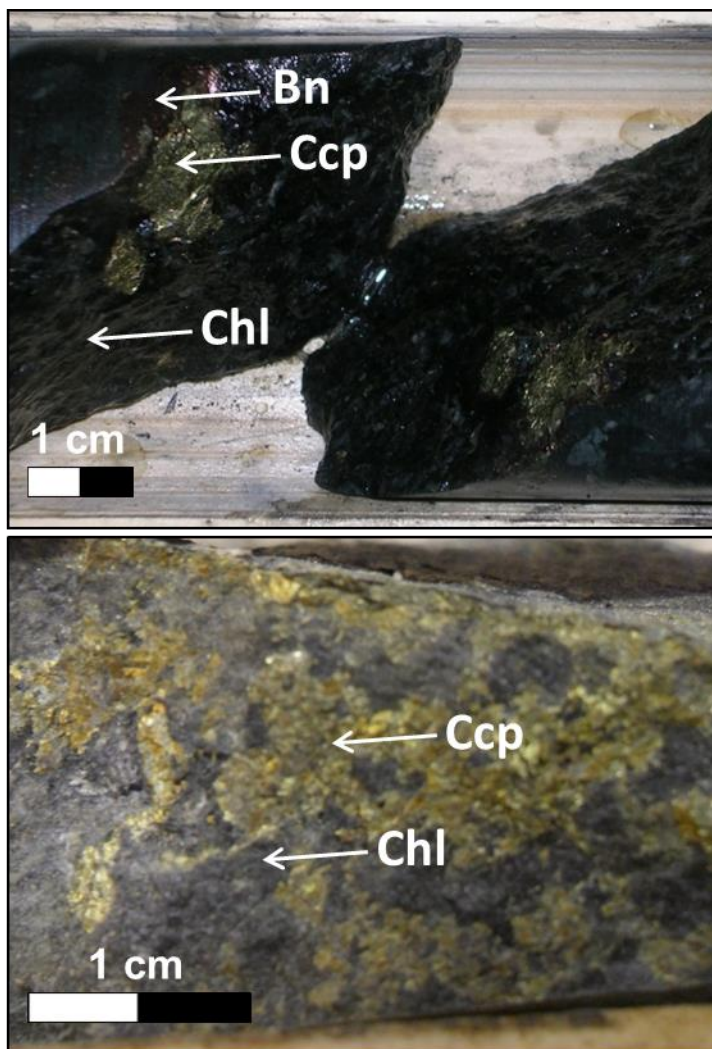


Figure 2.14 – Mineralization within fracture slip-surfaces: a) A chlorite fracture that contains blebby chalcopyrite and bornite mineralization, b) Another chlorite fracture surface that contains very blebby to semi-massive chalcopyrite mineralization

Mineralization at the GLD observed in two main settings: a thick, continuous basal main zone of mineralization and a thinner, discontinuous upper zone of mineralization at much lower grade. All mineralization is constrained to layers of heterogeneous gabbro, skeletal troctolite, and basal fine-grained gabbro (Units 3a, 3b, and 3c respectively) and has been traced for approximately 1650 meters along strike through drilling. The thickness of the deposit may be up to 200 m including the upper zone mineralization, but tends to be

discontinuous in the hanging-wall zone. The mineralization is enriched at the base or footwall of the deposit where higher grades and more consistent mineralization are observed. Pyrrhotite has only been observed higher up in the GLD stratigraphy, while bornite is observed predominantly within the basal zone of mineralization.

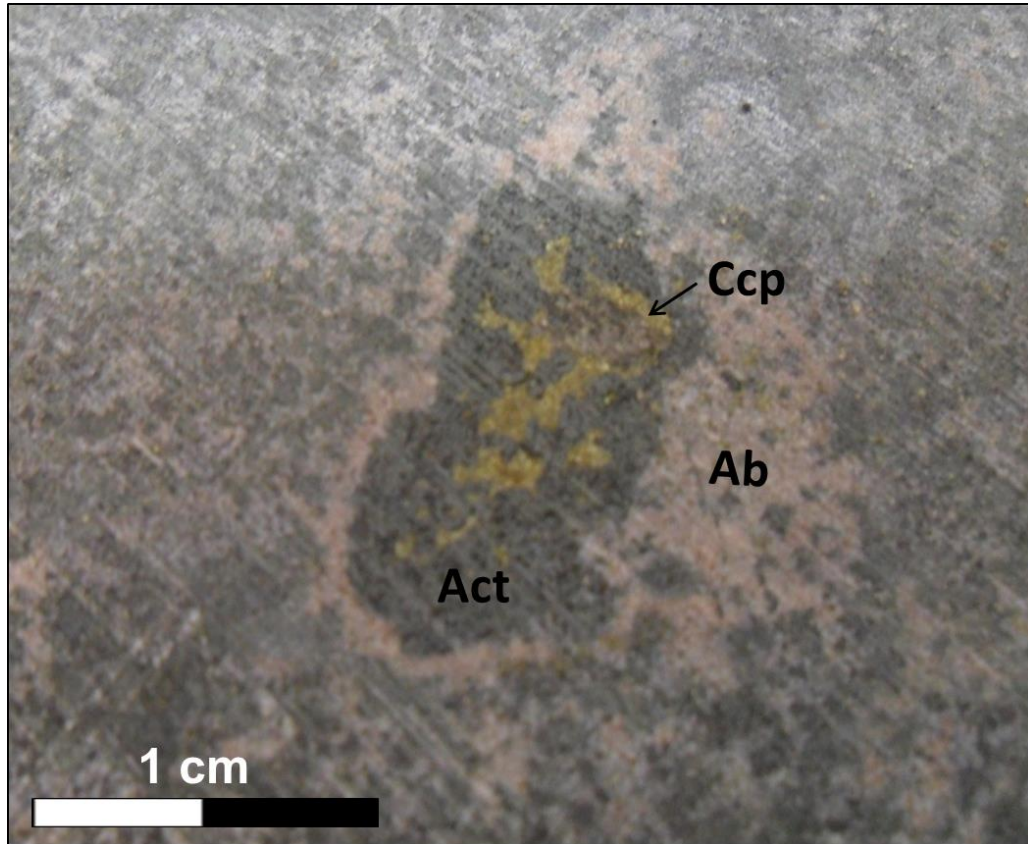


Figure 2.15 – Disseminated chalcopyrite occurring within an actinolite bleb, and surrounded by a thin ring of albite. This is a common sulfide texture within the heterogeneous gabbro.

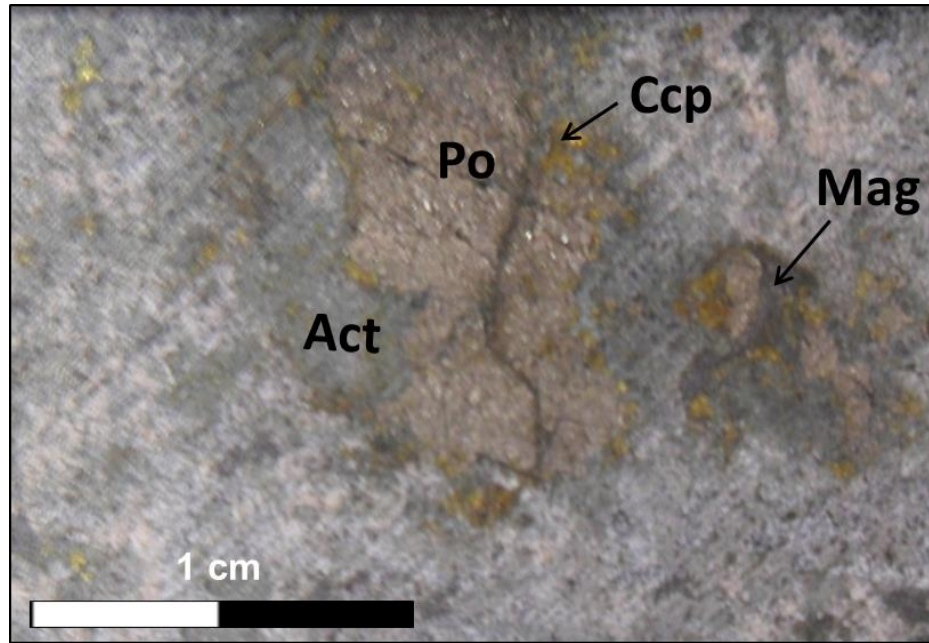


Figure 2.16 – Pyrrhotite mineralization occurring in close contact with actinolite alteration, and what appears to be secondary magnetite. Disseminated chalcopyrite is speckled within, or adjacent to the pyrrhotite mineralization.

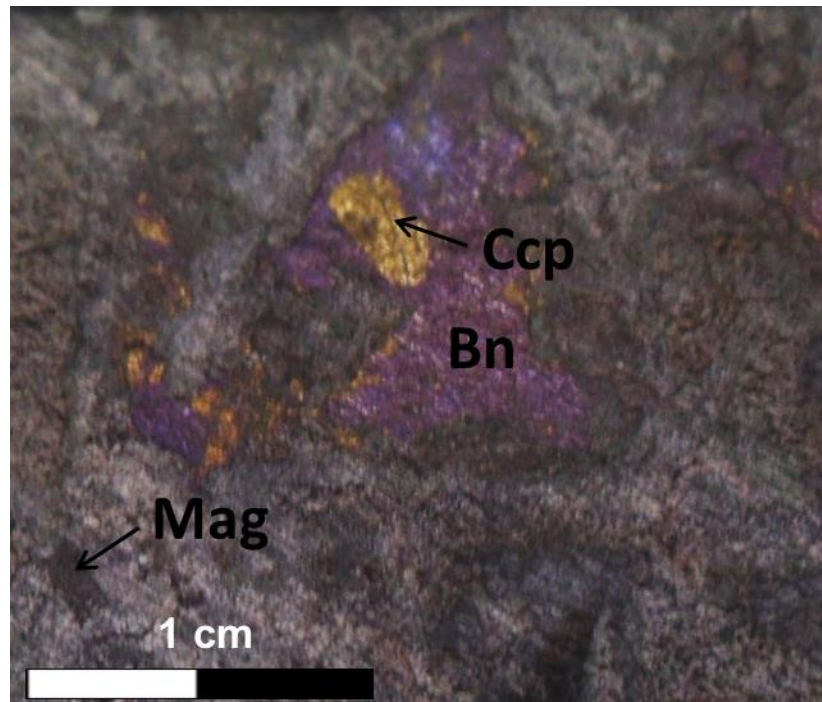


Figure 2.17 – An intergrowth of chalcopyrite and bornite, a common texture within the “main zone” of mineralization at the GLD.

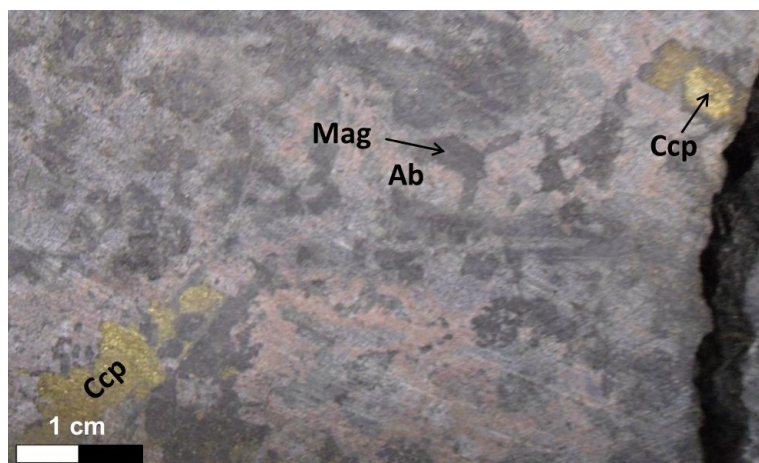


Figure 2.18 – Chalcopyrite mineralization near skeletal textured magnetite. Chalcopyrite is intergrown with a magnetite crystal in the top right of the image.

2.4.11 Sulfide Zonation at the Geordie Lake Deposit

The four study drill holes were re-logged during the summer of 2012 with an emphasis on the sulfide content. Figure 2.19 shows the results of the re-logging. The presence of chalcopyrite is indicated below the lithology drill hole log, whereas the presence of pyrrhotite and bornite are indicated above the lithology drill hole log. Chalcopyrite mineralization is present as disseminations, stringers, and blebs throughout all mineralized lithologies (heterogeneous gabbro, skeletal troctolite, and basal fine-grained gabbro). In drill hole G-10-16, chalcopyrite mineralization is also observed throughout both the plagioclase aligned gabbro, and the homogeneous gabbro as mainly very trace disseminations occurring within small actinolite pods, or chlorite fractures. Pyrrhotite is less common, and was only observed within drill holes G-10-16 and G-10-04, occurring within plagioclase aligned gabbro, homogeneous gabbro, and heterogeneous gabbro. Pyrrhotite is rarely observed within skeletal troctolite, with the only instances of pyrrhotite within skeletal troctolite occurring in drill hole G-10-04 in an interval that consists of alternations of skeletal troctolite and heterogeneous gabbro. Bornite is present predominantly within skeletal troctolite (in association with secondary magnetite as well as a thin layer of actinolite), and within heterogeneous gabbro that is proximal to skeletal troctolite. The strongest intervals of bornite mineralization exist at the base of the intrusion, near the syenitic contact.

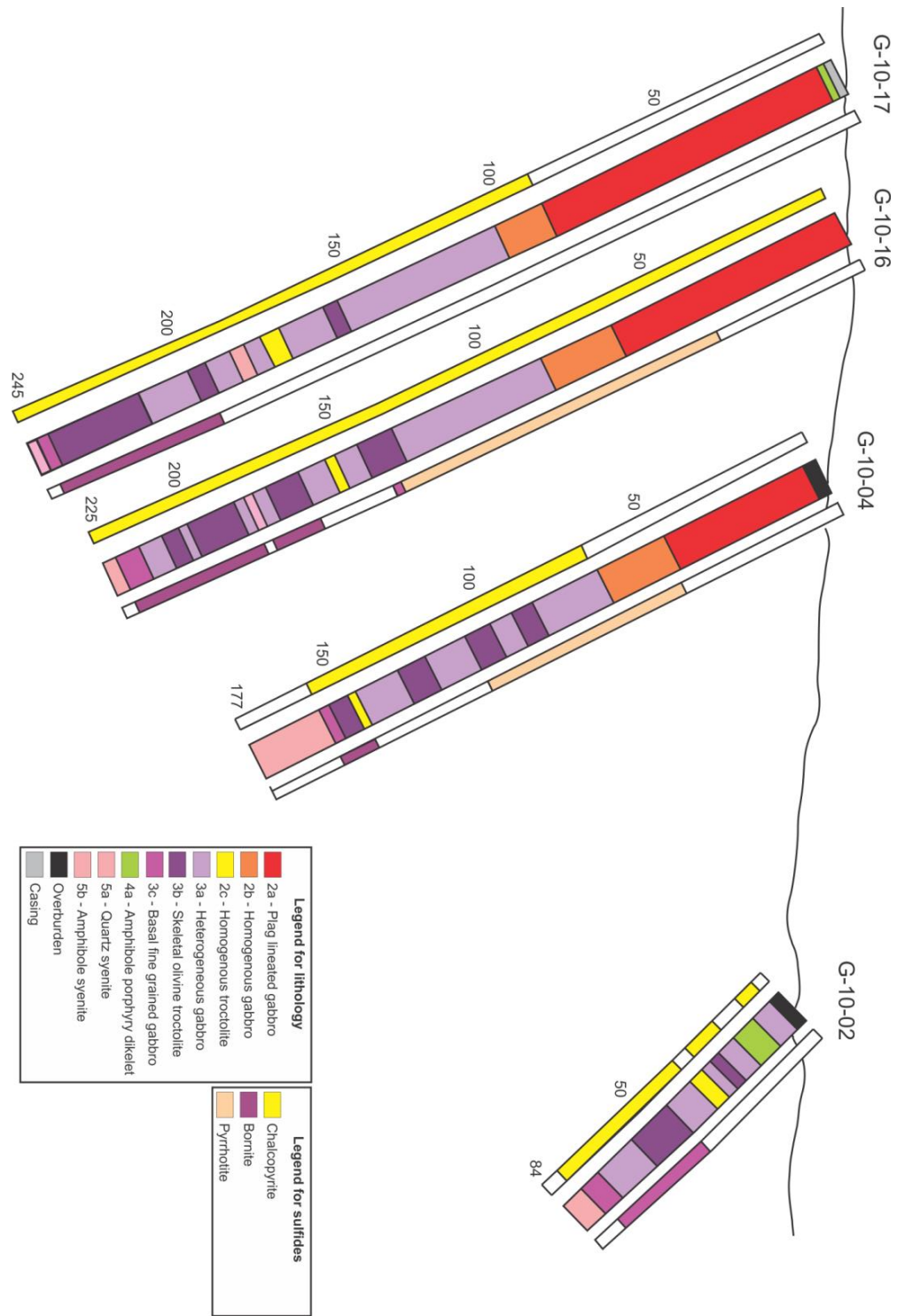


Figure 2.19 – The same north facing, east-west cross section of the GLD as in Figure 2.10, however this one shows the presence of sulfides within each drill-hole. To the left of each drill-hole, the presence of chalcopyrite is indicated within the yellow-shaded interval. To the right of each drill-hole, the presence of pyrrhotite is indicated by the orange-brown-shaded interval, while the presence of bornite is indicated by the purple-shaded interval. The numbers along each drill hole are units in meters.

Chapter 3

3 Methodology

In this chapter, both the sample gathering strategy and the analytical techniques used are discussed. The goals of sampling were to: 1) obtain a lithological suite that fully represents the GLD, and 2) sample the different mineralization styles present at the GLD, as well as the different alteration styles in order to evaluate whether or not there is relationship between the two. Furthermore, it became increasingly apparent during the course of the study that the surrounding syenites are important potentially as a heat source, which could have driven a hydrothermal system post-deposition at the GLD. Thus, both mineralized and unmineralized syenites were integrated into the sampling strategy.

3.1 Sample Collection

In order to well represent the variation in lithology and alteration at the GLD, a total of 92 samples were taken for whole rock geochemical analysis. Seventy samples were taken from drill-core (Figure 3.1), and 22 are from surface albite pod samples. Geochemistry used in this project were obtained from both: a) diamond drill core produced during an exploration drilling project conducted by Stillwater Canada Inc. (then Marathon-PGM) in the winter of 2010, and b) surface sampling conducted during the summer of 2012.

3.1.1 Diamond Drill Hole Selection Criteria

Due to the elongated shape of the GL deposit, four diamond drill holes (DDHs) in an east-west, north-facing cross-section were selected to best represent both the mineralized and unmineralized lithologies. The drill holes, from west to east are: G-10-17, G-10-16, G-10-04, and G-10-02. Holes G-10-16 and G-10-02 lie roughly along 5,407,400 m N (UTM), whereas holes G-10-17 and G-10-04 are both displaced 25 m to the north, and south respectively. G-10-17, G-10-16, and G-10-04 are all collared within the unmineralized plagioclase aligned gabbro, whereas G-10-02 is collared within mineralized, heterogeneous gabbro. Collar information for all four drill holes including northing, easting, elevation, dip at collar, azimuth and total depth is listed in Table 3.1.

All drill holes terminate within, on average, 8.7 meters after intersecting the contact between the eastern syenite and the GL gabbro.

Hole ID	Northing	Easting	Elevation (m)	Dip at Collar	Azimuth	Depth (m)
G-10-02	5407400	537735	340	-45	90	84
G-10-04	5407375	537612	340	-45	90	190
G-10-16	5407400	537575	272	-63	90	225
G-10-17	5407425	537550	238	-63	90	248

Table 3.1 – Collar information for all four drill-holes used in this study.

These four drill holes were chosen principally because (with the exception of G-10-02) they all intersect two separate zones of high grade Cu-PGE mineralization termed the Upper Zone mineralization, and the Main Zone mineralization. In addition, holes G-10-17, G-10-16, and G-10-04 intersect long intervals of unmineralized gabbro (units 2a and 2b) before intersecting mineralized lithologies (Units 3a, 3b and 3c). Hence, this cross section provides an opportunity to observe and compare continuities or discontinuities in lithology, mineralization (including metal ratios), alteration-types, and rock textures.

All drill core used in this study is NQ sized (47.6 mm in diameter). Mineralized drill core was sawed longitudinally and sampled in 2 m intervals for chemical analysis, as part of the exploration project carried out in the summer of 2010 by Stillwater Canada Inc. Chemical assay was performed at Accurassay Laboratories in Thunder Bay, Ontario. During this diamond drill program, all mineralized samples were analyzed for Cu, Ni, Ag, Au, Pt, Pd, and total S. The methods and detection limits for these analyses are fully described in Drennan and Fell, 2010. The mineralized samples that were used in this study were cut longitudinally from the remaining half core, and consequently, a quarter of original core was collected in 2 m intervals. Since unmineralized core was not assayed by Stillwater Canada Inc., unmineralized core was sampled in 1 m intervals and were cut in half longitudinally. The resulting half-core was collected for sampling. Witness samples (which best represented the textural variation of each 2 m interval) were kept in the event of sample loss or destruction during analysis.

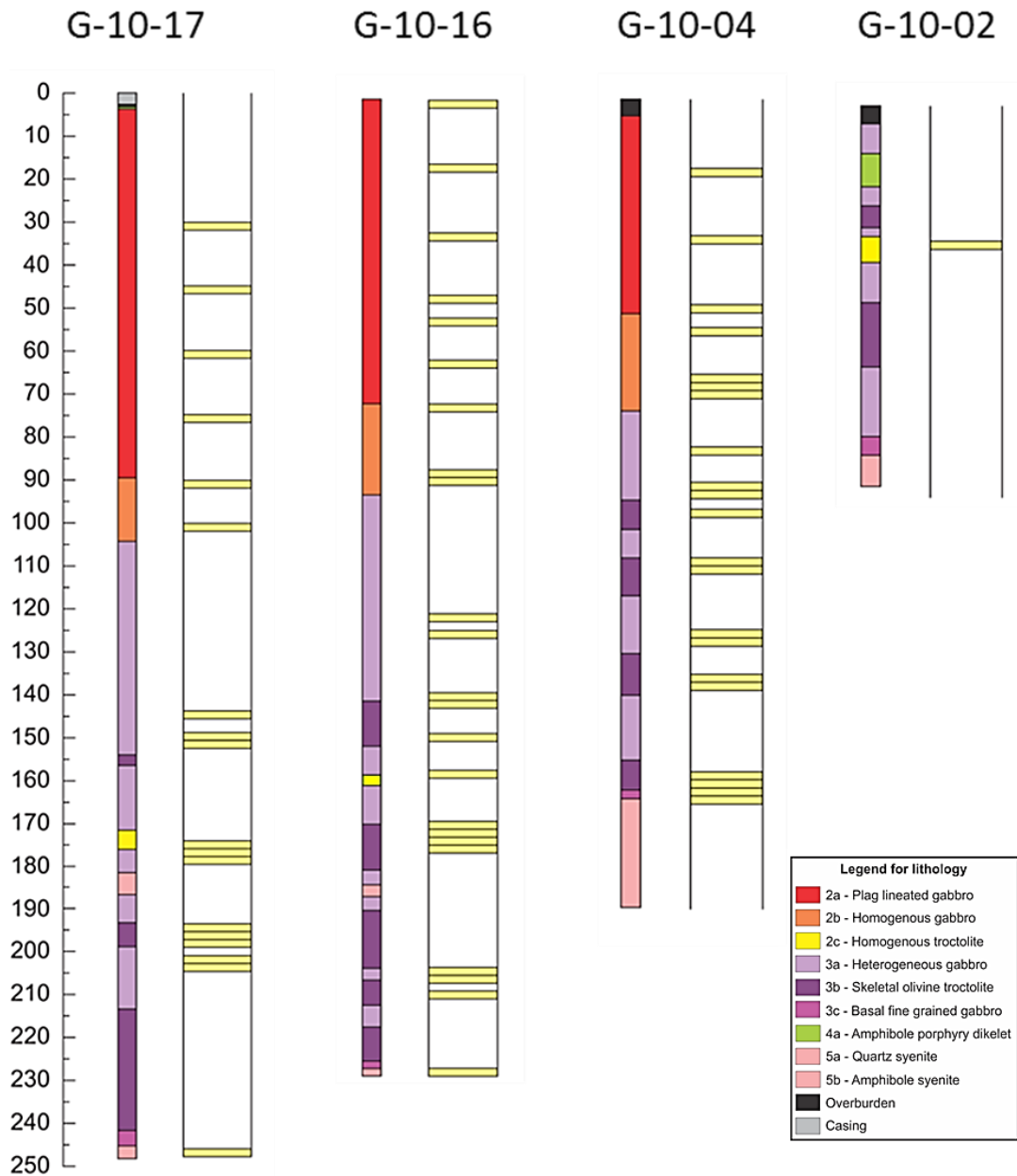


Figure 3.1 – Location of samples taken for geochemical analysis in all four drill-holes used in this study as indicated by the yellow bars. An additional 6 samples were taken from drill holes that were barren of mineralization (average grade of Cu <500 ppm and Pd <0.05 ppm), not shown on this image. The y-axis is depth in meters.

3.1.2 Albite Pod Selection Criteria

Three large albite pods on outcrop were also sampled in order to determine their alteration signatures relative to the host gabbro using trace element geochemistry and variations in $\delta^{18}\text{O}$ isotopic compositions. These albite pods were all located within 20m

of the basal syenite contact. The sampling method consisted of dividing each albite pod (ranging in size from 6 to 24cm across) into seven roughly 5 x 3.5 cm blocks that intersected the length of albite pod, with each block measuring up to 10 cm in depth. Each albite pod was photographed to record the progression from the most altered, to the least altered block. Albite Pod #3 (Figure 3.2) is the smallest albite pod, and upon observing a cross-section view of each block (Figure 3.3), it was decided that the degree of albitization is better represented by the cross-section views of each block, rather than a plan view transect of the pod. Albite Pod #5 contains a larger distribution of pink albite than Albite Pod #3, and is best represented by a plan view of the transect (Figure 3.4). Finally, the Discovery Outcrop Albite Pod was the largest albite pod observed in the field, and is also best represented by a plan view of the transect (Figure 3.5).

It should be noted that an approximately 1 cm 'crust' of surface weathering was removed before each sample was pulverized. This ensures that the $\delta^{18}\text{O}$ values of each block were not influenced by weathering. Each block has a representative photograph (see Appendix) which serves as verification of the amount of alteration present throughout each particular block. The trace element signatures of most altered to least altered samples coupled with precious metal values obtained from whole rock geochemistry can potentially provide an exploration vector for both the Geordie Lake and analogous deposits.

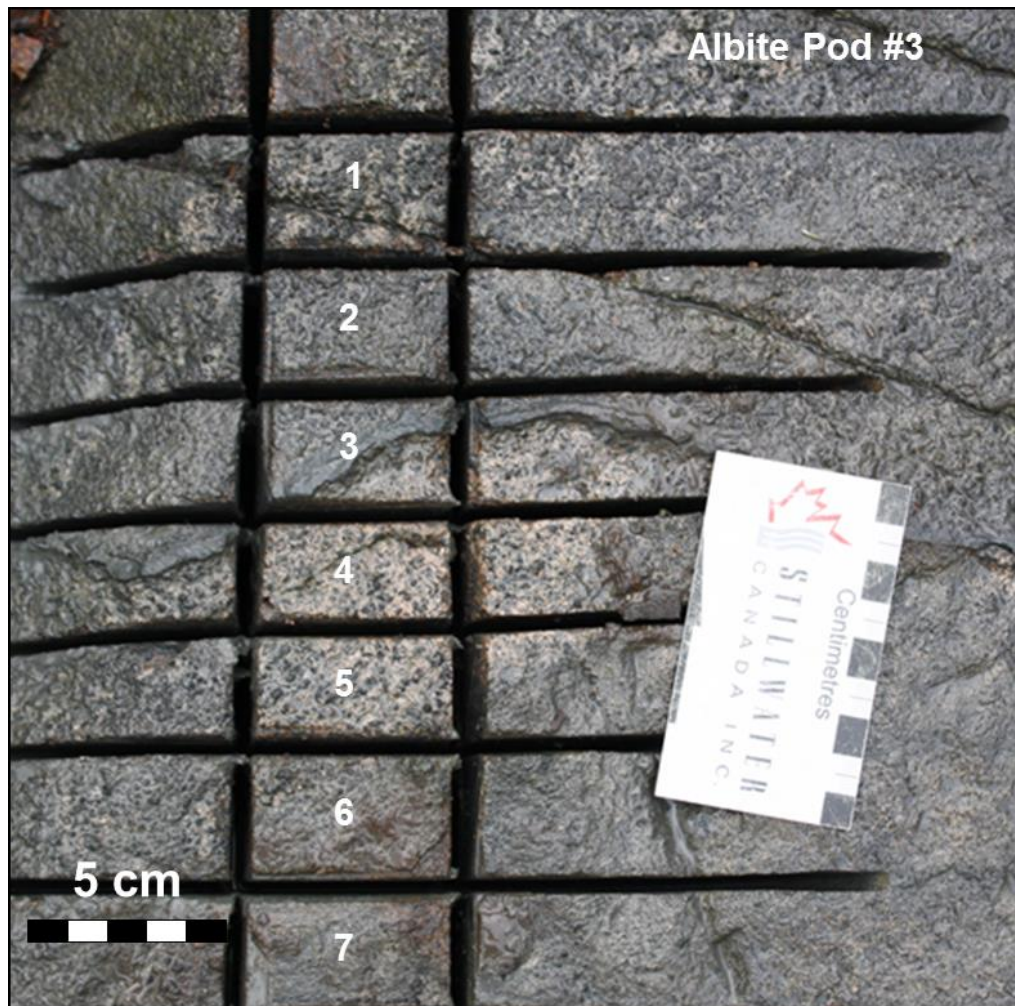


Figure 3.2 – Transect of Albite Pod #3, showing the cuts that were made. Blocks 1, 2, 6 and 7 contain no surface albitization, while blocks 4 and 5 are fully albitized on their surfaces. Block 3 is half albitized, and contains a 7 mm rim of chlorite-actinolite.

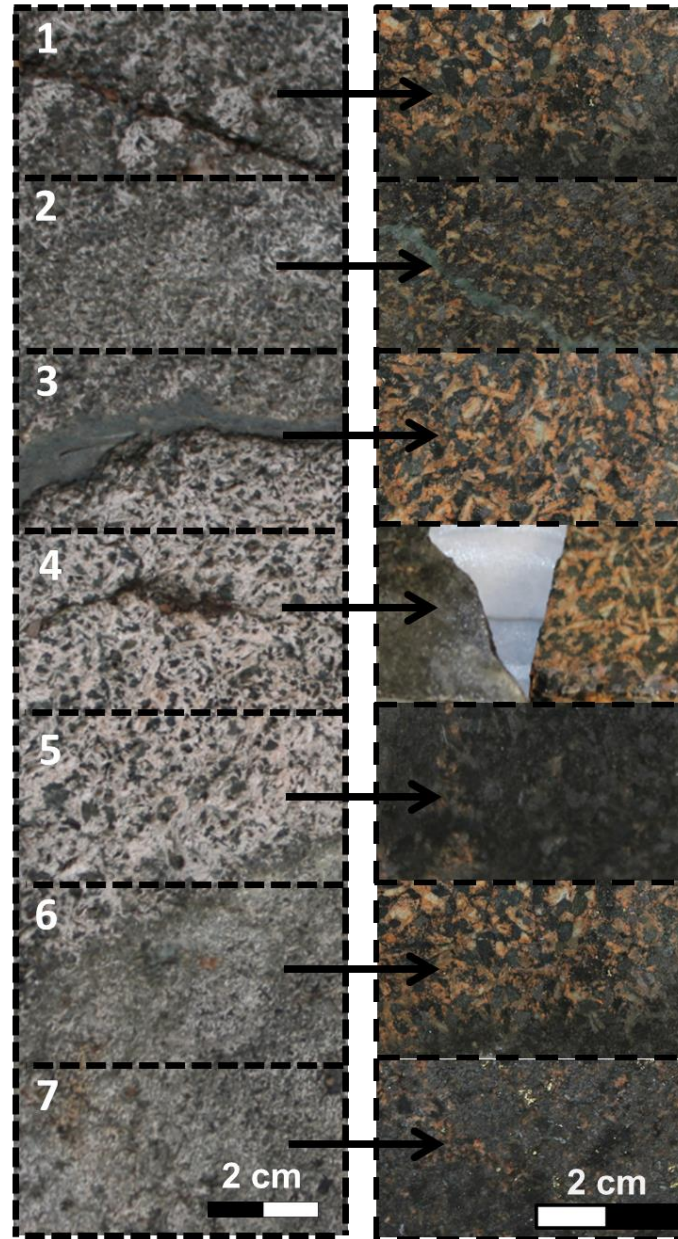


Figure 3.3 – Transect of Albitite Pod #3 shown again (on the left). The image on the right shows the cut blocks in cross section, which more accurately depicts the degree of albitization on each block since this particular albitite pod was not entirely continuous in depth. In cross section view, blocks 3, 4 and 6 contain the most albitization, while blocks 5 and 7 are the least albitized. Blocks 1 and 2 are weakly to moderately albitized respectively.



Figure 3.4 – Transect of Albite Pod #5, also showing the cuts that were made. Blocks 1 and 2 contain little to no surface albitization, while block 7 is moderately albitized on surface. Blocks 3, 4, 5, and 6 are pervasively albitized on surface.



Figure 3.5 – Transect of the Discovery Outcrop Albite Pod. Block 1 was visibly the most albitized on surface. Blocks 2, 3, 4, 5, and 6 exhibited decreasing albitization from block 2 onward. Blocks 7 and 8 showed little to no surface albitization. The albitization exhibited on surface is continuous in cross section.

3.2 Analytical Techniques

Both major and trace elements were analyzed and examined during the course of this project. Additionally, whole rock $\delta^{18}\text{O}$ was analyzed for 15 albitite pod samples, and 17 drill core samples (8 from G-10-17, and 7 from G-10-16). These samples were spaced in roughly 30 m intervals, starting from the top of the drill hole to the bottom, with no particular emphasis on lithology or alteration intensity. The majority of geochemical analyses were conducted at ALS Laboratories in Vancouver, British Columbia, and a

total of 6 duplicate samples were submitted in order to verify the consistency of all analyses. A suite of 15 samples were also analyzed for major elements in the Biotron at Western University in London, Ontario.

3.2.1 Major and Trace Element Geochemistry

Samples IM-1 to IM-15 were analyzed for major elements using X-ray fluorescence at the Geoanalysis Laboratory, located within the Biotron at Western University in London, Ontario with the assistance of Dr. Charlie Wu. These samples were all obtained from drill core. Sample preparation took place in the Rock Preparation Laboratory at Western University. Samples were first crushed using a Bico Chipmunk crusher and ground into granular pieces less than a few mm in diameter. After each sample was crushed, all tools and sample trays were cleaned with acetone solution in preparation for the next sample. Both crushing plates of the Bico Chipmunk crusher were also scrubbed with a brass bristle brush, and then wiped down with acetone. Crushed samples were then pulverized using a tungsten carbide ring mill. The ring mill was thoroughly cleaned with acetone in between sample runs. Pure silica sand was milled in between each sample in order to minimize contamination from the previous sample.

The majority of analyzed samples underwent preparation at ALS Laboratories in Vancouver, British Columbia. Samples were crushed using a fine jaw crusher which produced ~70% grains smaller than 2 mm (by passing a 2 mm Tyler 9 mesh US Std. No. 10 screen). The fine-grained material was then pulverized by a tungsten carbide ring and puck style grinding mill. This method resulted in 85% of the sample passing through a 75 micron (Tyler 2000) mesh, and hence, ensured a homogeneous powder. Silica sand cleaning between each sample run was also performed to prevent cross-contamination between samples.

Major elements were analyzed by X-ray fluorescence spectrometry (XRF) at ALS Laboratories in Vancouver, British Columbia. Samples were prepared by first drying to 100°C under a nitrogen atmosphere in order to drive off any absorbed H₂O, and then heated further to 1000°C under an oxygen atmosphere until a constant weight percentage

was determined. The sample was then fused with 9.0 g of Lithium Borate Flux (50% $\text{Li}_2\text{B}_4\text{O}_7$, and 50% LiBO_2), mixed well, and fused in an auto fluxer between 1050 - 1100°C. The remaining disk was then analyzed by XRF. The lower detection limit for each major element using this method is 0.01% (Rousseau, 2001).

Trace elements were analyzed using inductively coupled plasma mass spectroscopy (ICP-MS) at ALS Laboratories in Vancouver, British Columbia. A prepared sample was added to lithium metaborate flux (0.90 g), mixed well, and fused in a furnace at 1000°C. The resultant melt was then cooled and dissolved in 100 ml of 4% HNO_3 and 2% HCl_3 solution. This solution was then analyzed by ICP-MS. Pd, Pt, and Au were analyzed by inductively coupled plasma atomic emission spectroscopy (ICP-AES). A prepared sample was fused with a mixture of lead oxide, sodium carbonate and borax silica, in quartered with 6 mg of gold-free silver and then refined to yield a precious metal bead. The bead was digested for 2 minutes at high power by microwave in dilute nitric acid. The solution was then cooled, and then mixed with hydrochloric acid. The solution was digested for an additional 2 minutes at half power by microwave. The digested solution was then cooled, diluted to 4 ml with 2% hydrochloric acid, homogenized and then analyzed for gold, platinum and palladium by ICP-AES. The detection limits of trace elements using this method are summarized in Table 3.2. Cu and Ni were analyzed using a four-acid digestion method. The sample was digested in a mixture of nitric, perchloric and hydrofluoric acids. Perchloric acid was added to assist in oxidation of the sample, and to reduce the possibility of mechanical loss of sample as the solution was evaporated into moist salts. Elements were subsequently determined by ICP-AES (see Table 3.2 again for detection limits).

Sulfur was analyzed for total sulphur using a Leco sulphur analyzer. The sample was heated to approximately 1350 °C in an induction furnace while passing a stream of oxygen through the sample. Sulphur dioxide released from the sample was measured by an IR detection system and the total sulphur result was provided. Total ferrous iron (FeO) was analyzed by titration using H_2SO_4 -HF acid for digestion of the sample. The detection limit of the total S method is 0.01 – 50%.

Total PGE (including Pt, Pd, Rh, Ru, Ir, and Au) analysis was conducted on suite of 13 samples and was conducted at Geo Labs in Sudbury, Ontario. The method of analysis was a Nickel Sulfide Fire-Assay with an ICP-MS finish. The powdered sample was fused with a mixture of Ni and S to produce a nickel sulfide button. The nickel sulfide button was then dissolved in aqua regia, and followed by co-precipitation with Te to produce a concentrate containing all six precious metals. The concentrate was then analyzed by ICP-MS. Detection limits for all methods are summarized in Table 3.2 and 3.3.

Ba	0.5 – 10,000	Hf	0.2 – 10,000	Sn	1 – 10,000	W	1 – 10,000
Ce	0.5 – 10,000	Ho	0.1 – 10,000	Sr	0.1 – 10,000	Y	0.5 – 10,000
Cr	10 – 10,000	La	0.5 – 10,000	Ta	0.1 – 2,500	Yb	0.03 – 1,000
Cs	0.01 – 10,000	Lu	0.01 – 1,000	Tb	0.01 – 1,000	Zr	20 – 10,000
Dy	0.05 – 1,000	Nb	0.2 – 2,500	Th	0.05 – 1,000	Pd	0.005 – 10
Er	0.03 – 1,000	Nd	0.1 – 10,000	Tl	0.5 – 1,000	Pt	0.001 – 10
Eu	0.03 – 1,000	Pr	0.03 – 1,000	Tm	0.01 – 1,000	Au	0.001 – 10
Ga	0.1 – 1,000	Rb	0.2 – 10,000	U	0.05 – 1,000	Ni	1 – 10,000
Gd	0.05 – 1,000	Sm	0.03 – 1,000	V	5 – 10,000	Cu	1 – 10,000

Table 3.2 – The detection limits of trace elements analyzed in this study. All detection limits are measured in parts per million (ppm).

Au	0.22 – 3,600	Pd	0.12 – 4,800	Ru	0.08 – 8,000
Pt	0.17 – 4,700	Rh	0.02 – 970	Ir	0.01 – 1,900

Table 3.3 – The detection limits for PGE that were prepared using a Nickel Sulfide Fire-Assay method, and analyzed by ICP-MS. All detection limits are measured in parts per billion (ppb).

3.2.2 Oxygen Isotope Chemistry

Oxygen isotope analyses were performed in the Laboratory for Stable Isotope Science at Western University. Thirty-seven samples were analyzed in this study, ranging from drill-core samples to albite pod samples. The method used was based on the technique originally described by Clayton and Mayeda (1963) and modified by Borthwick and Harmon (1982). Approximately 9 milligrams of powdered samples were placed into spring-loaded stainless steel sample holders and let dry in a vacuum at 150°C overnight. The dried samples were subsequently placed under a dry nitrogen flow in nickel reaction vessels and were pretreated under vacuum at 300°C for 2 hours. They were then reacted

with chlorine trifluoride (ClF_3) reagent at 580°C for 18 hours. This allows for the liberation of oxygen from the silicate structure. The liberated oxygen is then converted to carbon dioxide (CO_2) via reaction with a headed graphite rod. Oxygen yields in the form of CO_2 were calculated in micromoles per milligram in order to determine the completion of the conversion. $\delta^{18}\text{O}$ values of CO_2 were finally measured using a dual-inlet DeltaPlus XL mass spectrometer. This method is able to provide an isotopic reproducibility of ± 0.1 to $\pm 0.2\%$, and the methods used to determine such a level of error is described in full detail by Clayton and Mayeda (1963),

3.2.3 Scanning Electron Microscopy

Polished thin sections were analyzed at the Nanofab Laboratory at Western University using a Zeiss Leo 1540 XB scanning electron microscope (SEM). Thin sections were first coated with 4 nm of osmium with a Filgen OPC80T osmium plasma coater prior to being mounted in the SEM in order to disperse charge. Elemental data was obtained using an Oxford Instruments INCA x-sight energy dispersive spectrometer (EDS) which was in conjunction to the 1540 XB microscope. Backscatter electron images were obtained at 15kV, and are a pictorial representation of the energy level of electrons that have been emitted from the primary beam, reacted with the sample's atoms, and subsequently rebounded back to be analyzed by the EDS attachment.

Chapter 4

4 Petrography

The following section is a petrographic review of the different lithologies present at the GLD that includes a summary of the different alteration and mineralization styles within each particular lithology. Of particular emphasis are mineralogies associated with Cu-sulfide mineralization (both primary and secondary mineralogy), and subsequently, the spatial associations of PGM within Cu-sulfide mineralization and the relationships of this mineralization with oxide and sulfide phases.

4.1 Umineralized Lithologies at the GLD

The GLD contains 3 unmineralized units that have consistently low grades of Cu (<500 ppm) and Pd (<0.05 ppm). Mineralization within these lithologies is constrained to very trace disseminations of chalcopyrite, and rarely, pyrrhotite. These lithologies are barren of mineralization despite being in close proximity to mineralized horizons at the GLD. Plagioclase aligned gabbro (Unit 2a) is the upper-most gabbroic unit, and is underlain by fine to medium-grained homogeneous gabbro (Unit 2b). Heterogeneous gabbro and skeletal troctolite are cross-cut by homogeneous troctolite (Unit 2c) deeper in the GLD stratigraphy.

4.1.1 Plagioclase Aligned Gabbro (Unit 2a)

The plagioclase aligned gabbro is the uppermost lithology in the stratigraphy of the GLD. A summary of the mineralogy and textural characteristics of plagioclase aligned gabbro are shown on Table 4.1. The alignment of the plagioclase crystals is variable; alignment is less pronounced closer to the gradational contact with homogeneous gabbro below. Figure 4.1 shows the texture of a typical plagioclase aligned gabbro. Plagioclase lath morphology at the top of the drill holes tends to be stubby and, less commonly, equant. Further down hole, these laths become longer and thinner. Plagioclase is commonly euhedral and albitized only at the rims within zones of weak alteration. The gabbro is also composed of clinopyroxene (8%), apatite (2%) and magnetite (7%).

Average values for plagioclase aligned gabbro (Unit 2a)							
Magmatic Minerals							
Mineral	Plagioclase	Clinopyroxene	Apatite		Magnetite		
Modal %	28-40%	5-15%	1-2%		5-10%		
Shape	Euhedral	Anhedral	Euhedral to subhedral		Anhedral to subhedral		
Grain size	3-15 mm	2-7 mm	<1-5 mm		<1-2 mm		
Comments	Forms euhedral laths that typically show distinct alignment	Interstitial to plagioclase, but mainly altered to actinolite or chlorite	Forms well defined needles that are especially prominent in regions of strong chlorite, actinolite and biotite alteration		Forms stubby grains		
Hydrothermal Minerals							
Mineral	Hornblende	Actinolite	Chlorite	Biotite	Epidote	Albite	Magnetite
Modal %	trace-1%	8-12%	1-7%	2-11%	<1%	8-14%	<1%
Shape	Anhedral	Anhedral, pseudo-morphic after Cpx	Patchy, replacement texture	Anhedral to subhedral	Anhedral	Anhedral, replacement of Pl	Disseminated
Grain size	<1 mm to	<1 – 3 mm	<1 – 2 mm	<1 – 3 mm	<1 mm	<1 – 4 mm	<1 – 2 mm
Comments	Pseudo-morphic after Cpx	Pseudo-morphic after Cpx	Patchy replacement of Cpx	Abundant in altered regions, manifests as reaction rims on magnetite	Occurs with chlorite-actinolite-biotite assemblages	Replaces Pl rims, or completely replaces Pl	Rarely replaces fine grained, disseminated Ccp
Sulfide Minerals							
Mineral	Chalcopyrite		Pyrite		Pyrrhotite		
Modal %	trace		trace		trace		
Shape	Disseminated to rarely blebby		Disseminated		Disseminated		
Grain size	<0.1 mm		<0.1 mm		<0.1 mm		
Comments	Commonly interstitial to actinolite, biotite, and less commonly chlorite		Occurs only alongside chalcopyrite, interstitial to actinolite, biotite and less commonly chlorite		Occurs alongside actinolite, chlorite, biotite		

Table 4.1 – Average mineral abundances based on visual estimations for plagioclase aligned gabbro (Unit 2a)

Clinopyroxene is medium-grained, and varies from subhedral to interstitial and ranges from being partially to wholly altered to actinolite, biotite, and chlorite. Coarse-grained apatite is commonly euhedral, elongate, and is enveloped by both clinopyroxene and plagioclase (Figure 4.2c and 4.2d) while fine-grained apatite needles are commonly found as inclusions within clinopyroxene, magnetite and actinolite-biotite-chlorite alteration zones. Magnetite occurs as anhedral to subhedral fine-grained stubby crystals less than 1.5 mm in size. Less commonly, magnetite grains exhibit irregular, skeletal morphologies (Figure 4.2a and 4.2b). These stubby (and primary) magnetite crystals exhibit ilmenite exsolution lamellae. Olivine is not observed in this lithology. The lower contact of the plagioclase aligned gabbro with the homogeneous gabbro is gradational

over 2 to 5 meters and is defined by the loss of plagioclase foliation. Plagioclase aligned gabbro is never found in contact with heterogeneous gabbro, skeletal troctolite, or basal fine-grained gabbro, all of which are ore-bearing lithologies.

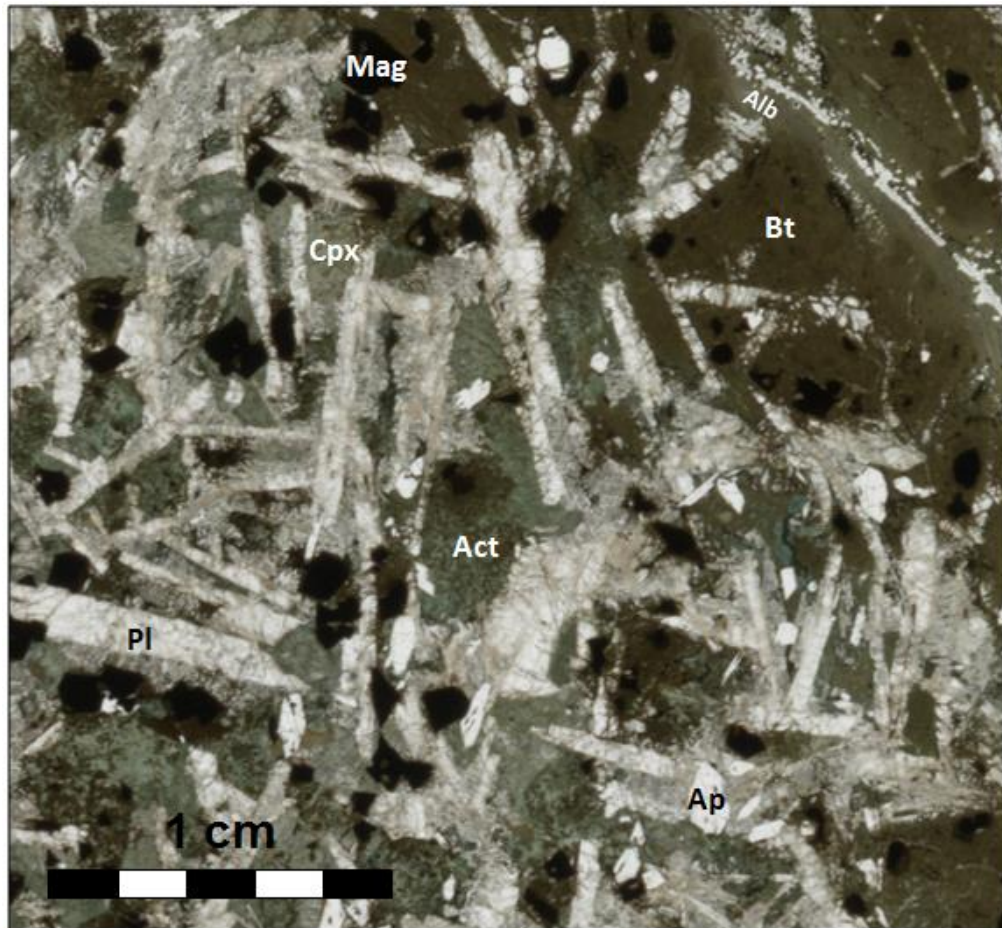


Figure 4.1 – Overall texture of the plagioclase aligned gabbro. Plagioclase alignment is weakly north-south in this image, with minor east-west alignment. East-west alignment is less common. In plane polarized light

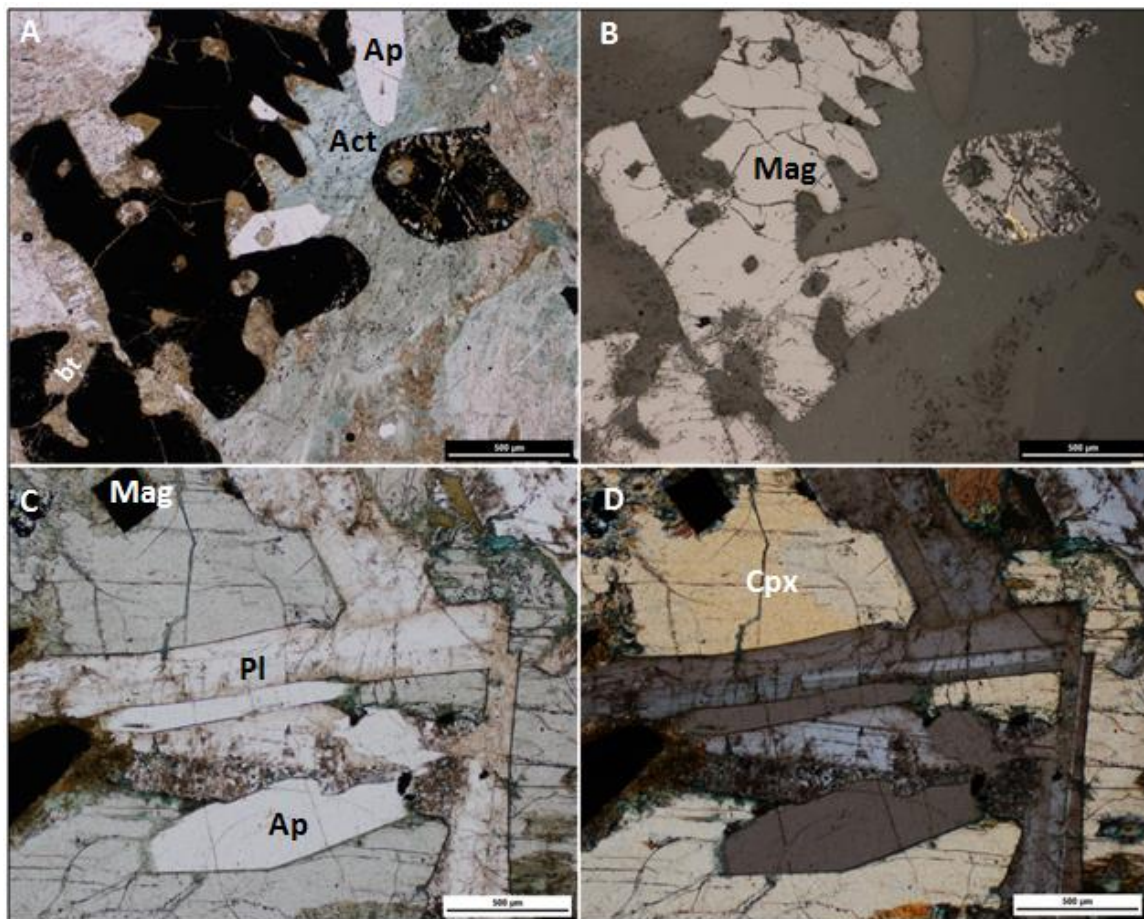


Figure 4.2 – **A)** Stubby, somewhat irregular skeletal magnetite crystals are rimmed by brown biotite and intergrown with chlorite that is pseudomorph after clinopyroxene. The magnetite grain on the right is enveloped by pervasive patchy chlorite alteration, **B)** The same image as in (A), the magnetite grain on the right side of the image contains small secondary inclusions of chalcopyrite that appears to be in close proximity to the chlorite alteration surrounding the magnetite grain, in reflected light, **C)** Two elongate apatite crystals being enveloped by clinopyroxene and plagioclase. The plagioclase and clinopyroxene form an ophitic texture, in PPL, **D)** The same image as in (C), but in XPL

4.1.1.1 Alteration

Alteration within plagioclase aligned gabbro is primarily manifested as local pseudomorph overprints or rims around plagioclase (albite altered), clinopyroxene (actinolite, chlorite and epidote altered), and magnetite (biotite rimmed), and that there is no evidence for any continuous, large-scale alteration halo. The bulk of alteration within the plagioclase aligned gabbro is constrained primarily to varying degrees of strongly pleochroic green actinolite and chlorite, as well as pleochroic brown biotite. Actinolite and chlorite are predominantly pseudomorph after clinopyroxene, and are manifested as

small blebs measuring <0.5 mm to a few mm in diameter. Figure 4.3 shows an example of pseudomorphic chlorite alteration (after clinopyroxene) as well as brown biotite that is concentrated within a zone that contains abundant magnetite, and forms a thin rim around magnetite grains. Biotite alteration is particularly strong where there is strong actinolite and chlorite alteration (Figure 4.4a). Where actinolite alteration is not pseudomorphic after clinopyroxene, it occurs in small (<0.5cm to 1cm) pods that result from the infilling of pore space. In these instances, actinolite is strongly associated with chalcopyrite or pyrrhotite.

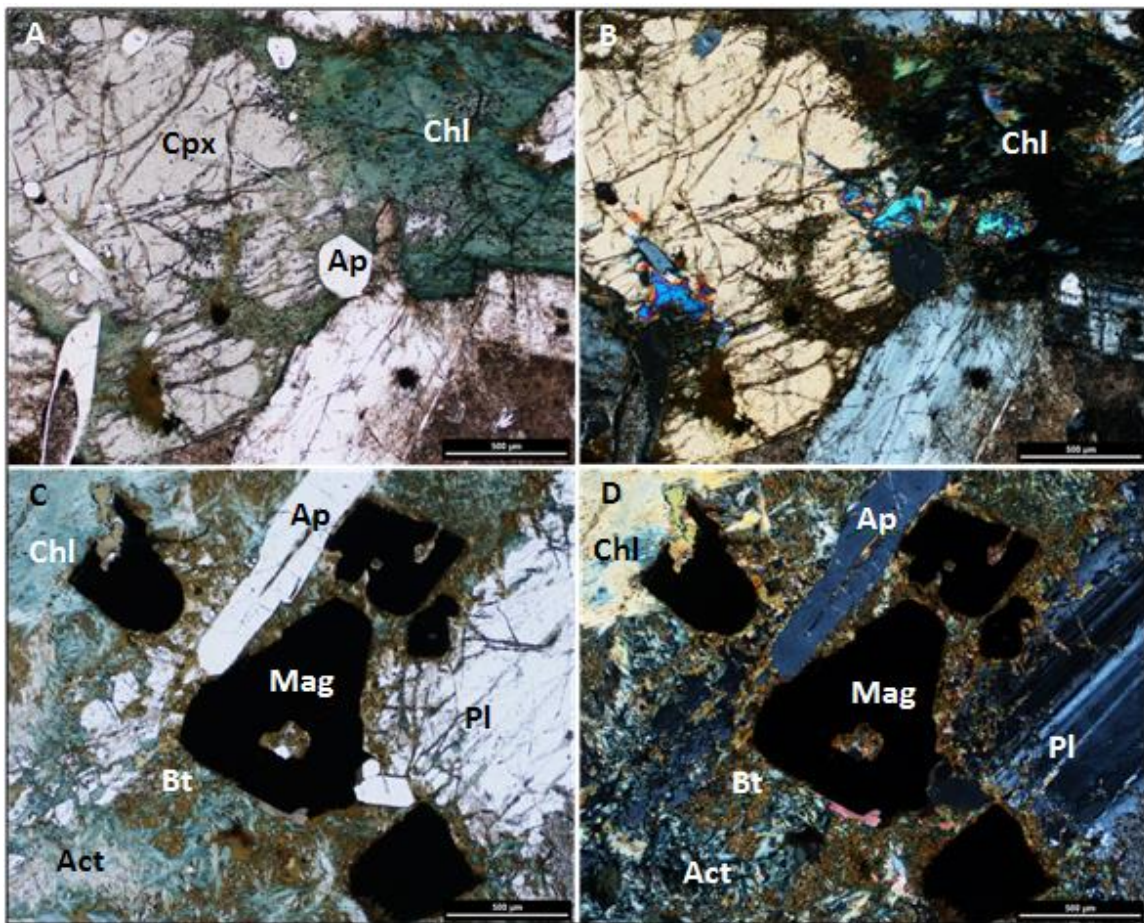


Figure 4.3 – A) Patchy chlorite alteration of clinopyroxene. Alteration is pervasive on the right side of the image, and alteration is also manifested within fractures coincident with clinopyroxene cleavage planes, in PPL, B) Same image as in (A), in XPL, C) Stubby, subhedral magnetite crystals are being enveloped by pervasive patchy to acicular chlorite alteration. Dirty-brown coloured biotite alteration is strongest near magnetite grains, D) The same image as in (C), but in XPL

Figure 4.4c and d shows a plane-polarized light (PPL) and reflected light thin section image where actinolite laths up to 0.5 mm are adjacent to a euhedral, hexagonal magnetite grain (with ilmenite exsolution lamellae) and include interstitial chalcopyrite and pyrrhotite. The same image as in Figure 4.4c is magnified in Figure 4.5 and shows the presence of albite alteration adjacent to the band of actinolite laths described in Figure 4.4c. Albite alteration commonly mantles plagioclase laths; however within the most altered patches, it completely overprints the previous mineralogy. Zones with such strong albite alteration contain up to 2-4% euhedral apatite.

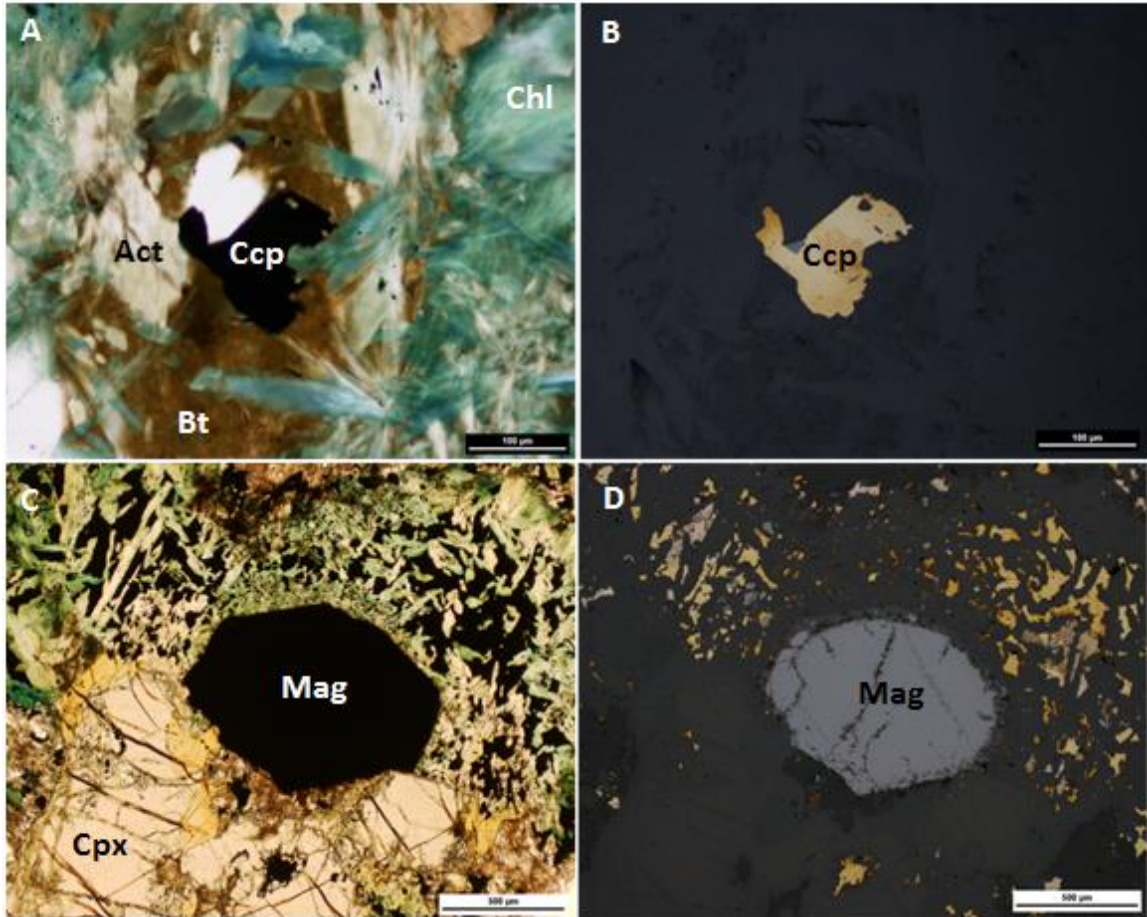


Figure 4.4 – **A)** Radially extending chlorite grains are intergrown with actinolite and dirty brown coloured biotite, enclosing a chalcopyrite grain. The original mineralogy that is overprinted by chlorite, actinolite and biotite is difficult to distinguish. In PPL **B)** Same image as in (A), showing the chalcopyrite grain in reflected light, **C)** A hexagonal, euhedral magnetite grain being enveloped by actinolite alteration at the top of the image, and in contact with a clinopyroxene grain at the bottom of the image. Secondary biotite is common at the margins of magnetite and clinopyroxene, particularly within zones of strong actinolite or chlorite alteration, **D)** The same image as in (C) showing the opaque minerals in the interstices of actinolite needles to be chalcopyrite and pyrite.

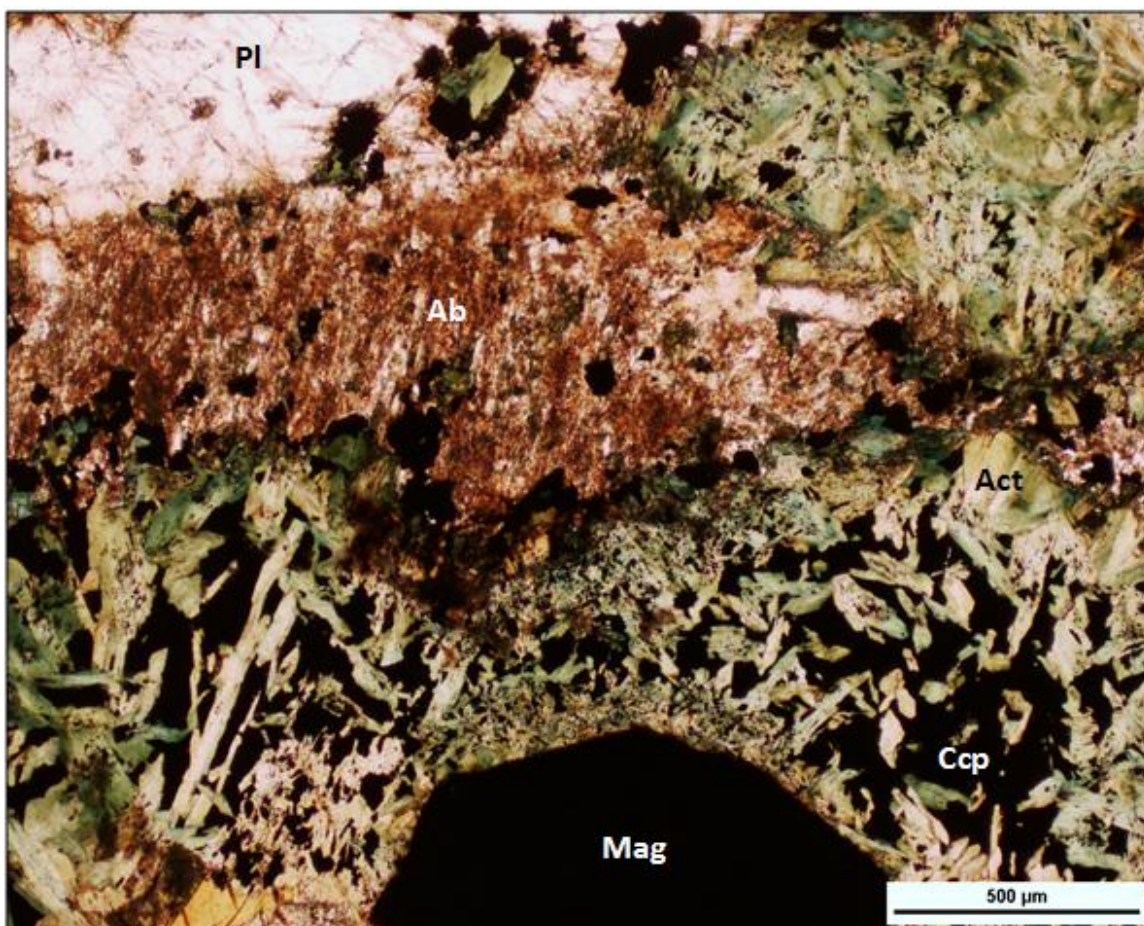


Figure 4.5 – A close up of the image in Figure 4.4c, showing the prominence of albite at the margins of strong actinolite alteration, and in this case, actinolite alteration that hosts chalcopyrite mineralization. In PPL

4.1.1.2 Mineralization

Sulfide mineralization within plagioclase aligned gabbro is scarce; however when present, it consists of disseminated chalcopyrite, pyrrhotite, and very sparsely, pyrite. This sulfide assemblage is hosted predominantly within blebs of actinolite, biotite, and less commonly, patchy chlorite that is pseudomorphic after clinopyroxene. Very small (<0.1 mm), disseminated blebs of chalcopyrite have been observed in spatial association with fine-grained biotite and calcite. Chalcopyrite blebs may be accompanied by pyrite, pyrrhotite, and secondary magnetite. No PGMs are found within this trace, disseminated

chalcopyrite mineralization, nor are PGMs found anywhere within primary and secondary silicate minerals.

4.1.2 Fine to Medium-Grained Homogeneous Gabbro (Unit 2b)

The fine to medium-grained homogeneous gabbro is mineralogically similar to the plagioclase aligned gabbro, except that it contains more clinopyroxene (~8%) and less plagioclase (~7%). Homogeneity is demonstrated by the constant modal percentages of plagioclase, clinopyroxene, magnetite and apatite (within 8 samples, averages are shown on Table 4.2). Plagioclase laths vary in size, between 4-12 mm in length with relatively high aspect ratios (7-10) of length to width. Virtually all plagioclase within this lithology is mantled by albite. Apatite is euhedral and is commonly enclosed by clinopyroxene grains. Clinopyroxene is medium-grained, subhedral to interstitial and partly to wholly altered to actinolite and chlorite (Figure 4.7). Very fine-grained, subhedral magnetite less commonly occur as inclusions within light green actinolite, biotite, and within clinopyroxene. Generally, euhedral magnetite (which is observed as equant, stubby grains) is present, and is commonly enclosed by a fine-grained rim of brown strongly-pleochroic biotite. Fine-grained apatite needles are present as inclusions in clinopyroxene, magnetite and actinolite-biotite alteration zones. Olivine may have been present as indicated by subhedral actinolite-chlorite pseudomorphs, however fresh olivine is not observed.

4.1.2.1 Alteration

The degree of alteration within the range of homogeneous gabbro samples is, overall, very uniform. As with the plagioclase aligned gabbro, green-alteration minerals within the homogeneous gabbro include actinolite, chlorite, and less commonly epidote. All three minerals are generally pseudomorphic after clinopyroxene, though the alteration of clinopyroxene ranges from patchy and sparse to extensive and pervasive (Figure 4.7). Roughly 40-50 % of clinopyroxene crystals are altered to strongly pleochroic green actinolite and chlorite. In some polished thin sections, over half of a clinopyroxene grain might exhibit actinolite alteration, whereas other clinopyroxene grains within the same polished section might exhibit only a small patch of actinolite alteration on the edge of a

Average values for homogeneous gabbro (Unit 2b)							
Magmatic Minerals							
Mineral	Plagioclase	Clinopyroxene		Apatite		Magnetite	
Modal %	28-38%	11-24%		1-4%		5-13%	
Shape	Euhedral	Anhedral		Euhedral to subhedral		Anhedral to subhedral	
Grain size	2-12 mm	2-9 mm		<1-5 mm		<1-2 mm	
Comments	Forms euhedral laths that show no alignment	Interstitial to plagioclase, but mainly altered to actinolite or chlorite		Forms well defined needles that are especially prominent in regions of strong chlorite, actinolite and biotite alteration		Forms stubby, equant crystals	
Hydrothermal Minerals							
Mineral	Hornblende	Actinolite	Chlorite	Biotite	Epidote	Albite	Magnetite
Modal %	Trace-1%	7-14%	2-8%	2-10%	<1%	7-16%	<1%
Shape	Anhedral	Anhedral, pseudo-morphic after Cpx	Patchy, replacement texture	Anhedral, irregular rims	Anhedral	Anhedral, frosty replacement of Pl	Disseminated
Grain size	<1-2 mm	<1 – 3 mm	<1 – 2 mm	<1 – 3 mm	<1 mm	<1 – 4 mm	<1 – 2 mm
Comments	Pseudo-morphic after Cpx	Pseudo-morphic after Cpx	Patchy replacement of Cpx	Abundant in the most altered regions, manifests as reaction rims on magnetite	Occurs with chlorite-actinolite-biotite assemblages	Sporadically replaces plagioclase rims, or completely replaces plagioclase	Rarely replaces fine grained, disseminated chalcopyrite
Sulfide Minerals							
Mineral	Chalcopyrite		Pyrite			Pyrrhotite	
Modal %	Trace		Trace			Trace	
Shape	Disseminated to rarely blebby		Disseminated			Disseminated	
Grain size	<0.1 mm		<0.1 mm			<0.1 mm	
Comments	Commonly interstitial to actinolite, biotite, and less commonly chlorite		Occurs only alongside chalcopyrite, interstitial to actinolite, biotite and less commonly chlorite			Occurs alongside actinolite, chlorite, biotite	

Table 4.2 – Average mineral abundances based on visual estimations for homogeneous gabbro (Unit 2b)

clinopyroxene grain. Actinolite and chlorite alteration are particularly extensive in and around the cleavage planes of clinopyroxene. Hornblende alteration of clinopyroxene is also observed, but not common. Reddish-brown, pleiochroic biotite commonly rims magnetite. Biotite rims around magnetite are notably thicker near regions of strong actinolite-chlorite and albite alteration. Epidote alteration is fine-grained, and is observed within zones of intense albitization. There are two varieties of chlorite alteration: patchy chlorite, and acicular, needle-like chlorite but both varieties are sporadic and are not

preferential to any particular mineral assemblage. Albite alteration is common, and is manifested either as mantling around plagioclase laths, or has fully replaced plagioclase. On average, approximately 13% albite exists within the homogeneous gabbro. Fine-grained apatite is ubiquitous within these zones of cloudy-grey albite.

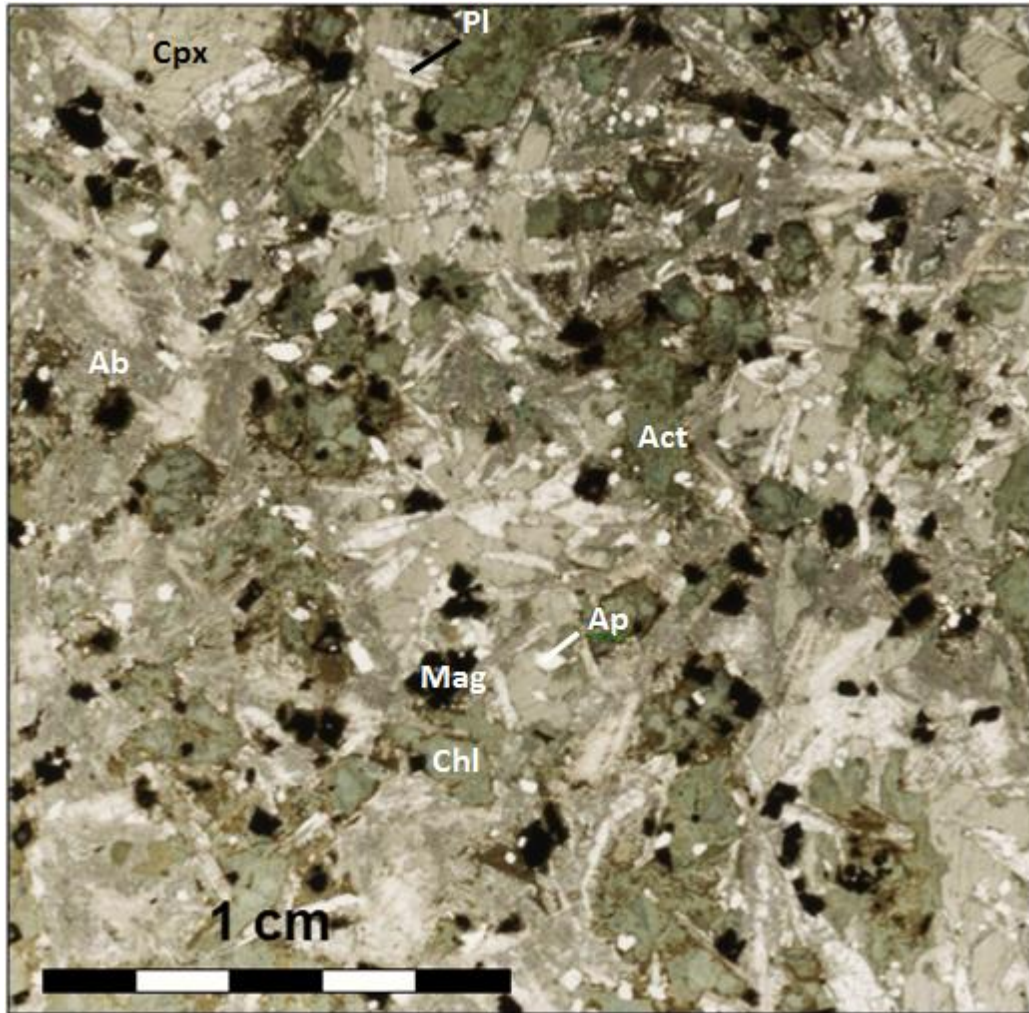


Figure 4.6 – General texture of the homogenous gabbro. The main distinction between the homogeneous gabbro and the plagioclase aligned gabbro is the alignment of plagioclase laths within the appropriately termed plagioclase aligned gabbro, and a smaller average grain size within the homogeneous gabbro. Modal mineralogy of the homogeneous gabbro does not differ much from that of the plagioclase aligned gabbro. Olivine may have been previously present, however, all that remains are patchy actinolite-chlorite pseudomorphs. In plane polarized light

4.1.2.2 Mineralization

Overall, the homogeneous gabbro is weakly mineralized. Where mineralization is present (in trace amounts), it is present as very weakly disseminated blebs of chalcopyrite and pyrite. Chalcopyrite and pyrite are spatially associated with actinolite, chlorite, and less commonly albite (but typically in spatial association with actinolite when associated with albite). Rarely, chalcopyrite may be present as an inclusion within strongly albitized plagioclase (Figure 4.8a). In this particular example, chalcopyrite occurs with millerite (Figure 4.8b), and hydrothermal magnetite (which contains no ilmenite exsolution lamellae). Very fine-grained actinolite is found at the margins of chalcopyrite. No PGMs are found within chalcopyrite grains, nor are they found as inclusions within silicate minerals.

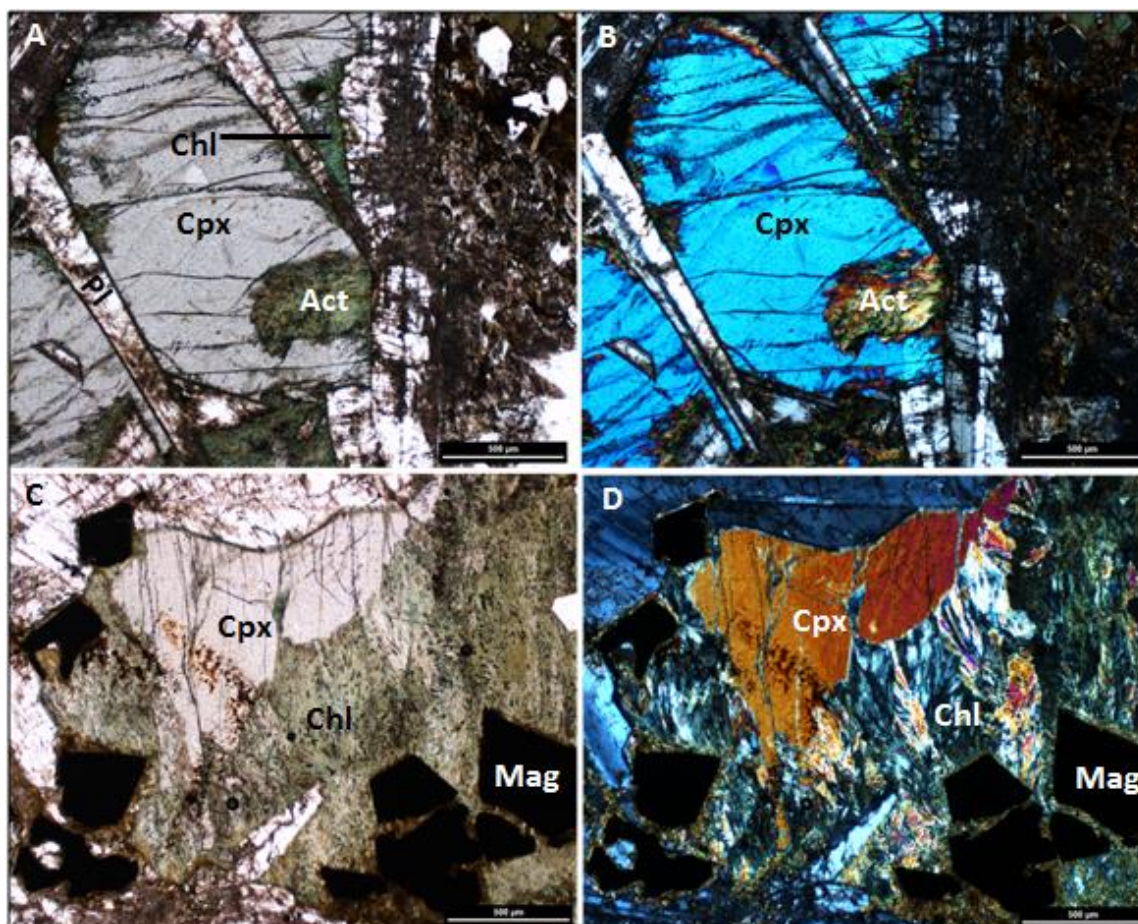


Figure 4.7 – **A**) Relatively minor, patchy actinolite alteration of clinopyroxene, in addition to wispy chlorite alteration, in PPL, **B**) The same image as in (A), but in XPL, **C**) Pervasive chlorite alteration of clinopyroxene from the bottom of the image moving upwards. Magnetite grains contain brown biotite rims within the region of chlorite alteration, **D**) The same image as in (C) but in XPL

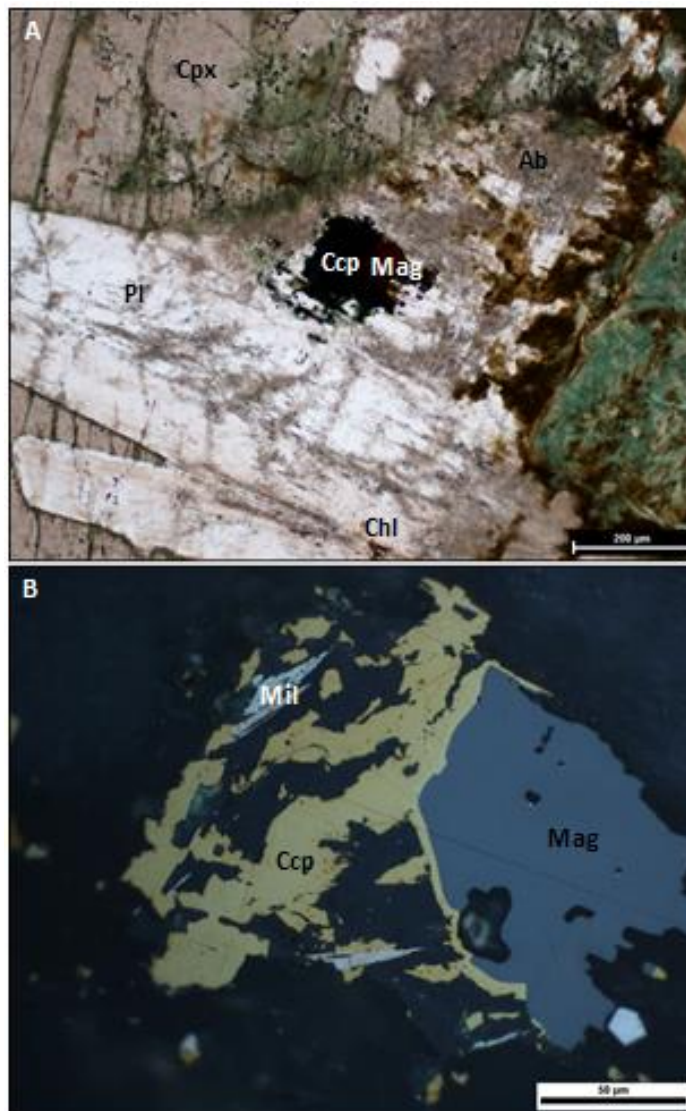


Figure 4.8 – **A**) An opaque mineral occurring as an inclusion in a plagioclase grain that exhibits dusty albite mantling. Very trace amounts of actinolite, chlorite or biotite surround the opaque inclusion, in PPL, **B**) The same image as in (A), but zoomed in on the opaque phase in reflected light. To the left, chalcopyrite hosts two roughly 20-30 µm grains of bladed millerite. To the right, magnetite appears to resorb chalcopyrite, and a thin but continuous wisp of chalcopyrite rims the magnetite grain.

4.1.3 Medium-Grained Homogeneous Troctolite (Unit 2c)

A mineralogical summary of the medium-grained homogeneous troctolite is shown on Table 4.3. The homogeneity in this lithology is defined by the constant grain size (~1 mm) of major mineral phases. The homogeneous troctolite consists of, in decreasing order of abundance: subhedral plagioclase, olivine, magnetite (commonly intergrown with olivine or occurring in variably sized clusters), interstitial clinopyroxene, and

ehedral apatite. Plagioclase is medium-grained (~5 mm), and subhedral since it is commonly altered to albite at its rims. Fine to medium-grained olivine is stubby and subhedral. Modal percentages of interstitial clinopyroxene is variable between samples, however clinopyroxene is more abundant farther away from the contact between the homogeneous troctolite and the surrounding heterogeneous gabbro. Very thin apatite needles up to 5 mm long are found as inclusions within clinopyroxene, magnetite, and particularly within zones of strong albitization.

4.1.3.1 Alteration

The most significant alteration consists of pink-albite alteration of plagioclase, strongly pleochroic reddish-brown biotite alteration around olivine and magnetite, and actinolite-chlorite alteration of clinopyroxene. Biotite alteration is commonly seen as an aureole around stubby olivine and magnetite grains (Figure 4.10a). Fine-grained magnetite is prevalent within olivine fracture planes (Figure 4.10b). In some instances, olivine is completely altered to fine-grained serpentine and actinolite. Figure 4.11 shows the typical texture of medium-grained homogeneous troctolite (top left of image) being overprinted by medium to strong albite alteration. Albite alteration ranges from thin mantling of plagioclase laths (in the least altered regions), to complete pervasive albite alteration of plagioclase and other relict, unidentifiable mineralogies. Fine-grained apatite is ubiquitous within regions of intense albitization. Alteration within this unit is not continuous on a large scale, but rather, patchy and localized.

4.1.3.2 Mineralization

The homogeneous troctolite is very poorly mineralized with rare disseminated chalcopyrite that is enveloped by an assemblage of strongly pleochroic green actinolite, chlorite, and biotite.

Homogeneous troctolite (Unit 2c)

Magmatic Minerals					
Mineral	Plagioclase	Olivine	Magnetite	Apatite	Clinopyroxene
Modal %	14-24%	12-22%	12-28%	2-7%	4-10%
Shape	Euhedral to subhedral	Subhedral, slightly skeletal grains	Stubby to equant	Euhedral	Anhedral
Grain size	<1 – 9 mm	<1 – 3 mm	<1 mm	<1 mm	<1 – 2 mm
Comments	Forms relatively stubby laths with aspect ratios of 2-5	Exhibit slightly skeletal textures, but commonly stubby grains	Very fine grained, stubby crystals that tend to occur near or at grain boundaries of olivine. Form little clusters	Occur mainly within cloudy, dusty-textured albite	When present, forms ophitic texture with plagioclase. Commonly altered to actinolite
Hydrothermal Minerals					
Mineral	Albite	Biotite	Actinolite	Chlorite	
Modal %	8-17%	6-15%	2-8%	trace-6%	
Shape	Anhedral	Anhedral	Anhedral	Anhedral	
Grain size	1 – 5 mm	~1 mm	<1 mm	<1 mm	
Comments	Occurs either as thin mantles of plagioclase, or 3 – 10 mm clouds that envelop olivine and magnetite in addition to plagioclase	Forms thin mantles around olivine grains and even thinner mantles around magnetite grains	Typically pseudomorphic after clinopyroxene	Occurs as pseudomorphs after clinopyroxene	
Sulfide Minerals					
Mineral	Chalcopyrite	Pyrrhotite		Pyrite	
Modal %	trace	trace		trace	
Shape	Disseminated	Disseminated		Disseminated	
Grain size	<1 mm	<1 mm		<1 mm	
Comments	Very trace, and occurs within zones of intense actinolite alteration	Only occurs proximal to chalcopyrite mineralization		Occurs within chalcopyrite mineralization	

Table 4.3 – Average mineral abundances based on visual estimations for homogeneous troctolite (Unit 2c)

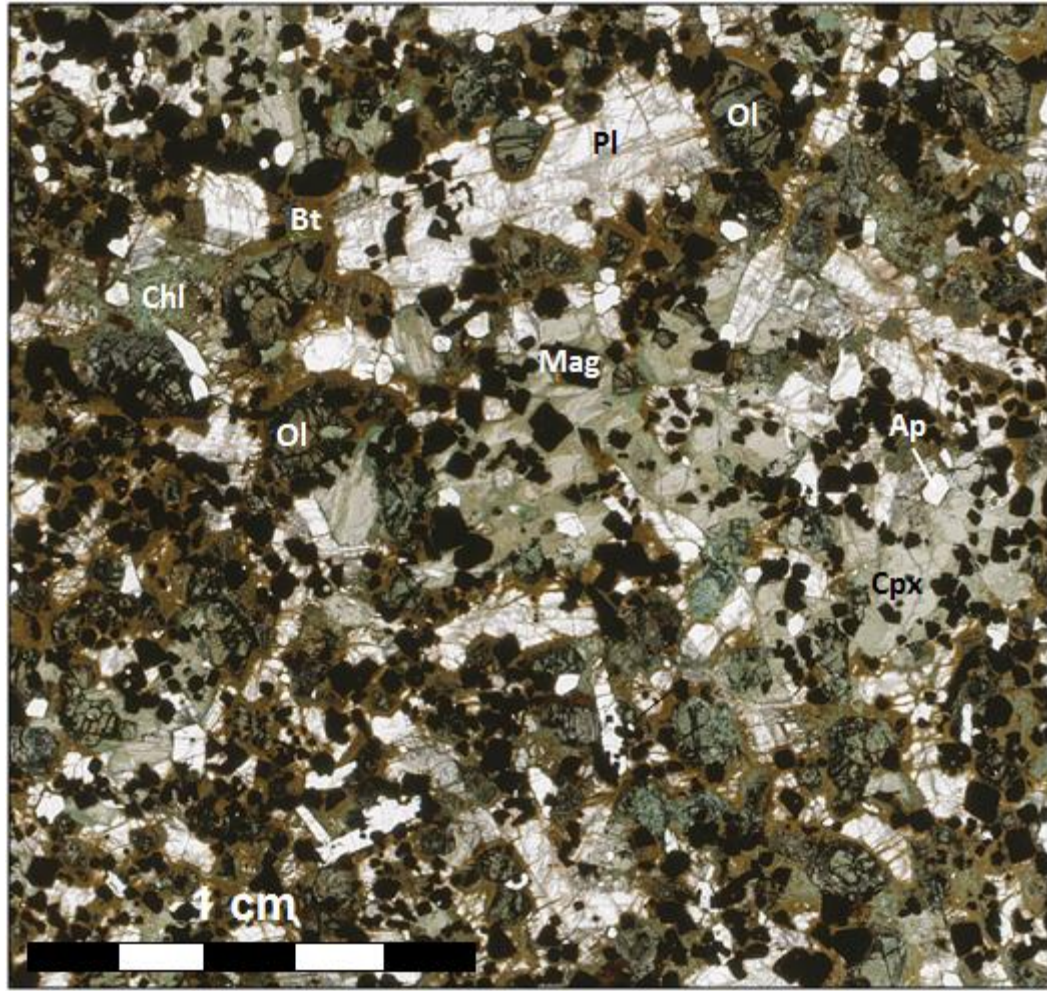


Figure 4.9 – General texture of homogenous troctolite. In plane polarized light

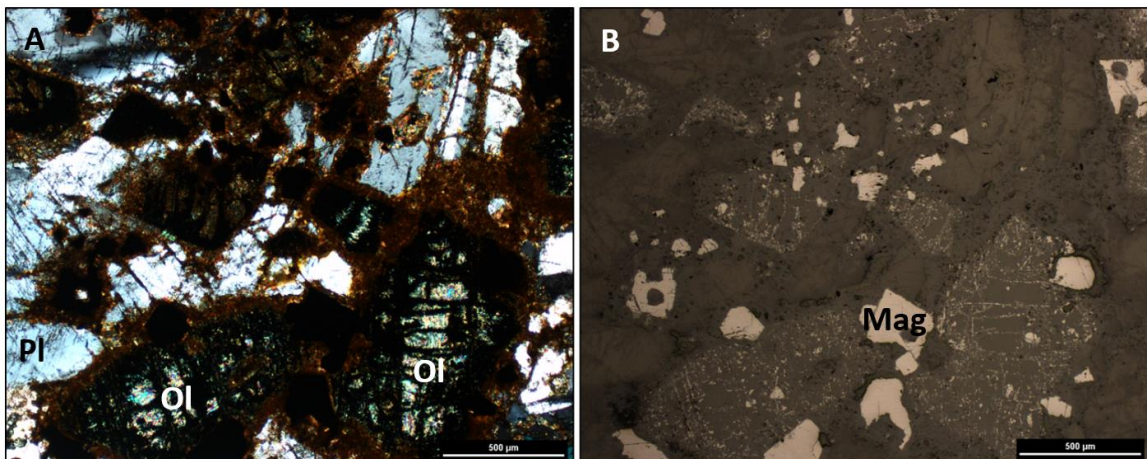


Figure 4.10 – **A**) Stubby grains of olivine within plagioclase are strongly rimmed by biotite, **B**) The same image as in **(A)**, however, in reflected light. Stubby grains of magnetite are intergrown with olivine. Secondary magnetite also occurs within the fractures of olivine grains.

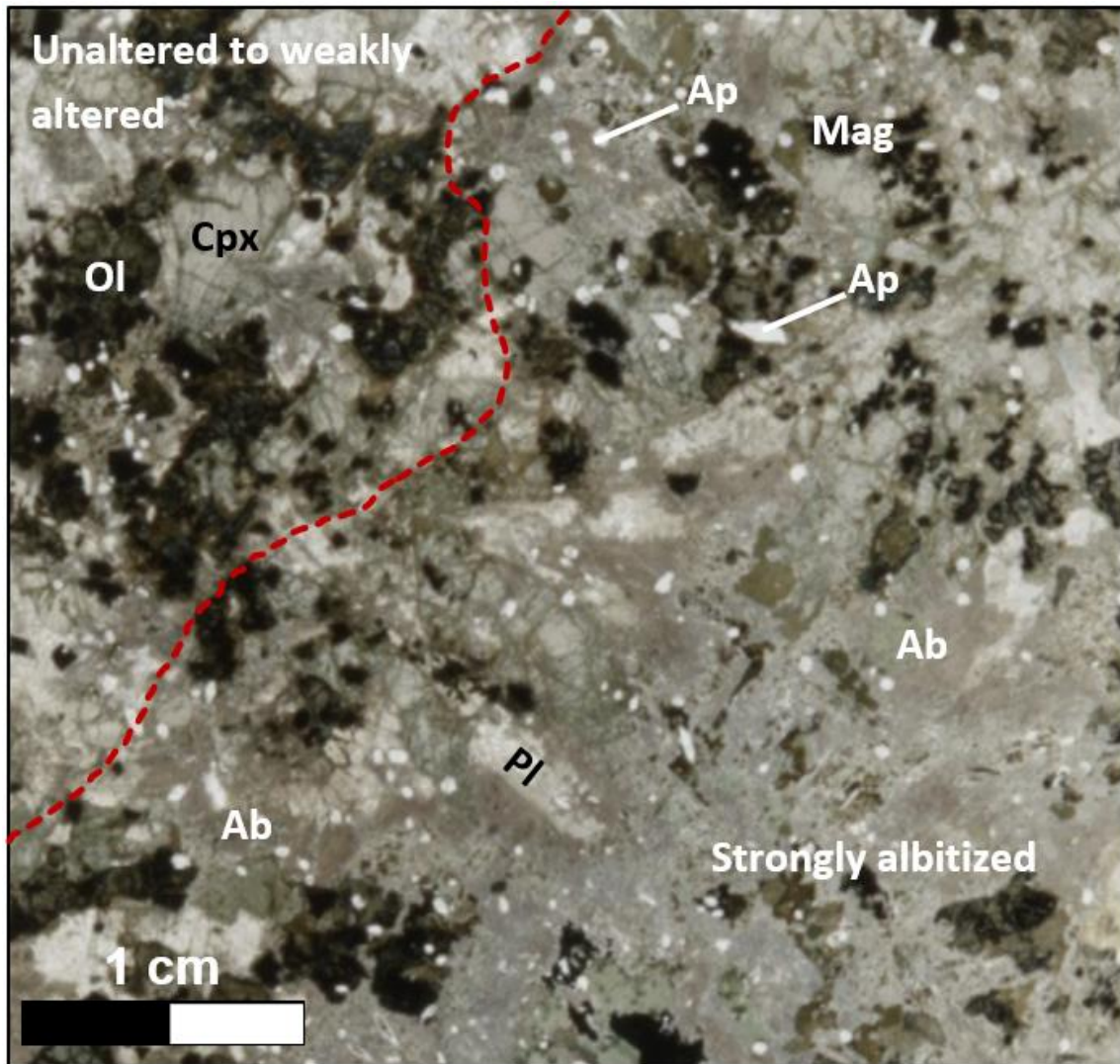


Figure 4.11 – Albite alteration within homogeneous troctolite. In the top left corner of the image, albitation is relatively low. Olivine, clinopyroxene, and plagioclase crystals are evident. In the lower right corner of the image, albitation is fairly intense and envelops olivine grains, as well as completely replacing plagioclase. Fine grained, euhedral apatite is common within these regions of intense albitation.

4.2 Mineralized Lithologies at the GLD

The mineralized lithologies at the GLD host all of the economic concentrations of Cu and PGE mineralization primarily in the form chalcopyrite and bornite. Cu mineralization may also be hosted by covellite, chalcocite, or digenite.

4.2.1 Heterogeneous Gabbro (Unit 3a)

A summary of the mineralogies that comprise the heterogeneous gabbro is shown in Table 4.4. Heterogeneity within this gabbro is not a result of primary magmatic features; rather, the heterogeneity that is observed is the product of albite-actinolite alteration. Plagioclase laths vary in size from medium-grained (~0.5 mm) subhedral laths with albite rims to very coarse-grained (up to 2 cm) subhedral laths with albite rims near the edges of albite pods. Figure 4.12 shows the general texture of the heterogeneous gabbro in plane polarized light. Ophitic textures dominate portions of unaltered heterogeneous gabbro. Where present, olivine varies from medium-grained subhedral grains to very coarse-grained (up to 1 cm) subhedral grains proximal to albite pods. Good (1994) first noted that olivine adjacent to albite pods is zoned. Very coarse to medium-grained skeletal olivine occurs sporadically within this unit. Medium to fine-grained skeletal to stubby magnetite is also locally present, and commonly associated with skeletal olivine. Anhedral clinopyroxene is subophitic to ophitic and is interstitial to olivine and plagioclase. Fine-grained subhedral to euhedral apatite is most abundant within albite-rich alteration zones (as seen in Figure 4.12), but may occur as inclusions within clinopyroxene.

4.2.1.1 Alteration

Using the term ‘heterogeneous’ as a descriptor for this gabbro was done in order to distinguish the lithology based on variable amounts of local alteration throughout the stratigraphy. The amount of alteration present within the heterogeneous gabbro is variable, sporadic, and typically patchy. The modal proportion of alteration does not vary significantly between samples used in this study. Alteration is noted by a variety of secondary minerals including (in decreasing modal abundances): albite, actinolite, biotite, chlorite, magnetite, serpentine, and epidote. The degree of albite alteration ranges from a weak albitization of plagioclase (on the upper right side of Figure 4.13a and b) to pervasive, randomly distributed medium-grained, granular albite pods and dikelets that are as small as 2 cm but up to 30 cm wide. Albite alteration has a very characteristic pink to orange, “dirty”, mottled texture (seen on the left side of Figure 4.13a and b, and in Figure 4.13c and d). Zones of strong albite alteration are invariably associated with fine-

Heterogeneous gabbro (Unit 3a)							
Magmatic Minerals							
Mineral	Plagioclase	Clinopyroxene	Olivine	Magnetite	Apatite		
Modal %	19-30%	22-35%	2-10%	3-6%	2-7%		
Shape	Euhedral to anhedral	Anhedral	Anhedral	Subhedral	Euhedral		
Grain size	2 – 5 mm	1 – 12 mm	1 – 5 mm	<1 – 3 mm	<1 mm		
Comments	Plagioclase, when unaltered, consists of laths with variable aspect ratios (3 to 8). Form ophitic textures with clinopyroxene	Unzoned, and poikilitically enclose plagioclase, magnetite and apatite.	Typically occur as strongly altered clusters, appear to have faint skeletal textures	Occurs as equant, and less commonly skeletal grains	Fine grained and randomly dispersed through the lithology, though more common in the most albitized zones		
Hydrothermal Minerals							
Mineral	Albite	Actinolite	Biotite	Chlorite	Epidote	Magnetite	Serpentine
Modal %	16-28%	5-15%	3-9%	5-8%	trace-1%	1-5%	trace-1%
Shape	Anhedral, cloud-like pods	Bladed	Anhedral	Anhedral, radial masses	Anhedral	Anhedral, disseminated	Anhedral, dusty
Grain size	<1 – 4 mm, mainly as fine grained aggregates	<1 mm – 4 mm	<1 mm – 2 mm	<1 mm – 2 mm	<1 mm	<1 mm	<1 mm
Comments	Cloudy aggregates that fully replace plagioclase, and envelop proximal mineralogy, sometimes leaving relict ophitic textures	Commonly present proximal to chalcopyrite blebs	Occurs as brown replacement of magnetite and olivine rims	Radial clusters that are commonly pseudomorphic after clinopyroxene and olivine	Very fine grained replacement product of clinopyroxene	Occur as disseminations within strongly altered regions that contain magmatic magnetite, also fill fractures of skeletal olivine	Rarely occurs as alteration mineral of plagioclase
Sulfide Minerals							
Mineral	Chalcopyrite	Bornite	Pyrrhotite	Pyrite	Digenite	Galena	Millerite
Modal %	1%	0.5%	<0.5%	trace	trace	trace	trace
Shape	Anhedral, blebby to disseminated	Exsolution lamellae	Anhedral, disseminated	Anhedral	Exsolution lamellae	Equant inclusions	Bladed, lath-like
Grain size	<1 – 10 mm	<1 – 6 mm	<1 – 4 mm	<1 mm	<1 mm	<1 mm	<1 mm
Comments	Blebby to disseminated aggregates cluster within pods of actinolite, common within the altered regions	Present as exsolution within Ccp, typically host PGE	Present with Ccp as disseminated aggregates, rarely blebby	Hosted by pyrrhotite and Ccp, commonly cross-cuts both Ccp and Po	Occurs within bornite	Occurs as inclusions, or adjacent to Ccp and Bn	Has a bladed habit, occurs within Bn grains

Table 4.4 – Average mineral abundances based on visual estimations for heterogeneous gabbro (Unit 3a)

grained, sporadically disseminated apatite (up to 10% as inclusions within albite) (also seen in Figure 4.13c and d). Actinolite, biotite and chlorite alteration is also localized and often associated with albite alteration. Clinopyroxene is commonly pseudomorphed by actinolite, chlorite, and biotite alteration. Figure 4.14a and (b) shows actinolite alteration of clinopyroxene within the cleavage planes and fractures, with albite alteration after plagioclase in the bottom left corner. However, actinolite and chlorite alteration is most abundant in the presence of chalcopyrite (Figure 4.14c and d). Greenish-brown biotite alteration is commonly associated with actinolite and chlorite alteration. Olivine, where present, may be weakly to strongly altered to a very fine-grained (<0.1 mm) assemblage of serpentine, actinolite and magnetite.

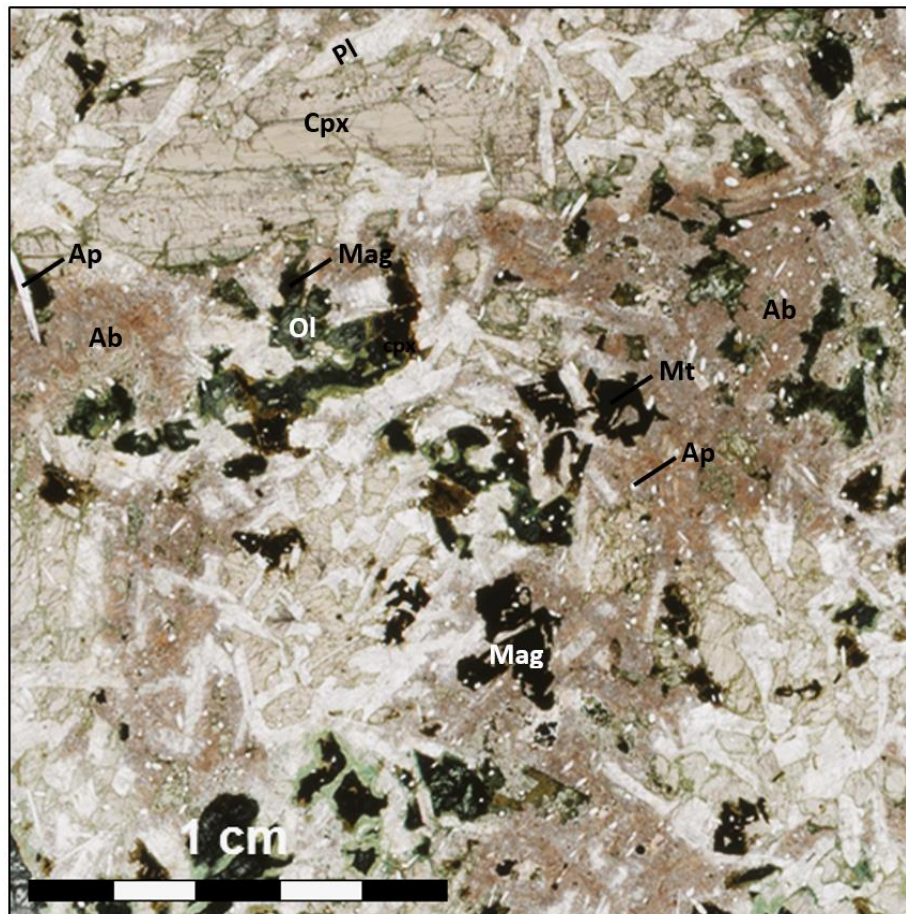


Figure 4.12 – General texture of heterogeneous gabbro. In plane polarized light

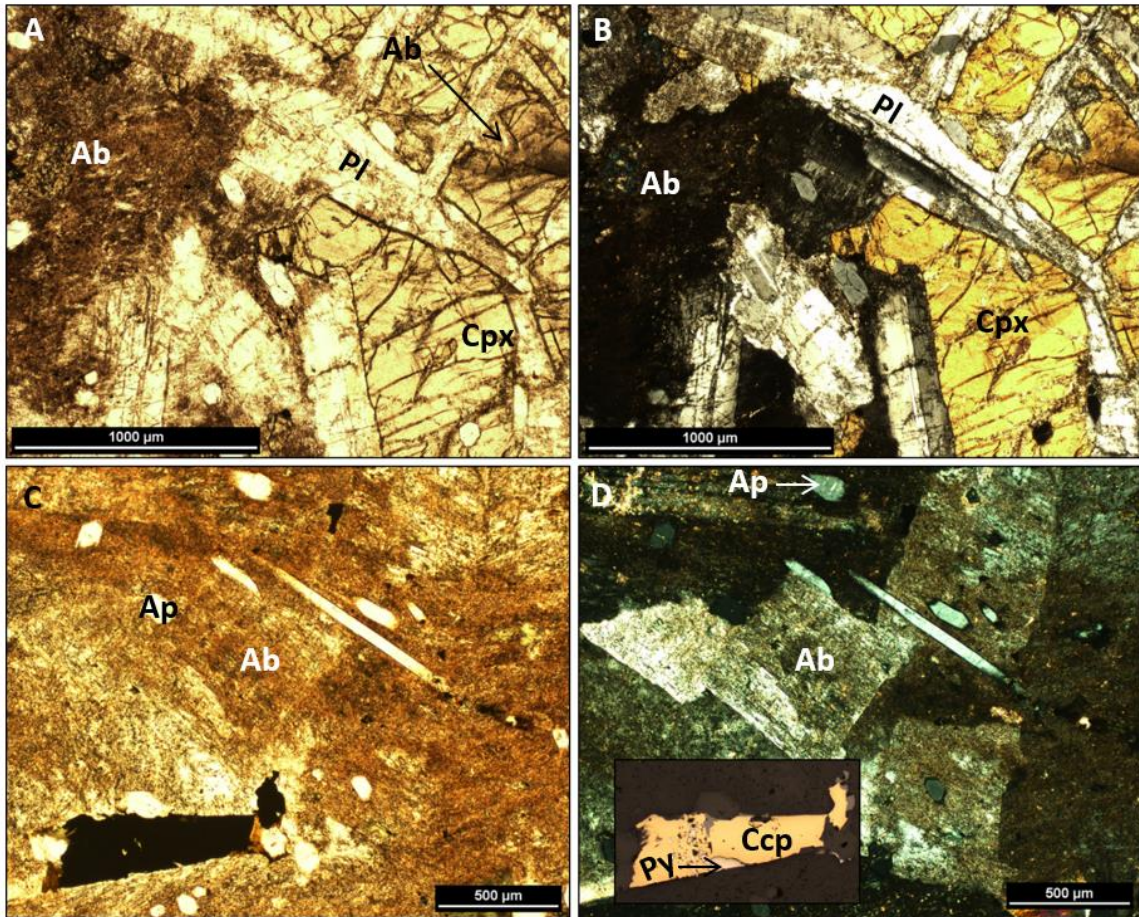


Figure 4.13 – **A**) A PPL image showing a thin section that has fresh gabbro on the right side of the image and strong albitization on the left side of the image. **B**) The same image as in (A), but in XPL. This demonstrates the patchy nature of albitization. **C**) A local zone of strong albitization within a heterogeneous gabbro sample. Reddish-brown albite with apatite inclusions dominate in this PPL image. An opaque mineral is seen in the bottom left portion of the image, **D**) The same image in XPL with an inset in the bottom left corner that is shown in reflected light. Albite grains are more prominent in this image. The reflected light inset shows that the opaque mineral is mainly chalcopyrite with minor pyrite. The chalcopyrite-pyrite grain is bounded by mostly albite, with minor biotite and apatite.

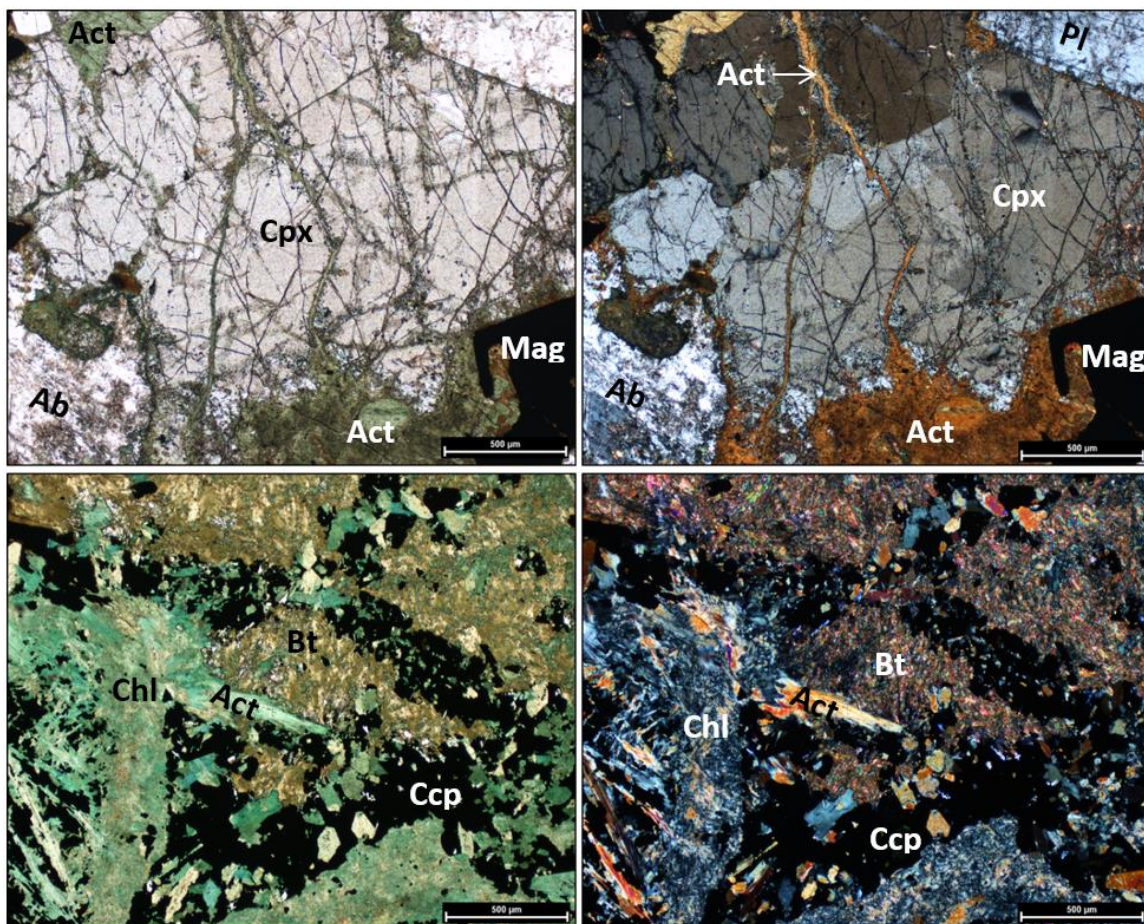


Figure 4.14 – **A**) A predominantly fresh clinopyroxene grain exhibiting actinolite alteration within fractures and cleavage planes (in PPL), **B**) The same image in (A) but in XPL, **C**) Green actinolite alteration, in addition to fine grained greenish-brown biotite is intergrown with an opaque mineral (chalcopyrite). Image is in PPL, **D**) The same image as in (C) but in XPL

4.2.1.2 Sulfide Mineralization

Sulfide mineralization within heterogeneous gabbro is manifested primarily as blebs or disseminations of chalcopyrite, bornite, or pyrrhotite with minor pyrite. Within the heterogeneous gabbro, there are two distinct assemblages of sulfide mineralization. Higher in the Geordie Lake stratigraphy (refer to Figure 2.19 in Chapter 2 for a cross section of the Geordie Lake deposit), within the horizon of heterogeneous gabbro that occurs up to 40 m beneath homogeneous gabbro and adjacent to skeletal troctolite is a portion of mineralization that was historically termed the “Upper Zone mineralization” (Drennan and Fell, 2010). A very characteristic trait of Upper Zone mineralization in heterogeneous gabbro is the ubiquitous association of actinolite (and invariably, albite) to

sulfide mineralization. Actinolite pods such as the one shown in Figure 4.15 contain variable amounts of calcite that is also interstitial to actinolite laths. Figure 4.16 (a) and (b) show the spatial association of pyrrhotite, chalcopyrite and pyrite to secondary actinolite with minor biotite and chlorite, while Figure 4.16 (c) and (d) shows the spatial association of a single chalcopyrite grain with actinolite alteration. Chalcopyrite is the most common sulfide within Upper Zone mineralized heterogeneous gabbro. Pyrrhotite is the next most abundant sulfide mineral, followed by pyrite, pentlandite, millerite, sphalerite, and galena. Figure 4.17 shows the various different textures and assemblages of chalcopyrite, pyrrhotite, pyrite, and pentlandite and sphalerite. Figure 4.17 (a) shows a chalcopyrite grain with pyrrhotite lamellae, and pyrite inclusions. The sphalerite grain near the top of the image has irregular grain boundaries, and is hosted by the chalcopyrite grain. Figure 4.17 (b) shows a large chalcopyrite grain in contact with a large pyrrhotite grain. Sphalerite is again hosted by chalcopyrite. Pyrite grains are at the margins of chalcopyrite (to the far right of the image). In Figure 4.17 (c), a large apatite grain is thinly rimmed by pyrite and surrounded by pyrrhotite on the left, and pyrite+chalcopyrite on the right. In Figure 4.17 (d), grains of pentlandite, millerite, and pyrite are hosted within a larger grain of pyrrhotite. Within Upper Zone mineralization, there is a notable absence of bornite.

Lower in the Geordie Lake stratigraphy, adjacent to the basal syenite contact is a zone of mineralization that has been referred to as the “Main Zone mineralization” (Drennan and Fell, 2010). The Main Zone mineralization is a thick, continuous, tabular body of primarily disseminated to blebby chalcopyrite and bornite mineralization. This Main Zone of mineralization is hosted by two lithologies: heterogeneous gabbro, and skeletal troctolite. Only mineralization within the heterogeneous gabbro will be described in this sub-section. Figure 4.18 (a) and (b) shows a bleb of chalcopyrite with minor bornite occurring within a small pod of actinolite. Main Zone mineralization within heterogeneous gabbro contains bornite, whereas Upper Zone mineralization does not. Pyrrhotite is not observed within the Main Zone mineralization horizon.

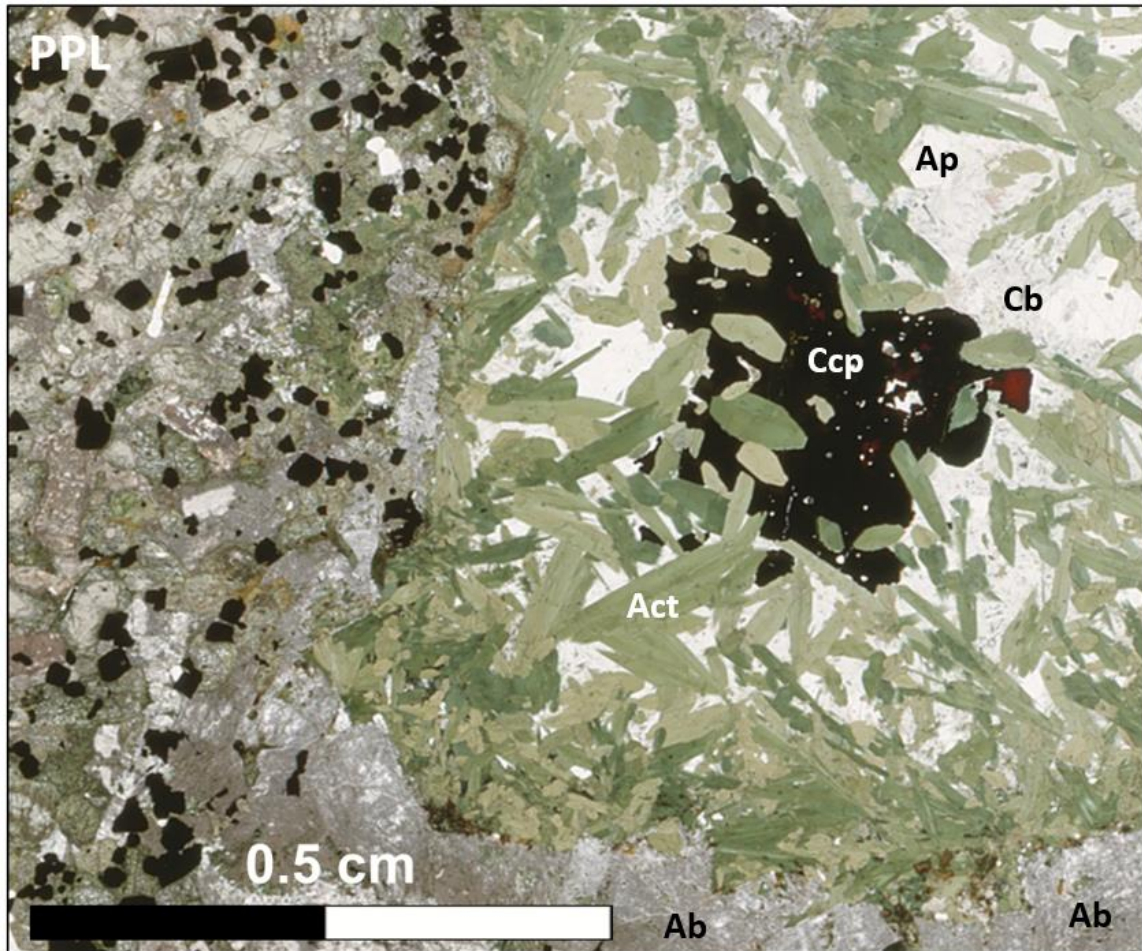


Figure 4.15 – Chalcopyrite mineralization occurring interstitial to actinolite laths. Chalcopyrite is enveloped by actinolite laths, as well as calcite and apatite.

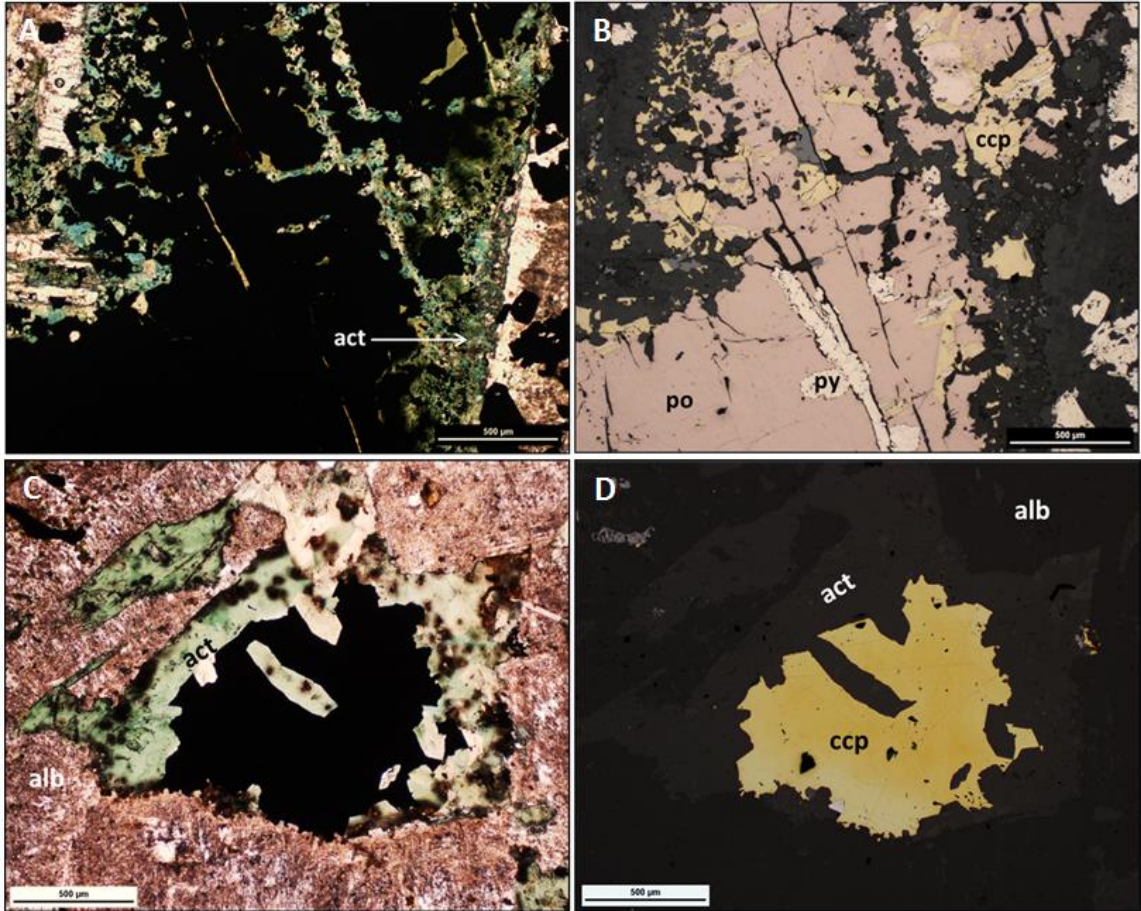


Figure 4.16 – **A**) Sulfide (opaque) mineralization that is spatially associated with mainly actinolite, and lesser chlorite alteration, in PPL, **B**) The same image as in (A) shows that the opaque sulfide is mainly pyrrhotite with disseminated chalcopyrite, and secondary pyrite that replaces pyrrhotite primarily at the margins of pyrrhotite and actinolite, in reflected light, **C**) Sulfide (opaque) mineralization that is occurring interstitial to actinolite, in PPL, **D**) The same image as in (C), but showing that the opaque sulfide is chalcopyrite with wormy, myrmekitic-textured bornite intergrowth, in reflected light

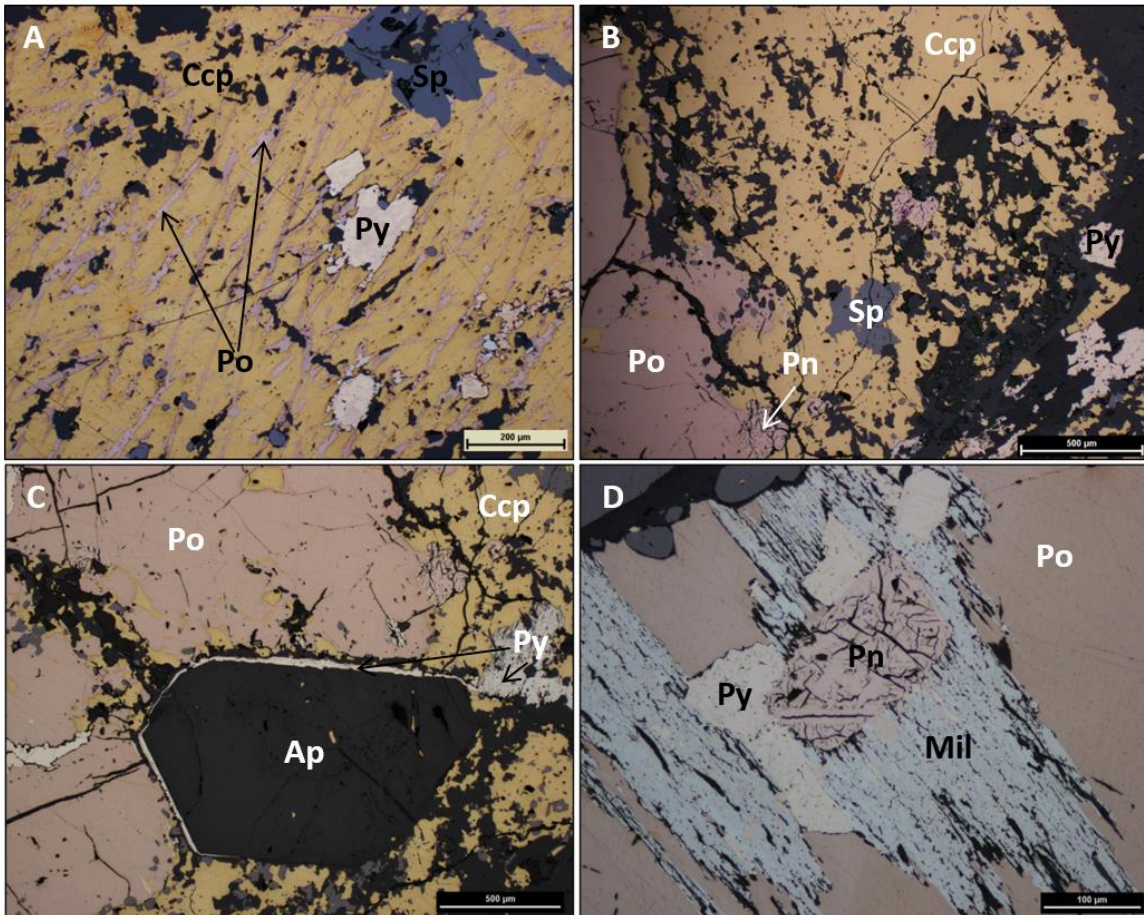


Figure 4.17 – A) Chalcopyrite containing lamellae of pyrrhotite, and inclusions of pyrite. Pyrite is commonly associated with secondary silicate minerals, commonly actinolite, B) Chalcopyrite grain with abundant inclusions of gangue (actinolite). Bottom left of the image is pyrrhotite, and the bottom right of the image is pyrite, C) Pyrrhotite grain on the left side of the image, and chalcopyrite on the right side. A large apatite crystal is at the center of the image, and around it is a thin rim of pyrite, D) Inclusions of pentlandite, millerite, and pyrite are hosted by a pyrrhotite grain.

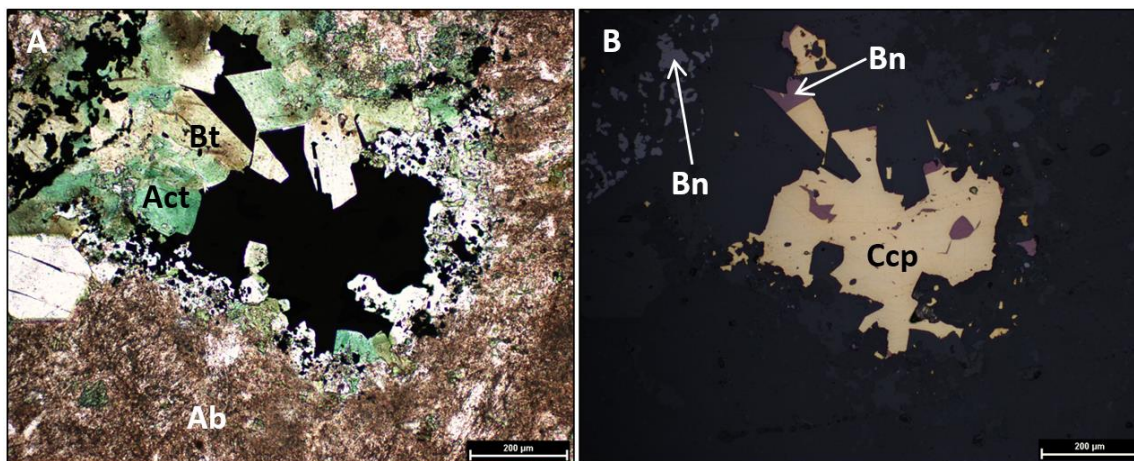


Figure 4.18 – A) An opaque mineral is completely enveloped by actinolite, and biotite. The bright white mineral surrounding the opaque mineral is also actinolite; however they are oriented perpendicular to the C-axis and appear to be colourless. This mineral assemblage is further enveloped by albite alteration. B) The opaque mineral is predominantly chalcopyrite with minor bornite occurring interstitial to actinolite laths.

4.2.1.3 PGE Mineralization

PGE mineralization within the heterogeneous gabbro is hosted primarily by blebs of chalcopyrite and bornite intergrowths. These sulfide blebs are also associated with blebby to pods of actinolite. The only PGM found within heterogeneous gabbro during the course of this study are palladium arsenides, and palladium antimonides. These PGM occur either exclusively within chalcopyrite or bornite blebs or at the margins of sulfide and secondary silicate minerals. PGM were not found within silicate minerals.

4.2.2 Skeletal Troctolite (Unit 3b)

The skeletal augite troctolite is distinguished primarily by the abundance of skeletal olivine and accessory skeletal magnetite. A summary of skeletal troctolite is shown in Table 4.5. The skeletal olivine grains are typically coarse-grained (~1cm) dendritic olivines hosted in a matrix of medium to coarse-grained plagioclase. These skeletal olivine grains may reach up to 5 cm in length, and approximately 2 cm in width. Figure 4.19 shows an example of a long, continuous dendritic olivine grain. Locally, the sizes of skeletal olivine grains do not vary significantly as most olivine grains are fairly uniform with only a maximum of ~20 % variation in absolute size within each thin section. These skeletal olivine grains were first described by Mulja (1989; 1991) and analyses showed

them to be slightly fayalitic (Fo_{44-49}) and unzoned. Plagioclase laths range in size from <1 mm, to 6 mm, though this size range ultimately depends on the size of the olivine grains they are interstitial to. The aspect ratio of these plagioclase grains is relatively low (between 2 to 4). Where present, clinopyroxene is anhedral and coarse-grained, and may enclose plagioclase laths in an ophitic texture. Skeletal magnetite grains are primarily fine-grained, however may reach lengths of 5 mm. One particular thin section exhibits a very prominent bimodal variation in grain size (Figure 4.20) where grains of apatite, chalcopyrite and bornite (opaque), magnetite (opaque), albite altered plagioclase laths, reddish-brown pleochroic biotite, and serpentized skeletal olivine grains are all between 1-8 mm and are surrounded by fine-grained (<2 mm) plagioclase and olivine.

4.2.2.1 Alteration

Alteration within skeletal troctolite is primarily manifested as secondary actinolite and chlorite, which both occur as fine-grained, acicular crystals that mantle olivine, magnetite, and clinopyroxene. The degree of actinolite and chlorite alteration is sporadic between samples, and there is no corresponding increase or decrease in the magnitude of alteration with changing depth through the Geordie Lake stratigraphy. Figure 4.21 illustrates the difference between a relatively fresh sample of skeletal troctolite, and an altered sample. Clusters of fine-grained, secondary green biotite are commonly intergrown with actinolite and chlorite in zones where such alteration is strong. Samples of rubbly skeletal troctolite that are proximal to small-scale faults contain significantly more chlorite, with slightly less actinolite alteration. In regions where actinolite and chlorite alteration are prevalent, olivine is strongly serpentized, and plagioclase is strongly sericitized. Brown, anhedral biotite is also common as reaction coronas around magnetite crystals, and serpentized olivine. Secondary, fine-grained magnetite typically occurs around the irregular fractures of skeletal olivine grains (Figure 4.21d). Figure 4.22 (a) shows the location of an olivine grain in thin section (in a red dashed square, top right of image) and Figure 4.22 (b) shows a backscatter electron (BSE) image indicating an inset where Figure 4.22 (c) is zoomed in on a skeletal olivine fracture plane. Olivine fractures are infilled with both magnetite, and silicate gangue. Albite alteration of plagioclase is occurs at a much smaller scale than it does within heterogeneous gabbro.

Average values for skeletal troctolite (Unit 3b)								
Magmatic Minerals								
Mineral	Plagioclase	Olivine	Clino- pyroxene	Apatite	Biotite	Horn- blende	Magnetite	
Modal %	12-22%	18-32%	9-17%	1-5%	1-3%	Trace-1%	4-9%	
Shape	Subhedral to anhedral	Skeletal, dendritic, harrisitic	Anhedral	Euhedral	Subhedral	Subhedral	Skeletal, to stubby, equant grains	
Grain size	1 – 5 mm	3 mm – 5 cm	1 – 6 mm	<1 – 2 mm	<1 – 4 mm	1 – 3 mm	1 – 6 mm	
Comments	Less than 1 – 4 mm in width	Crystals up to 5 cm in length, set within a granular matrix of plagioclase	Coarse grained and poikilically enclose plagioclase and rarely olivine	Crystals that are randomly dispersed through the lithology	Brown, exhibit high relief and occur near clinopyroxene	Brown, exhibit high relief and occur near clinopyroxene	Skeletal textured, though stubby, equant grains occur in regions of disseminated magnetite	
Hydrothermal Minerals								
Mineral	Chlorite	Actinolite	Sericite	Epidote	Biotite	Mag- netite	Serpent- ine	Albite
Modal %	1-5%	3-10%	4-8%	Trace-1%	1-5%	3-8%	1-3%	2-6%
Shape	Anhedral	Anhedral	Anhedral	Anhedral	Sub- hedral	Sub- hedral	Anhedral	Anhedral
Grainsize	<1 – 2 mm	<1 – 3 mm	<1 mm	<1 mm	<1 – 2 mm	<1 mm	<1 mm	<1 mm
Comments	Alters rims of skeletal olivine, clinopyroxene	Pseudomorphic after clinopyroxene where present	Alters plagioclase that occurs within interstitial to serpentinized olivine	Occurs within zones of strong actinolite, biotite and chlorite alteration	Manifested as coronas around olivine and magnetite	Lack ilmenite exsolution lamellae	Alters skeletal olivine grains, and is within larger zones of alteration	Altered plagioclase, associated with actinolite
Sulfide Minerals								
Mineral	Chalcopyrite	Bornite	Covellite	Digenite	Galena	Millerite	Pent- landite	
Modal %	1-3%	1%	Trace	Trace	Trace	Trace	Trace	
Shape	Anhedral	Wormy intergrowths	Anhedral	Anhedral, wormy	Anhedral	Lath-like, anhedral	Anhedral	
Grain size	<1 mm – 5 mm	<1 mm – 3 mm	<1 mm	<1 mm	<1 mm	<1 mm	<1 mm	
Comments	Interstitial to plagioclase laths, or occurs in actinolite-chlorite-biotite assemblages	Exsolution within chalcopyrite	Occurs as exsolution within bornite	Occurs as exsolution within bornite	Inclusions within Ccp and bornite, or at grain boundaries	Commonly occurs within bornite grains	Only observed within bornite grains	

Table 4.5 – Average mineral abundances based on visual estimations for skeletal troctolite (Unit 3b)



Figure 4.19 – General texture of the skeletal troctolite. Plagioclase is interstitial to skeletal olivine grains, but commonly altered to sericite.

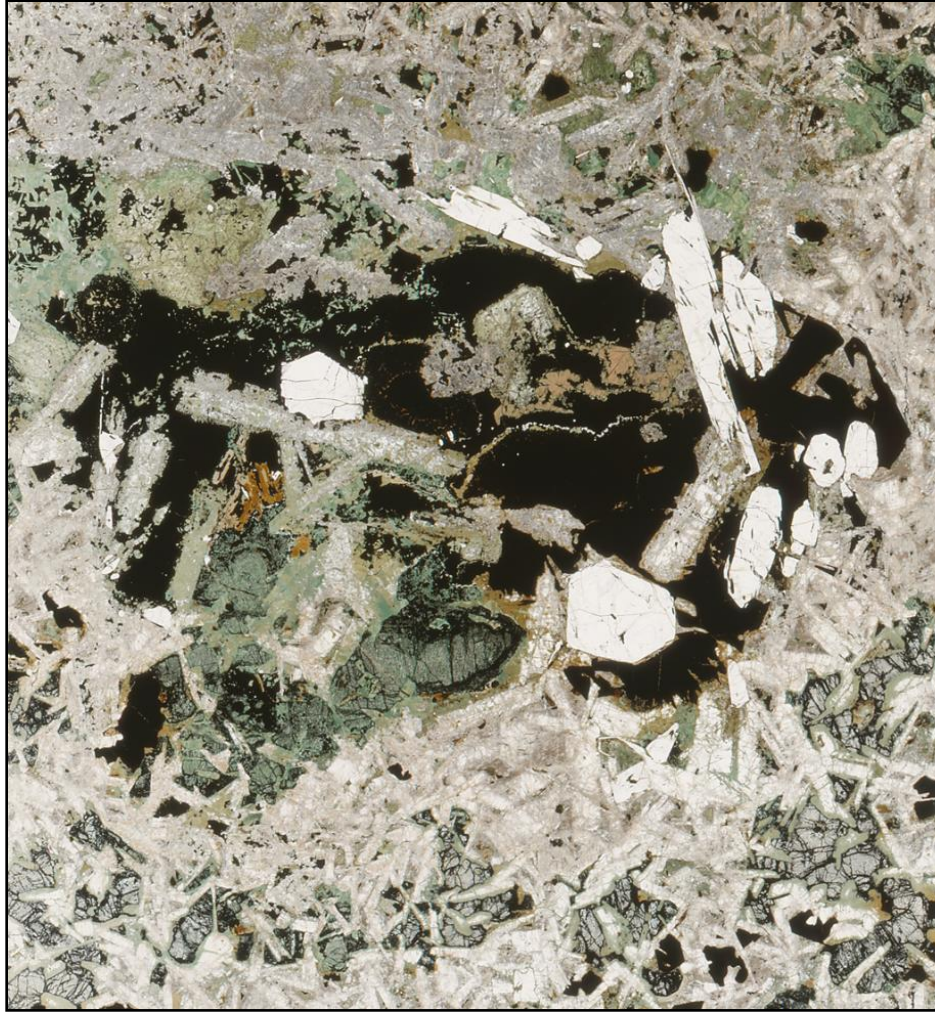


Figure 4.20 – PPL image showing bimodal variation in grain size that may be observed within skeletal troctolite samples.

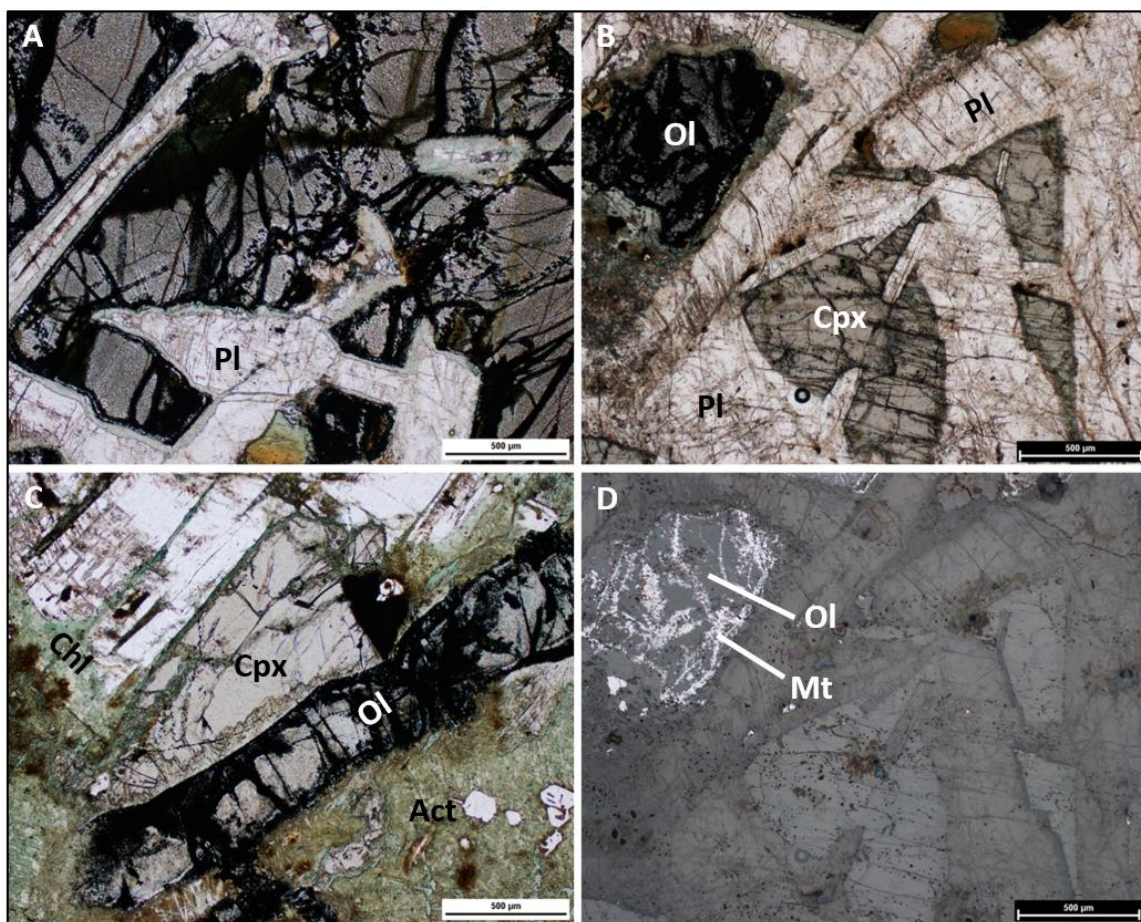


Figure 4.21 – A) Images of the general texture, in PPL, of primarily unaltered (or very weakly altered) skeletal troctolite. Plagioclase laths are enveloped by olivine, however a thin ring of chlorite is visible at the margin of plagioclase and olivine, **B)** Plagioclase and clinopyroxene are the dominant constituents in this image (in PPL). This sample is very weakly altered. Clinopyroxene is interstitial within the triangular interstices of plagioclase, while olivine is present in the top right corner of the image, **C)** Alteration is quite evident in this image (in PPL), with pervasive actinolite alteration of clinopyroxene at the bottom of the image, and chlorite alteration of plagioclase at the center-left side of the image. Plagioclase is weakly to moderately sericitized, **D)** The same image as in (b), however in reflected light. The olivine grain in the top left corner of the image shows that the olivine fractures contain appreciable amounts of secondary magnetite.

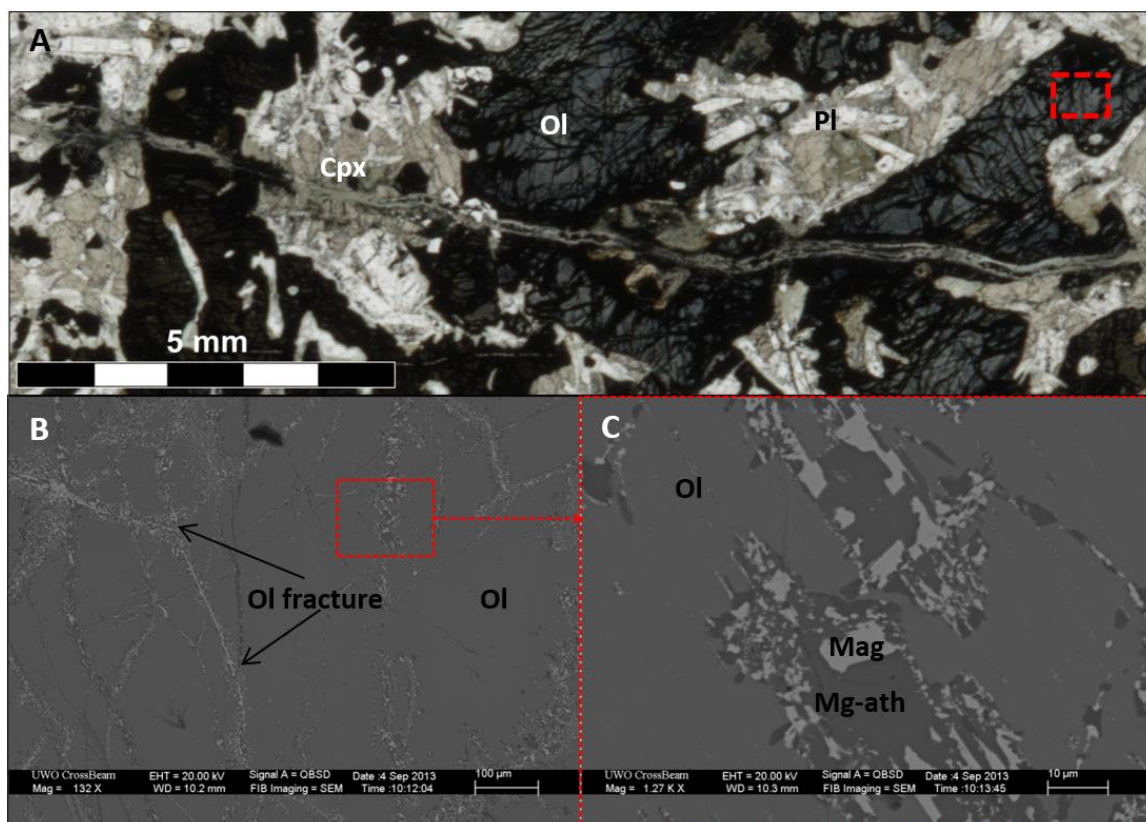


Figure 4.22 – **A**) A PPL image of a skeletal troctolite thin section sample, showing skeletal olivine grains with abundant fractures. A dashed red box highlights the spot that was zoomed in on in **(B)**, **B**) A BSE image which shows what a skeletal olivine grain looks like up close. The fracture planes of the olivine grain are pale and mottled. The spot with the dashed red box is further zoomed in on image **(C)**, **C**) A close up of the fracture plane within a skeletal olivine grain show that it is made up of two predominant minerals: magnetite (mt), and perhaps magnesioanthophyllite (Mg-ath)

4.2.2.2 Sulfide Mineralization

Sulfide mineralization within skeletal troctolite occurs within Upper Zone and Main Zone mineralization horizons. Mineralization within the Upper Zone consists of predominantly chalcopyrite and bornite, and is associated with only minor actinolite and chlorite alteration. Fine-grained horizons of cumulate magnetite are strongly associated with sulfide mineralization in the Upper Zone. Chalcopyrite and bornite is commonly blebby and between 1-9 mm in diameter, but may be disseminated in the presence of strong actinolite alteration. Disseminated chalcopyrite and bornite is strongly associated with disseminated magnetite.

In the Main Zone of mineralization, sulfides that exist within skeletal troctolite are composed of more copper-rich species including chalcocite (Cu_2S), and covellite (CuS). Figure 4.23 (a) shows an image of an angular sulfide mineral in PPL. Figure 4.23 (b) shows that the opaque mineral is chalcopyrite, which occurs within the triangular interstices that are developed by interlocking plagioclase laths. Figure 4.24 (a) shows another opaque mineral, but this time within a region of strong actinolite and albite alteration. Actinolite grains are included in the lower portion of the opaque grain. In Figure 4.24 (b), the uppermost portion of the opaque mineral is magnetite, while the lower portion is composed of chalcopyrite, bornite, and pyrite. Hence, the portion of the opaque with a strong association to actinolite contains the Cu-sulfides. Fractures of skeletal olivine, plagioclase, and clinopyroxene are commonly filled by disseminations of chalcopyrite and secondary magnetite. Figure 4.25 (a) shows a plane-polarized light (PPL) image of a skeletal olivine grain (reddish-brown) with an infilled fracture (middle of image). The red-dashed box is zoomed in on Figure 4.25 (b), which is shown in reflected light. The reflected light image shows the composition of the opaque mineral, which it made up of magnetite at the outer margins, and chalcocite with wormy bornite intergrowth in the middle. Figures 4.25 (c) shows a similar mineralogical assemblage with bornite and chalcocite intergrowth at the top of the image, while the bottom portion is made up of disseminated magnetite with minor disseminated specks of bornite. Figure 4.26 shows the association between primary skeletal magnetite, and chalcopyrite+bornite mineralization. A skeletal magnetite grain with ilmenite exsolution lamellae are in contact with a chalcopyrite bleb which contains bornite exsolution. The chalcopyrite bleb is also associated with small specks of albite, and actinolite. Figure 4.27 shows another skeletal magnetite grain that contains strong ilmenite exsolution lamellae. The skeletal magnetite grain has inclusions of actinolite. These inclusions of actinolite are rimmed by secondary magnetite (which contains no ilmenite exsolution) and chalcopyrite. Figure 4.28 shows another magnetite grain with prominent ilmenite exsolution lamellae. This grain is rimmed by chlorite to an extent, and is completely enclosed by actinolite. Blebs of chalcopyrite replace magnetite, but do not replace ilmenite.

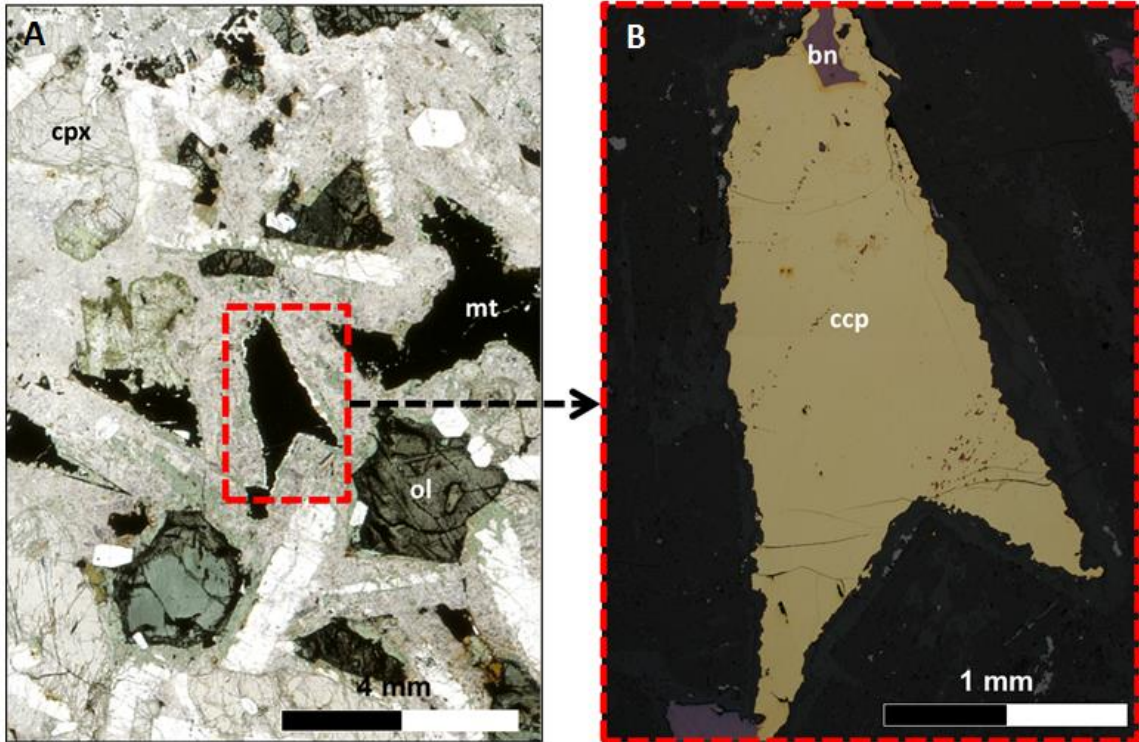


Figure 4.23 – Typical unaltered sulfide mineralization within skeletal troctolite. **A)** An opaque mineral (chalcopyrite), highlighted in the red-dashed square, is completely enveloped by plagioclase forming planar contacts with the slightly albitized edges of the plagioclase laths, in plane polarized light, **B)** Shows the opaque mineral, in reflected light, to be chalcopyrite with bornite inclusions, in reflected light

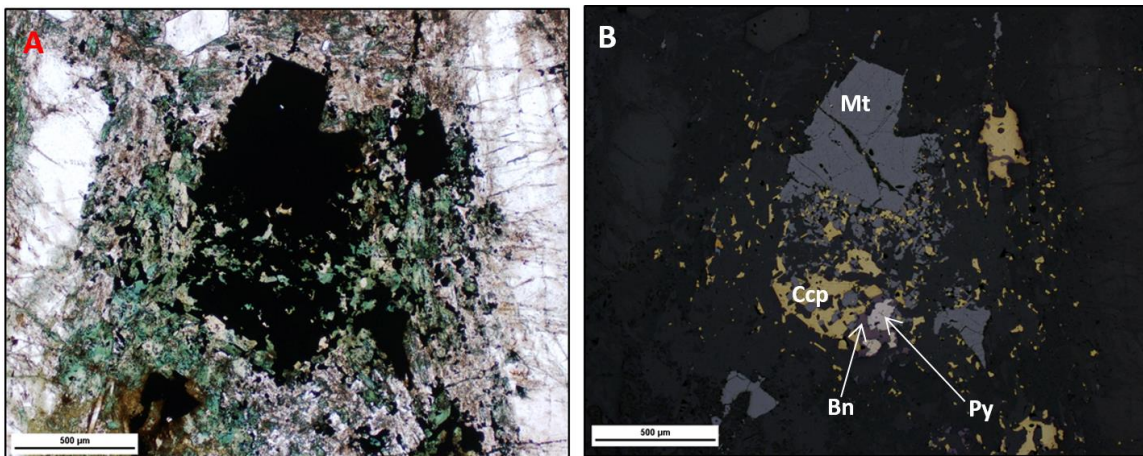


Figure 4.24 – **A)** An opaque mineral is fully enclosed by albite and actinolite. Farther out from the albite and actinolite alteration are plagioclase laths (on either side). The top of the opaque bleb exhibits a rigid, nearly right-angled morphology. **B)** A reflected light image of the opaque bleb show a magmatic magnetite grain (exhibiting ilmenite exsolution lamellae) at the top, while the bottom of the bleb is made up of chalcopyrite, bornite, and pyrite

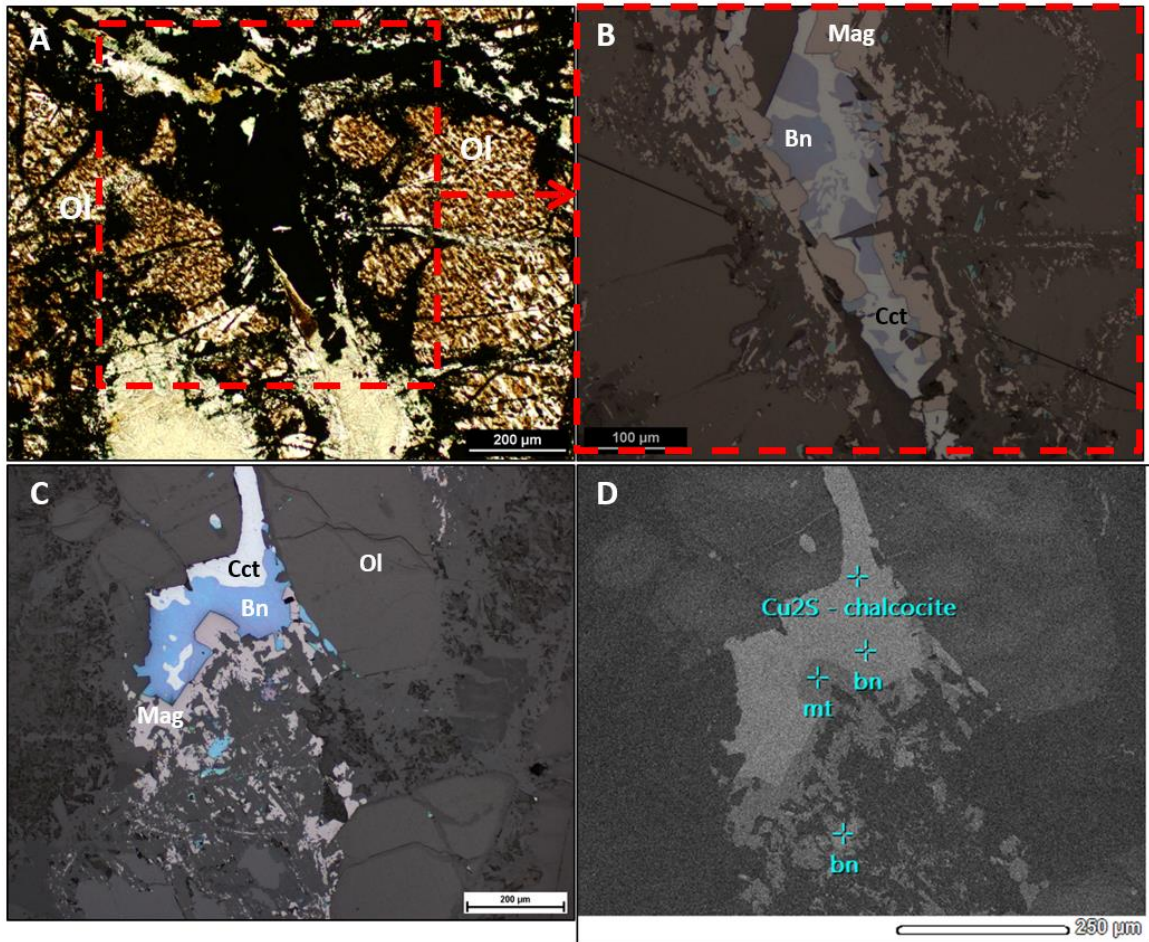


Figure 4.25 – **A**) An opaque mineral occurs at the boundary between olivine grains. **B**) A zoomed in reflected light image of the opaque bleb shows that the bleb is composed of magnetite (on the outer portion), bornite and chalcocite (in the inner portion). **C**) Another sulfide bleb from the same sample shows a similar assemblage of magnetite, bornite and chalcocite occurring at the margin of an olivine grain. **D**) A back-scatter electron image of the same grain shown in (C) with points which indicate the mineral that was identified using energy-dispersive X-ray spectroscopy (EDS)

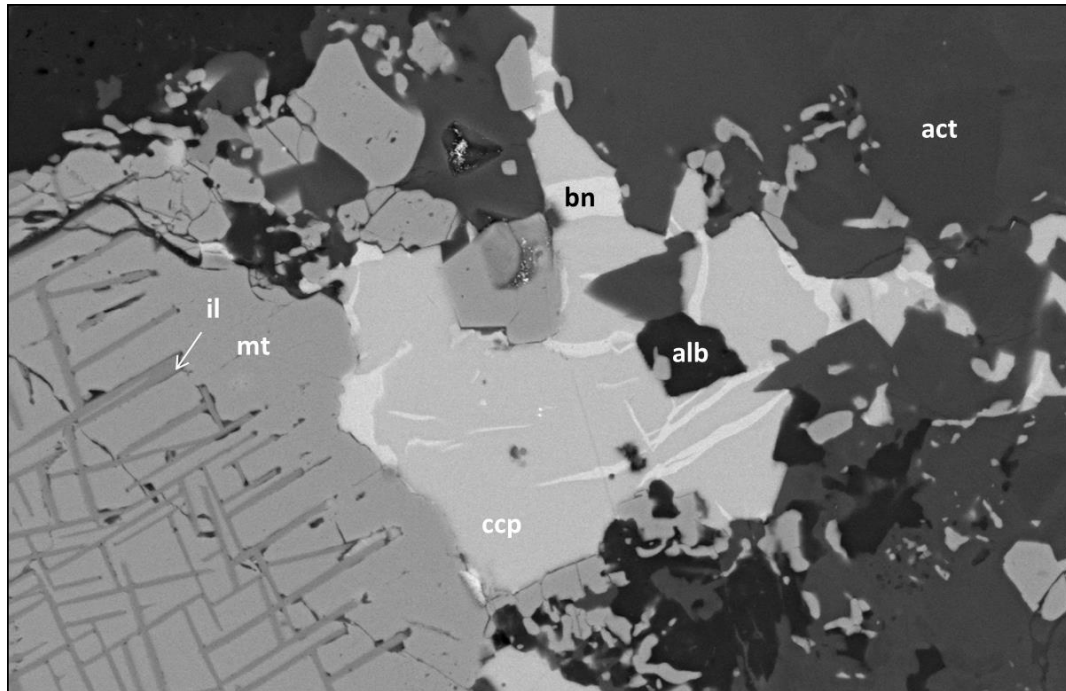


Figure 4.26 – A BSE image of an edge of a skeletal magnetite grain. The magnetite grain contains visible exsolution lamellae of ilmenite. At the margin of the magnetite grain, there is a bleb of chalcopyrite with intergrown bornite.

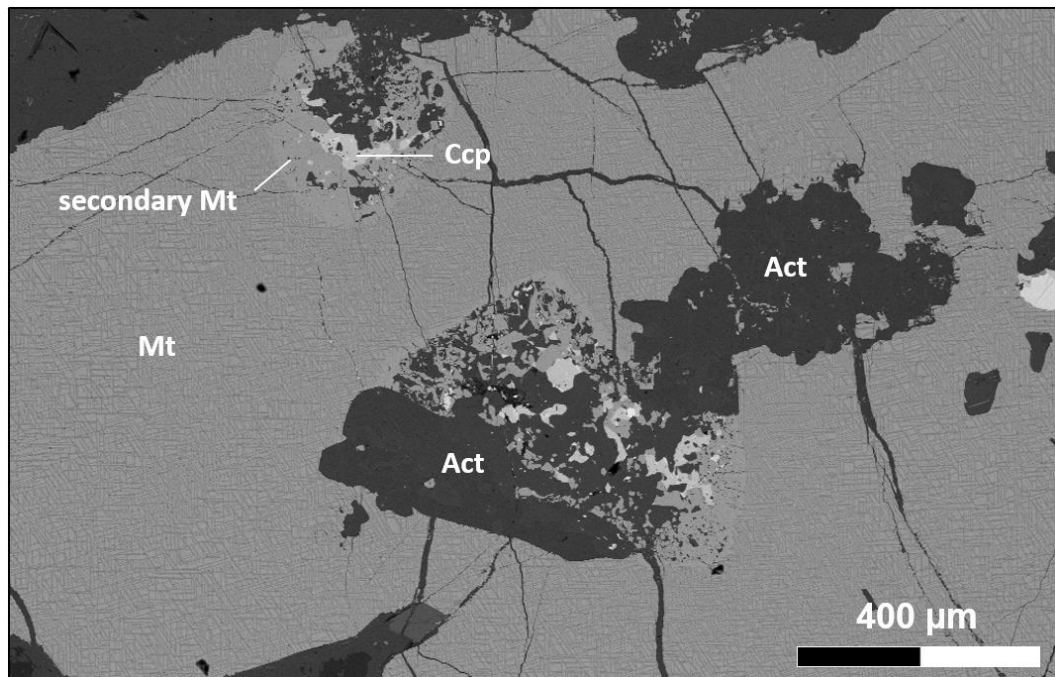


Figure 4.27 – A BSE image of a subhedral magnetite grain containing inclusions of actinolite. The magnetite grain contains visible exsolution lamellae of ilmenite. At the margin of actinolite and the magnetite grain, disseminated chalcopyrite and appears to have formed as a secondary product. This chalcopyrite is intergrown with secondary magnetite that does not contain any ilmenite exsolution lamellae. This is quite evident in the upper left portion of the image, by virtue of a halo of secondary magnetite extending radially from the mixture of actinolite and chalcopyrite.

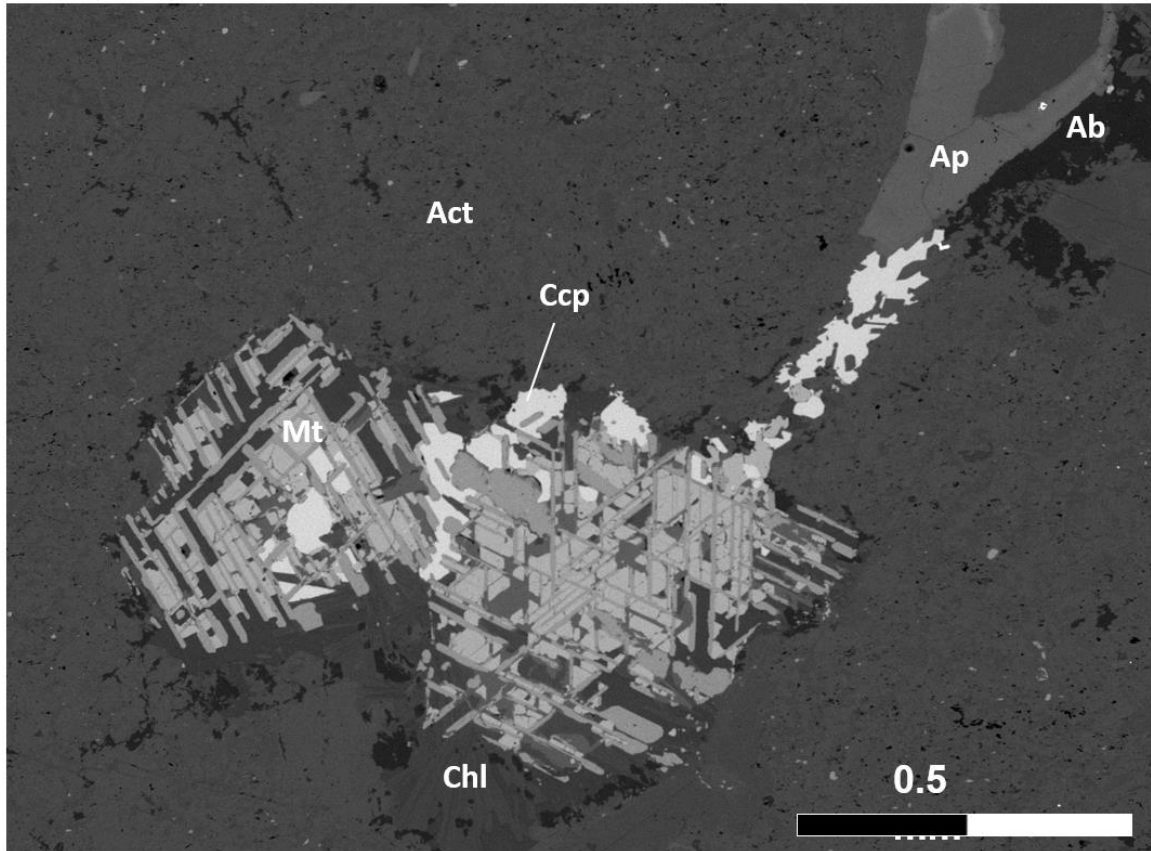


Figure 4.28 – A BSE image of a magmatic magnetite grain with ilmenite exsolution lamellae, enclosed by chlorite, actinolite and epidote. Portions of the magnetite grain that are in contact with these secondary silicate minerals contain small blebs of chalcopyrite, which in some instances, envelop ilmenite exsolution lamellae. This likely indicates that chalcopyrite was a sulfide liquid when it collected around the magnetite crystal, rather than having formed as a secondary alteration product.

4.2.2.3 PGE Mineralization

Platinum group minerals within the skeletal troctolite lithology are dominantly in the form of palladium tellurides, arsenides, and antimonides (as defined by SEM-EDS). The occurrence of PGM is limited to: 1) the grain boundaries between chalcopyrite-bornite hosts and adjacent silicate minerals, and 2) the grain boundaries between chalcopyrite and bornite exsolution, and 3) These PGM tend to be euhedral within chalcopyrite and bornite, but exhibit irregular boundaries with the adjacent silicate minerals.

The PGM found within the skeletal troctolite are dominantly palladium-rich minerals. PGM commonly occur as very small inclusions (<5 μm) hosted primarily by bornite and

chalcopyrite (Figure 4.29). Coarser PGM (~40 μm) occur at the margins of Cu-sulfide grains and secondary silicates including actinolite, sericite and biotite. In the skeletal textured gabbro, PGM are not only unique to chalcopyrite and bornite, but are also hosted within secondary magnetite occurring at the margin of skeletal olivine and heavily sericitized plagioclase. The most common palladium minerals include palladium-arsenides, palladium-tellurides, and less commonly, palladium-antimonides and palladium-bismuthides.

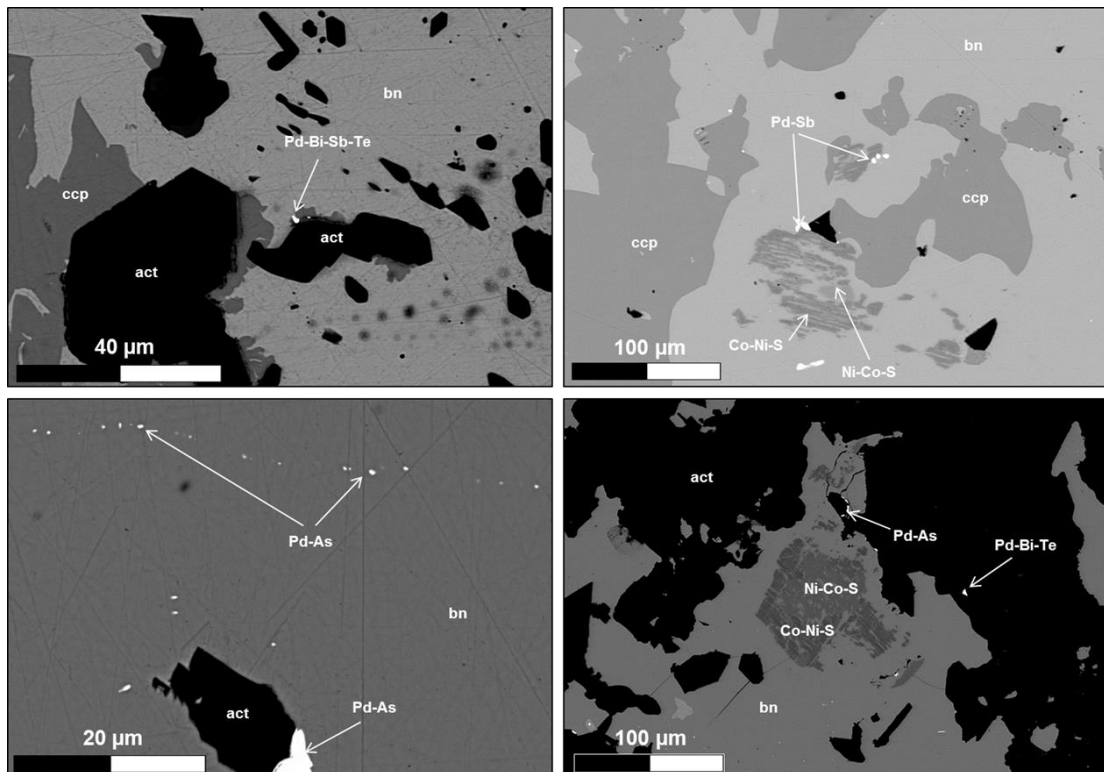


Figure 4.29 – The occurrences of PGM within skeletal troctolite. **A)** A Pd grain is shown at the grain boundary of bornite and actinolite. This Pd+Bi+Sb+Te grain appears to have nucleated particularly well in a crevasse within the sulfide, even protruding into the secondary silicate mineral actinolite, **B)** A few Pd-antimonide grains straddle the margins of bornite and chalcopyrite (middle-top of the image), while another Pd-antimonide grain occurs at the margin of bornite, pentlandite, and actinolite. **C)** A Pd-arsenide looks to have nucleated at the grain boundary of an actinolite inclusion within bornite (bottom of image). In the top portion of the image, a trail of Pd-arsenide inclusions occur in bornite, with an average grain size of <math><1 \mu\text{m}</math>. A Pd-telluride forms within an inlet in a larger bornite grain, and shares grain boundaries with chalcopyrite and actinolite, **D)** A Pd-antimonide grain occurs at the margin of bornite and actinolite (top of image). Slightly to the bottom right of this grain is a Pd-bismuth-telluride that is completely hosted by actinolite, and is not touching a bornite grain.

4.2.3 Basal Fine-Grained Gabbro (Unit 3c)

The basal fine-grained gabbro is the only lithology that occurs solely at the contact of footwall syenite. It consists of stubby plagioclase laths with low aspect ratios, and these plagioclase laths form an ophitic texture with interstitial clinopyroxene which

Average values for basal fine grained gabbro (Unit 3c)						
Magmatic Minerals						
Mineral	Plagioclase	Olivine	Clinopyroxene	Apatite	Biotite	Magnetite
Modal %	28-40%	4-8%	11-17%	2-5%	trace-1%	2-7%
Shape	Subhedral to anhedral	Skeletal, dendritic, harrisitic	Anhedral	Euhedral	Subhedral	Skeletal, to stubby, equant grains
Grain size	1 – 10 mm	1 – 4 mm	1 – 6 mm	<1 – 4 mm	<1 – 2 mm	1 – 4 mm
Comments	Less than 1 – 4 mm in width	Up to 5 cm in length, set within a granular matrix	When present, is coarse grained and poikilitically encloses plagioclase, magnetite and rarely olivine	Fine-grained crystals randomly dispersed through the lithology	Very brown, exhibit well defined boundaries and occur near clinopyroxene	Commonly skeletal textured, though stubby, equant grains occur in regions of fine grained disseminated magnetite
Hydrothermal Minerals						
Mineral	Actinolite	Sericite	Epidote	Biotite	Magnetite	Serpentine
Modal %	2-6%	Trace-1%	Trace-2%	3-5%	2-8%	trace-1%
Shape	Anhedral	Anhedral	Anhedral	Anhedral to subhedral	Subhedral	Anhedral
Grain size	<1 – 2 mm	<1 mm	<1 mm	<1 – 2 mm	<1 mm	<1 mm
Comments	Pseudo-morphic after clinopyroxene where present, also alters skeletal olivine grains	Alters plagioclase that occurs within interstices of serpentinized olivine	Occurs within zones of strong actinolite, biotite and chlorite alteration	Typically manifested as subsolidus coronas around olivine and magnetite	Lack ilmenite exsolution lamellae	Alters skeletal olivine, is commonly associated with larger zones of alteration
Sulfide Minerals						
Mineral	Chalcopyrite	Bornite	Covellite	Digenite	Galena	Millerite
Modal %	1-4%	1%	Trace	Trace	Trace	Trace
Shape	Anhedral	Wormy intergrowths	Anhedral	Anhedral, wormy	Anhedral	Lath-like, anhedral
Grain size	<1 mm – 5 mm	<1 mm – 3 mm	<1 mm	<1 mm	<1 mm	<1 mm
Comments	Interstitial to plagioclase laths, or occurs within actinolite-chlorite-biotite assemblages	Exsolution within chalcopyrite	Occurs as exsolution within bornite	Occurs as exsolution within bornite	Commonly as inclusions within chalcopyrite and bornite, or at grain boundaries	Commonly occurs within bornite grains

Table 4.6 – Average mineral abundances for basal fine grained gabbro (Unit 3c)

poikilitically encloses plagioclase. Clinopyroxene is commonly fresh, unzoned, and significantly more abundant than in the skeletal troctolite (Table 4.6). Figure 4.30 shows the general texture of the basal fine-grained gabbro in PPL. Sulfide grains including chalcopyrite and bornite tend to have strongly defined, planar contacts with plagioclase, olivine, and clinopyroxene. Alteration within the basal fine-grained gabbro is typically weak, except near the syenite.

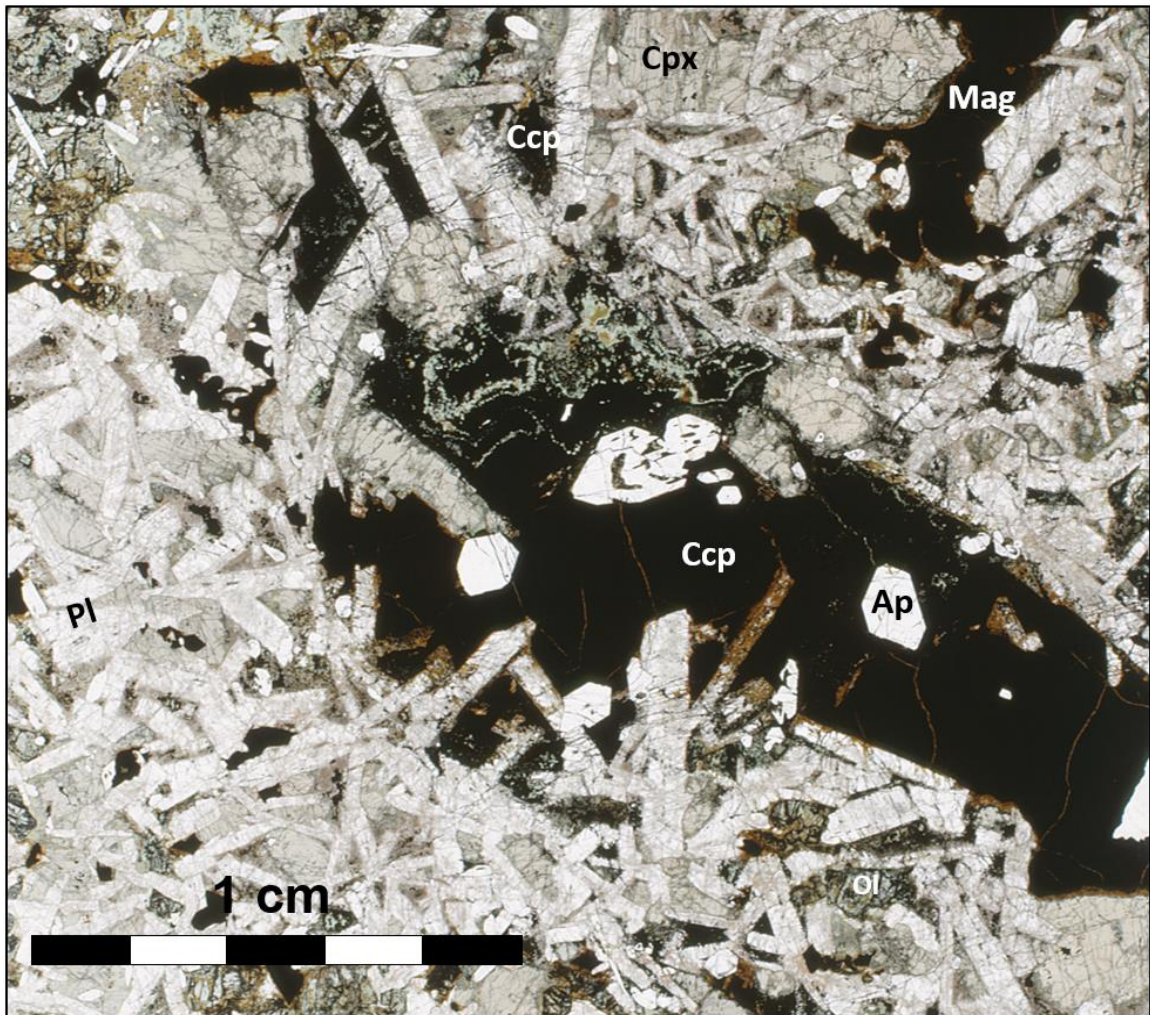


Figure 4.30 – General texture of the basal fine grained gabbro. Mineral abbreviations: Ccp – chalcopyrite, plag – plagioclase, act – actinolite, Cpx – clinopyroxene. In plane polarized light

4.2.3.1 Alteration

Albite alteration is not nearly as common within the basal fine-grained gabbro as it is within the heterogeneous gabbro, though within some zones near syenite, albite alteration is relatively intense. The other alteration minerals within the basal fine-grained gabbro

are actinolite, biotite, epidote, which alter margins of clinopyroxene and olivine grains, and sericite which alters plagioclase grains. Serpentine rarely alters stubby olivine crystals.

4.2.3.2 Mineralization

Mineralization within the basal fine-grained gabbro consists mainly of blebby, interstitial chalcopyrite and bornite (Figure 4.31). One notable feature of mineralization within the basal fine-grained gabbro is the lack of, or the scarcity of actinolite, chlorite or biotite proximal to chalcopyrite and bornite relative to all other lithologies. Sulfide mineralization typically occurs within the interstices of plagioclase laths. Bornite occurs as exsolution within chalcopyrite. Figure 4.32 shows a BSE image of a plagioclase lath (top right of the image) with a rim of chalcopyrite to the bottom left of it. The rim of chalcopyrite contains many inclusions of disseminated magnetite. As you continue to move to the bottom left of the image, there is a solid rim of magnetite. Hence, it appears as though chalcopyrite has been replaced by magnetite.

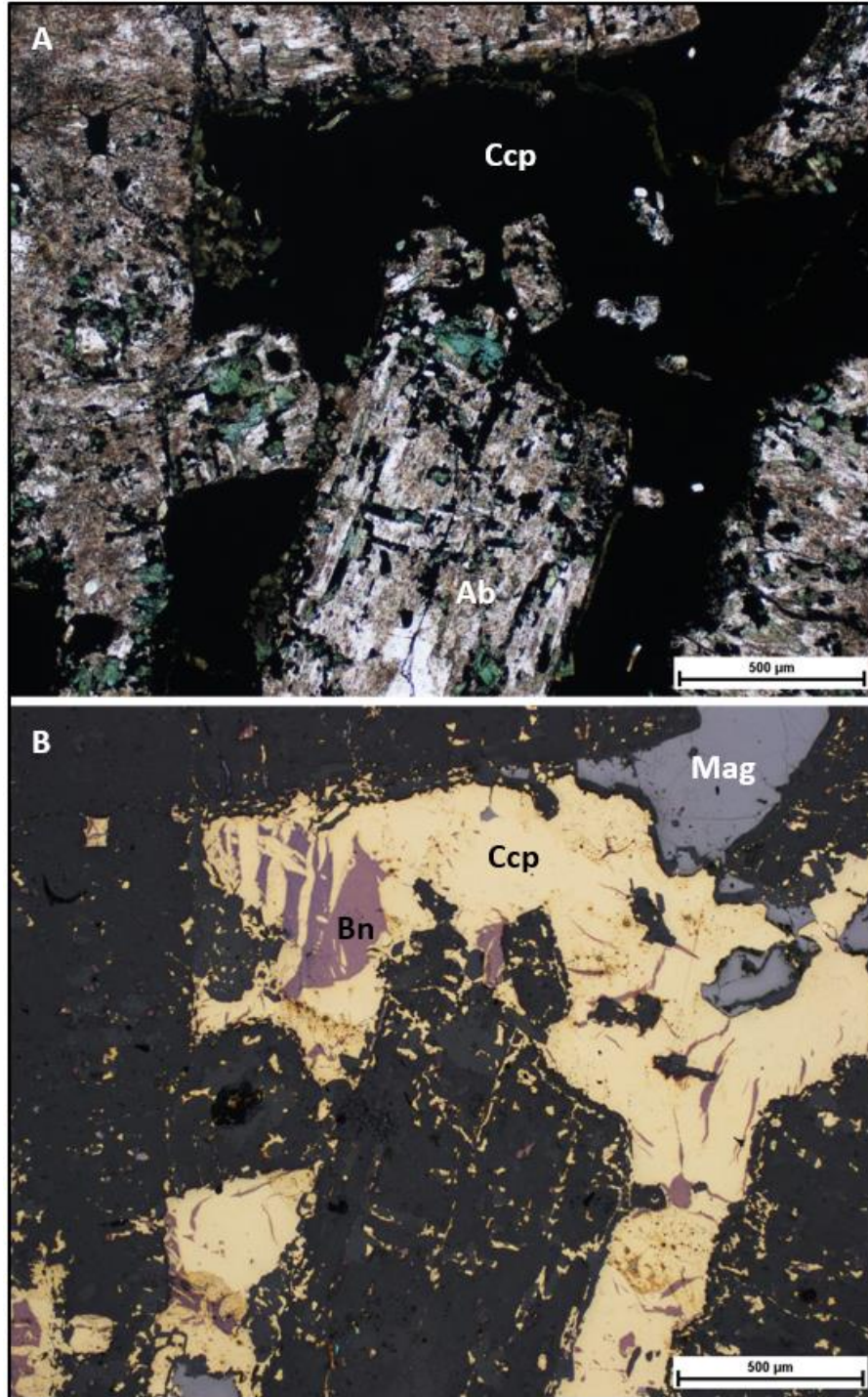


Figure 4.31 – **A**) Opaque mineral occurring interstitial to albitized plagioclase laths, and as inclusions that follow plagioclase 90 degree cleavage planes. Note that there is significantly less chlorite and actinolite associated with chalcopyrite mineralization as is typical with most GLD sulfide mineralization. Image is in PPL. **B**) The same image as in (a), but in reflected light, showing that the opaque mineral is chalcopyrite with bornite exsolution.

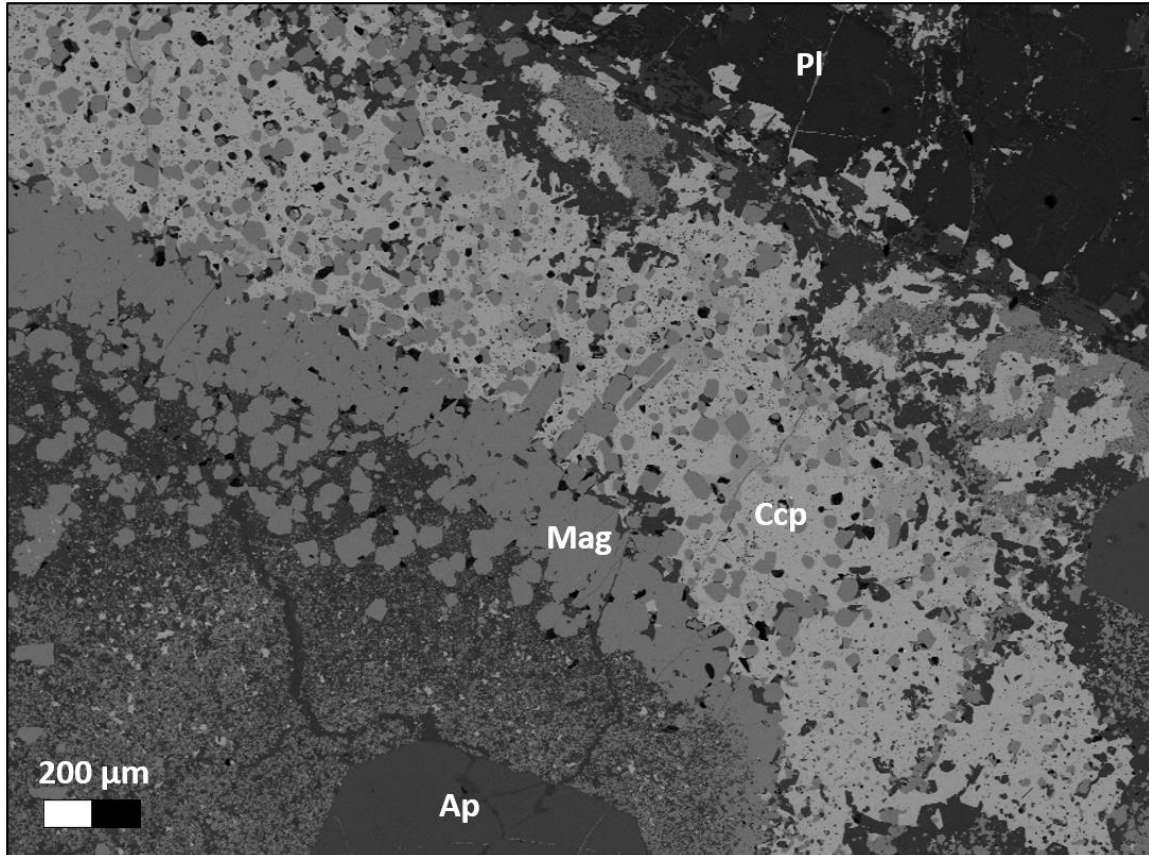


Figure 4.32 – A BSE image of chalcopyrite being resorbed by hydrothermal magnetite. The chalcopyrite grain shares a grain boundary with plagioclase to the top right of the image, with very sparse secondary silicate alteration.

4.3 Syenite

The syenite at the base of the Geordie Lake Deposit is fine-grained, and sacchroidal with abundant intergrowths of albite and potassium feldspar (Figure 4.33). Figure 4.33 (a) shows a general texture of the fine-grained syenite, with intergrowths of sacchroidal, dirty-brown albite, and white potassium feldspar. Figure 4.33 (b) shows that these intergrowths of albite and potassium feldspar are slightly perthitic, which is in agreement with the same observation made by Good and Crocket (1994). Figure 4.34 (a) shows the cross-cutting relationship between syenite and the basal fine-grained gabbro. The contact is apparently quite diffuse. Figure 4.34 (b) shows a PPL image of a region where syenite almost completely envelops fine-grained gabbro. Syenite farther away from the contact (over 5 m) is coarse-grained, and had a distinct interlocking texture containing potassium feldspar, plagioclase, magnetite, and augite as well lesser hornblende and apatite.

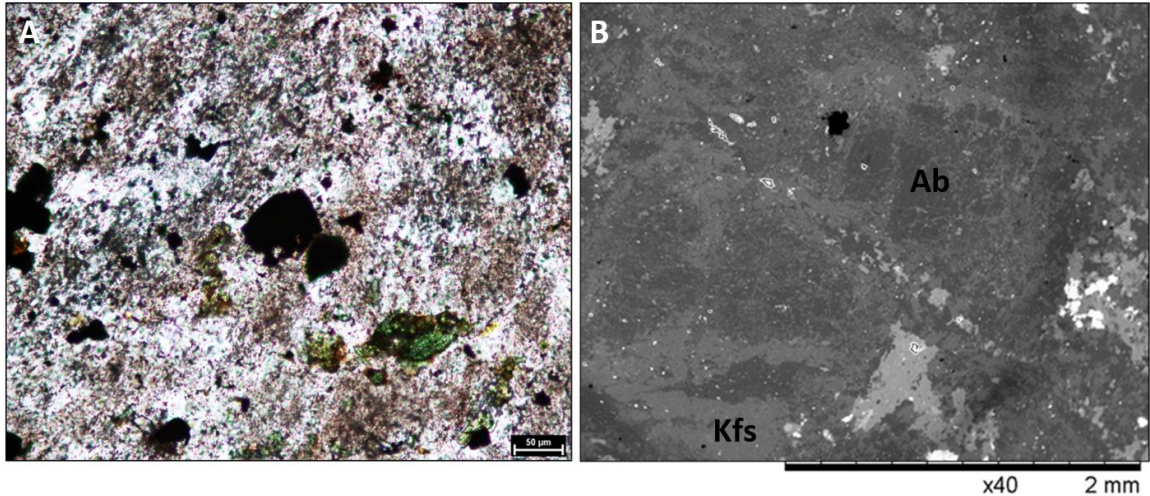


Figure 4.33 – **A**) A photomicrograph in PPL showing the general texture of fine grained syenite very near the contact of the Geordie Lake deposit. The mineralogy is difficult to distinguish due to the fine grained nature of the syenite. **B**) A BSE image of the general texture within syenite sample in (A). The dark patches are almost end-member albite, while the light patches are almost end-member potassium feldspar

4.3.1 Mineralization

The different styles of mineralization within the fine-grained syenite at the margin of the Geordie Lake gabbro are shown in Figure 4.35. In parts of the syenite dominated by granular potassium feldspar (over 5 m from the contact), it is common to observe sphalerite intergrown with chalcopyrite as shown on Figure 4.35 (a) and (b). However, within portions of the syenite that contain intergrowths of albite and potassium feldspar, mainly chalcopyrite is common as shown on Figure 4.35 (c) to (f). Chalcopyrite that occurs within these portions of syenite is commonly associated with actinolite, while chalcopyrite and sphalerite intergrowths are not associated with actinolite, but rather, occur within potassium feldspar.

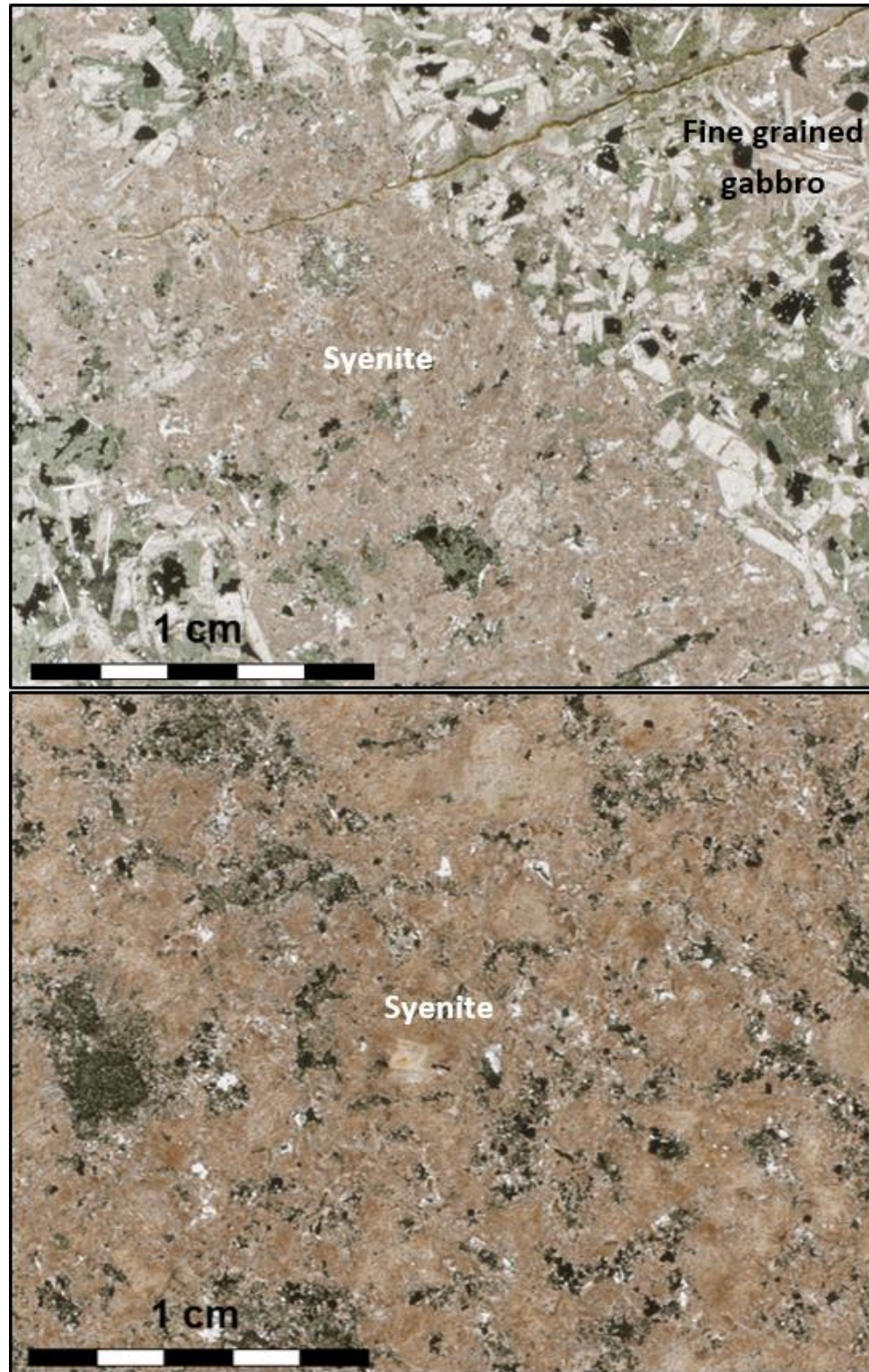


Figure 4.34 – A) Amphibole syenite beginning to envelope basal fine grained gabbro, B) Amphibole syenite fully enveloping basal fine grained gabbro. In plane polarized light

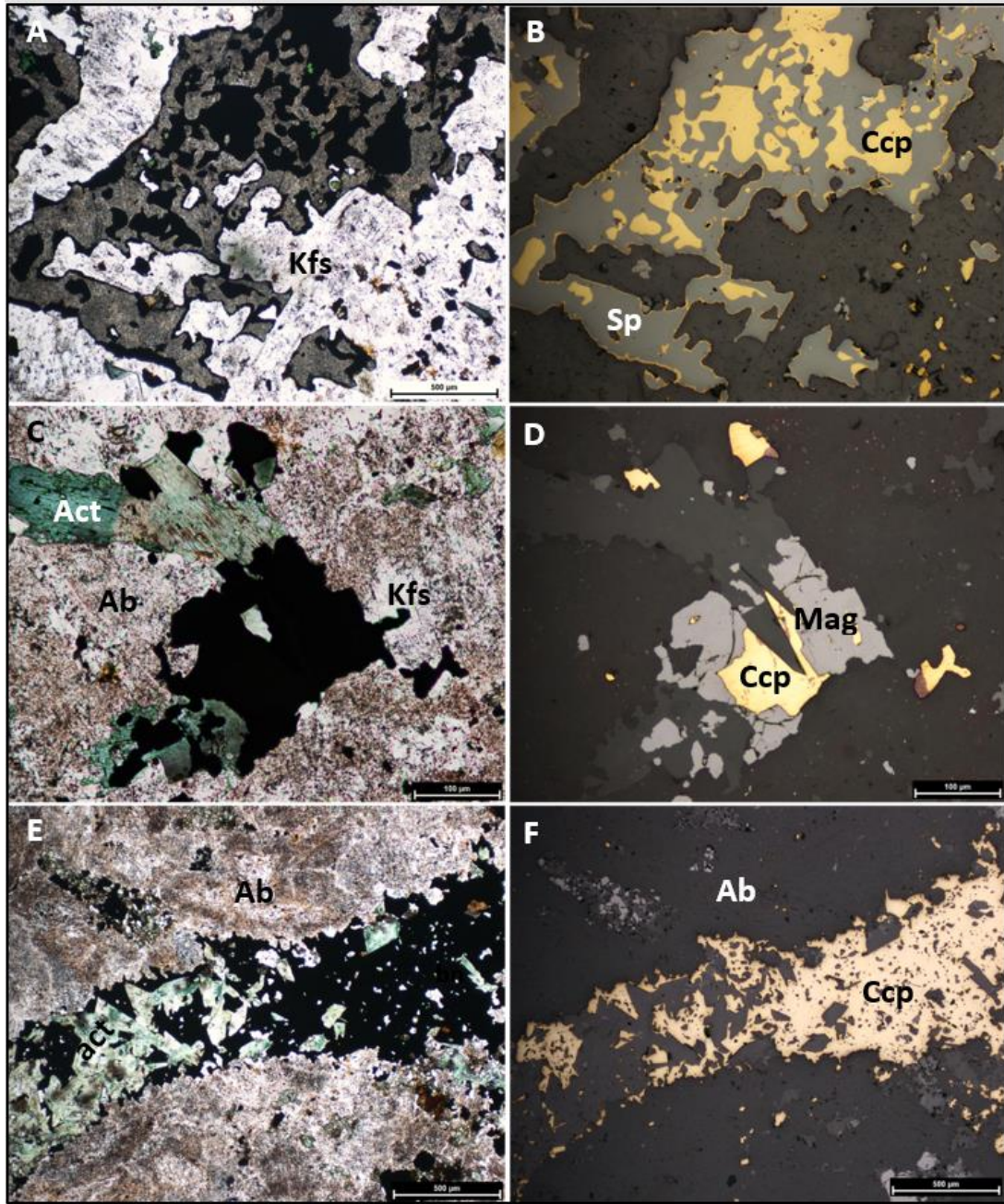


Figure 4.35 – **A**) A photomicrograph in PPL showing an irregularly shaped bleb of a cloudy grey to brown mineral with opaque inclusions. The irregular bleb is completely enveloped by potassium feldspar, **B**) The same image as in (A), however, in reflected light. The cloudy grey to brown mineral is sphalerite, while the opaque inclusions are chalcopyrite intergrowths within sphalerite, **C**) Another photomicrograph in PPL which shows an irregular opaque mineral inclusion within an intergrowth of albite and potassium feldspar, **D**) The same image as in (C), however in reflected light shows the opaque minerals are an intergrowth of chalcopyrite and magnetite. Bornite occurs at the margin of smaller chalcopyrite grains within the same image, **E**) A small veinlet of an opaque mineral occurs within albite. The veinlet contains a fair amount of euhedral to subhedral actinolite, which appears to be altering the opaque mineral. **F**) The same image as in (E), but in reflected light shows that the opaque mineral is chalcopyrite

4.4 Albite Pods at the GLD

Three different albite pods were sampled in order to understand the corresponding mineralogical and chemical variations from the most albitized portions of the albite pod, to the least altered portions. Albite Pod #3 was the first albite pod to be sampled (Figure 3.3 in Chapter 3) and contains seven sample blocks. Figure 4.36 shows the variable degrees of alteration within Albite Pod #3. Figure 4.36 (a) is a fairly fresh, coarse-grained ophitic gabbro with primary plagioclase, clinopyroxene and magnetite. In Figure 4.36 (b), Block 3 is also coarse-grained, but contains significant albite, actinolite and chlorite alteration. Block 5 in Figure 4.36 (c) shows very weak alteration, is medium-grained, and contains a primary assemblage of plagioclase, clinopyroxene and magnetite. Finally, Block 7 in Figure 4.36 (d) is fine-grained and contains moderate albite and actinolite alteration that is pseudomorphic after plagioclase, and clinopyroxene respectively.

Albite Pod #5 contains patchy, sporadic albite alteration that is very strongly spatially associated with actinolite alteration within all seven sample blocks taken during a transect of the Albite Pod (shown in Figure 3.4 in Chapter 3). A progressive sequence of sample blocks shown in Figure 4.37 demonstrates the extent of alteration that is present within every other block. The main alteration assemblage includes dirty-brown texture albite, intergrown with deep green actinolite that is pseudomorphic after plagioclase and clinopyroxene respectively. Medium to fine-grained apatite is common within the sugary-textured albite. Figure 4.38 (a) and (b) show unaltered portions of Blocks 1 and 3 within Albite Pod #5. The unaltered portions contain roughly equal proportions of plagioclase and clinopyroxene, with lesser magnetite. The amount of alteration present within Blocks 1 to 7 is variable and sporadic. The style of mineralization within Albite Pod #5 is constrained to small blebs and disseminations of chalcopyrite that are spatially associated with euhedral to subhedral actinolite (Figure 4.38 c & d).

The Discovery Outcrop Albite Pod contains a very progressive order of most altered sample (Block 1), to the least altered sample (Block 8). This progression of alteration is summarized in Figure 4.39, where the general textures of Blocks 1, 3, 5, and 7 respectively are shown in PPL to view the extent of alteration within each block. Where

alteration is pervasive, albite and actinolite alteration completely overprint the primary mineralogy. This is observed within Blocks 1 and 3 in Figure 4.39 (a) and (b). Where alteration is less significant, the primary mineralogy includes plagioclase, clinopyroxene, skeletal olivine, skeletal magnetite, and apatite. Despite the level of alteration changing gradually from Block 1 to Block 8, the amount of copper and platinum group element mineralization does not correspond to the degree of alteration.

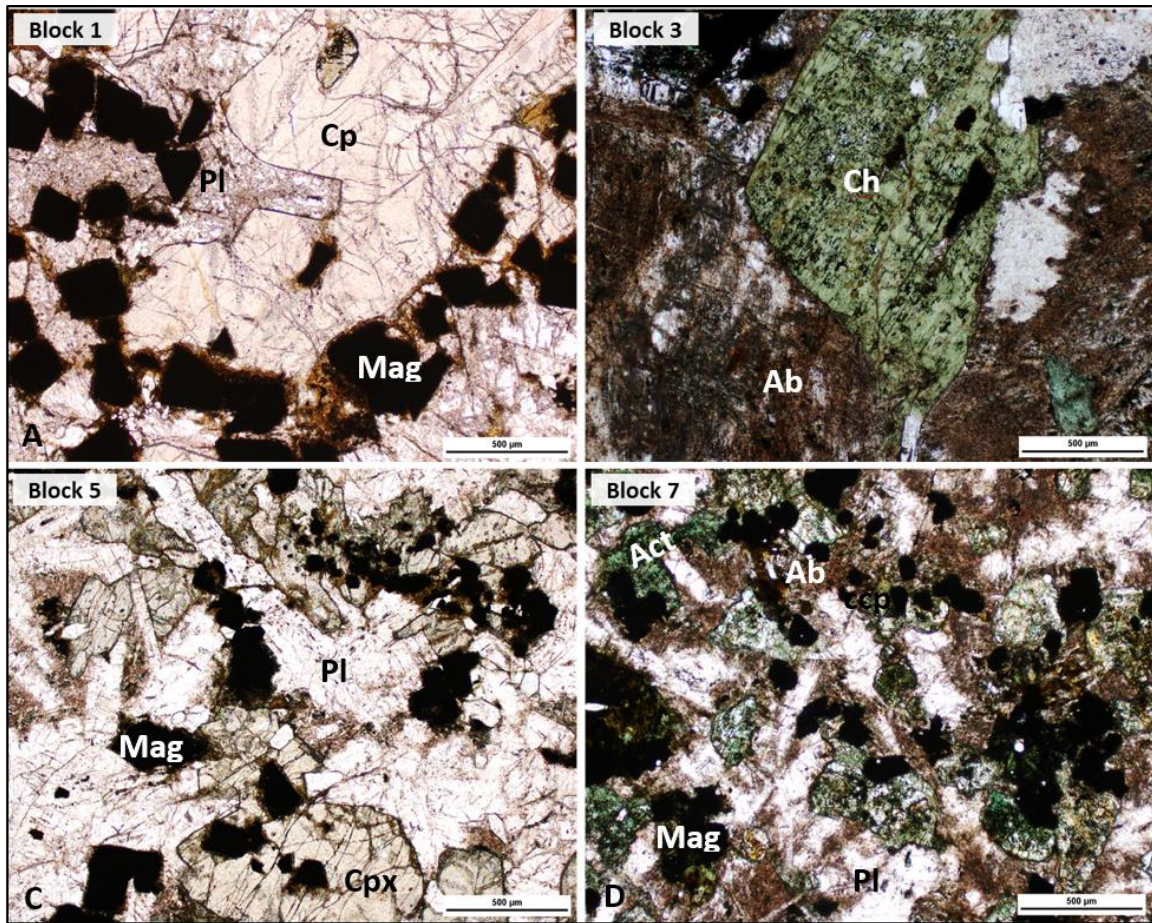


Figure 4.36 – **A**) A photomicrograph in PPL showing the general texture of Block 1. There is limited alteration, but when present, it is manifested as dusty mantling of plagioclase laths, and thin biotite rimming of magnetite grains. Overall grain size is coarse, **B**) A photomicrograph in PPL showing the general texture of Block 3. Alteration is quite strong, and is exhibited by strong (dirty brown) albite alteration of plagioclase, in addition to green pseudomorphic actinolite alteration of clinopyroxene. Grain size is coarse. **C**) Another photomicrograph in PPL which shows the general texture of Block 5. There is slight albite alteration of plagioclase rims, and thin biotite rims have formed around magnetite grains. However, overall, the primary igneous texture is very little disturbed. **D**) A photomicrograph in PPL showing the general texture of Block 7. Grain size is fine, and alteration is prevalent in the form of pseudomorphic actinolite alteration of clinopyroxene, as well as partial to complete albite alteration of plagioclase, and biotite alteration of magnetite rims.

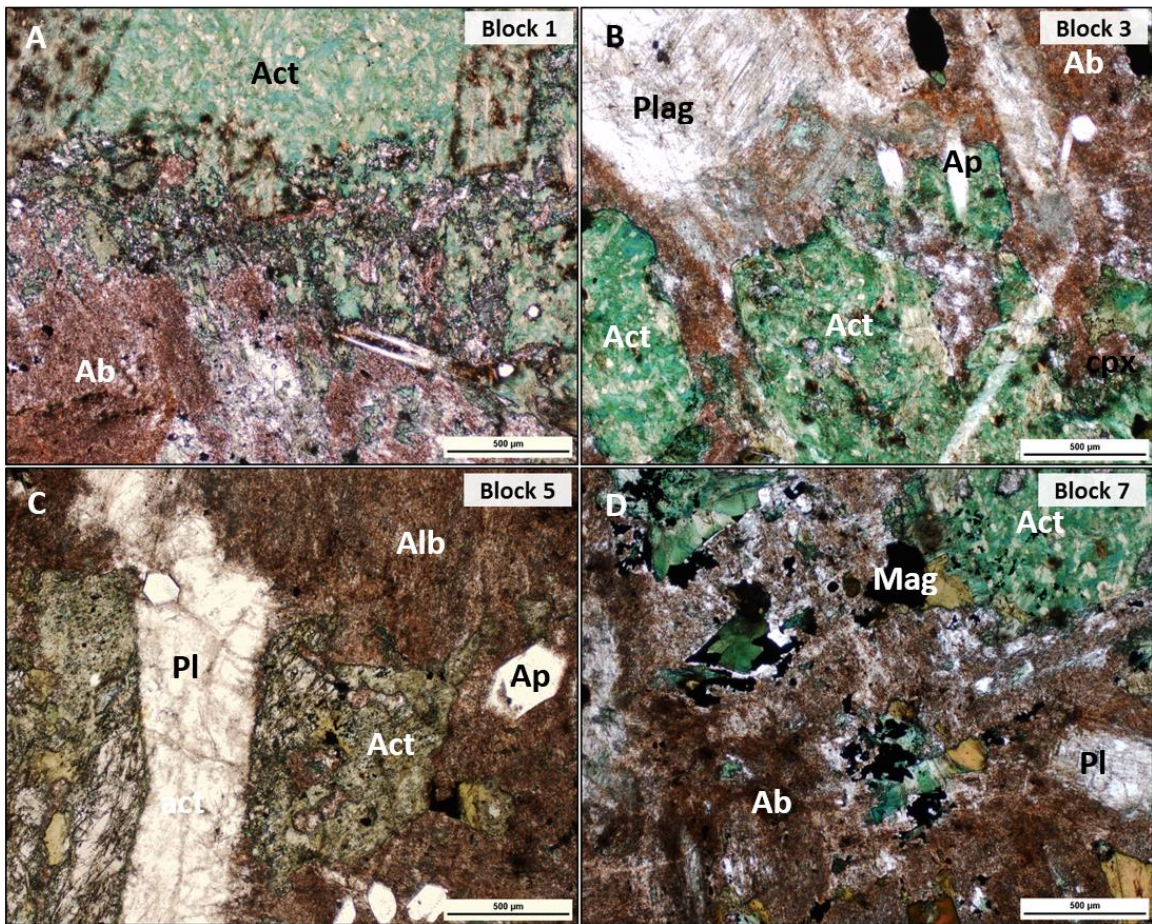


Figure 4.37 – A to D) Photomicrographs in PPL showing the general texture of sample Blocks #1, #3, #5 and #7 within Albite Pod #5. The alteration mineral assemblages are all similar within all these various blocks, including primarily albite and actinolite that are pseudomorphic after plagioclase, and actinolite respectively. The proportion of albite to actinolite is relatively constant from block to block.

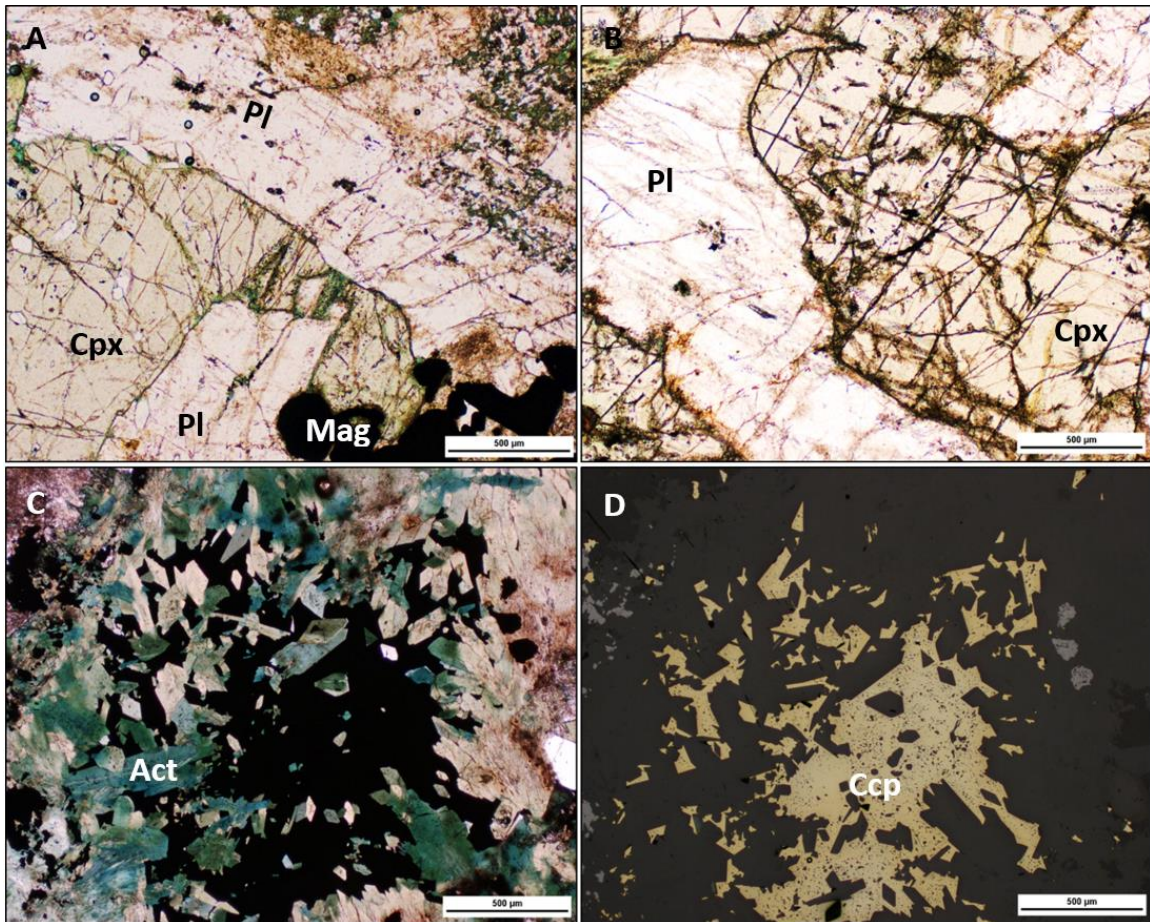


Figure 4.38 – A to B) Photomicrographs in PPL showing the texture of the unaltered portions of Block #1 and #3 in Albite Pod #5. Plagioclase shows slight mantling of albite, which clinopyroxene shows slight alteration to actinolite at the margins of fractures, **C)** The mineralization style observed in Albite Pod #5 in PPL, where actinolite grains are clustered together, and are euhedral, surrounding interstitial chalcopyrite, **D)** The same image as in (C), but in reflected light showing chalcopyrite interstitial to actinolite.

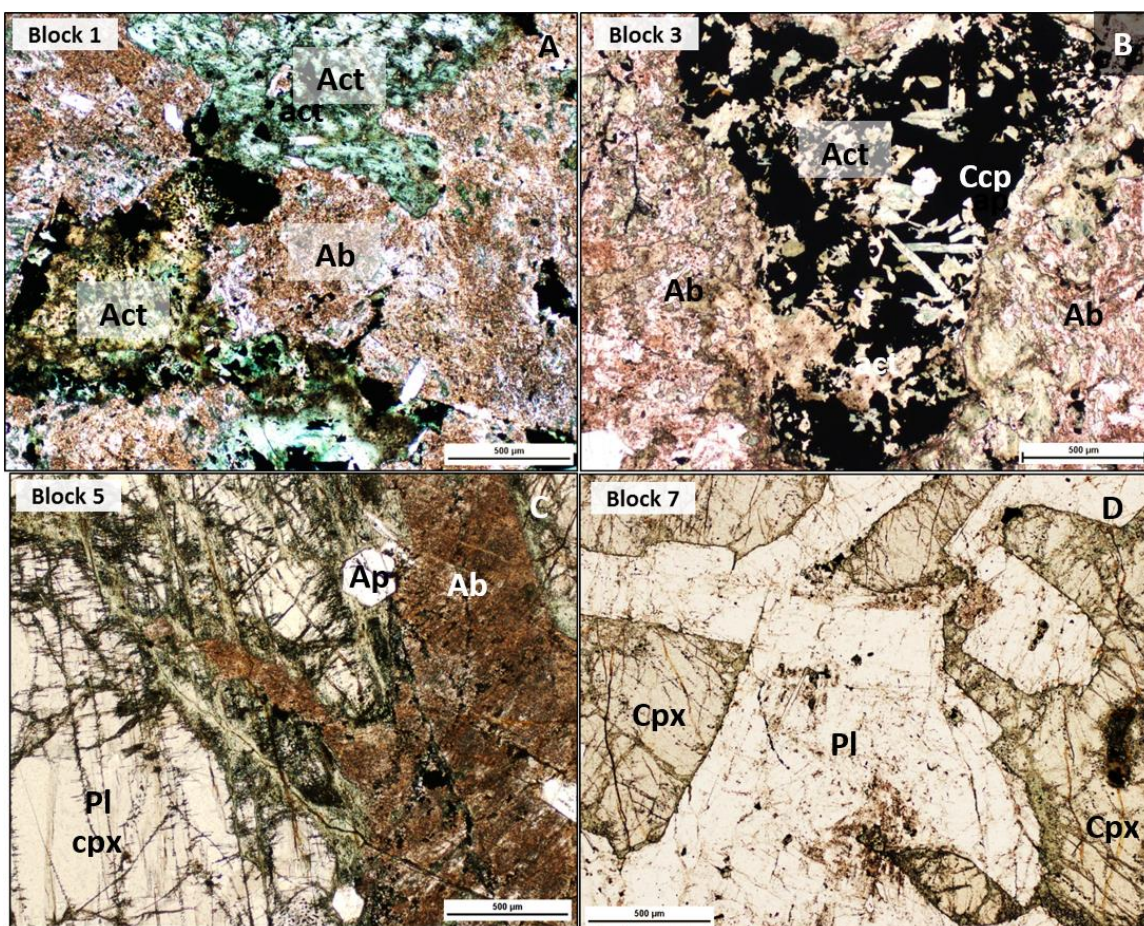


Figure 4.39 – **A**) A photomicrograph in PPL showing the general texture of sample Block #1 in the Discovery Outcrop Albite Pod. The mineralogy is dominated by mainly albite, and actinolite that is pseudomorphic after clinopyroxene, **B**) A photomicrograph in PPL which shows the general texture of Block #3 in the Discovery Outcrop Albite Pod. Alteration is still quite pervasive, featuring mainly cloudy-brown, saccharoidal albite pods along with patches of actinolite. Actinolite is commonly intergrown with chalcopyrite, which also occurs adjacent to the albite pods, **C**) Photomicrograph of Block #5 in the Discovery Outcrop Albite Pod in PPL. A dark brown albite bleb fills in heavy fractures within a clinopyroxene grain, and is intergrown with fine grained actinolite. Clinopyroxene in this sample is, overall, quite unaltered, **D**) A photomicrograph in PPL of the general texture within sample Block #7 in the Discovery Outcrop Albite Pod, showing that the overall texture is quite unaltered, particularly relative to the other blocks within the Discovery Outcrop Albite Pod. Ophitic textures are created by euhedral plagioclase and interstitial clinopyroxene

The sulfide mineralization within the Discovery Outcrop Albite Pod is quite different from anywhere else documented within the Geordie Lake deposit. The most common sulfide assemblages within the Discovery Outcrop Albite Pod include that of chalcopyrite, bornite, and covellite with lesser pyrite, and less commonly pentlandite, sphalerite, and galena. Figure 4.40 shows the associations of chalcopyrite to magnetite, bornite, and covellite. All bornite within these particular samples exhibit strong Widmanstätten textures with faint chalcopyrite lamellae. In Figure 4.40 (a), Coarse-

grained magnetite (with ilmenite exsolution lamellae) contain inclusions of chalcopyrite. Chalcopyrite primarily occurs at the rims and within fractures of magnetite in this reflected light image. In Figure 4.40 (b), chalcopyrite and bornite occur in proximity to magnetite. Bornite grains are rimmed by covellite. Figure 4.40 (c) shows a grain of chalcopyrite with actinolite inclusions, and bornite exsolution. This chalcopyrite grain is hosted within a larger magnetite grain. Figure 4.40 (d) shows the Widmanstätten texture exhibited by bornite, which contains chalcopyrite lamellae. Fractures within this bornite grain are rimmed by covellite.

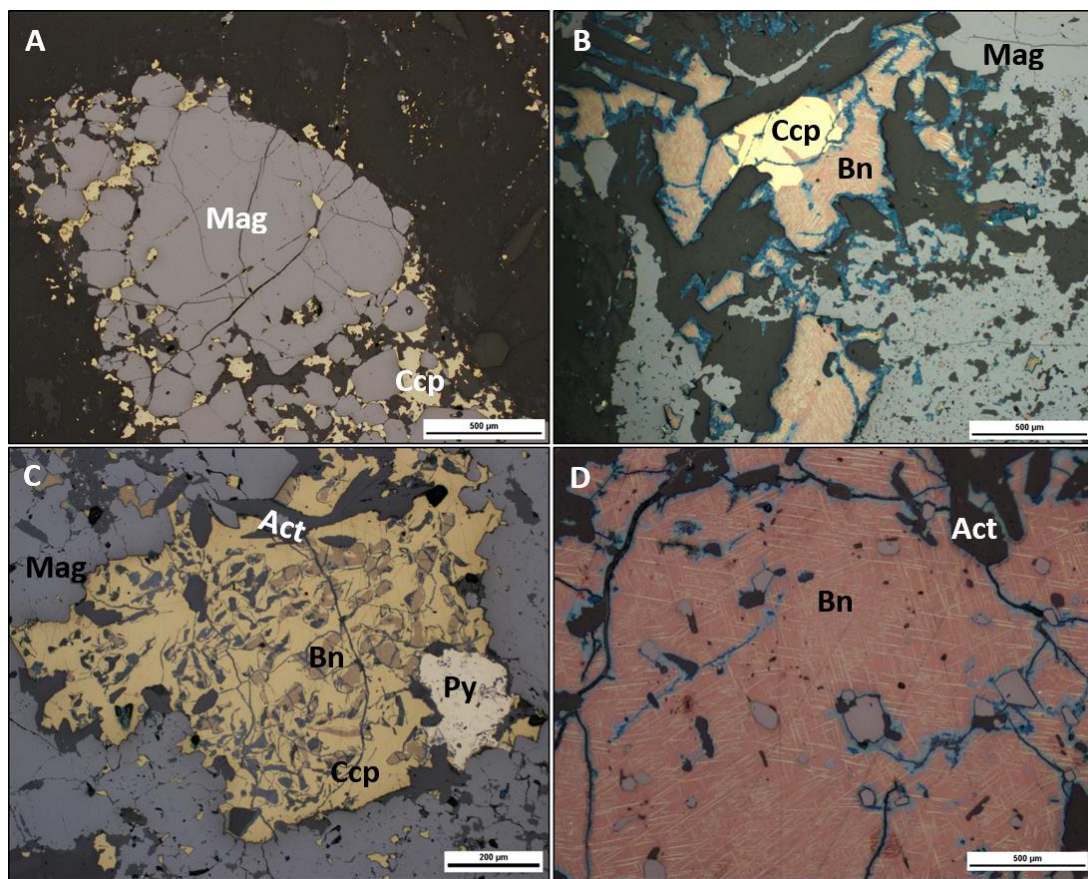


Figure 4.40 – **A)** A reflected light image of one mineralization style observed within the Discovery Outcrop Albite Pod sample blocks. A coarse grained magnetite grain contains fine grained inclusions of chalcopyrite, which contains even finer grained bornite exsolution, **B)** A reflected light photomicrograph which shows a large grain of bornite intergrown with chalcopyrite. The rims of the bornite grains are altered to covellite (in blue), **C)** Photomicrograph in reflected light of a large chalcopyrite grain, with abundant bornite and covellite intergrowths. As in (B), covellite tends to be associated with the fracture planes of the chalcopyrite grain. The large chalcopyrite grain is completely enclosed by magnetite. A pyrite grain occurs at the right margin of the chalcopyrite grain, presumably as an alteration mineral. **D)** A reflected light image close-up of bornite within the Discovery Outcrop Albite Pod. Bornite tends to exhibit thin lamellae of chalcopyrite in a Widmanstätten pattern

Chapter 5

5 Geochemistry

5.1 Results of Major and Trace Element Geochemistry

The major element data include the sample name, drill hole, sample depth (in meters), and the lithology name and unit number. A summary of major element data for 13 samples of plagioclase aligned gabbro is shown in Table 5.1. Major element data for 9 samples of homogeneous gabbro, as well as 3 samples of homogeneous troctolite are shown in Table 5.2. The degree of alteration within homogeneous gabbro samples is generally weak, and hence, they are not sorted on the basis of varying degrees of alteration.

The major element geochemistry for heterogeneous gabbro is shown on Tables 5.3 and 5.4, and include three highly albitized heterogeneous gabbro samples, seven heterogeneous gabbro samples that exhibiting moderate albitization in addition to moderate actinolite alteration, and seven heterogeneous gabbro samples exhibiting weak albitization. Table 5.4 also shows the major element data for three samples of unmineralized skeletal troctolite, and three samples of unmineralized syenite. Note that samples which were analyzed for major elements at the Biotron facility at Western University (IM-1 to IM-15) do not include FeO data.

Mg-numbers of minerals such as olivine and clinopyroxene decrease upwards in a fractional crystallization trend. The Mg-number is calculated by using Formula 5.1. However, due to the amount of ferrous iron present in magnetite, a trend using simply whole rock Mg-numbers may be skewed by the presence of magnetite. Therefore, the whole rock magnesium number (Mg #) for each sample is calculated by first assuming that all of the Fe₂O₃ is contained in magnetite. This assumption is confirmed by plotting Fe₂O₃ versus TiO₂, which yields a linear correlation between the two (except for within the skeletal troctolite samples which are a cumulate phase) (Figure 5.1). This assumption

would be erroneous if there was sufficient chalcopyrite, pyrrhotite or pyrite in the rock to influence the amount of iron, but given the low weight percentage of sulfur (0.14% average) it is reasoned that the amount of iron present within sulfide is negligible. The number of moles of FeO and Fe₂O₃ are then calculated. Since the chemical formula of magnetite is Fe₂O₃·FeO, 1 mole of FeO is used up for every mole of Fe₂O₃ in order to make magnetite. The remaining amount of FeO in moles becomes the residual amount of FeO (FeO_r). The residual molar FeO_r used in the calculation of the Mg # which is as follows:

$$Mg\# = \frac{(mole \% MgO)}{(mole \% MgO) + (mole \% FeO_r)} \quad (5.1)$$

Heterogeneous gabbro was sampled based on the varying degrees of alteration, and were sorted into three groups based on visual modal percentages established during core logging: 1) highly albitized heterogeneous gabbro, 2) moderately albitized heterogeneous gabbro, and 3) weakly albitized heterogeneous gabbro. Good and Crocket (1994) described a spatial association between both disseminated sulfides and PGM with the pervasive albite pods, which is in agreement with what was observed in this study. Thus, the purpose of grouping samples based on the degree of albitization was to distinguish: 1) whether the more intensely albitized samples were more enriched in Cu and Pd, and 2) whether there is a notable variation in major and trace elements between the most and least albitized samples. Actinolite alteration is also present within albite altered samples; however, the degree of actinolite alteration is variable, and for the purpose of examining the link between Cu-PGE mineralization and albitization, the degree of actinolite alteration within these heterogeneous gabbro samples was not considered.

Skeletal troctolite samples were sorted on four criteria: 1) skeletal troctolite with low actinolite/biotite/chlorite alteration, 2) skeletal troctolite occurring within 2 m of faulted, rubbly rock, 3) skeletal troctolite with high actinolite/biotite/chlorite alteration, and 4) skeletal troctolite that has a variable degree of actinolite alteration, but is barren of mineralization. As discussed in Chapter 4, the green-alteration (including actinolite/biotite/chlorite alteration) in the skeletal troctolite lithology consists of varying

proportions of actinolite, chlorite, biotite, and minor epidote. Since there is a clear spatial association between the green-alteration minerals (predominantly actinolite) and Cu-sulfide-PGM mineralization, the purpose of grouping the skeletal troctolite samples according to varying intensities of green alteration minerals was to distinguish: 1) whether the most intensely green-altered skeletal troctolite samples were in fact the most highly enriched in Cu and Pd, and 2) the major and trace element variations between the most and least altered samples. The selections of samples that contain a variable degree of actinolite/biotite/chlorite alteration (but barren of mineralization) came much later in this study, and they were selected in order to provide more insight on the major and trace element variations between mineralized and unmineralized samples, since all previously selected skeletal troctolite samples with varying degrees of alteration contained some degree of Cu-PGE mineralization as they are contained within the GLD. Hence, these unmineralized samples (which are located far from the mineralized zone of the GL intrusion) were sampled in order to gain an understanding of the geochemical variations between mineralized and unmineralized skeletal troctolite samples.

Table 5.5 shows major element data for skeletal troctolite samples with low actinolite/biotite/chlorite alteration, and those that occur within 2 m of rubbly, faulted rock. Samples within the rubbly interval exhibit chlorite alteration at fracture margins in the form of slickensides. Disseminated to blebby, and rarely semi-massive chalcopyrite mineralization is commonly inter-grown with fracture-controlled chlorite alteration. Table 5.6 shows major element data for skeletal troctolite samples with high actinolite alteration.

Major element geochemistry for all albite pod samples is shown in Tables 5.7 and 5.8. It should be noted that Albite Pods #3 and #5 exhibit sparse, disseminated chalcopyrite mineralization that is associated with actinolite alteration within the albitized regions of the samples. On the other hand, the Discovery Outcrop Albite Pod samples contain strong, blebby to disseminated chalcopyrite-bornite mineralization that is primarily associated with actinolite alteration, and enveloped by albite alteration.

A summary of trace element data for all plagioclase aligned gabbro, homogeneous gabbro, and homogeneous troctolite samples are shown on Tables 5.9 and 5.10. Trace element data include rare earth elements (REE), Cu, Ni, Pd, and Pt. Table 5.9 includes trace element data for 13 plagioclase aligned gabbro samples (Unit 2a). Table 5.10 contains trace element data for 9 samples of homogeneous gabbro (Unit 2b), and 3 samples of homogeneous troctolite (Unit 2c).

All trace element geochemistry for heterogeneous gabbro, skeletal troctolite, basal fine-grained gabbro and syenite are shown on Tables 5.11 – 5.14. Tables 5.11 and 5.12 include trace element data for 17 heterogeneous gabbro, 3 unmineralized skeletal troctolite, and 3 unmineralized syenite samples, while Tables 5.13 and 5.14 include trace element data for 19 skeletal troctolite, 1 basal fine-grained gabbro, and 2 basal syenite samples. The trace element data for all albite pod samples are shown on Tables 5.15 and 5.16. Whole rock PGE data is shown on Table 5.17.

Sample	IM-UM-10	IM-UM-11	IM-UM-12	IM-UM-16	IM-UM-17	IM-UM-18	IM-UM-19	IM-UM-2	IM-UM-20	IM-UM-3	IM-UM-4	IM-UM-7	IM-UM-8	IM-UM-9
Drillhole	G-10-16	G-10-16	G-10-16	G-10-17	G-10-17	G-10-17	G-10-17	G-10-04	G-10-17	G-10-04	G-10-04	G-10-16	G-10-16	G-10-16
Depth (m)	45	50	60	15.62	30	45	60	15	75.57	30.3	45	0	15	30.36
Lithology	Coarse grained gabbro with plagioclase alignment (2a)													
SiO ₂	47.70	45.40	46.60	44.90	45.30	46.10	45.50	44.90	46.40	46.40	44.80	43.00	46.30	45.90
Al ₂ O ₃	14.80	13.10	14.00	13.15	13.00	13.70	13.85	13.75	13.90	14.35	14.35	12.90	14.60	13.90
FeO	12.35	13.30	11.90	12.95	12.60	12.25	12.65	12.45	11.70	11.95	13.45	13.60	11.55	11.55
Fe ₂ O ₃	17.85	19.90	16.85	19.45	19.25	17.75	18.35	18.40	17.20	17.45	18.20	21.20	17.20	18.45
CaO	8.07	8.04	8.18	7.42	8.62	7.70	7.59	7.87	8.03	8.05	7.06	7.10	8.01	7.74
MgO	4.04	5.37	4.07	5.05	4.95	4.06	4.28	4.50	4.05	4.09	4.22	5.60	4.04	4.38
Na ₂ O	3.79	3.16	3.60	3.39	3.20	3.75	3.44	3.11	3.62	3.60	3.16	3.18	3.80	3.43
K ₂ O	1.67	1.50	1.56	1.46	1.50	1.64	1.71	1.60	1.63	1.56	2.47	1.92	1.57	1.64
TiO ₂	2.12	2.20	2.01	2.21	2.25	2.14	2.15	2.10	2.00	2.07	2.09	2.39	1.96	2.15
MnO	0.27	0.30	0.26	0.29	0.28	0.27	0.27	0.27	0.26	0.25	0.26	0.31	0.25	0.28
P ₂ O ₅	0.87	1.05	0.85	0.92	1.20	0.98	0.89	0.83	0.89	0.84	0.95	0.85	1.00	0.85
L.O.I.	0.35	0.48	0.44	0.94	0.40	0.55	0.46	0.66	0.61	0.31	0.72	0.49	0.57	0.30
S	0.03	0.01	0.03	0.02	0.02	0.02	0.03	0.03	0.04	0.04	0.04	0.02	0.03	0.03
TOTAL	101.56	100.51	98.45	99.20	99.97	98.66	98.52	98.02	98.63	99.01	98.32	98.96	99.33	99.05

Table 5.1 – Major element geochemistry of all plagioclase aligned gabbro samples (Unit 2a) in wt. %

Sample	IM-16	IM-40	IM-UM-13	IM-UM-14	IM-UM-21	IM-UM-22	IM-UM-5	IM-UM-6	IM-41	IM-UM-1	IM-UM-23
Drillhole	G-10-04	G-10-16	G-10-16	G-10-16	G-10-17	G-10-17	G-10-04	G-10-04	G-10-16	G-10-02	G-10-17
Depth (m)	62	86	69.64	85	90	100	50	60.38	154	30	175
Lithology	Medium grained homogenous gabbro (2b)								Medium grained homogenous troctolite (2c)		
SiO ₂	46.41	46.33	47.70	47.20	46.50	46.20	48.00	47.80	45.32	46.10	45.90
Al ₂ O ₃	13.92	13.89	14.35	13.60	13.60	12.70	14.30	13.80	13.01	12.20	12.30
FeO	12.20	11.90	12.15	12.05	12.35	13.15	12.10	12.25	10.90	11.50	11.00
Fe ₂ O ₃	17.72	17.86	18.05	17.80	18.00	19.35	18.05	17.80	18.72	18.70	18.55
CaO	7.76	7.70	7.71	7.61	7.63	7.27	7.67	7.83	8.05	8.26	7.50
MgO	4.08	4.19	4.19	3.95	4.18	4.36	4.07	3.92	4.79	3.96	4.53
Na ₂ O	3.60	3.63	3.74	3.76	3.56	3.55	3.94	3.77	3.68	3.72	3.83
K ₂ O	1.95	2.01	1.89	2.08	1.89	2.10	1.81	1.91	1.75	1.73	2.01
TiO ₂	2.03	2.08	2.05	2.06	2.08	2.22	2.08	2.08	2.18	2.21	2.07
MnO	0.28	0.27	0.27	0.27	0.28	0.30	0.26	0.28	0.28	0.30	0.30
P ₂ O ₅	1.03	1.05	0.97	1.05	0.98	1.04	1.00	1.06	1.06	1.16	1.05
L.O.I.	0.32	0.52	0.72	0.61	0.45	0.62	0.51	0.59	0.26	1.27	0.82
S	0.05	0.04	0.03	0.03	0.03	0.08	0.05	0.05	0.04	0.04	0.03
TOTAL	99.15	99.57	101.67	100.02	99.18	99.79	101.74	100.89	99.14	99.65	98.89

Table 5.2 – Major element geochemistry of all medium grained homogeneous gabbro samples (Unit 2b), and medium grained homogenous troctolite samples (Unit 2c) in wt. %

Sample	IM-14	IM-34	IM-35	IM-2	IM-20	IM-33	IM-38	IM-39	IM-5	IM-9
Drillhole	G-10-17	G-10-17	G-10-17	G-10-04	G-10-04	G-10-17	G-10-17	G-10-17	G-10-04	G-10-16
Depth (m)	178	150	176	76	116	148	202	206	118	122
Lithology	Strongly albitized, heterogeneous gabbro (3a)			Heterogeneous w/ moderate alteration (3a)						
SiO ₂	39.69	43.02	46.88	42.97	46.29	43.19	44.03	45.16	46.91	45.25
Al ₂ O ₃	9.95	12.96	13.94	12.82	13.84	12.71	13.21	13.70	13.33	12.72
FeO	-	12.15	10.40	-	9.76	12.65	11.00	10.10	-	-
Fe ₂ O ₃	26.66	21.43	17.51	22.89	17.31	22.24	19.35	18.79	17.56	19.84
CaO	6.87	7.64	7.61	7.16	8.17	7.29	7.89	7.93	7.72	7.48
MgO	8.23	5.15	4.30	4.33	4.10	4.73	5.46	5.30	4.18	4.49
Na ₂ O	2.49	3.29	3.83	3.37	3.71	3.50	3.46	3.72	3.86	3.39
K ₂ O	1.06	1.52	2.01	1.57	1.91	1.40	1.32	1.46	1.93	2.29
TiO ₂	2.13	2.56	1.93	2.83	2.03	2.49	1.68	1.72	1.98	2.42
MnO	0.30	0.30	0.28	0.25	0.27	0.29	0.28	0.28	0.26	0.25
P ₂ O ₅	0.88	0.97	1.00	1.01	1.13	0.97	0.90	0.93	1.07	0.98
L.O.I.	0.57	0.33	0.48	0.36	0.32	0.25	1.53	0.52	0.33	0.17
S	0.41	0.13	0.06	0.40	0.03	0.24	0.15	0.14	0.09	0.04
TOTAL	99.24	99.30	99.83	99.96	99.11	99.30	99.26	99.65	99.22	99.32

Table 5.3 – Major element geochemistry of heterogeneous gabbro samples (Unit 3a) in wt. %. The first three are highly albitized samples, while the last seven are samples which exhibited a moderate degree of albite alteration. Total iron is reported as Fe₂O₃ and FeO is not included in the total.

Sample	IM-13	IM-17	IM-18	IM-15	IM-25	IM-30	IM-3	IM-32	IM-40	IM-41	IM-42	IM-UM-25	IM-UM-26	IM-UM-27
Drillhole	G-10-17	G-10-04	G-10-04	G-10-17	G-10-16	G-10-16	G-10-04	G-10-16	G-00-03	G-00-05	G-02-01	G-00-03	G-06-03	G-00-04
Depth (m)	144	86	90	196	118	200	84	146	75	42.67	38.11	179.87	431.41	110.06
Lithology	Weakly albitized heterogeneous gabbro (3a)								Unmineralized skeletal (3b)			Unmineralized syenite (5a)		
SiO ₂	47.18	42.73	43.40	45.00	45.25	44.08	42.04	43.94	39.8	40.2	44.2	55.4	56.1	60.4
Al ₂ O ₃	13.03	12.81	12.86	13.60	13.21	11.59	11.87	12.91	8.23	9.69	12.05	14.25	14.4	14.7
FeO	-	13.10	13.40	-	12.00	11.70	-	12.20	15	17.6	10.55	9.05	9.29	5.92
Fe ₂ O ₃	17.47	21.26	21.49	19.82	19.79	21.40	24.37	20.91	25	26.5	20.5	13.45	13.7	8.52
CaO	7.77	7.99	7.41	7.52	7.81	8.10	6.96	7.38	5.93	5.9	7.02	4.5	4.91	3.68
MgO	3.86	4.99	5.56	5.43	4.57	5.65	5.35	5.24	11.75	10.3	8.11	1.02	0.71	1.18
Na ₂ O	3.94	3.03	3.01	3.74	3.55	3.41	2.99	3.25	1.92	1.5	3.13	4.69	5.11	4.66
K ₂ O	2.19	1.56	1.57	1.22	1.70	1.50	1.51	1.85	1.21	1.65	1.41	4.27	4.18	4.31
TiO ₂	2.02	2.57	2.41	1.74	2.30	2.29	2.97	2.37	1.08	1.92	1.29	1.25	1.13	0.87
MnO	0.25	0.28	0.30	0.23	0.28	0.38	0.27	0.29	0.43	0.4	0.32	0.35	0.29	0.2
P ₂ O ₅	1.13	0.96	0.97	0.84	1.08	1.03	0.86	0.91	0.6	0.61	0.76	0.33	0.31	0.28
L.O.I.	0.47	0.76	0.20	0.51	0.25	0.31	0.24	0.35	2.15	0.74	0.66	0.5	0.18	0.78
S	0.07	0.06	0.06	0.20	0.08	0.14	0.28	0.06	0.06	0.02	0.04	0.01	0.04	0.01
TOTAL	99.38	99.00	99.24	99.85	99.87	99.88	99.71	99.46	98.16	99.43	99.49	100.02	101.06	99.59

Table 5.4 – Major element geochemistry of weakly albitized heterogeneous gabbro samples (Unit 3a), unmineralized skeletal troctolite (Unit 3b), and unmineralized syenite (Unit 5a) in wt. %. Total iron is reported as Fe₂O₃ and FeO is not included in the total.

Sample	IM-23	IM-24	IM-31	IM-7	IM-10	IM-11	IM-26	IM-28	IM-29	IM-4
Drillhole	G-10-04	G-10-04	G-10-16	G-10-04	G-10-16	G-10-16	G-10-16	G-10-16	G-10-16	G-10-04
Depth (m)	146	148	206	150	138	172	136	168	170	100
Lithology	Skeletal w/ low alteration (3b)				Skeletal near fault (rubbly) (3b)					
SiO ₂	41.25	42.03	41.25	42.24	37.57	40.78	44.76	40.29	38.94	40.88
Al ₂ O ₃	9.55	12.30	10.42	10.09	10.30	10.52	13.27	9.72	9.41	11.36
FeO	3.87	13.05	13.40	-	-	-	11.50	15.20	16.00	-
Fe ₂ O ₃	25.95	22.04	24.18	24.92	29.91	25.10	19.74	26.47	27.33	26.17
CaO	5.92	7.60	8.51	6.34	5.77	7.03	7.75	6.73	5.94	6.49
MgO	10.98	7.57	8.06	9.63	7.55	8.10	5.04	8.87	10.29	4.94
Na ₂ O	2.05	2.67	2.61	2.20	1.98	2.52	3.53	2.15	1.69	3.24
K ₂ O	1.05	1.01	1.03	1.08	1.68	1.02	1.50	1.39	1.03	1.38
TiO ₂	1.62	1.73	2.00	1.27	3.69	2.12	2.24	2.48	2.33	3.25
MnO	0.39	0.32	0.37	0.32	0.31	0.30	0.29	0.38	0.41	0.25
P ₂ O ₅	0.72	0.87	1.30	0.76	0.66	0.92	1.05	1.03	0.77	0.89
L.O.I.	-0.14	0.45	-0.03	0.15	0.04	0.44	0.38	0.33	1.12	0.33
S	0.16	0.39	0.27	0.50	0.07	0.39	0.05	0.11	0.10	1.24
TOTAL	99.50	98.98	99.97	99.50	99.53	99.24	99.60	99.95	99.36	100.42

Table 5.5 – Major element geochemistry of skeletal troctolite samples (Unit 3b) in wt. %. The first are weakly altered skeletal troctolites, while the next six are skeletal troctolites which were sampled within 2 m of faulted (and very rubbly) drill core. Total iron is reported as Fe₂O₃ and FeO is not included in the total.

Sample Drillhole Depth (m)	IM-12 G-10-16 202	IM-19 G-10-04 102	IM-21 G-10-04 126	IM-27 G-10-16 166	IM-22 G-10-04 128	IM-36 G-10-17 192	IM-37 G-10-17 194	IM-6 G-10-04 126	IM-8 G-10-04 152	IM-UM-15 G-10-16 224	IM-UM-24 G-10-17 246.5
Lithology	Skeletal w/ high actinolite alteration (3b)								Basal gabbro (3c)	Mineralized syenite (5a)	
SiO ₂	42.15	35.46	40.62	41.57	41.72	42.22	39.24	41.26	41.10	58.80	60.40
Al ₂ O ₃	10.05	10.33	9.91	10.35	10.25	11.18	8.59	9.71	10.84	14.10	14.50
FeO	-	15.80	16.35	14.50	14.60	12.35	16.55	-	-	5.17	4.71
Fe ₂ O ₃	24.35	31.84	26.53	24.06	24.33	22.70	28.44	25.79	25.86	9.23	8.93
CaO	6.49	6.18	6.12	5.92	6.51	6.38	5.32	6.53	7.13	3.27	2.60
MgO	9.61	6.10	10.21	9.47	10.45	8.59	11.41	10.05	7.33	0.98	0.95
Na ₂ O	2.39	2.20	2.04	2.01	2.10	2.66	1.68	2.01	2.49	4.98	5.78
K ₂ O	1.25	1.18	1.10	2.02	1.10	1.38	1.04	1.02	1.20	4.81	4.91
TiO ₂	1.55	4.44	1.76	1.77	1.46	1.99	1.97	1.76	1.62	0.82	0.79
MnO	0.33	0.35	0.38	0.38	0.37	0.34	0.42	0.31	0.31	0.30	0.30
P ₂ O ₅	0.62	0.78	0.73	0.68	0.81	0.81	0.70	0.80	0.86	0.25	0.21
L.O.I.	0.00	0.14	0.42	0.74	0.74	1.19	0.54	0.24	0.03	0.52	0.44
S	0.15	0.16	0.17	0.05	0.19	0.06	0.11	0.20	0.58	0.20	0.17
TOTAL	98.94	99.16	99.99	99.02	100.03	99.50	99.46	99.68	99.35	98.26	99.98

Table 5.6 – Major element geochemistry of: skeletal troctolite samples (Unit 3b) which exhibit a high degree of actinolite alteration, basal fine grained gabbro (Unit 3c), and mineralized syenite that is in contact with the overlying mineralized gabbro (Unit 5). Units are in wt. %. Total iron is reported as Fe₂O₃ and FeO is not included in the total.

Sample	AB-3-1	AB-3-2	AB-3-3	AB-3-4	AB-3-5	AB-3-6	AB-3-7	AB-5-1	AB-5-2	AB-5-3	AB-5-4	AB-5-5	AB-5-6	AB-5-7
Pod	Albite Pod #3							Albite Pod #5						
Block #	1	2	3	4	5	6	7	1	2	3	4	5	6	7
SiO ₂	43.5	41.9	50.7	45.4	44.3	49	43.4	42.2	45.5	46	45.7	45.9	45.5	45.3
Al ₂ O ₃	12.55	12.3	14.15	13.2	13.1	13.6	12.6	11.35	13	13.3	12.95	13	13	12.4
FeO	11.15	12.05	7.65	10.4	10.6	8.78	11.4	14.3	11.4	10.9	11.4	11.8	11.8	13
Fe ₂ O ₃	22	24.3	14.9	20.8	21.2	16.9	21.9	26	20.4	19.05	19.9	19.9	19.8	21.4
CaO	8.34	8.15	6.95	7.67	8.32	7.47	8.91	6.25	7.88	7.93	8.43	8.32	8.12	7.54
MgO	4.49	4.29	3.27	3.84	4.1	3.56	4.17	5.04	4.44	4.21	4.34	4.5	4.53	4.88
Na ₂ O	3.56	3.39	5.5	4.26	3.83	4.93	3.56	3.41	4.2	4.37	4.2	4.15	4.04	3.75
K ₂ O	1.9	1.72	1	1.56	1.56	1.12	1.65	1.29	0.99	0.98	0.88	0.96	1.02	1.1
TiO ₂	2.55	2.98	1.28	2.55	2.53	1.7	2.59	3.3	2.24	2.2	2.49	2.29	2.2	2.67
MnO	0.32	0.35	0.23	0.3	0.34	0.27	0.29	0.4	0.33	0.32	0.34	0.34	0.34	0.35
P ₂ O ₅	1.1	1.12	1.08	1.17	1.14	1.12	1.27	0.88	1.29	1.35	1.41	1.49	1.56	1.14
L.O.I.	1.11	0.37	1.37	0.87	0.43	1.05	0.47	0.69	1.01	0.91	0.84	0.8	0.83	0.53
S	0.02	0.05	0.04	0.02	0.04	0.04	0.2	0.04	0.04	0.03	0.02	0.03	0.04	0.04
TOTAL	100.33	100.55	99.10	100.77	100.46	99.71	100.54	100.16	100.31	99.74	100.66	100.88	100.15	100.57

Table 5.7 – Major element geochemistry of samples from Albite Pod #3 and Albite Pod #5 in wt. %. Total iron is reported as Fe₂O₃ and FeO is not included in the total.

Sample	AB-D-1	AB-D-2	AB-D-3	AB-D-4	AB-D-5	AB-D-6	AB-D-7	AB-D-8
Pod	Discovery Outcrop							
Block #	1	2	3	4	5	6	7	8
SiO ₂	51.3	48.6	49	48.3	44.3	46.3	45.8	45.4
Al ₂ O ₃	12.75	12.55	13.55	13.05	10.4	12.7	13.35	13.2
FeO	10.85	11.85	11.2	10.95	14.2	11.4	10.25	10.25
Fe ₂ O ₃	19.2	19.35	18.25	18.45	23.6	21.4	19.3	19.3
CaO	4.62	6.47	6.45	6.62	6.7	6.97	9.18	8.72
MgO	2.81	4.45	4.51	5.11	5.92	5.76	5.1	5.35
Na ₂ O	6.12	4.72	4.84	4.47	3.54	3.77	3.71	3.62
K ₂ O	0.44	0.51	0.51	0.62	0.65	0.8	0.71	0.82
TiO ₂	1.36	0.93	0.94	0.94	1.42	1.44	2.18	1.91
MnO	0.27	0.31	0.3	0.32	0.39	0.35	0.32	0.32
P ₂ O ₅	0.63	0.58	0.51	0.7	0.96	0.86	1.3	1.23
L.O.I.	0.82	0.39	0.44	0.55	0.8	0.73	0.35	0.53
S	0.64	0.54	0.54	0.41	0.69	0.27	0.13	0.12
TOTAL	100.14	99.01	99.40	98.99	98.57	100.62	101.08	99.99

Table 5.8 – Major element geochemistry of the Discovery Outcrop Albite Pod in wt. %. Total iron is reported as Fe₂O₃ and FeO is not included in the total.

Sample	IM-UM-10	IM-UM-11	IM-UM-12	IM-UM-16	IM-UM-17	IM-UM-18	IM-UM-19	IM-UM-2	IM-UM-20	IM-UM-3	IM-UM-4	IM-UM-7	IM-UM-8	IM-UM-9
Drillhole	G-10-16	G-10-16	G-10-16	G-10-17	G-10-17	G-10-17	G-10-17	G-10-04	G-10-17	G-10-04	G-10-04	G-10-16	G-10-16	G-10-16
Depth (m)	45	50	60	15.62	30	45	60	15	75.57	30.3	45	0	15	30.36
Description	Coarse grained gabbro with plagioclase alignment (2a)													
Ba	1010	873	1050	919	923	1040	1045	1035	1115	984	1495	1095	1060	990
Ce	172.5	161.5	178	165	171	185.5	180	165.5	189.5	177.5	199.5	168.5	169.5	168.5
Cr	10	10	10	10	10	10	10	10	10	10	10	10	10	10
Cs	2.18	1.48	2.02	2.64	1.98	3.35	2.76	1.86	3.65	2.16	3.39	3.83	2	1.61
Dy	6.95	6.6	7.17	6.81	7.06	7.56	6.9	6.72	7.59	7.23	7.84	7.12	6.83	6.74
Er	3.78	3.69	3.89	3.71	3.77	4.06	3.85	3.65	4.12	3.92	4.38	3.9	3.7	3.66
Eu	3.47	3.26	3.53	3.38	3.53	3.75	3.52	3.32	3.72	3.54	3.76	3.49	3.49	3.35
Ga	21.3	18.8	20.7	19.6	19.4	20.5	20.4	21	21.1	22.3	23.5	22.3	21.1	20.3
Gd	9.51	9.24	9.9	9.69	10.3	10.6	9.8	9.21	10.45	9.73	10.65	9.55	9.4	9.22
Hf	4.8	4.3	5	4.7	4.3	5.2	4.9	4.5	5.3	5.1	5.7	4.8	4.6	4.8
Ho	1.38	1.33	1.41	1.37	1.45	1.51	1.38	1.36	1.48	1.46	1.61	1.42	1.4	1.35
La	87	80.1	89.5	80.7	83.8	93.2	90.1	82.7	93.7	88.5	99.3	83.3	84	83
Lu	0.55	0.51	0.56	0.54	0.54	0.6	0.56	0.53	0.6	0.56	0.62	0.56	0.52	0.53
Nb	78.6	68.1	79.4	73.2	69.8	81.9	79.4	74.3	84.5	79.8	90.7	74.1	71.8	74.6
Nd	73.2	69.6	74.5	69.9	73.9	79	74.7	69.9	78.5	75.3	84.7	72.1	72.7	71
Pr	20	18.9	20.8	19.05	19.95	21.6	20.7	19.35	21.7	20.8	23.5	19.75	19.8	19.5
Rb	53.7	46.1	52	47.6	49.7	55.1	57.1	53.2	65.4	55.5	87.1	67.8	50	51.4
Sm	12	11.35	12.3	11.65	12.25	12.95	12.2	11.55	13.05	12.35	13.8	12	12.05	11.75
Sr	660	570	654	576	592	586	639	645	647	694	666	650	675	637
Ta	3.7	3.4	3.9	3.7	3.4	4.1	3.9	3.7	4	4	4.5	3.7	3.5	3.7
Tb	1.33	1.29	1.34	1.3	1.35	1.43	1.34	1.27	1.44	1.36	1.51	1.31	1.31	1.31
Th	9.17	8.26	9.48	8.88	8.19	10.05	9.46	9.12	9.83	9.81	11.4	9.4	8.99	9.11
Tm	0.56	0.51	0.57	0.54	0.55	0.57	0.56	0.54	0.6	0.56	0.63	0.55	0.53	0.51
U	2.77	2.48	2.88	2.65	2.47	2.97	2.78	2.69	3.02	2.93	3.37	2.74	2.61	2.95
V	679	780	673	750	770	699	722	751	688	748	698	933	661	737
Y	35	33.4	35.9	33.6	35	37.2	35.1	34.2	38	37	41.5	35.5	35	33.8
Yb	3.49	3.22	3.55	3.36	3.32	3.8	3.55	3.37	3.7	3.61	4.03	3.44	3.38	3.44
Zr	227	198	230	212	199	238	227	215	243	240	269	224	215	220
Cu	231	180	252	219	178	209	200	251	273	284	252	210	212	274
Pd	0.016	0.008	0.011	0.053	0.022	0.011	0.007	0.02	0.018	0.029	0.016	0.048	0.018	0.024
Pt	0.005	0.005	0.005	0.014	0.005	0.006	0.007	0.006	0.005	0.005	0.005	0.016	0.006	0.009
Ni	39	58	37	55	46	39	44	49	34	39	37	62	37	47

Table 5.9 – Trace element geochemistry of all plagioclase aligned gabbro samples (Unit 2a). All values are in parts per million (ppm).

Sample	IM-16	IM-40	IM-UM-13	IM-UM-14	IM-UM-21	IM-UM-22	IM-UM-5	IM-UM-6	IM-41	IM-UM-1	IM-UM-23
Drillhole	G-10-04	G-10-16	G-10-16	G-10-16	G-10-17	G-10-17	G-10-04	G-10-04	G-10-16	G-10-02	G-10-17
Depth (m)	62	86	69.64	85	90	100	50	60.38	154	30	175
Description	Medium grained homogenous gabbro (2b)								Medium grained homogenous troctolite (2c)		
Ba	1245	991	1200	1185	1095	1235	1080	1175	1015	1150	1150
Ce	214	190.5	203	209	191	216	193	212	197	220	207
Cr	10	10	10	10	10	10	10	10	20	20	20
Cs	2.42	3.49	2.79	3.85	3.91	3.97	2.72	2.43	3.82	1.84	4.08
Dy	8.66	7.95	7.81	8.16	7.61	8.46	7.81	8.48	8.07	9.29	8.26
Er	4.88	4.38	4.19	4.41	4.12	4.57	4.18	4.76	4.51	4.96	4.45
Eu	3.94	3.64	3.7	3.77	3.63	3.96	3.81	4.03	3.85	4.42	3.87
Ga	22.8	19.8	21.6	20.6	19.8	20.6	22.8	22.3	21.1	20.7	19.5
Gd	11.85	10.85	10.6	11.4	10.75	11.95	10.6	10.6	10.6	10.6	10.6
Hf	6.3	5.7	5.5	5.6	5.2	6	5.3	6	5.7	5.7	5.5
Ho	1.8	1.64	1.56	1.64	1.52	1.68	1.59	1.72	1.66	1.82	1.62
La	103.5	91	101	103.5	95.7	107	95.9	106	93.1	107.5	103
Lu	0.69	0.64	0.62	0.66	0.6	0.66	0.6	0.67	0.65	0.71	0.64
Nb	101	89.9	89.2	93.6	87.4	98.2	88.5	96.2	94	96.5	94.5
Nd	94.7	81.7	83.7	85.6	78.4	88.9	82.8	89.6	86.5	95.9	85.6
Pr	23.8	20.8	23.1	23.8	21.9	24.6	22.9	24.9	22	25.8	23.3
Rb	68.9	71.9	63.9	76.8	74.5	77.7	64.1	68.4	68.2	61.6	71.4
Sm	15.5	13.4	13.7	14.15	12.95	14.6	13.5	14.8	14.35	15.75	14.3
Sr	611	557	676	583	583	556	669	667	564	590	541
Ta	4.9	4.4	4.3	4.5	4.2	4.7	4.3	4.8	4.7	4.8	4.6
Tb	1.63	1.5	1.45	1.56	1.48	1.59	1.48	1.63	1.53	1.77	1.57
Th	12.55	11.65	10.9	11.2	10.35	11.1	10.35	12.3	10.9	10.2	10.45
Tm	0.7	0.65	0.63	0.65	0.6	0.69	0.6	0.69	0.65	0.72	0.67
U	3.56	3.27	3.21	3.27	3.08	3.31	3.08	3.57	3.21	3.02	3.03
V	560	515	635	549	605	650	654	603	602	579	487
Y	46.1	40.3	40	41.1	37.8	42.2	40.2	43.5	42.9	45.7	40
Yb	4.41	4.11	3.83	4.05	3.83	4.26	3.98	4.26	4.05	4.47	4.14
Zr	280	250	270	271	246	277	258	283	240	257	257
Cu	261	244	217	239	232	502	271	274	238	419	250
Pd	0.029	0.023	0.013	0.027	0.017	0.031	0.027	0.02	0.023	0.036	0.025
Pt	0.005	0.005	0.005	0.009	0.006	0.007	0.005	0.006	0.006	0.008	0.007
Ni	34	27	40	35	41	46	39	31	31	32	43

Table 5.10 – Trace element geochemistry of all medium grained homogeneous gabbro samples (Unit 2b), and medium grained homogenous troctolite samples (Unit 2c). All values are in parts per million (ppm).

Sample Drillhole	IM-14 G-10-17	IM-34 G-10-17	IM-35 G-10-17	IM-2 G-10-04	IM-20 G-10-04	IM-33 G-10-17	IM-38 G-10-17	IM-39 G-10-17	IM-5 G-10-04	IM-9 G-10-16
Depth (m)	178	150	176	76	116	148	202	206	118	122
Description	Heterogeneous gabbro w/ strong albite alteration (3a)			Heterogeneous w/ moderate albite alteration (3a)						
Ba	631	930	1035	1030	1220	886	953	869	1255	1085
Ce	114.5	173.5	206	165	201	182.5	147	154.5	216	182.5
Cr	57	30	10	18	10	20	10	10	16	21
Cs	2.53	2.83	3.94	1.51	4.13	3.37	2.01	2.8	2.69	5.65
Dy	5.08	7.09	8.17	6.77	8.16	7.3	6.29	6.27	8.61	7.78
Er	2.8	3.99	4.65	3.96	4.47	4.03	3.55	3.42	4.83	4.55
Eu	3.87	3.87	3.87	3.87	3.87	3.87	3.87	3.87	3.87	3.87
Ga	15.1	22.2	22.1	20.3	22.2	21.5	17.7	18.7	21.4	19.8
Gd	10.6	10.6	10.6	10.6	10.6	10.6	10.6	10.6	10.6	10.6
Hf	3.4	5	6.3	4.6	5.3	5.3	4.6	4.1	6.2	6
Ho	1.01	1.47	1.72	1.38	1.68	1.52	1.29	1.29	1.79	1.57
La	59.1	82.4	99.4	85.6	95.2	87.1	73.4	73	113	95
Lu	0.4	0.56	0.68	0.56	0.63	0.6	0.52	0.49	0.74	0.64
Nb	48.8	80.9	95.6	78.2	93.7	85.5	69.7	71	108.5	87.9
Nd	51.5	77.2	87.6	71.4	90.7	80.8	67.4	68.3	96	76.9
Pr	14.65	19.2	22.5	21	22.6	20.1	17.15	17.1	26.4	22.7
Rb	38.3	55.3	70	51	65.5	54	46	48.3	62.2	110.5
Sm	9.24	12.8	14.35	12.6	15.05	13.3	10.95	11.45	15.65	13.45
Sr	460	594	601	554	629	553	702	652	584	490
Ta	2.3	3.9	4.6	3.8	4.4	4.2	3.4	3.4	5.1	4.2
Tb	0.89	1.34	1.52	1.21	1.55	1.4	1.2	1.17	1.51	1.39
Th	5.66	9.5	13.3	9.43	10.1	10.75	8.57	7.83	12.9	11.05
Tm	0.37	0.56	0.68	0.53	0.64	0.58	0.5	0.48	0.71	0.6
U	1.42	2.72	3.72	2.28	2.88	2.97	2.43	2.25	3.78	2.88
V	615	938	516	819	514	858	448	429	414	591
Y	24.8	38	44.1	35	43.3	39.2	33	33.4	48.9	39.1
Yb	2.4	3.5	4.14	3.37	4	3.75	3.2	3.03	4.65	4.04
Zr	137	220	280	193	230	230	200	190	283	247
Cu	6383	956	257	1725	259	3392	2600	1856	368	285
Pd	1.075	0.089	0.023	0.106	0.027	0.323	0.298	0.199	0.041	0.053
Pt	0.071	0.007	0.005	0.013	0.005	0.019	0.015	0.012	0.009	0.01
Ni	20	61	28	60	33	83	94	91	28	34

Table 5.11 – Trace element geochemistry of heterogeneous gabbro samples (Unit 3a). The first three are highly albitized samples, while the last seven are samples which exhibited a moderate degree of alteration (both pink albitization, and green actinolite alteration). All values are in parts per million (ppm).

Sample Drillhole	IM-13 G-10-17	IM-17 G-10-04	IM-18 G-10-04	IM-25 G-10-16	IM-27 G-10-16	IM-3 G-10-04	IM-32 G-10-16	IM-40 G-00-03	IM-41 G-00-05	IM-42 G-02-01	IM-UM-25 G-00-03	IM-UM-26 G-06-03	IM-UM-27 G-00-04
Depth (m)	144	86	90	118	166	84	146	75	42.67	38.11	179.87	431.41	110.06
Description	Heterogeneous gabbro w/ weak albite alteration (3a)							Unmineralized skeletal (3b)			Unmineralized syenite (5a)		
Ba	1255	1020	912	919	797	904	902	107.5	104	135.5	345	289	338
Ce	203	171	176	202	135.5	161	195	20	40	20	10	10	10
Cr	5	20	20	10	30	17	30	6.29	5.25	3.74	3.45	5.38	1.56
Cs	2.89	2.81	1.86	5.05	4.74	2.32	4.87	4.58	4.26	5.64	13.9	11.95	12.35
Dy	8.61	7.2	7.01	7.98	5.69	6.37	7.67	1.99	2.03	2.79	4.94	5.05	4.04
Er	5.19	4.02	3.87	4.44	3.18	3.65	4.32	12.9	16.7	17	26.2	25.5	24.1
Eu	3.87	3.87	3.87	3.87	3.87	3.87	3.87	5.9	5.94	7.32	15.65	13.7	14.2
Ga	19.5	21.8	21.4	21.4	17.1	21.3	22.8	2.7	2.9	3.4	12.4	9.2	13.4
Gd	10.6	10.6	10.6	10.6	10.6	10.6	10.6	0.87	0.94	1.12	2.61	2.36	2.41
Hf	6.3	4.8	5.1	6	4.1	4.3	6.2	53.1	51.1	66.3	174	144.5	174.5
Ho	1.81	1.51	1.45	1.67	1.17	1.32	1.61	0.36	0.4	0.44	1.21	1.09	1.1
La	105.5	80.4	84	97.5	68.1	83.9	93.7	50.1	53.6	63.5	216	189.5	243
Lu	0.72	0.58	0.56	0.65	0.47	0.55	0.65	47.4	45.4	59.5	132.5	114.5	125
Nb	101	77.1	79.9	92.4	68.7	80	90.3	12.6	12.25	15.9	38.1	32.6	36.2
Nd	88.2	76.9	75.8	88.4	60.8	72.4	84.6	0.006	0.005	0.007	0.005	0.005	0.005
Pr	25.7	18.9	19.2	22.3	15.5	19.7	21.3	8.24	7.86	10.3	21.7	18.65	20.5
Rb	75.4	63.6	55.4	75.1	64.9	53.4	73.3	367	265	533	330	384	205
Sm	15.35	12.7	12.5	14.6	10.05	11.6	13.75	2	2.2	2.6	9	7.4	10.1
Sr	581	585	580	569	394	524	559	0.84	0.78	0.99	2.37	1.96	2.03
Ta	4.8	3.8	3.9	4.5	3.3	3.7	4.5	5.18	5.85	6.96	26.1	18.65	27.1
Tb	1.55	1.35	1.34	1.5	1.07	1.11	1.44	1.6	<0.5	<0.5	<0.5	0.5	<0.5
Th	12.5	9.43	10.1	11.7	8.57	9.53	12.25	0.4	0.35	0.45	1.16	1.05	1.04
Tm	0.69	0.58	0.56	0.65	0.46	0.53	0.64	1.63	1.79	2.04	7.39	5.8	8.27
U	3.26	2.7	2.85	3.22	2.43	2.72	3.41	271	705	313	6	7	26
V	353	860	821	651	625	992	864	2	1	1	2	2	2
Y	43.7	38.3	37.4	42.7	30.5	35.7	41.2	23.8	23.6	29.2	69.4	61.7	64.1
Yb	4.39	3.51	3.55	4.08	2.97	3.31	4.04	2.36	2.27	2.97	8	6.98	7.04
Zr	268	210	220	270	180	202	270	141	148	181	624	490	679
Cu	324	957	543	317	228	1550	1196	213	93	271	83	170	5
Pd	0.047	0.106	0.08	0.062	0.084	0.178	0.118	0.064	0.03	0.054	0.001	0.001	0.001
Pt	0.013	0.01	0.007	0.005	0.005	0.018	0.009	2	1	2	5	5	6
Ni	32	78	59	29	63	88	51	191	152	114	1	3	2

Table 5.12 – Trace element geochemistry of weakly albitized heterogeneous gabbro samples (Unit 3a), unmineralized skeletal troctolite (Unit 3b), and unmineralized syenite (Unit 5a). All values are in parts per million (ppm).

Sample Drillhole	IM-23 G-10-04	IM-24 G-10-04	IM-30 G-10-16	IM-31 G-10-16	IM-7 G-10-04	IM-10 G-10-16	IM-11 G-10-16	IM-26 G-10-16	IM-28 G-10-16	IM-29 G-10-16	IM-4 G-10-04
Depth (m)	146	148	200	206	150	138	172	136	168	170	100
Description	Skeletal w/ low actinolite alteration (3b)					Skeletal near fault (rubbly) (3b)					
Ba	565	719	871	612	743	828	670	943	761	576	847
Ce	113.5	114	211	137	109.5	110.5	119	184	138	114	183.5
Cr	40	30	10	20	21	20	36	20	40	70	30
Cs	4.3	6.12	5.85	4.58	4.38	1.82	2.68	1.68	2.8	3.26	1.87
Dy	5.01	4.92	8.49	6.18	4.67	4.64	5.11	7.46	6.04	4.95	6.59
Er	2.79	2.7	4.74	3.22	2.72	2.7	2.88	4.08	3.35	2.81	3.92
Eu	3.87	3.87	3.87	3.87	3.87	3.87	3.87	3.87	3.87	3.87	3.87
Ga	14.6	16.7	21.9	17	13.8	19.9	16.3	20.1	17.8	17.3	20.9
Gd	10.6	10.6	10.6	10.6	10.6	10.6	10.6	10.6	10.6	10.6	10.6
Hf	3.8	3.1	6.3	3	3.2	3.7	3.3	5.1	3.9	3.4	5.3
Ho	1.06	1.01	1.76	1.25	0.96	0.97	1.03	1.56	1.24	1.05	1.39
La	57.1	56.9	100	66.4	57	57.6	60.7	86.7	67.9	56	95.4
Lu	0.42	0.37	0.68	0.43	0.38	0.39	0.4	0.58	0.47	0.41	0.58
Nb	52.2	50.7	102.5	46	48.1	59.2	54.1	79.9	61.6	56.9	87.8
Nd	52	53.2	93.1	70.1	47.3	47.4	53.1	79.8	64.6	53.6	78.6
Pr	13.05	13.3	23.3	16.65	13.9	14.1	15.2	20.1	16.25	13.25	22
Rb	41.8	38.5	64.5	47.4	41.4	52.4	40	49.9	52.4	42.2	46.9
Sm	8.56	8.83	15.4	11.8	8.3	8.23	9.24	13.1	10.85	8.95	12.7
Sr	409	604	546	582	442	350	471	599	407	375	469
Ta	2.6	2.5	5	2.2	2.3	2.9	2.6	4	3	2.8	4.4
Tb	0.96	0.95	1.6	1.16	0.83	0.84	0.94	1.43	1.18	0.96	1.19
Th	7.24	6.1	11.85	5.36	6.45	6.17	6.02	10.55	7.59	6.44	12.45
Tm	0.42	0.38	0.67	0.45	0.36	0.37	0.37	0.59	0.47	0.4	0.57
U	2.01	1.74	3.31	1.54	1.54	1.54	1.45	2.95	2.13	1.81	3.56
V	544	576	501	597	315	1530	603	679	909	1020	1100
Y	26.1	26.2	46.4	33	23.6	23.5	26	38.9	31.7	26.7	37.8
Yb	2.61	2.36	4.23	2.78	2.38	2.4	2.44	3.71	2.97	2.52	3.65
Zr	160	140	280	130	134	154	134	220	160	150	239
Cu	2001	7220	4432	4249	11203	793	6676	605	2208	1819	13243
Pd	1.115	1.585	0.316	0.596	1.685	0.178	1.32	0.054	0.39	0.417	1.32
Pt	0.062	0.066	0.023	0.05	0.075	0.017	0.061	0.005	0.023	0.024	0.092
Ni	119	200	127	157	252	98	164	44	93	129	276

Table 5.13 – Trace element geochemistry of skeletal troctolite samples (Unit 3b). The first are weakly altered skeletal troctolites, while the next six are skeletal troctolites which were sampled within 2 m of faulted (and very rubbly) drill core. All values are in parts per million (ppm).

Sample Drillhole	IM-12 G-10-16	IM-15 G-10-17	IM-19 G-10-04	IM-21 G-10-04	IM-22 G-10-04	IM-36 G-10-17	IM-37 G-10-17	IM-6 G-10-04	IM-8 G-10-04	IM-UM-15 G-10-16	IM-UM-24 G-10-17
Depth (m)	202	196	102	126	128	192	194	126	152	224	246.5
Description	Skeletal w/ moderate to high actinolite alteration (3b)								Basal gabbro (3c)	Mineralized syenite (5a)	
Ba	698	965	706	581	522	738	523	602	689	1840	1640
Ce	111.5	147.5	121.5	112	118.5	136	113.5	106.5	116	365	397
Cr	10	22	170	40	20	30	70	32	5	10	10
Cs	4.01	2.14	1.54	3.54	3.53	2.93	3.06	2.56	5.53	1.19	1.35
Dy	4.89	6.04	5.29	4.86	5.22	5.96	4.69	4.6	5.14	11.95	12.25
Er	2.82	3.3	2.88	2.71	2.9	3.28	2.62	2.65	2.91	6.86	7.23
Eu	3.87	3.87	3.87	3.87	3.87	3.87	3.87	3.87	3.87	3.87	3.87
Ga	15	19.2	22.4	15.5	15.3	17.9	15.7	14.6	14.7	23.4	24.1
Gd	10.6	10.6	10.6	10.6	10.6	10.6	10.6	10.6	10.6	10.6	10.6
Hf	3.4	3.9	4.2	3.4	3.5	4	3.2	3	3.4	15.3	18.2
Ho	0.97	1.23	1.08	1	1.09	1.24	0.97	0.95	1.01	2.48	2.55
La	57.6	76.7	59.9	55.6	58.7	68	55.7	54.8	59.8	189	206
Lu	0.42	0.5	0.43	0.39	0.42	0.49	0.39	0.38	0.4	1.06	1.16
Nb	49.4	73	66.5	53.1	50.8	67.3	54.1	47.1	51	241	283
Nd	48.5	68.1	56	52.4	55.8	62	51.8	47	51.7	127.5	135.5
Pr	14.25	18	14.1	12.9	13.8	15.6	13.05	13.65	15.15	38.9	40.8
Rb	54	40.4	38.8	41.3	41.8	50.4	40.1	37.6	60.1	164	173
Sm	8.67	10.75	9.27	8.66	9.39	10.4	8.56	8.39	9.39	19.55	20.7
Sr	458	713	442	409	484	478	330	366	497	234	199
Ta	2.3	3.5	3.5	2.5	2.5	3.2	2.6	2.2	2.4	11.8	14
Tb	0.88	1.08	0.98	0.91	1	1.12	0.89	0.83	0.93	2.2	2.28
Th	6.2	8.31	7.45	6.45	6.77	8.36	6.49	5.65	6.04	30.5	35.1
Tm	0.39	0.47	0.42	0.38	0.41	0.47	0.38	0.34	0.38	1.05	1.14
U	1.56	2.31	2.14	1.87	1.9	2.28	1.85	1.31	1.49	9.06	10.35
V	391	410	2020	634	472	669	817	536	372	25	22
Y	24.6	33.1	27.8	25.8	27.3	31.9	25.6	22.9	25.8	62	64
Yb	2.56	3.1	2.68	2.49	2.58	2.97	2.38	2.16	2.48	6.77	7.41
Zr	149	175	180	150	150	180	150	121	137	731	881
Cu	3229	3770	1427	5069	3704	607	2599	4149	12677	2270	2570
Pd	0.584	0.427	0.391	0.724	0.544	0.18	0.71	0.97	1.31	0.356	0.325
Pt	0.048	0.023	0.029	0.033	0.051	0.01	0.044	0.035	0.083	0.022	0.017
Ni	178	155	133	147	168	85	140	147	260	21	27

Table 5.14 – Trace element geochemistry of: skeletal troctolite samples (Unit 3b) which exhibit a high degree of actinolite alteration, basal fine grained gabbro (Unit 3c), and mineralized syenite that is in contact with the overlying mineralized gabbro (Unit 5). All values are in parts per million (ppm).

Sample	AB-3-1	AB-3-2	AB-3-3	AB-3-4	AB-3-5	AB-3-6	AB-3-7	AB-5-1	AB-5-2	AB-5-3	AB-5-4	AB-5-5	AB-5-6	AB-5-7
Pod	Albite Pod #3							Albite Pod #5						
Block #	1	2	3	4	5	6	7	1	2	3	4	5	6	7
Ba	1210	1080	649	870	965	694	1035	910	931	916	905	909	948	978
Ce	177	168.5	256	203	183.5	246	179.5	188	207	208	204	212	214	191
Cr	30	30	10	20	20	10	10	60	20	10	10	10	10	20
Cs	4.5	3.14	1.04	2.07	2.76	1.31	2.61	2.86	3.9	2.98	2.1	2.27	2.55	2.8
Dy	7.18	6.96	10.05	8.2	7.68	10.1	7.94	7.76	8.39	8.72	8.72	8.66	9.04	8.25
Er	3.93	3.7	5.56	4.39	4.15	5.57	4.28	4.42	4.62	4.73	4.73	4.79	4.77	4.55
Eu	3.12	3.34	3.74	3.61	3.42	3.78	3.9	3.56	4.06	4.11	4.19	4.19	4.26	3.83
Ga	22.1	23.4	21.9	23.7	22.7	22.6	23.1	23.6	22	21.7	22.6	22.1	21.8	22.4
Gd	9.94	9.6	13	11.2	10.55	13.1	11.35	10.5	11.8	12.05	12.35	12.6	12.85	11.7
Hf	4.7	5	7.3	5.7	5.3	7.2	4.8	5.8	5.1	5.1	5.1	5.2	5.4	5.3
Ho	1.47	1.39	2.03	1.65	1.56	2.03	1.57	1.54	1.74	1.73	1.74	1.76	1.79	1.67
La	91.2	84.8	141.5	107	95.4	134	90	96.3	105.5	105	102.5	107.5	106.5	98
Lu	0.56	0.55	0.82	0.65	0.6	0.81	0.61	0.65	0.66	0.64	0.68	0.66	0.68	0.65
Nb	79.5	83.7	127	102.5	92.6	122.5	85.8	96.9	90.7	87.7	92.4	89.2	88.6	95.4
Nd	79	76.4	107	88.4	82.9	104	82.5	81.4	94.8	94.3	93.4	95.1	95.9	84.5
Pr	21.3	20.3	29.6	24.6	21.8	29	21.7	22.4	25.1	25.2	24.9	25.8	26	23
Rb	68.9	63.5	30.2	54.7	57.9	36.3	62.4	46.2	37.7	36.1	32.4	35.7	39.3	43.1
Sm	12.85	12.5	16.85	14.45	13.3	16.75	13.65	13.3	15.1	15.35	15.4	15.65	15.3	13.65
Sr	441	523	606	535	586	587	598	525	644	639	650	644	660	600
Ta	3.8	4.1	5.7	4.7	4.4	5.7	4.1	4.6	4.2	4.2	4.3	4.3	4.3	4.6
Tb	1.35	1.27	1.83	1.53	1.43	1.83	1.48	1.4	1.58	1.6	1.65	1.63	1.67	1.55
Th	9.02	8.84	15.5	11.05	9.94	15.15	8.5	12.15	10	10.25	9.45	10.35	10.3	9.94
Tm	0.56	0.53	0.81	0.64	0.58	0.8	0.59	0.62	0.65	0.65	0.67	0.67	0.7	0.65
U	2.38	2.39	3.7	2.85	2.59	3.76	2.52	3.39	2.84	2.89	2.7	2.87	2.97	2.93
V	855	1010	241	880	755	360	746	1270	604	531	651	580	553	770
Y	37.7	35.9	53	43	39.7	51.7	40.5	40.8	45.1	44.5	45.5	46.1	46.3	42.3
Yb	3.57	3.49	5.18	4.16	3.71	5.13	3.82	3.99	4.19	4.2	4.22	4.26	4.29	4.03
Zr	220	226	354	269	247	342	222	281	247	231	234	243	249	252
Cu	201	670	776	439	625	914	2970	439	366	285	202	357	361	370
Pd	0.016	0.134	0.009	0.01	0.046	0.008	0.386	0.251	0.05	0.046	0.029	0.035	0.023	0.087
Pt	0.005	0.008	0.005	0.005	0.005	0.005	0.024	0.014	0.006	0.007	0.007	0.009	0.007	0.007
Ni	50	62	29	47	49	32	66	90	43	33	28	32	32	44

Table 5.15 – Trace element geochemistry of samples from Albite Pod #3 and Albite Pod #5. All values are in parts per million (ppm).

Sample	AB-D-1	AB-D-2	AB-D-3	AB-D-4	AB-D-5	AB-D-6	AB-D-7	AB-D-8
Pod	Discovery Outcrop							
Block #	1	2	3	4	5	6	7	8
Ba	345	757	846	872	732	874	799	832
Ce	205	202	192	177	185.5	155	156.5	145
Cr	10	10	10	10	10	10	20	20
Cs	0.61	1.96	2.09	1.92	1.88	2.47	2.67	2.9
Dy	9.4	8.11	7.55	7.3	7.9	6.6	6.81	6.26
Er	5.58	4.75	4.37	4.15	4.42	3.68	3.64	3.43
Eu	3.23	3.53	3.25	3.17	3.2	3.04	3.38	3.17
Ga	20.9	19.6	20	19.2	18.1	19	20.1	20
Gd	11.4	10.55	9.58	9.61	10.75	9.2	10.2	9.34
Hf	10.5	7.5	7.4	6.4	6.4	5.4	4.7	4.1
Ho	1.93	1.67	1.55	1.51	1.63	1.34	1.36	1.28
La	102.5	106	102	91.8	94.6	80	79.5	73.6
Lu	0.88	0.74	0.68	0.64	0.65	0.54	0.49	0.48
Nb	150.5	103	106.5	91.9	100	83.3	76.9	73.7
Nd	85.9	82.8	78	71.9	79.9	65.7	71.2	65
Pr	24.2	23.3	22.3	20.5	22.1	18.4	19	17.65
Rb	11.8	17.3	21.2	26.1	28.2	35	32.1	37.7
Sm	14.05	13.3	12.25	11.5	12.85	10.65	11.55	10.7
Sr	458	748	792	723	535	658	716	703
Ta	7.6	5	5.1	4.6	4.9	4	3.6	3.3
Tb	1.67	1.48	1.36	1.34	1.47	1.23	1.31	1.23
Th	26.3	14.5	15.8	13.6	12.4	10.9	8.37	7.99
Tm	0.81	0.69	0.66	0.61	0.64	0.54	0.51	0.48
U	5.65	4	4.47	3.82	3.59	3.2	2.42	2.27
V	198	171	180	201	339	320	562	465
Y	49	44.1	41.2	39.1	41.8	35	35.4	33.3
Yb	5.51	4.53	4.24	3.98	4.18	3.51	3.19	3.05
Zr	506	372	369	307	310	267	217	190
Cu	9750	11600	11550	9420	13700	6590	3580	3580
Pd	1.255	2.66	1.2	1.055	1.96	0.906	0.494	0.506
Pt	0.077	0.112	0.081	0.075	0.097	0.058	0.033	0.034
Ni	299	301	253	226	334	212	129	129

Table 5.16 – Trace element geochemistry of the Discovery Outcrop Albite Pod. All values are in parts per million (ppm).

Sample	IM-3	IM-8	IM-12	IM-29	IM-32	IM-37	IM-38	IM-UM-15	IM-UM-24
Drillhole	G-10-04	G-10-04	G-10-16	G-10-16	G-10-16	G-10-17	G-10-17	G-10-16	G-10-16
Depth (m)	84	152	202	170	146	194	202	224	246.5
Lithology	3a	3c	3b	3b	3a	3b	3a	5a	5a
Au	10.00	113.00	103.00	31.90	23.60	49.10	19.00	20.40	27.30
Ir	0.05	0.04	0.02	0.03	0.02	0.04	0.02	0.01	0.01
Pd	173	1346	713	455	134	649	303	368	338
Pt	12.90	81.70	31.00	27.00	9.77	43.90	16.30	22.70	18.00
Rh	4.01	8.21	6.72	4.46	2.28	8.71	4.00	0.04	0.21
Ru	0.09	0.33	0.37	0.96	0.17	1.12	0.23	0.08	0.08

Table 5.17 – PGE data for a sample suite chosen based on high Pd values. All values are in parts per billion (ppb).

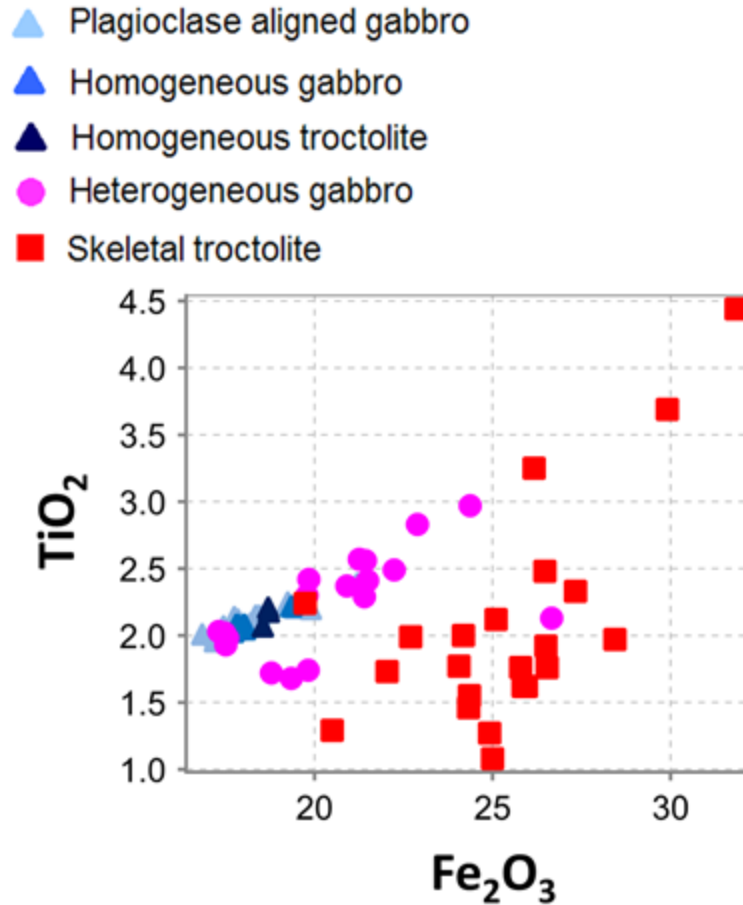


Figure 5.1 – A plot of Fe_2O_3 versus TiO_2 . With the exception of skeletal troctolite samples (and some heterogeneous gabbro samples that contained lenses of skeletal troctolite), samples show a linear correlation between Ti and Fe which indicates that Ti is all contained in magnetite. Units for the oxides are in wt. % and the Mg # is the molar $\text{Mg}/(\text{Mg}+\text{Fe})$ ratio.

5.1.1 Down-hole Whole Rock Geochemistry

Whole rock major element geochemistry down each study drill hole is shown on Figures 5.2 – 5.4, and whole rock trace element geochemistry down each study drill hole is shown on Figures 5.5 – 5.7. While the sampling strategy was not to continuously sample down each drill hole in equal intervals, there are still enough data points to adequately describe down-hole major and trace element variations caused by certain phenomenon, including new intrusions of magma or an abundance of by secondary alteration.

In Figures 5.2 to 5.4, a few recurring trends are discernable. Within the unmineralized gabbros, major element abundances are nearly constant, and are generally unchanged, with the exception of an increase in SiO_2 and Na_2O that is observed at the contact

between plagioclase aligned gabbro (in red) and homogeneous gabbro (in orange) in Figure 5.2 and Figure 5.3. However, the range in variation is quite small and a similar variation is not observed in Figure 5.4. In Figure 5.3, at approximately 50 m depth, there is a small spike in the MgO content (slightly more than 1% MgO than proximal samples). This same sample point exhibits a negligible change in Mg #, which is in agreement with the petrological observation that the sample merely contains more clinopyroxene relative to other proximal samples.

The most obvious major element variations are observed within the alternating intervals of heterogeneous gabbro and skeletal troctolite (the lithologies shown in light and dark purple respectively). In all of Figures 5.2 – 5.4, there is a clear decrease in SiO₂, Na₂O, and K₂O within intervals of skeletal troctolite (in dark purple), but an increase in MgO, TiO₂, and Fe₂O₃. These are attributed to abundant skeletal olivine, skeletal magnetite, and clinopyroxene relative to plagioclase within the skeletal troctolite samples. The variation in Mg # between heterogeneous gabbro and skeletal troctolite samples is much more gradual and less saw-tooth patterned in Figures 5.2 to 5.4. Overall, with the exception of skeletal troctolite sample points, the range in major element data between plagioclase aligned gabbro, homogeneous gabbro, homogeneous troctolite, and heterogeneous gabbro is small and hence, these units are geochemically similar. The skeletal troctolite samples (as well as the lone basal fine-grained gabbro sample in Figure 5.2) are generally more enriched in MgO, Fe₂O₃, TiO₂ and have greater Mg-numbers, but are more depleted in SiO₂, CaO, Na₂O and K₂O than the rest of the dataset.

Figures 5.5 – 5.7 also show very limited trace element variations between the plagioclase aligned gabbro, homogeneous gabbro, homogeneous troctolite, and heterogeneous gabbro. Skeletal troctolite samples on average have lower concentrations of trace elements than all of the other lithologies. For example, the highest concentration of Zr in any sample in Figure 5.5 is 283 ppm which occurs within medium-grained homogeneous gabbro at 60.38 m, while the lowest concentration of 121 ppm occurs within skeletal troctolite at 126 m.

In order to negate any influence alteration may have played the relative gain or loss of major elements, Figures 5.8 – 5.10 show down-hole plots compared to CIPW norm calculated values. CIPW norm values were calculated for anorthite, albite, magnetite, and diopside using the method outlined in Winter, 2014. In Figure 5.8 (hole G-10-04), anorthite content shows little variation from top to bottom, whereas the albite content fluctuates, particularly at ~115 m where it reaches a maximum value within heterogeneous gabbro. Magnetite content is steady within heterogeneous and homogeneous gabbro, but fluctuates greatly between heterogeneous gabbro and skeletal troctolite. Diopside content also fluctuates, particularly between heterogeneous and skeletal troctolite samples. Similar trends are seen in Figures 5.9 and 5.10, with relatively consistent values of anorthite, albite, magnetite and diopside within plagioclase aligned and homogeneous gabbros. The greatest fluctuations in data are seen again within heterogeneous gabbro and skeletal troctolite.

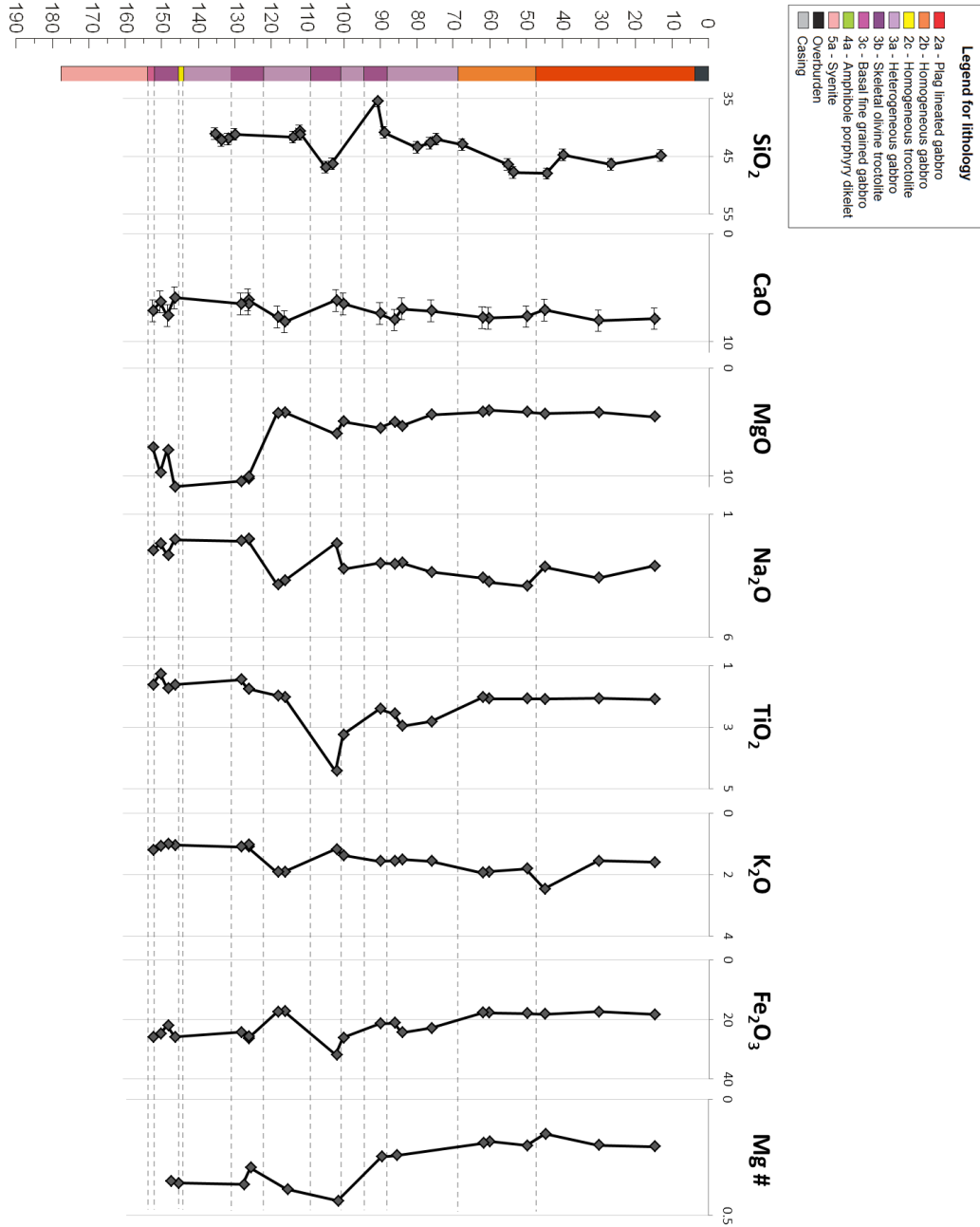


Figure 5.2 – Down-hole plot of major elements for drill hole G-10-04, and additionally, the down-hole variation in Mg #. Units for the oxides are in wt. % and the Mg # is the molar Mg/(Mg+Fe) ratio. The y-axis is depth in meters.

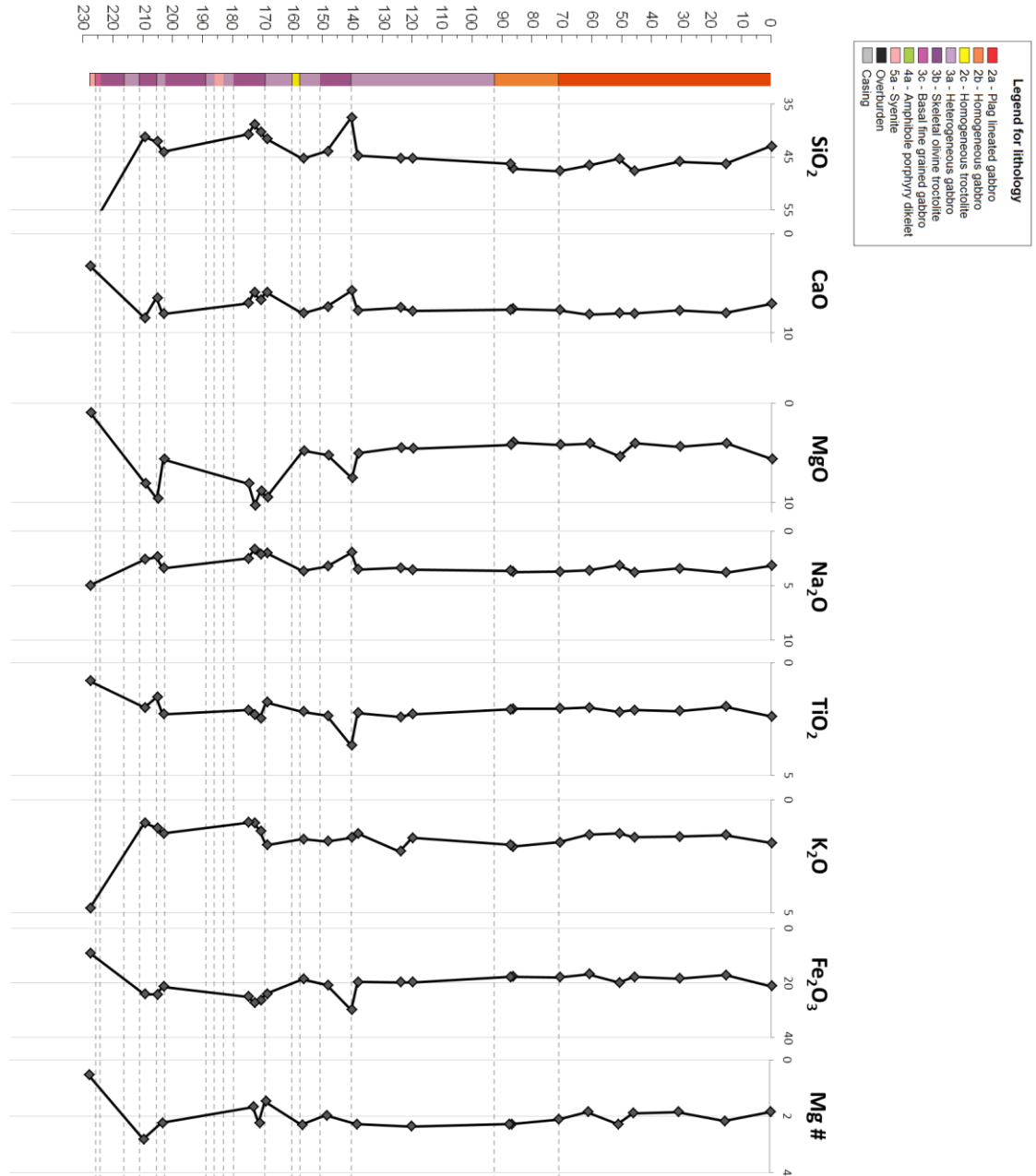


Figure 5.3 – Down-hole plot of major elements for drill hole G-10-16, and additionally, the down-hole variation in Mg #. Units for the oxides are in wt. % and the Mg # is the molar Mg/(Mg+Fe) ratio. The y-axis is depth in meters.

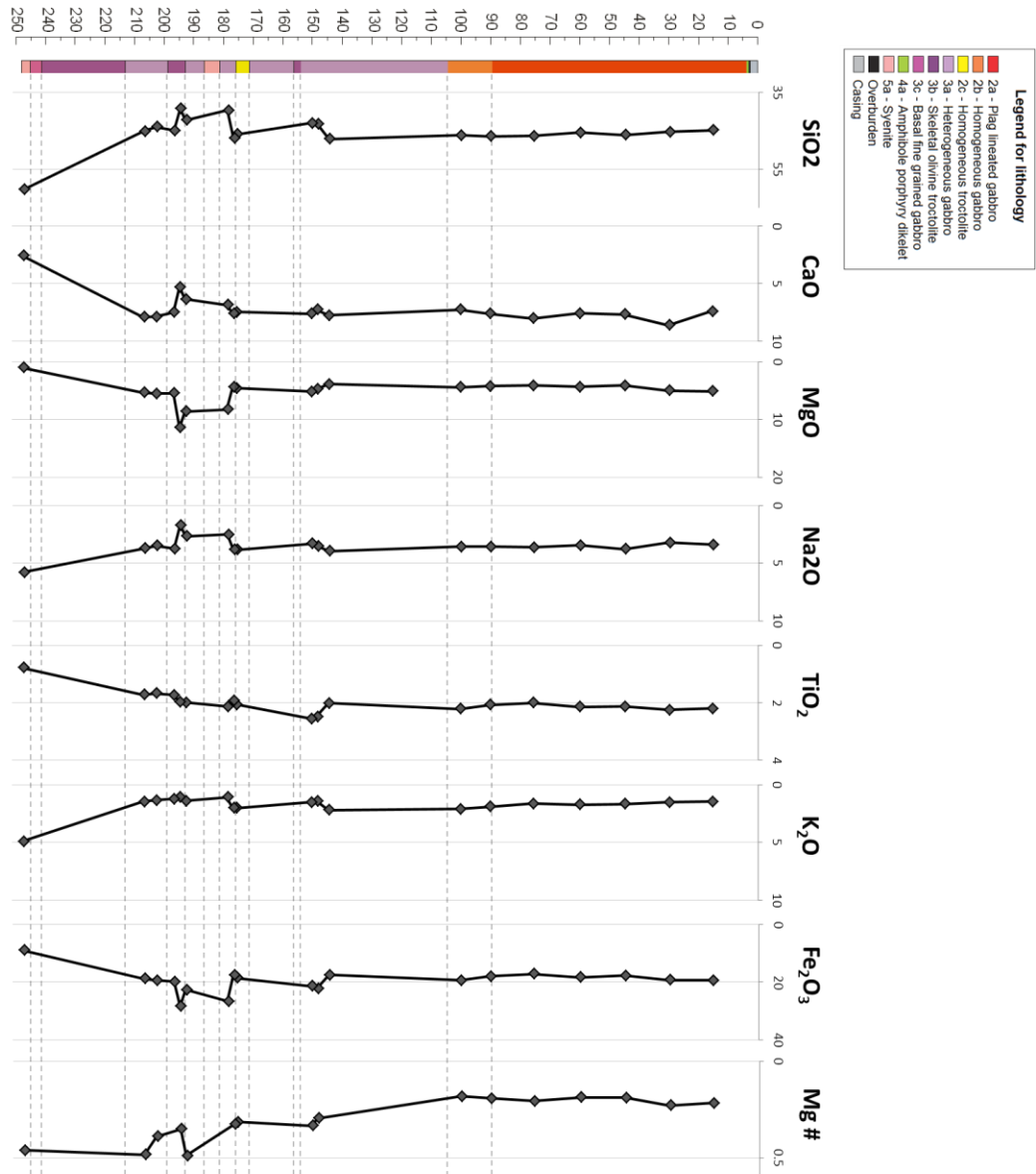


Figure 5.4 – Down-hole plot of major elements for drill hole G-10-17, and additionally, the down-hole variation in Mg #. Units for the oxides are in wt. % and the Mg # is the molar Mg/(Mg+Fe) ratio. The y-axis is depth in meters.

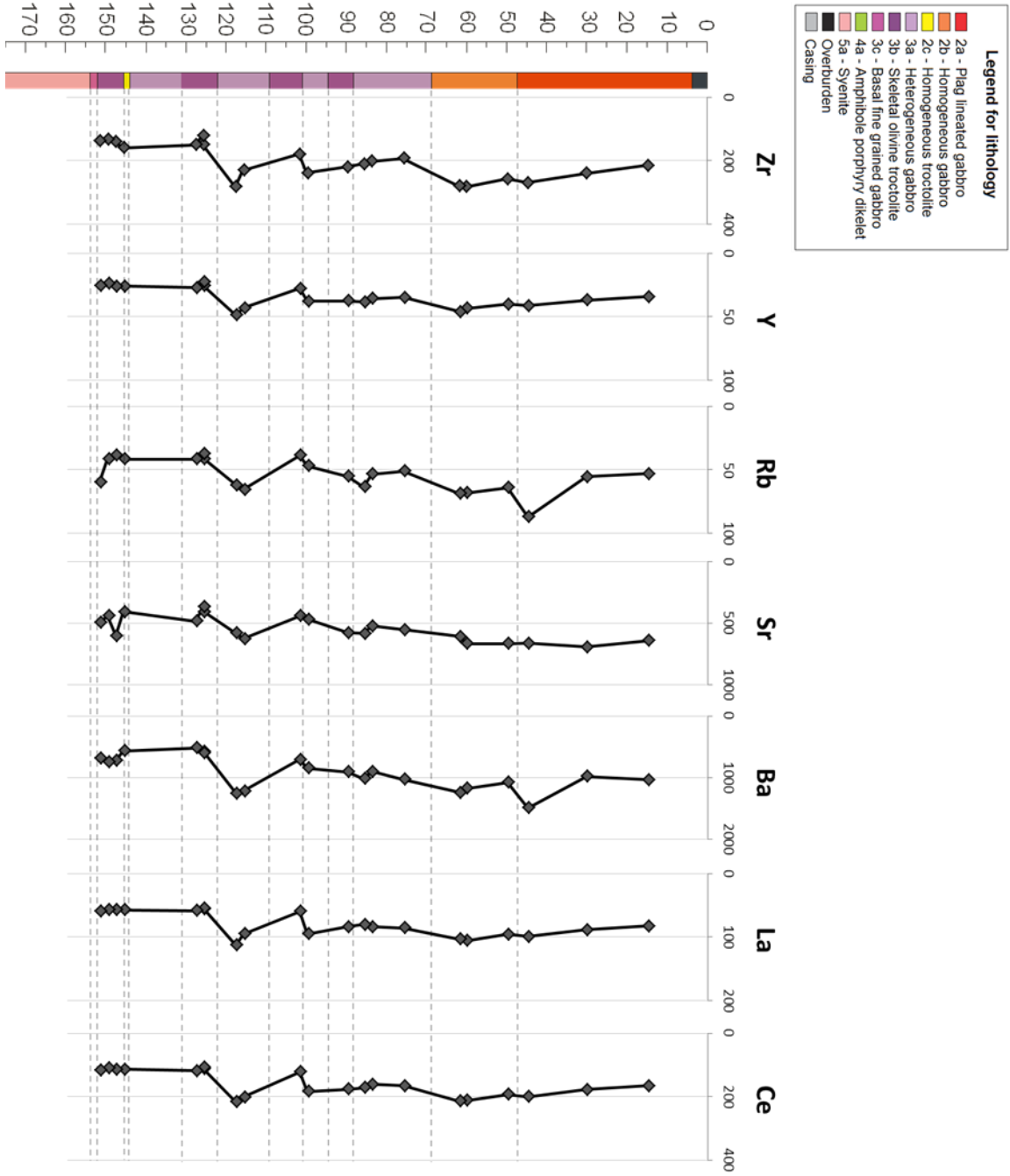


Figure 5.5 – Down-hole plot of trace elements for drill hole G-10-04. The x-axis is in parts per million (ppm), and the y-axis is in meters.

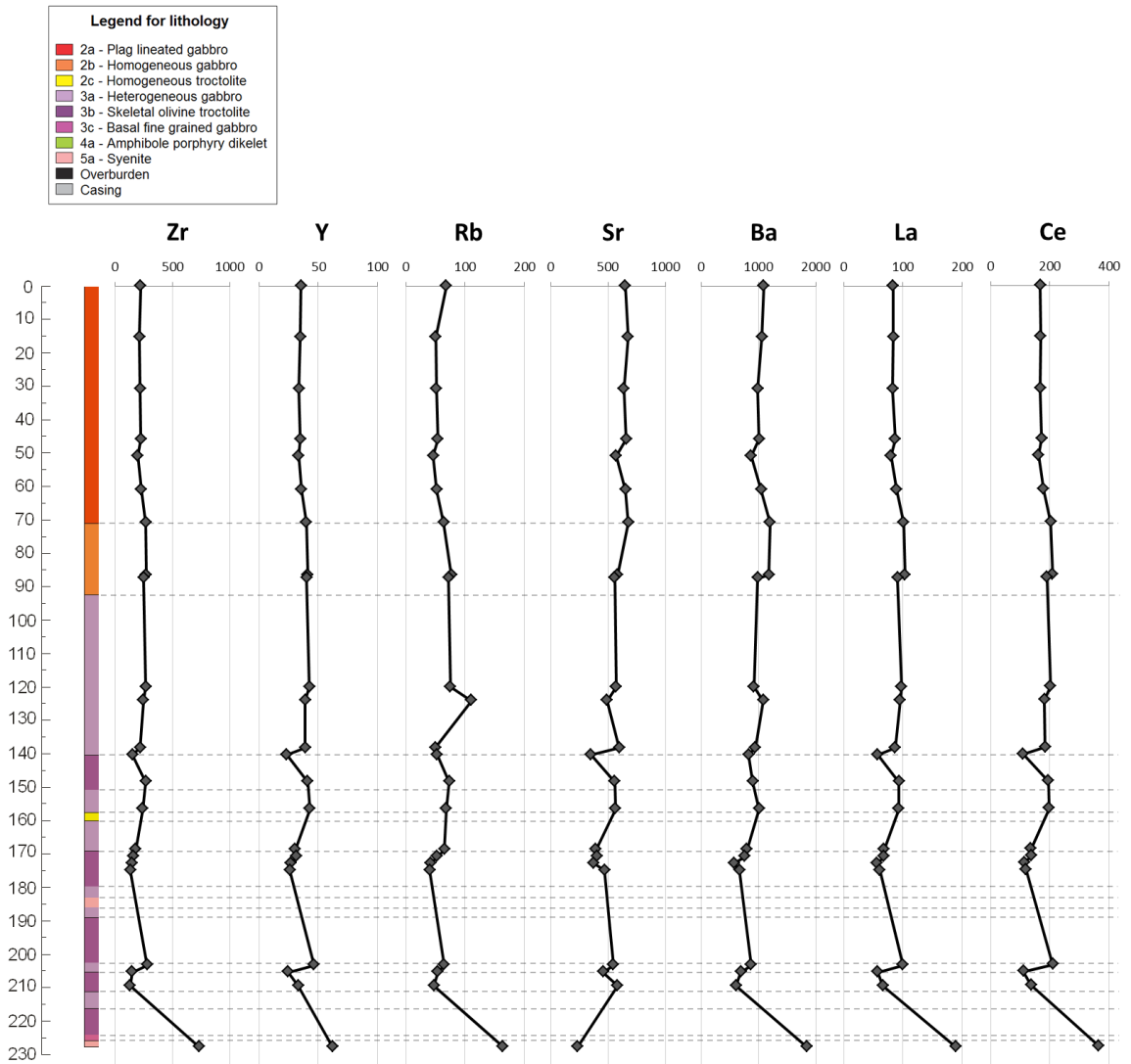


Figure 5.6 – Down-hole plot of trace elements for drill hole G-10-16. The x-axis is in parts per million (ppm), and the y-axis is in meters.

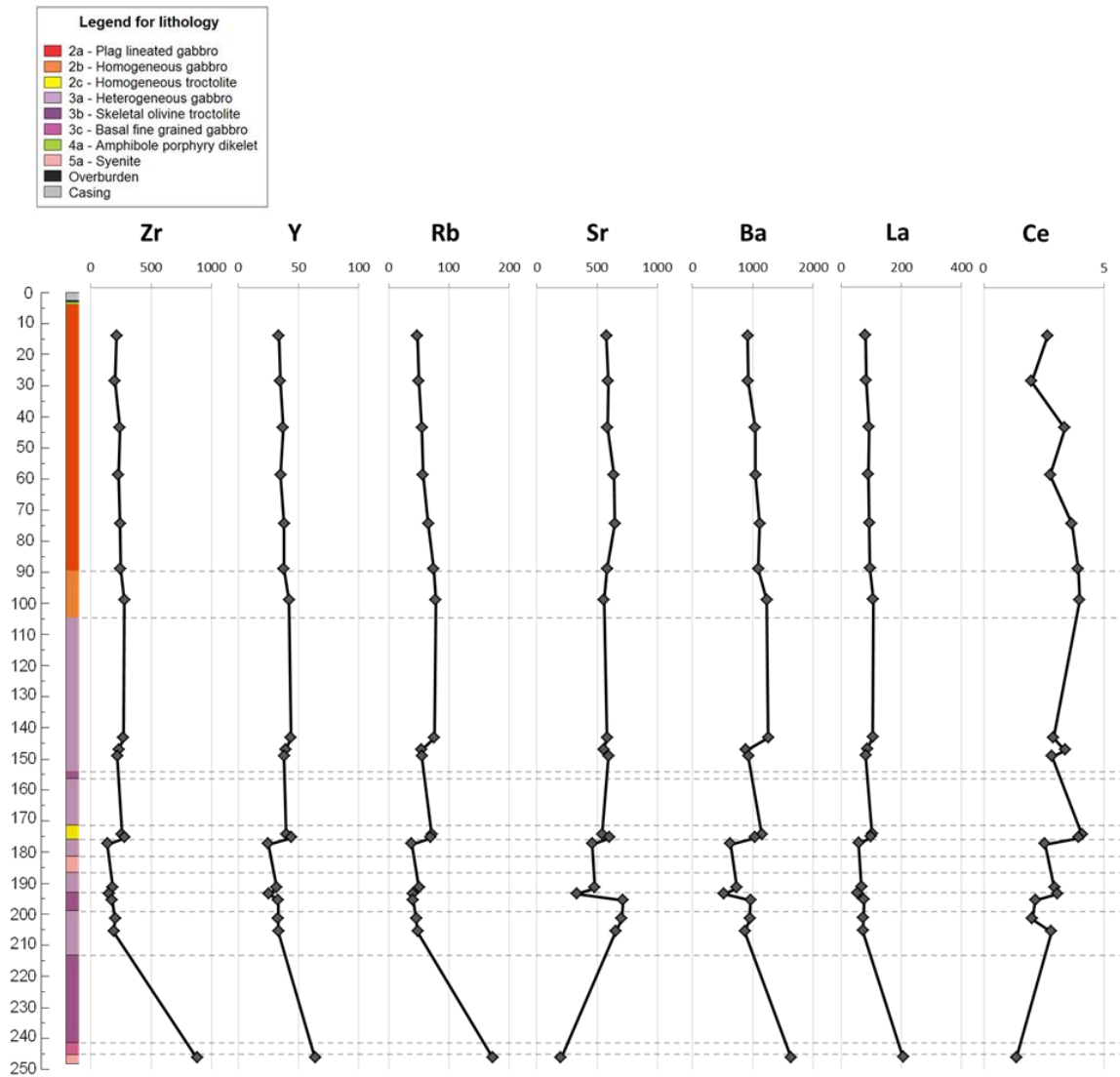


Figure 5.7 – Down-hole plot of trace elements for drill hole G-10-17. The x-axis is in parts per million (ppm), and the y-axis is in meters.

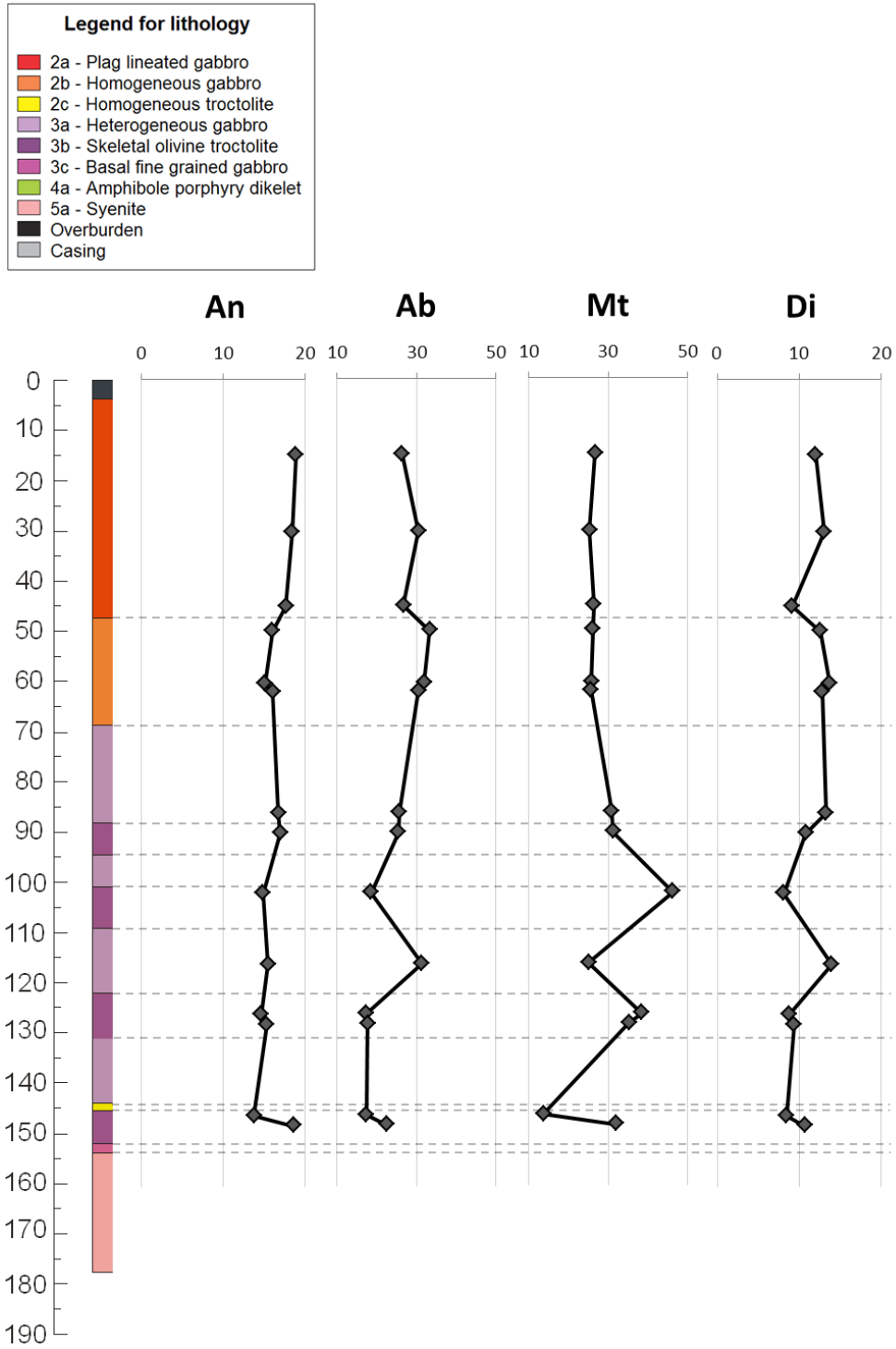


Figure 5.8 – CIPW normalized values for anorthite (An), albite (Ab), magnetite (Mt), and Diopside (Di) plotted versus decreasing depth in drill hole G-10-04. The x-axis is the calculated modal % for each mineral. The y-axis is depth in meters.

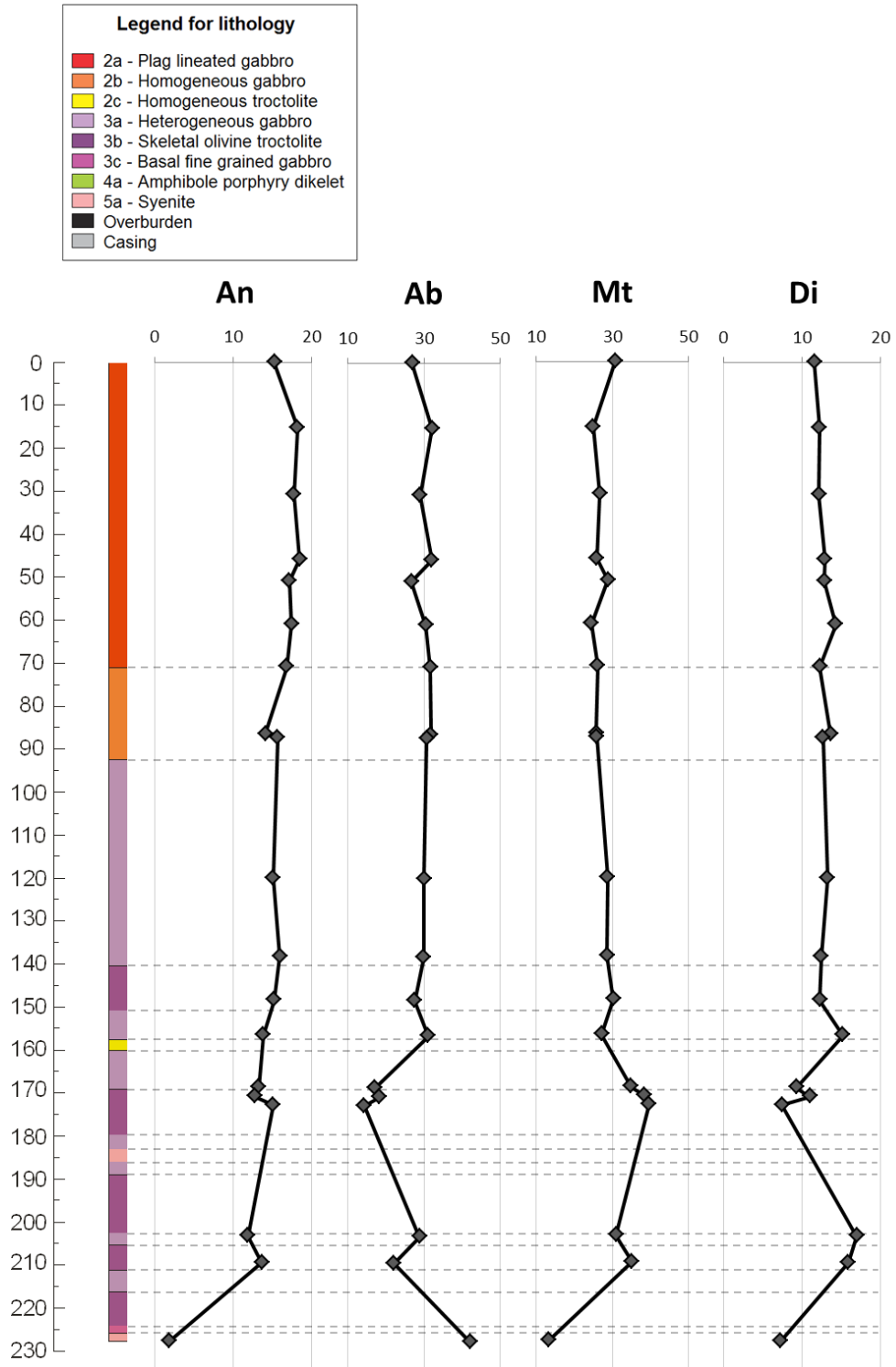


Figure 5.9 – CIPW normalized values for anorthite (An), albite (Ab), magnetite (Mt), and Diopside (Di) plotted versus decreasing depth in drill hole G-10-16. The x-axis is the calculated modal % for each mineral. The y-axis is depth in meters.

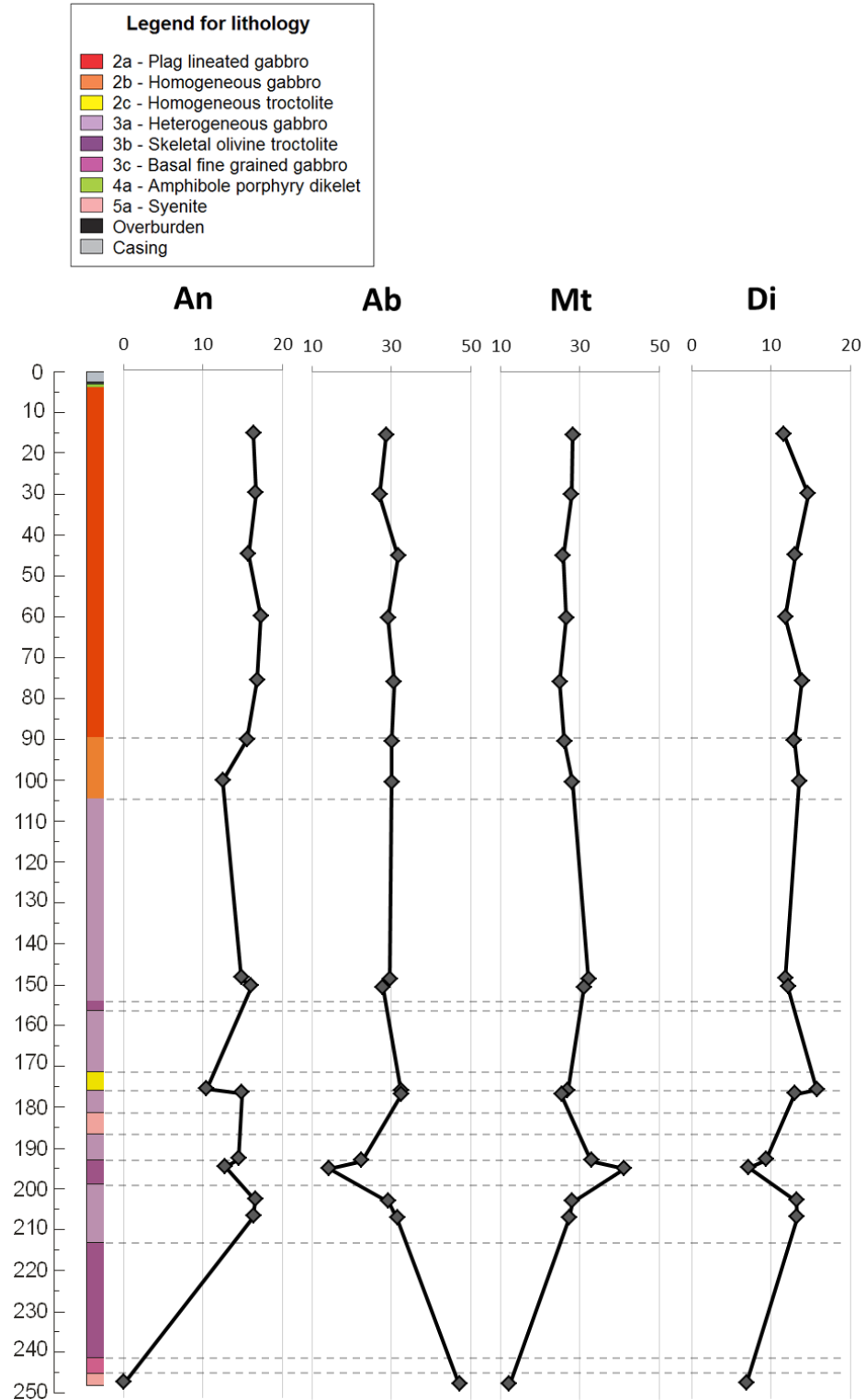


Figure 5.10 – CIPW normalized values for anorthite (An), albite (Ab), magnetite (Mt), and Diopside (Di) plotted versus decreasing depth in drill hole G-10-17. The x-axis is the calculated modal % for each mineral. The y-axis is depth in meters.

5.1.2 Albite Pod Transect Geochemistry

The variations in major element geochemistry of the albite pods are shown in Figures 5.11 to 5.13. Figure 5.11 shows Albite Pod #3, where seven equal sized blocks that represent various levels of alteration were analyzed. The most altered region (block 3) contains relative enrichment in SiO_2 , Na_2O and a very slight enrichment in Al_2O_3 . However, there is a marked decrease in Fe_2O_3 , TiO_2 , and K_2O . In Figure 5.12, Albite Pod #5 shows very little major element variation altogether. Block #1 contains the least amount of SiO_2 , Al_2O_3 , and Na_2O , but contains the most MgO , Fe_2O_3 , Na_2O , TiO_2 , and K_2O . The remaining samples indicate little to no major element variation. The Discovery Outcrop Albite Pod (Figure 5.13) shows the most major element variation, which mostly corresponds to the intensity of alteration. SiO_2 and Na_2O values are highest in Block 1 (the most altered block), and these values steadily decrease down the transect towards Block 8, with the exception of Block #5 which has very low values of SiO_2 and Na_2O relative to all other blocks. Of particular note is the decrease in Al_2O_3 within Block 5, and the increase in Fe_2O_3 . In thin section, these anomalous values are the result of relatively abundant skeletal olivine in Block 5, which also corresponds to a local increase in MgO . The amount of albitization generally decreases steadily from Block 1 (which is the most albitized block) to Block 8 (the least albitized block).

The variation in trace element geochemistry of the albite pods is demonstrated in Figures 5.14 to 5.16. In Figure 5.13, Albite Pod #3 contains relative depletions in Zr, Y, and La (considered immobile, incompatible elements) in comparison to Rb, and Ba (considered mobile trace elements). The relative enrichment and depletion of these elements is strongest at the margins of the albite pod (blocks 3 and 6). In Figure 5.15, Albite Pod #5 exhibits very little trace element variation, similar to the lack of variation in major element chemistry. The Discovery Outcrop Albite Pod shows the most notable variations in trace element geochemistry. Zr and La steadily decrease from Block 1 to Block 8, while Rb exhibits an opposite trend and shows steady enrichment from Block 1 to Block 8. The trend of Y is similar to that of Zr and La, however with one anomalous point in Block 5. Sr and Ba are most enriched through Blocks #2-4, and Sr shows steady enrichment from Blocks 5-7 with a slight depletion in Block 8.

Figures 5.17 to 5.19 show the CIPW normalized values for the albite pod transects. Figure 5.17 shows a transect of Albite Pod #3. Block 3, which is the most altered block, contains the least amount of anorthite, and the most albite. Samples with relatively high albite tend to have low magnetite as well. Diopside is generally unchanged. Figure 5.18 shows a transect of Albite Pod #5 with CIPW normalized values plotted. Block 1 has relatively low anorthite, albite, and diopside, but high magnetite. Blocks 2-7 show fairly consistent values of anorthite, albite and magnetite. Normalized diopside values are greatest in block 4. Figure 5.19 shows a transect of the Discovery Outcrop Albite Pod. Anorthite steadily increases from blocks 1 to 4, and is again depleted in block 5. Between blocks 5 and 8, anorthite again steadily increases. Albite values are greatest in block 1, and decrease up to block 5. From block 5 to 8, albite is fairly constant. Magnetite is generally constant, with a slight enrichment in block 5.

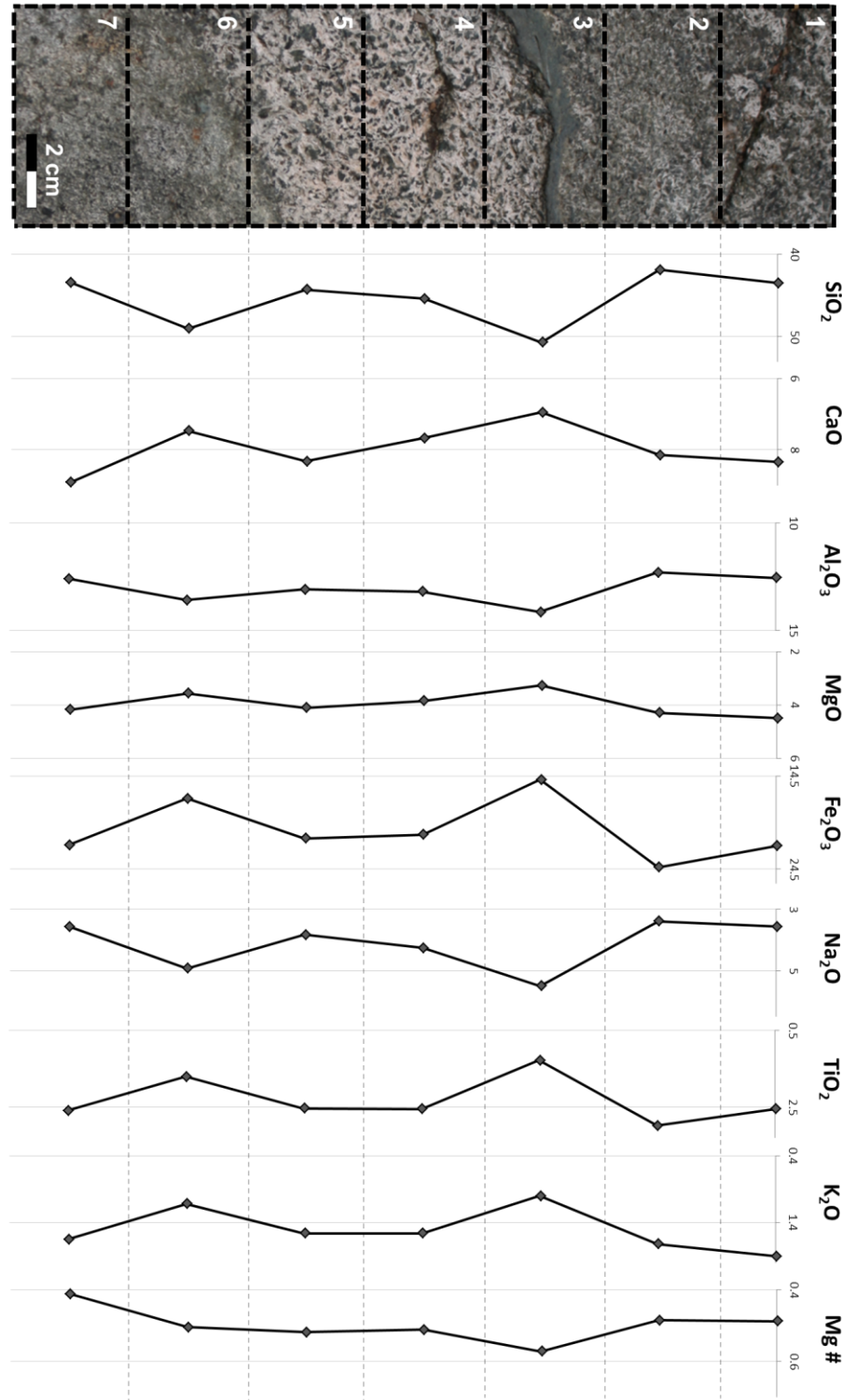


Figure 5.11 – A representation of samples from a transect of Albite Pod #3 is shown on the left (separated into blocks) with corresponding major element geochemistry to the right. The variation in Mg # is also shown. Units for the oxides are in wt. % and the Mg # is the molar Mg/(Mg+Fe) ratio.

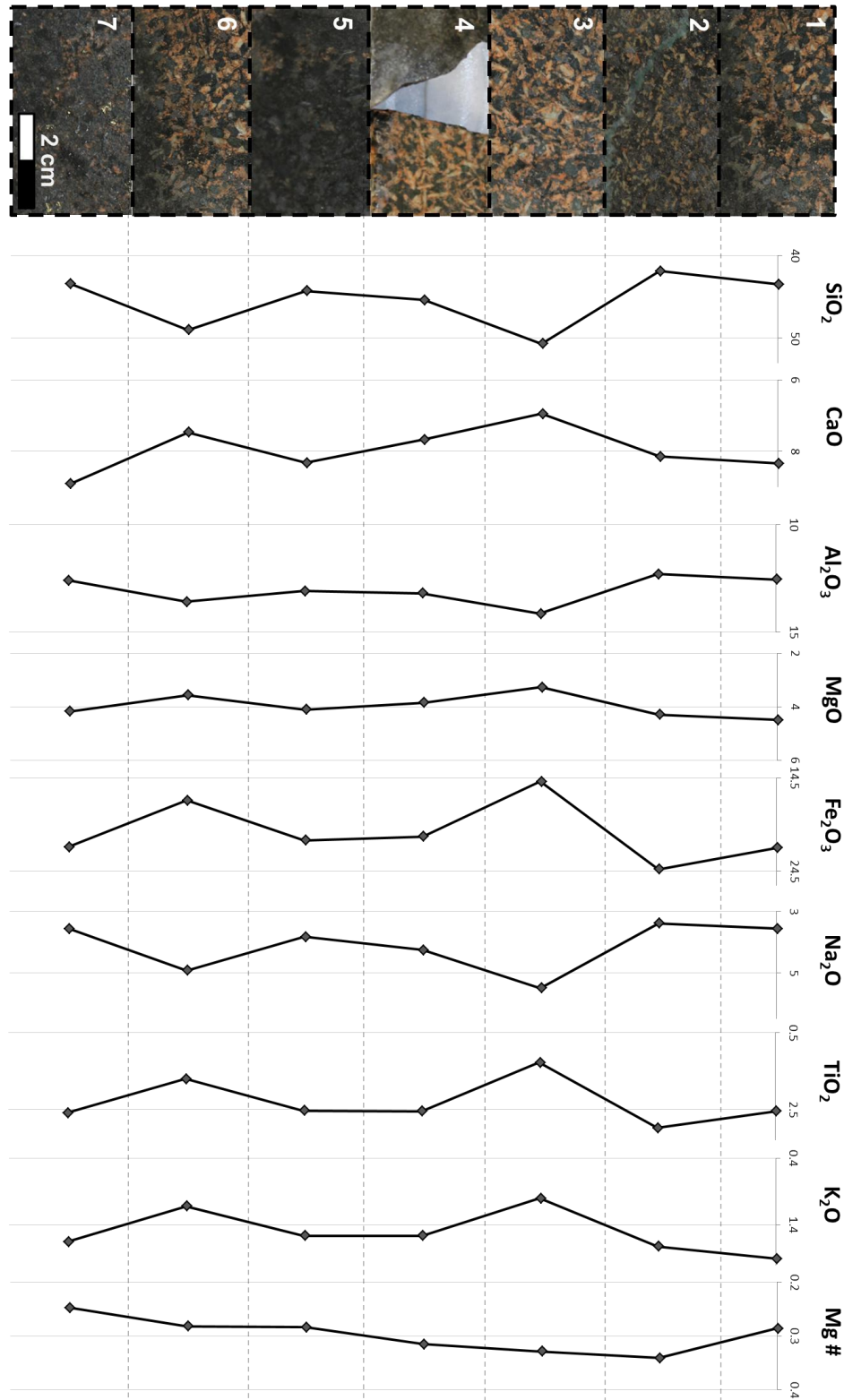


Figure 5.12 – A transect of Albite Pod #5 is shown on the left (separated into blocks) with corresponding major element geochemistry to the right. The variation in Mg # is also shown. Units for the oxides are in wt. % and the Mg # is the molar Mg/(Mg+Fe) ratio.

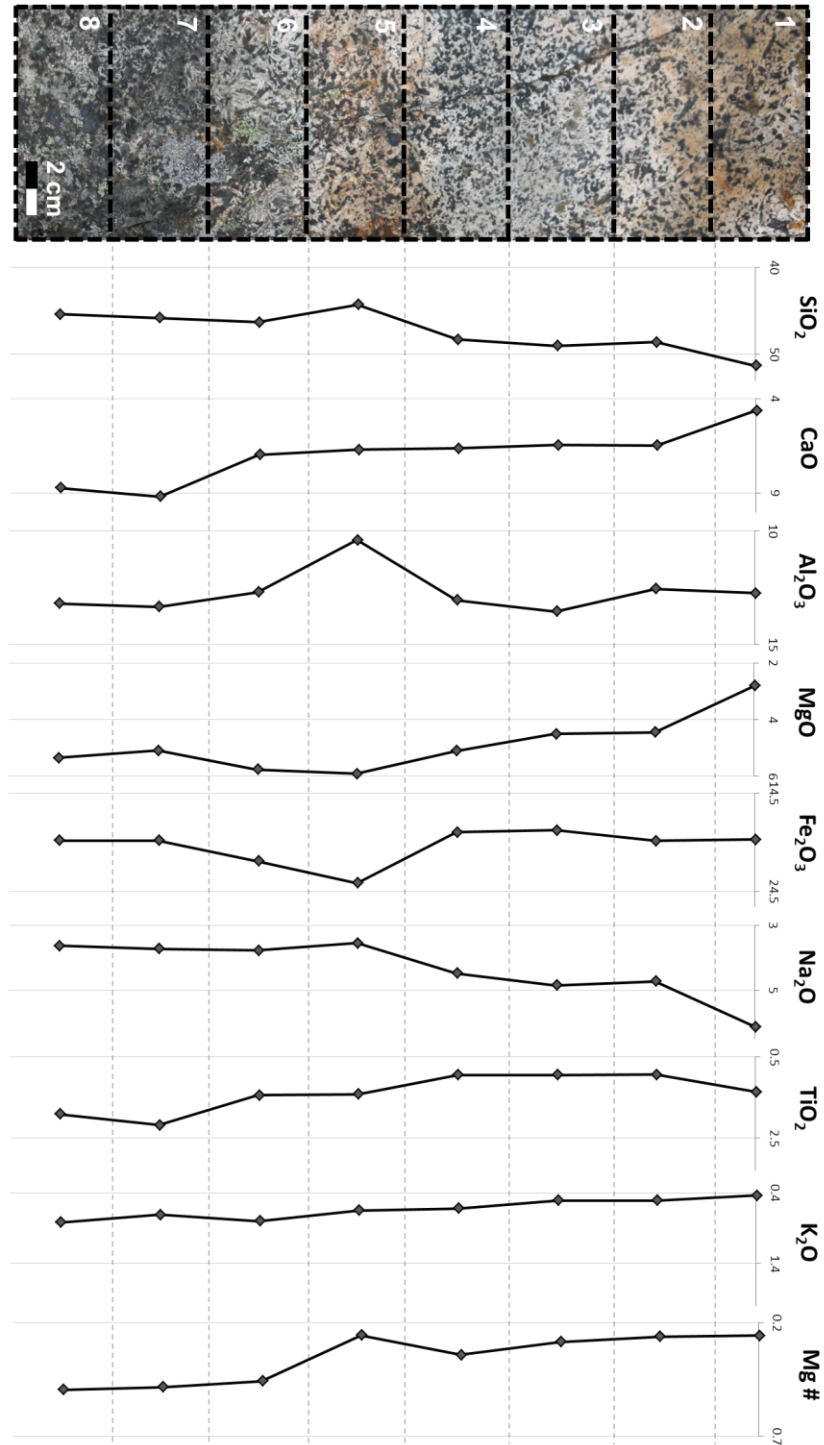


Figure 5.13 – A transect of the Discovery Outcrop Albite Pod is shown on the left (separated into blocks) with corresponding major element geochemistry to the right. The variation in Mg # is also shown. Units for the oxides are in wt. % and the Mg # is the molar Mg/(Mg+Fe) ratio.

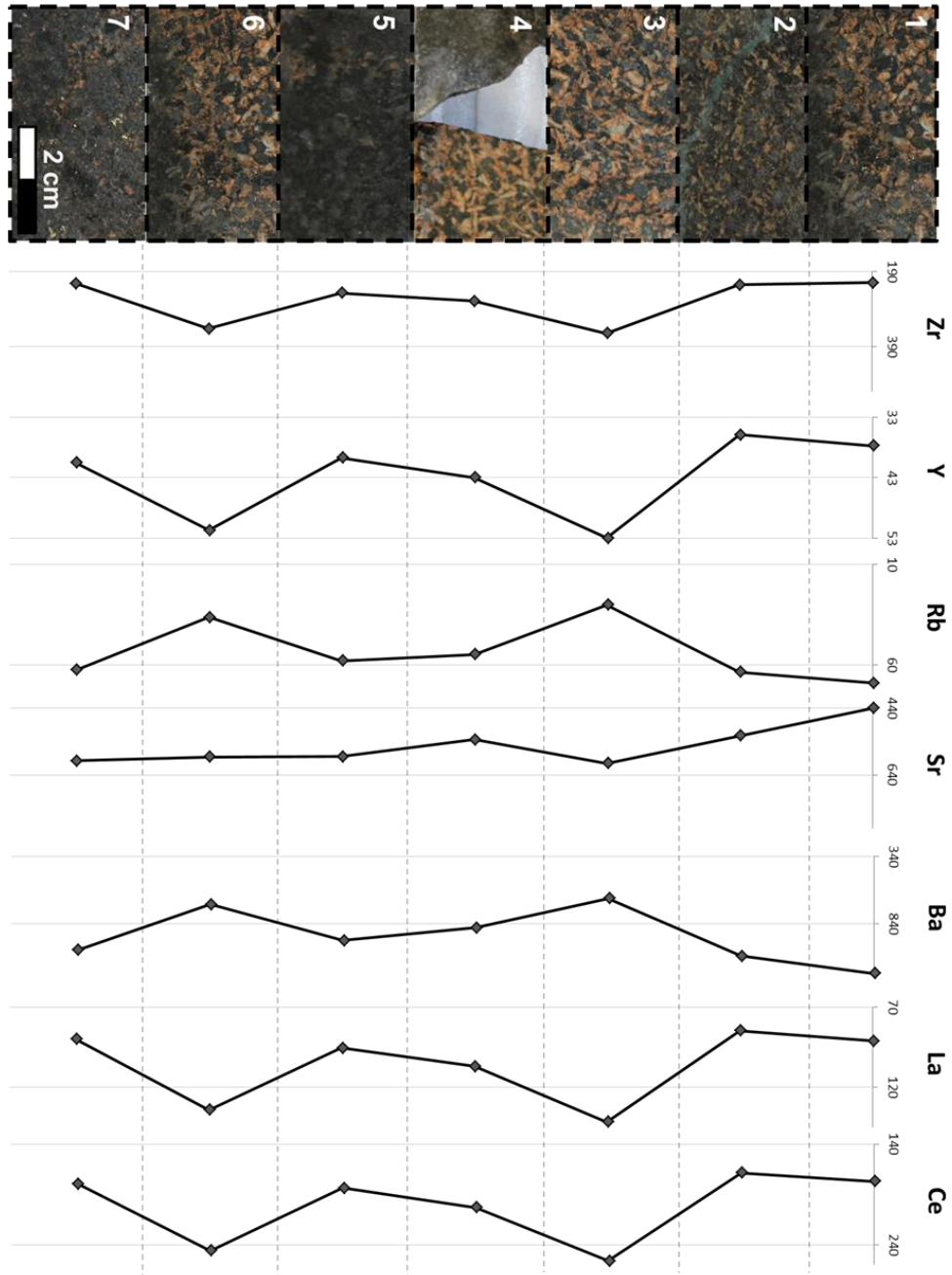


Figure 5.14 – A transect of Albite Pod #3 is shown on the left (separated into blocks) with corresponding trace element geochemistry to the right. The x-axis values are in parts per million (ppm).

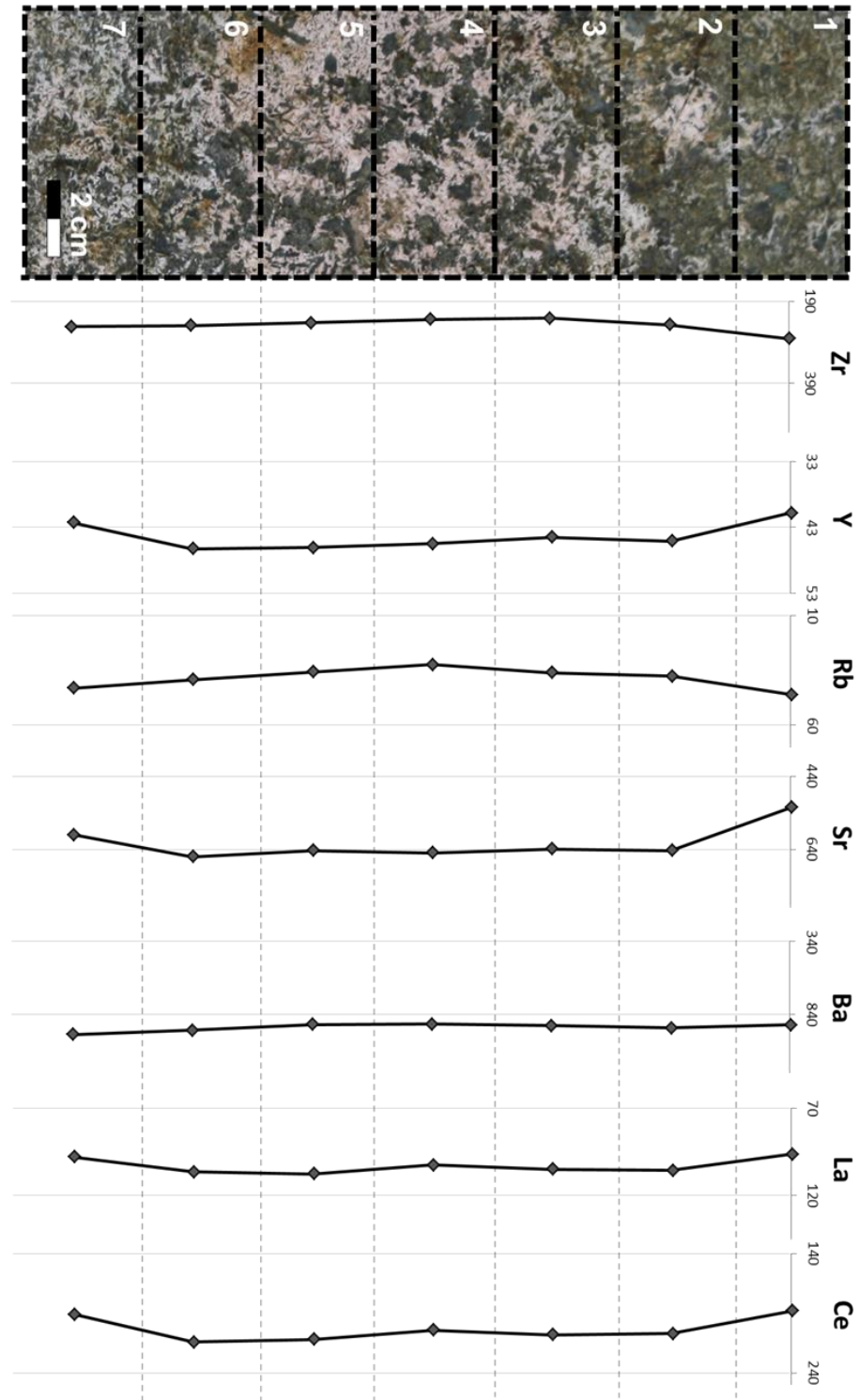


Figure 5.15 – A transect of Albite Pod #5 is shown on the left (separated into blocks) with corresponding trace element geochemistry to the right. The x-axis values are in parts per million (ppm).

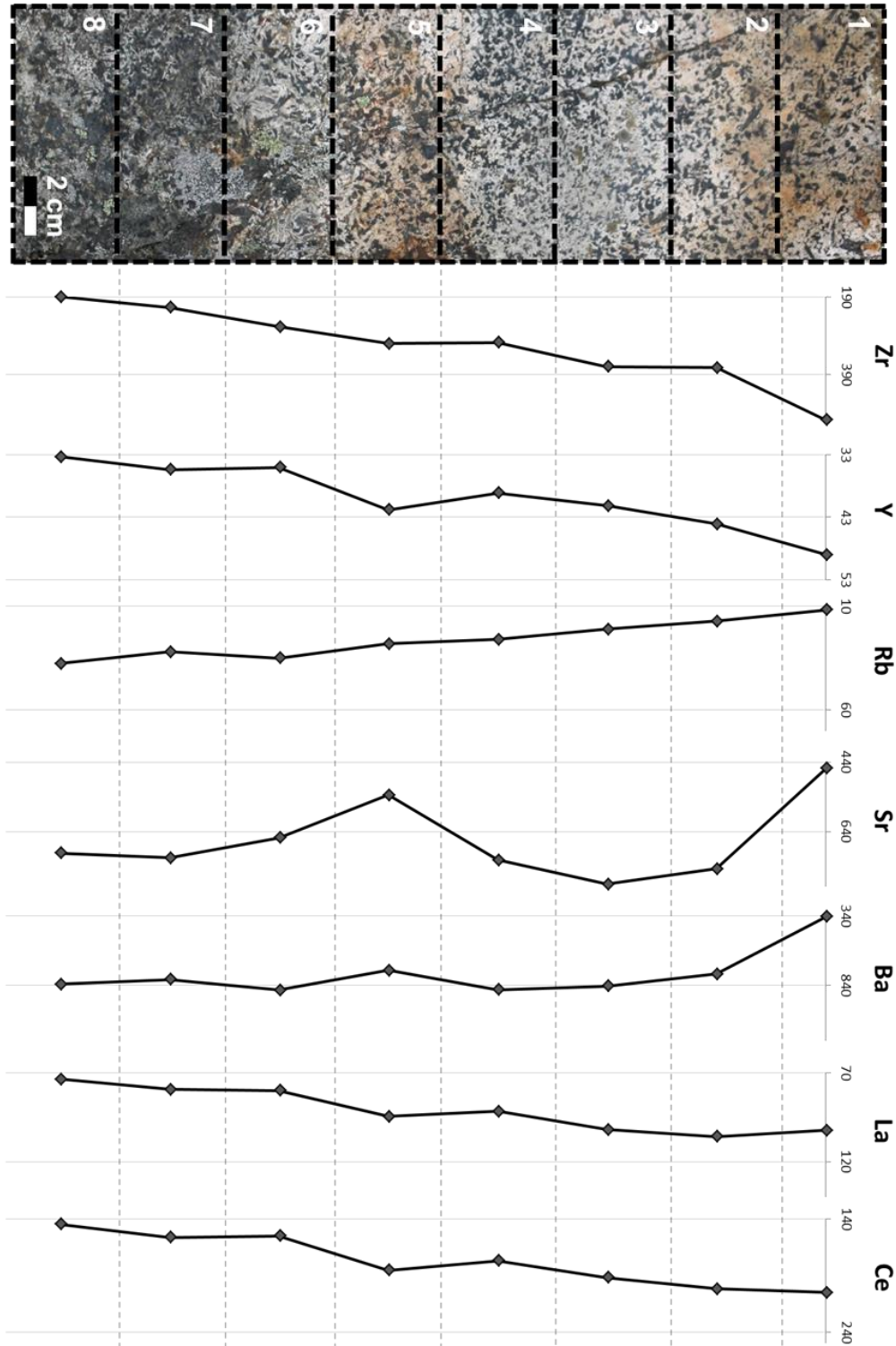


Figure 5.16 – A transect of the Discovery Outcrop Albite Pod is shown on the left (separated into blocks) with corresponding major element geochemistry to the right. The x-axis values are in parts per million (ppm).

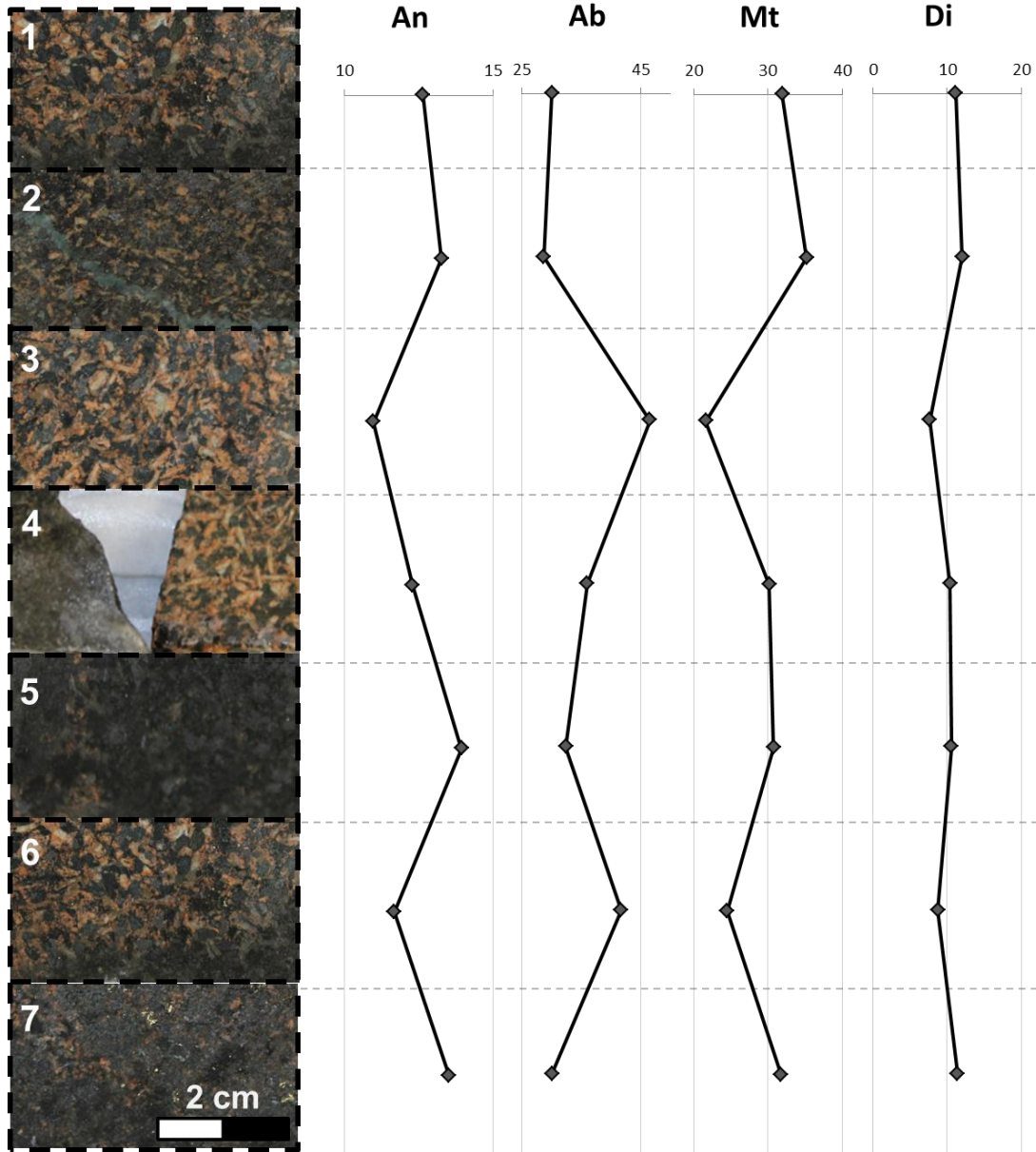


Figure 5.17 – CIPW normalized values for anorthite (An), albite (Ab), magnetite (Mt), and Diopside (Di) plotted to correspond with each sample block from Albite Pod #3 (shown on the left). Blocks 1 and 2 and 5 and 7 exhibit weak to moderate albite alteration, while blocks 4 and 5 exhibit strong albite alteration. Block 3 shows strong actinolite and albite alteration. Blocks 6 and 7 show little to no albite alteration. The x-axis is the calculated modal % for each mineral.

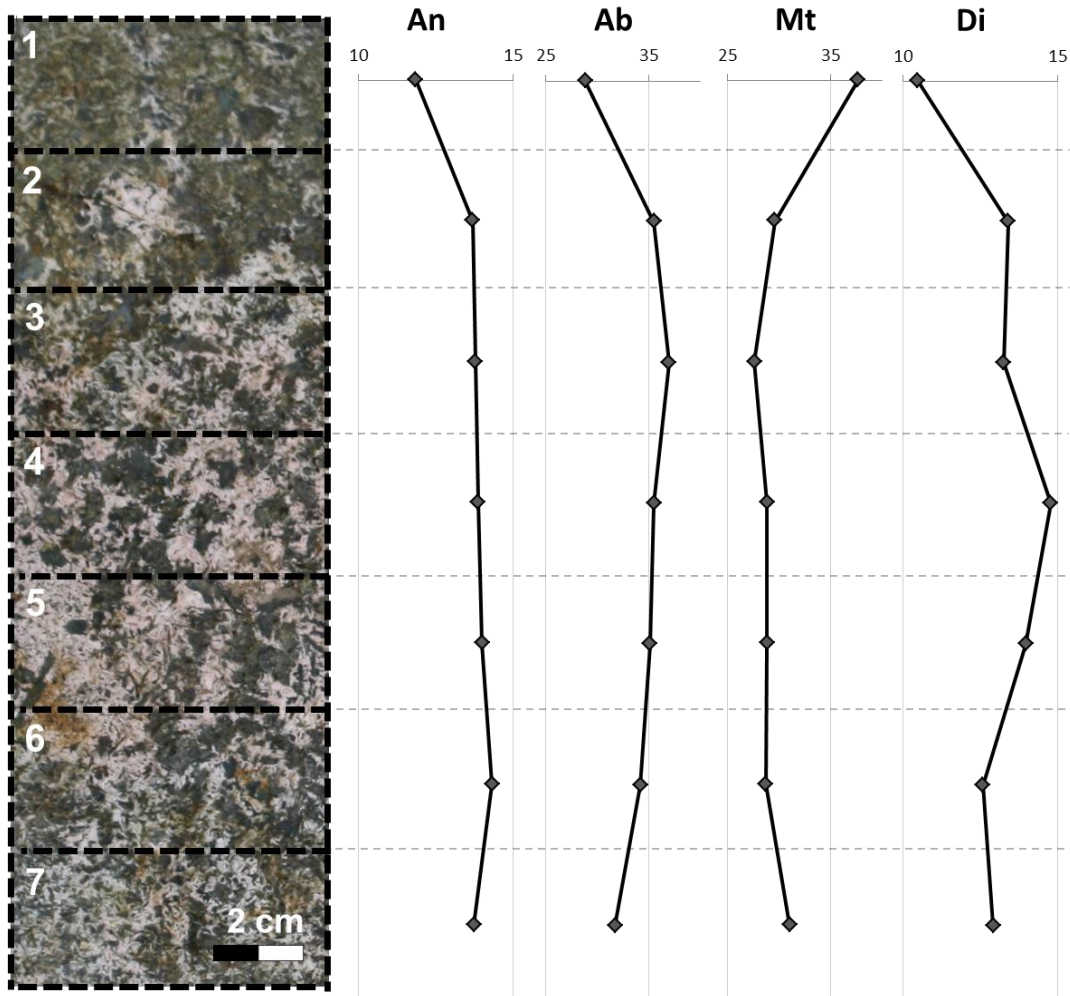


Figure 5.18 – CIPW normalized values for anorthite (An), albite (Ab), magnetite (Mt), and Diopside (Di) plotted to correspond with each sample block from Albite Pod #5 (shown on the left). Block 1 exhibits weak albite alteration, while block 2 shows a weak to moderate albite alteration. Blocks 3, 4 and 5 exhibit strong albite alteration, while blocks 6 and 7 contain moderate albite alteration. The x-axis is the calculated modal % for each mineral.

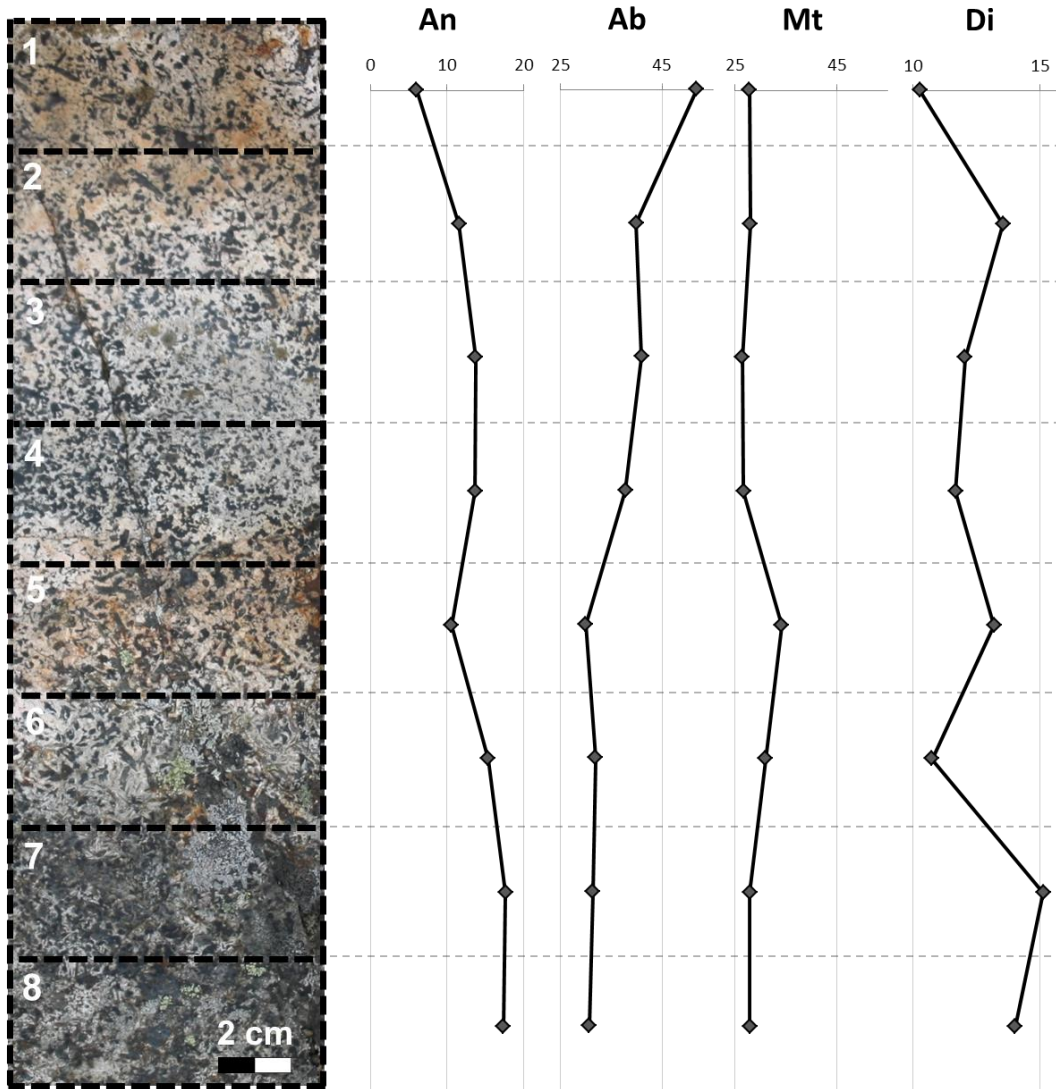


Figure 5.19 – CIPW normalized values for anorthite (An), albite (Ab), magnetite (Mt), and Diopside (Di) plotted to correspond with each sample block from the Discovery Outcrop Albite Pod (shown on the left). Block 1 exhibits the strongest degree of albite alteration, and the degree of albite alteration appears to decrease steadily towards block 8, with the exception of block 5 which appears to be the second most pink-albitized block. The x-axis is the calculated modal % for each mineral.

5.1.3 Major and Trace Element Geochemistry

Figure 5.20 are a series of Harker diagrams which show the major elements of the least altered samples plotted against silica (with syenite plotted as reference points). Fe_2O_3 decreases with increasing SiO_2 , while Na_2O increases with increasing SiO_2 . Figure 5.21 is similar to Figure 5.20, except that the fields for the least altered lithologies is

superimposed over all of the data. An orange shaded field with a dashed border represents the field in which the least altered data points plotted. The most altered samples, particularly from the heterogeneous gabbro sample suite, do not diverge far from the field of least altered samples. Among the skeletal troctolite samples, there are more data points that do not fit within the least altered field in each of the bivariate plots. However, the major element geochemistry of these outward-lying skeletal troctolite data points could be more influenced by the fact that they contain very high modal abundances of skeletal olivine (between 20 to 30%). As an overall trend, the following elements increase with increasing SiO_2 : Al_2O_3 , CaO , Na_2O , and P_2O_5 . Conversely, the following elements decrease with increasing SiO_2 : Fe_2O_3 , TiO_2 , and MnO . There is a particular clear separation in the data set in the plot of MgO vs SiO_2 , as the skeletal troctolite samples are richer in MgO than the rest of the data set, and they show no correlation with increasing SiO_2 while the remaining data points show a decreasing trend with increasing SiO_2 . Another separation of data points is apparent in the TiO_2 vs SiO_2 plot, where skeletal troctolite samples plot in a fairly tight cluster. The remaining samples show a negative correlation with increasing SiO_2 , thus implying that among them an increase in SiO_2 results in a decrease of TiO_2 .

Albite pod samples enriched in Na_2O and depleted in K_2O relative to all other samples. Samples from Albite Pod #5 also contain much more P_2O than all other samples, while samples from the Discovery Outcrop Albite Pod contain less P_2O . This is due to the varying amounts of apatite between the two pods. It should also be noted that pod samples are distinctly different from syenite.

Figure 5.22 is similar in principle to the Harker diagram in Figure 5.20, except that the x-axis is Mg # rather than SiO_2 . Only the least altered lithologies are plotted in this figure. In general, skeletal troctolite samples plot separately from all the other lithologies due to relatively high Mg #s. Figure 5.23 is similar to Figure 5.22, except that all of the lithologies are plotted. The least altered samples are shown in the orange shaded field. With the exception of albite pod samples and a few skeletal troctolite data points, the

majority of altered samples plot within the least altered fields, indicating little variation between altered and least altered samples.

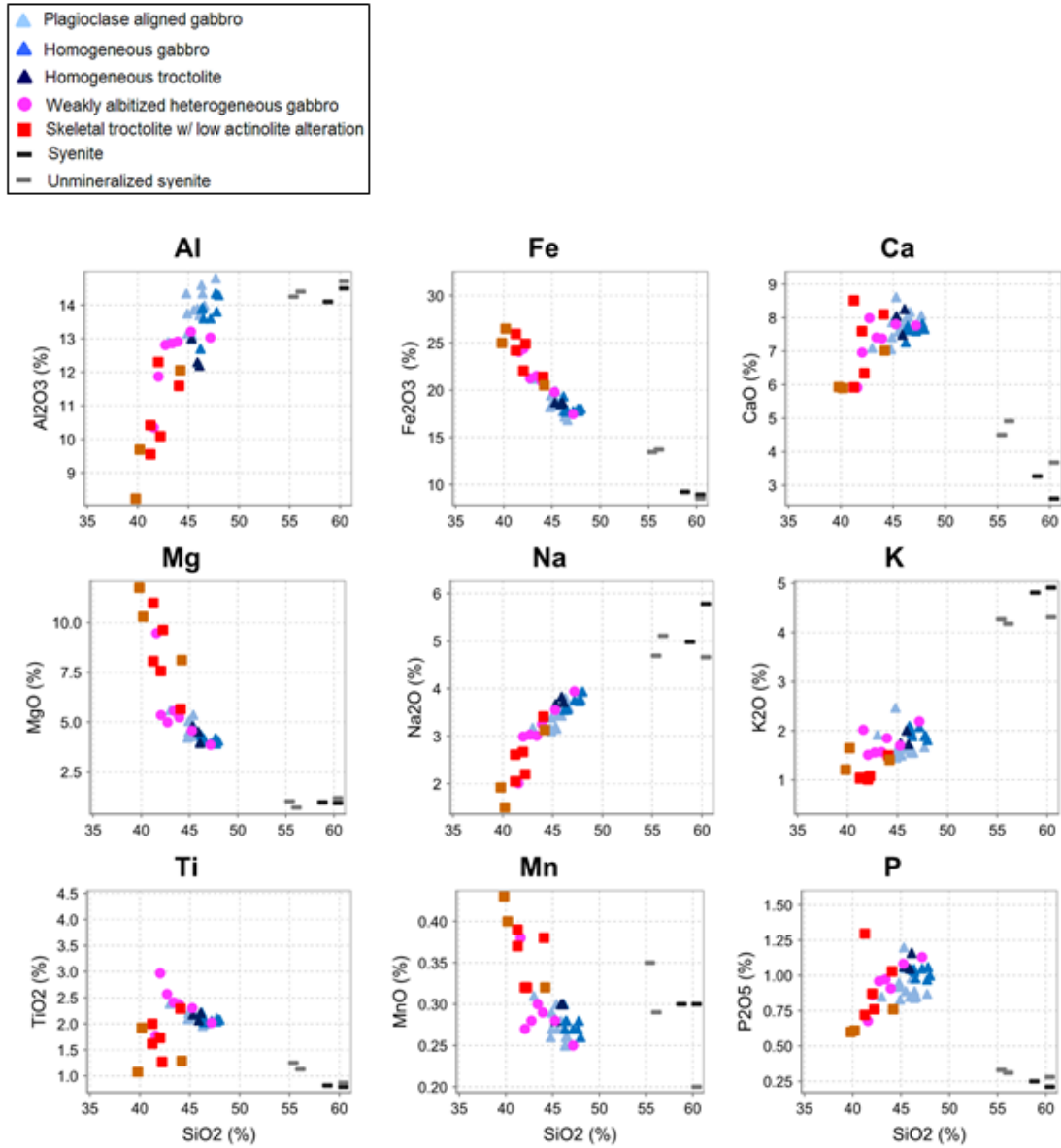


Figure 5.20 – Harker diagram (major elements plotted against SiO₂) for the least altered GLD suite of samples. The X-axis for all diagrams is SiO₂

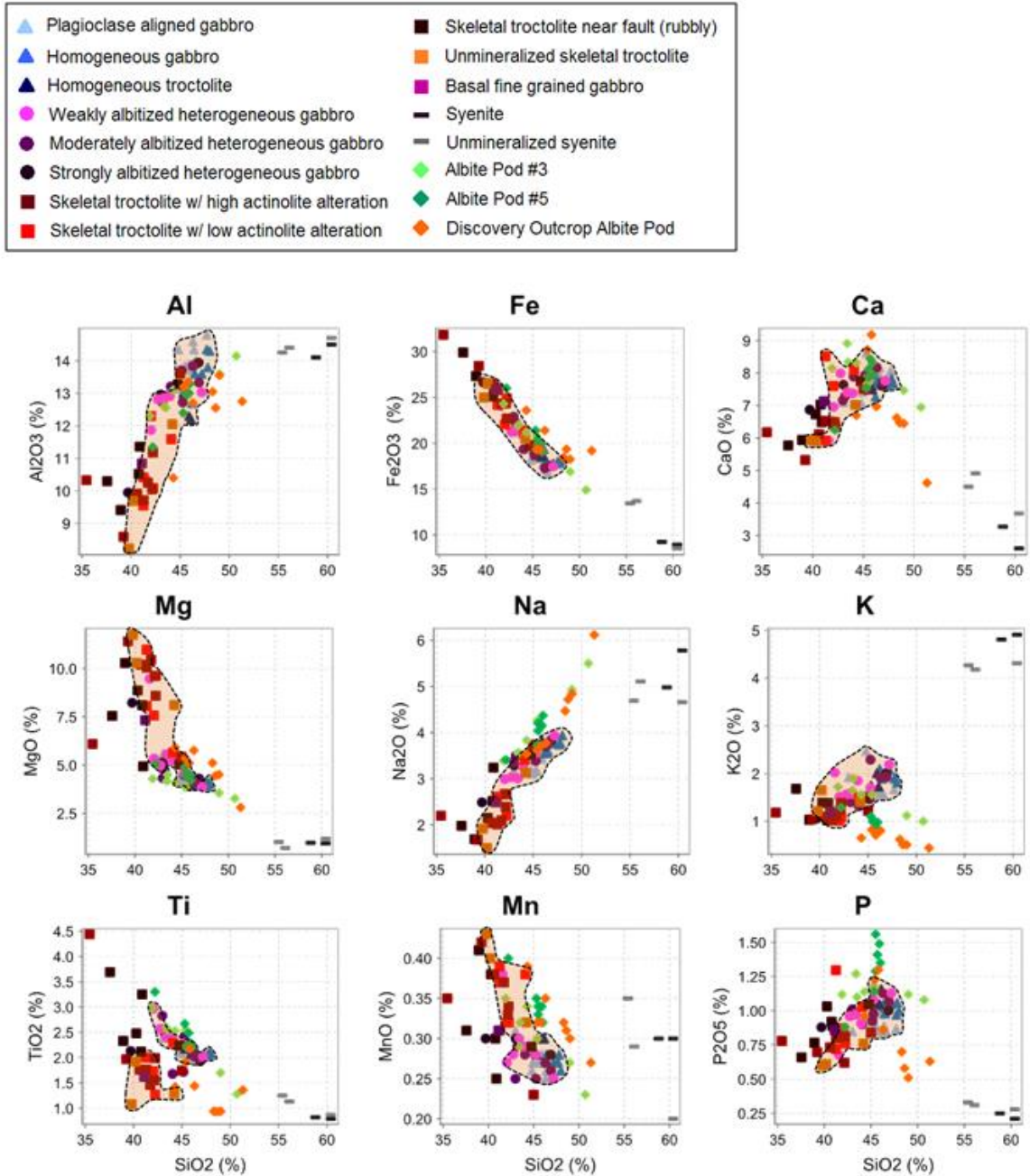


Figure 5.21 – Harker diagram for the all GLD suite of samples with the field for the least altered lithologies superimposed as an orange shaded and bordered field

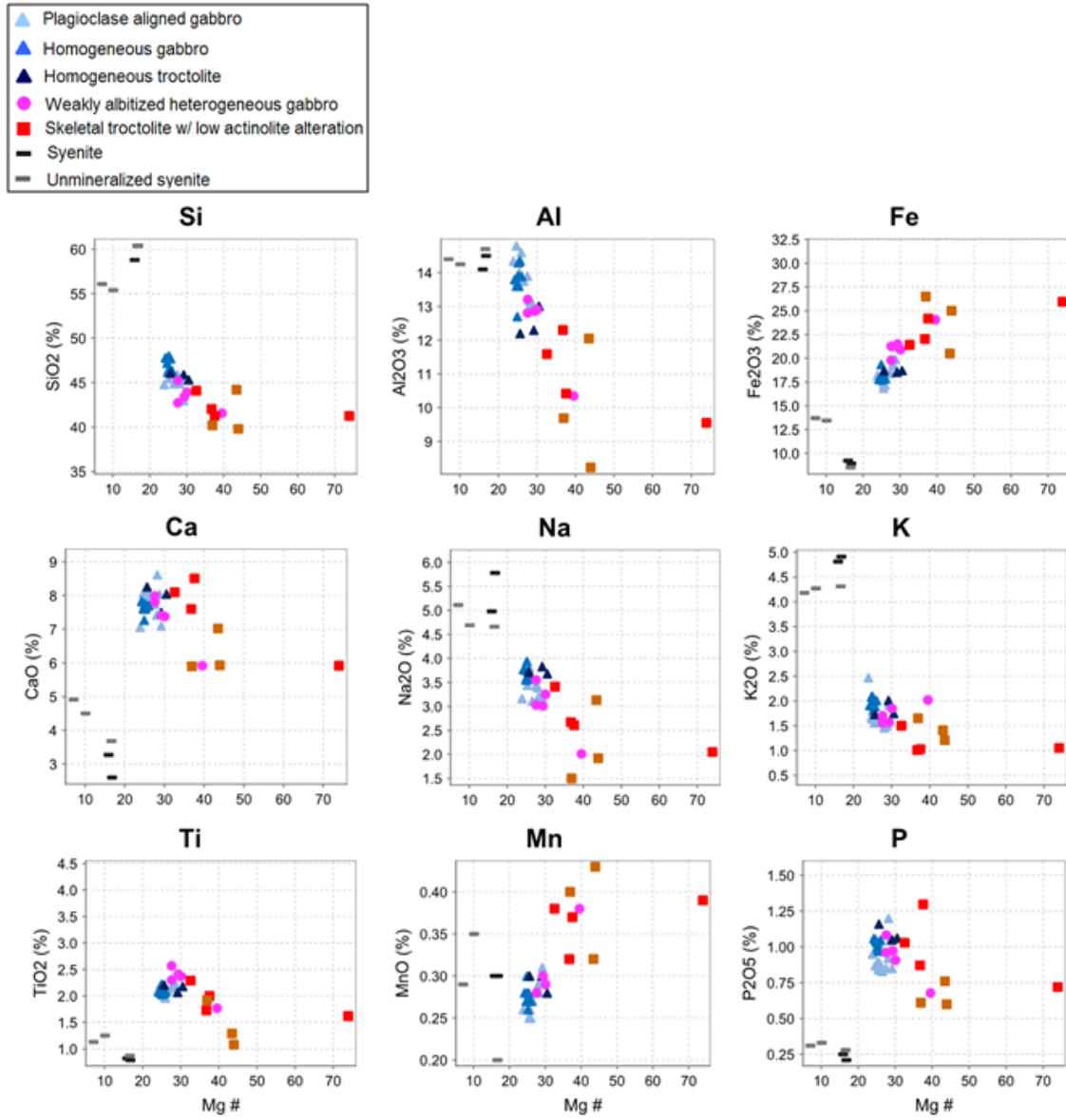


Figure 5.22 – Bivariate diagrams with Mg # plotted against major elements for the least altered GLD suite of samples. The X-axis for all diagrams is Mg #

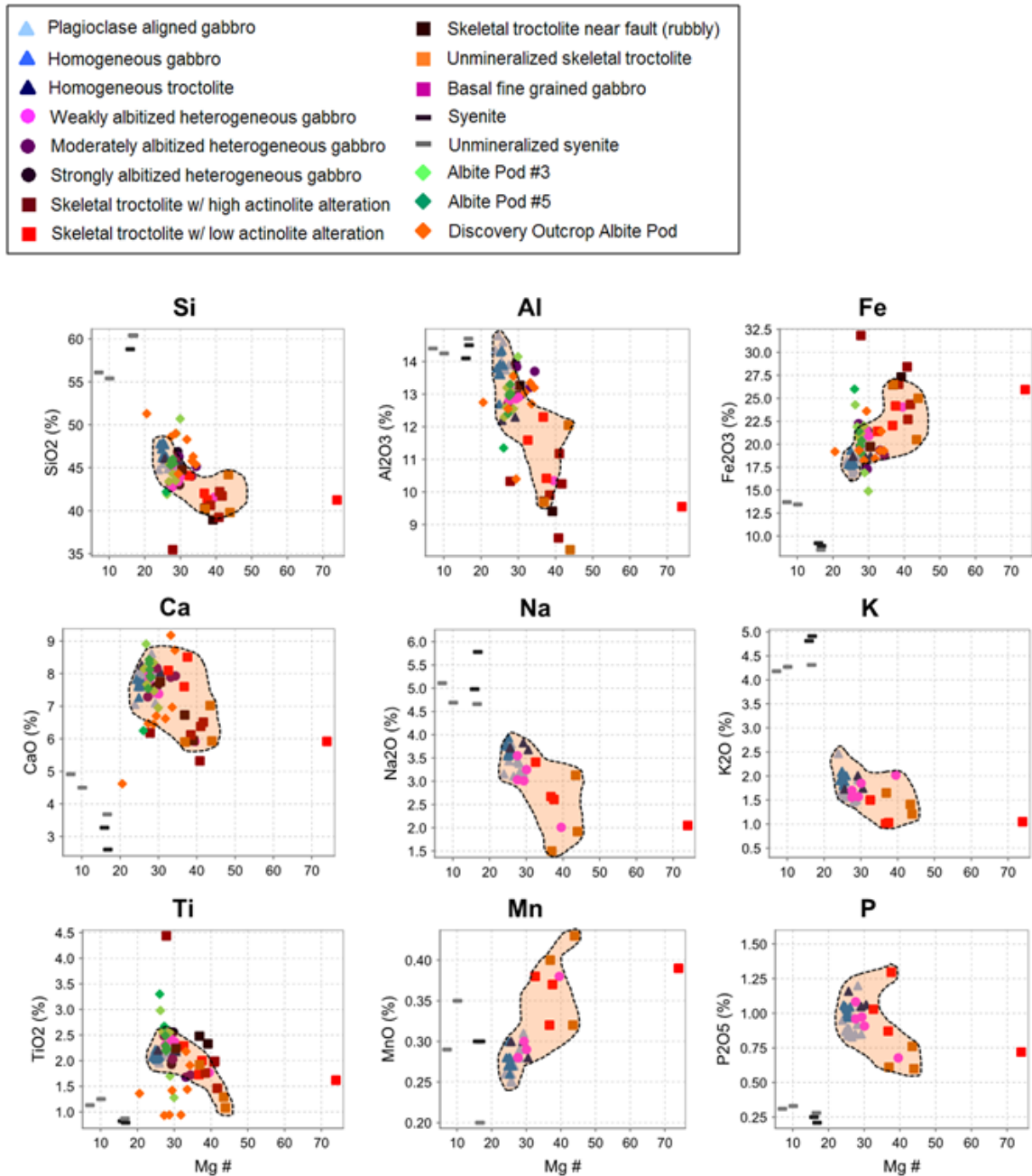


Figure 5.23 – Mg # diagrams for the all GLD suite of samples with the field for the least altered lithologies superimposed as an orange shaded and bordered field

REE profiles of the unmineralized gabbros (plagioclase aligned and homogeneous gabbro), skeletal troctolite and heterogeneous gabbro are shown on Figure 5.24a. Syenite is also plotted for reference. The REE trends are very similar, and hence, infer that the rocks are cogenetic. There is also a notable absence of any Eu-anomaly. Albite pod samples are shown in Figure 5.24b, and also appear to be cogenetic. Notably, trace

elements within albite pod samples are depleted relative to syenite, indicating that the albite pods are indeed different from the syenite.

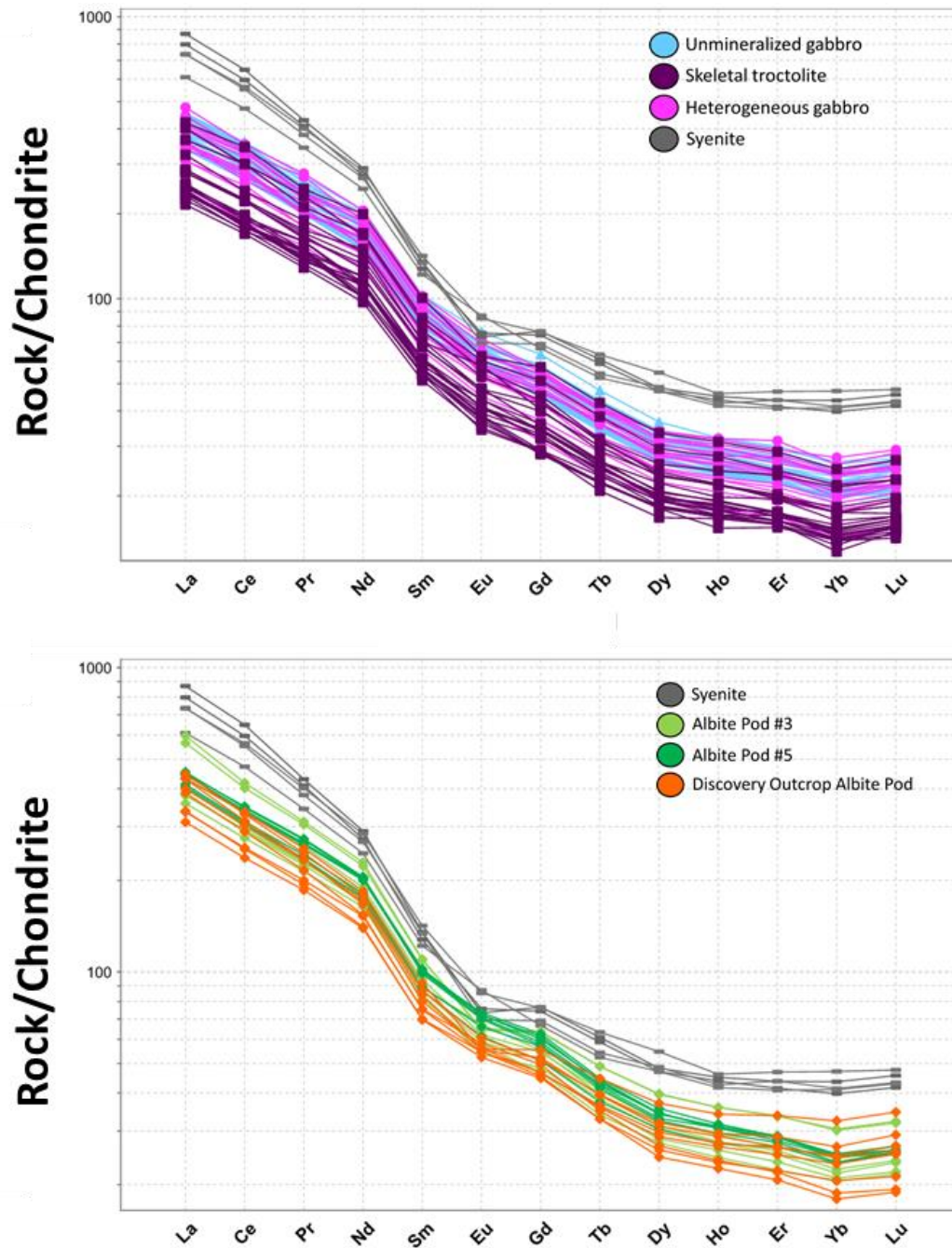


Figure 5.24 – (A) Chondrite normalized spider diagram with all drill-core samples arranged by lithology type, (B) Chondrite normalized spider diagram with all albite pod samples plotted. Syenite samples are plotted on both for reference. Chondrite values are from Sun and McDonough, 1989.

REE are regarded as the most useful of all trace elements, and REE studies have yielded important applications in igneous petrology (Rollinson, 1993). The REE all share very similar chemical and physical properties, mainly due to the fact that they all form stable 3+ ions of similar size. Differences in chemical behaviour between REE arise from the small but steady decreases in their ionic sizes with increasing atomic number. These small differences in size control their preferential enrichment and depletions during a number of petrologic processes, causing the REE to become fractionated relative to each other (Rollinson, 1993). For this reason, the incompatible elements were plotted on REE and multi-element variation (spider) diagrams (figures where general patterns and trends of trace elements give a general indication of the parental magmas compositions). Figure 5.24 (a) shows all GLD samples with the exception of albite pod samples plotted with syenite samples on a chondrite normalized spider diagram, with values obtained from Sun and McDonough, 1989. Skeletal troctolite samples are relatively depleted in rare-earth elements compared to heterogeneous gabbro, and syenite samples. In Figure 5.24 (b), albite pod samples are plotted relative to syenite samples. Albite pod samples are much more enriched in rare-earth elements compared to skeletal troctolite samples, but plot in similar ranges to heterogeneous gabbro. Syenite samples are much more enriched in the REE relative to all other Geordie Lake lithologies. There is a slightly negative europium anomaly within some syenite samples. No europium anomaly is observed within any other samples.

Zr, and Y are high field strength elements with high charge to radius ratios. Thus, they are not easily transported in aqueous fluids and have a tendency to remain impervious to metasomatism (Pearce and Norry, 1979). Figure 5.25 shows a log-log bivariate plot of Zr versus Y. Dashed lines are plotted, which indicate ratios of Zr/Y of 55, 60, and 65 (from left to right). Plagioclase aligned and homogeneous gabbro samples generally plot along a ratio of 65, while all other least altered samples plot roughly within the range of 55 to 65.

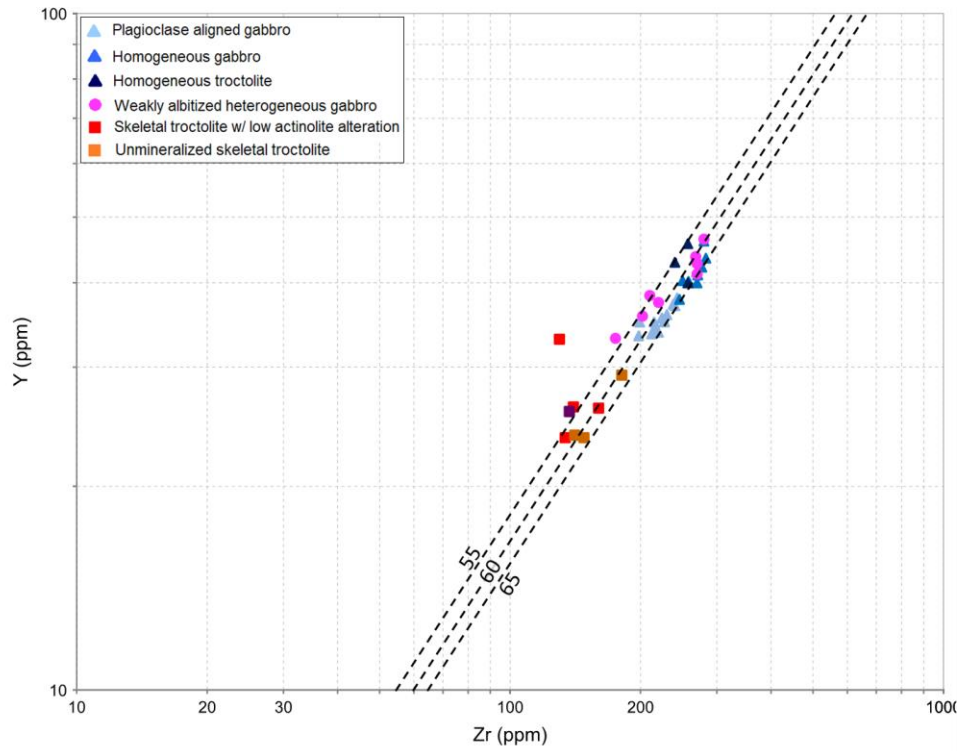


Figure 5.25 – Plot of Zr vs Y (in ppm) for all unaltered samples. The dashed lines represent $Zr/Y=55$, 60 and 65 respectively.

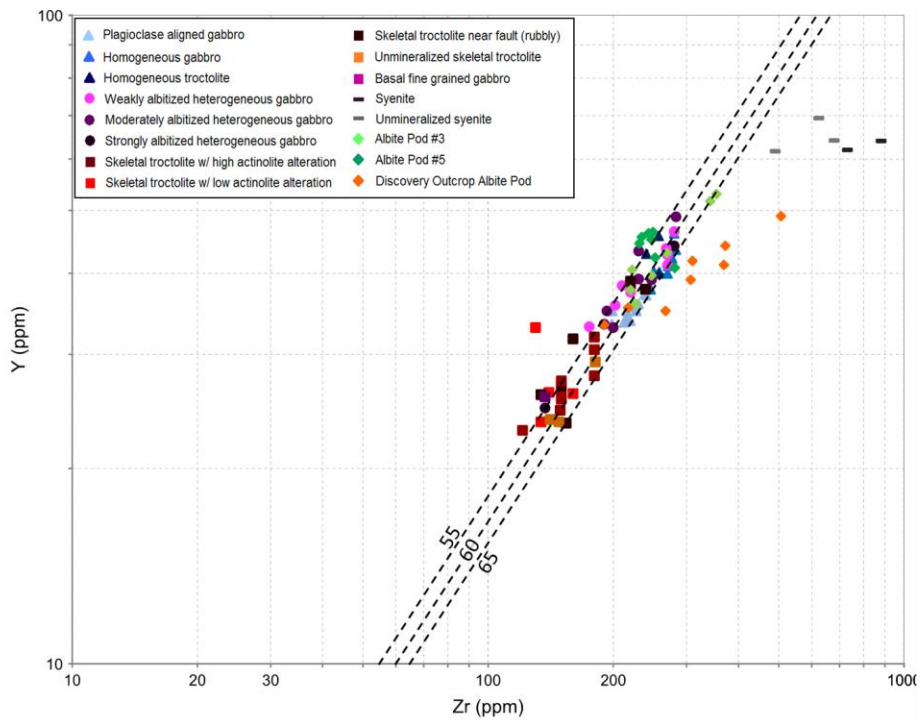


Figure 5.26 – Plot of Zr vs Y (in ppm) for all samples. The dashed lines represent $Zr/Y=55$, 60 and 65 respectively.

Figure 5.26 shows the same diagram as 5.25, except with all samples plotted. All samples largely plot within, or very near the range of Zr/Y of 55 to 65 with the only exception being the Discovery Outcrop albite pod samples. La vs Yb is shown on Figure 5.27, and shows a constant ratio of 25 (as a dashed black line). In Figure 5.28, both altered and least altered samples are plotted on the same diagram. Plagioclase aligned and homogeneous gabbro mainly plot below this ratio, while heterogeneous gabbro and skeletal troctolite plot above it, indicating that these units are still inherently different, regardless of the level of alteration.

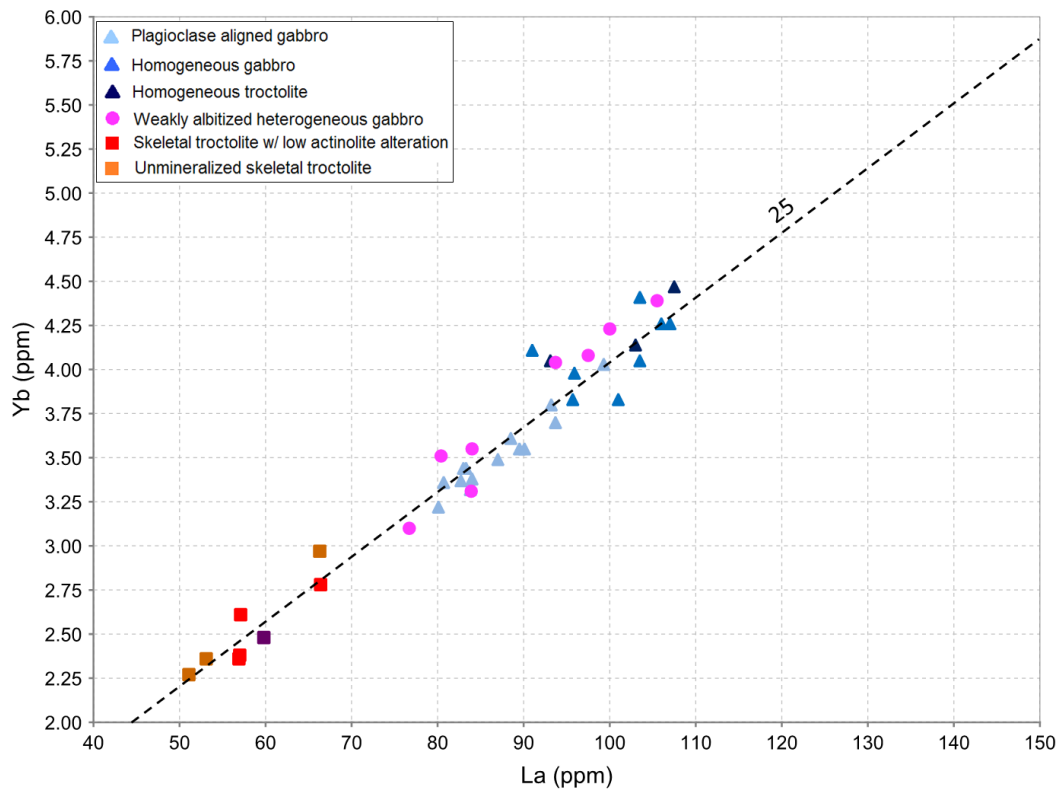


Figure 5.27 – Plot of La vs Yb with only unaltered samples plotted. The dashed line represents $La/Yb=25$

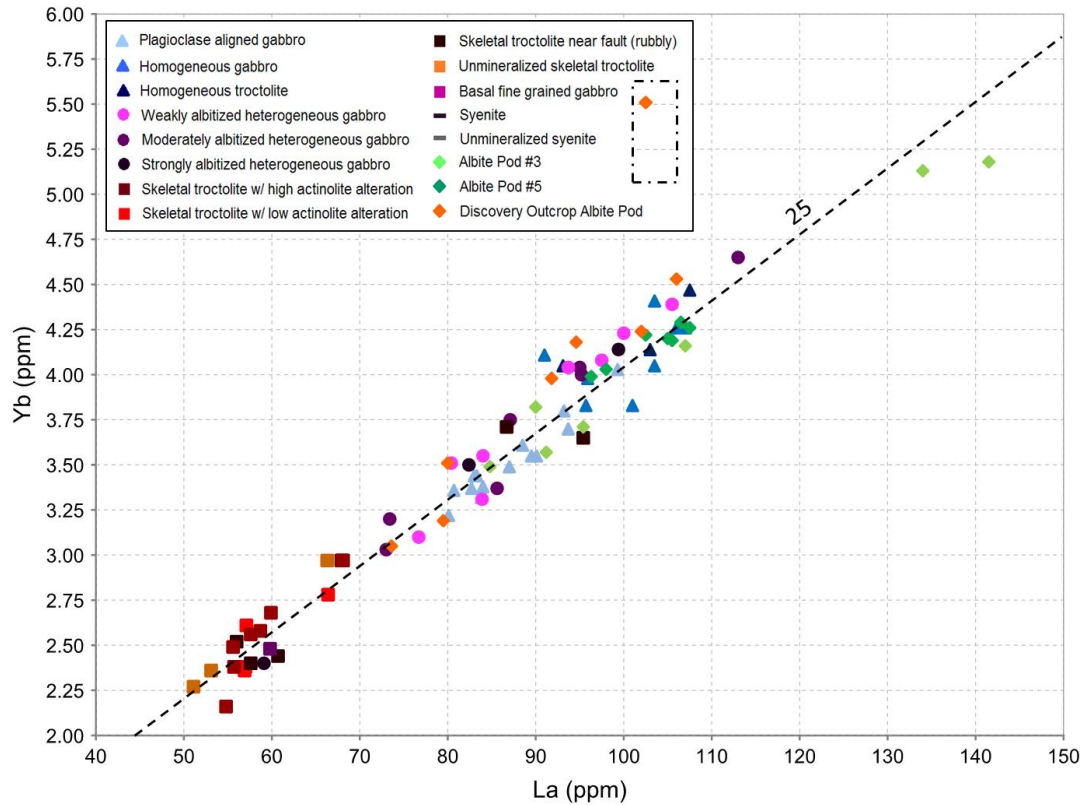


Figure 5.28 – Plot of La vs Yb with all samples plotted. The dashed line $La/Yb=25$

Figure 5.29 utilizes the differences observed in the Zr vs Y and La vs Yb to further distinguish each lithology. Only least samples are plotted, and we can see that plagioclase aligned gabbro is indeed unique from heterogeneous gabbro and skeletal troctolite. Figure 5.30 shows the same diagram as Figure 5.29, but with all the samples plotted. The altered samples predominantly plot within the red dashed field, indicating little variance between altered and least altered samples. In order to test whether sodium addition is occurring, Figure 5.31 plots Zr vs Na_2O with only the least altered samples. Samples predominantly plot within the ratios of $Zr/Na_2O = 50$, and 90. Figure 5.32 shows the same plot but with all samples plotted. Generally, Na_2O increases as Zr increases. The majority of the sample points do remain within the margins of the plagioclase ratios of 50, and 90, indicating a consistent ratio of plagioclase regardless of the level of alteration. Figure 5.33 shows a linear plot of Zr vs Rb with the least altered samples plotted. Except for skeletal troctolite samples (squares), all other least altered samples show an increase in Rb with an increase in Zr. Figure 5.34 shows all samples plotted, and vaguely shows that

there still remains a positive correlation with higher Zr and higher Rb values. Curiously, albite pod samples do not follow this trend but rather show that higher Zr values result in lower Rb values. Notably, the Discovery Outcrop albite pod samples show that Rb generally depletes steadily from the least altered sample (AB-D-8) to the most altered sample (AB-D-1). Within the least altered samples, Rb has a very strong relationship with K_2O (Figure 5.35). A similar plot is shown on Figure 5.36 with all samples plotted. This plot shows that altered samples still show a strong positive correlation between Rb and K_2O . Discovery Outcrop albite pod samples show that higher K_2O results in higher Rb. Figure 5.37 is a plot of K_2O and Zr, which shows a fairly linear correlation between the two elements. Figure 5.38 shows the same diagram, with all samples plotted. This diagram shows once again that the albite pod samples behave differently from the rest of the GL samples, since the most albitized samples contain the least amount of K_2O .

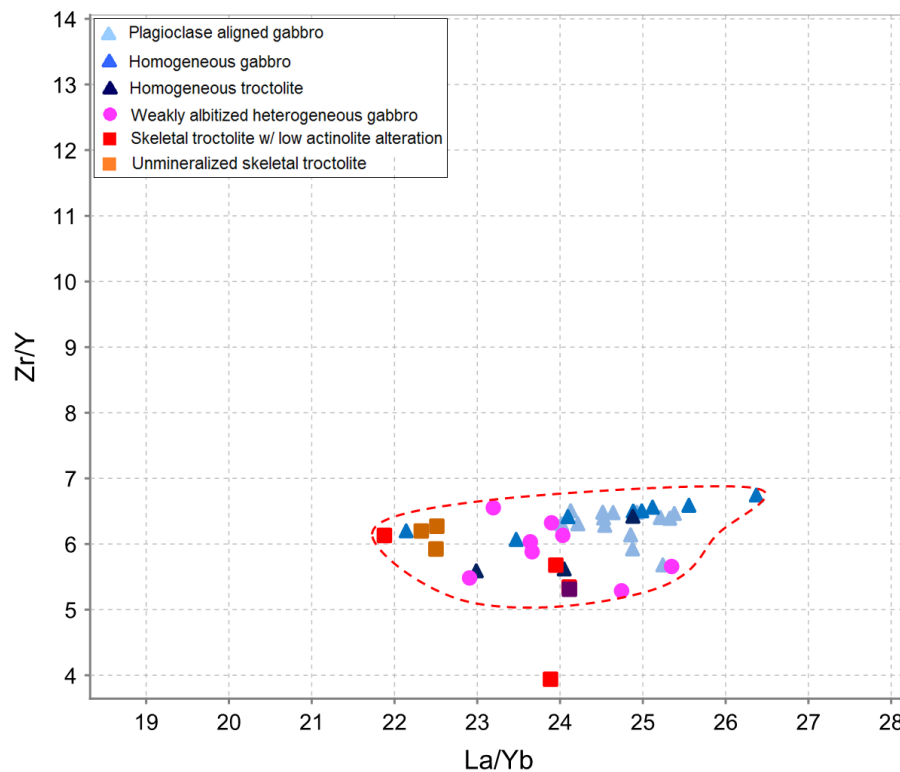


Figure 5.29 – A plot of La/Yb vs. Zr/Y with only unaltered samples plotted. The dashed red area indicates the field for unaltered samples. Wt. % ratios are used in this figure.

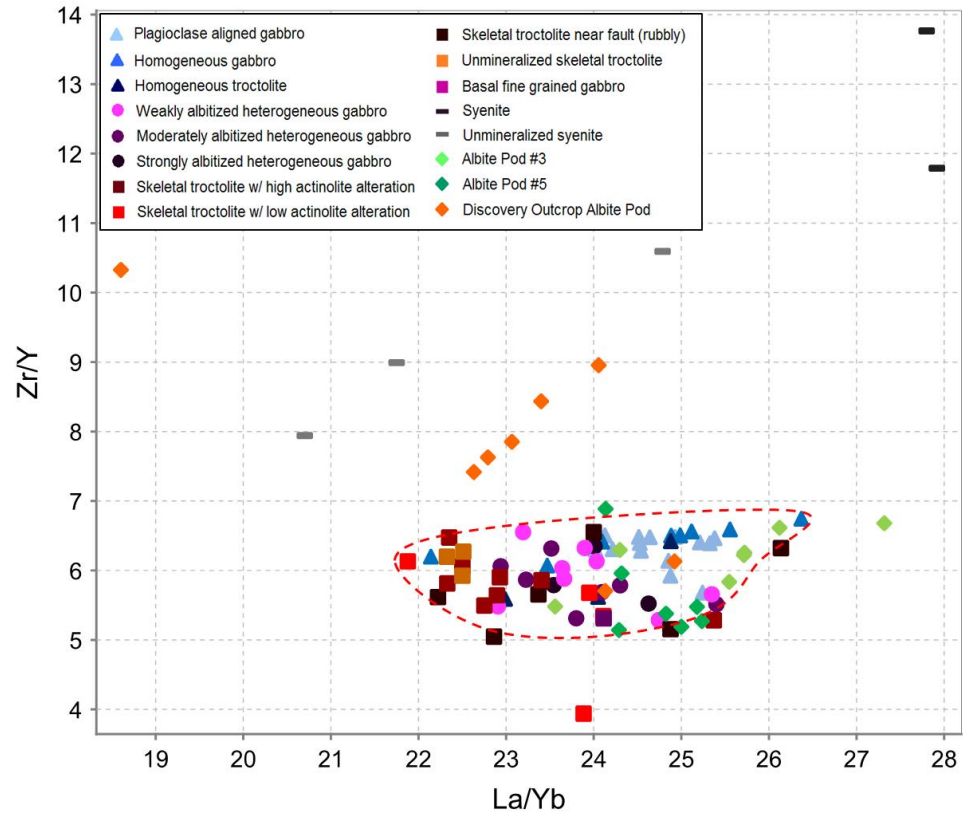


Figure 5.30 – A plot of La/Yb vs. Zr/Y with only all samples plotted. The dashed red area indicates the field for unaltered samples. Wt. % ratios are used in this figure.

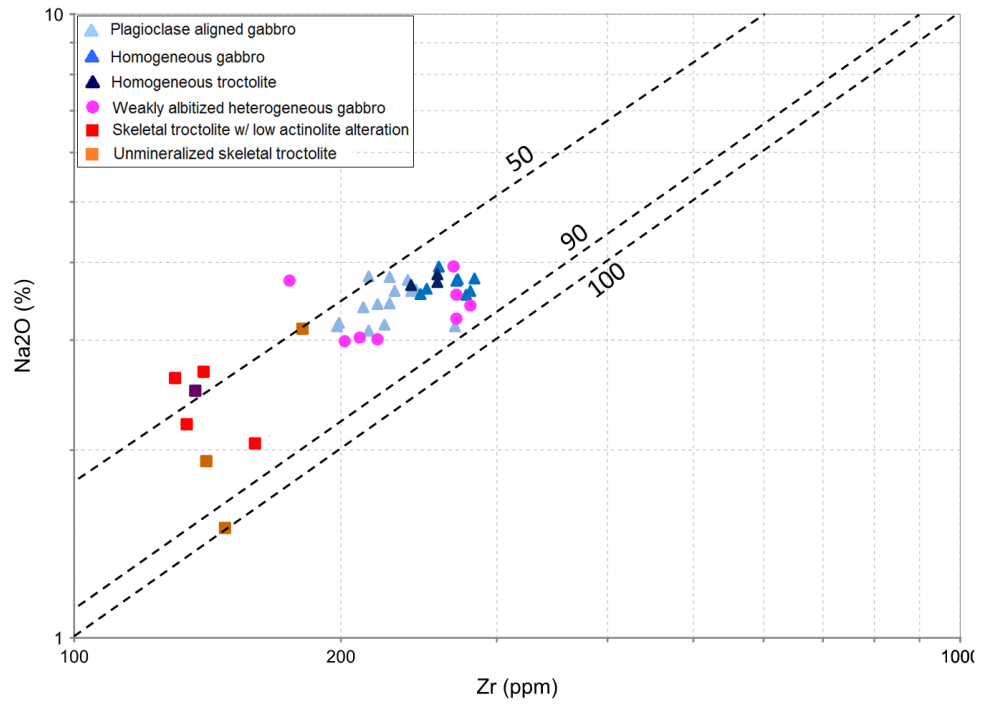


Figure 5.31 – A plot of Zr vs. Na₂O with unaltered samples plotted. The dashed black lines, from top to bottom indicate ratios of Zr/Na₂O=50, 90 and 100 respectively.

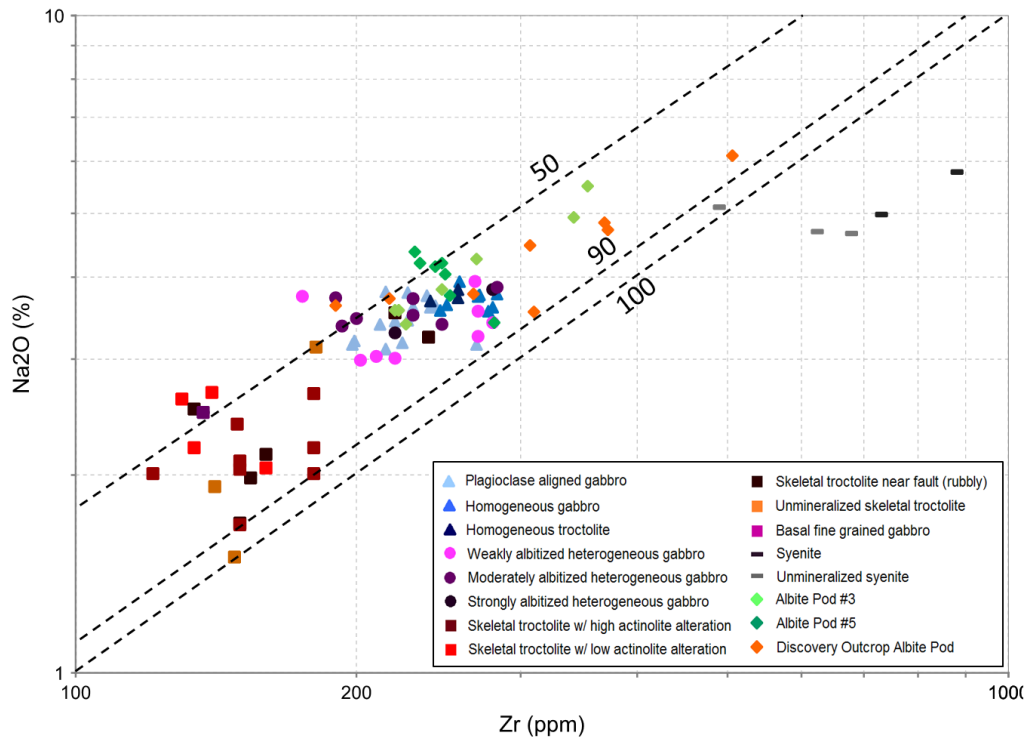


Figure 5.32 – A plot of Zr vs. Na₂O with all samples plotted. The dashed black lines, from top to bottom indicate ratios of Zr/Na₂O=50, 90 and 100 respectively.

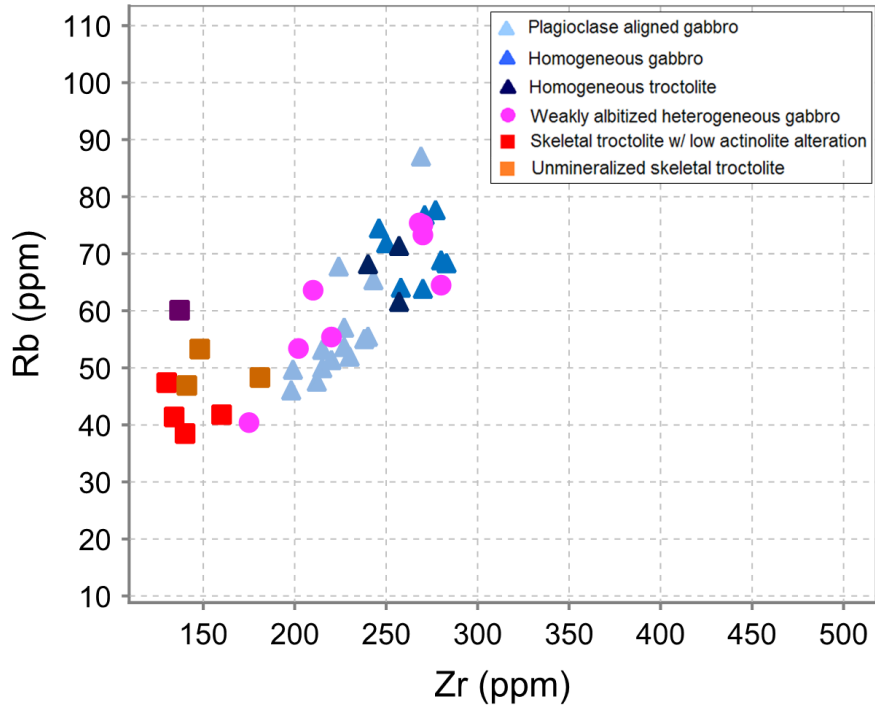


Figure 5.33 – A plot of Zr vs. Rb with only unaltered samples plotted

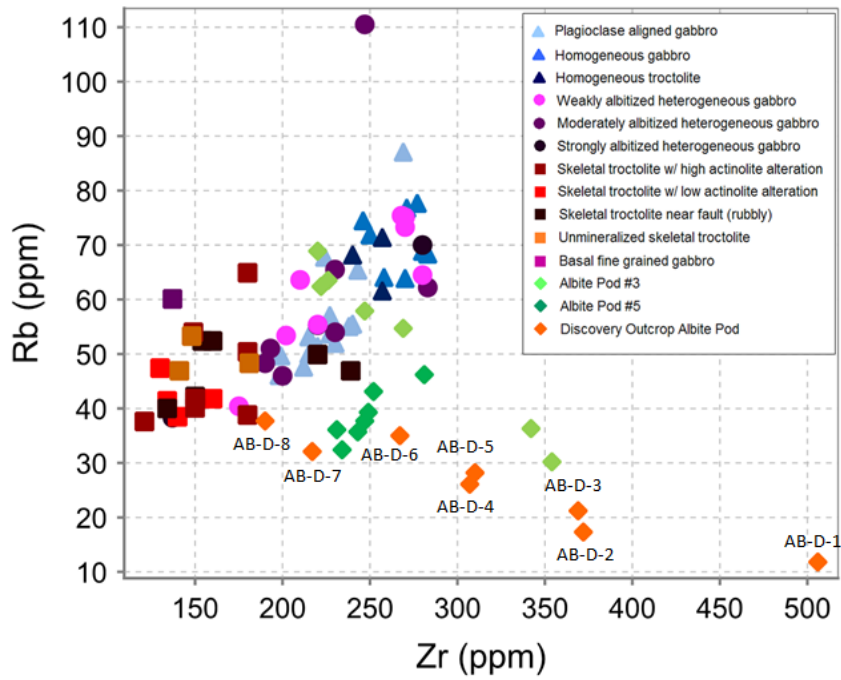


Figure 5.34 – A plot of Zr vs. Rb with all samples plotted

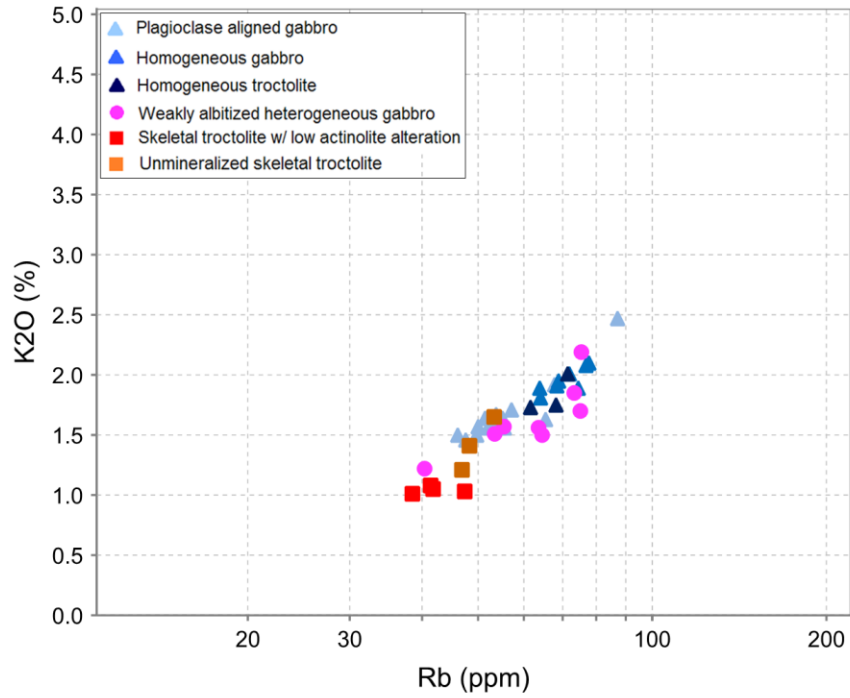


Figure 5.35 – A plot of Rb vs K_2O with only unaltered samples plotted. K_2O is in wt. %.

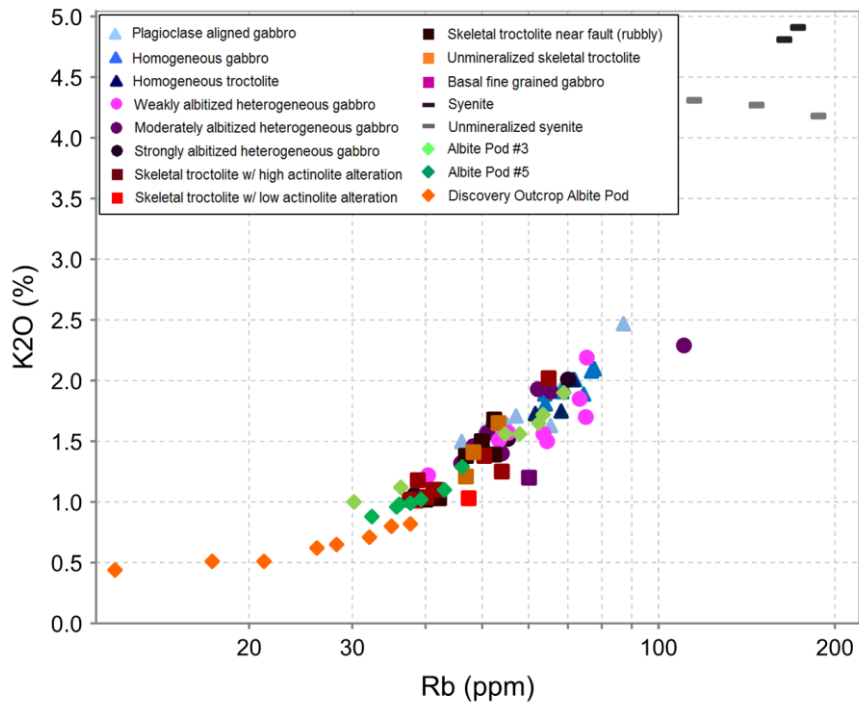


Figure 5.36 – A plot of Rb vs K_2O with all samples plotted. K_2O is in wt. %.

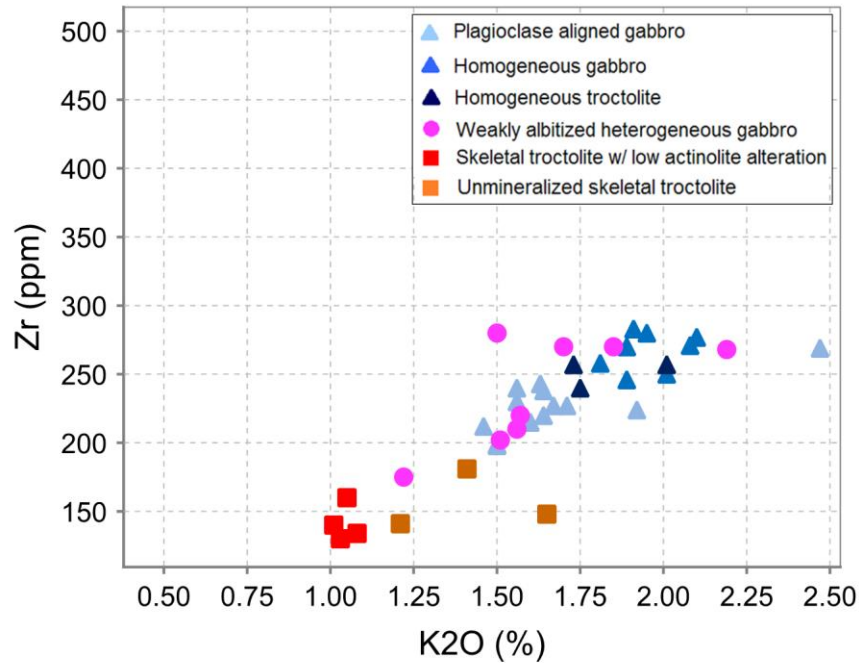


Figure 5.37 – A plot of K_2O vs. Zr. K_2O and Zr have a moderate linear correlation. Only unaltered samples are plotted in this diagram. K_2O is in wt. %.

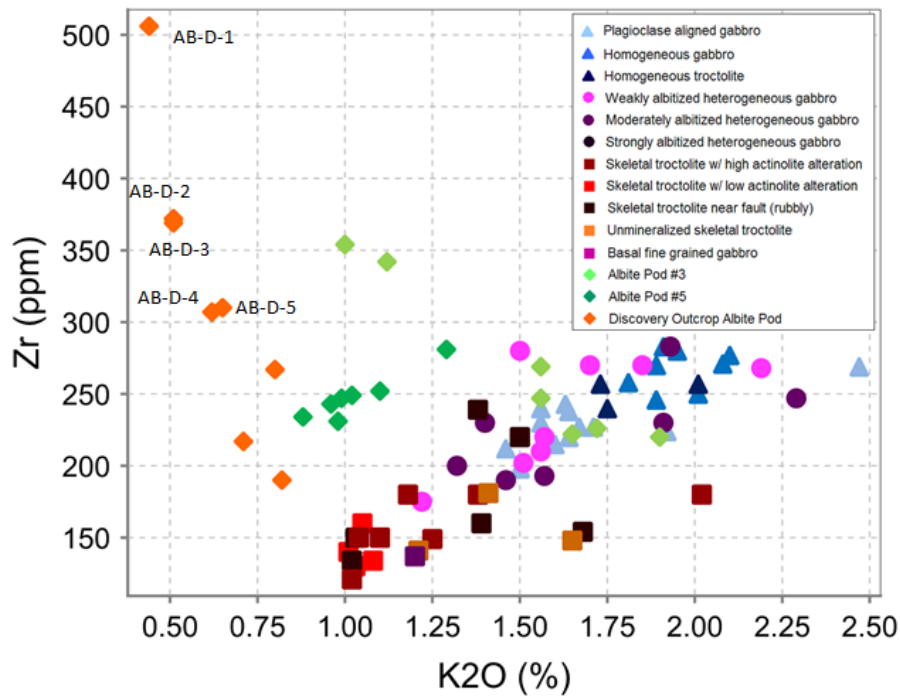


Figure 5.38 – A plot of K_2O vs. Zr with all samples plotted. Altered samples show more scatter in the data. Albite pod samples with the least amount of K_2O are the most albitized samples. K_2O is in wt. %.

5.1.4 Cu-PGE Diagrams and Down Hole Metal Ratios

Cu is the most abundant ore metal at the GLD, whereas Pd is the most abundant PGE. Figure 5.39 shows a log-log plot of Cu vs Pd with ratio lines for reference. The leftmost dashed line represents a ratio of $\text{Cu/Pd} = 3000$, while the rightmost dashed line represents a ratio of $\text{Cu/Pd} = 10,000$. Only weakly altered samples are shown on this plot. Most of the heterogeneous gabbro and skeletal troctolite samples have Cu/Pd ratios of 3000 to 10,000 lines. By contrast, most plagioclase aligned and homogeneous gabbro samples have Cu/Pd ratios of $> 10,000$. Figure 5.40 shows the same plot, but with all samples plotted. Most heterogeneous gabbro and skeletal troctolite samples plot within Cu/Pd ratios of 3,000 and 10,000, as do the albite pod samples and the majority of plagioclase aligned and homogeneous gabbro samples have Cu/Pd ratios of $>10,000$. Figure 5.41 shows a plot of Pd vs Cu/Pd with the least altered samples plotted. Dashed lines are shown between Cu/Pd values of 1000 and 10,000, and they indicate typical mantle values (Barnes et al., 1993). Almost all of the heterogeneous gabbro and skeletal troctolite data points plot within mantle values. Plagioclase aligned gabbro and homogeneous gabbro samples mainly plot outside of the field for mantle values. The homogeneous troctolite have values close to the upper limit for mantle rocks. Notably, the two plagioclase aligned gabbro samples with low Cu/Pd values at the two uppermost samples in DDHs G-10-16, and G-10-17. Some plagioclase aligned gabbro samples contain Cu/Pd ratios as high as $\sim 22,500$. These samples in particular occur lower in the stratigraphy, nearer to the mineralized and Pd-rich skeletal troctolite. Figure 5.42 shows the same plot as in Figure 5.41, but with all samples plotted. Samples from Albite Pod #3 and #5 follow the trend of unmineralized samples, while Discovery Outcrop Albite Pod samples plot among mineralized heterogeneous and skeletal troctolite samples. Unmineralized samples (<0.1 ppm Pd) show a steadily decreasing Cu/Pd ratio as Pd increases, while mineralized samples (>0.1 ppm Pd) mostly cluster between a ratio of 1000 and 10,000 Cu/Pd , with the exception of a few heterogeneous gabbro samples. The most Pd-rich samples were analyzed for Ir, Pt, Pd and Au content and show that, relative to mantle, GL samples are depleted in Ir and Ru, while values of Rh, Pt, Pd, and Au show enrichment over mantle

values (Figure 5.43). Syenite samples contain significantly less Rh than the rest of the sample suite.

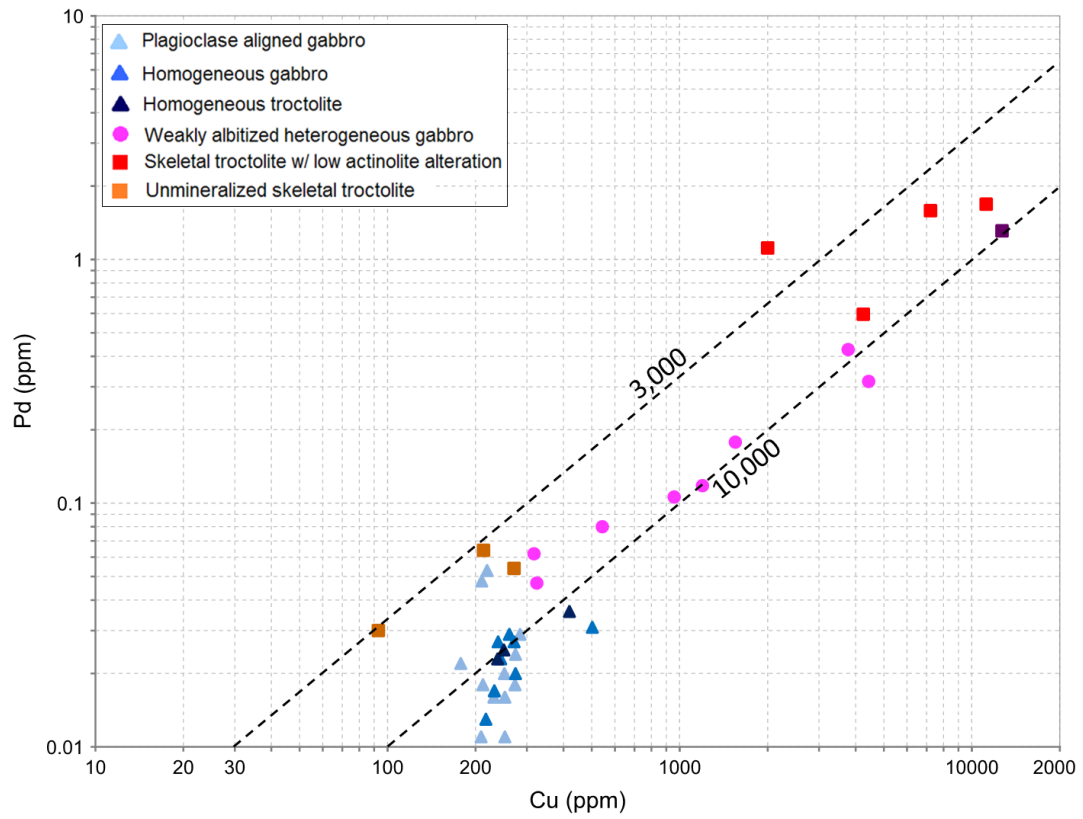


Figure 5.39 – A plot of Cu vs. Pd with two lines which represent the ratio of Cu/Pd (3000, and 10,000 from left to right). Only unaltered samples are plotted in this diagram.

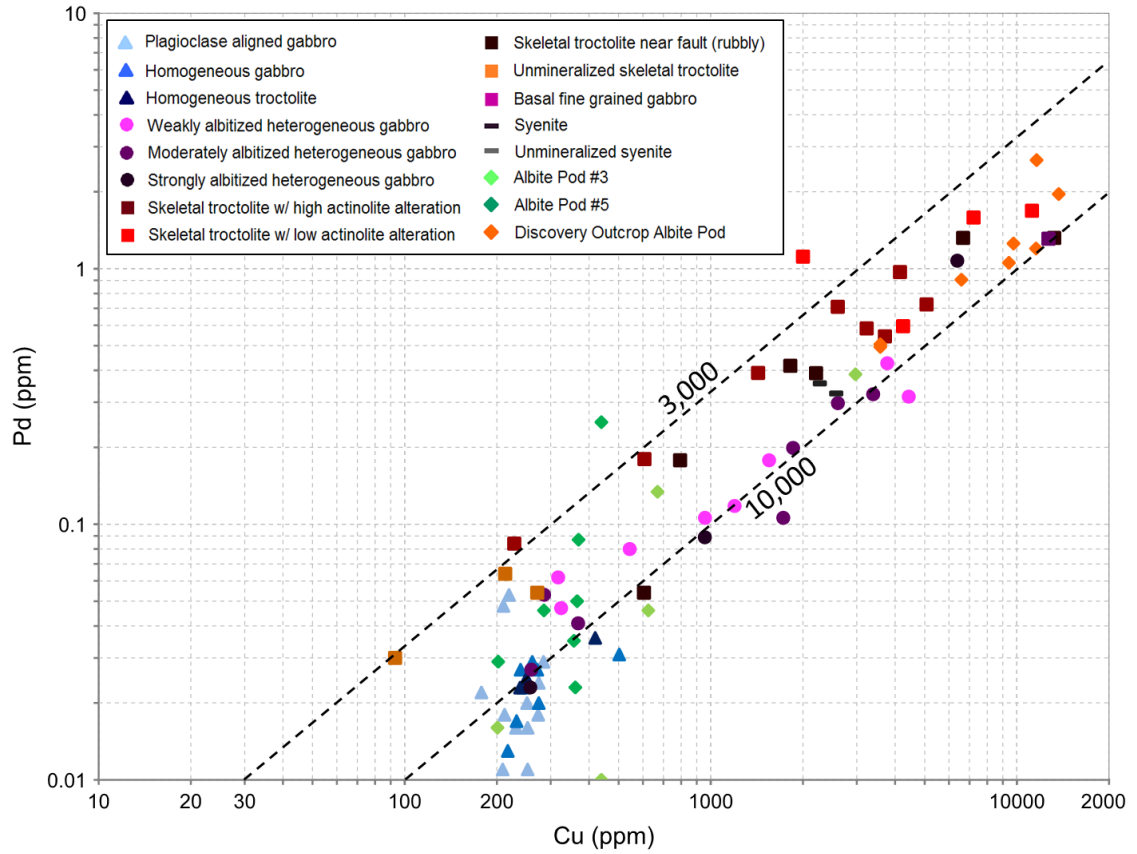


Figure 5.40 – A plot of Cu vs. Pd with two lines which represent the ratio of Cu/Pd (3000, and 10,000 from left to right). All samples are plotted in this diagram.

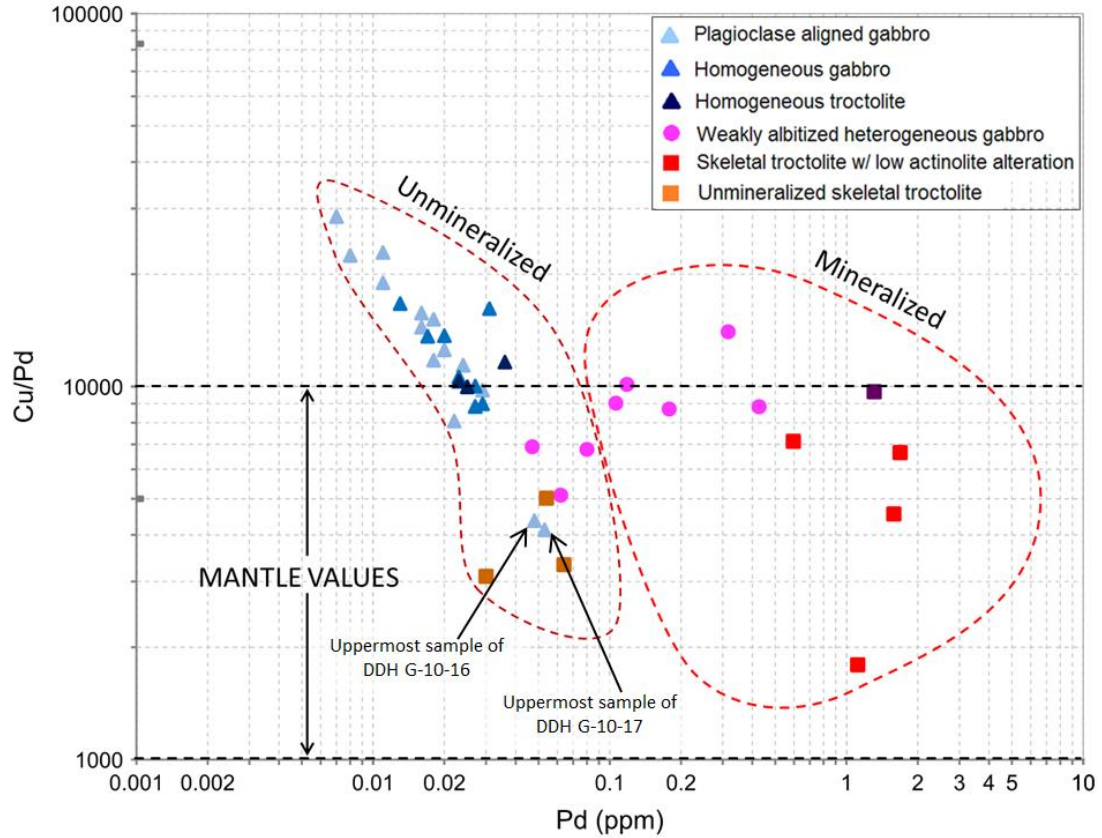


Figure 5.41 – A plot of Pd vs. Cu/Pd with all samples plotted. The field indicated by the dashed lines represents the Cu/Pd ratio typical of the mantle (Barnes et al., 1993). Cu/Pd is a wt. % ratio.

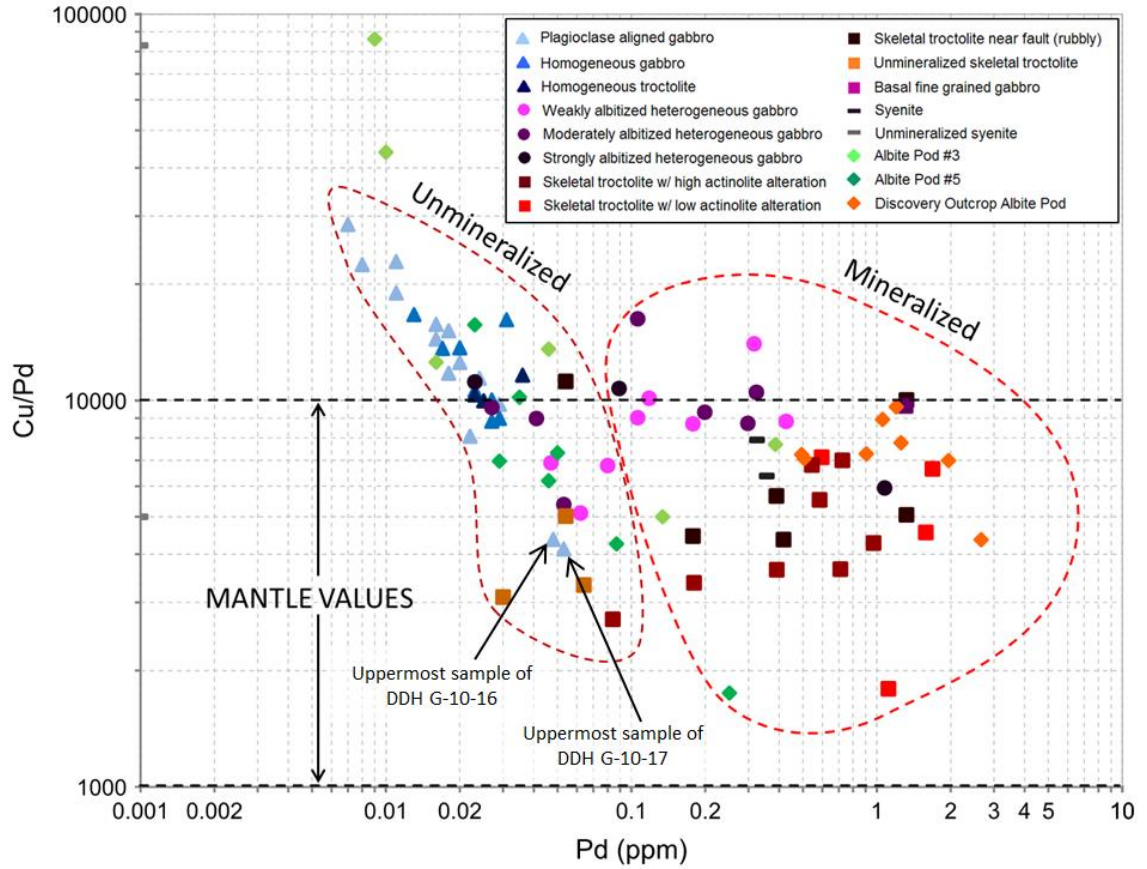


Figure 5.42 – A plot of Pd vs. Cu/Pd with only unaltered samples plotted. The field indicated by the dashed lines represents the Cu/Pd ratio typical of the mantle (Barnes et al., 1993). Cu/Pd is a wt. % ratio.

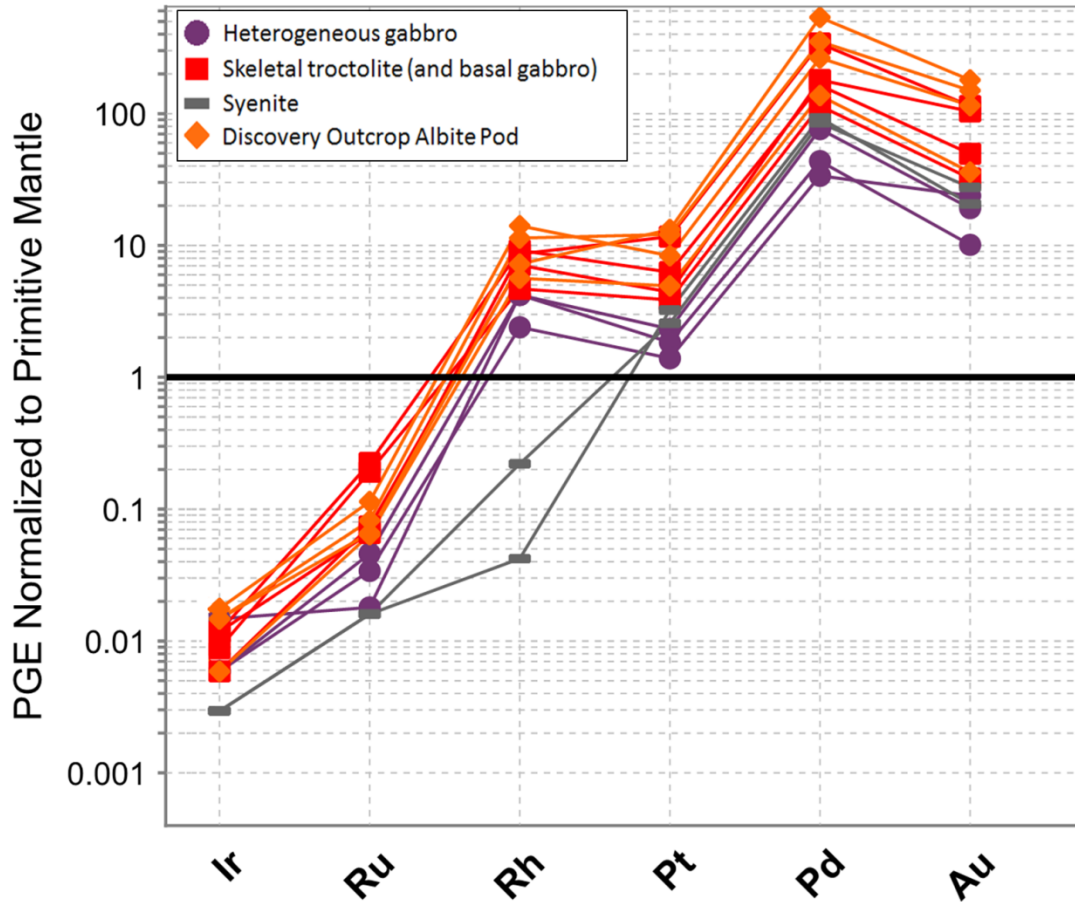


Figure 5.43 – A plot of PGE and Au normalized to mantle values (using data from Taylor and McLennan, 1985).

Understanding the relationship between lithologies and metal ratios is an important step in determining the deposition style (whether magmatic or hydrothermal) of copper-sulfides and associated platinum-group elements at the GLD. Figures 5.44 – 5.47 show the down-hole distribution of metals at the GLD including Cu, Ni, and Pd, and the variation in down-hole metal ratios including Pd/Pt, Cu/S, Cu/Pd, Ni/Pd and Ni/Cu. In mafic rocks, the proportions of Cu, Ni and Pd are typically controlled by the distribution of sulfides, chromite, olivine, and potentially platinum-group minerals (Barnes et al., 1988). Sulfides have been shown to act as ‘collectors’ of PGEs during the early formation stages of PGE deposits. Hence, an understanding of if and when sulfide segregation occurred is valuable from a prospecting point of view. Metal ratios can offer insight as to

whether or not sulfide segregation occurred due to the high partition coefficients that PGEs have (>1000) into sulfides than does Ni or Cu. As a result, sulfide segregation drastically changes the ratios of PGE in comparison to Ni and Cu. However, olivine crystallization must be considered before analyzing differences between Ni and Cu, since Ni and Cu have similar partition coefficients into olivine (Rajamani and Naldrett, 1978; Barnes and Ripley, 2016).

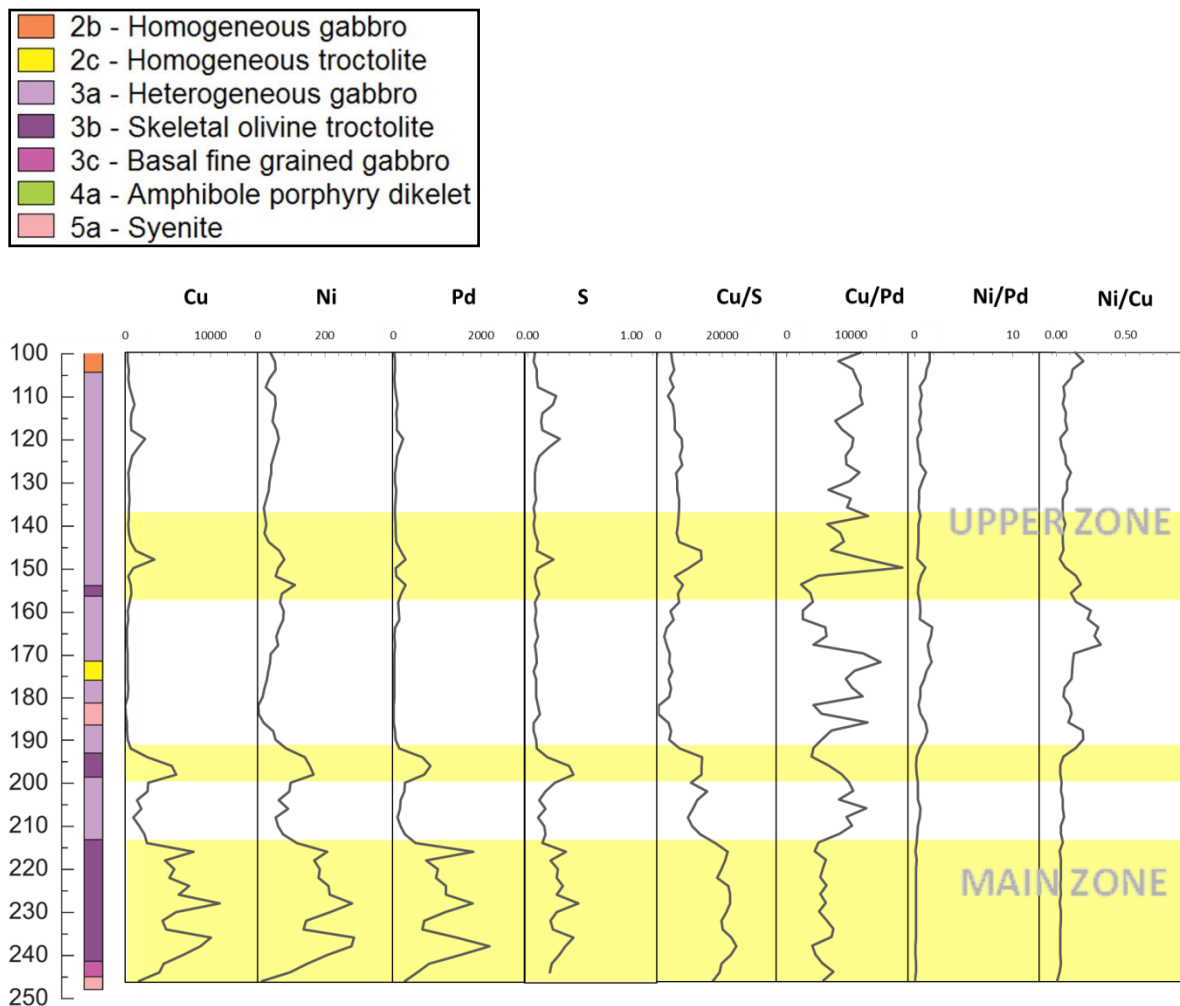


Figure 5.44 – Down-hole metal summary of drill hole G-10-17, with Cu, Ni, and Pd (ppm). Metal ratios include Cu/S, Cu/Pd, Ni/Pd and Ni/Cu as wt. % ratios. The y-axis is depth in meters.

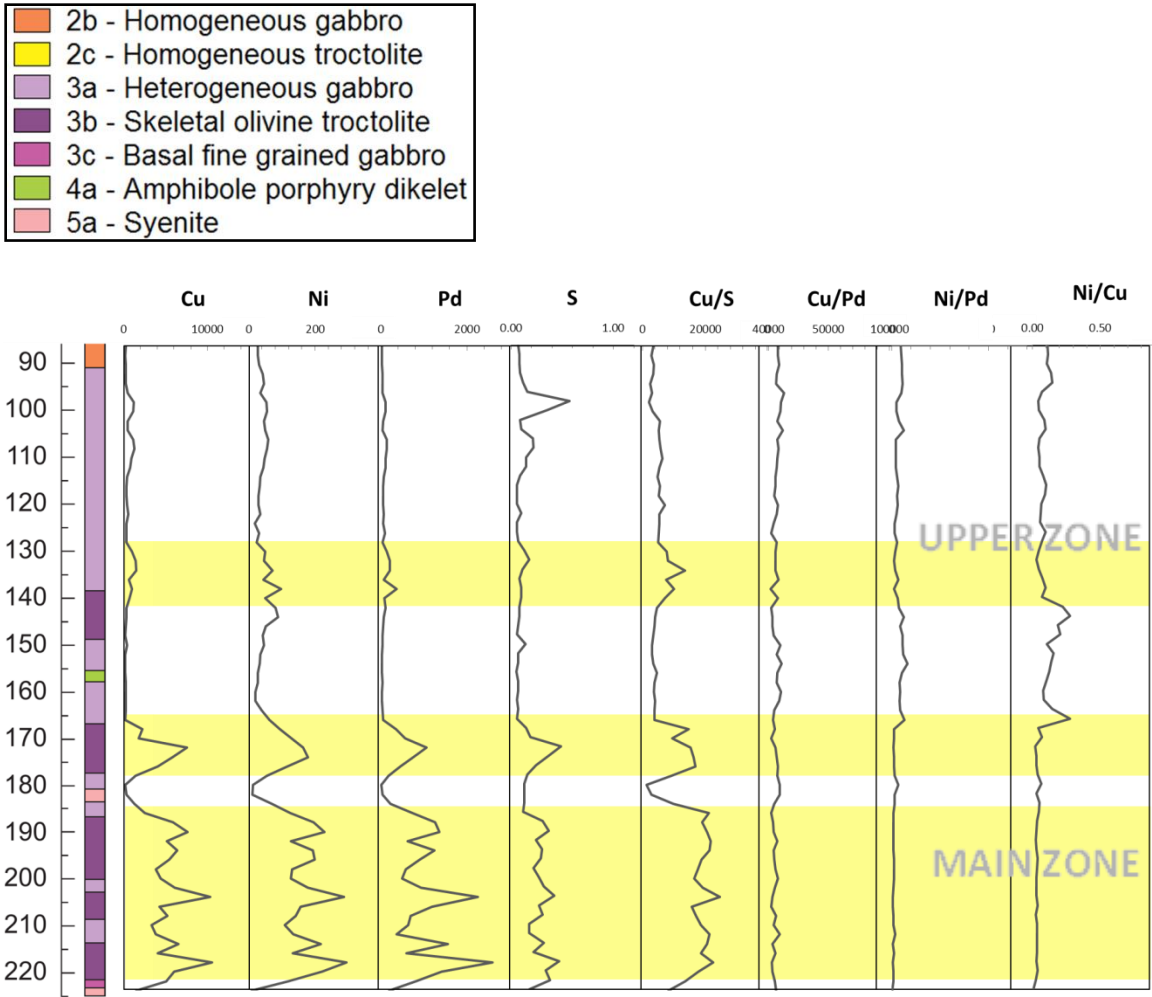


Figure 5.45 – Down-hole metal summary of drill hole G-10-16, with Cu, Ni, and Pd (ppm). Metal ratios include Cu/S, Cu/Pd, Ni/Pd and Ni/Cu as wt. % ratios. The y-axis is depth in meters.

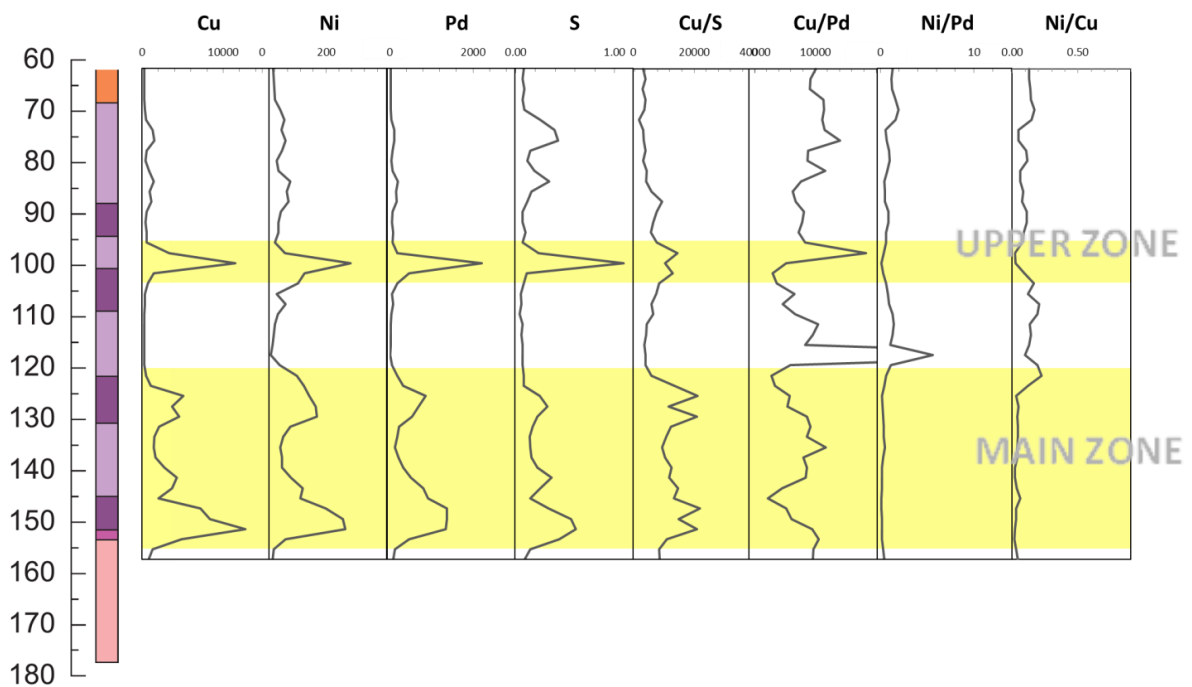
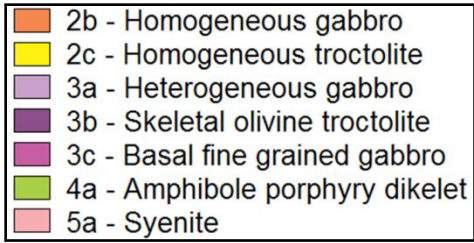


Figure 5.46– Down-hole metal summary of drill hole G-10-04, with Cu, Ni, and Pd (ppm) as well as S (%). Metal ratios include Cu/S, Cu/Pd, Ni/Pd and Ni/Cu as wt. % ratios. The y-axis is depth in meters.

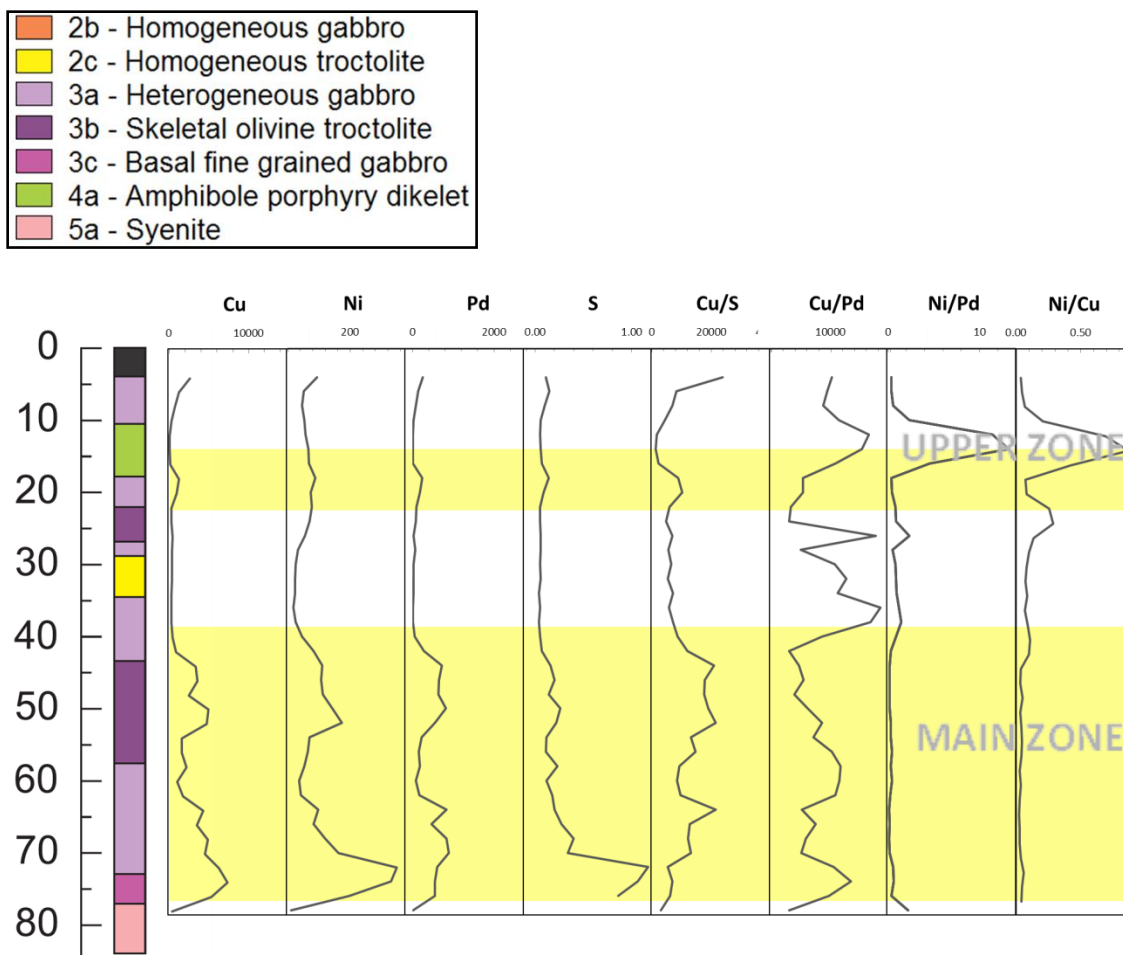


Figure 5.47 – Down-hole metal summary of drill hole G-10-02, with Cu, Ni, and Pd (ppm). Metal ratios include Cu/S, Cu/Pd, Ni/Pd and Ni/Cu as wt. % ratios. The y-axis is depth in meters.

5.1.4.1 Drill Hole G-10-17

Figure 5.44 shows the down-hole distribution of Cu, Ni, and Pd along with ratios of Cu/S, Cu/Pd, Ni/Pd and Ni/Cu in drill hole G-10-17. The yellow fields highlight the depths at which Cu mineralization locally peaks. At 148 m, Cu reaches a local maximum value of 0.339 wt. %, but then gradually decreases further down hole until reaching trace values. This moderately Cu-rich interval is termed the “Upper Zone” of mineralization, and is also observed in holes G-10-16 and G-10-04. Concurrent with the minor spike in Cu is also an increase in Ni (80 ppm) and Pd (279 ppm). Metal ratios also demonstrate a

corresponding change, particularly with Cu/S which is fairly static until the Upper Zone mineralization is intersected, at which point they too show local peaks that correspond to high Cu values. Once away from the Upper Zone mineralization at 152 m, metal values show no significant fluctuation and metal ratios are sporadic until 194 m, at which point Cu surges from 0.061 wt. % to 0.2599 wt. %. From 194 m to the end of hole at 248 m, Cu values range from a low of 0.093 wt. % to a high of 1.10 wt. %. This interval marks the “Main Zone” of mineralization. Ni, Cu and Pd all appear to increase proportionally. Not coincidentally, this Main Zone mineralization occurs directly below a thin layer of syenite at 182 m, and the particularly strong Cu, Ni, and Pd mineralization occurs within the skeletal troctolite unit. Petrography and SEM work shows that Ni, Cu and Pd are all sequestered into sulfide phases, primarily chalcopyrite, bornite, millerite, and what appears to be altered pentlandite (with varying amounts of Co substituting in for Ni), and a variety of PGM including those that have integrated Ni into their structure.

5.1.4.2 Drill Hole G-10-16

Figure 5.45 shows the down-hole distribution of Cu, Ni, and Pd along with ratios of Cu/S, Cu/Pd, Ni/Pd and Ni/Cu in drill hole G-10-16. As mentioned previously, the yellow fields highlight the depths at which Cu mineralization occurs at or very near 0.10 wt. %. At 98 m, Cu reaches a local maximum value of 0.124 wt. % and remains roughly around same value until 114 m. Cu mineralization again remains negligible until 130 m, at which point once again reaches a local maximum of 0.100 wt. %. This small lens of mineralization continues until 140 m, with values between 0.061 wt. % and 0.149 wt. %. Unlike the first described interval of Cu-mineralization, the second described interval of mineralization contains concurrent peaks in Ni, and Pd-mineralization. Hence, it is likely that the second interval of mineralization is continuous with the Upper Zone mineralization in drill hole G-10-17. Cu/S exhibit peak values which correspond to locally high Cu values, while Ni/Pd and Ni/Cu ratios are low. At 168 m, and coincident with a lithological change to the skeletal unit, begins the Main Zone mineralization. The range in Cu values in this interval (not including the low values associated with the syenite intrusion at 180 m) is from a low of 0.148 wt. % to a high of 1.05 wt. %. Ni and Pd values correlate well to fluctuations in Cu. The ratio of Cu/S increases with higher

values of Cu, while Ni/Pd and Ni/Cu decreases as Cu values increase. Cu/Pd generally shows an inverse trend with increasing Cu, thus indicating that the proportion of Pd is much higher than the proportion of Cu in the most strongly mineralized intervals. As noted previously, metal values are generally much higher within the skeletal troctolite unit, as opposed to the heterogeneous unit.

5.1.4.3 Drill Hole G-10-04

Figure 5.46 shows the down-hole distribution of Cu, Ni, and Pd along with ratios of Cu/S, Cu/Pd, Ni/Pd and Ni/Cu in drill hole G-10-04. The first significant peak in Cu mineralization occurs at 98 m, at which point it peaks from 543 ppm to 3331 ppm. This strongly mineralized interval ends at 104 m, containing a maximum of 1.15 wt. % Cu, and a minimum of 0.143 wt. % Cu. Coincident with this mineralized Cu interval are also peaks in Ni (maximum 276 ppm, minimum 72 ppm) and Pd (maximum 2214 ppm, minimum 182 ppm). Cu/S, Cu/Pd, Ni/Pd and Ni/Cu generally show a decrease at this maximum Cu value. This indicates that at that particular maximum Cu value, S is locally enriched relative to Cu, while Pd is relatively more enriched than Cu, and that Cu is more enriched than Ni. Mineralogically, this interval contains abundant skeletal olivine intergrown with skeletal to stubby, equant grains of magnetite. Blebby to disseminated chalcopyrite is commonly hosted by an actinolite-chlorite-biotite alteration assemblage that is pseudomorphic after clinopyroxene. This interval is the Upper Zone mineralization, which was also observed in drill holes G-10-17, and G-10-16. At 124 m, and at the contact between heterogeneous gabbro (Unit 3a) and skeletal troctolite (Unit 3b), Cu again drastically increases and remains at elevated values until the basal syenite contact. This interval is continuous with the Main Zone mineralization also observed in drill holes G-10-17, and G-10-16. During this interval, Cu ranges from a minimum of 0.109 wt. % to a maximum of 1.28 wt. %. Overall, Ni and Pd values both vary proportionally to Cu. Metal ratios Cu/Pd, Ni/Pd and Ni/Cu are predominantly unchanged in the Main Zone, while Cu/S varies somewhat proportionally to the varying, yet elevated amounts of Cu. From 110-120 m, Pd values are remarkably depleted relative to all unmineralized intervals, while Cu values are steady with similarly unmineralized intervals.

5.1.4.4 Drill Hole G-10-02

Figure 5.47 shows the down-hole distribution of Cu, Ni, and Pd along with ratios of Cu/S, Cu/Pd, Ni/Pd and Ni/Cu in drill hole G-10-02. This drill hole is unique from the other drill holes in that it collared directly into the heterogeneous gabbro (Unit 3a) which is stratigraphically lower than the unmineralized gabbros, and hence does not ever intersect any plagioclase lined gabbro (Unit 2a) or homogeneous gabbro (Unit 2b). At 4 m, Cu values peak at 0.263 wt. %, but sharply declines to negligible values between 10 and 16 m as a result of the intrusion of an amphibole porphyry dikelet (Unit 4a). At 18 m, directly after the change in lithology from the amphibole porphyry dikelet (Unit 4a) to the heterogeneous gabbro (Unit 3a), Cu values again increase from 0.016 wt. % to 0.124 wt. %. This zone of Cu-mineralization likely corresponds to Upper Zone mineralization that is observed in all of the other study drill holes. Peaks in Ni, and Pd values also mimic the peaks in Cu. Overall, the ratio of Cu/S increases proportionally to high values of Cu, Ni and Pd, while Ni/Pd and Ni/Cu mostly decrease proportionally to high values of Cu, Ni, and Pd. The ratio of Cu/Pd largely decreases upon increasing Cu, Ni and Pd. After 22 m, Cu mineralization stays below 0.045 wt. % until 42 m, at which point Cu surges to 0.084 wt. %. Between 42 m and near the end of the hole at 72 m, Cu values stay within a maximum of 0.735 wt. %, and a minimum of 0.102 wt. %. This 30 m zone of mineralization is continuous with the Main Zone mineralization that is observed in all of the other study drill holes. Throughout this mineralized interval, Ni and Pd maximum and minimum values mimic those of Cu. The Cu/S ratio also mimics the trends of Cu, Ni and Pd, while Cu/Pd is largely a reversal of the peaks created by high Cu, Ni and Pd values. Ratios of Ni/Pd and Ni/Cu are also constant.

Chapter 6

6 Stable $\delta^{18}\text{O}$ Isotopes

6.1 Down-hole Whole Rock Oxygen Isotopes

A total of 23 drill-core samples were analyzed for whole rock $\delta^{18}\text{O}$ content. 17 of these samples were from drill-holes G-10-17 and G-10-16. In order to display the large scale variation in whole rock $\delta^{18}\text{O}$ values at the GLD, the whole rock $\delta^{18}\text{O}$ values of these two particular drill holes (G-10-17 and G-10-16) are plotted adjacent to the down-hole logs of each respective drill-hole (Figure 6.1). There is an apparent decrease in $\delta^{18}\text{O}$ values down-hole towards the basal syenite contact in both holes G-10-16 and G-10-17.

Plagioclase aligned gabbro, which is the uppermost lithology at the Geordie Lake deposit, contains a range of whole rock $\delta^{18}\text{O}$ values from 6.0 ± 0.1 ‰ to 4.6 ± 0.1 ‰. Figure 6.2 compares the petrographic characteristics of a sample that has a $\delta^{18}\text{O}$ value of 6.0 ± 0.1 ‰ to a sample with a $\delta^{18}\text{O}$ value of 4.6 ± 0.1 ‰. Both samples contain similar modal amounts of primary plagioclase, clinopyroxene, plus magnetite as well as secondary actinolite, and biotite. Homogeneous gabbro, which is stratigraphically below than the plagioclase aligned gabbro, contain whole rock $\delta^{18}\text{O}$ values that range from 4.1 ± 0.1 ‰ to 3.6 ± 0.1 ‰, and the samples with these different values exhibit no significant variation in modal mineralogy and alteration. Whole rock $\delta^{18}\text{O}$ values within heterogeneous gabbro are comparatively lower on average, with a range of $\delta^{18}\text{O}$ values from 4.2 ± 0.1 ‰, to 2.4 ± 0.1 ‰. Heterogeneous gabbro samples with the uppermost and lowermost values of $\delta^{18}\text{O}$ are also petrographically similar with the exception of slightly more fine grained magnetite in the sample with $\delta^{18}\text{O}$ value of 2.4 ± 0.1 ‰ (Figure 6.3). Skeletal troctolite, on average, contain the most depleted values of $\delta^{18}\text{O}$, with a maximum whole rock $\delta^{18}\text{O}$ value of 3.2 ± 0.1 ‰, and a minimum whole rock $\delta^{18}\text{O}$ value of 1.9 ± 0.1 ‰. In Figure 6.4, a sample with a whole rock $\delta^{18}\text{O}$ value of 1.9 ± 0.1 ‰ is compared to a sample with a whole rock $\delta^{18}\text{O}$ value of 3.2 ± 0.1 ‰. The greatest dissimilarity between the two samples is grain size. Sample IM-30 (Figure 6.5a) is fine grained (<0.5 mm), whereas IM-29 (Figure 6.5b) is mainly medium to coarse grained (~1 mm). Additionally, sample IM-30 consists

mainly of albite-altered (pinkish-brown) fine grained plagioclase with disseminated fine grained magnetite and apatite, while IM-29 consists predominantly of fresh coarse grained clinopyroxene, skeletal olivine, plagioclase, as well as fine grained magnetite and accessory apatite. Thus, the more altered and finer-grained sample contains a comparatively lower whole rock $\delta^{18}\text{O}$ value.

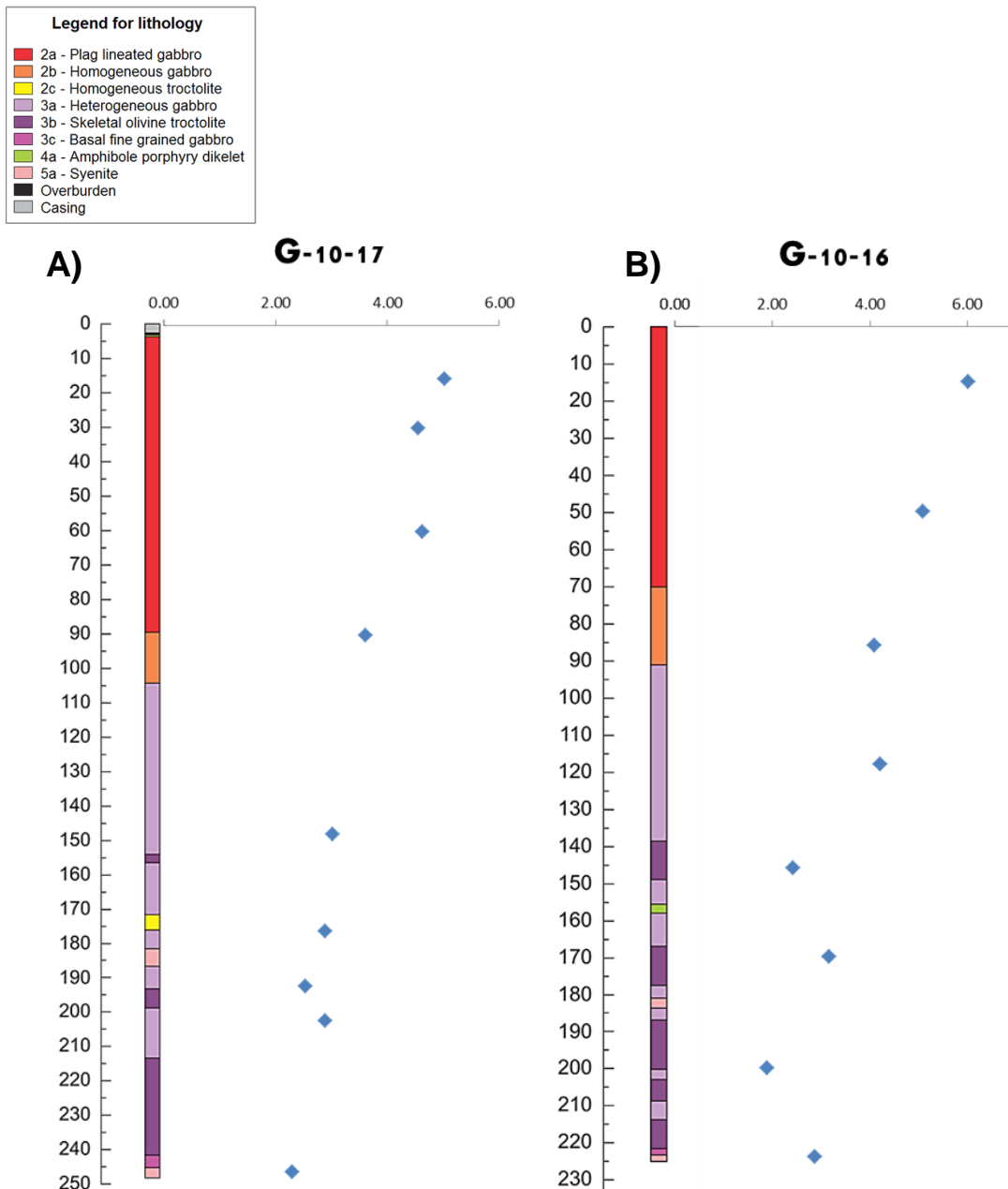


Figure 6.1 – Down-hole plots of drill hole G-10-17 (A) and G-10-16 (B) showing whole rock $\delta^{18}\text{O}$ values that correspond to where each sample was taken. Generally, $\delta^{18}\text{O}$ values show a decrease going down-hole. The x-axis represents $\delta^{18}\text{O}$ values in ‰, and the y-axis is depth in m.

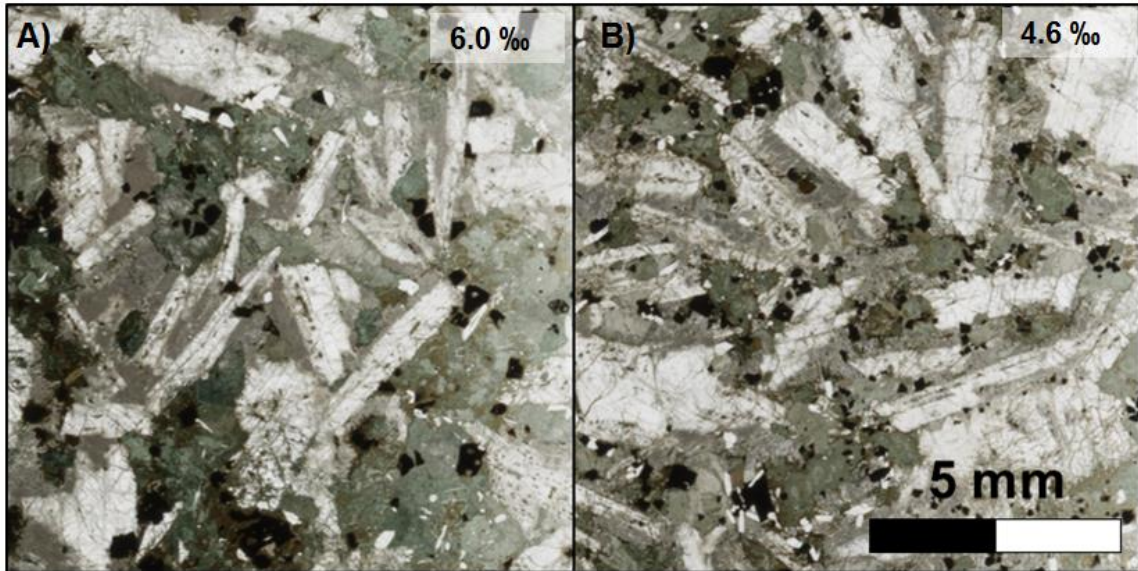


Figure 6.2 – Comparison of plagioclase aligned gabbro samples with variable whole rock $\delta^{18}\text{O}$ values. (A) Sample IM-UM-8 contains a whole rock $\delta^{18}\text{O}$ value of 6.0 ‰; (B) Sample IM-UM-17 contains a whole rock $\delta^{18}\text{O}$ value of 4.6 ‰. Both images are in PPL

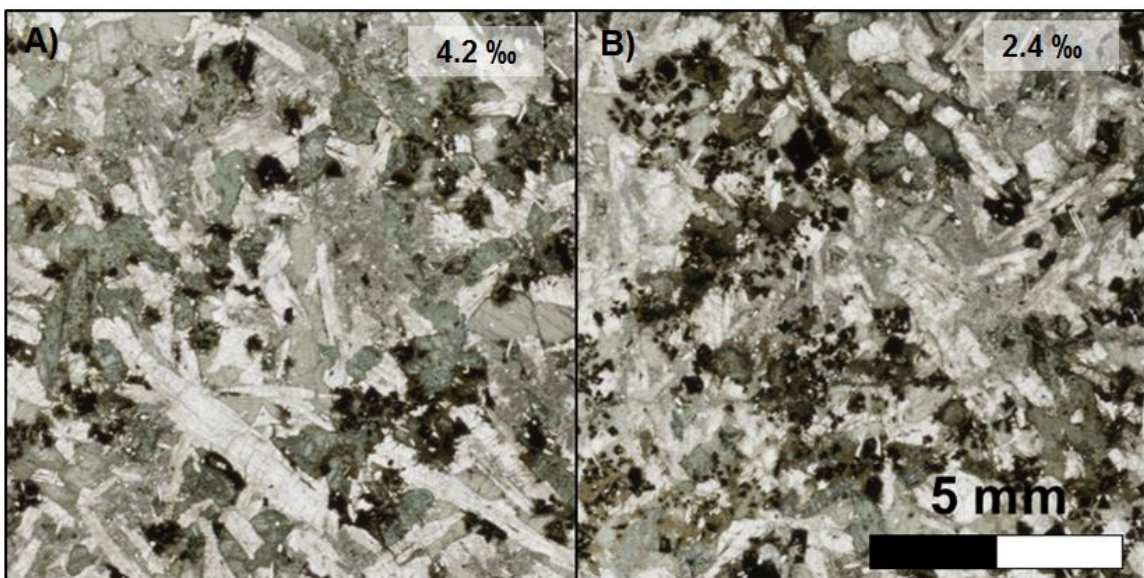


Figure 6.3 – Comparison of weakly albitized heterogeneous gabbro samples with variable whole rock $\delta^{18}\text{O}$ values. (A) Sample IM-25 contains a whole rock $\delta^{18}\text{O}$ value of 4.2 ‰; (B) Sample IM-32 contains a whole rock $\delta^{18}\text{O}$ value of 2.4 ‰. Both images are in PPL

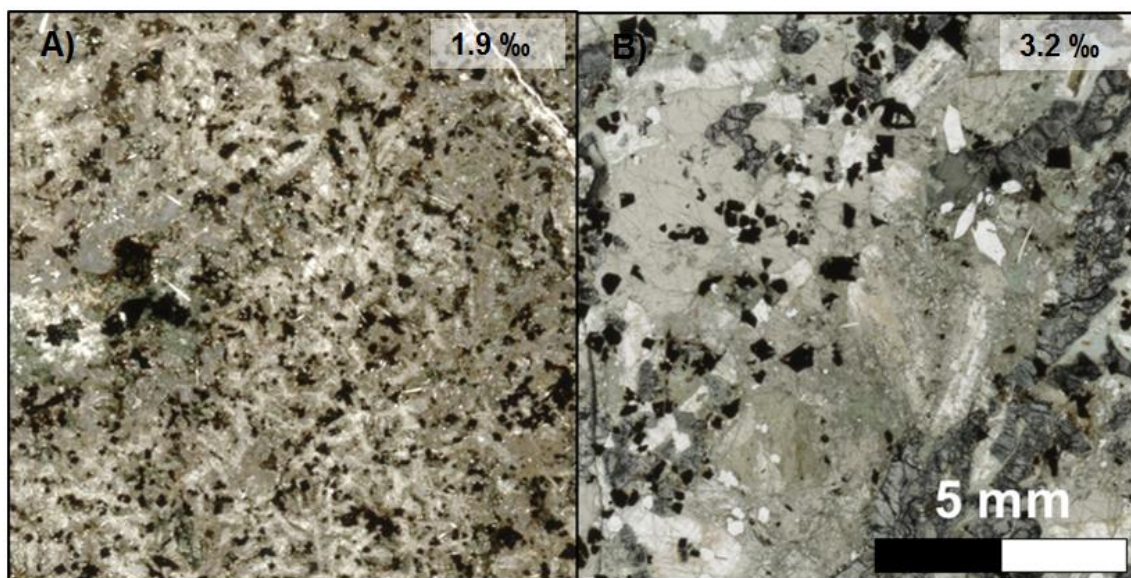


Figure 6.4 – A comparison of skeletal troctolite samples with varying $\delta^{18}\text{O}$ values. (A) Sample IM-30 contains a whole rock $\delta^{18}\text{O}$ value of 1.9 ‰, (B) Sample IM-29 contains a whole rock $\delta^{18}\text{O}$ value of 3.2 ‰. Both images are in PPL

Figure 6.5 shows the whole rock $\delta^{18}\text{O}$ values of all down-hole samples plotted against SiO_2 , Fe_2O_3 , Na_2O , CaO , K_2O , and MgO . Whole rock $\delta^{18}\text{O}$ values tend to increase in skeletal troctolite samples with increasing Fe_2O_3 and MgO . Conversely, increasing $\delta^{18}\text{O}$ values favours lower amounts of SiO_2 , Na_2O , and CaO in skeletal troctolite samples. Within the syenite samples (dark and light grey dashes), CaO mainly increases as whole rock $\delta^{18}\text{O}$ values increase, while K_2O decreases with increasing whole rock $\delta^{18}\text{O}$ values. Figure 6.6 shows the same samples plotted on a bivariate plot of Mg # versus $\delta^{18}\text{O}$. Generally, this diagram shows that a higher Mg # results in a lower $\delta^{18}\text{O}$ value, particularly among skeletal troctolite and heterogeneous gabbro samples. Figure 6.7 shows the ratio of $\text{Na}/(\text{Na}+\text{Ca})$ in moles plotted against $\delta^{18}\text{O}$ values, since the most abundant alteration mineral present at the GLD is albite. In this plot, we can see three distinct trends (circled by a dashed red line on the plot): first is that of decreasing $\text{Na}/(\text{Na}+\text{Ca})$ with increasing $\delta^{18}\text{O}$ values in syenite samples, second is decreasing $\text{Na}/(\text{Na}+\text{Ca})$ with increasing $\delta^{18}\text{O}$ values in skeletal troctolite samples, and finally, constant $\text{Na}/(\text{Na}+\text{Ca})$ with increasing $\delta^{18}\text{O}$. Figure 6.8 shows a comparison of whole rock $\delta^{18}\text{O}$ values plotted against CIPW normative albite (Figure 6.8a) and anorthite (Figure 6.8b). Figure 6.8c and (d) also show whole rock $\delta^{18}\text{O}$ values plotted versus CIPW normative magnetite and diopside.

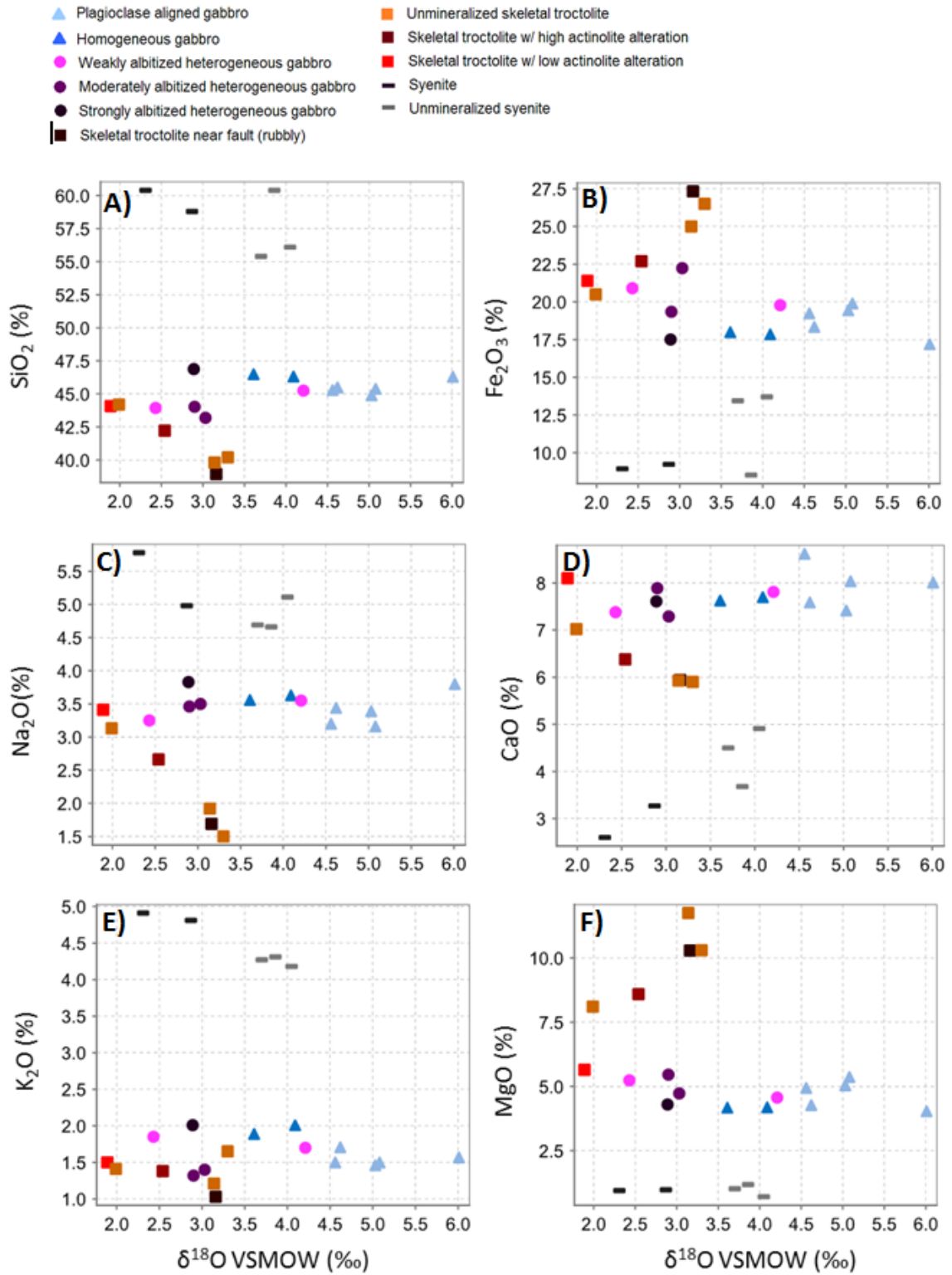


Figure 6.5 – Whole rock $\delta^{18}\text{O}$ values are plotted against the following major element oxides: **A)** SiO₂, **B)** Fe₂O₃, **C)** Na₂O, **D)** CaO, **E)** K₂O, and **F)** MgO.

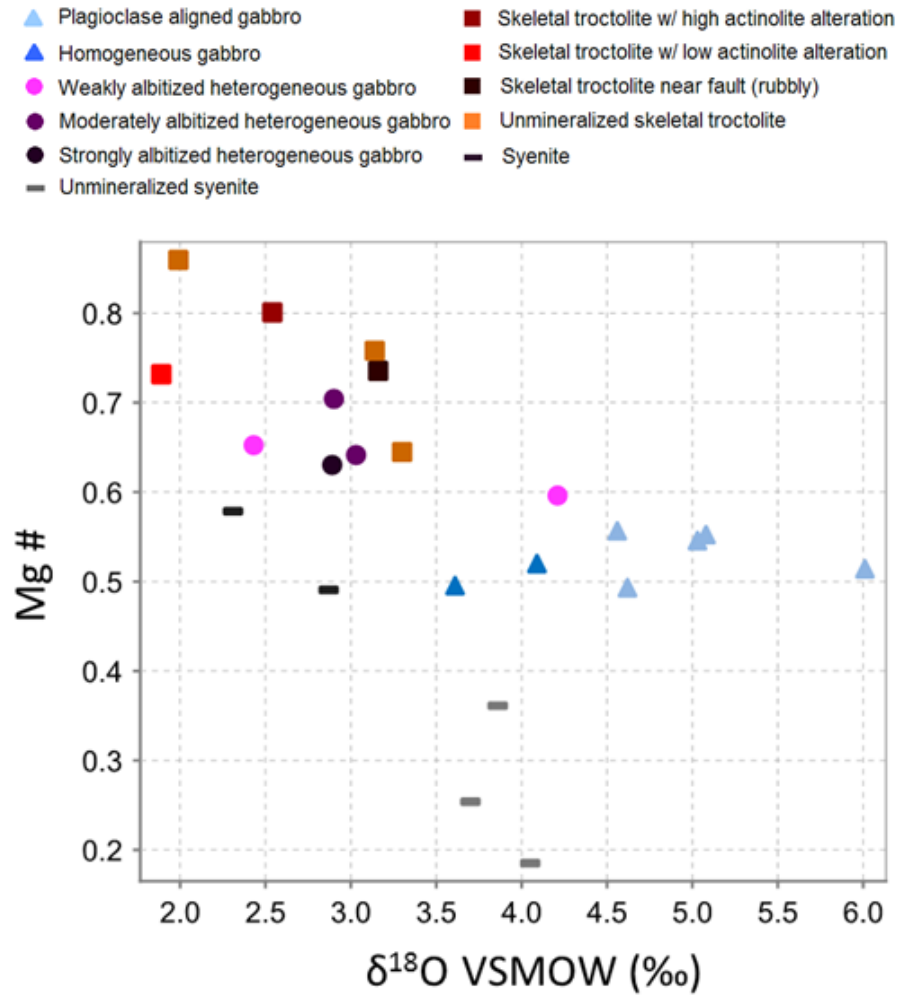


Figure 6.6 – Whole rock $\delta^{18}\text{O}$ values are plotted versus Mg #. The Mg # was calculated based on the residual FeO content, assuming that all Fe_2O_3 partitioned into magnetite (as described in Chapter 5)

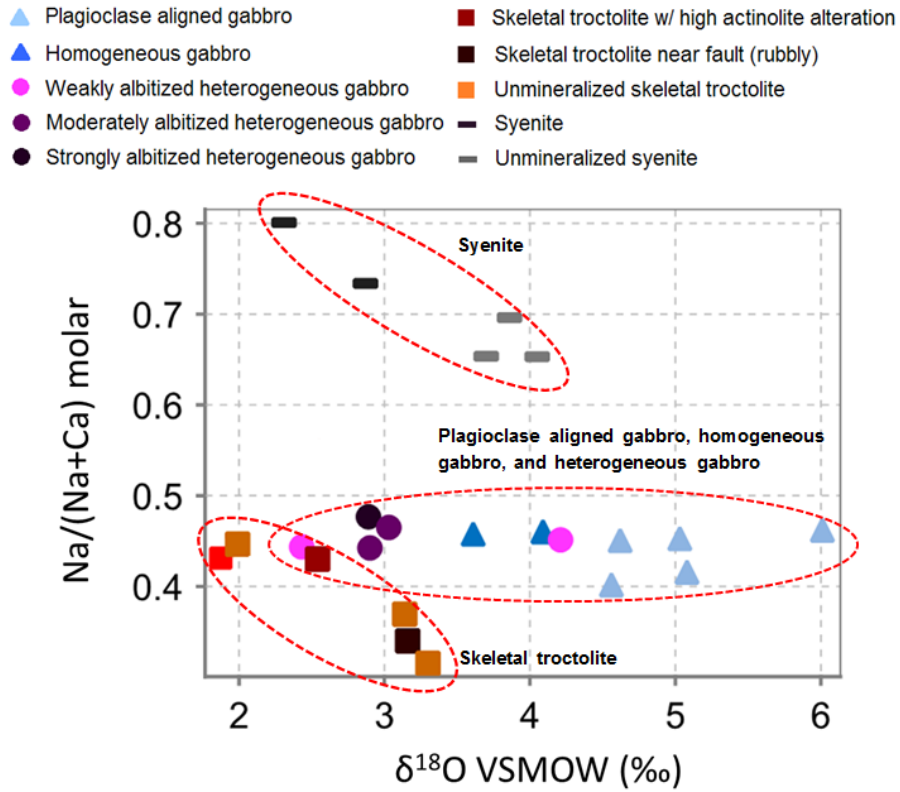


Figure 6.7 – Whole rock $\delta^{18}\text{O}$ values are plotted versus a ratio of Na relative to Na+Ca in moles. This ratio represents the amount of albite relative to anorthite, where a higher ratio represents more albite relative to anorthite.

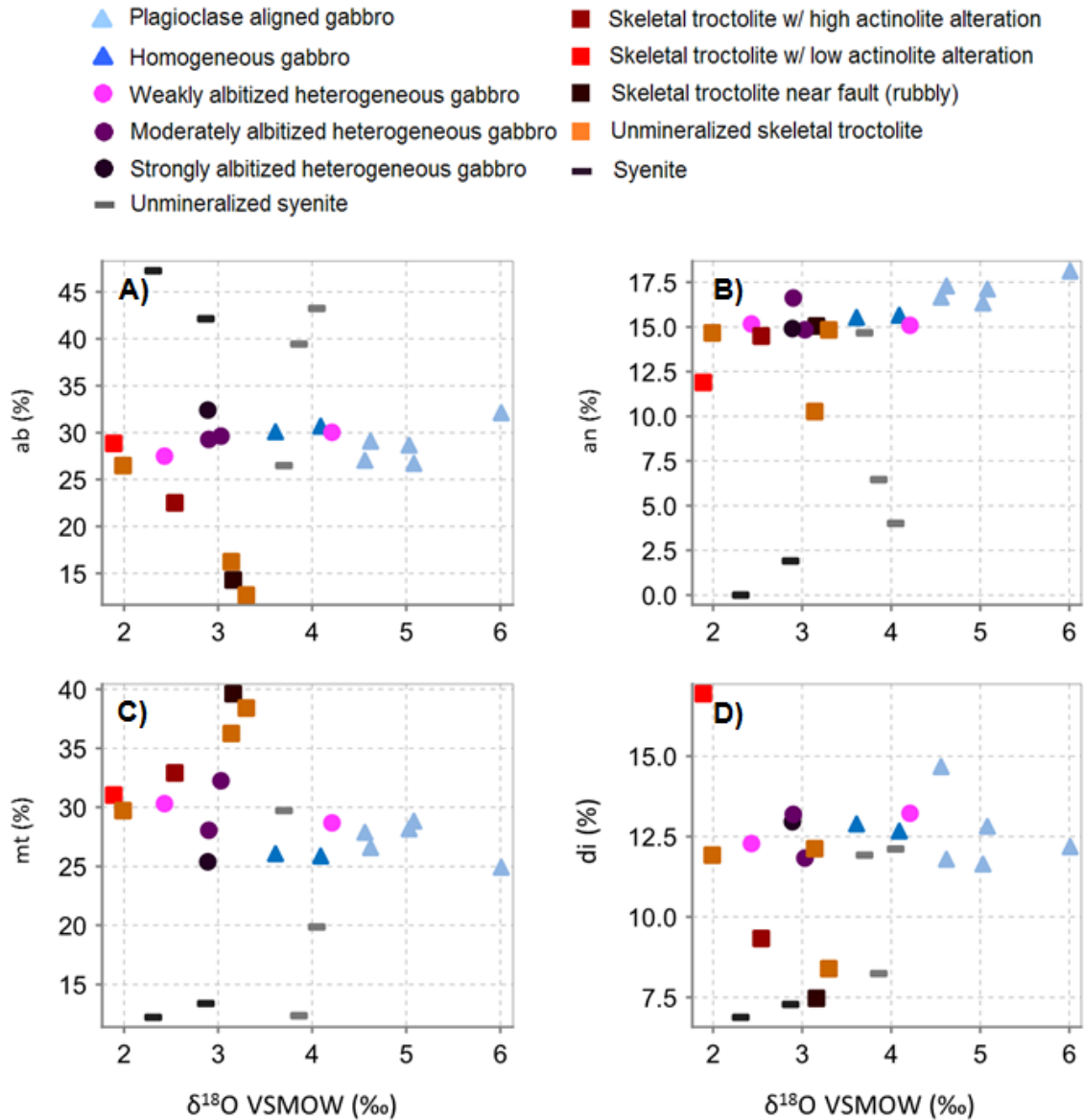


Figure 6.8 – Whole rock $\delta^{18}\text{O}$ values are plotted versus CIPW normative mineral modal percentages (as calculated in Chapter 5). **A)** There is no discernable trend with regard to the effect of increasing albite (%) relative to whole rock $\delta^{18}\text{O}$ values of heterogeneous gabbro (circles) plagioclase aligned gabbro and homogeneous gabbro (both represented by triangles). Decreasing amounts of albite correlate to an increase in $\delta^{18}\text{O}$ values for skeletal troctolite samples (squares), **B)** Increasing $\delta^{18}\text{O}$ values generally increase with increasing amounts of anorthite (%), **C)** Within skeletal troctolite samples, an increase in $\delta^{18}\text{O}$ values correlate to an increase in normative magnetite, **D)** Increasing $\delta^{18}\text{O}$ values do not correspond to any changes in CIPW normative percentages of diopside. Values on the y-axis are in calculated weight percent.

In Figure 6.8a, there is a clear correlation between increasing whole rock $\delta^{18}\text{O}$ values and decreasing normative albite content within skeletal troctolite samples (which are denoted

by square sample points). In Figure 6.8b, increasing whole rock $\delta^{18}\text{O}$ values correlate to an increase in normative anorthite content for most of the data points, with the exception of two skeletal troctolite samples. In Figure 6.8c, skeletal troctolite samples show a positive correlation between whole rock $\delta^{18}\text{O}$ values, and normative magnetite content. All other data points show relative scatter. Figure 6.8d shows no relationship between normative diopside content, and whole rock $\delta^{18}\text{O}$ values.

Figure 6.9 (a) shows whole rock $\delta^{18}\text{O}$ values plotted against Cu (ppm), while Figure 6.9 (b) shows whole rock $\delta^{18}\text{O}$ values versus Pd (ppm). In both plots, we see that Cu and Pd are enriched (containing <1,000 ppm Cu and <0.1 ppm Pd) only within those samples that have whole rock $\delta^{18}\text{O}$ values <3.2±0.1 ‰, and this is indicated by the light orange shaded region. It should be noted that whole rock $\delta^{18}\text{O}$ values less than 3.2±0.1 ‰ occur no more than 80 m above the contact between the GLI and the basal syenite. However, beneath this contact and deeper into the syenite, we see whole rock $\delta^{18}\text{O}$ values of 3.7±0.1 ‰, 4.1±0.1 ‰, and 3.9±0.1 ‰ at distances of 82.33 m, 65.41 m, and 18.99 m respectively below the GL-syenite contact.

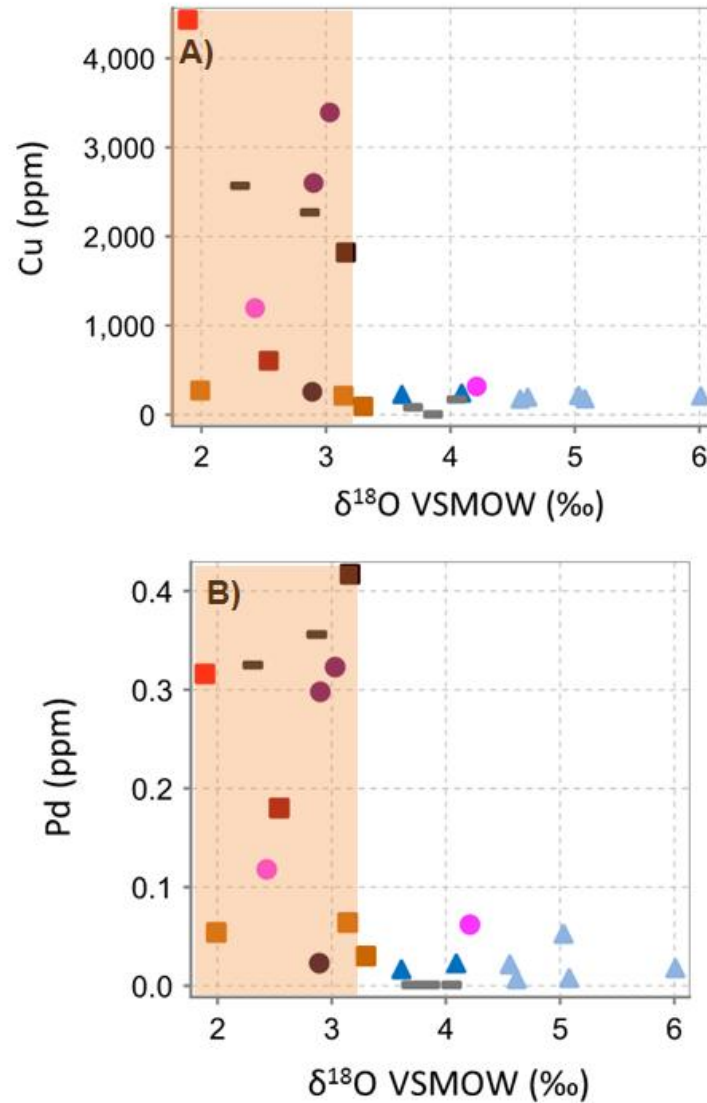
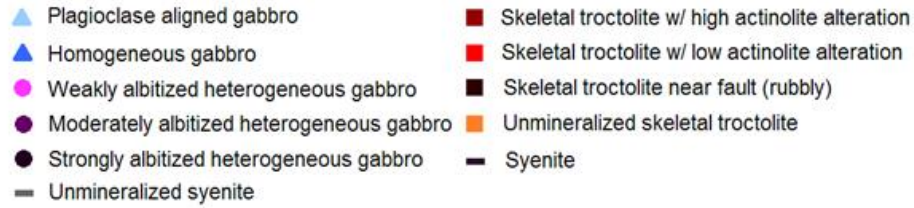


Figure 6.9 – Whole rock $\delta^{18}\text{O}$ values are plotted versus: **A)** Cu (in ppm) where the light orange shaded region shows the field which contains the last sample to have >1,000 ppm Cu, **B)** Pd (ppm) where the light orange shaded region also denotes the field which contains the last sample to have >0.1 ppm Pd

6.2 Albite Pod Whole Rock Oxygen Isotopes

Two of three albite pods transects that were sampled during course of this study were analyzed for whole rock oxygen isotope contents. These albite pods are the Discovery Outcrop Albite Pod and Albite Pod #3 (Figures 6.11 and Figure 6.12 respectively).

6.2.1 Discovery Outcrop Albite Pod

Figure 6.10 shows an image of the transect taken from the Discovery Outcrop Albite Pod, as well as three thin section photos that correspond to blocks 1, 4 and 7 respectively. The thin section photos demonstrate the extent of albitization (a pinkish, mottled texture) within each of the mentioned blocks, and also indicate the whole rock $\delta^{18}\text{O}$ value of each sample. Block 1 is the most altered sample within this particular transect, and exhibits complete albitization of plagioclase. Albitization is so pervasive, that in some sections of Block 1, only cloudy pink albite is visible with no relicts of previous mineralogy. These albite grains also have roughly 120° grain boundaries with each other. Block 4 shows moderate albitization of plagioclase, and appears to be intermediate to the most albitized and the least albitized blocks. Block 7 shows virtually no albitization of plagioclase or other surrounding minerals. However, Block 1 (most altered) has a whole rock $\delta^{18}\text{O}$ value of 2.7 ± 0.1 ‰, while Block 7 (least altered) has a whole rock $\delta^{18}\text{O}$ value of 1.4 ± 0.1 ‰.

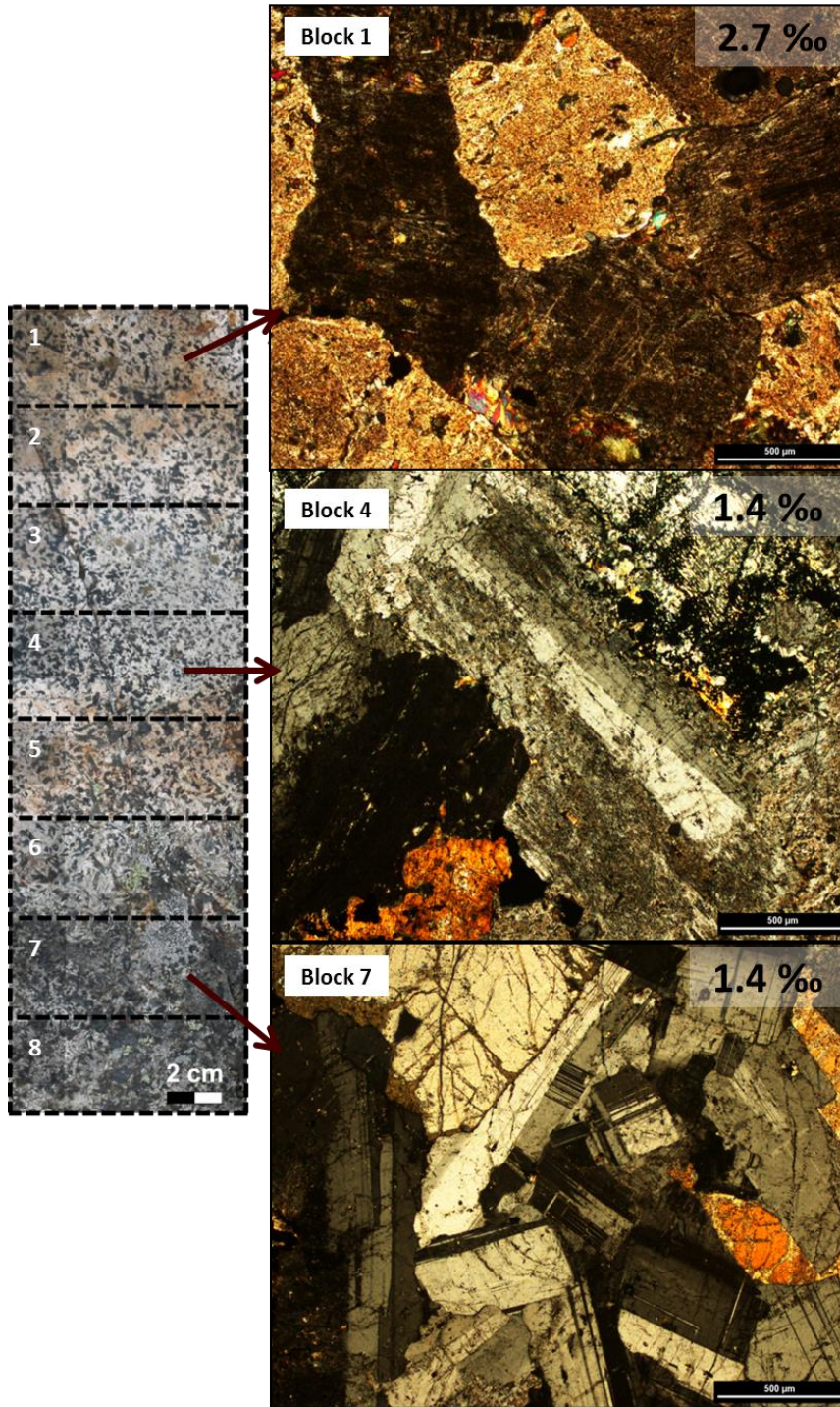


Figure 6.10 – The left side of the image shows the transect that was made over the Discovery Outcrop Albite Pod, with eight evenly sized sections comprising the transect. The uppermost portion of the albite pod (Block 1) was thought to represent the ‘most altered’ portion of the albite pod, while Block 8 was believed to represent the ‘least altered’ section. On the right of the image, the photomicrographs (in XPL) confirm that Block 1 is indeed the most altered by exhibiting complete albitization of all previous mineralogy. Block 4 is moderately albitized, and finally, Block 7 and subsequently Block 8 are the least altered.

6.2.2 Albite Pod #3

Figure 6.11 shows blocks 1 to 7 within Albite Pod #3. To the right of sample pictures are three thin section images that show the petrographic variations of blocks 1, 4, and 7.

Block 1 is medium-grained with frosty-white laths of plagioclase enveloped by a thin network of pink albite, mottled by dark, coarse grained clinopyroxene. The presence of fine to medium grained stubby magnetite crystals is much more evident in thin section.

Alteration within Block 1 is limited to moderate albitization of plagioclase, and biotite rimming of magnetite. Macroscopically, one of the most albitized blocks within Albite Pod #3 is Block 4. The corresponding thin section photo to the right is also in agreement with the latter observation. Plagioclase exhibits near complete albitization, which shows as a cloudy, dirty-looking network of relict plagioclase. Clinopyroxene within these networks of albite are completely altered to actinolite (high order yellow birefringence).

Block 7 is fine grained and predominantly consists of plagioclase, clinopyroxene, and magnetite. The corresponding thin section photo of Block 7 shows only minor albite alteration within the bottom right side of the image, but overall, is subjected to very little secondary alteration. Block 1 has a whole rock $\delta^{18}\text{O}$ value of 2.0 ± 0.1 ‰, while Block 4, one of the most albitized blocks in the transect, has an identical whole rock $\delta^{18}\text{O}$ value of 2.0 ± 0.1 ‰. Block 7 is slightly more enriched in the heavy ^{18}O isotope, with a whole rock $\delta^{18}\text{O}$ value of 2.5 ± 0.1 ‰.

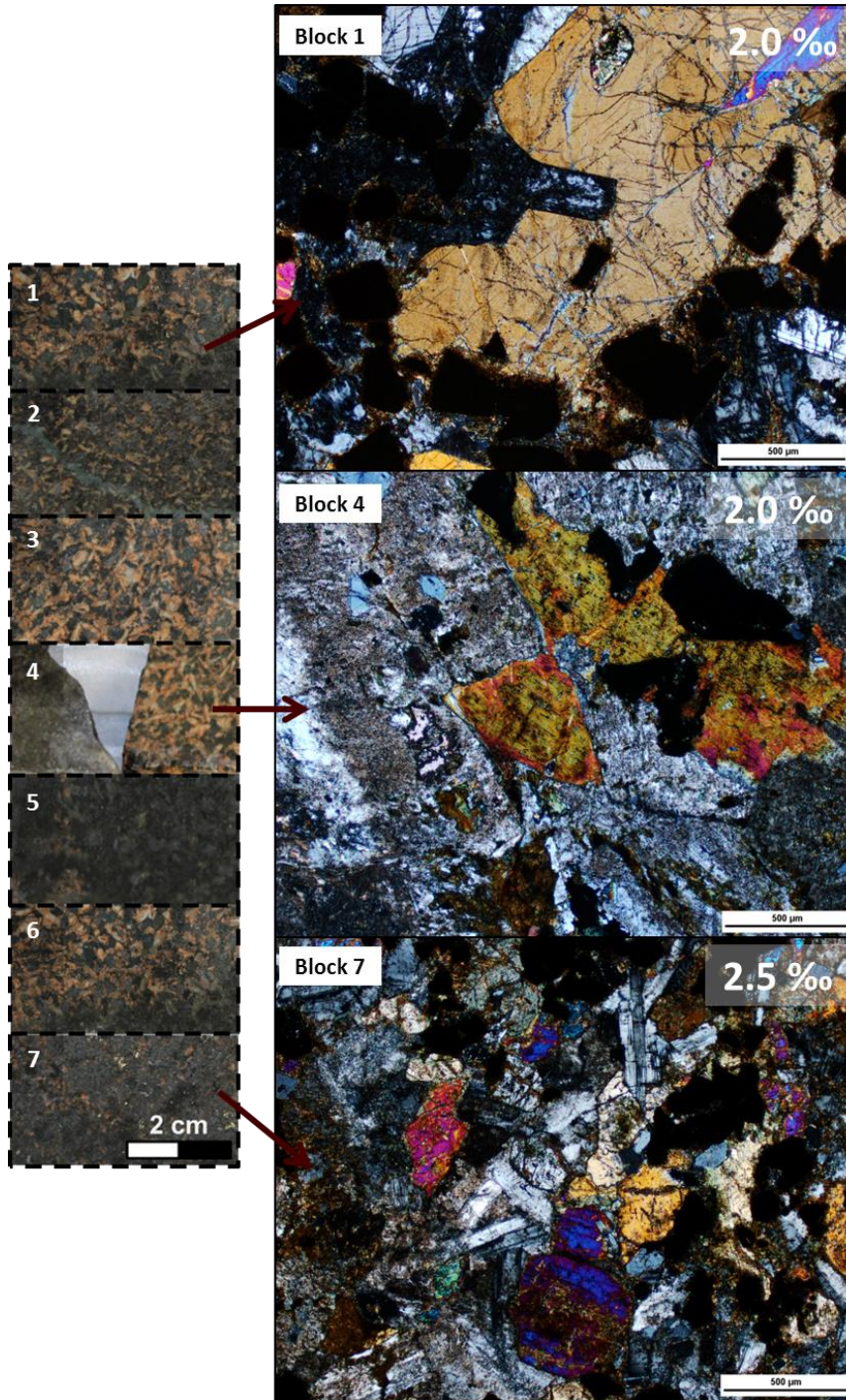


Figure 6.11 – The left side of the image shows the samples that were taken from Albite Pod #3, with seven evenly sized sections comprising a transect of the pod. The uppermost portion of the albite pod (Block 1) contains abundant medium grained, stubby magnetite, while clinopyroxene appear to be mainly unaltered. Block 4 contains significant albization of plagioclase, and clinopyroxene is altered to actinolite and chlorite. Finally, Block 7 contains very strong actinolite alteration of clinopyroxene, in addition to albization of plagioclase, however Block 7 contains up to 4% chalcopyrite (opaque in thin section photo). All thin section photos are in XPL

6.2.3 Relationship Between Albite Pod Oxygen Isotopes and Geochemistry

Figure 6.12 shows the relationship between Mg # and $\delta^{18}\text{O}$. The non to weakly albitized samples from the Discovery Outcrop albite pod have the lowest Mg numbers, while the three most albitized samples from the Discovery Outcrop albite pod and all of the samples from Albite Pod #3 have comparably higher Mg numbers. The whole rock $\delta^{18}\text{O}$ values do not correlate to any change in Mg number among the most altered Discovery Outcrop samples, while the non to weakly albitized samples show a trend where the Mg # decreases as the whole rock $\delta^{18}\text{O}$ values increase. Figure 6.13 uses a molar ratio of $\text{Na}/(\text{Na}+\text{Ca})$ in order to test the correlation between albitite alteration and whole rock $\delta^{18}\text{O}$ values. While Figure 6.7 showed that an increase in whole rock $\delta^{18}\text{O}$ values corresponds to a decrease in $\text{Na}/(\text{Na}+\text{Ca})$ within skeletal troctolite samples, the same plot shows only scatter with regard to albitite pod samples. A similar outcome is apparent in Figure 6.14, where variations in CIPW normative values show scatter relative to changing whole rock $\delta^{18}\text{O}$ values. Figure 6.15 shows the relationship between whole rock $\delta^{18}\text{O}$ values and Cu, and Pd respectively. Figure 6.15a shows that any samples with a whole rock $\delta^{18}\text{O}$ value of greater than 2.9 ± 0.1 ‰ contain less than 1000 ppm Cu, while Figure 6.15b shows that any samples with a whole rock $\delta^{18}\text{O}$ value of greater than 2.9 ± 0.1 ‰ contain trace amounts of Pd.

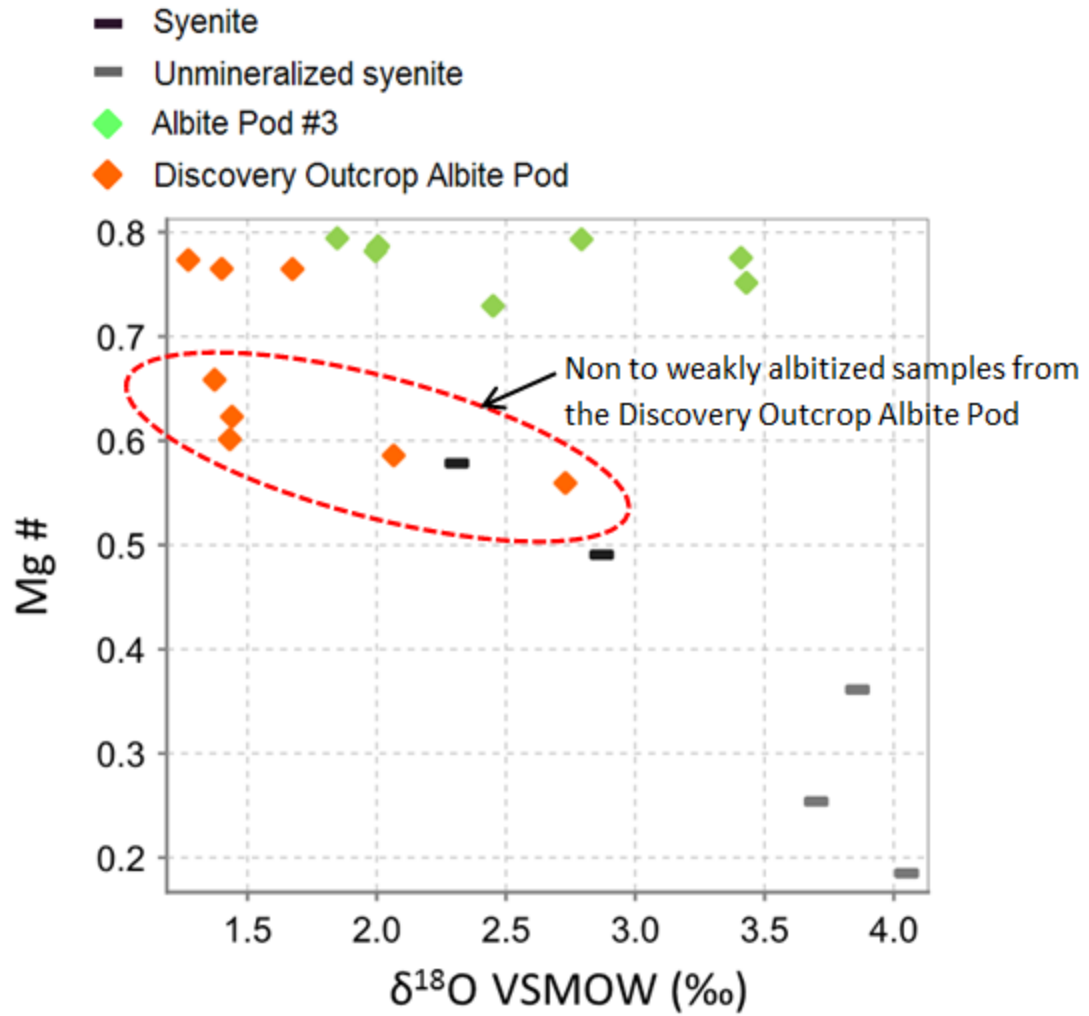


Figure 6.12 – Whole rock $\delta^{18}\text{O}$ values are plotted versus Mg #. The Mg # was calculated based on the residual FeO content, assuming that all Fe_2O_3 partitioned into magnetite (as described in Chapter 5)

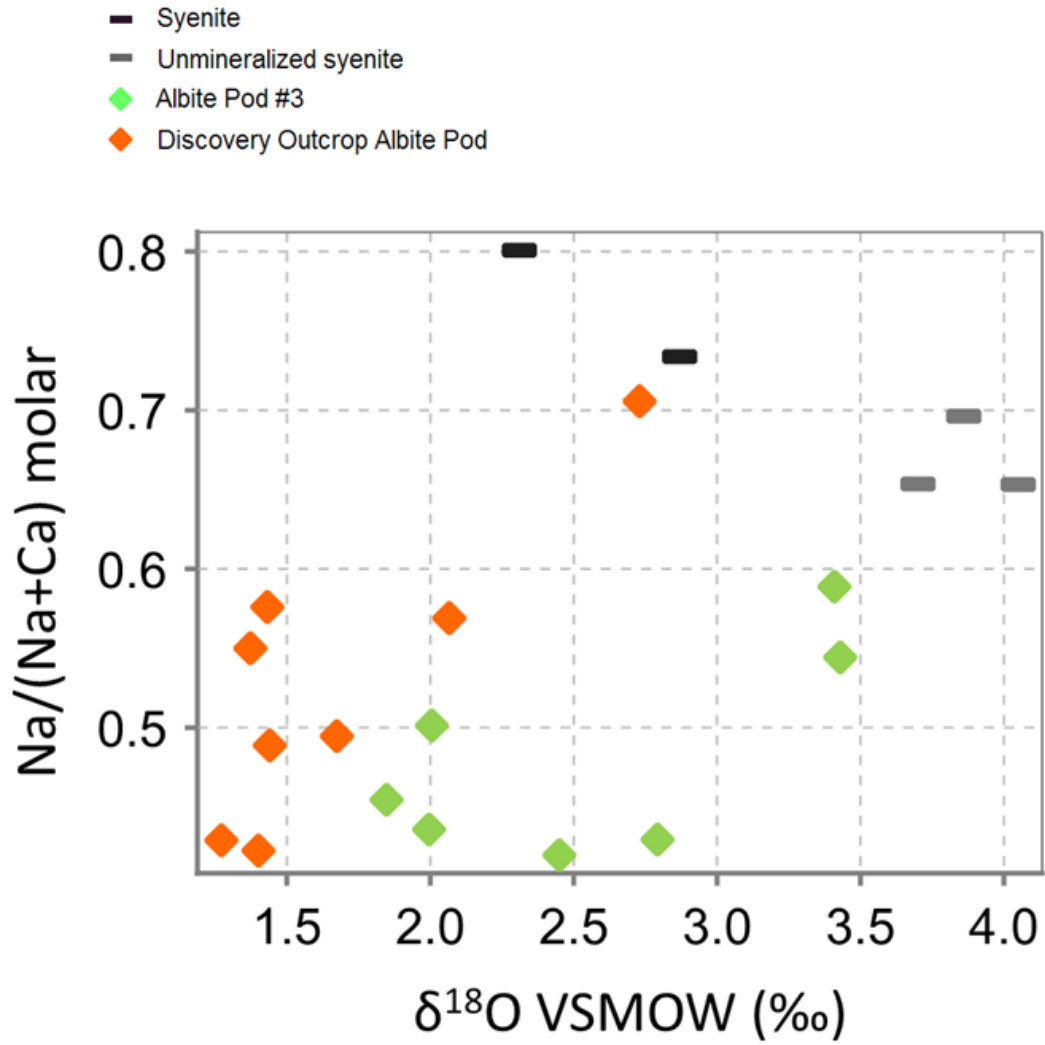


Figure 6.13 – Whole rock δ¹⁸O values are plotted versus a ratio of Na relative to Na+Ca in moles. This ratio represents the amount of albite relative to anorthite, where a higher ratio represents more albite relative to anorthite.

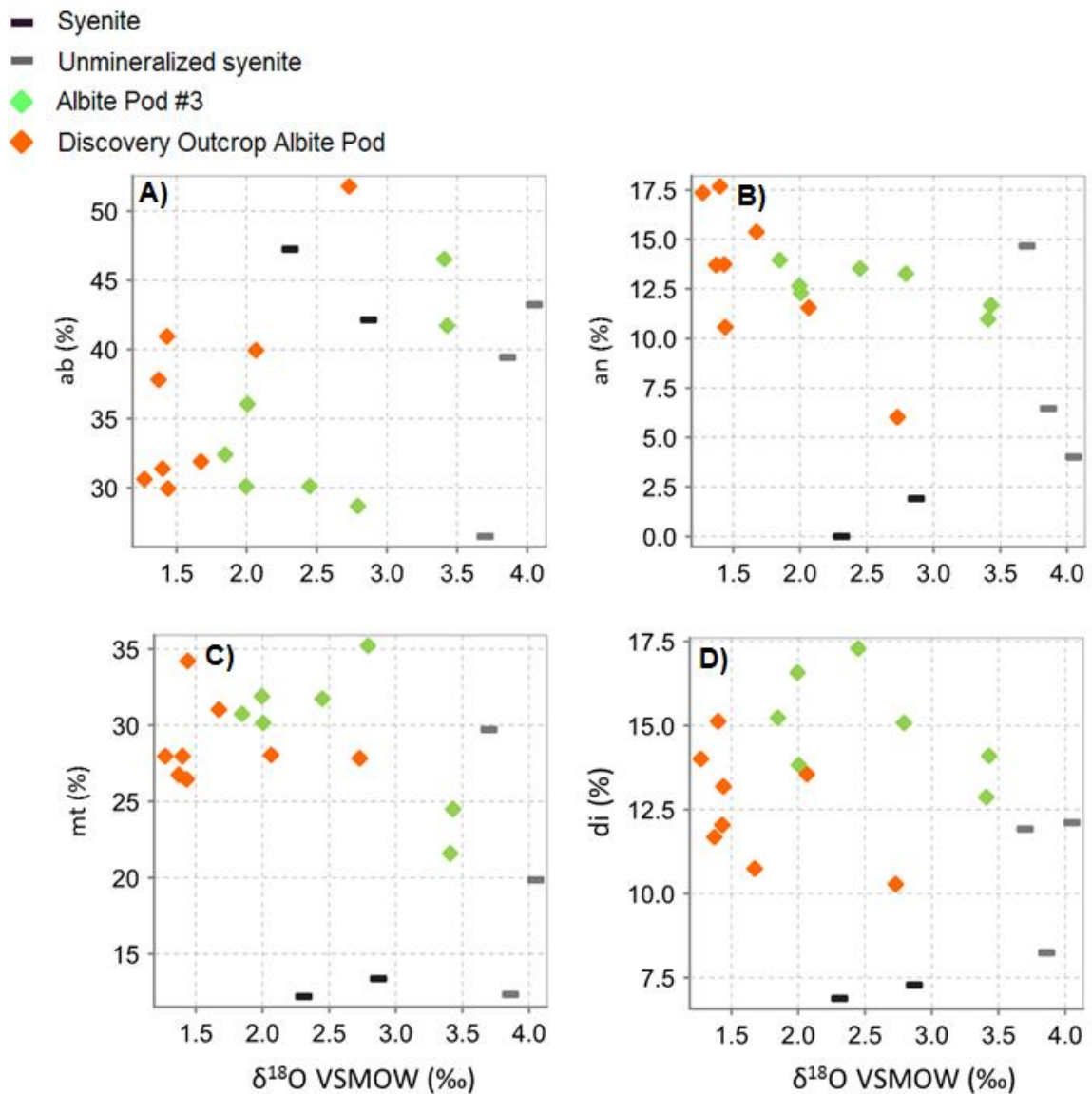


Figure 6.14 – A to D) A comparison between $\delta^{18}\text{O}$ values and CIPW normalized values for albite, anorthite, magnetite, and diopside show no discernable trends within albite pod samples. Values on the y-axis are in calculated weight percent.

- Syenite
- Unmineralized syenite
- ◆ Albite Pod #3
- ◆ Discovery Outcrop Albite Pod

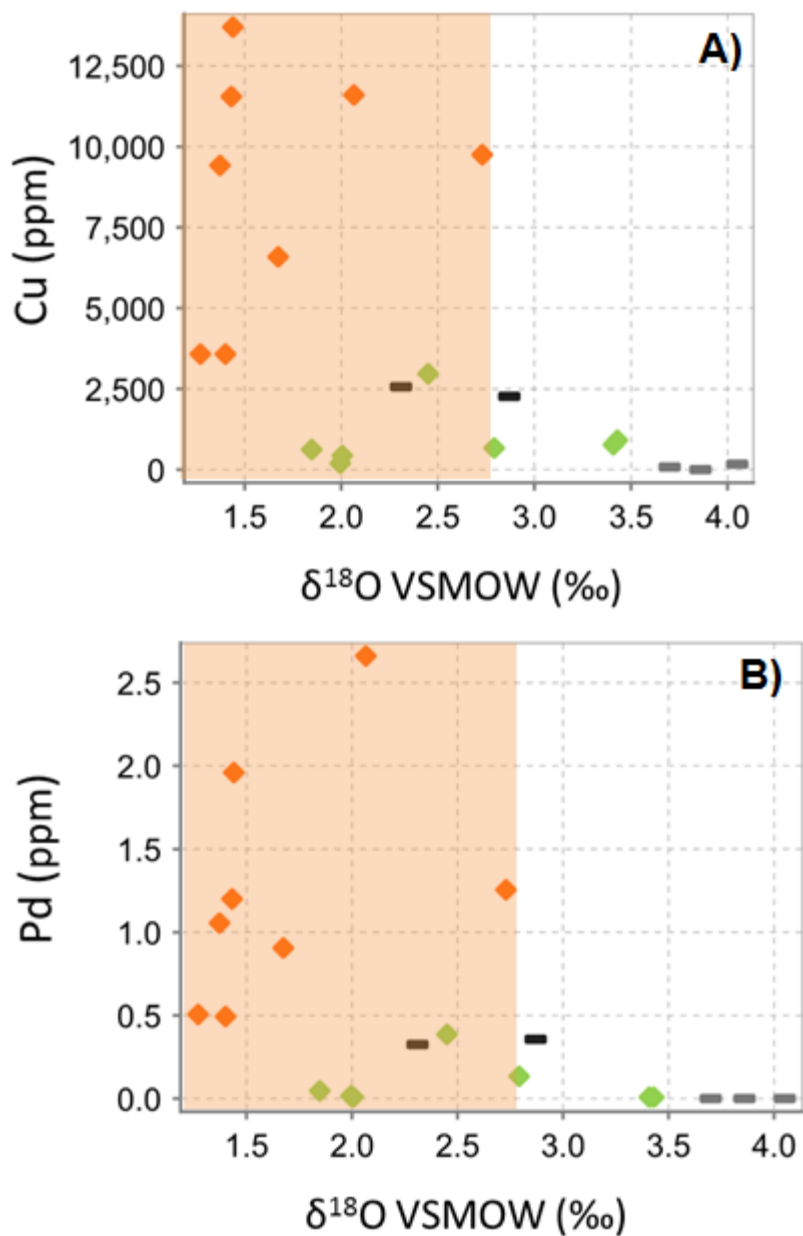


Figure 6.15 – Whole rock $\delta^{18}\text{O}$ values are plotted versus: **A)** Cu (in ppm) where the light orange shaded region shows the field which contains the last sample to have $>1,000$ ppm Cu, **B)** Pd (ppm) where the light orange shaded region also denotes the field which contains the last sample to have >0.1 ppm Pd

Chapter 7

7 Discussion and Conclusion

Two models of Cu-PGE emplacement, and ultimately, the enrichment of ore are being considered at the GLD: 1) a magmatic origin, whereby Cu-sulfides and associated PGE-mineralization crystallized from a relatively evolved sulfide melt that arose after sulfide saturation was attained (Mulja and Mitchell, 1991), and 2) a magmatic-hydrothermal origin, whereby Cu-sulfides and associated PGE-mineralization formed from a fluid derived from the highly evolved magma that is also responsible for forming the albite pods (Good and Crocket, 1994).

7.1 Discussion of Geochemical Data

High MgO, TiO₂, and Fe₂O₃ values of skeletal troctolite (Figure 5.21) indicate that the skeletal troctolite is likely a cumulate that is enriched in these major elements due to the abundance of skeletal olivine, and skeletal magnetite. The skeletal texture infers that these minerals were formed from rapid quenching caused by a substantial degree of undercooling. The down-hole plots (Figures 5.2-5.4) also show that the skeletal troctolite is depleted in SiO₂ relative to all other lithologies, which is consistent with it being a skeletal olivine cumulate with accessory skeletal magnetite.

Highly incompatible trace elements can be used to monitor the degree of fractionation and magmatic affinity (Maclean and Barret, 1993), and the incompatible element enrichment may be modelled using the Rayleigh fractionation equation:

$$C_i = C_o F^{D-1} \quad 7.1$$

Where C_o and C_i represent the concentrations of an incompatible element within initial and fractionated magmas respectively; F is the fraction of remaining magma, and D is the bulk (solid/melt) distribution coefficient. When D is sufficiently small (at ~0.05 for Zr) it may be utilized to monitor the fractionation process (Maclean and Barrett, 1993). Figure 5.25 shows the least altered lithologies plotted on a Zr vs. Y diagram, while Figure 5.26

shows all of the samples including the altered ones plotted on the same diagram. Both unaltered and altered samples plot linearly (except for albite pod samples), which further support the hypothesis that the GLD is derived from a fractionated melt. There are subtle variations in trace element chemistry, particularly in Figures 5.27 and 5.28, which shows that the skeletal troctolite contains lower amounts of La and Yb than the rest of the sample suite, while heterogeneous gabbro, plagioclase aligned gabbro and homogeneous gabbro show a steady increase in La and Yb values. This again is consistent with fractionation, and indicates that the skeletal troctolite is more primitive than the heterogeneous gabbro, plagioclase aligned gabbro and skeletal troctolite. The lone basal fine grained gabbro sample consistently plots among skeletal troctolite data points, which indicates that it is genetically similar to skeletal troctolite.

7.2 Discussion of Geology

The emplacement of the Geordie Lake intrusion, which hosts the Geordie Lake deposit, was believed by Mulja and Mitchell (1990, 1991) to have intruded into contemporaneous syenites of the Coldwell alkaline complex. This was based on what they interpreted to be recrystallization textures within syenite that is adjacent to the Geordie Lake contact, in addition to the presence of sulfides extending out from the Geordie Lake intrusion, into the syenite. However, Good and Crocket (1994) interpreted the granular texture of alkali feldspar grains within syenite near the contact to be braided perthite, rather than a recrystallization feature. Sufficient field evidence from this study shows that the GLI was emplaced prior to the emplacement of syenite. Figure 2.12 shows a xenolith of GL gabbro within syenite, indicating that syenite intruded after the emplacement of the GLI. The GLD consists of six distinct lithologies, as summarized in this study. Trace element geochemistry shows that all of these lithologies are contemporaneous (Figure 5.24), since the trend lines of each lithology on chondrite normalized spider diagrams are all parallel with one another. A sequence from most primitive to least primitive as follows: skeletal troctolite/basal fine grained gabbro → heterogeneous gabbro/homogeneous gabbro/plagioclase aligned gabbro → syenite. One of the key characteristics of the plagioclase aligned gabbro (which is stratigraphically the uppermost unit) is the alignment of plagioclase laths. This indicates movement within the magma after

plagioclase had already formed. Homogeneous gabbro is geochemically similar to plagioclase aligned gabbro (Figures 5.19 and 5.21), but was grouped distinctly due to the distinct lack of plagioclase alignment. Since the contact between both units is gradational, it is likely that the plagioclase aligned gabbro formed from the same magma as homogeneous gabbro, but differ only on the basis of a moving versus in-situ magma. Homogeneous troctolite is also geochemically similar to plagioclase aligned gabbro, with the exception of being slightly more aluminum-rich (Figure 5.19). It is commonly enclosed by heterogeneous gabbro, and occurs lower in the GL stratigraphy than plagioclase aligned and homogeneous gabbro. Homogeneous troctolite occurs in between the Upper and Main Zone of mineralization (Figure 5.44 and 5.47) which suggests that it could have been intruded after the ore-bearing units were deposited, and ore deposition had already occurred. Heterogeneous gabbro share a similar trace element pattern with plagioclase aligned gabbro, and homogeneous gabbro, which suggests that these units are cogenetic. Heterogeneous gabbro is different from plagioclase aligned gabbro and homogeneous gabbro in that it hosts a significant amount of albite alteration that is manifested as albite pods. These albite pods have been shown to have a close spatial association with actinolite alteration, which in turn hosts the majority of chalcopyrite, pyrrhotite, and bornite mineralization (Figures 4.15, 4.16 and 4.18). Basal fine grained gabbro and skeletal troctolite are the most primitive, since they contain the lowest concentration of trace elements and highest Mg #. The abundance of skeletal olivine within skeletal troctolite relative to all other lithologies at the GLD is also consistent with the notion that it was the first to form, since the skeletal texture implies supercooling (Donaldson, 1976), and thus, it likely cooled first.

7.2.1 Significance of Alteration at the GLD

Alteration at the GLD is undoubtedly prevalent, primarily in the form of albite and actinolite alteration. Good and Crocket (1994) observed that disseminated sulfides and palladium minerals had a spatial association with albite pods. Chalcopyrite and bornite are invariably intergrown with actinolite, and actinolite is strongly associated with albite (Figure 2.16). This is due to the fact that actinolite commonly replaces clinopyroxene, while albite replaces plagioclase. Plagioclase and clinopyroxene comprise the ophitic

texture that is common to the Geordie Lake lithologies. This spatial association is observed predominantly within heterogeneous gabbro and more rarely, within homogeneous gabbro and plagioclase aligned gabbro. Albitization is also observed in skeletal troctolite, as noted within observations of the Discovery Outcrop Albite pod, which exhibits strong Cu-PGE mineralization. However, there is no evidence to suggest that mineralization is the result of alteration and this is particularly observed in Figure 5.40 where samples of skeletal troctolite with low actinolite alteration contain similar amounts Cu and Pd than samples which exhibited stronger actinolite alteration. The same can be said about heterogeneous gabbro (in Figure 5.40) in that the most albitized samples do not exhibit any favourable Cu or Pd enrichment over weakly altered samples. Figures 5.20 and 5.21 show a series of bivariate diagrams that compare various major element oxides to SiO_2 , which indicates that altered samples are geochemically similar to unaltered samples. This observation suggests that the elements responsible for the pervasive alteration were likely sourced from local fluids (within the GLD) rather than from an outside source, since we do not observe any significant gain or loss of elements with the exception of the albite pod samples. Albite pod samples have higher amounts of Na, but lower amounts of K while the most albitized Discovery Outcrop albite pod samples contain lower amounts of Ca. Higher amounts of Na and lower amounts of Ca were expected since albite alteration itself is a replacement of Ca-bearing plagioclase with Na-rich albite. The loss of K in albite samples could also be due to the replacement of biotite (the main K-bearing mineral) by albite. However, in Figure 5.24 we see that albite pod samples are cogenetic with rest of the GLD sample suite, albeit with higher trace element concentrations. This agrees with the observation made by Good and Crocket (1994) that the albite pod formed from fluid that was derived from the highly evolved magma responsible for forming the GLD. Albite and actinolite likely formed from the same fluid, and based on the recurring spatial association that they share, it is probable that they formed contemporaneously. For future work, oxygen isotope analyses of mineral separates would provide a clearer answer as to whether or not these two mineral phases were indeed contemporaneous.

7.3 Mineralization and Metal Ratios

Results from core logging show that the GLD consists of a three mineralized lithologies: heterogeneous gabbro, skeletal troctolite, and basal fine grained gabbro. Syenite exhibits mineralization at the contact with the GLD, but is barren of mineralization up to a few metres below the contact. There are two zones within the GLD stratigraphy that exhibit strong mineralization: the Upper Zone, and Main Zone. Metal ratios are useful in understanding the conditions during which sulfides were first formed (Barnes et al., 1993). Metal ratios such as Cu/Pd are sensitive to changes in R-factor, which was summarized by Campbell and Naldrett (1979) as the ratio of silicate magma to sulfide liquid within a magmatic system (Eqn. 5.1):

$$R \text{ factor} = \frac{(\text{mass of silicate liquid})}{(\text{mass of sulfide liquid})} \quad (7.2)$$

Campbell and Naldrett (1979) also demonstrated how the composition of sulfides could be modeled using a recalculation to one-hundred percent sulfide approach, using the equilibrium fractionation equation:

$$\frac{C_C}{C_L} = \frac{D(R+1)}{R+D} \quad (7.3)$$

where C_c = concentration of the element in the sulfide, $C_c =$ concentration of the element in the silicate liquid, D = the partition coefficient of the element between sulfide and silicate liquid, and R = the ratio of silicate to sulfide liquid. However, making use of the one-hundred percent sulfide approach can be challenging particularly because S is typically mobile and so the amount of S remaining in the rock might not be fully representative of its original igneous composition. As well, most Cu-Ni-PGE exploration programs tend to only focus on analyzing drill-core for Ni, Cu, Pt and Pd (Barnes et al., 1988). Thus, the differences between the partition coefficients for Ni, Cu, Pt and Pd into a sulfide liquid allows the use of Pd/Pt, Cu/Pd, Ni/Pd, and Ni/Cu in modeling the genesis of Cu-PGE rich deposits, such as the GLD.

In Figure 5.39, Cu is plotted versus Pd, and boundaries of ratios 3,000 (which is the upper limit of all but one sample) to 10,000 values are superimposed. Mantle rocks fall within a Cu/Pd range of 1,000 to 10,000 (Barnes et al., 1993). The Cu/Pd ratio is dependent on the R-factor, and as the R-factor of system increases, so does the enrichment factor for Pd relative to Cu. This is explained by the high partition coefficient that Pd has into a sulfide melt (Barnes et al., 1993). Figure 5.41 shows a bivariate plot of Pd vs the ratio of Cu/Pd. Mineralized samples easily fall within the mantle values of Cu/Pd, indicating that the metals are likely mantle derived. Most notably, however, the majority of plagioclase aligned gabbro and homogeneous gabbro samples (both unmineralized lithologies) plot above the mantle boundary lines. This could be due to a large depletion in Pd relative to Cu. It is possible that Pd was scavenged from the underlying magma (which formed Pd-rich skeletal troctolite and heterogeneous gabbro) after the formation of sulfide melt, leaving the plagioclase aligned and homogeneous gabbros relatively barren of Pd. Alternatively, it could represent an enrichment of Cu relative to Pd, which would result in a lower value of Cu/Pd. This too is quite plausible given the observation of chalcopyrite within localized zones of alteration within plagioclase aligned and homogeneous gabbro samples (Figure 4.4 and 4.8).

Naldrett and Duke (1980) pointed out that Archean komatiite-related deposits have relatively low Pd/Ir ratios, while those related to progressively less mafic magmas have progressively higher ratios. Figure 5.43 is a PGE profile normalized to mantle values (data from Taylor and McClellon, 1985) and shows that mineralized samples at the GLD have low values of Ir, and Ru, but are enriched in Rh, Pt, and particularly Pd and Au relative to mantle values. The two mineralized syenite samples have low Rh values relative to the rest of the sample set, and relative to mantle values. Thus, this observation indicates that the GL magma was highly evolved at the time of emplacement.

7.3.1 Upper Zone Mineralization

The Upper Zone of mineralization is characterized by mainly chalcopyrite and pyrrhotite mineralization (Chapter 4). In Figures 5.44-5.47, the Upper Zone Cu-Pd mineralization is shown to be a continuous horizon, ranging from roughly 4-10 m in thickness and with an

average Cu grade of 0.231 wt. %, and Pd grade of 475 ppb (based on data from the four drill holes used in this study). Cu/S ratios are observed to increase along with increasing Cu and Pd, while Cu/Pd and Ni/Pd ratios exhibit inconsistent trends. In a magmatic sulfide model, a noticeable variation in Cu/Pd ratios of the silicate rocks proximal to horizons of sulfide mineralization is expected to delineate these horizons, since the strongly chalcophile Pd would be preferentially depleted during sulfide segregation from the silicate magma (Maier et al., 1998). However, this is not the case with Cu/Pd in and around the Upper Zone mineralization. The ratio of Ni/Cu generally decreases with increasing Cu and Pd, which also does not agree with a sulfide segregation model since Ni has a higher partition coefficient (150) than Cu (50) into sulfide liquid over silicate liquid in the FeS-FeO-SiO₂ system at 1,150 C and 1 bar pressure (MacLean and Shimazaki, 1976). Thus, metal ratios in the Upper Zone of mineralization do not support a magmatic sulfide model, which is consistent with a lack of magmatic textures in the Upper Zone.

7.3.2 Main Zone Mineralization

The main zone of mineralization is characterized by mainly chalcopyrite and bornite mineralization (Chapter 4). In Figures 5.44-5.47, the intersection of the Main Zone Cu-Pd mineralization ranges in thickness from 34-58 m, with an average total Cu grade of 0.444 wt. %, and Pd grade of 741 ppm (based on data from the four drill holes used in this study). Cu/Pd ratios fluctuate and are void of any apparent trends. Intervals that contain the highest values of Cu and Pd are coincident with sections of skeletal troctolite. Petrographically, these intervals contain significant chalcopyrite and bornite mineralization (Figures 4.23 and 4.24).

7.4 Discussion of Whole Rock Oxygen Isotopes

The fractionation that oxygen isotopes undergo is particularly useful in addressing a variety of problems that arise in attempting to understand ore deposition, including: 1) the conditions as well as the processes involved in mineral and rock formation, 2) the origin and evolution of magmas, 3) the extent of interaction between magma and country rock, 4) the nature of fluids that are involved in geological processes (i.e., magmatic or

metamorphic), and 5) the extent of interaction between rocks and circulating fluids (Turi, 1988). Heated groundwater that percolates through rocks surrounding a cooling igneous pluton can interact with certain unstable minerals in the rocks, which may release various metals into solution. These metals can ultimately be redeposited within open fractures and cavities, or via replacement of other minerals in the country rocks. Such hydrothermal mineral deposits may form within the body of the igneous intrusive, in the adjacent country rocks, or in both. The ore minerals in such deposits typically include native gold and silver as well as sulfides of Fe, Cu, Ni, Co, Zn and Pb which form at decreasing temperatures and hence at increasing distances from the igneous intrusives which are the source of the heat that drives the convection cells of groundwater (Faure and Mensing, 2005).

7.4.1 Discussion of Down-hole Whole Rock Oxygen Isotopes

The plagioclase aligned gabbro, which is the uppermost lithology at the Geordie Lake deposit, contains whole rock $\delta^{18}\text{O}$ values that are most consistent with magmatic values. Typically, gabbro formed by partial melting from the mantle has a $\delta^{18}\text{O}$ value of 5-7 ‰ (VSMOW) for whole rocks (Eiler, 2001). There is a systematic decrease in whole rock $\delta^{18}\text{O}$ values moving down the GLD stratigraphy, with values as low as 1.9 ± 0.1 ‰ in skeletal troctolite samples near the basal syenite contact. Figure 6.2 shows a comparison of two plagioclase aligned gabbro samples with $\delta^{18}\text{O}$ value of 6.0 ± 0.1 ‰ to a sample with a $\delta^{18}\text{O}$ value of 4.6 ± 0.1 ‰. Both samples contain similar modal amounts of primary plagioclase, clinopyroxene, plus magnetite as well as secondary actinolite, and biotite. Homogeneous gabbro, which is stratigraphically below than the plagioclase aligned gabbro, contain whole rock $\delta^{18}\text{O}$ values that range from 4.1 ± 0.1 ‰ to 3.6 ± 0.1 ‰, and the samples with these different values exhibit no significant variation in modal mineralogy and alteration. Petrographically, there is no obvious increase in the degree of alteration within rocks that have higher whole rock $\delta^{18}\text{O}$ values compared to those that have lower whole rock $\delta^{18}\text{O}$. Interaction with hydrothermal fluids can cause the $\delta^{18}\text{O}$ value of an igneous rock to change as a result of exchange of oxygen between the rock and the fluid. However, evidence of hydrothermal alteration is usually evident in the form of typical alteration textures overprinting primary igneous texture (Staudigel et al., 1995). Magmas

with unusual whole rock oxygen isotope compositions outside of a $\delta^{18}\text{O}$ range of 5-7 ‰ do exist, albeit quite rarely. Muehlenbachs et al. (1972) documented fresh volcanic flows from Iceland with $\delta^{18}\text{O}$ values as low as 2 ‰. While Muehlenbachs et al. (1972) had no conclusive explanation as to how such depleted $\delta^{18}\text{O}$ values could exist within fresh basalt, they speculated that such low $\delta^{18}\text{O}$ values are either the result of superficial depletion of O^{18} at crustal levels, or that they are the result of an exceptional property or process from within the mantle beneath Iceland (Muehlenbachs, 1974). Conversely, Turi and Taylor (1976) showed unaltered flows from Pleistocene volcanoes north of Rome, Italy to have $\delta^{18}\text{O}$ values as high as 13 ‰. Such high values of $\delta^{18}\text{O}$ are indicative of formation by either melting, or large-scale assimilation of high ^{18}O sedimentary rock (Turi and Taylor, 1976).

This could suggest that there are two pulses of magma, where one has a low $\delta^{18}\text{O}$ value, which the other has a normal $\delta^{18}\text{O}$ value. The low $\delta^{18}\text{O}$ magma could have resulted from the melting of a hydrothermally altered rock, thus explaining the lack of alteration and primary magmatic textures in samples with low whole rock $\delta^{18}\text{O}$ values (Figure 6.10). But given the similarities in major and trace element data, the source rock must have been comagmatic with the subsequent magma.

7.4.2 Discussion of Whole Rock Oxygen Isotopes in Albite Pods

The transect of the Discovery Outcrop Albite Pod with corresponding whole rock oxygen isotope values in Figure 6.10 demonstrates that the least altered sample (Block 7) has the lowest whole rock $\delta^{18}\text{O}$ value, while the most altered sample (Block 1) has the highest whole rock $\delta^{18}\text{O}$ value. This suggests that the low whole rock $\delta^{18}\text{O}$ values in the rock are not related to hydrothermal alteration. However, the albite altered rocks have the highest local whole rock $\delta^{18}\text{O}$ values, which could be the result of interaction with magmatic fluids with normal $\delta^{18}\text{O}$ values. Another example of the negligible effect that small-scale alteration has on the whole rock $\delta^{18}\text{O}$ values is shown on Figure 6.11 which shows a fresh sample (Block 1) and an altered sample (Block 4). Both samples have whole rock $\delta^{18}\text{O}$ values of 2.0 ± 0.1 ‰ despite the obvious difference in the degree of alteration of each

sample, further suggesting that hydrothermal alteration is not the correct mechanism for decreasing whole rock $\delta^{18}\text{O}$ values with depth at the GLD.

7.5 Conclusion

The GLD was likely derived from an evolved, mafic melt with mantle derived sulfides. The evidence presented in this study indicates that mineralization is predominantly bound to the skeletal troctolite unit. The sulfide textures within skeletal troctolite indicate that they formed magmatically. However, the close spatial association between chalcopyrite and actinolite/albite also supports the notion that some sulfides were later remobilized. Samples containing high amounts of actinolite and albite alteration are not discernable from unaltered samples using whole and trace element geochemistry. This implies that alteration was likely the product of interaction between rock and fluid sourced from the same magma, rather than from an outside source. Trace element geochemistry shows that fractionation played a role in the evolution of the GLD lithologies, and a crystallization sequence is as follows: skeletal troctolite/basal fine grained gabbro \rightarrow heterogeneous gabbro/homogeneous gabbro/plagioclase aligned gabbro \rightarrow syenite. The geochemistry of albite pod samples show that they are also cogenetic with the rest of the GL sample quite, but much more evolved. This supports the model that the GLD was a primarily magmatic deposit, with late stage hydrothermal remobilization of metals by fluids that were sourced from the original magma.

References

- Arndt, N.T., Czamanske, G., Walker, R.J., Chauvel, C., and Fedorenko, V., 2003, Geochemistry and origin of the intrusive hosts of the Noril'sk-Talnakh Cu-Ni-PGE sulfide deposits: *Economic Geology*, v. 98, p. 495-515.
- Barnes, S.J., Naldrett, A.J., and Gorton, M.P., 1985, The origin of platinum group element concentrations in terrestrial magmas: *Chemical Geology*, v. 53, p. 303-323.
- Barnes, S.J., Couture, J.F., Sawyer, E.W., and Bouchaib, C., 1993, Nickel-copper occurrences in the Belleterre-Angliers Belt of the Pontiac Subprovince and the use of Cu-Pd ratios in interpreting platinum-group element distributions: *Economic Geology*, v. 88, p. 1402-1418.
- Barnes, S.J., and Lightfoot, P.C., 2005, Formation of magmatic nickel sulfide deposits and processes affecting their copper and platinum group element content, in Hedenquist, J.W., Thompson, J.F.H., Goldfarb, R.J., and Richards, J.P., eds., *Economic Geology—One hundredth anniversary volume 1905–2005*: Littleton, Colorado, Society of Economic Geologists, p. 179–213.
- Barnes, S.J., and Gomwe, T.S., 2011, The Pd Deposits of the Lac des Iles Complex, Northwestern Ontario: *Economic Geology*, v. 17, p. 351-370.
- Barnes, S.J., and Ripley, E.M., 2016, Highly Siderophile and Strongly Chalcophile Elements in Magmatic Ore Deposits: *Reviews in Mineralogy and Geochemistry*, v.81, p. 725-774.
- Barrie C.T., MacTavish A.D., Walford P.C., Chataway R. and Middaugh R., 2002, Contact-type and Magnetite Reef-type Pd-Cu Mineralization in Ferroan Olivine Gabbros of the Coldwell Complex, Ontario. In *The Geology, Geochemistry, Mineralogy and Mineral Beneficiation of Platinum-Group Elements* (ed. LJ Cabri), Ottawa Ontario. Can Inst Min Me. Special Volume 54, p. 321-337.
- Beakhouse, G.P. 1991. Winnipeg River subprovince. In *Geology of Ontario*. Edited by P.C. Thurston, H.R. Williams, R.H. Sutcliffe and G.M. Stott. Ontario Geological Survey, Special Vol. 4, Part 1. pp. 279–301.
- Borthwick, J., and Harmon, R.S., 1982, A note regarding CiF_3 as an alternative to BrF_5 for oxygen isotope analyses: *Geochimica et Cosmochimica Acta*, v. 49 (9), p. 1665-1668.
- Boudreau, A., Djon, L., Tchalikian, A., and Corkery, J., 2014, The Lac Des Iles Palladium Deposit, Ontario, Canada part I. The effect of variable alteration on the Offset Zone: *Miner Deposita*, v. 49, p. 625-654

Campbell, I.H., and Naldrett, A.J., 1979, The influence of silicate:sulfide ratios on the geochemistry of magmatic sulfides: *Economic Geology and the Bulletin of the Society of Economic Geologists*, v.6, p. 1503-1506.

Card, K.D., and Ciesielski, A., 1986, Subdivisions of the Superior Province of the Canadian Shield: *Geoscience Canada*, v. 13, p. 5-13.

Card, K.D., and Poulsen, H., 1998, Geology and mineral deposits of the Superior Province of the Canadian Shield. In *Geology of Ontario*. Ontario Geological Survey, Vol. 7, p. 13-194.

Cawthorn, R.G., 1999, The platinum and palladium resources of the Bushveld Complex. *South African Journal of Science*: v. 95, p. 481-489.

Corfu, F., and Stott, G.M. 1996. Hf isotopic composition and age constraints on the evolution of the Archean central Uchi Subprovince, Ontario, Canada. *Precambrian Research*, 78: 53–63.

Corfu, F., and Stott, G.M., 1998, Shebandowan greenstone belt, western Superior Province; U–Pb ages, tectonic implications and correlations: *Geological Society of America Bulletin*, v. 110, p. 1467–1484.

Chacko et al., 2001, *in* Valley and Cole (Eds.), *Stable Isotope Geochemistry, Reviews of Mineralogy and Geochemistry*, Virginia Polytechnic Institute. 43:1 – 81. Blacksburg, VA.

Chai, G. and Naldrett, A.J., 1992, Characteristics of Ni-Cu-PGE mineralization and genesis of the Jinchuan Deposit, Northwest China. *Economic Geology*, v. 87, p. 1475-1495.

Clayton, R.N., and Mayeda, T.K., 1963, The use of bromine pentafluoride in the extraction of oxygen from oxides and silicates for isotopic analysis: *Geochimica et Cosmochimica Acta*, v. 27, p. 43-52.

Cundari, R., 2012, Geology and geochemistry of Midcontinent Rift-related igneous rocks: Unpublished MSc thesis, Lakehead University, Thunder Bay, Ontario, 154 pp.

Davis, D.W., and Paces, J.B., 1990, Time resolution of geologic events on the Keweenaw Peninsula and implications for development of the Midcontinent Rift System: *Earth Planetary Science Letters*, v. 97, p. 54-64.

Davis, D.W., Sutcliffe, R.H., 1985, U-Pb ages from the Nipigon plate and northern Lake Superior: *Geological Society of American Bulletin*, v. 96, p. 1572-1579.

Ding, X, Ripley, E.M., and Li, C., 2012, PGE geochemistry of the Eagle Ni-Cu-(PGE) deposit, Upper Michigan: constraints on ore genesis in a dynamic magma conduit: *Miner Deposita*, v. 47, p. 89-104.

Djon, M.L.N., and Barnes, S.J., 2012, Changes in sulfides and platinum-group minerals with the degree of alteration in the Roby, Twilight, and High Grade Zones of the Lac des Iles Complex, Ontario, Canada: *Mineralium Deposita*, v. 47, p. 875-896.

Donaldson, C.H., 1976, An experimental investigation of olivine morphology: *Contributions to Mineralogy and Petrology*, v. 57, pp. 187-213.

Drennan, M., and Fell, M., 2010, Marathon PGM Corporation, NI 43-101 Technical Report and Resource Estimate: Update for the Geordie Lake Property Northern Ontario, June 4, 2010

Eiler, J.M., 2001, Oxygen isotope variation of basaltic lavas and upper mantle rocks (*in* *Stable isotope geochemistry*): *Reviews in Mineralogy and Geochemistry*, v. 43, p. 319-364.

Eckstrand, O.R., and Hulbert, L.J., 2007, Magmatic nickel-copper-platinum group element deposits, in Goodfellow, W.D., ed., *Mineral deposits of Canada—A synthesis of major deposit-types, district metallogeny, the evolution of geological provinces, and exploration methods*: Geological Association of Canada, Mineral Deposits Division, Special Publication No. 5, p. 205–222.

Farrow, D., Johnson, M., 2012, Cardero Resource Corporation, NI 43-101 Technical Report on the Titac Ilmenite Exploration Project, Minnesota, USA, January 27, 2012.

Faure, G., and Mensing, T.M., 2005, *Isotopes: Principles and Application*: John Wiley & Sons, New Jersey, pp.1-897

Fedorenko, V.A., 1991, Tectonic control of magmatism and regularities of Ni-bearing localities in the northwestern Siberian Platform: *Soviet Geology and Geophysics*, v. 32, p. 41-47.

Fralick, P., Purdon, R.H., and Davis, D.W., 2006a. Neoproterozoic trans-subprovince sediment transport in western Superior Province; *Canadian Journal of Earth Sciences*, v. 43, p. 1055-1070.

Gal, B., Molnar, F., and Peterson, D.M., 2011, Cu-Ni-PGE Mineralization in the South Filson Creek Area, South Kawishiwi Intrusion, Duluth Complex: *Mineralization Styles and Magmatic Hydrothermal Processes*: *Economic Geology*, v. 106, p. 481-509.

Good, D.J., Epstein, R., McLean, K., Linnen, R.L., and Samson, I.M., 2015, Evolution of the Main Zone at the Marathon Cu-PGE Sulfide Deposit, Midcontinent Rift, Canada: *Spatial Relationships in a Magma Conduit Setting*: *Economic Geology*, v. 110, p. 953-1008.

Good, D. and J. Crocket, 1994: Genesis of the Marathon Cu-Platinum-Group Element Deposit, Port Coldwell Alkalic Complex, Ontario: *A Midcontinent Rift-Related Magmatic Sulfide Deposit*: *Economic Geology*, v. 89, p. 131—149.

Green, J.C., and Fitz, T.J., 1993, Extensive felsic lavas and rheognimbrites in the Keweenaw Midcontinent Rift plateau volcanics, Minnesota: petrographic and field recognition: *Journal of Volcanology and Geothermal Research*, v. 54, p. 177.-196

Hilliard, H.E., 2003, Platinum-group metals: U.S. Geological Survey Mineral Commodity Summaries 2003, p. 126-127. (Also available online at <http://minerals.er.usgs.gov/minerals/pubs/commodity/platinum/550303.pdf>.)

Hinchev, J.G., and Hattori, K.H., 2005, Magmatic mineralization and hydrothermal enrichment of the High Grade Zone at the Lac des Iles palladium mine, northern Ontario, Canada: *Mineralium Deposita*, v. 40, p. 13-23.

Hoefs, J., 2004, *Stable Isotope Geochemistry*: Springer, Berlin, 5th edition, 340 pp.

Hoffman, P.F., 1989, Precambrian geology and tectonic history of North America, in *The Geology of North America: An Overview*, The Geology of North America, Volume A, Geological Society of America, p.447-512

Heaman, L.M., and Machado, N., 1992, Timing and origin of midcontinent rift alkaline magmatism, North America: evidence from the Coldwell Complex: *Contributions to Mineralogy and Petrology*, v. 110, p. 289-303

Hutchinson, D.R., White, R.S., Cannon, W.F., Schulz, K.J., 1990, Keweenaw hot spot; geophysical evidence for a 1.1 Ga mantle plume beneath the Midcontinent Rift System: *Journal of Geophysical Research*, v. 10, p. 869-884.

Jago, B., 1980, *Geology of a portion of the western contact margin: The Coldwell Complex*, BSc thesis, Lakehead University, Thunder Bay, Ontario.

Kanitpanyacharoen, W., and Boudreau, A.E., 2013, Sulfide-associated mineral assemblages in the Bushveld Complex, South Africa: platinum-group element enrichment by vapor refining by chloride-carbonate fluids: *Miner Deposita*, v. 48, p. 193-210.

Keays, R.R., Lightfoot, P.C., Hamlyn, P.R., 2011, Sulfide saturation history of the Stillwater Complex Montana: chemostratigraphic variation in platinum group elements: *Mineral Deposita*, v. 47, p. 151-173

Keays, R.R., Lightfoot, P.C., 2002, *Exploration for Platinum-Group Element (PGE) Deposits in*

Mafic and Ultramafic Rocks [ext. abs.]: International Platinum Symposium, 9th, Billings, Montana, 2002, Extended Abstracts, p. 1-4

Lavigne, M.J., and Michaud, M.J., 2001, *Geology of North American Palladium Ltd's Roby Zone Deposit, Lac des Iles*: *Exploration and Mining Geology*, v. 10, p. 1-17.

Lilley, F.E.M., 1964, An analysis of the magnetic features of the Port Coldwell intrusive; unpublished MSc. thesis. University of Western Ontario, London, Ontario, 69 pp.

Listerud, W.H., and Meineke, D.G., 1977, Mineral resources of a portion of the Duluth Complex and adjacent rocks in St. Louis and Lake Counties, northeastern Minnesota: Hibbing, Minn., Minnesota Department of Natural Resources, Division of Minerals Report 93, 74p.

Macdonald, A.J., Brugmann, G.E., Naldrett, A.J., 1989, Coeval felsic mafic and ultramafic magmas: Magma mixing during formation of PGE-rich Ni-Cu sulfides at Lac des Iles Ontario Canada *in* Magmatic sulfides – the Zimbabwe volume (eds. Prendergast, M.D., and Jones, M.J.): Institute of Mining and Metal London, p. 139-150.

MacLean, W.H., and Shimazaki, H., 1976, The Partition of Co, Ni, Cu, and Zn between Sulfide and Silicate Liquids: *Economic Geology*, v. 71, p. 1049-1057

MacLean and Shizamaki, 1976 – the partition of Co, Ni, Cu, and Zn between Sulfide and Silicate Liquids

Mahoney, J.J., and Coffin, M.F., eds. 1997, Large Igneous Provinces: Continental, Oceanic, and Planetary Flood Volcanism. *Geophysical Monograph 100*, American Geophysical Union, Washington D.C., 438 pp.

Maier, W., Barnes, S.J., De Klerk, W.J., Teigler, B., and Mitchell, A.A., 1996, Cu/Pd and Cu/Pt of silicate rocks in the Bushveld Complex: implications for platinum-group element exploration: *Economic Geology*, v. 91, p. 1151–1158

Maier, W.D., Barnes, S.J., and de Waal, S.A., 1998, Exploration for magmatic Ni-Cu-PGE sulphide deposits: a review of recent advances in the use of geochemical tools, and their application to some South African ores: *South African Journal of Geology*, v. 101.3, p. 237-253.

Maier, W.D., 2005, Platinum-group element (PGE) deposits and occurrences: Mineralization styles, genetic concepts, and exploration criteria: *Journal of African Earth Sciences*, v. 41, p. 165-191.

McDonough, W., Sun, S., Ringwood, A., Jagoutz, E., and Hofmann, A., 1992, Potassium, rubidium, and cesium in the Earth and Moon and the evolution of the mantle of the Earth: *Geochimica et Cosmochimica Acta*, v. 56, p. 1001-1012

Mitchell, R.H., and Platt, R.G., 1978, Mafic mineralogy of Ferroaugite syenite from the Coldwell alkaline complex, Ontario, Canada: *Journal of Petrology*, v. 19, p. 627-651

- Mitchell, R.H., Platt, R.G., Lukosius-Sanders, J., Artist-Downey, M., Moogk-Pickard, S., 1993, Petrology of syenites from centre III of the Coldwell alkaline complex, northwestern Ontario, Canada: *Canadian Journal of Earth Sciences*, v. 30, p. 145-158
- Mitchell, R.H., Platt, R.G., Cheadle, S.P., 1983, A gravity study of the Coldwell Complex, northwestern Ontario, and its petrological significance: *Canadian Journal of Earth Sciences*, v. 20, p. 1631-1638
- Miller, J.D. Jr., and Ripley, E.M., 1996, Layered intrusions of the Duluth Complex Minnesota USA *in Layered Intrusions* (ed. Cawthorn, R.G.), Elsevier, pp. 257-301.
- Miller, J.D. Jr., Green, J.C., Severson, M.J., Chandler, V.W., Hauck, S.A., Peterson, D.E., and Wahl, T.E., 2002, Geology and mineral potential of the Duluth Complex and related rocks of northeastern Minnesota: *Minnesota Geological Survey Report of Investigations*, v. 58, 207 p
- Miller, J.D., Green, J.C., Severson, M.J., Chandler, V.W., Hauck, S.A., Peterson, D.M., and Wahl, T.E., 2002, Geology and mineral potential of the Duluth Complex and related rocks of northeastern Minnesota: *Minnesota Geological Survey Report of Investigations*, v. 58, pp. 207
- Muehlenbachs, K., and Clayton, R.N., 1972, Oxygen isotope studies of fresh and weathered submarine basalts: *Canadian Journal of Earth Sciences*, v. 9, p. 172-184.
- Muehlenbachs, K., Anderson, A.T., 1974, Low-¹⁸O basalts from Iceland: *Geochemica et Cosmochimica Acta*, v. 38, p. 577-588.
- Mulja, T., and Mitchell, R.H., 1991, The Geordie Lake Intrusion, Coldwell complex, Ontario: a palladium and tellurium-rich disseminated sulfide occurrence derived from an evolved tholeiitic magma: *Economic Geology*, v. 86, p. 1050-1069.
- Mungall, J.E., 2007, Crystallization of magmatic sulfides: An empirical model and application to Sudbury ores: *Geochemica et Cosmochimica Acta*, v. 71, p. 2809-2819.
- Naldrett, A.J., 2004, *Magmatic sulfide deposits—Geology, geochemistry, and exploration*: Berlin, Springer-Verlag, 727 p
- Naldrett A. J., Asif, M., Gorbachev, N.S., Kuniylov, V., Stekhin, A. I., Fedorenko, V. A., and Lightfoot, P. C., 1994, The composition of the Ni-Cu ores of the Oktyabr'sky Deposit, Noril'sk Region: *Ont. Geol. Surv. Spec.*, v. 5, p. 357–371.
- Naldrett A. J., Asif, M., Schandl, E., Searcy, T., Morrison, G. G., Binney, W. P. and Moore, C., 1999, Platinum-group elements in the Sudbury ores: Significance with respect to the origin of different ore zones and to the exploration for footwall ore bodies: *Economic Geology*, v. 94, p. 185–210.

- Nicol, D.W., 1990, Assimilation of basic xenoliths within center 3 syenites of the Coldwell alkaline complex, Ontario, MSc Thesis, Lakehead University, Thunder Bay, Ontario.
- Palmer, H.C., Davis, D.W., 1987, Paleomagnetism and U-Pb Geochronology of Volcanic Rocks from Michipicoten Island, Lake Superior: Precise calibration of the Keweenawan polar wander track: *Precambrian Research*, v. 37, p. 157-171.
- Palacas, James G. (1995). "Superior Province (051)". National Oil and Gas Assessment. United States Geological Survey. Retrieved 2007-06-10.
- Pearce, J., and Cann, J., 1973, Tectonic setting of basic volcanic rocks determined using trace element analyses: *Earth and Planetary Science Letters*, v.19, p. 290-300.
- Pearce, J.A., and Norry, M.J., 1979, Petrogenetic Implications of Ti, Zr, Y, and Nb Variations in Volcanic Rocks: *Contributions to Mineralogy and Petrology*, v. 69, p. 33-47
- Percival, J.A, and West, G.F., 1994, The Kapuskasing Uplift: A geological and geophysical synthesis: *Canadian Journal of Earth Sciences*, v. 31: p. 1256–1286.
- Percival, J.A., Sanborn-Barrie, M., Skulski, T., Stott, G.M., Helmstaedt, H., and White, D.J., 2006. Tectonic evolution of the western Superior Province from NARMAP and Lithoprobe studies: *Canadian Journal of Earth Sciences*, v. 43: p. 1085-1117.
- Percival, J., 2007. Geology and Metallogeny of the Superior Province, Canada. In Goodfellow, w., ed., *Mineral Deposits of Canada: A Synthesis of Major Deposit Types, District Metallogeny, the Evolution of Geological Provinces, and Exploration Methods*: Geological Association of Canada, Mineral Deposits Division, Special Publication No. 5, p. 903-928.
- Polat, A., and Kerrich, R., 1999, Formation of an Archean tectonic melange in the Schreiber–Hemlo greenstone belt, Superior Province, Canada; implications for Archean subduction–accretion process.: *Tectonics*, p. 18, v. 733–755.
- Polat, A., Kerrich, R., and Wyman, D.A., 1998, The late Archean Schreiber-Hemlo and White River-Dayohessarah greenstone belts, Superior Province: collages of oceanic plateaus, oceanic arcs, and subduction-accretion complexes: *Tectonophysics*, v. 289, p. 295-326
- Puritch, E.J., Orava, D., Armstrong, T., Yassa, A., Gowans, R., Wislesky, I., and Jacobs, C., 2009, Marathon PGM Corporation, NI 43-101 Technical Report on the Updated Mineral Resource Estimate and Feasibility Study for the Marathon PGM-Cu Project, Marathon, Ontario, Canada, February 2, 2009.
- Puskas, F.P., 1967, The geology of the Port Coldwell area: Ontario Department of Mines, Thunder Bay, Ontario, Open File Report 5104.

Puskas, F.P., 1970, The Port Coldwell Alkali Complex: Institute of Lake Superior Geology, v. 16, p. 1-17.

Rio Tinto, Conceptual Estimate, Rio Tinto press release, 2008.
http://www.riotinto.com/documents/ReportsPublications/Nickel-Copper_exploration_target_at_Tamarack.pdf

Ripley, E.M., 1986, Applications of stable isotope studies to problems of magmatic sulfide ore genesis with special reference to the Duluth Complex Minnesota *in* Geology and Metallogeny of Copper Deposits (eds. Friedrich, G.H., Genkin, A.D., Naldrett, A.J., Ridge, J.D., Sillitoe, R.H., and Vokes, F.M.): Society for Geology Applied to Ore Deposits Special Publication 4, Springer-Verlag, Berlin-Heidelberg, p. 25-42.

Ripley, E.M., 2014, Ni-Cu-PGE Mineralization in the Partridge River, South Kawishiwi, and Eagle Intrusions: A Review of Contrasting Styles of Sulfide-Rich Occurrences in the Midcontinent Rift System: *Economic Geology*, v. 109, p. 309-324.

Rousseau, R.M., 2001, Detection limit and estimate of uncertainty of analytical XRF results: *The Rigaku Journal*, v. 2, p. 1-15

Sage, R.P., Lightfoot, P.C., and Doherty, W. 1996. Geochemical characteristics of granitoid rocks from within the Archean Michipicoten greenstone belt, Wawa Subprovince, Superior Province, Canada; implications for source regions and tectonic evolution: *Precambrian Research*, v. 76, p. 155–190.

Schulz, K.J., Chandler, V.W., Nicholson, S.W., Piatak, N., Seal, R.P., Woodruff, L.G., and Zientek, M.L., Magmatic Sulfide-Rich Nickel-Copper Deposits Related to Picrate and (or) Tholeiitic Basalt Dike-Sill Complexes: A Preliminary Deposit Model: USGS Open File Report, 2010, U.S. Department of the Interior, U.S. Geological Survey, 31 pp

Severson, M.J., 1994, Igneous stratigraphy of the South Kawishiwi intrusion, Duluth Complex Minnesota: Duluth, Minnesota, Natural Resources Research Institute, Technical Report 95-26, 185 p.

Shaw, C., 1997, The petrology of the layered gabbro intrusion, eastern gabbro, Coldwell alkaline complex, Northwestern Ontario, Canada: evidence for multiple phases of intrusion in a ring dyke. *Lithos*: v. 40, p. 243-259.

Shervais, J.W., 1982, Ti-V plots and the petrogenesis of modern and ophiolitic lavas: *Earth and Planetary Science Letters*, v. 59, p. 101-118.

Sluzhenikin, S.F., Distler, V.V., Dyuzhikov, O.A., Kravtsov, V.F., Kunilov, V.E., Laputina, I.P., and Turovtsev, D.M., 1994, Low-sulphide platinum mineralization in the Noril'sk differentiated intrusive bodies: *Geology of Ore Deposits*, v. 36, p. 171-195.

- Song, X.Y., Keays, R.R., Zhou, M.F., Qi, L., Ihlenfeld, C., and Xiao, J.F., 2009, Siderophile and chalcophile elemental constraints on the origin of the Jinchuan Ni-Cu-(PGE) sulfide deposit, NW China: *Geochimica et Cosmochimica Acta*, v. 73, p. 404-424.
- Staudigel, H., Davies, G.R., Hart, S.R., Marchant, K.M., Smith, B.M., 1995, Large-scale isotopic Sr, Nd and O isotopic anatomy of altered oceanic crust - DSDP/ODP sites 417/418: *Earth Planet Sci Letters*, v. 130, p. 169-185.
- Stone, D., Lavigne, M.J., Schnieders, B., Scott, J., Wagner, D., 2003, Regional geology of the Lac des Iles Area. Summary of field work and other activities – Open File Report 6120, Ontario Geological Survey 15-11 – p. 15-25.
- Stott, G. M., Corkery, M.T., Percival, J.A., Simard, M. and Goutier, J., 2011, A revised terrane subdivision of the Superior Province. *In: Summary of Field Work and Other Activities*, 2010, Geological Survey, Open File Report 6260, p. 201-210.
- Sun, S., and McDonough, W.F., 1989, Chemical and isotopic systematics of oceanic basalts: implications for mantle composition and processes (*in Magmatism in the Ocean Basins*, Edited by A.D. Saunders and M.J. Norry): Geological Society London Special Publication, v. 42, p. 313-345
- Sun, S., 1982, Chemical composition and origin of the earth's primitive mantle: *Geochimica et Cosmochimica Acta*, v. 46, p. 179-192.
- Sutcliffe, R.H., 1986, Regional geology of the Lac des Iles area District of Thunder Bay: Ontario Geological Survey Miscellaneous Paper, v. 132, p. 70-75.
- Sutphin, D.M., and Page, N.J., 1986, Platinum-group metals - International Strategic Minerals Inventory summary report: U.S. Geological Survey Circular, v. 930-E, 34 pp.
- Taylor, H.P. Jr., and Turi, B., 1976, High-¹⁸O Igneous Rocks from the Tuscan Magmatic Province, Italy: *Contributions to Mineralogy and Petrology*, v. 55, p. 33-54.
- Taylor, H.P., 1974, The application of oxygen and hydrogen isotope studies to problems of hydrothermal alteration and ore deposition: *Economic Geology*, v. 69, p. 843-883
- Taylor S.R., and McLennan, S.M., 1985, *The continental crust: its composition and evolution*: Blackwell Scientific Publication, Carlton, 312 pp.
- Thériault, R.D., and Barnes, S.J., 2000, Origin of Cu-Ni-PGE sulfide mineralization in the Partidge River Intrusion, Duluth Complex, Minnesota: *Economic Geology*, v. 95, p. 929-944.
- Thomas, D.G., Melnyk, J., Gormely, L., Searston, S., and Kulla, G., 2011, Magma Metals Limited, NI 43-101 Technical Report on Preliminary Assessment, March 17, 2011.
- Thurston, P.C., 1991. Archean Geology of Ontario: Introduction, in *Geology of Ontario*, Ontario Geological Survey, Special volume 4, Part, 73-98.

- Todd S.G., Keith D.W., Leroy L.W., Schissel D.J., Mann E.L., Irvine T.N., 1982, The J-M platinum-palladium reef of the Stillwater Complex, Montana: I. stratigraphy and petrology. *Economic Geology*, v. 77, p. 1454–1480
- Turi, B., 1986, Stable Isotope Geochemistry of Travertines: Chapter 5 *in*: Fritz, P., Fontes, J.C (Eds.), *The Terrestrial Environment, Handbook of Environmental Isotope Geochemistry*, Elsevier Amsterdam, v. 2., pp. 207–238.
- Walker, E.C., Sutcliffe, R.H., Shaw, C.S.J., Shore, G.T., Penczak, R.S., 1993, Precambrian geology of the Coldwell Alkaline Complex, Ontario Geological Survey, Open File Report, v. 5868, 30 pp.
- Ware, A., 2007, The Geology of the Eagle Nickel Copper Deposit: Michigan Basin Geological Society, Abstract. <http://www.mbgs.org/newsletters/2007/01-07.pdf>
- Watkinson D.H. and Ohnenstetter D., 1992, Hydrothermal origin of platinum-group mineralization in the Two Duck Lake intrusion, Coldwell Complex, northwestern Ontario: *Canadian Mineralogist*, v. 30, p. 121-13.
- Watkinson, D.H., and Dahl, R., 1988, Platinum-group mineral precipitation from fluids in pegmatitic gabbro: Two Duck Lake Intrusion, Coldwell Complex, Ontario. *In* *Geo-Platinum '87*, Edited by H.M. Prichard, P.J. Potts, J.F.W. Bowles and S.J. Cribb, Elsevier, London, p. 237.
- Winter, J.D., 2014, *Principles of Igneous and Metamorphic Petrology Second Edition*: New York, Prentice Hall, 737 pp.
- Van Schmus, W.R. and Hinze, W.J., 1985, The midcontinent rift system: *Annual Review of Earth Planetary Sciences*, v. 13, p. 345-383.
- Williams, H.R., Stott, G.M., Thurston, P.C., Sutcliffe, R.H., Bennett, G., Easton, R.M. and Armstrong, D.K., 1992, Tectonic evolution of Ontario: summary and synthesis. *In* *Geology of Ontario*. Ontario Geological Survey., Spec. Vol. 4(2), p. 1253-1332.
- Williams, H.R., Stott, G.M., Heather, K.B., Muir, T.L. and Sage, R.P., 1991, Wawa Subprovince. *In*: *Geology of Ontario*, Ontario Geological Survey, Special Volume 4, Part I. P. 485-539.
- Williams, H.R., 1990, Quetico Subprovince. *In*: *Geology of Ontario*, Ontario Geological Survey, Special Volume 4, Part I. p. 383-409.
- Young, D.A., 2003, *Mind Over Magma*, Princeton University Press., Princeton, NJ, Chapters 17, 28, and 29.
- Zientak, M.L., 2012, *Magmatic Ore Deposits in Layered Intrusions – Descriptive Model for Reef-Type PGE and Contact-Type Cu-Ni-PGE Deposits*: U.S. Department of the Interior, U.S. Geological Survey, 54 pp.

Appendix

Appendix 1 – SEM-EDS Data

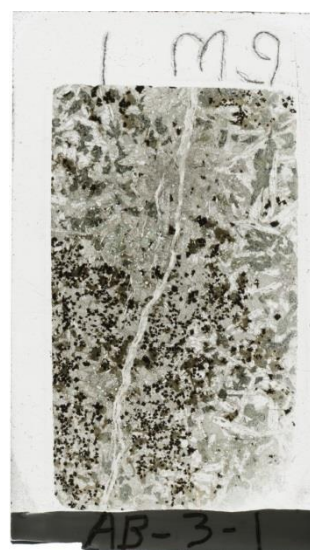
Due to the length and large file size, the SEM portion of the appendix is available on a jump drive provided by the author. If you are accessing this document from outside Western University, please contact the author for the necessary files.

Appendix 2 – Petrographic Reports

Note: All values are in weight % except for Cu and Pd, which are in parts per million (ppm).

Northing: 5407634			Easting: 537722
Sample name	Location	Depth	Lithology
AB-3-1	Albite Pod	Surface sample	Heterogeneous gabbro

Hand Sample	Thin section
-------------	--------------



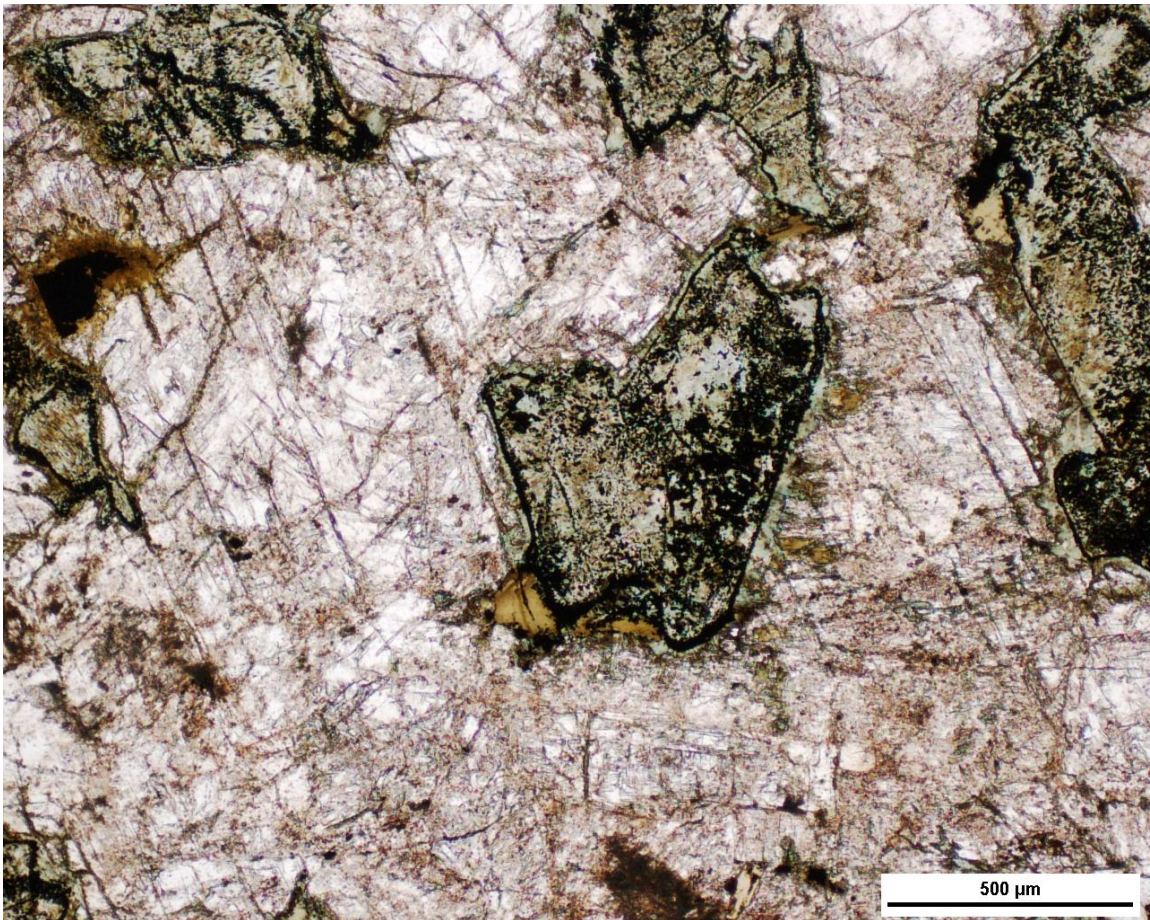
Albitization is localized to pods 3-4 cm in diameter and thin mantling of plagioclase laths. Actinolite alteration, and/or chloritization occurs as a smeared dark green band adjacent to regions of strong albitization. Albite alteration is characterized by small pods consisting of networked albite grains. Euhedral, sugary apatite is common (~5 modal percent) within albite alteration.

Geochemistry of Sample														
SiO ₂	Al ₂ O ₃	FeO	Fe ₂ O ₃	CaO	MgO	Na ₂ O	K ₂ O	TiO ₂	MnO	P ₂ O ₅	L.O.I.	S	Cu	Pd
43	12.6	11.2	22	8.3	4.49	3.56	1.9	2.6	0.32	1.1	1.11	0.02	201	0.016

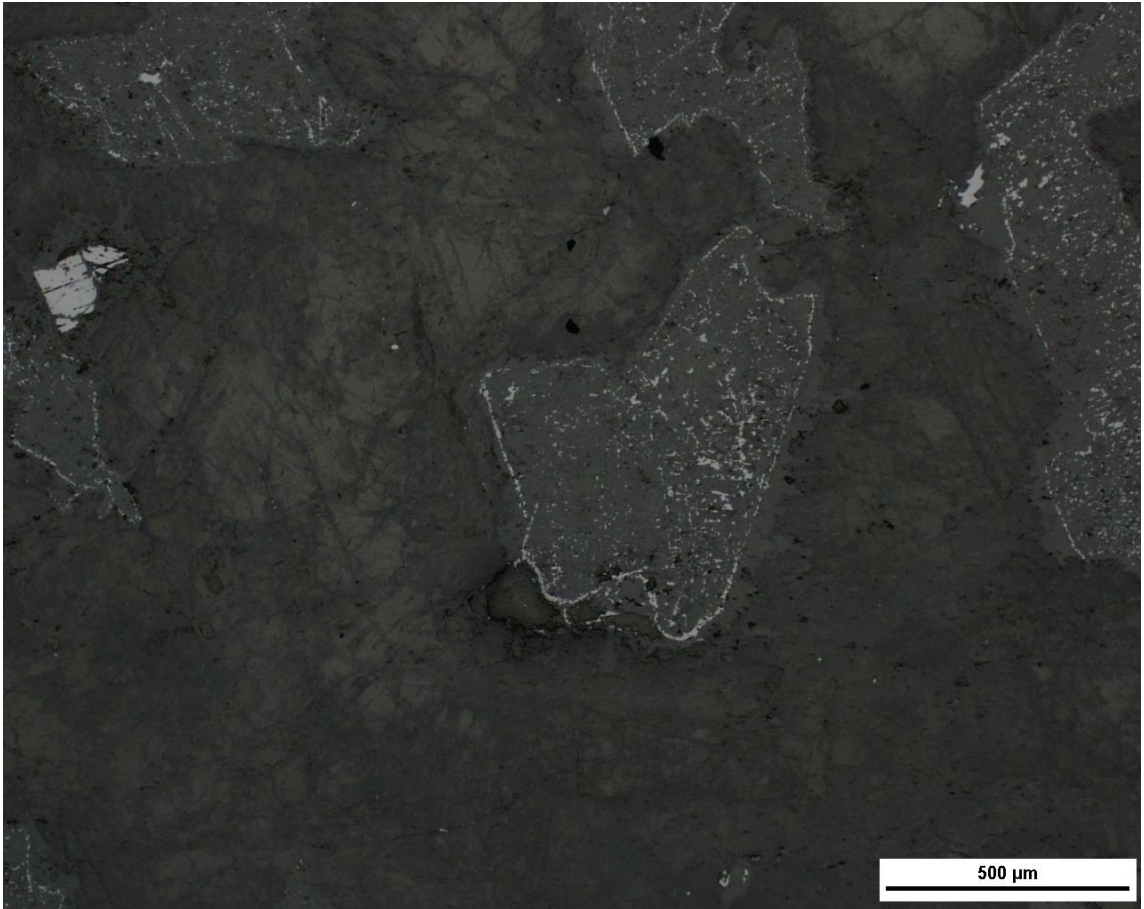
Thin Section Petrography			
Silicates			
Mineral	Modal %	Grainsize	Description
Plagioclase	27	1-3mm	Euhedral laths, albitized at rims when near regions of strong albite alteration

Albite	22	1-4mm	Regions of the section are strongly albitized, overprinting all other minerals except opaques (sulfides)
Biotite	4	1mm	Thinly rims magnetite grains
Actinolite	1	<1mm	Very weak alteration of Cpx
Magnetite	7	<1-1mm	Bottom left portion of thin section contains ~15% disseminated, euhedral to subhedral magnetite
Olivine	13	1-2mm	Stubby, to irregular shaped grains with high relief
Clinopyroxene	19	1-3mm	Interstitial to plag, low to medium relief
Apatite	1	<1mm	Abundant in zones of strong albite alteration
Epidote	Tr	<1mm	Rare, but associated with weak actinolite alteration
Carbonate	3	1-2mm	Is contained within thin veinlet that cuts the entire section
Serpentine	3	<1mm	Present as product of weak to moderate olivine alteration
Sulfides			
Mineral	Modal %	Dominant Grainsize	Description
Chalcopyrite	Tr	<1mm	Weak disseminated and associated with actinolite alteration near magnetite, and albite alteration

Photomicrographs



Olivine grains are enclosed by a large plagioclase grain. Biotite (brown small grain) borders the olivine grain (center). Olivine is weakly serpentinized. In PPL.



Same image as above, but in reflected light. The olivine grain contains magnetite at its fractures (bright grey).

Northing: 5407634		Easting: 537722	
Sample name	Location	Depth	Lithology

AB-3-2	Albite Pod	Surface sample	Heterogeneous gabbro
--------	------------	----------------	----------------------

Hand Sample	Thin section
--------------------	---------------------

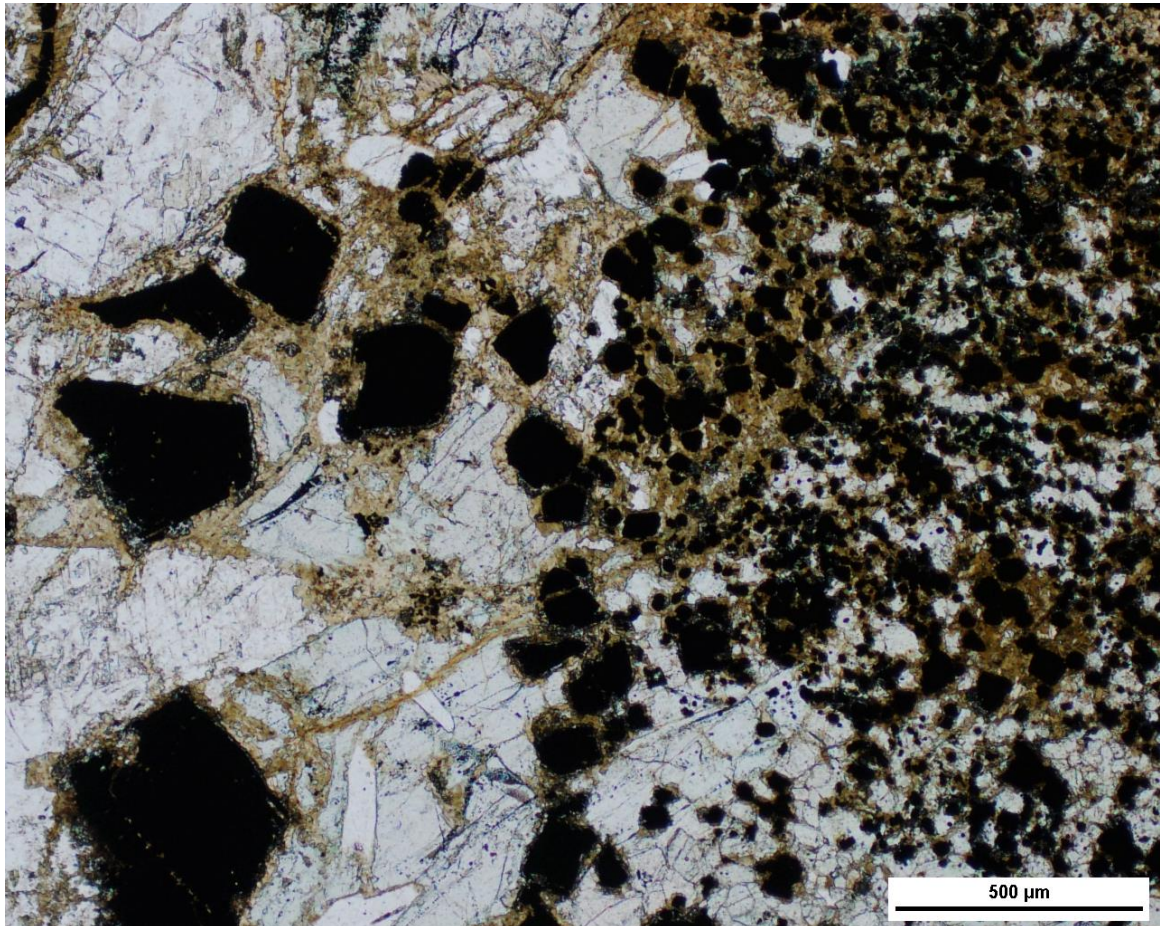


Geochemistry of Sample														
SiO ₂	Al ₂ O ₃	FeO	Fe ₂ O ₃	CaO	MgO	Na ₂ O	K ₂ O	TiO ₂	MnO	P ₂ O ₅	L.O.I.	S	Cu	Pd
41.9	12.3	12.05	24.3	8.15	4.29	3.39	1.72	2.98	0.35	1.12	0.37	0.05	670	0.134

Thin Section Petrography			
Silicates			
Mineral	Modal %	Grainsize	Description
Plagioclase	21	1-3mm	Euhedral to subhedral laths, albitized at rims when near regions of strong albite alteration
Albite	25	1-4mm	The upper two-thirds of this section is strongly albitized, dirty-brown coloured and frosty textured
Biotite	4	1mm	Strongly alters rims and even cores of magnetite grains
Actinolite	3	<1mm	Pseudomorphic after Cpx grains that are interstitial to albitized plagioclase laths
Magnetite	6	<1-1mm	Irregular shaped, almost skeletal textured
Olivine	4	1mm	High relief, strongly serpentinized. Irregular shaped grains
Clinopyroxene	11	1-3mm	Interstitial to plag, low to medium relief
Apatite	2	<1mm	Abundant in zones of strong albite alteration
Epidote	Tr	<1mm	Rare, but associated with weak actinolite alteration. Pistachio green coloured
Carbonate	3	1-2mm	Is contained within thin veinlet that cuts the bottom portion of the thin section
Chlorite	7	1-3mm	Also contained within thin veinlet at the bottom portion of the thin section, associated with carbonate
Sulfides			

Mineral	Modal %	Dominant Grainsize	Description
Chalcopyrite	Tr	<1mm	Weak disseminated and associated with actinolite alteration near magnetite, and albite alteration

Photomicrographs



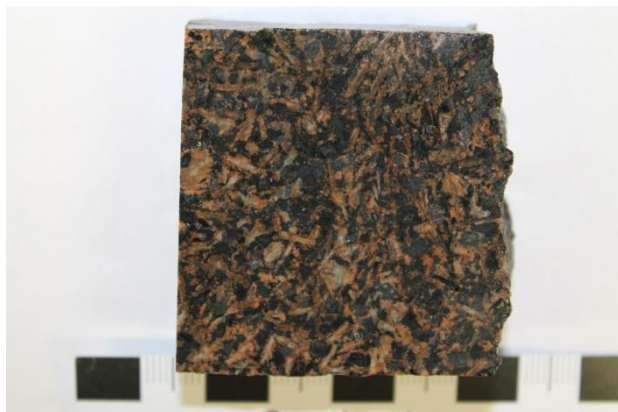
Stubby fine grained magnetite crystals are disseminated at the right side of the image. On the left side, magnetite is stubby and equant and larger. Magnetite grains are rimmed by brown biotite.

Northing: 5407634

Easting: 537722

Sample name	Location	Depth	Lithology
AB-3-3	Albite Pod	Surface sample	Heterogeneous gabbro

Hand Sample	Thin section
-------------	--------------



Geochemistry of Sample														
SiO ₂	Al ₂ O ₃	FeO	Fe ₂ O ₃	CaO	MgO	Na ₂ O	K ₂ O	TiO ₂	MnO	P ₂ O ₅	L.O.I.	S	Cu	Pd
50.7	14.15	7.65	14.9	6.95	3.27	5.5	1	1.28	0.23	1.08	1.37	0.04	776	0.009

Thin Section Petrography			
Silicates			
Mineral	Modal %	Grainsize	Description
Plagioclase	19	1-3mm	Euhedral to subhedral laths, albitized at rims when near regions of strong albite alteration
Albite	51	1-4mm	Pervasive in this sample, overprints plagioclase in bottom half of section and envelops act-altered Cpx
Biotite	4	1mm	Strongly alters rims and even cores of magnetite grains
Actinolite	8	<1mm	Pseudomorphic after Cpx grains that are interstitial to albitized plagioclase laths
Magnetite	6	<1-1mm	Irregular shaped, almost skeletal textured
Olivine	3	1mm	High relief, strongly serpentinized. Irregular shaped grains
Clinopyroxene	2	1-3mm	Interstitial to plag, low to medium relief – predominantly altered to act in this section.
Apatite	3	<1mm	Abundant in zones of strong albite alteration
Carbonate	Tr	<1mm	Fine grained, associated with chlorite in upper left portion of thin section
Chlorite	4	1-3mm	Also contained within thin veinlet at the bottom portion of the thin section, associated with carbonate
Sulfides			

Mineral	Modal %	Dominant Grainsize	Description
Chalcopyrite	Tr	<1mm	Weak disseminated and associated with actinolite alteration near magnetite, and albite alteration

Photomicrographs



General texture of alteration in this sample. Middle grain (light green) is a serpentinized olivine grain, and it is enveloped by albite. An actinolite grain (forest green) is also contained by albite alteration.

Northing: 5407634

Easting: 537722

Sample name	Location	Depth	Lithology
AB-3-4	Albite Pod	Surface sample	Heterogeneous gabbro

Hand Sample	Thin section
-------------	--------------



Plagioclase laths weakly aligned perpendicular to the core length, plagioclase grains on average $\sim <1.5\text{cm}$, interstitial clinopyroxene and very little to no olivine. Magnetite is subhedral forming rounded clusters of $\sim 0.5\text{cm}$.

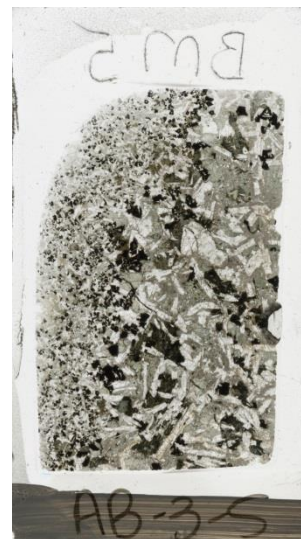
Geochemistry of Sample														
SiO ₂	Al ₂ O ₃	FeO	Fe ₂ O ₃	CaO	MgO	Na ₂ O	K ₂ O	TiO ₂	MnO	P ₂ O ₅	L.O.I.	S	Cu	Pd
45.4	13.2	10.4	20.8	7.67	3.84	4.26	1.56	2.55	0.3	1.17	0.87	0.02	439	0.01

Thin Section Petrography			
Silicates			
Mineral	Modal %	Grainsize	Description
Plagioclase	19	1-3mm	Euhedral to subhedral laths
Albite	55	1-4mm	Pervasive in this sample, overprints plagioclase in bottom half of section and envelops act-altered Cpx. Typically interstitial to plagioclase
Biotite	4	1-3mm	Strongly alters rims and even cores of magnetite grains
Actinolite	6	<1mm	Pseudomorphic after Cpx grains that are interstitial to albitized plagioclase laths
Magnetite	7	<1-1mm	Irregular shaped, almost skeletal textured
Olivine	2	1mm	High relief, strongly serpentinized. Irregular shaped grains
Clinopyroxene	2	1-3mm	Interstitial to plag, low to medium relief – predominantly altered to act in this section.
Apatite	2	<1mm	Abundant in zones of strong albite alteration
Chlorite	1	1-3mm	Occurs proximal to actinolite, deep green coloured

Sulfides			
Mineral	Modal %	Dominant Grainsize	Description
Chalcopyrite	Tr	<1mm	Weak disseminated and associated with actinolite alteration near magnetite, and albite alteration

Northing: 5407634			Easting: 537722
Sample name	Location	Depth	Lithology
AB-3-5	Albite Pod	Surface sample	Heterogeneous gabbro

Hand Sample	Thin section
-------------	--------------



Geochemistry of Sample														
SiO ₂	Al ₂ O ₃	FeO	Fe ₂ O ₃	CaO	MgO	Na ₂ O	K ₂ O	TiO ₂	MnO	P ₂ O ₅	L.O.I.	S	Cu	Pd
44.3	13.1	10.6	21.2	8.32	4.1	3.83	1.56	2.53	0.34	1.14	0.43	0.04	625	0.046

Thin Section Petrography			
Silicates			
Mineral	Modal %	Grainsize	Description
Plagioclase	37	1-3mm	Euhedral to subhedral laths
Albite	20	1-4mm	Pervasive in this sample, overprints plagioclase in bottom half of section and envelops act-altered Cpx. Typically interstitial to plagioclase
Biotite	4	1-3mm	Strongly alters rims and even cores of magnetite grains
Actinolite	6	<1mm	Pseudomorphic after Cpx grains that are interstitial to albitized plagioclase laths
Magnetite	8	<1-1mm	Irregular shaped, some are skeletal textured
Olivine	5	1mm	High relief, serpentinized. Irregular shaped grains
Clinopyroxene	16	1-3mm	Interstitial to plag, low to medium relief – albitized on the right side of the thin section
Apatite	2	<1mm	Abundant in zones of strong albite alteration
Chlorite	1	1-3mm	Occurs proximal to actinolite, deep green coloured
Serpentine	1	<1mm	Weak alteration of olivine
Sulfides			

Mineral	Modal %	Dominant Grainsize	Description
Chalcopyrite	Tr	<1mm	Weak disseminated and associated with actinolite alteration near magnetite, and albite alteration

Northing: 5407634			Easting: 537722
Sample name	Location	Depth	Lithology
AB-3-6	Albite Pod	Surface sample	Heterogeneous gabbro

Hand Sample	Thin section
-------------	--------------



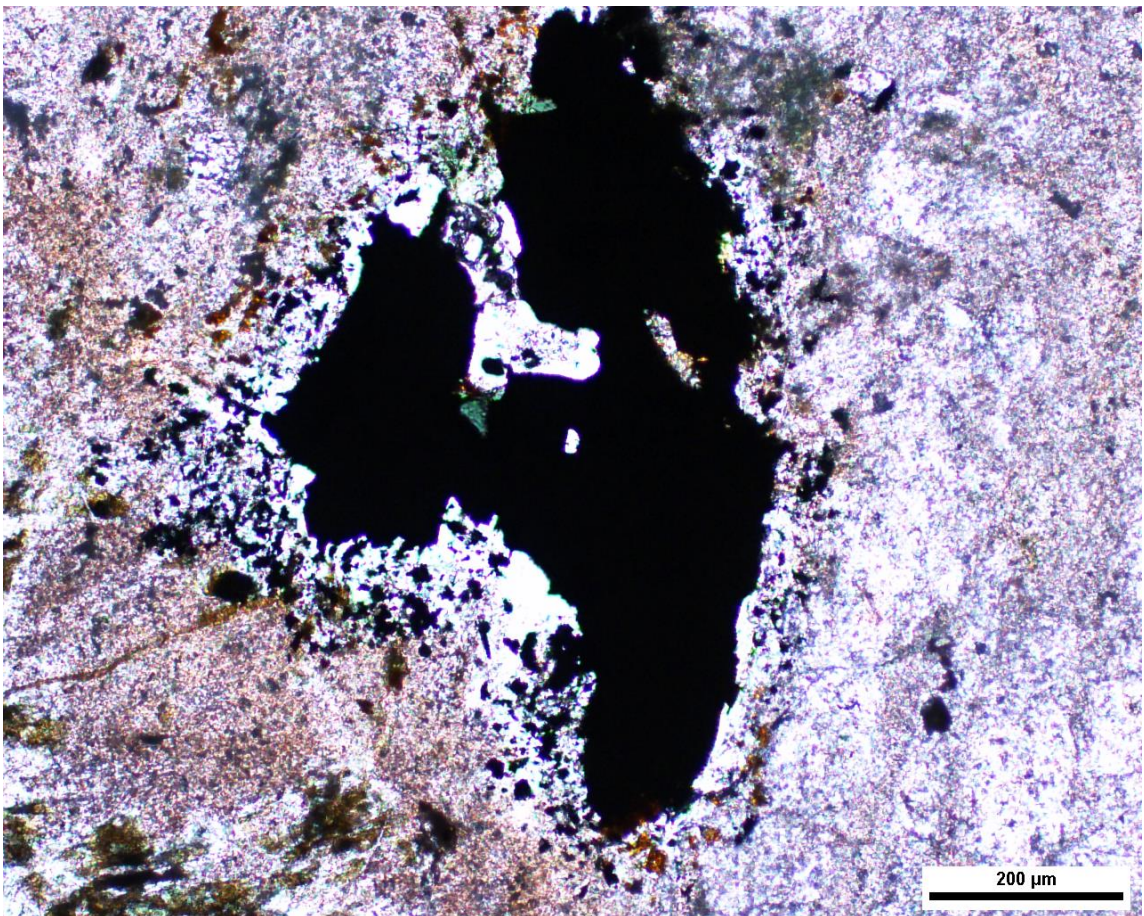
Plagioclase laths weakly aligned perpendicular to the core length, plagioclase grains on average $\sim <1.5\text{cm}$, interstitial clinopyroxene and very little to no olivine. Magnetite is subhedral forming rounded clusters of $\sim 0.5\text{cm}$.

Geochemistry of Sample														
SiO ₂	Al ₂ O ₃	FeO	Fe ₂ O ₃	CaO	MgO	Na ₂ O	K ₂ O	TiO ₂	MnO	P ₂ O ₅	L.O.I.	S	Cu	Pd
49	13.6	8.78	16.9	7.47	3.56	4.93	1.12	1.7	0.27	1.12	1.05	0.04	914	0.008

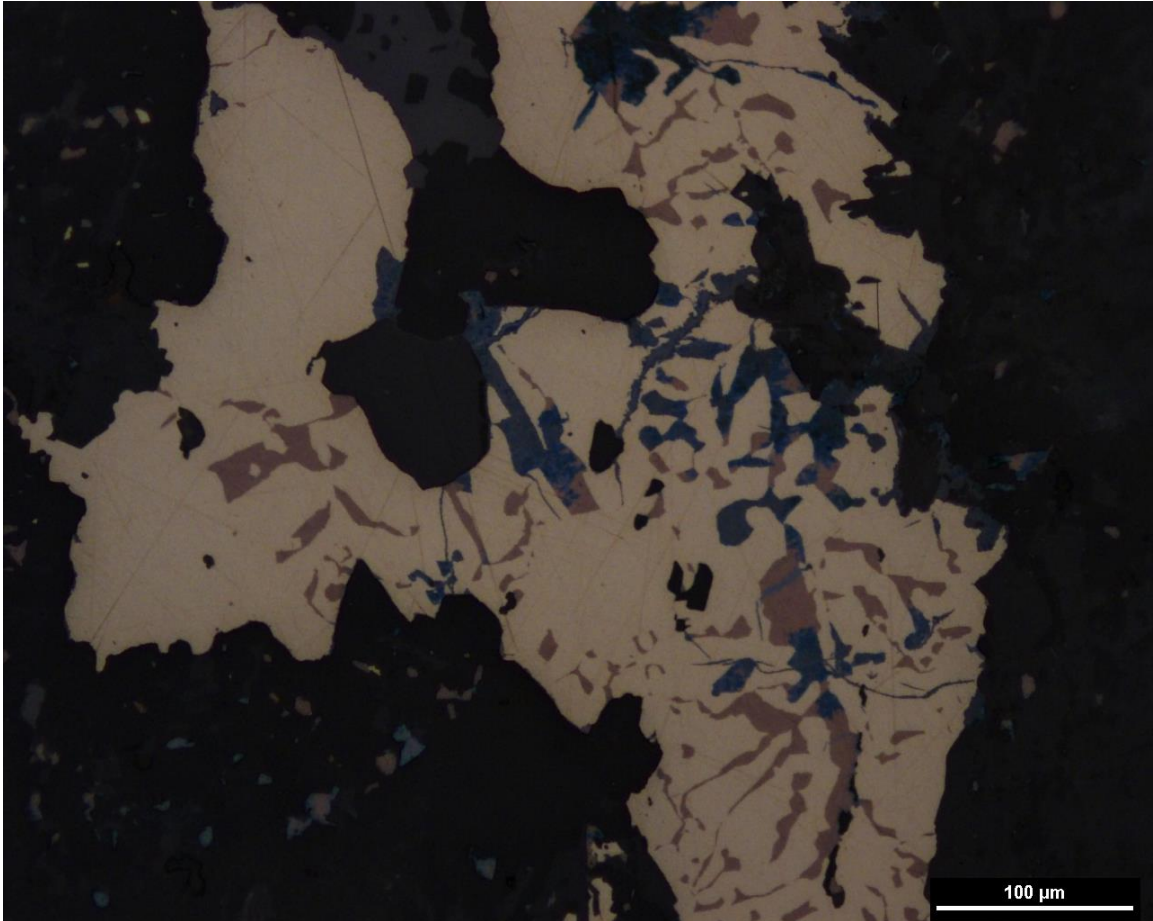
Thin Section Petrography			
Silicates			
Mineral	Modal %	Grainsize	Description
Plagioclase	15	1-3mm	Euhedral to subhedral laths, generally are strongly albitized
Albite	61	1-4mm	Pervasive in this sample, overprints plagioclase in bottom half of section and envelops act-altered Cpx. Typically interstitial to plagioclase
Biotite	5	1-3mm	Strongly alters rims and less commonly, cores of magnetite grains
Actinolite	6	<1mm	Pseudomorphic after Cpx grains that are interstitial to albitized plagioclase laths
Magnetite	7	<1-1mm	Irregular shaped, some are skeletal textured
Olivine	2	1mm	High relief, serpentinized. Irregular shaped grains
Clinopyroxene	1	1-3mm	Pervasively altered to act, particularly in regions of strong albite alteration

Apatite	2	<1mm	Abundant throughout, disseminated especially within albite alteration
Chlorite	1	1-3mm	Occurs proximal to actinolite, deep green coloured
Serpentine	Tr	<1mm	Weak alteration of olivine
Carbonate	Tr	<1mm	Associated with actinolite, particularly around Ccp
Sulfides			
Mineral	Modal %	Dominant Grainsize	Description
Chalcopyrite	Tr	<1mm	Weak disseminated and associated with actinolite alteration near magnetite, and albite alteration
Bornite	Tr	<1mm	Occurs as exsolution within chalcopyrite
Chalcocite	Tr	<1mm	Occurs as exsolution within chalcopyrite

Photomicrographs



An opaque bleb is surrounded by albite, carbonate, and lesser actinolite. In PPL.



The same image as above but zoomed in. The opaque bleb is a chalcopyrite grain that also hosts bornite and chalcocite exsolution. In reflected light.

Northing: 5407634			Easting: 537722
Sample name	Location	Depth	Lithology
AB-3-7	Albite Pod	Surface sample	Heterogeneous gabbro

Hand Sample	Thin section
-------------	--------------



Geochemistry of Sample														
SiO ₂	Al ₂ O ₃	FeO	Fe ₂ O ₃	CaO	MgO	Na ₂ O	K ₂ O	TiO ₂	MnO	P ₂ O ₅	L.O.I.	S	Cu	Pd
43.5	12.55	11.15	22	8.34	4.49	3.56	1.9	2.55	0.32	1.1	1.11	0.02	201	0.016

Thin Section Petrography			
Silicates			
Mineral	Modal %	Grainsize	Description
Plagioclase	30	1-3mm	Euhedral to subhedral laths, generally are strongly albitized
Albite	35	1-4mm	Pervasive in this sample, interstitial to plagioclase and magnetite
Biotite	7	1-3mm	Strongly alters rims and less commonly, cores of magnetite grains
Actinolite	4	<1mm	Pseudomorphic after Cpx grains that are interstitial to albitized plagioclase laths
Magnetite	17	<1-1mm	Fine grained and disseminated
Olivine	1	1mm	High relief, serpentinized. Irregular shaped grains, quite rare in this section
Clinopyroxene	2	1-3mm	Pervasively altered to act, particularly in regions of strong albite alteration
Apatite	2	<1mm	Abundant throughout, disseminated especially within albite alteration
Chlorite	1	1-3mm	Occurs proximal to actinolite, deep green coloured
Serpentine	Tr	<1mm	Weak alteration of olivine
Sulfides			
Mineral	Modal %	Dominant Grainsize	Description
Chalcopyrite	Tr	<1mm	Weak disseminated and associated with actinolite alteration near

			magnetite, and albite alteration
Northing: 5407585		Easting: 537717	
Sample name	Location	Depth	Lithology
AB-5-1	Albite Pod	Surface sample	Heterogeneous gabbro

Hand Sample	Thin section
--------------------	---------------------

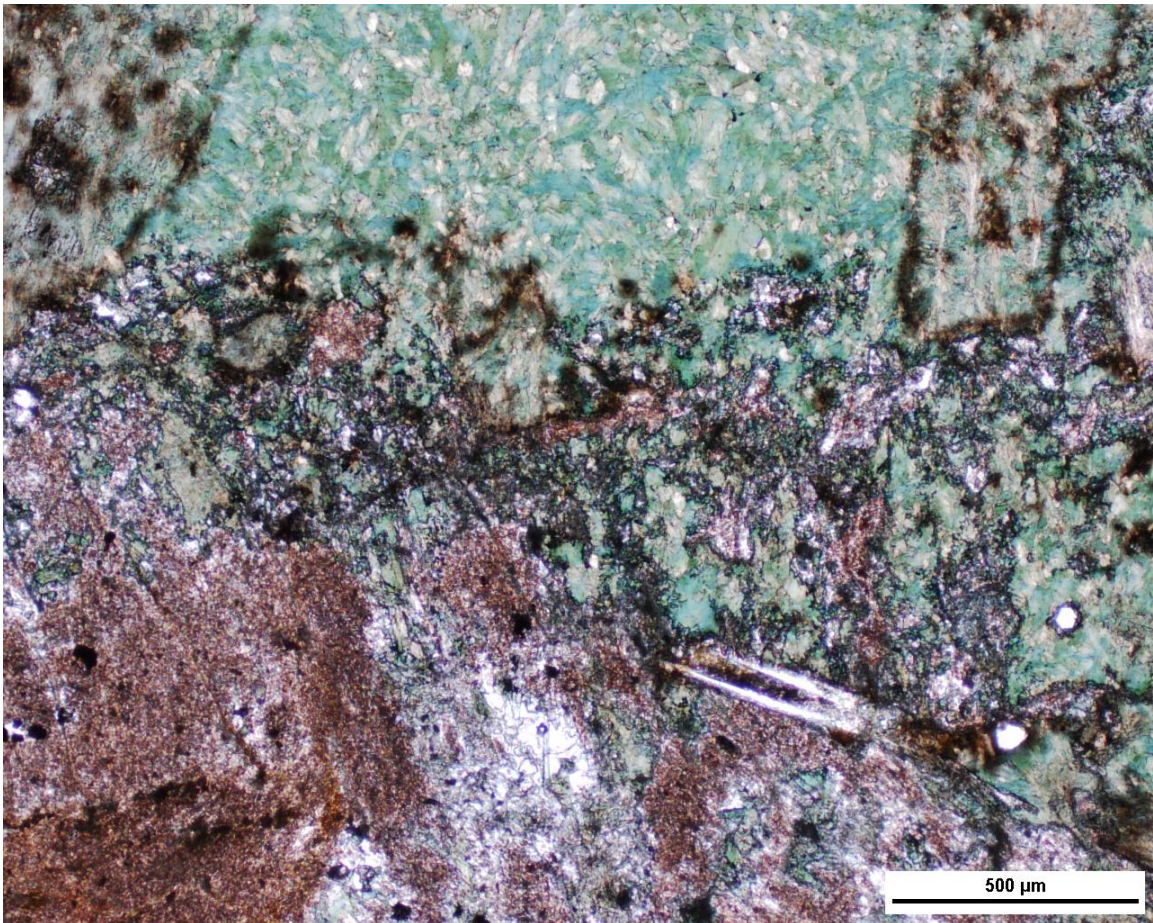


Geochemistry of Sample														
SiO ₂	Al ₂ O ₃	FeO	Fe ₂ O ₃	CaO	MgO	Na ₂ O	K ₂ O	TiO ₂	MnO	P ₂ O ₅	L.O.I.	S	Cu	Pd
42.2	11.35	14.3	26	6.25	5.04	3.41	1.29	3.3	0.4	0.88	0.69	0.04	439	0.251

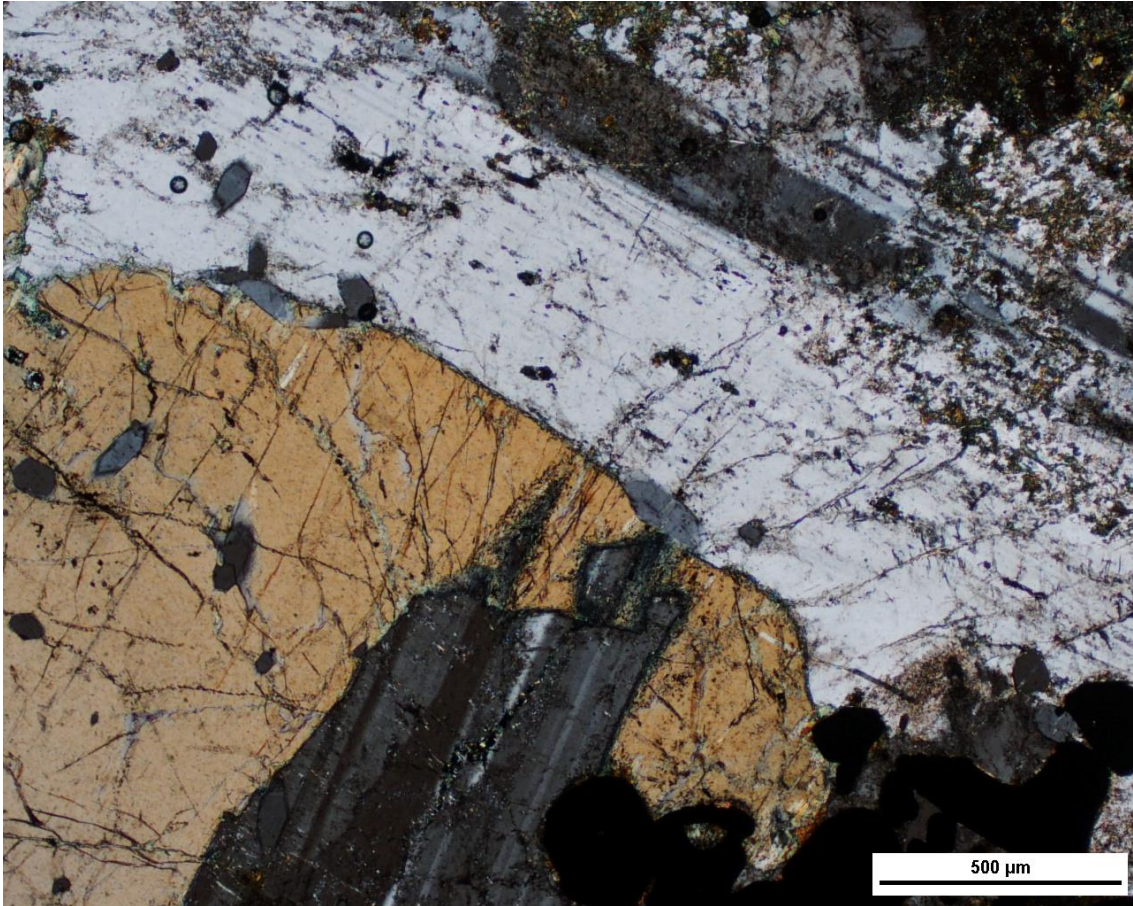
Thin Section Petrography			
Silicates			
Mineral	Modal %	Grainsize	Description
Plagioclase	28	1-3mm	Euhedral to subhedral laths, fresh outside of the albite/actinolite pod
Albite	23	1-4mm	Forms a pod/ring of alteration around actinolite pod
Biotite	4	1-3mm	Alters the rims of magnetite grains
Actinolite	16	<1mm	Forms a pod in the middle-right of the thin section
Magnetite	10	<1-1mm	Irregular shaped, some are skeletal textured. Euhedral to subhedral. Forms a faint ring of cumulates around albite and actinolite pod.
Clinopyroxene	14	1-3mm	Generally fresh outside of the albite/actinolite pod. Forms ophitic texture with plag
Apatite	<1	<1mm	Disseminated within albite alteration
Chlorite	3	1-3mm	Intergrown with actinolite
Epidote	1	<1mm	Intergrown with chl/act
Carbonate	Tr	<1mm	Associated with actinolite, particularly around Ccp
Sulfides			
Mineral	Modal	Dominant	Description

	%	Grainsize	
Chalcopyrite	Tr	<1mm	Weak disseminated and associated with actinolite alteration near magnetite, and albite alteration
Bornite	Tr	<1mm	Occurs as exsolution within chalcopyrite
Chalcocite	Tr	<1mm	Occurs as exsolution within chalcopyrite

Photomicrographs



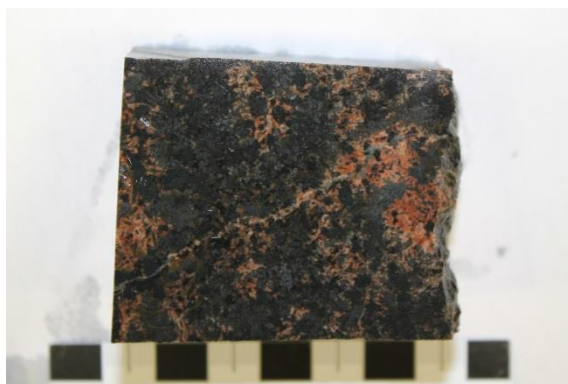
The texture of the boundary between albite (bottom, dirty brown) and actinolite alteration. In PPL.



A relatively fresh texture in the same thin section, showing ophitic plagioclase and clinopyroxene. Magnetite is at the bottom right of the image, and is subhedral. In XPL.

Northing: 5407585			Easting: 537717
Sample name	Location	Depth	Lithology
AB-5-2	Albite Pod	Surface sample	Heterogeneous gabbro

Hand Sample	Thin section
-------------	--------------



Geochemistry of Sample														
SiO ₂	Al ₂ O ₃	FeO	Fe ₂ O ₃	CaO	MgO	Na ₂ O	K ₂ O	TiO ₂	MnO	P ₂ O ₅	L.O.I.	S	Cu	Pd
45.5	13	11.4	20.4	7.88	4.44	4.2	0.99	2.24	0.33	1.29	1.01	0.04	366	0.05

Thin Section Petrography			
Silicates			
Mineral	Modal %	Grainsize	Description
Plagioclase	17	1-3mm	Euhedral to subhedral laths, fresh outside of the albite/actinolite pod
Albite	51	1-4mm	Is pervasive in this thin section, and completely encloses actinolite alteration.
Biotite	1	1-3mm	Alters the rims of magnetite grains
Actinolite	16	<1mm	Forms a pod in the middle-right of the thin section
Magnetite	5	<1-2mm	Irregular shaped, some are skeletal textured. Euhedral to subhedral
Clinopyroxene	6	1-3mm	Generally fresh outside of the albite/actinolite pod. Forms ophitic texture with plag
Apatite	<1	<1mm	Disseminated within albite alteration
Chlorite	3	1-3mm	Intergrown with actinolite
Epidote	Tr	<1mm	Intergrown with chl/act
Carbonate	Tr	<1mm	Associated with actinolite, particularly around Ccp
Sulfides			

Mineral	Modal %	Dominant Grainsize	Description
Chalcopyrite	Tr	<1mm	Weak disseminated and associated with actinolite alteration at middle to bottom-right of the thin section

Northing: 5407585			Easting: 537717
Sample name	Location	Depth	Lithology
AB-5-3	Albite Pod	Surface sample	Heterogeneous gabbro

Hand Sample	Thin section
-------------	--------------

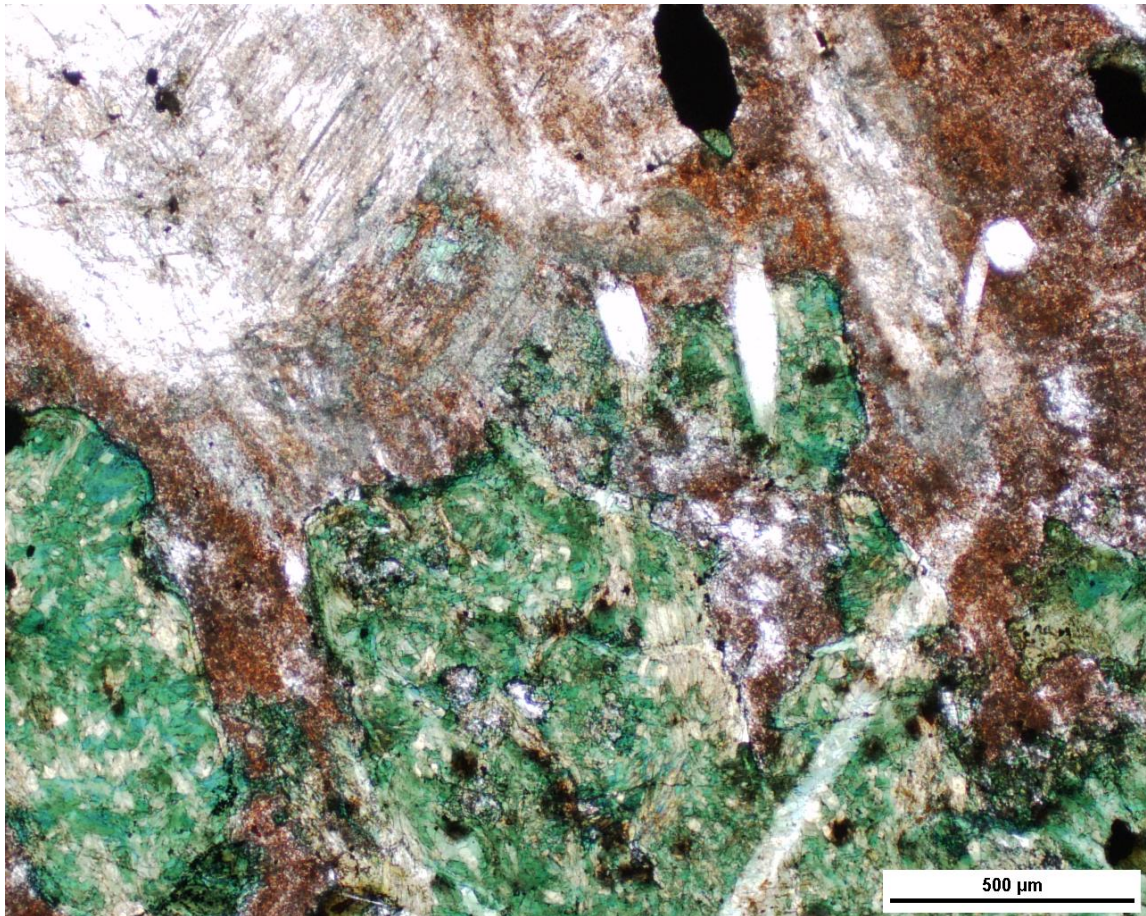


Geochemistry of Sample														
SiO ₂	Al ₂ O ₃	FeO	Fe ₂ O ₃	CaO	MgO	Na ₂ O	K ₂ O	TiO ₂	MnO	P ₂ O ₅	L.O.I.	S	Cu	Pd
46	13.3	10.9	19.05	7.93	4.21	4.37	0.98	2.2	0.32	1.35	0.91	0.03	285	0.046

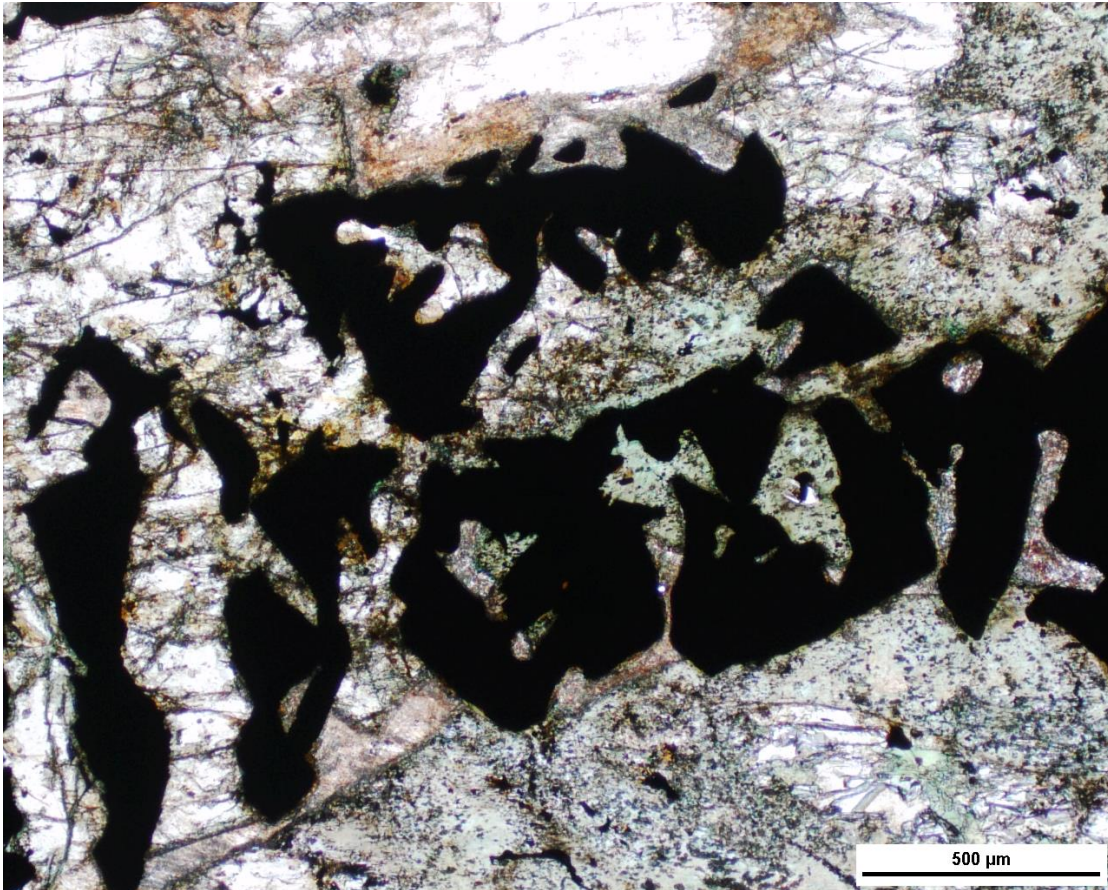
Thin Section Petrography			
Silicates			
Mineral	Modal %	Grainsize	Description
Plagioclase	28	1-3mm	Euhedral to subhedral laths, fresh outside of the albite/actinolite pod
Albite	38	1-4mm	Is pervasive in this thin section, and completely encloses actinolite alteration.
Biotite	1	<1mm	Alters the rims of magnetite grains
Actinolite	4	<1mm	Strongly alters Cpx in the regions of strong albitization
Magnetite	5	<1-3mm	Irregular shaped, most are skeletal textured. Euhedral to subhedral
Clinopyroxene	19	1-3mm	Fresh outside of the albitized regions of the thin section, low relief and forms ophitic texture with plag
Olivine	1	1mm	Only one olivine grain found in this section, has high relief and fractures that are infilled by magnetite
Apatite	2	<1mm	Disseminated within albite alteration
Chlorite	1	<1mm	Intergrown with act alteration
Epidote	Tr	<1mm	Intergrown with chl/act
Carbonate	Tr	<1mm	Associated with actinolite, particularly around Ccp
Sulfides			

Mineral	Modal %	Dominant Grainsize	Description
Chalcopyrite	Tr	<1mm	Weak disseminated and associated with actinolite alteration at middle to bottom-right of the thin section

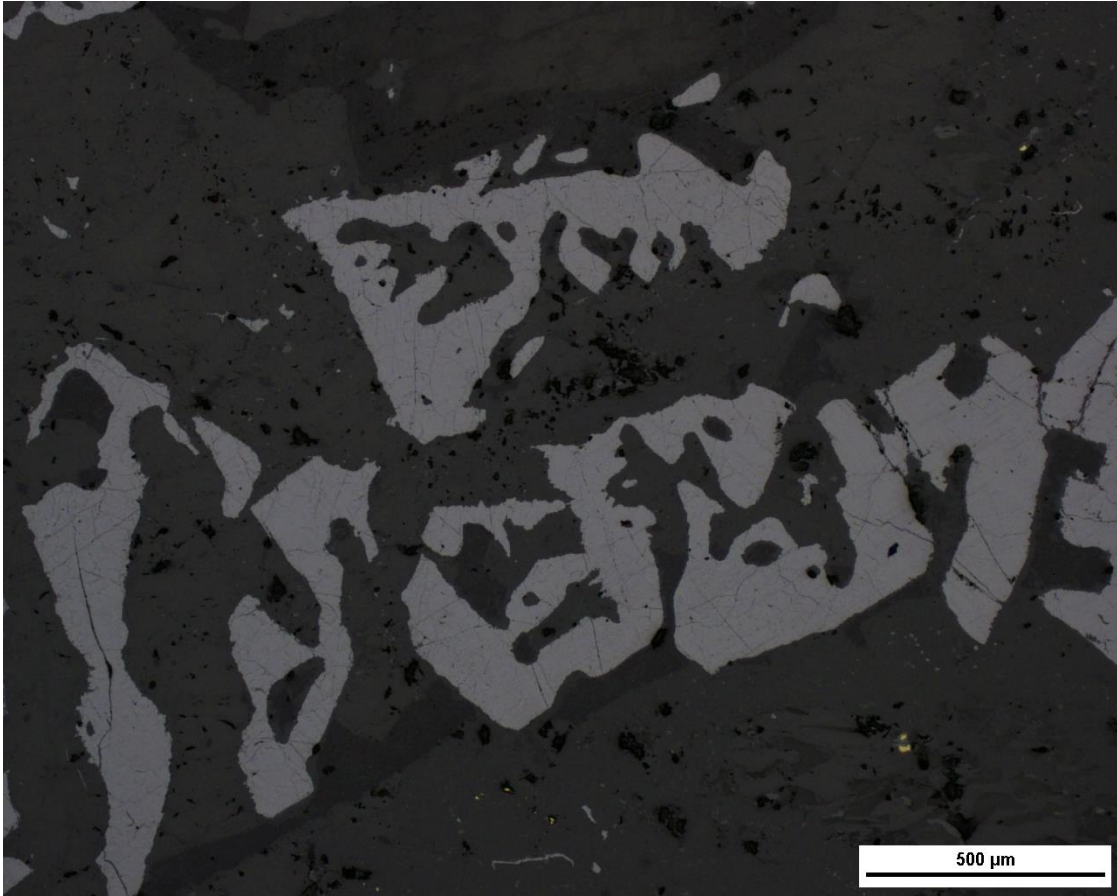
Photomicrographs



A typical altered texture of this sample in PPL. Albite alteration and actinolite alteration are very common. Albite alters plag (top of image), while actinolite alters Cpx (bottom of image).



Skeletal magnetite grains are enclosed by plagioclase and clinopyroxene. Biotite weakly rims some of the magnetite grains. In PPL.



Same image as above, but in reflected light. Skeletal magnetite grains exhibit ilmenite exsolution lamellae.

Northing: 5407585			Easting: 537717
Sample name	Location	Depth	Lithology
AB-5-4	Albite Pod	Surface sample	Heterogeneous gabbro

Hand Sample	Thin section
-------------	--------------



Geochemistry of Sample														
SiO ₂	Al ₂ O ₃	FeO	Fe ₂ O ₃	CaO	MgO	Na ₂ O	K ₂ O	TiO ₂	MnO	P ₂ O ₅	L.O.I.	S	Cu	Pd
45.7	12.95	11.4	19.9	8.43	4.34	4.2	0.88	2.49	0.34	1.41	0.84	0.02	202	0.029

Thin Section Petrography			
Silicates			
Mineral	Modal %	Grainsize	Description
Plagioclase	31	1-3mm	Euhedral to subhedral laths, fresh outside of the albite/actinolite pod
Albite	30	1-4mm	Is pervasive in this thin section, and completely encloses actinolite alteration.
Biotite	1	<1mm	Alters the rims of magnetite grains
Actinolite	4	<1mm	Strongly alters Cpx in the regions of strong albitization
Magnetite	6	<1-3mm	Irregular shaped, most are skeletal textured. Euhedral to subhedral
Clinopyroxene	19	1-3mm	Fresh outside of the albitized regions of the thin section, low relief and forms ophitic texture with plag
Apatite	2	<1mm	Disseminated within albite alteration
Chlorite	1	<1mm	Intergrown with act alteration
Epidote	Tr	<1mm	Intergrown with chl/act, pistachio green in PPL
Carbonate	Tr	<1mm	Associated with actinolite, particularly around Ccp
Sulfides			

Mineral	Modal %	Dominant Grainsize	Description
Chalcopyrite	Tr	<1mm	Weak disseminated and associated with actinolite alteration

Northing: 5407585			Easting: 537717
Sample name	Location	Depth	Lithology
AB-5-5	Albite Pod	Surface sample	Heterogeneous gabbro

Hand Sample	Thin section
-------------	--------------



Geochemistry of Sample															
SiO ₂	Al ₂ O ₃	FeO	Fe ₂ O ₃	CaO	MgO	Na ₂ O	K ₂ O	TiO ₂	MnO	P ₂ O ₅	L.O.I.	S	Cu	Pd	
45.9	13	11.8	19.9	8.32	4.5	4.15	0.96	2.29	0.34	1.49	0.8	0.03	357	0.035	

Thin Section Petrography			
Silicates			
Mineral	Modal %	Grainsize	Description
Plagioclase	32	1-3mm	Euhedral to subhedral laths, fresh outside of the albite/actinolite pod
Albite	33	1-4mm	Is pervasive in this thin section, and completely encloses actinolite alteration.
Biotite	1	<1mm	Alters the rims of magnetite grains
Actinolite	4	<1mm	Strongly alters Cpx in the regions of strong albitization
Magnetite	5	<1-3mm	Irregular shaped, most are skeletal textured. Euhedral to subhedral
Clinopyroxene	21	1-3mm	Fresh outside of the albitized regions of the thin section, low relief and forms ophitic texture with plag
Apatite	2	<1mm	Disseminated within albite alteration
Chlorite	1	<1mm	Intergrown with act alteration
Epidote	Tr	<1mm	Intergrown with chl/act, pistachio green in PPL
Sulfides			

Mineral	Modal %	Dominant Grainsize	Description
Chalcopyrite	Tr	<1mm	Rare, but a few specks are present with actinolite alteration

Northing: 5407585		Easting: 537717	
Sample name	Location	Depth	Lithology
AB-5-6	Albite Pod	Surface sample	Heterogeneous gabbro

Hand Sample	Thin section
-------------	--------------



Geochemistry of Sample														
SiO ₂	Al ₂ O ₃	FeO	Fe ₂ O ₃	CaO	MgO	Na ₂ O	K ₂ O	TiO ₂	MnO	P ₂ O ₅	L.O.I.	S	Cu	Pd
45.5	13	11.8	19.8	8.12	4.53	4.04	1.02	2.2	0.34	1.56	0.83	0.04	361	0.023

Thin Section Petrography			
Silicates			
Mineral	Modal %	Grainsize	Description
Plagioclase	25	1-3mm	Euhedral to subhedral laths, fresh outside of the albite/actinolite pod. Rims are strongly albite altered on the left side of the thin section
Albite	48	1-4mm	The entire left side of the thin section is strongly albitized. Dirty-brown, sandy textured
Biotite	2	<1mm	Alters the rims of magnetite grains
Actinolite	4	<1mm	Strongly alters Cpx in the regions of strong albitization, pseudomorphic after Cpx
Magnetite	6	<1-3mm	Irregular shaped, most are skeletal textured. Euhedral to subhedral
Clinopyroxene	12	1-3mm	Fresh outside of the albitized regions of the thin section, low relief and forms ophitic texture with plag
Apatite	2	<1mm	Disseminated within albite alteration
Olivine	Tr	1mm	Rare, but has high relief and magnetite infilled fractures

Chlorite	1	<1mm	Intergrown with act alteration
Epidote	Tr	<1mm	Intergrown with chl/act, pistachio green in PPL
Sulfides			
Mineral	Modal %	Dominant Grainsize	Description
Chalcopyrite	Tr	<1mm	Rare, but a few specks are present with actinolite alteration

Northing: 5407585			Easting: 537717
Sample name	Location	Depth	Lithology
AB-5-7	Albite Pod	Surface sample	Heterogeneous gabbro

Hand Sample	Thin section
-------------	--------------

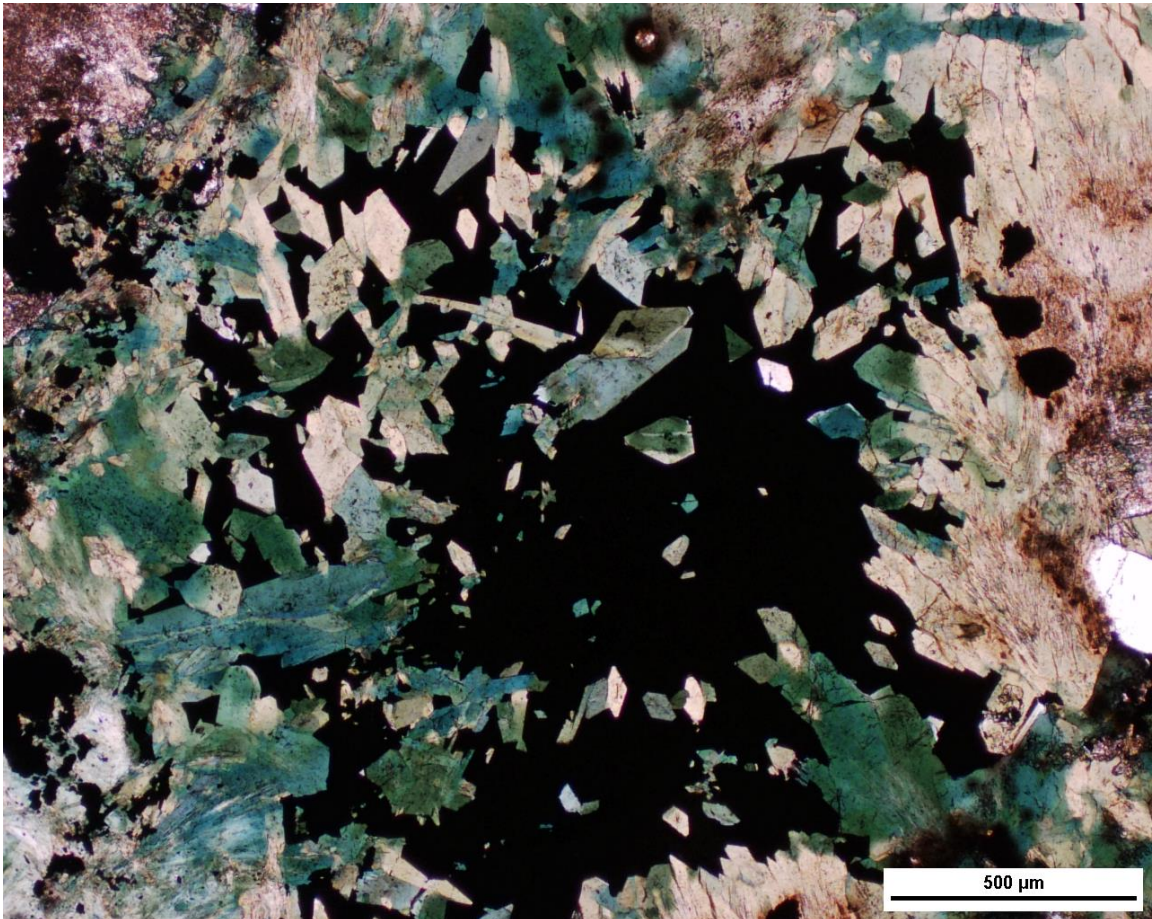


Geochemistry of Sample															
SiO ₂	Al ₂ O ₃	FeO	Fe ₂ O ₃	CaO	MgO	Na ₂ O	K ₂ O	TiO ₂	MnO	P ₂ O ₅	L.O.I.	S	Cu	Pd	
45.3	12.4	13	21.4	7.54	4.88	3.75	1.1	2.67	0.35	1.14	0.53	0.04	370	0.087	

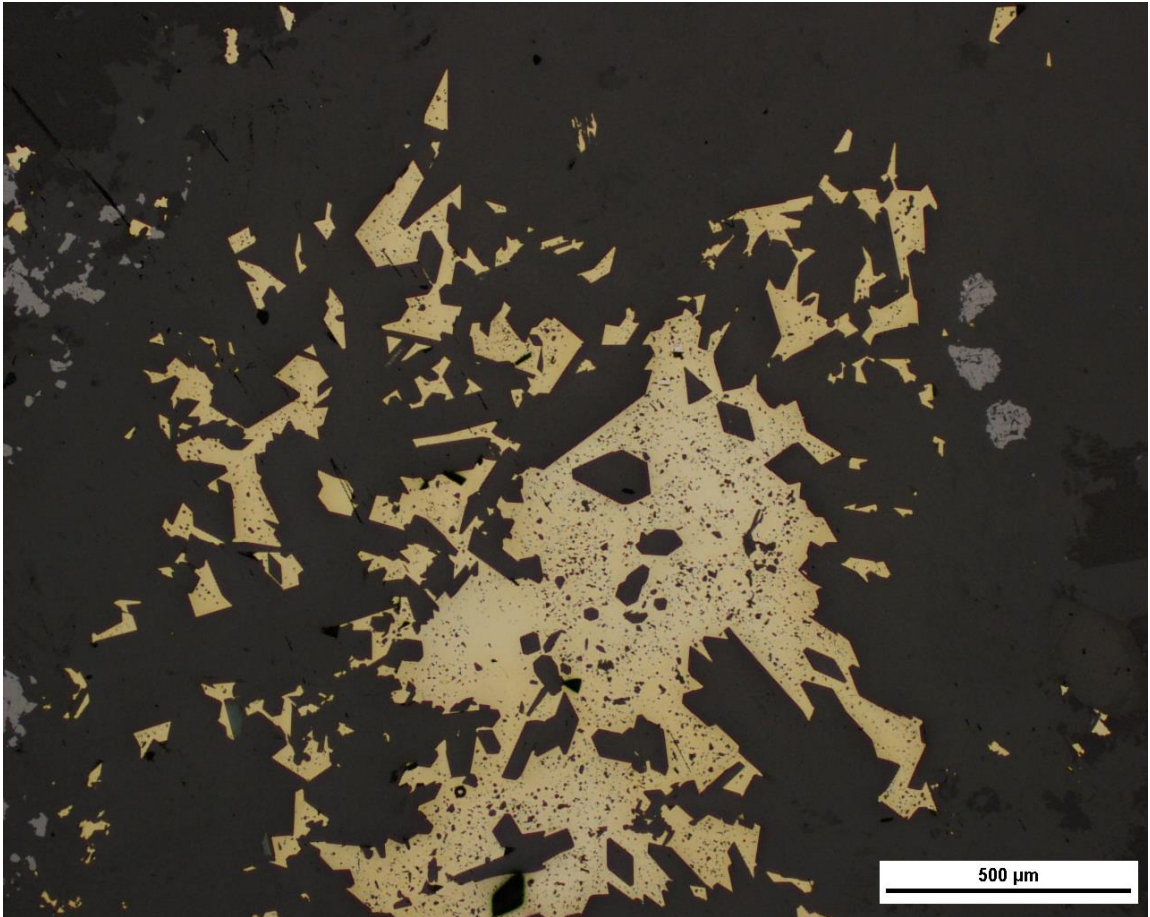
Thin Section Petrography			
Silicates			
Mineral	Modal %	Grainsize	Description
Plagioclase	31	1-3mm	Euhedral to subhedral laths, fresh outside of the albite/actinolite pod. Rims are strongly albite altered on the left side of the thin section
Albite	36	1-4mm	The entire left side of the thin section is strongly albitized. Dirty-brown, sandy textured
Biotite	3	<1mm	Alters the rims of magnetite grains
Actinolite	5	<1mm	Strongly alters Cpx in the regions of strong albitization, pseudomorphic after Cpx. Also intergrown with chalcopyrite, and engulfed by albite alteration
Magnetite	6	<1-2mm	Irregular shaped, most are skeletal textured. Euhedral to subhedral
Clinopyroxene	16	1-3mm	Fresh outside of the albitized regions of the thin section, low relief and forms ophitic texture with plag
Apatite	2	<1mm	Disseminated within albite alteration
Olivine	Tr	1mm	Rare, but has high relief and magnetite infilled fractures
Serpentine	Tr	<1mm	Weakly alters olivine

Chlorite	1	<1mm	Intergrown with act alteration
Epidote	Tr	<1mm	Intergrown with chl/act, pistachio green in PPL
Sulfides			
Mineral	Modal %	Dominant Grainsize	Description
Chalcopyrite	Tr	<1mm	Intergrown with actinolite, and enveloped by albite alteration. Occurs as fine grained blebs to disseminated

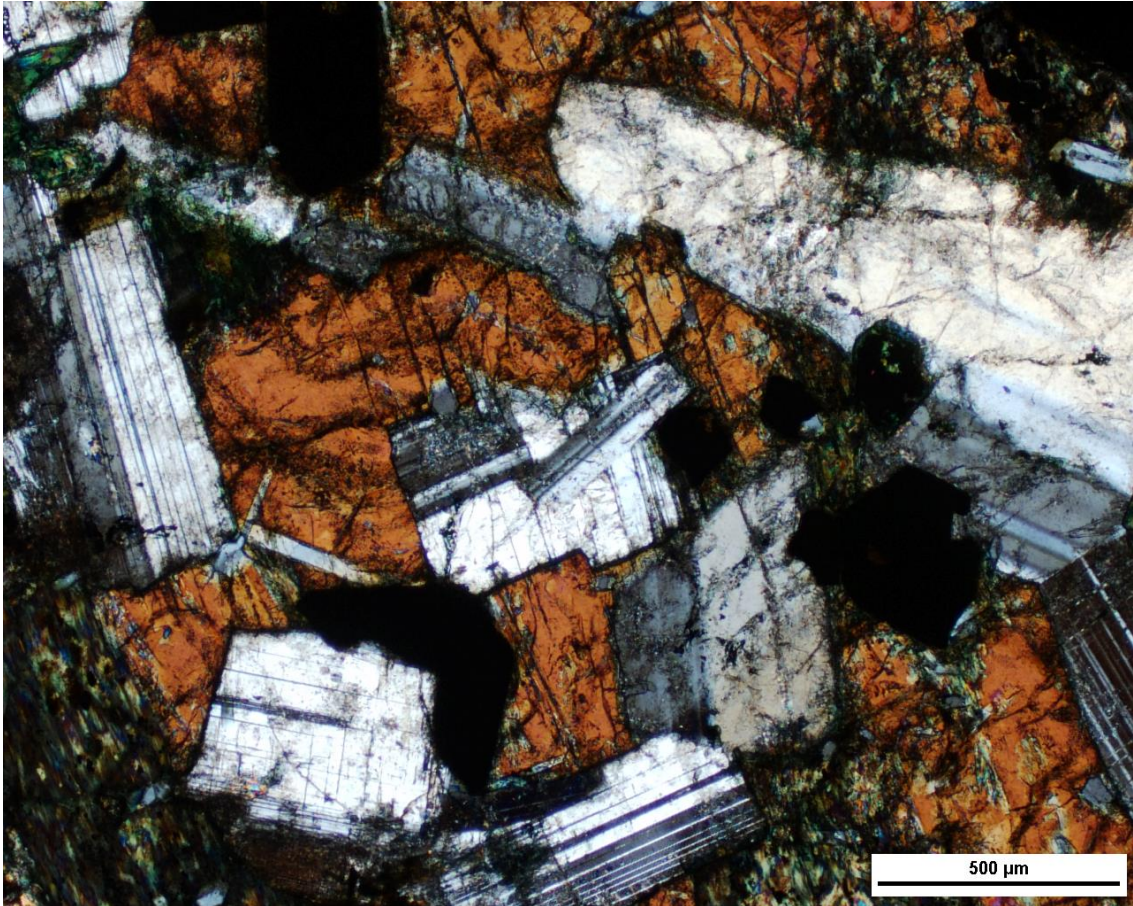
Photomicrographs



An opaque mineral is intergrown with radial actinolite laths. Albite alteration is visible in the top left of the section. In PPL.



The same image as above, but in reflected light. The opaque mineral is chalcopyrite.



A generally unaltered texture from the left side of the thin section. Opaques are magnetite. Plagioclase and clinopyroxene form an ophitic texture. In XPL.

Northing: 5407551			Easting: 537795
Sample name	Location	Depth	Lithology
AB-5-7	Albite Pod	Surface sample	Heterogeneous gabbro

Hand Sample	Thin section
-------------	--------------



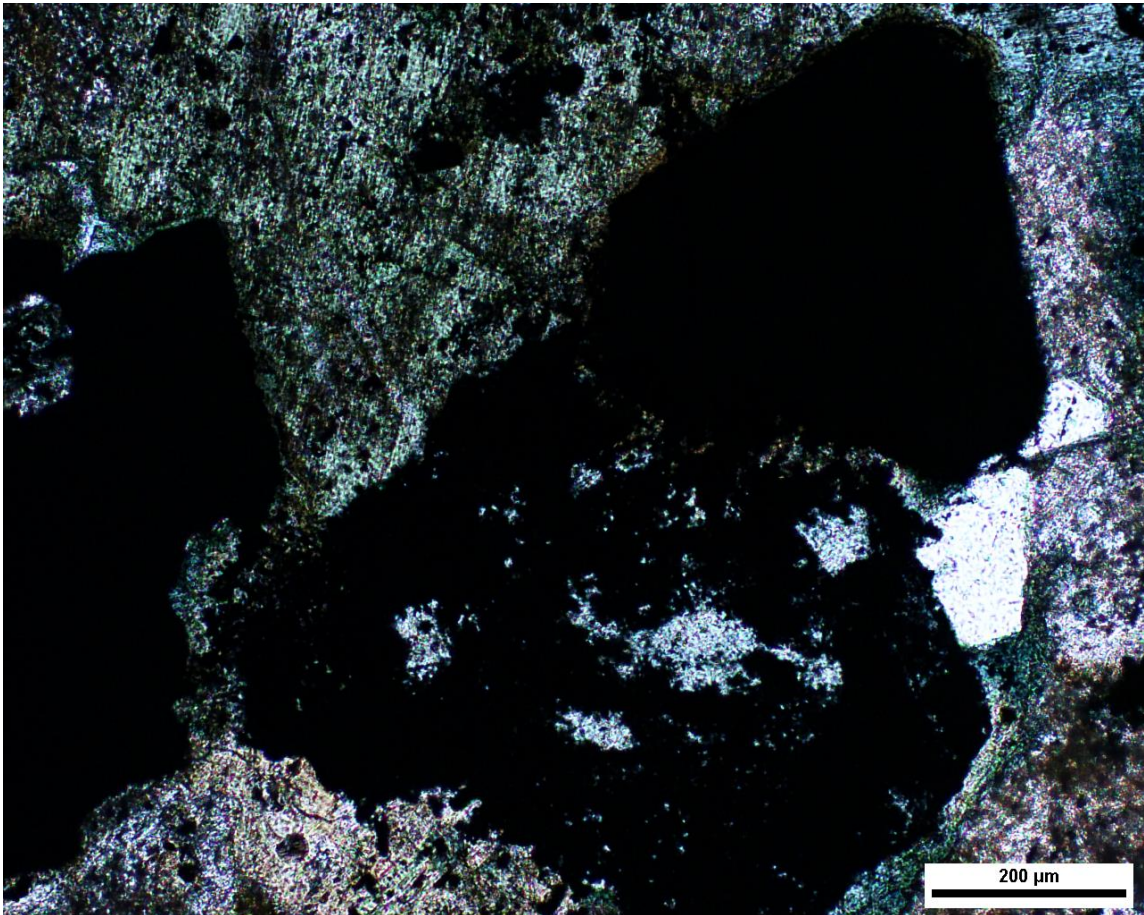
There is some very fine disseminated chalcopyrite visible. Blue-grey plagioclase laths comprise most of the sample with interstitial black clinopyroxene or magnetite. Apatite is also common, resulting in a fairly sugary texture.

Geochemistry of Sample														
SiO ₂	Al ₂ O ₃	FeO	Fe ₂ O ₃	CaO	MgO	Na ₂ O	K ₂ O	TiO ₂	MnO	P ₂ O ₅	L.O.I.	S	Cu	Pd
51.3	12.75	10.85	19.2	4.62	2.81	6.12	0.44	1.36	0.27	0.63	0.82	0.64	9750	1.255

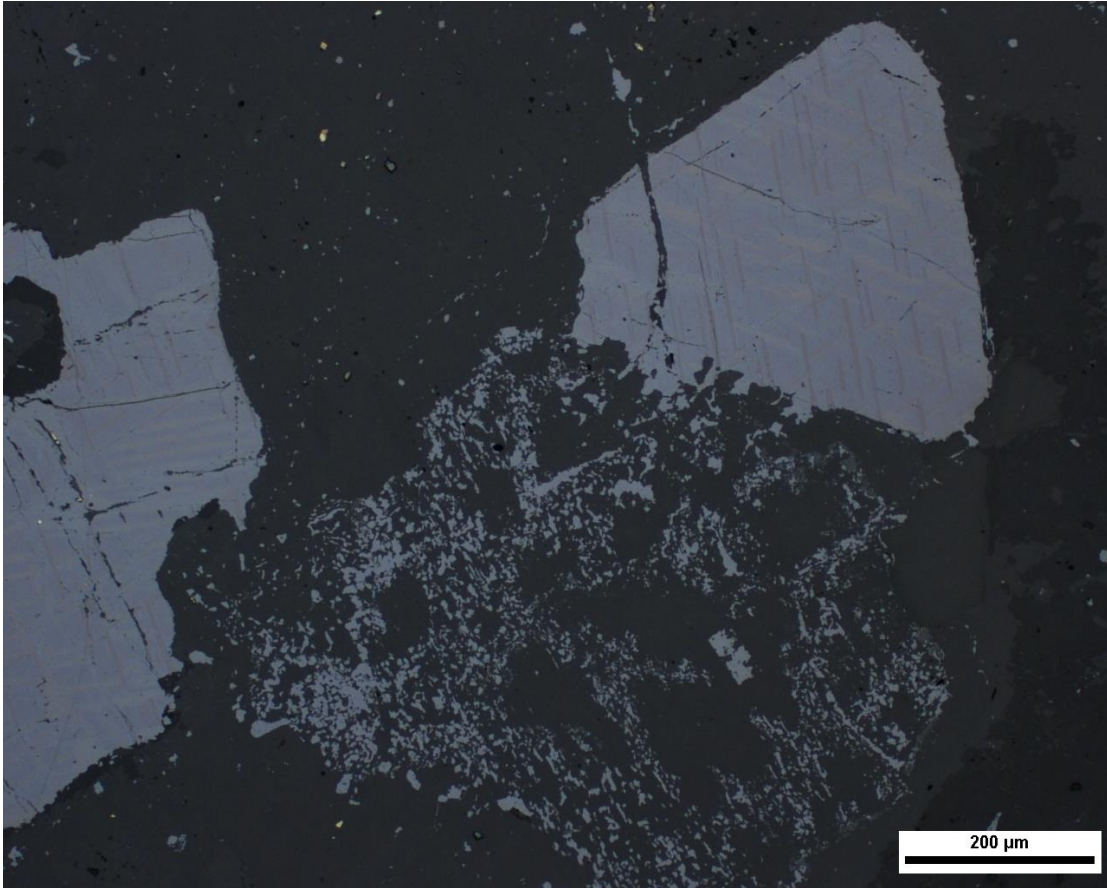
Thin Section Petrography			
Silicates			
Mineral	Modal %	Grainsize	Description
Plagioclase	24	1-5mm	Cores of plagioclase laths are preserved in some sections, however some regions are completely albitized
Albite	35	1-7mm	Dirty-brown textured and in some zones, completely overprints plagioclase, and fully envelops altered Cpx grains as well as magnetite and Ccp + bn
Biotite	2	<1mm	Rims magnetite grains (foxy brown coloured), green biotite is rarely observed near actinolite alteration
Actinolite	2	1-2mm	Pseudomorphic alteration of Cpx, however albite alteration overprints a lot of secondary alteration minerals
Magnetite	5	<1-3mm	Irregular shaped, equant grains that are generally euhedral
Olivine	11	1-3mm	Grains are stubby, and subhedral. Fractures are infilled by magnetite
Clinopyroxene	4	1-2mm	Not common. A few fresh grains are observed, but generally most primary mineralogy has been overprinted by albite alteration
Apatite	2	<1mm	Very common in regions of strong albitization.

Serpentine	3	<1mm	Olivine grains are lightly serpentinized. Pseudomorphic even.
Chlorite	2	<1mm	Less commonly associated with serpentine alteration
Sulfides			
Mineral	Modal %	Dominant Grainsize	Description
Chalcopyrite	2	1-3mm	Interstitial to albitized plagioclase. Associated with fine grained actinolite
Bornite	<1	<1mm	Associated with Ccp blebs as exsolution lamellae
Covellite	Tr	<1mm	Commonly found at the fracture planes of Ccp and bn
Digenite	Tr	<1mm	Commonly found at the fracture planes of Ccp and bn, associated with covellite
Galena	Tr	<1mm	Less commonly found within Ccp and bn exsolution
Pentlandite	Tr	<1mm	Less commonly found at margins of Ccp and secondary alteration

Photomicrographs



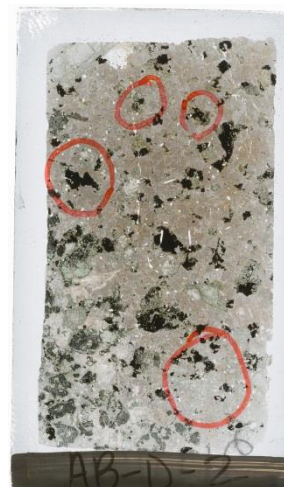
Magnetite grain is being destroyed by surrounding albite alteration. Image is in PPL.



The same image as above, but shown in reflected light. The magnetite grain appears to be destroyed by secondary alteration.

Northing: 5407551			Easting: 537795
Sample name	Location	Depth	Lithology
AB-D-2	Albite Pod	Surface sample	Heterogeneous gabbro

Hand Sample	Thin section
-------------	--------------

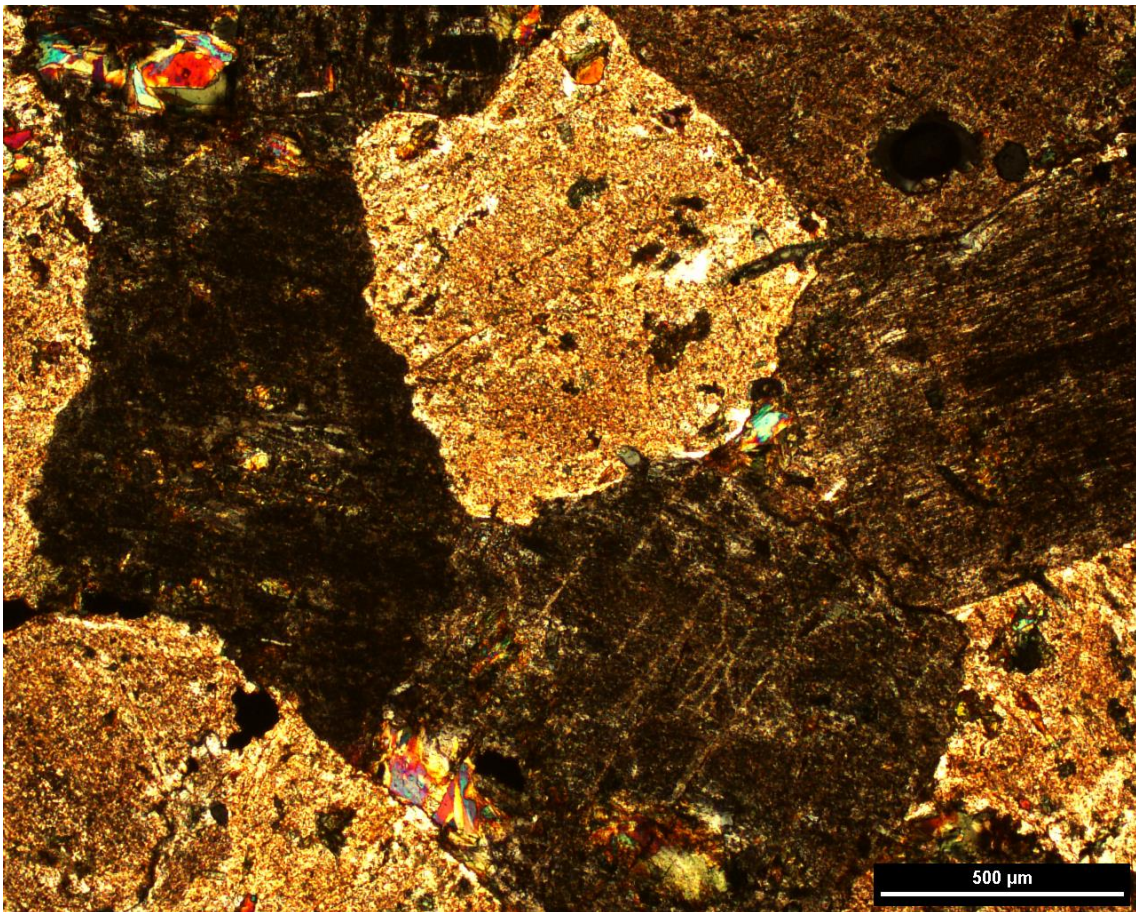


Geochemistry of Sample														
SiO ₂	Al ₂ O ₃	FeO	Fe ₂ O ₃	CaO	MgO	Na ₂ O	K ₂ O	TiO ₂	MnO	P ₂ O ₅	L.O.I.	S	Cu	Pd
48.6	12.55	11.85	19.35	6.47	4.45	4.72	0.51	0.93	0.31	0.58	0.39	0.54	11600	2.66

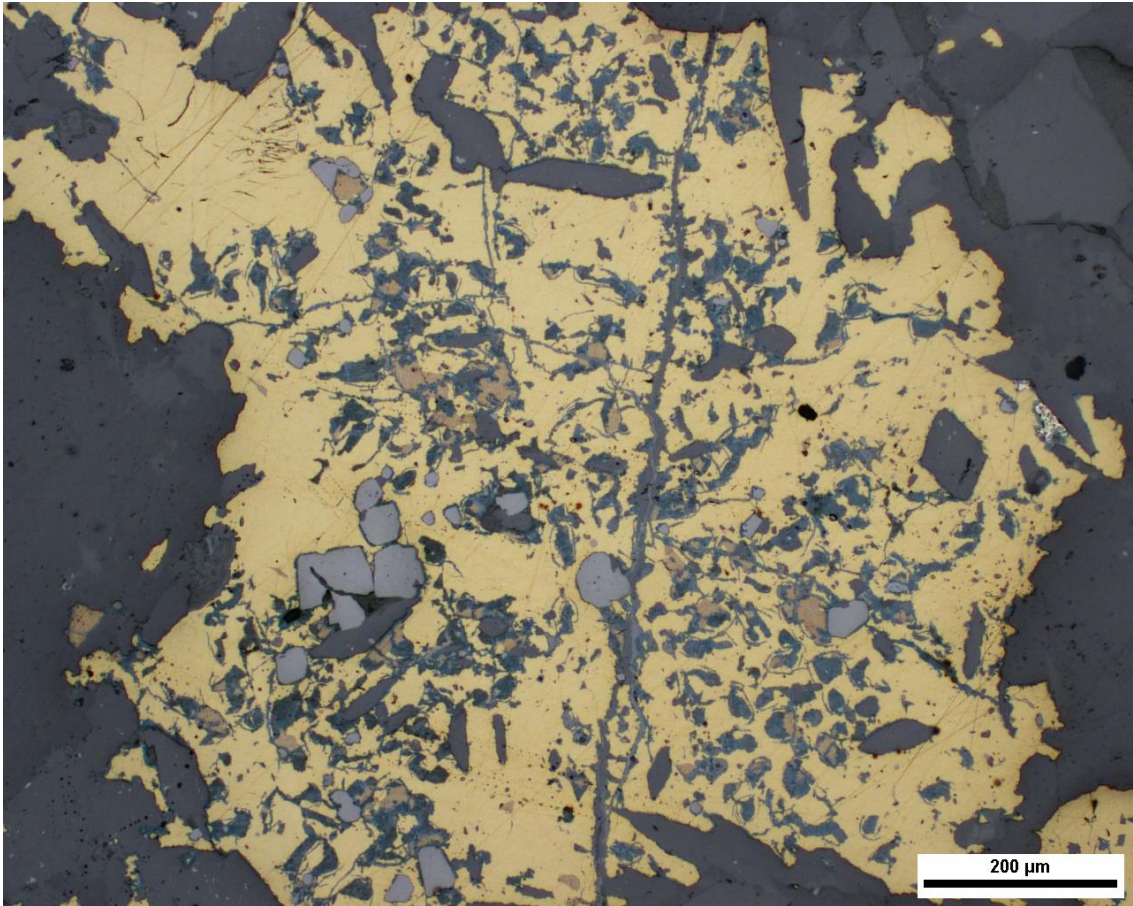
Thin Section Petrography			
Silicates			
Mineral	Modal %	Grainsize	Description
Plagioclase	3	1-5mm	Plagioclase is entirely albitized in this thin section. Relict plagioclase grains are rare to see relative to all other thin sections
Albite	63	1-7mm	Dirty-brown textured and in some zones, completely overprints plagioclase, and fully envelops altered Cpx grains as well as magnetite and Ccp + bn
Biotite	2	<1mm	Rims magnetite grains (foxy brown coloured), green biotite is rarely observed near actinolite alteration
Actinolite	2	1-2mm	Pseudomorphic alteration of Cpx, however albite alteration overprints a lot of secondary alteration minerals
Magnetite	3	<1-3mm	Irregular shaped, equant grains that are generally euhedral
Olivine	12	1-3mm	Grains are stubby, and subhedral. Fractures are infilled by magnetite
Clinopyroxene	4	1-2mm	Not common. A few fresh grains are observed, but generally most primary mineralogy has been overprinted by albite alteration
Apatite	3	<1mm	Very common in regions of strong albitization.
Serpentine	3	<1mm	Olivine grains are lightly serpentinized.
Chlorite	2	<1mm	Less commonly associated with serpentine alteration

Sulfides			
Mineral	Modal %	Dominant Grainsize	Description
Chalcopyrite	2	1-3mm	Interstitial to albitized plagioclase. Associated with fine grained actinolite
Bornite	<1	<1mm	Associated with Ccp blebs as exsolution lamellae
Covellite	Tr	<1mm	Commonly found at the fracture planes of Ccp and bn
Digenite	Tr	<1mm	Commonly found at the fracture planes of Ccp and bn, associated with covellite
Galena	Tr	<1mm	Less commonly found within Ccp and bn exsolution
Pentlandite	Tr	<1mm	Less commonly found at margins of Ccp and secondary alteration

Photomicrographs



A texture typical of this thin section; strong albitization overprints almost all primary mineralogy. The albite grains form 120 degree grain boundaries. In XPL.



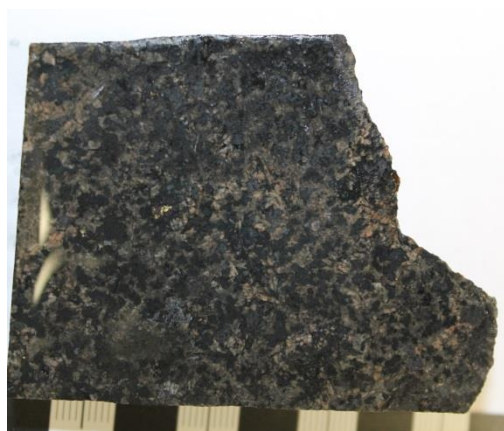
A typical sulfide texture in the Discovery Outcrop albite pod; major sulfides include chalcopyrite (in yellow), as well as bornite (purple-brown) and covellite (blue). In reflected light.



A close up of the image above, showing bornite (brownish-purple) within a chalcopyrite grain. The fractures of the chalcopyrite grain contain covellite (blue). In reflected light. The white coloured grains are pentlandite (grey-white), and galena (bright white).

Northing: 5407551			Easting: 537795
Sample name	Location	Depth	Lithology
AB-D-3	Albite Pod	Surface sample	Heterogeneous gabbro

Hand Sample	Thin section
-------------	--------------



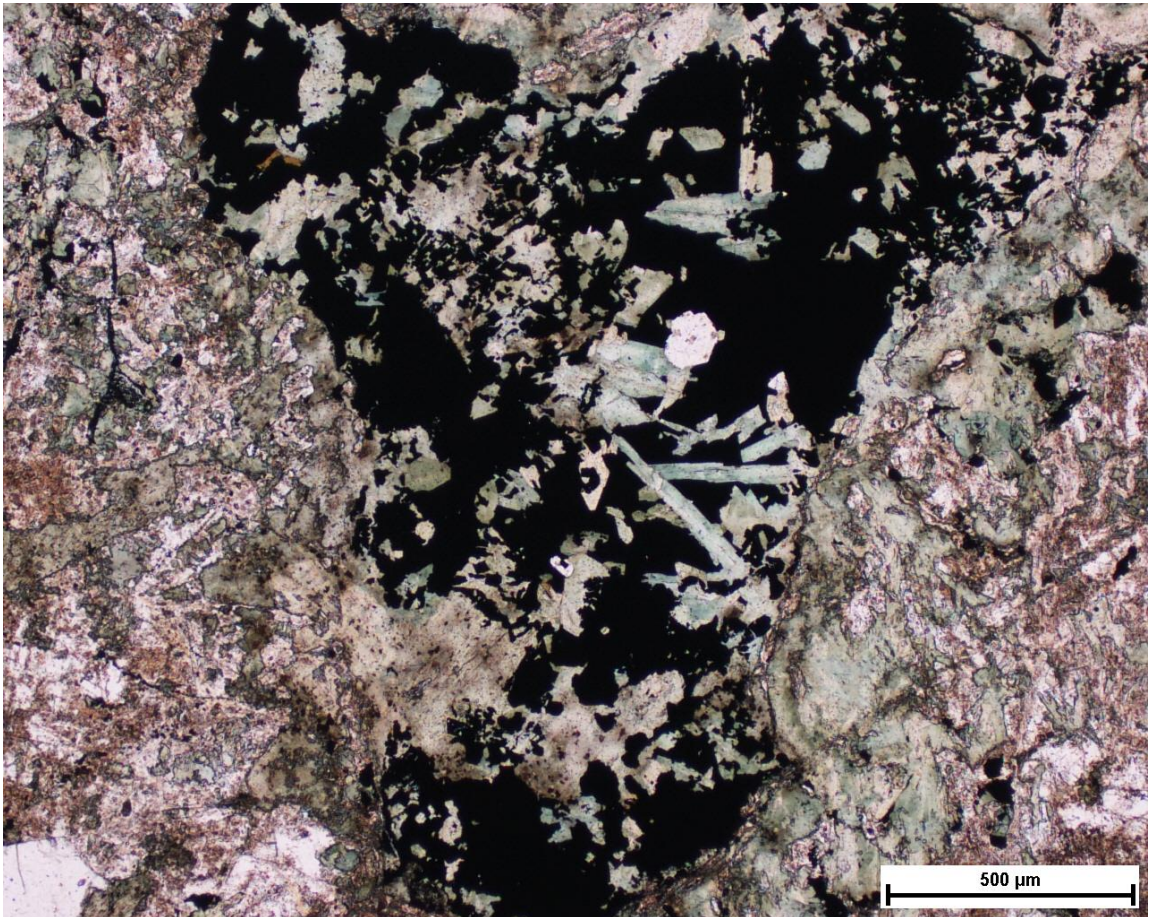
Sample is abundant in dark, almost black olivine grains (~40%) that appear inter-grown. Plagioclase laths are not clearly visible; most feldspar occurs as disseminated pink albite. Chalcopyrite is also disseminated, but occurs in close spatial association with actinolite alteration.

Geochemistry of Sample														
SiO ₂	Al ₂ O ₃	FeO	Fe ₂ O ₃	CaO	MgO	Na ₂ O	K ₂ O	TiO ₂	MnO	P ₂ O ₅	L.O.I.	S	Cu	Pd
49	13.55	11.2	18.25	6.45	4.51	4.84	0.51	0.94	0.3	0.51	0.44	0.54	11550	1.2

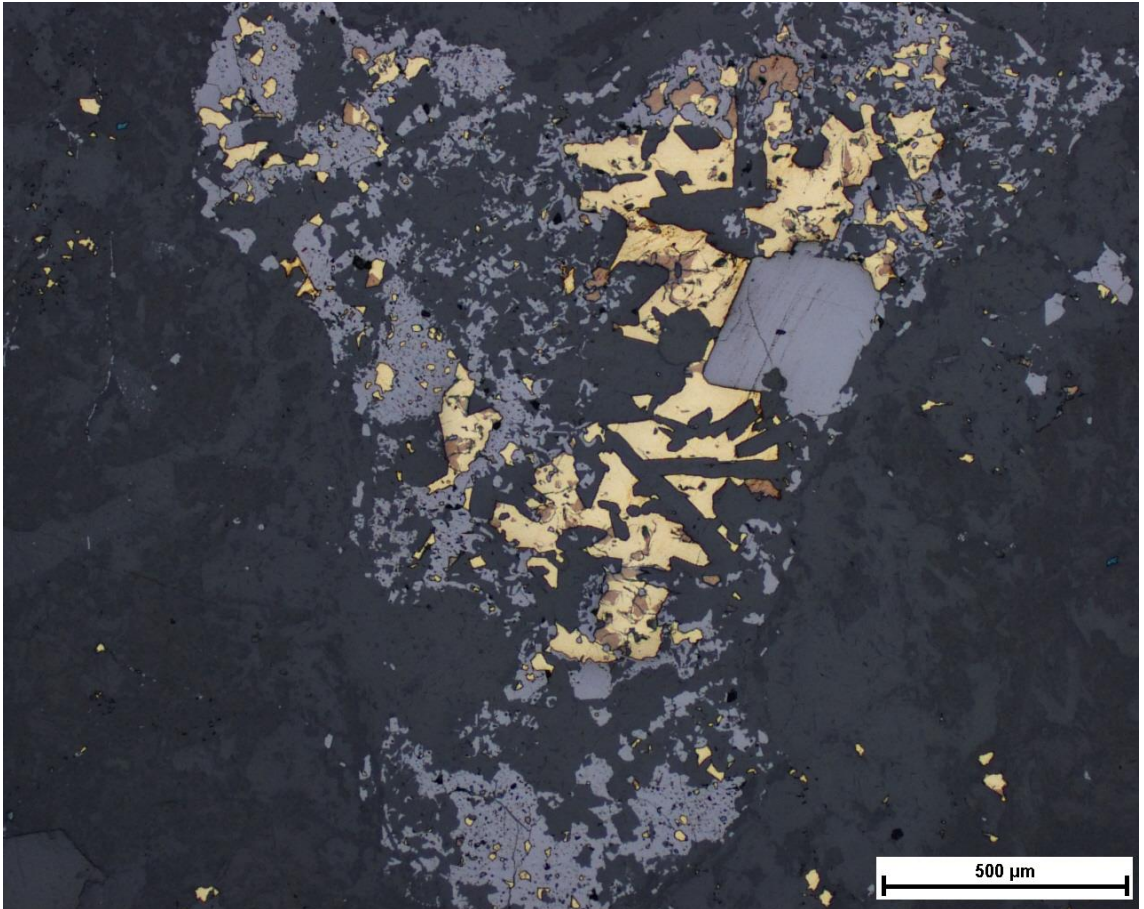
Thin Section Petrography			
Silicates			
Mineral	Modal %	Grainsize	Description
Plagioclase	8	1-3mm	Mainly albitized, though some relatively fresh grains are observed.
Albite	57	1-5mm	Dirty-brown textured and in some zones, completely overprints plagioclase, and fully envelops altered Cpx grains as well as magnetite
Biotite	2	<1mm	Rims magnetite grains (foxy brown coloured), green biotite is observed near actinolite alteration though not commonly
Actinolite	1	1-2mm	Pseudomorphic alteration of Cpx, however albite alteration overprints a lot of secondary alteration minerals
Magnetite	2	1mm	Euhedral to subhedral, generally disseminated throughout sample
Olivine	26	1-4mm	Most grains are skeletal textured, while some are stubby and irregularly shaped. Fractures are infilled by magnetite
Clinopyroxene	4	1mm	Not common. A few scarce fresh grains are observed, but generally most primary mineralogy has been overprinted by albite alteration
Apatite	3	<1mm	Common in regions of strong albitization.

Serpentine	3	<1mm	Olivine grains are lightly serpentinized.
Chlorite	2	<1mm	Less commonly associated with serpentine alteration
Sulfides			
Mineral	Modal %	Dominant Grainsize	Description
Chalcopyrite	2	1-3mm	Interstitial to albitized plagioclase. Associated with fine grained actinolite
Bornite	<1	<1mm	Associated with Ccp blebs as exsolution lamellae
Covellite	Tr	<1mm	Commonly found at the fracture planes of Ccp and bn
Chalcocite	Tr	<1mm	Commonly found at the fracture planes of Ccp and bn, associated with covellite
Galena	Tr	<1mm	Less commonly found within Ccp and bn exsolution
Pentlandite	Tr	<1mm	Less commonly found at margins of Ccp and secondary alteration

Photomicrographs



An opaque grain is surrounded by albite alteration. Actinolite laths are strongly associated with the opaque grain. In XPL.



Same image as above but in reflected light. The opaque mineral is predominantly magnetite (grey), with chalcopyrite (yellow) and bornite (purple-brown). Chalcopyrite is also disseminated within magnetite grain.

Northing: 5407551			Easting: 537795
Sample name	Location	Depth	Lithology
AB-D-4	Albite Pod	Surface sample	Heterogeneous gabbro

Hand Sample	Thin section
-------------	--------------

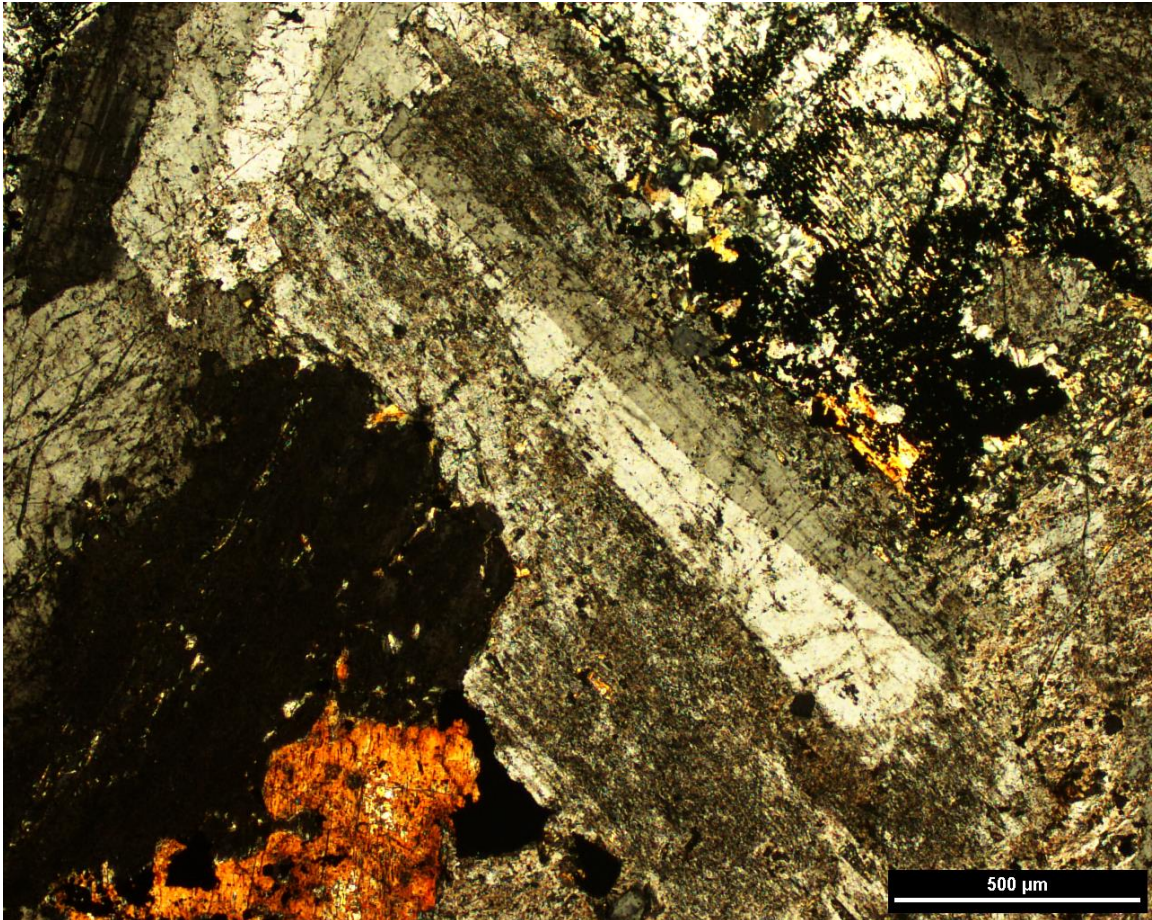


Geochemistry of Sample														
SiO ₂	Al ₂ O ₃	FeO	Fe ₂ O ₃	CaO	MgO	Na ₂ O	K ₂ O	TiO ₂	MnO	P ₂ O ₅	L.O.I.	S	Cu	Pd
48.3	13.05	10.95	18.45	6.62	5.11	4.47	0.62	0.94	0.32	0.7	0.55	0.41	9420	1.055

Thin Section Petrography			
Silicates			
Mineral	Modal %	Grainsize	Description
Plagioclase	25	1-3mm	Mainly albitized, though some relatively fresh grains are observed.
Albite	33	1-5mm	Dirty-brown textured and in some zones, completely overprints plagioclase, and fully envelops altered Cpx grains as well as magnetite. Faintly rims some plagioclase grains in the less albitized regions
Biotite	2	<1mm	Rims magnetite grains (foxy brown coloured), green biotite is observed near actinolite alteration though not commonly
Actinolite	2	1-2mm	Pseudomorphic alteration of Cpx, however albite alteration overprints a lot of secondary alteration minerals
Magnetite	3	1mm	Generally skeletal or irregular shaped.
Olivine	18	1-4mm	Most grains are skeletal textured, while some are stubby and irregularly shaped. Fractures are infilled by magnetite
Clinopyroxene	10	1mm	Not common. A few scarce fresh grains are observed, but generally most primary mineralogy has been overprinted by albite alteration
Apatite	1	<1mm	Common in regions of strong albitization.
Serpentine	2	<1mm	Olivine grains are lightly serpentinized.
Chlorite	2	<1mm	Less commonly associated with serpentine alteration
Sulfides			
Mineral	Modal %	Dominant Grainsize	Description

Chalcopyrite	1	1-3mm	Interstitial to albitized plagioclase. Associated with fine grained actinolite
Bornite	<1	<1mm	Associated with Ccp blebs as exsolution lamellae
Covellite	Tr	<1mm	Commonly found at the fracture planes of Ccp and bn
Chalcocite	Tr	<1mm	Commonly found at the fracture planes of Ccp and bn, associated with covellite
Galena	Tr	<1mm	Less commonly found within Ccp and bn exsolution
Pentlandite	Tr	<1mm	Less commonly found at margins of Ccp and secondary alteration

Photomicrographs



An ophitic textured plagioclase and clinopyroxene are overprinted by moderate albite alteration. In XPL.

Northing: 5407551			Easting: 537795
Sample name	Location	Depth	Lithology
AB-D-5	Albite Pod	Surface sample	Heterogeneous gabbro

Hand Sample	Thin section
-------------	--------------



Geochemistry of Sample														
SiO ₂	Al ₂ O ₃	FeO	Fe ₂ O ₃	CaO	MgO	Na ₂ O	K ₂ O	TiO ₂	MnO	P ₂ O ₅	L.O.I.	S	Cu	Pd
44.3	10.4	14.2	23.6	6.7	5.92	3.54	0.65	1.42	0.39	0.96	0.8	0.69	13700	1.96

Thin Section Petrography			
Silicates			
Mineral	Modal %	Grainsize	Description
Plagioclase	23	1-3mm	Mainly albitized, though some relatively fresh grains are observed.
Albite	33	1-5mm	Dirty-brown textured and in some zones, completely overprints plagioclase, and fully envelops altered Cpx grains as well as magnetite. Faintly rims some plagioclase grains in the less albitized regions
Biotite	1	<1mm	Rims magnetite grains (foxy brown coloured), green biotite is observed near actinolite alteration though not commonly
Actinolite	4	1-2mm	Pseudomorphic alteration of Cpx, however albite alteration overprints a lot of secondary alteration minerals
Magnetite	3	1mm	Generally skeletal or irregular shaped.
Olivine	17	1-4mm	Olivine has high optic relief and magnetite altered fractures
Clinopyroxene	16	1mm	Medium relief, and when unaltered, is interstitial to plagioclase.
Apatite	2	<1mm	Common in regions of strong albitization.
Serpentine	Tr	<1mm	Olivine grains are lightly serpentinized.
Chlorite	1	<1mm	Associated with actinolite alteration
Sulfides			
Mineral	Modal %	Dominant Grainsize	Description

Chalcopyrite	1	1-3mm	Interstitial to albitized plagioclase. Associated with fine grained actinolite
Bornite	Tr	<1mm	Associated with Ccp blebs as exsolution lamellae
Covellite	Tr	<1mm	Commonly found at the fracture planes of Ccp and bn
Chalcocite	Tr	<1mm	Commonly found at the fracture planes of Ccp and bn, associated with covellite
Galena	Tr	<1mm	Less commonly found within Ccp and bn exsolution
Pentlandite	Tr	<1mm	Less commonly found at margins of Ccp and secondary alteration

Photomicrographs

Northing: 5407551			Easting: 537795
Sample name	Location	Depth	Lithology
AB-D-6	Albite Pod	Surface sample	Heterogeneous gabbro

Hand Sample	Thin section
-------------	--------------

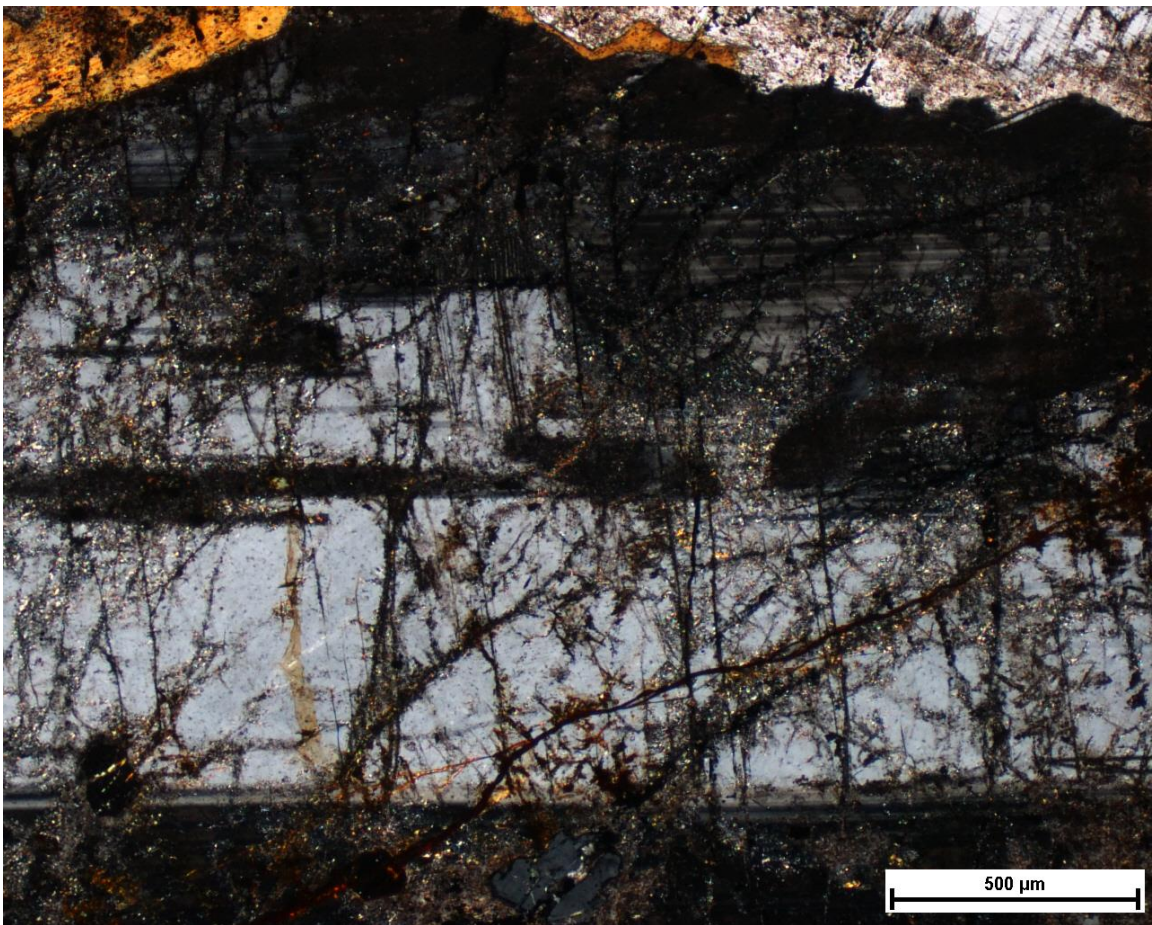


Geochemistry of Sample														
SiO ₂	Al ₂ O ₃	FeO	Fe ₂ O ₃	CaO	MgO	Na ₂ O	K ₂ O	TiO ₂	MnO	P ₂ O ₅	L.O.I.	S	Cu	Pd
46.3	12.7	11.4	21.4	6.97	5.76	3.77	0.8	1.44	0.35	0.86	0.73	0.27	6590	0.906

Thin Section Petrography			
Silicates			
Mineral	Modal %	Grainsize	Description
Plagioclase	29	1-5mm	Mainly fresh, especially at the bottom half of the section. Plagioclase grains are relatively albitized in the upper half of the section. Fracture planes are reddish-brown, and albitized
Albite	16	1-2mm	Dirty-brown textured and in some zones, completely overprints plagioclase, and fully envelops altered Cpx grains as well as magnetite. Faintly rims some plagioclase grains in the less albitized regions
Biotite	1	<1mm	Rims magnetite grains (foxy brown coloured), green biotite is observed near actinolite alteration though not commonly
Actinolite	4	<1-2mm	Pseudomorphic alteration of Cpx, however albite alteration overprints a lot of secondary alteration minerals
Magnetite	3	1mm	Generally skeletal or irregular shaped, subhedral to euhedral
Olivine	21	1-4mm	Olivine has high optic relief and magnetite altered fractures, dark grey coloured
Clinopyroxene	23	1mm	Medium relief, and when unaltered, is interstitial to plagioclase, shows good cleavage
Apatite	1	<1mm	Common in regions of strong albitization.
Serpentine	Tr	<1mm	Olivine grains are lightly serpentinized.

Chlorite	1	<1mm	Associated with actinolite alteration
Sulfides			
Mineral	Modal %	Dominant Grainsize	Description
Chalcopyrite	1	1-2mm	Interstitial to albitized plagioclase. Associated with fine grained actinolite
Bornite	Tr	<1mm	Associated with Ccp blebs as exsolution lamellae
Covellite	Tr	<1mm	Commonly found at the fracture planes of Ccp and bn
Chalcocite	Tr	<1mm	Commonly found at the fracture planes of Ccp and bn, associated with covellite
Galena	Tr	<1mm	Less commonly found within Ccp and bn exsolution
Pentlandite	Tr	<1mm	Less commonly found at margins of Ccp and secondary alteration

Photomicrographs



A plagioclase grain in XPL. Fractures within plagioclase are altered to a reddish-brown, and portions adjacent to this reddish-brown alteration are albite altered.

Northing: 5407551		Easting: 537795	
Sample name	Location	Depth	Lithology
AB-D-7	Albite Pod	Surface sample	Heterogeneous gabbro

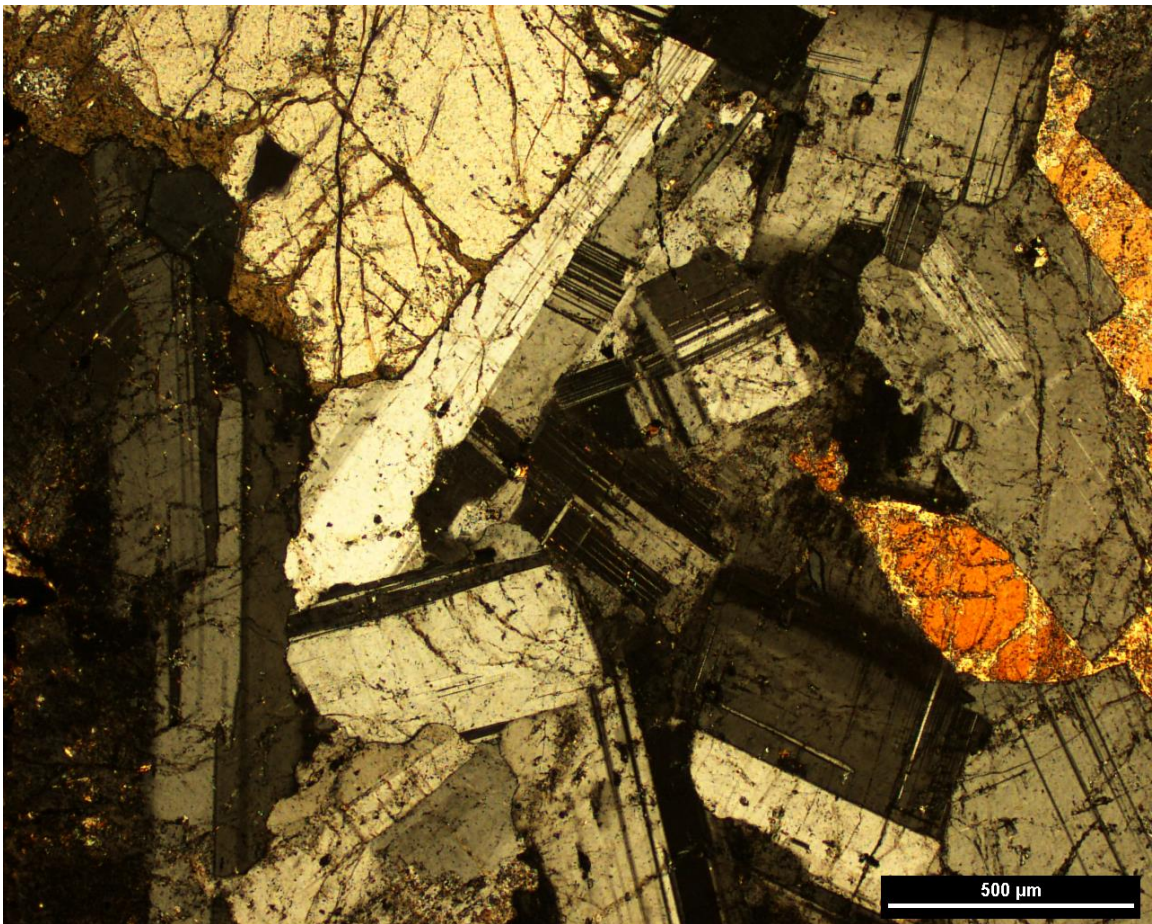
Hand Sample	Thin section
-------------	--------------



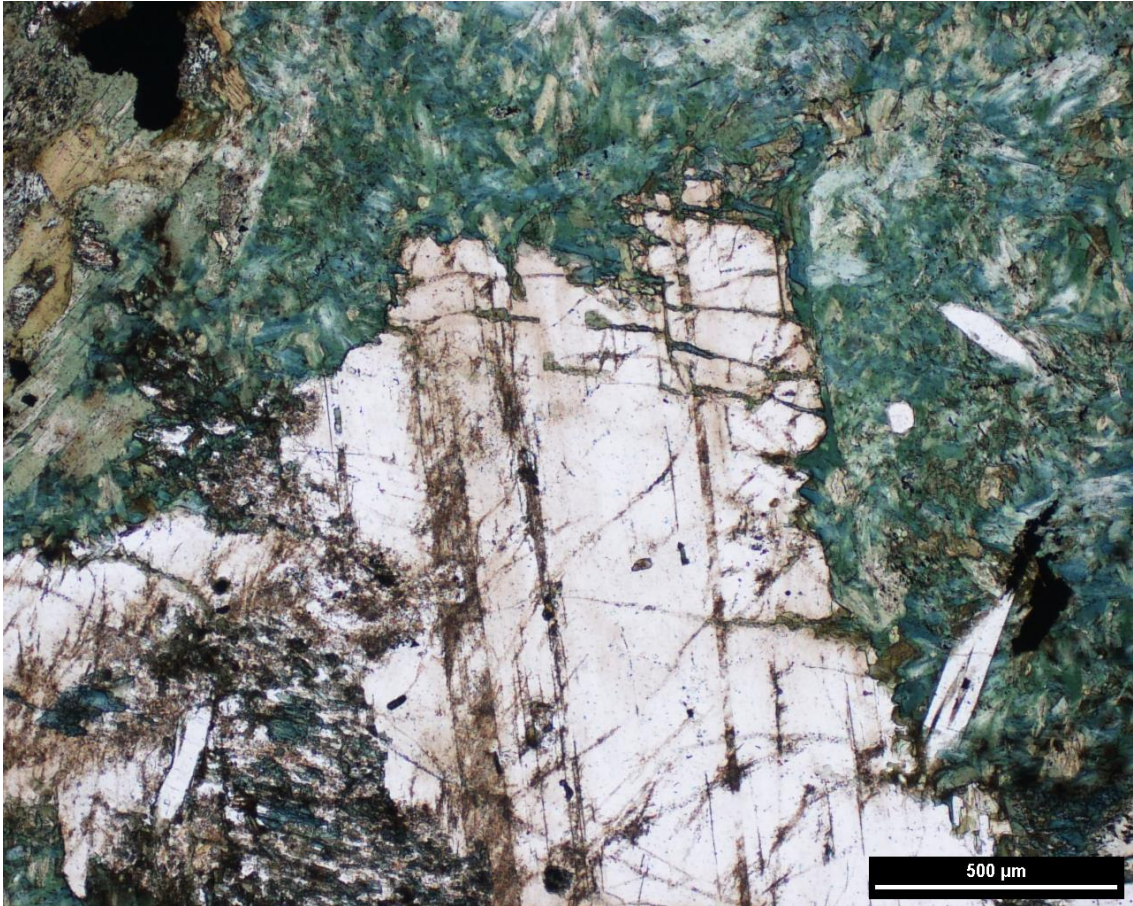
Geochemistry of Sample														
SiO ₂	Al ₂ O ₃	FeO	Fe ₂ O ₃	CaO	MgO	Na ₂ O	K ₂ O	TiO ₂	MnO	P ₂ O ₅	L.O.I.	S	Cu	Pd
45.8	13.35	10.25	19.3	9.18	5.1	3.71	0.71	2.18	0.32	1.3	0.35	0.13	3580	0.494

Thin Section Petrography			
Silicates			
Mineral	Modal %	Grainsize	Description
Plagioclase	36	1-5mm	Plagioclase grains are overwhelmingly fresh in this section. Form an ophitic texture with Cpx
Albite	3	1-2mm	Very weak albite mantling of plagioclase laths is present in some portions of the section
Biotite	2	<1mm	Rims magnetite grains (foxy brown coloured), greenish-brown biotite is observed near actinolite
Actinolite	3	<1-2mm	Pseudomorphic alteration of Cpx, however albite alteration overprints a lot of secondary alteration minerals. Forms acicular blades
Magnetite	9	1mm	Generally skeletal or irregular shaped, subhedral to euhedral
Olivine	21	1-4mm	Olivine has high optic relief and magnetite altered fractures, dark grey coloured and very stubby.
Clinopyroxene	23	1mm	Medium to low relief, and when unaltered, is interstitial to plagioclase, shows good cleavage
Apatite	<1	<1mm	Common in regions of strong albitization
Serpentine	1	<1mm	Olivine grains are lightly serpentinized at fracture planes and at rims, especially in contact with Cpx
Chlorite	1	<1mm	Associated with actinolite alteration

Sulfides			
Mineral	Modal %	Dominant Grainsize	Description
Chalcopyrite	1	1-2mm	Interstitial to albitized plagioclase. Associated with fine grained actinolite
Bornite	Tr	<1mm	Associated with Ccp blebs as exsolution lamellae
Covellite	Tr	<1mm	Commonly found at the fracture planes of Ccp and bn
Chalcocite	Tr	<1mm	Commonly found at the fracture planes of Ccp and bn, associated with covellite
Galena	Tr	<1mm	Less commonly found within Ccp and bn exsolution
Pentlandite	Tr	<1mm	Less commonly found at margins of Ccp and secondary alteration



A very common texture in this section, fresh plagioclase and Cpx are intergrown forming an ophitic texture. In XPL.



Less commonly, actinolite and biotite are pseudomorphic after a Cpx grain (middle white grain). In PPL.

Northing: 5407551

Easting: 537795

Sample name	Location	Depth	Lithology
AB-D-8	Albite Pod	Surface sample	Heterogeneous gabbro

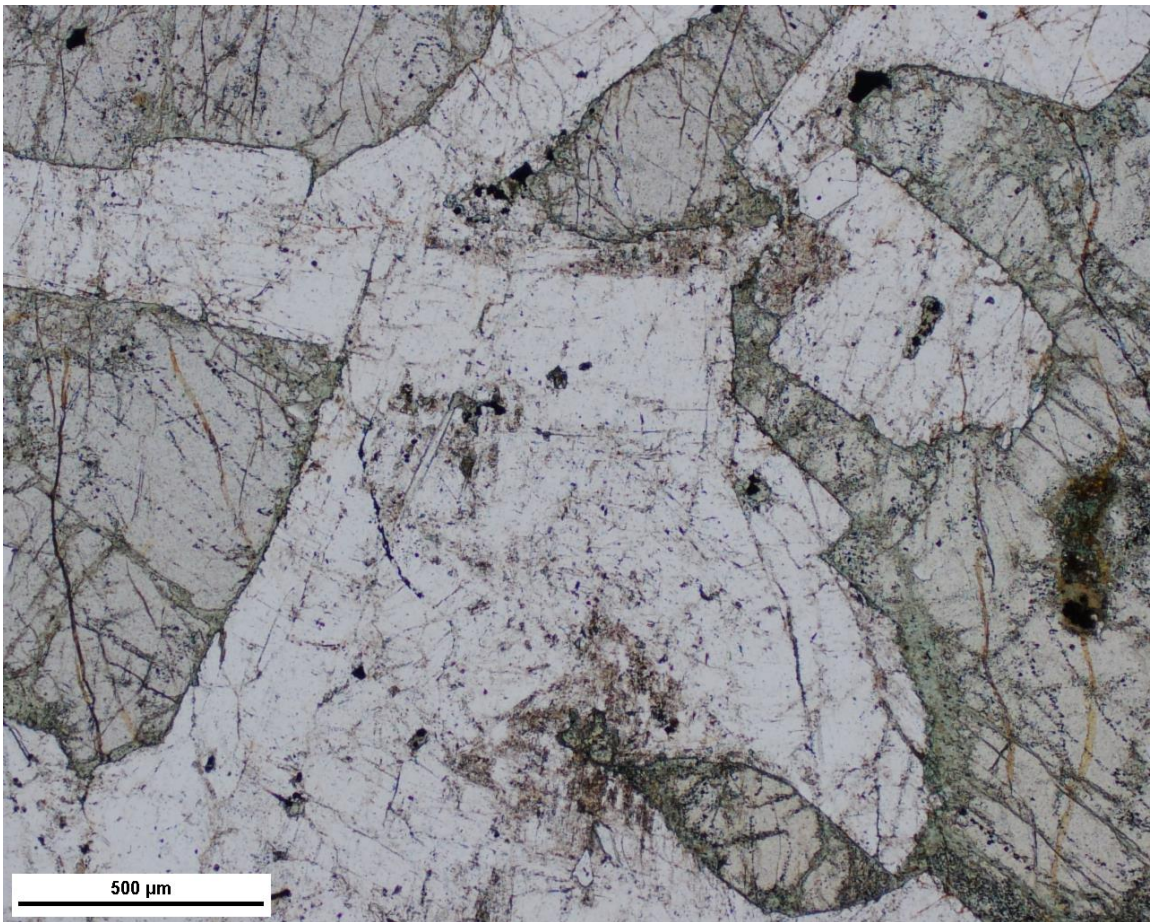
Hand Sample	Thin section
-------------	--------------



Geochemistry of Sample														
SiO ₂	Al ₂ O ₃	FeO	Fe ₂ O ₃	CaO	MgO	Na ₂ O	K ₂ O	TiO ₂	MnO	P ₂ O ₅	L.O.I.	S	Cu	Pd
45.4	13.2	10.25	19.3	8.72	5.35	3.62	0.82	1.91	0.32	1.23	0.53	0.12	3580	0.506

Thin Section Petrography			
Silicates			
Mineral	Modal %	Grainsize	Description
Plagioclase	35	1-5mm	Plagioclase grains are mostly fresh in this section. Form an ophitic texture with Cpx
Albite	18	1-2mm	Very weak to intense albite mantling of plagioclase laths is present in some portions of the section
Biotite	2	<1mm	Rims magnetite grains (foxy brown coloured), greenish-brown biotite is observed near actinolite
Actinolite	3	<1-2mm	Pseudomorphic alteration of Cpx, however albite alteration overprints a lot of secondary alteration minerals. Forms acicular blades
Magnetite	5	1mm	Generally skeletal or irregular shaped, subhedral to euhedral
Olivine	13	1-4mm	Olivine has high optic relief and magnetite altered fractures, dark grey coloured and very stubby.
Clinopyroxene	22	1mm	Medium to low relief, and when unaltered, is interstitial to plagioclase, shows good cleavage
Apatite	<1	<1mm	Common in regions of strong albitization
Serpentine	1	<1mm	Olivine grains are lightly serpentinized at fracture planes and at rims, especially in contact with Cpx
Chlorite	1	<1mm	Associated with actinolite alteration

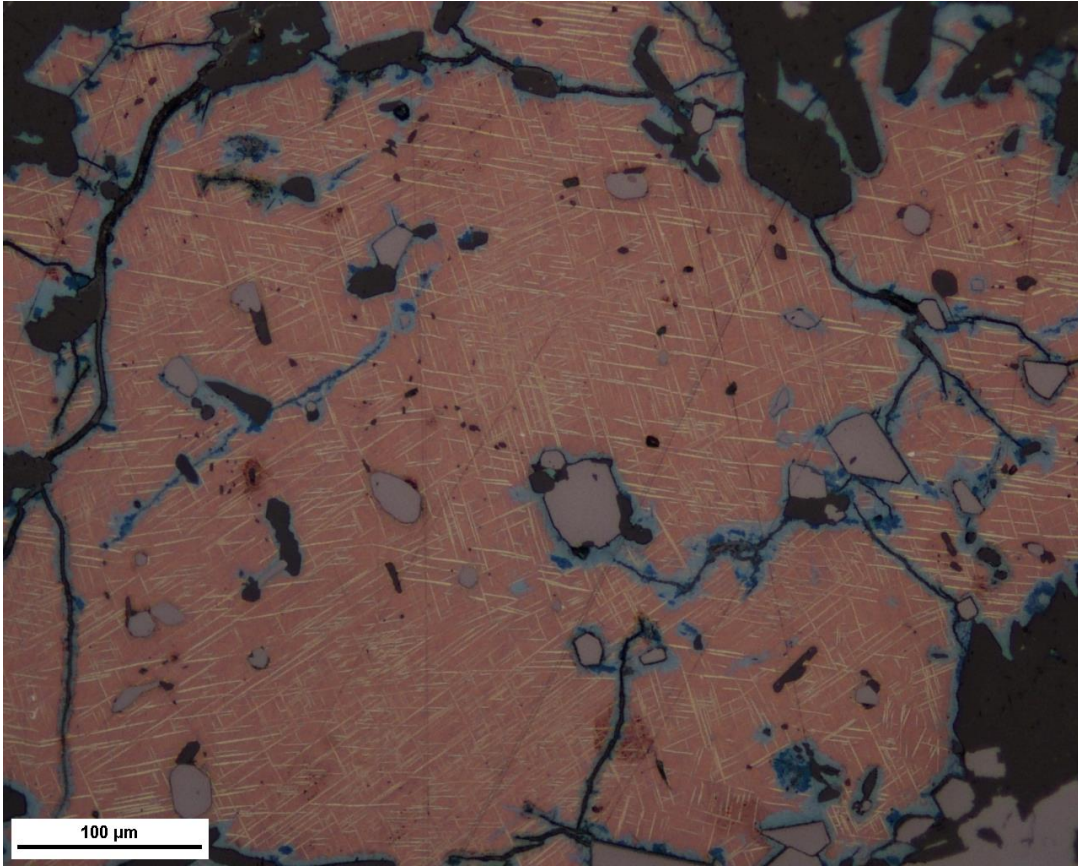
Sulfides			
Mineral	Modal %	Dominant Grainsize	Description
Chalcopyrite	1	1-2mm	Interstitial to albitized plagioclase. Associated with fine grained actinolite
Bornite	Tr	<1mm	Associated with Ccp blebs as exsolution lamellae
Covellite	Tr	<1mm	Commonly found at the fracture planes of Ccp and bn
Chalcocite	Tr	<1mm	Commonly found at the fracture planes of Ccp and bn, associated with covellite
Galena	Tr	<1mm	Less commonly found within Ccp and bn exsolution
Pentlandite	Tr	<1mm	Less commonly found at margins of Ccp and secondary alteration



General, unaltered texture. Large grain to the center of the image is plagioclase. CPX is adjacent, slightly darker. In PPL



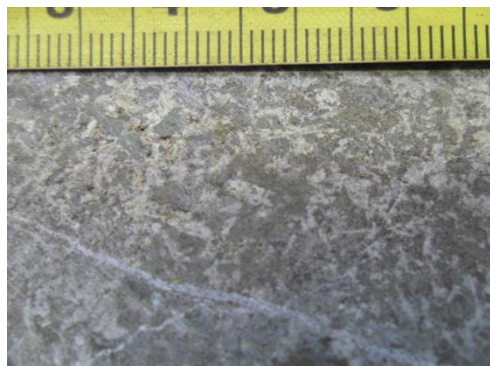
Same image as above, in XPL.



Widmanstätten texture, with exsolution of chalcopyrite within a bornite host grain.

Sample name	Drill-hole	Depth	Lithology
G-10-04-76m-1	G-10-04	76-78m	Heterogeneous gabbro

Hand Sample	Thin section
-------------	--------------



Consists primarily of euhedral plagioclase with interstitial clinopyroxene. Section is x-cut by a carbonate fracture.

Geochemistry of Sample														
SiO ₂	Al ₂ O ₃	FeO	Fe ₂ O ₃	CaO	MgO	Na ₂ O	K ₂ O	TiO ₂	MnO	P ₂ O ₅	L.O.I.	S	Cu	Pd
46.41	13.92	12.2	17.72	7.76	4.08	3.6	1.95	2.03	0.28	1.028	0.32	0.05	261	0.029

Thin Section Petrography			
Silicates			
Mineral	Modal %	Grainsize	Description
Plagioclase	20	1-3mm	Laths are strongly altered to albite. Only cores of plag laths are visible
Albite	22	1-4mm	Alters the outer margins of plagioclase and in some instances, completely alters plag
Biotite	9	1-2mm	Rims stubby magnetite grains
Actinolite	12	1-2mm	Alters clinopyroxene
Magnetite	7	<1mm	Euhedral stubby grains are disseminated throughout
Olivine	1	<1mm	Rare but is seen adjacent to a Cpx grain
Chlorite	6	1-4mm	Commonly occurs near actinolite and biotite alteration zones
Clinopyroxene	17	1-3mm	Interstitial to plagioclase
Apatite	4	<1mm	Common in strong zones of albitization
Epidote	2	<1mm	Associated with actinolite and chlorite alteration
Sulfides			
Mineral	Modal %	Dominant Grainsize	Description

Chalcopyrite	<1	<1mm	Occurs near larger magnetite grains that are spatially associated with actinolite
Bornite	tr	<1mm	Rare, occurs in contact with chalcopyrite

Sample name	Drill-hole	Depth	Lithology
G-10-16-118m-1	G-10-16	118-120m	Heterogeneous gabbro

Hand Sample	Thin section
-------------	--------------



Geochemistry of Sample														
SiO ₂	Al ₂ O ₃	FeO	Fe ₂ O ₃	CaO	MgO	Na ₂ O	K ₂ O	TiO ₂	MnO	P ₂ O ₅	L.O.I.	S	Cu	Pd
45.25	13.21	12	19.79	7.81	4.57	3.55	1.7	2.3	0.28	1.083	0.25	0.08	317	0.062

Thin Section Petrography			
Silicates			
Mineral	Modal %	Grainsize	Description
Plagioclase	7	1-3mm	Predominantly altered to albite
Albite	60	3-15mm	Forms a pervasive network of dirty pink alteration
Biotite	1	<1mm	Forms thin mantles around magnetite
Actinolite	13	1-4mm	Alters CPX pervasively
Magnetite	3	<1mm	Forms equant to skeletal grains
Clinopyroxene	7	<1mm	Is almost completely altered to actinolite, only remnants of CPX grains are left
Apatite	2	<1-2mm	Stubby grains to needle-like crystals
Epidote	3	1-2mm	Associated with actinolite alteration
Chlorite	2	1-2mm	Associated with actinolite and epidote alteration
Sulfides			
Mineral	Modal %	Dominant Grainsize	Description
Chalcopyrite	2	1mm	Typically interstitial to albite altered plagioclase, associated with actinolite alteration
Bornite	<1	<1mm	Associated with chalcopyrite

Sample name	Drill-hole	Depth	Lithology
G-10-16-118m-2	G-10-16	118-120m	Heterogeneous gabbro

Hand Sample	Thin section
-------------	--------------



Geochemistry of Sample														
SiO ₂	Al ₂ O ₃	FeO	Fe ₂ O ₃	CaO	MgO	Na ₂ O	K ₂ O	TiO ₂	MnO	P ₂ O ₅	L.O.I.	S	Cu	Pd
45.25	13.21	12	19.79	7.81	4.57	3.55	1.7	2.3	0.28	1.083	0.25	0.08	317	0.062

Thin Section Petrography			
Silicates			
Mineral	Modal %	Grainsize	Description
Plagioclase	11	1-3mm	Predominantly altered to albite
Albite	47	<1-12mm	Forms a pervasive network of dirty pink alteration. Commonly encloses actinolite altered CPX
Biotite	3	<1mm	Forms thin mantles around magnetite. Also is associated with actinolite/epidote/chlorite
Actinolite	17	1-4mm	Alters CPX pervasively
Magnetite	8	<1mm	Forms equant to skeletal grains
Clinopyroxene	6	<1mm	Is almost completely altered to actinolite, only remnants of CPX grains are left
Apatite	4	<1-2mm	Stubby grains to needle-like crystals. Very common within albite alteration
Epidote	2	1-2mm	Associated with actinolite alteration
Chlorite	2	1-2mm	Associated with actinolite and epidote alteration
Sulfides			
Mineral	Modal %	Dominant Grainsize	Description

Chalcopyrite	tr	<1mm	Uncommon in this section; very small specks in association with actinolite alteration and proximal to magnetite
--------------	----	------	---

Sample name	Drill-hole	Depth	Lithology
G-10-16-138m-1	G-10-16	138-140m	Skeletal troctolite

Hand Sample	Thin section
-------------	--------------



Sample contains abundant fine-grained magnetite and sugary-white apatite. Some sections of the sample contain higher proportions of clinopyroxene and plagioclase.

Geochemistry of Sample														
SiO ₂	Al ₂ O ₃	FeO	Fe ₂ O ₃	CaO	MgO	Na ₂ O	K ₂ O	TiO ₂	MnO	P ₂ O ₅	L.O.I.	S	Cu	Pd
-	-	-	-	-	-	-	-	-	-	-	-	0.10	1004	0.361

Thin Section Petrography			
Silicates			
Mineral	Modal %	Grainsize	Description
Plagioclase	19	1-3mm	Generally fresh, no significant albite alteration is present.
Albite	1	<1mm	Rare in this sample, only present in thin mantles near weak actinolite alteration
Biotite	13	<1-2mm	Commonly forms brown mantles around magnetite grains, and are interlocking forming a pervasive network around grains
Actinolite	5	1-2mm	Weakly alters CPX
Magnetite	40	<1-2mm	Forms stubby disseminated grains, are slightly networked. Irregular shaped sometimes
Clinopyroxene	14	<1-2mm	Generally fresh, is anhedral and appears to have formed after magnetite
Apatite	7	1-3mm	Stubby to needle-like grains
Epidote	1	<1mm	Associated with weak actinolite alteration

Sulfides			
Mineral	Modal %	Dominant Grainsize	Description
Chalcopyrite	tr	<1mm	Uncommon in this section; very fine grained where present, associated with biotite and magnetite

Sample name	Drill-hole	Depth	Lithology
--------------------	-------------------	--------------	------------------

G-10-16-138m-2	G-10-16	138-140m	Skeletal troctolite
----------------	---------	----------	---------------------

Hand Sample	Thin section
--------------------	---------------------



Cumulate fine grained magnetite, section is cross-cut by a carbonate-chl vein.

Geochemistry of Sample														
SiO ₂	Al ₂ O ₃	FeO	Fe ₂ O ₃	CaO	MgO	Na ₂ O	K ₂ O	TiO ₂	MnO	P ₂ O ₅	L.O.I.	S	Cu	Pd
-	-	-	-	-	-	-	-	-	-	-	-	0.10	1004	0.361

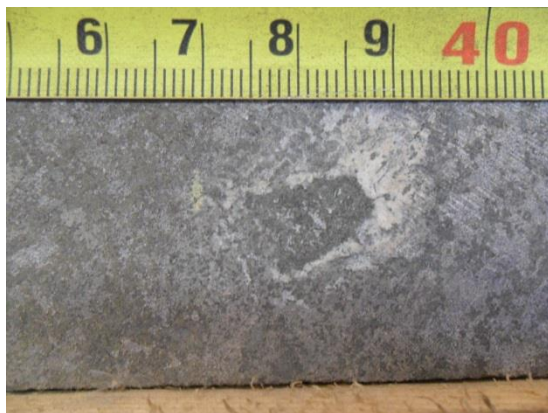
Thin Section Petrography			
Silicates			
Mineral	Modal %	Grainsize	Description
Plagioclase	20	1-3mm	Generally fresh, no significant albite alteration is present.
Albite	4	<1mm	Rare in this sample, only present in thin mantles near weak actinolite alteration
Biotite	6	<1-2mm	Commonly forms brown mantles around magnetite grains, and are interlocking forming a pervasive network around grains
Actinolite	4	1-2mm	Weakly alters CPX
Magnetite	28	<1-2mm	Forms stubby disseminated grains, are slightly networked. Irregular shaped sometimes
Clinopyroxene	18	<1-2mm	Generally fresh, is anhedral and appears to have formed after magnetite
Apatite	6	1-3mm	Stubby to needle-like grains
Epidote	1	<1mm	Associated with weak actinolite alteration
Chlorite	4	1-2mm	Found exclusively within cross-cutting vein
Carbonate	3	1-2mm	Found exclusively within cross-cutting vein
Sericite	5	1-2mm	Alteration of plagioclase along the cross-cutting chl-carb vein
Sulfides			

Mineral	Modal %	Dominant Grainsize	Description
Chalcopyrite	1	<1mm	Very fine grained where present, associated with biotite and magnetite
Bornite	Tr	<1mm	Associated with chalcopyrite

Sample name	Drill-hole	Depth	Lithology
--------------------	-------------------	--------------	------------------

G-10-16-140m-1	G-10-16	140-142m	Skeletal troctolite
----------------	---------	----------	---------------------

Hand Sample	Thin section
--------------------	---------------------



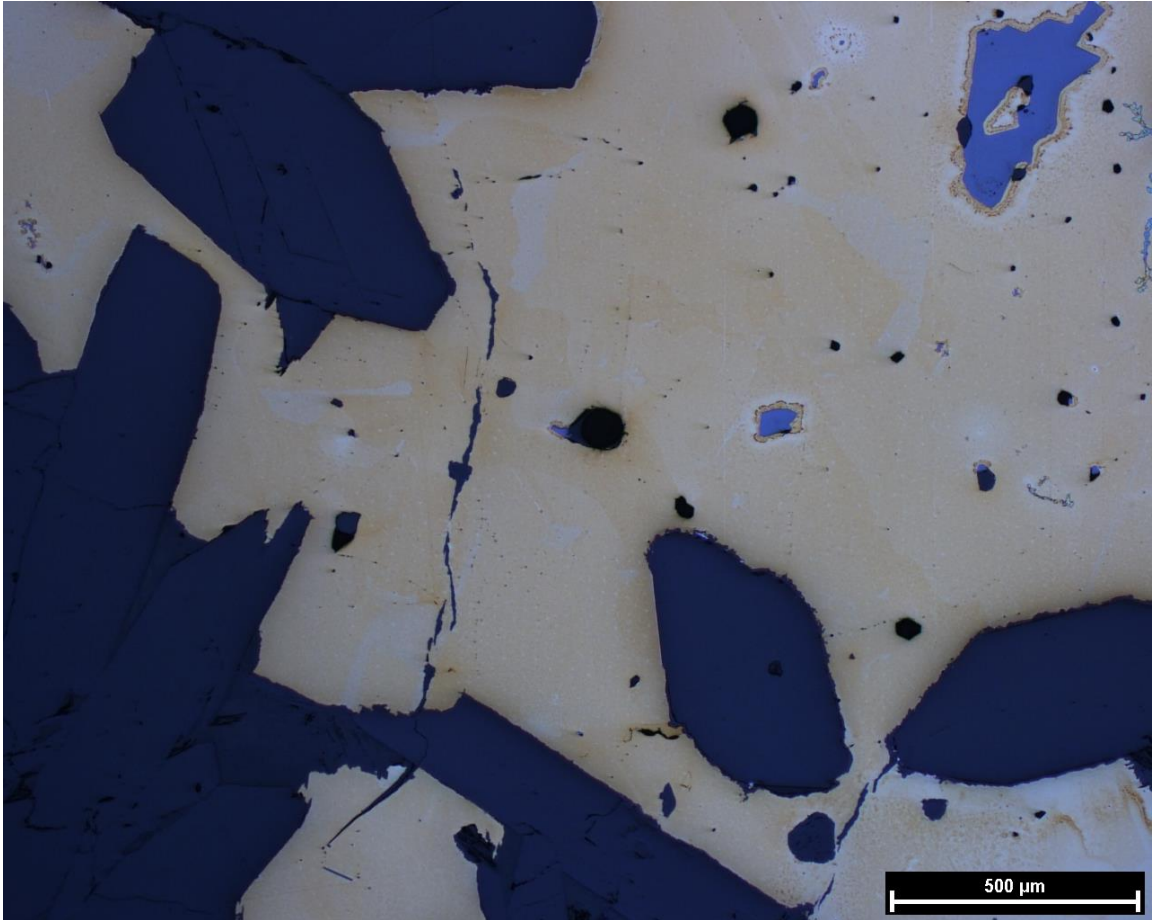
Plagioclase laths weakly aligned perpendicular to the core length, plagioclase grains on average $\sim <1.5\text{cm}$, interstitial clinopyroxene and very little to no olivine. Magnetite is subhedral forming rounded clusters of $\sim 0.5\text{cm}$.

Geochemistry of Sample														
SiO ₂	Al ₂ O ₃	FeO	Fe ₂ O ₃	CaO	MgO	Na ₂ O	K ₂ O	TiO ₂	MnO	P ₂ O ₅	L.O.I.	S	Cu	Pd
-	-	-	-	-	-	-	-	-	-	-	-	0.10	714	0.08

Thin Section Petrography			
Silicates			
Mineral	Modal %	Grainsize	Description
Plagioclase	28	1-3mm	Typically mantled by albite, forms a weak ophitic texture with Cpx in weakly altered sections
Albite	19	1-5mm	Strong albite alteration is present around actinolite pod. Also mantles plagioclase laths
Biotite	2	<1mm	Associated with intense actinolite alteration
Actinolite	15	1-3mm	Forms acicular euhedral crystals within the actinolite pod. Otherwise is pseudomorphous after Cpx
Magnetite	14	<1-1mm	Stubby, equant grains. Disseminated throughout section, not including within actinolite pod
Clinopyroxene	14	1-3mm	Interstitial to plagioclase and magnetite
Apatite	2	1-2mm	Forms equant stubby to elongated crystals, depending on crystal orientation
Epidote	1	<1mm	Pistachio green-brown coloured, associated with actinolite alteration of Cpx
Carbonate	3	1-2mm	Interstitial to actinolite laths in actinolite pod, engulfs chalcopyrite
Sulfides			

Mineral	Modal %	Dominant Grainsize	Description
Chalcopyrite	2	1-3mm	Blebbly when interstitial to actinolite and carbonate
Pentlandite	Tr	<1mm	Spatially associated with Ccp
Galena	Tr	<1mm	Spatially associated with Ccp
Millerite	Tr	<1mm	Spatially associated with Ccp

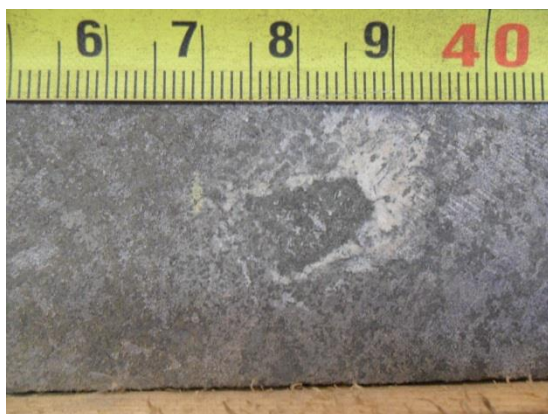
Photomicrographs



Reflected image of Ccp grain within the actinolite pod (in yellow). Sulfide grain is predominantly Ccp with trace pentlandite, galena, and millerite.

Sample name	Drill-hole	Depth	Lithology
G-10-16-140m-1	G-10-16	140-142m	Skeletal troctolite

Hand Sample	Thin section
-------------	--------------



Geochemistry of Sample															
SiO ₂	Al ₂ O ₃	FeO	Fe ₂ O ₃	CaO	MgO	Na ₂ O	K ₂ O	TiO ₂	MnO	P ₂ O ₅	L.O.I.	S	Cu	Pd	
-	-	-	-	-	-	-	-	-	-	-	-	0.10	714	0.08	

Thin Section Petrography			
Silicates			
Mineral	Modal %	Grainsize	Description
Plagioclase	27	1-4mm	Forms ophitic texture with Cpx, is altered to albite in patches of the section
Albite	21	1-3mm	Strong albite alteration is present around actinolite pod. Also mantles plagioclase laths
Biotite	2	<1mm	Associated with intense actinolite alteration
Actinolite	18	1-2mm	Associated with patchy albite alteration, typically encloses sulfides
Magnetite	14	<1-1mm	Stubby, equant grains. Disseminated throughout section
Clinopyroxene	14	1-3mm	Interstitial to plagioclase and magnetite
Apatite	2	1-2mm	Forms equant stubby to elongated crystals, depending on crystal orientation
Epidote	1	<1mm	Pistachio green-brown coloured, associated with actinolite alteration of Cpx
Sulfides			
Mineral	Modal %	Dominant Grainsize	Description
Chalcopyrite	1	1-3mm	Interstitial to albite altered plagioclase laths
Bornite	Tr	<1mm	Spatially associated with Ccp

Sample name	Drill-hole	Depth	Lithology
-------------	------------	-------	-----------

G-10-16-172m-1	G-10-16	172-174m	Skeletal troctolite
----------------	---------	----------	---------------------

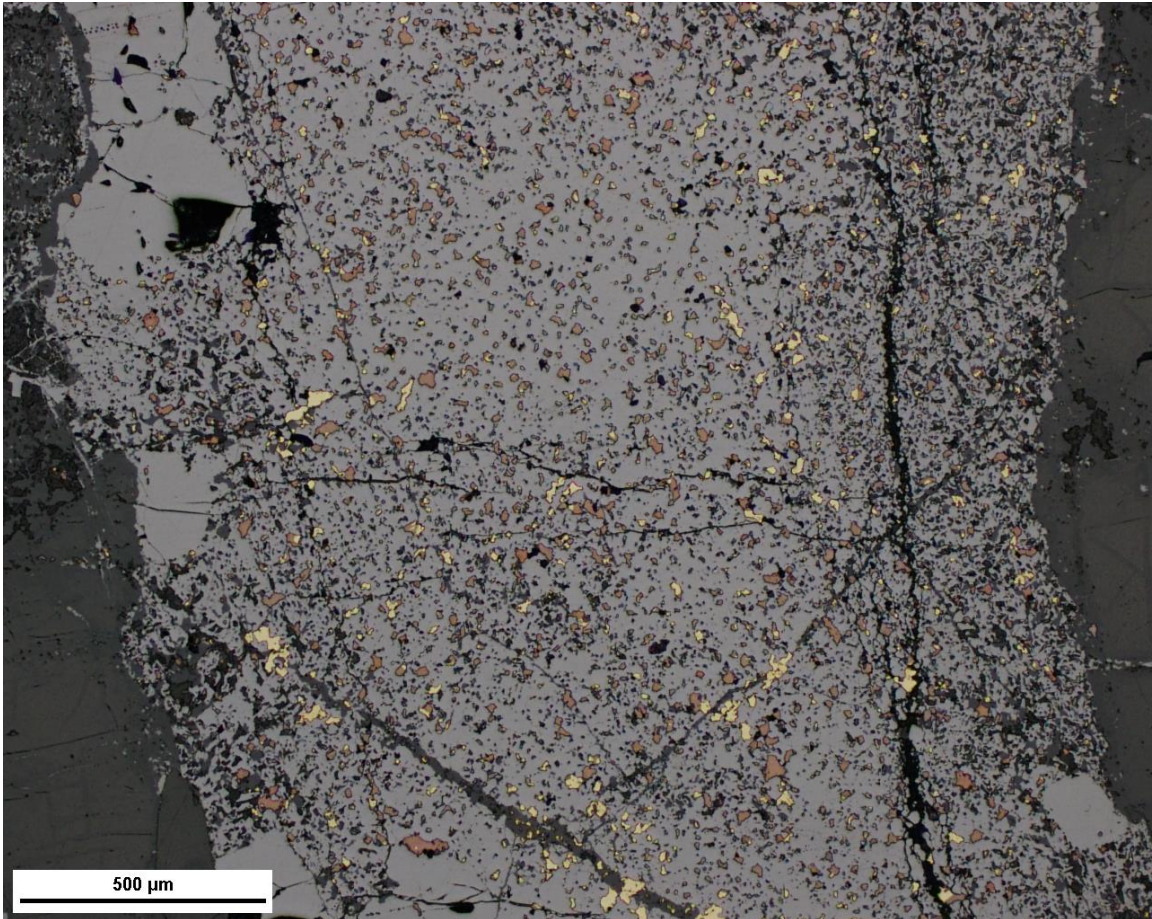
Hand Sample	Thin section
--------------------	---------------------



Geochemistry of Sample														
SiO ₂	Al ₂ O ₃	FeO	Fe ₂ O ₃	CaO	MgO	Na ₂ O	K ₂ O	TiO ₂	MnO	P ₂ O ₅	L.O.I.	S	Cu	Pd
-	-	-	-	-	-	-	-	-	-	-	-	0.49	7534	1.061

Thin Section Petrography			
Silicates			
Mineral	Modal %	Grainsize	Description
Plagioclase	21	1-2mm	Fresh, and forms ophitic texture with Cpx
Olivine	36	1-7mm	Skeletal, harrisitic and forms branches.
Biotite	1	<1mm	Rims irregular shaped magnetite crystals
Magnetite	14	<1-1mm	Irregular shaped. Also forms a large vein through the middle of the section
Clinopyroxene	26	1-3mm	Interstitial to plagioclase, fresh.
Apatite	<1	<1mm	Forms equant stubby to elongated crystals, depending on crystal orientation
Sulfides			
Mineral	Modal %	Dominant Grainsize	Description
Chalcopyrite	1	<1mm	Disseminated within large magnetite vein
Bornite	1	<1mm	Disseminated within large magnetite vein

Photomicrographs



Disseminated Ccp and bn within the large mt vein in the middle of the section.

Sample name	Drill-hole	Depth	Lithology
-------------	------------	-------	-----------

G-10-16-172m-2	G-10-16	172-174m	Skeletal troctolite
----------------	---------	----------	---------------------

Hand Sample	Thin section
--------------------	---------------------



Geochemistry of Sample														
SiO ₂	Al ₂ O ₃	FeO	Fe ₂ O ₃	CaO	MgO	Na ₂ O	K ₂ O	TiO ₂	MnO	P ₂ O ₅	L.O.I.	S	Cu	Pd
-	-	-	-	-	-	-	-	-	-	-	-	0.49	7534	1.061

Thin Section Petrography			
Silicates			
Mineral	Modal %	Grainsize	Description
Plagioclase	28	1-2mm	Forms ophitic texture with Cpx
Olivine	22	1-7mm	Skeletal, harrisitic and forms branches.
Biotite	1	<1mm	Weakly rims magnetite crystals
Magnetite	2	<1-1mm	Weakly disseminated throughout section
Clinopyroxene	26	1-3mm	Interstitial to plagioclase, generally altered to actinolite.
Apatite	<1	<1mm	Forms equant stubby to elongated crystals, depending on crystal orientation
Albite	15	<1-3mm	Alters rims and forms dusty mantles around plagioclase grains
Actinolite	4	1-2mm	Weakly alters Cpx that is interstitial to plagioclase
Epidote	1	<1mm	Associated with actinolite alteration
Chlorite	<1	<1mm	Associated with actinolite alteration
Sericite	1	<1-1mm	Alters rims of plagioclase in contact with skeletal olivine
Sulfides			
Mineral	Modal %	Dominant Grainsize	Description
Chalcopyrite	<1	<1mm	Interstitial to plagioclase that exhibits albite alteration

Sample name	Drill-hole	Depth	Lithology
G-10-16-172m-3	G-10-16	172-174m	Skeletal troctolite

Hand Sample	Thin section
-------------	--------------



Geochemistry of Sample														
SiO ₂	Al ₂ O ₃	FeO	Fe ₂ O ₃	CaO	MgO	Na ₂ O	K ₂ O	TiO ₂	MnO	P ₂ O ₅	L.O.I.	S	Cu	Pd
-	-	-	-	-	-	-	-	-	-	-	-	0.49	7534	1.061

Thin Section Petrography			
Silicates			
Mineral	Modal %	Grainsize	Description
Plagioclase	35	1-3mm	Forms ophitic texture with Cpx
Olivine	14	1-2mm	Stubby, to equant grains with high relief
Biotite	1	<1mm	Weakly rims magnetite crystals
Magnetite	9	<1-1mm	Fine grained and disseminated at the bottom of the section, otherwise subhedral and irregular shaped
Clinopyroxene	31	1-3mm	Interstitial to plagioclase, generally altered to actinolite.
Apatite	1	<1mm	Forms equant stubby to elongated crystals, depending on crystal orientation
Albite	2	<1-3mm	Weak mantling of plagioclase laths
Actinolite	4	1-2mm	Occurs with chalcopyrite, bladed
Chlorite	<1	<1mm	Associated with actinolite alteration
Sericite	1	<1-1mm	Alters rims of plagioclase in contact with skeletal olivine
Sulfides			
Mineral	Modal %	Dominant Grainsize	Description
Chalcopyrite	2	<1mm	Interstitial to plagioclase that exhibit weak albite alteration. Occurs alongside actinolite

Bornite	<1		Occurs as exsolution within Ccp
---------	----	--	---------------------------------

Sample name	Drill-hole	Depth	Lithology
G-10-16-172m-4	G-10-16	172-174m	Skeletal troctolite

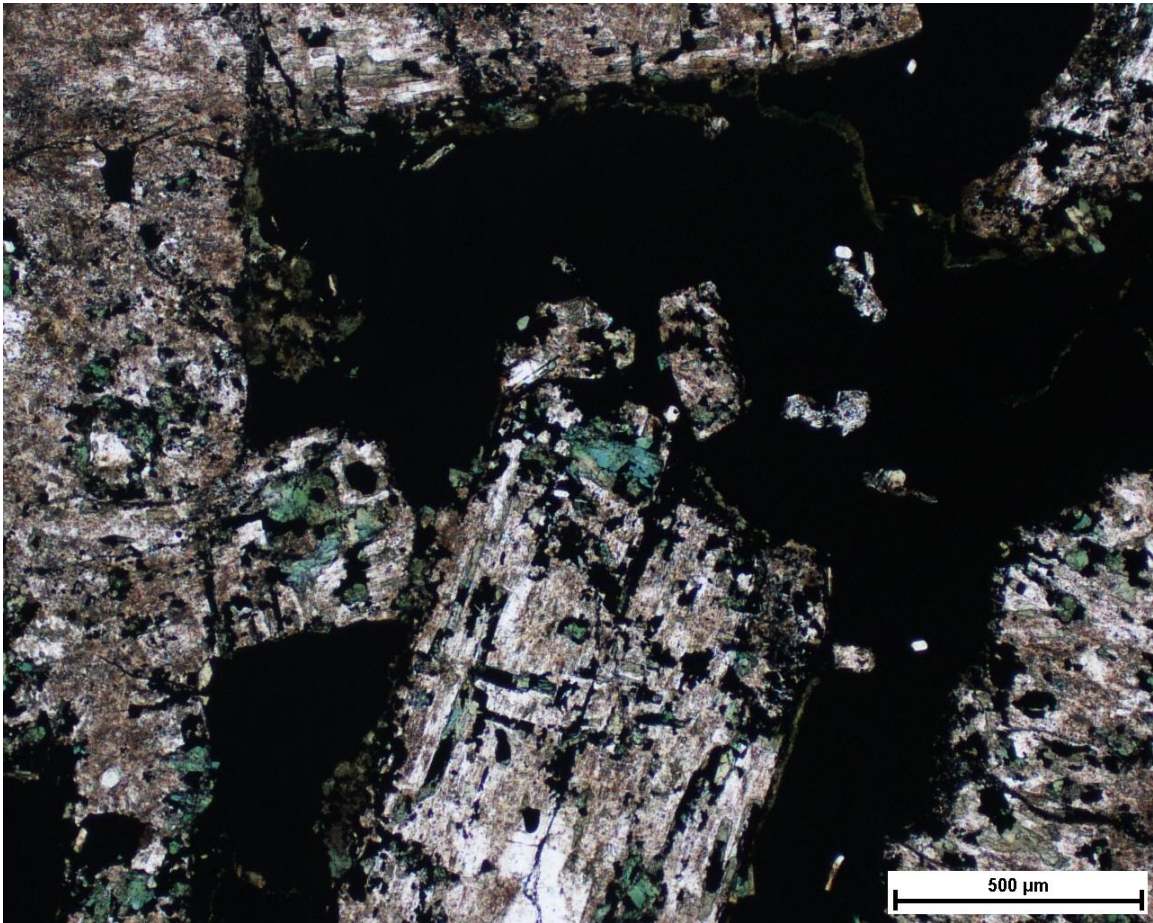
Hand Sample	Thin section
-------------	--------------



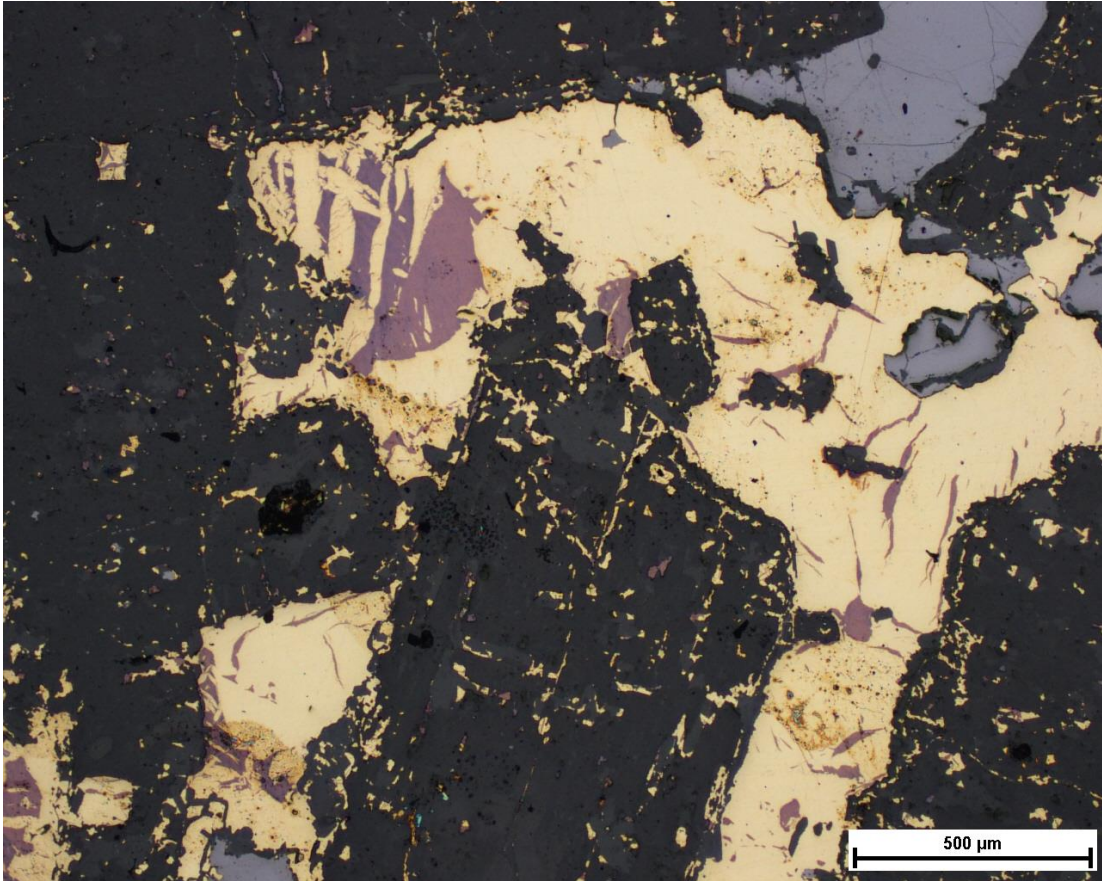
Geochemistry of Sample														
SiO ₂	Al ₂ O ₃	FeO	Fe ₂ O ₃	CaO	MgO	Na ₂ O	K ₂ O	TiO ₂	MnO	P ₂ O ₅	L.O.I.	S	Cu	Pd
-	-	-	-	-	-	-	-	-	-	-	-	0.49	7534	1.061

Thin Section Petrography			
Silicates			
Mineral	Modal %	Grainsize	Description
Plagioclase	27	1-3mm	Forms ophitic texture with Cpx, medium relief
Olivine	31	1-2mm	Stubby, equant to skeletal/harrisitic grains with high relief
Biotite	2	<1mm	Weakly rims magnetite crystals
Magnetite	4	<1-1mm	Fine grained and disseminated
Clinopyroxene	22	1-3mm	Interstitial to plagioclase, generally altered to actinolite.
Apatite	<1	<1mm	Forms equant stubby to elongated crystals, depending on crystal orientation
Albite	3	<1-3mm	Weak mantling of plagioclase laths
Actinolite	2	1-2mm	Occurs with chalcopyrite, bladed
Chlorite	<1	<1mm	Associated with actinolite alteration
Sericite	8	<1-1mm	Alters rims of plagioclase in contact with skeletal olivine
Sulfides			
Mineral	Modal %	Dominant Grainsize	Description
Chalcopyrite	1	<1mm	Interstitial to plagioclase that exhibits moderate albite alteration. Occurs alongside actinolite
Bornite	<1		Occurs as exsolution within Ccp

Photomicrographs



An opaque mineral is interstitial to plagioclase laths that have been moderately albitized. Actinolite alteration (green) also occurs with the albite alteration. In PPL.



The same image as above but in reflected light. The opaque mineral is chalcopyrite (yellow) and contains bornite exsolution (purple). Magnetite (grey) is in the top right of the image, and contains ilmenite exsolution lamellae.

Sample name	Drill-hole	Depth	Lithology
IM-16	G-10-04	62-64m	Plag lineated gabbro

Thin section

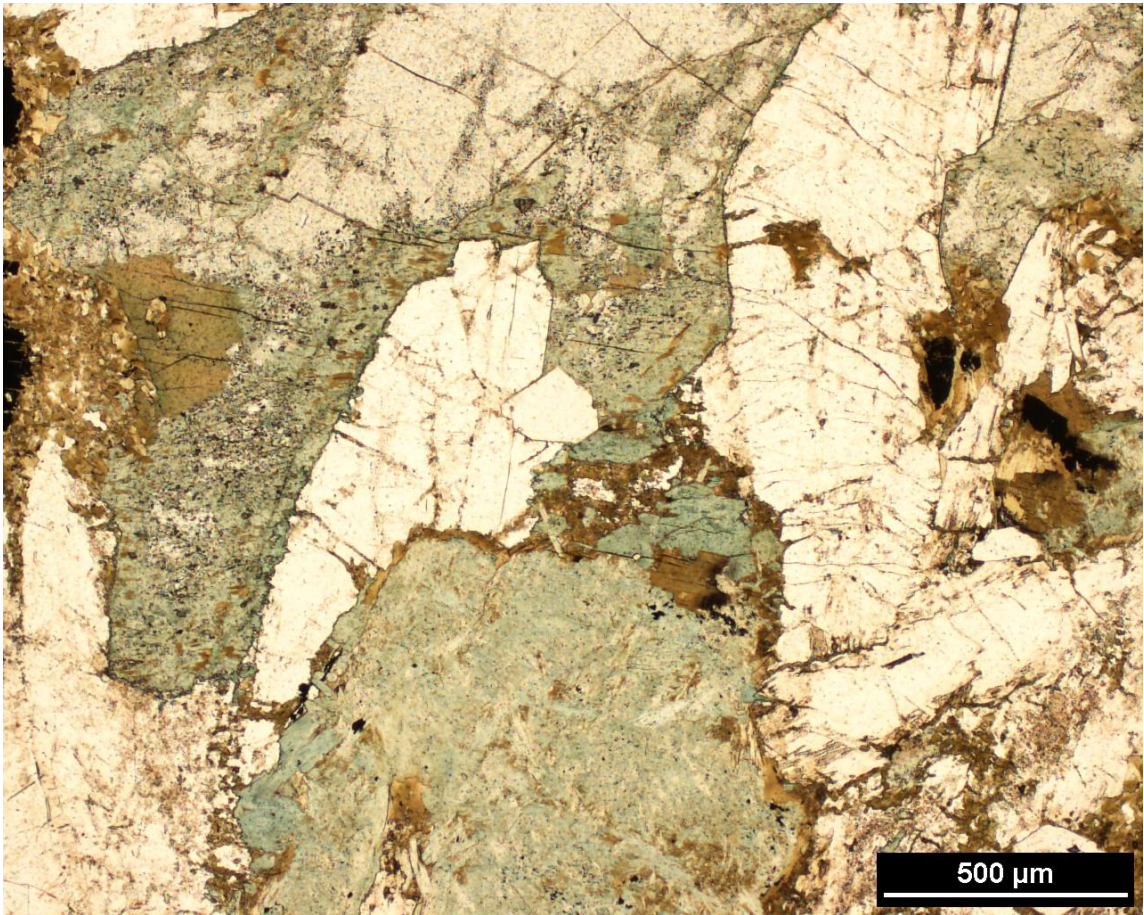


Plagioclase laths weakly aligned perpendicular to the core length, plagioclase grains on average $\sim <1.5\text{mm}$, with interstitial clinopyroxene. Magnetite is subhedral forming rounded clusters of $\sim 0.5\text{cm}$.

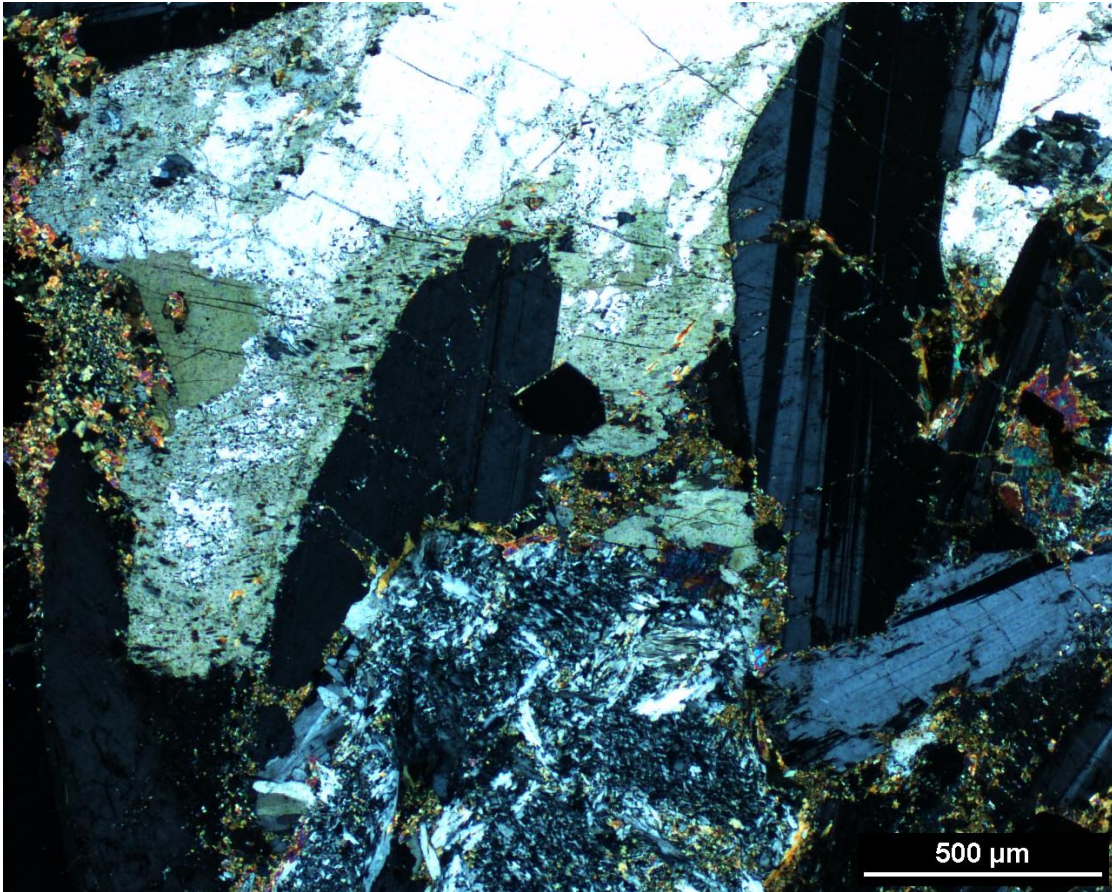
Geochemistry of Sample														
SiO ₂	Al ₂ O ₃	FeO	Fe ₂ O ₃	CaO	MgO	Na ₂ O	K ₂ O	TiO ₂	MnO	P ₂ O ₅	L.O.I.	S	Cu	Pd
46.41	13.92	12.2	17.72	7.76	4.08	3.6	1.95	2.03	0.28	1.028	0.32	0.05	261	0.029

Thin Section Petrography			
Silicates			
Mineral	Modal %	Grainsize	Description
Plagioclase	35	1-5mm	Euhedral laths exhibiting weak alignment in NS and EW orientations
Albite	4	1-3mm	Weakly replaces plag rims
Biotite	8	1mm	Rims equant magnetite grains. Appears greenish brown
Actinolite	15	1-2mm	Alters clinopyroxene, commonly associated with biotite and chlorite
Magnetite	5	1-2mm	Forms equant, stubby subhedral grains. Weakly disseminated
Chlorite	1	1-2mm	Occurs only near actinolite and biotite alteration zones
Clinopyroxene	29	2-4mm	Interstitial to plagioclase, anhedral. Commonly altered to actinolite
Apatite	3	1-2mm	Euhedral, stubby to elongated grains. Common near albite alteration
Epidote	tr	<1mm	Uncommon, but occurs near actinolite/chlorite alteration
Sulfides			
Mineral	Modal %	Dominant Grainsize	Description
Chalcopyrite	tr	<1mm	Very trace disseminations within actinolite blebs

Photomicrographs



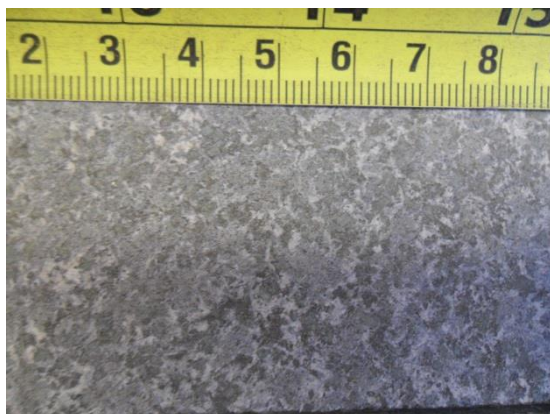
Actinolite alteration in green of CPX. Brown grains are biotite. In PPL



Plag laths are grey-black exhibiting twinning. Same image as above in XPL.

Sample name	Drill-hole	Depth	Lithology
IM-25	G-10-16	118-120m	Heterogeneous gabbro

Hand Sample	Thin section
-------------	--------------



Geochemistry of Sample														
SiO ₂	Al ₂ O ₃	FeO	Fe ₂ O ₃	CaO	MgO	Na ₂ O	K ₂ O	TiO ₂	MnO	P ₂ O ₅	L.O.I.	S	Cu	Pd
45.25	13.21	12	19.79	7.81	4.57	3.55	1.7	2.3	0.28	1.083	0.25	0.08	317	0.062

Thin Section Petrography			
Silicates			
Mineral	Modal %	Grainsize	Description
Plagioclase	36	1-5mm	Forms ophitic texture with Cpx
Biotite	1	<1mm	Weakly rims magnetite grains
Magnetite	9	<1-1mm	Fine grained and disseminated. Grains are blocky
Clinopyroxene	31	1-3mm	Interstitial to plagioclase, generally are altered to actinolite.
Apatite	1	<1mm	Forms equant stubby to elongated crystals, depending on crystal orientation. Occurs prominently in zones of albite alteration
Albite	8	<1-3mm	Weak mantling of plagioclase laths, and can be observed fully altering plag laths
Actinolite	8	1-2mm	Pseudomorphic after Cpx, strongly associated with albite alteration
Chlorite	1	<1mm	Associated with actinolite alteration
Sulfides			
Mineral	Modal %	Dominant Grainsize	Description
Chalcopyrite	Tr	<1mm	Fine grained and disseminated, occurs alongside actinolite

Sample name	Drill-hole	Depth	Lithology
IM-26	G-10-16	136-138m	Heterogeneous gabbro

Hand Sample	Thin section
-------------	--------------



Geochemistry of Sample														
SiO ₂	Al ₂ O ₃	FeO	Fe ₂ O ₃	CaO	MgO	Na ₂ O	K ₂ O	TiO ₂	MnO	P ₂ O ₅	L.O.I.	S	Cu	Pd
44.76	13.27	11.5	19.74	7.75	5.04	3.53	1.5	2.24	0.29	1.048	0.38	0.05	605	0.054

Thin Section Petrography			
Silicates			
Mineral	Modal %	Grainsize	Description
Plagioclase	37	1-3mm	Forms ophitic texture with Cpx
Biotite	1	<1mm	Weakly rims magnetite grains
Magnetite	7	<1-2mm	Grains are skeletal to stubby, occur alongside Cpx and plag
Clinopyroxene	35	1-3mm	Interstitial to plagioclase, generally are altered to actinolite.
Apatite	1	<1mm	Occurs prominently in zones of albite alteration
Albite	13	<1-4mm	Forms a pod 4-7mm in diameter, completely overprints previous minerals in this pod
Actinolite	6	1-2mm	Pseudomorphic after Cpx, strongly associated with albite pod
Chlorite	Tr	<1mm	Associated with actinolite alteration
Sulfides			
Mineral	Modal %	Dominant Grainsize	Description
Chalcopyrite	Tr	<1mm	Fine grained and disseminated, occurs alongside actinolite particularly within albite pod

Sample name	Drill-hole	Depth	Lithology
IM-27	G-10-16	166-168m	Skeletal troctolite

Hand Sample	Thin section
-------------	--------------



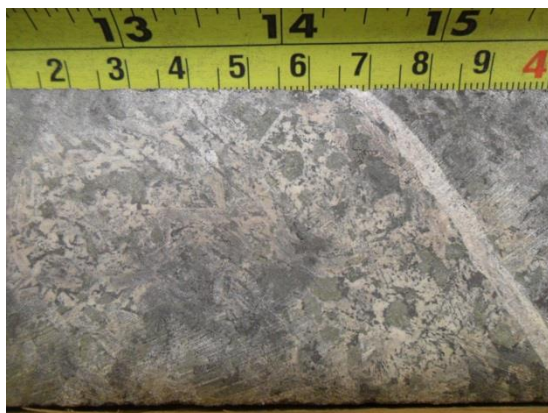
Geochemistry of Sample														
SiO ₂	Al ₂ O ₃	FeO	Fe ₂ O ₃	CaO	MgO	Na ₂ O	K ₂ O	TiO ₂	MnO	P ₂ O ₅	L.O.I.	S	Cu	Pd
41.57	10.35	14.5	24.06	5.92	9.47	2.01	2.02	1.77	0.38	0.678	0.74	0.05	228	0.084

Thin Section Petrography			
Silicates			
Mineral	Modal %	Grainsize	Description
Plagioclase	32	1-3mm	Forms ophitic texture with Cpx
Biotite	4	<1mm	Weakly rims magnetite grains, but also occurs with actinolite that is pseudomorphic after Cpx
Magnetite	7	<1-2mm	Grains are skeletal to stubby, occur alongside Cpx and plag
Clinopyroxene	19	1-3mm	Interstitial to plagioclase, generally are altered to actinolite.
Apatite	1	<1mm	Occurs prominently in zones of albite alteration
Olivine	27	1-5mm	Skeletal textured, euhedral to subhedral
Sericite	4	1-2mm	Strongly alters rims of olivine where in contact with plagioclase
Albite	2	<1mm	Weak alteration of plagioclase in some sections
Actinolite	5	1-2mm	Pseudomorphic after Cpx that is interstitial to weakly albitized plagioclase
Chlorite	Tr	<1mm	Associated with actinolite alteration
Sulfides			
Mineral	Modal %	Dominant Grainsize	Description
Chalcopyrite	Tr	<1mm	Fine grained and disseminated, occurs alongside actinolite near magnetite

			grains
--	--	--	--------

Sample name	Drill-hole	Depth	Lithology
IM-28	G-10-16	168-170m	Skeletal troctolite

Hand Sample	Thin section
-------------	--------------

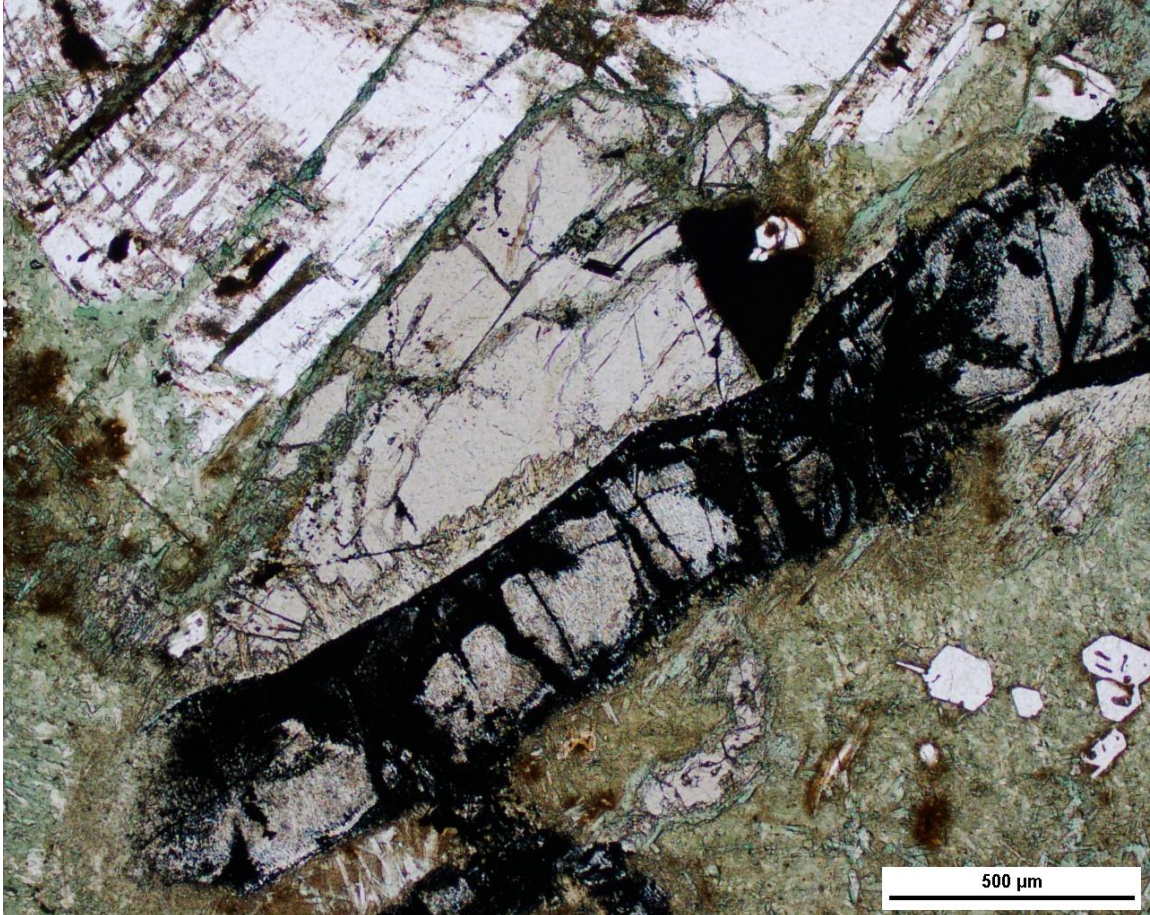


Geochemistry of Sample														
SiO ₂	Al ₂ O ₃	FeO	Fe ₂ O ₃	CaO	MgO	Na ₂ O	K ₂ O	TiO ₂	MnO	P ₂ O ₅	L.O.I.	S	Cu	Pd
40.29	9.72	15.2	26.47	6.73	8.87	2.15	1.39	2.48	0.38	1.032	0.33	0.11	2208	0.39

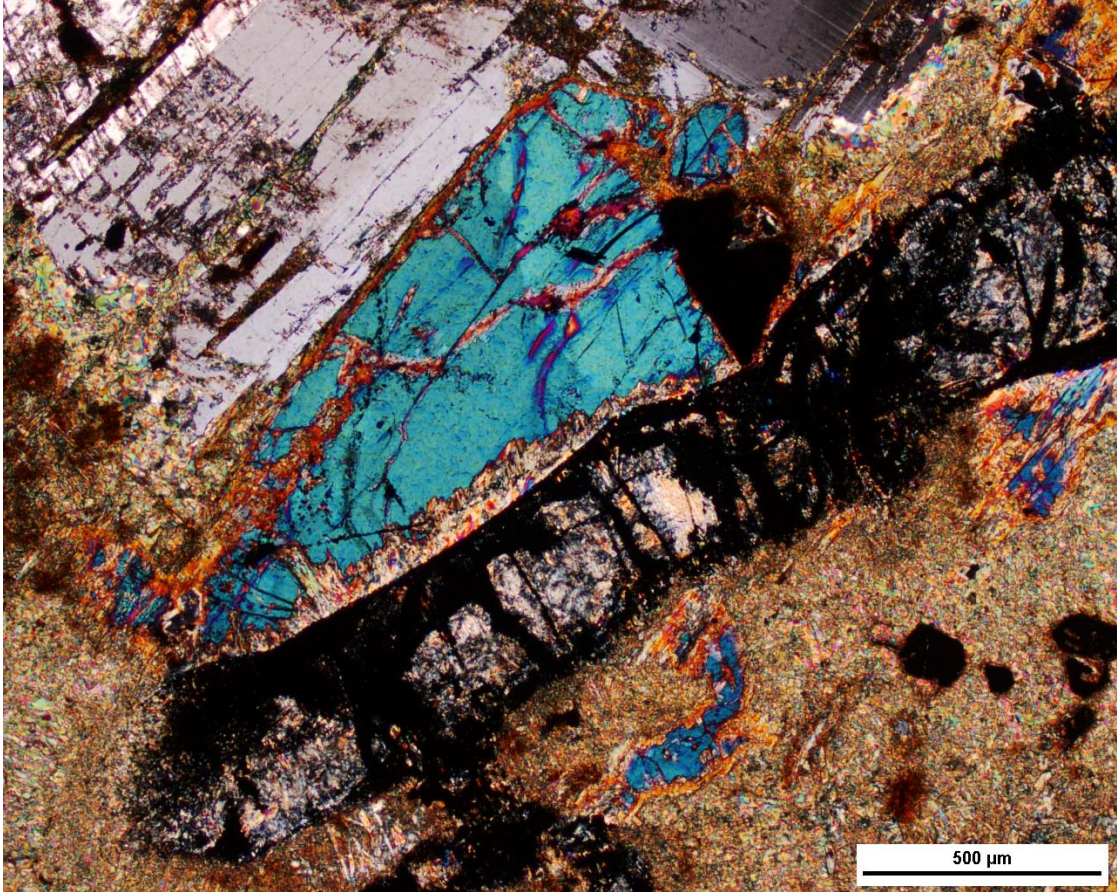
Thin Section Petrography			
Silicates			
Mineral	Modal %	Grainsize	Description
Plagioclase	28	1-3mm	Forms weak ophitic texture with Cpx, generally euhedral to subhedral and encloses skeletal olivine grains
Biotite	8	<1mm	Rims skeletal magnetite grains as well as olivine grains, green to foxy brown in PPL
Magnetite	9	<1-2mm	Grains are skeletal to stubby, occur alongside Cpx and plag
Clinopyroxene	7	1-2mm	Interstitial to plagioclase, generally fresh
Apatite	1	<1mm	Disseminated, euhedral with medium relief
Olivine	24	1-5mm	Skeletal textured, euhedral to subhedral
Sericite	2	1-2mm	Weakly alters rims of olivine where in contact with plagioclase
Albite	3	<1mm	Weak alteration of plagioclase rims. Cloudy grey
Actinolite	18	1-2mm	Pseudomorphic after Cpx that is interstitial to skeletal olivine
Chlorite	Tr	<1mm	Associated with actinolite alteration
Sulfides			
Mineral	Modal %	Dominant Grainsize	Description

Chalcopyrite	Tr	<1mm	Fine grained and disseminated, occurs alongside biotite/sericite near magnetite and olivine grains
--------------	----	------	--

Photomicrographs



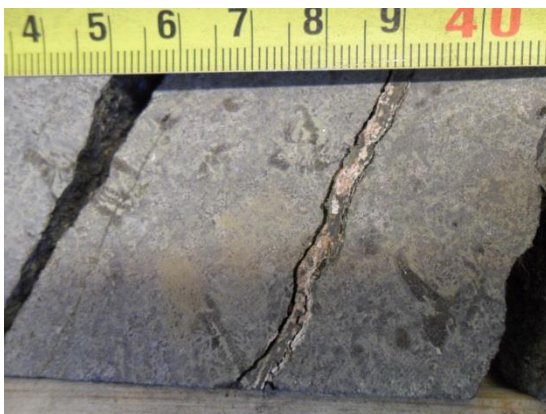
A skeletal olivine grain is bordered by a Cpx grain above it (light brown, center), while below, Cpx is altered to biotite (foxy brown) and actinolite (green). In PPL



Same image as above, but in XPL. Actinolite is pseudomorphic after Cpx.

Sample name	Drill-hole	Depth	Lithology
IM-29	G-10-16	170-172m	Skeletal troctolite

Hand Sample	Thin section
-------------	--------------

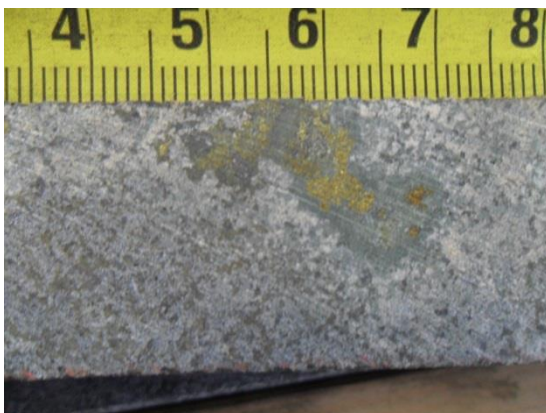


Geochemistry of Sample														
SiO ₂	Al ₂ O ₃	FeO	Fe ₂ O ₃	CaO	MgO	Na ₂ O	K ₂ O	TiO ₂	MnO	P ₂ O ₅	L.O.I.	S	Cu	Pd
38.94	9.41	16	27.33	5.94	10.29	1.69	1.03	2.33	0.41	0.767	1.12	0.1	1819	0.417

Thin Section Petrography			
Silicates			
Mineral	Modal %	Grainsize	Description
Plagioclase	13	1-3mm	Forms weak ophitic texture with Cpx, generally euhedral to subhedral
Biotite	1	<1mm	Rims skeletal magnetite grains, foxy brown in PPL
Magnetite	13	<1-2mm	Grains are skeletal to stubby, occur alongside Cpx and plag
Clinopyroxene	36	1-4mm	Generally fresh, light brown in PPL and medium relief
Apatite	1	<1mm	Disseminated, euhedral with medium relief
Olivine	27	1-2mm	Stubby to slightly skeletal textured, high relief
Albite	3	<1mm	Weak alteration of plagioclase rims. Cloudy grey
Actinolite	6	1-2mm	Pseudomorphic after Cpx that is interstitial to albitized plagioclase
Chlorite	Tr	<1mm	Associated with actinolite alteration
Sulfides			
Mineral	Modal %	Dominant Grainsize	Description
Chalcopyrite	1	<1mm	Fine grained and disseminated, occurs alongside actinolite/biotite alteration, near the most albitized portion of the thin section
Bornite	Tr	<1mm	Associated with Ccp mineralization as exsolution lamellae

Sample name	Drill-hole	Depth	Lithology
IM-30	G-10-16	200-202m	Skeletal but some heterogeneous gabbro mixed

Hand Sample	Thin section
-------------	--------------

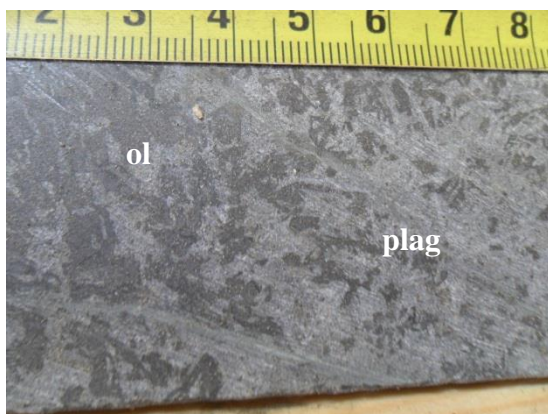


Geochemistry of Sample														
SiO ₂	Al ₂ O ₃	FeO	Fe ₂ O ₃	CaO	MgO	Na ₂ O	K ₂ O	TiO ₂	MnO	P ₂ O ₅	L.O.I.	S	Cu	Pd
44.08	11.59	11.7	21.4	8.1	5.65	3.41	1.5	2.29	0.38	1.029	0.31	0.14	4432	0.316

Thin Section Petrography			
Silicates			
Mineral	Modal %	Grainsize	Description
Plagioclase	26	1mm	Forms weak ophitic texture with Cpx, generally subhedral
Biotite	1	<1mm	Weakly rims magnetite grains
Magnetite	15	1mm	Grains are generally stubby and disseminated
Clinopyroxene	12	1-2mm	Generally altered to actinolite, especially when near albite alteration
Apatite	1	<1mm	Disseminated, euhedral with medium relief
Albite	37	<1mm	Prominent patches of cloudy grey to brown form a connected network of alteration throughout the section
Actinolite	5	1-2mm	Pseudomorphic after Cpx that is interstitial to albitized plagioclase
Chlorite	Tr	<1mm	Associated with actinolite alteration
Carbonate	1	<1mm	Patchy, cloudlike with high birefringence in XPL. Associated with actinolite alteration
Sulfides			
Mineral	Modal %	Dominant Grainsize	Description
Chalcopyrite	2	<1mm	Fine grained and disseminated, occurs alongside actinolite/biotite alteration, near the most albitized portion of the thin section
Bornite	Tr	<1mm	Associated with Ccp mineralization as exsolution lamellae
Pentlandite	Tr	<1mm	Associated with bornite, and Ccp

Sample name	Drill-hole	Depth	Lithology
IM-31	G-10-16	206-208m	Skeletal troctolite

Hand Sample	Thin section
-------------	--------------



Medium to mainly coarse grained dark grey to black skeletal olivine grains with interstitial frosty white plagioclase inter-grown with minor light grey clinopyroxene. Appears to have very minor actinolite (green) alteration. Very trace disseminated chalcopyrite is visible in the slightly greener (actinolite altered) patches of plagioclase.

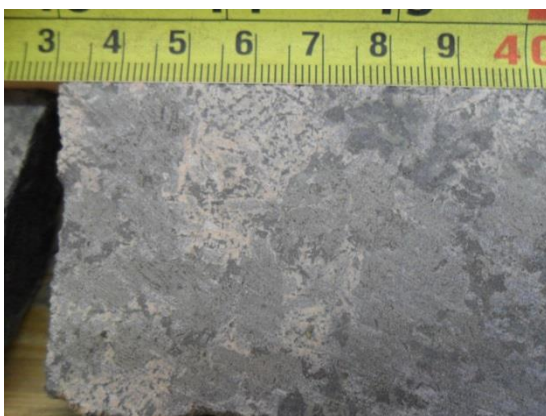
Geochemistry of Sample														
SiO ₂	Al ₂ O ₃	FeO	Fe ₂ O ₃	CaO	MgO	Na ₂ O	K ₂ O	TiO ₂	MnO	P ₂ O ₅	L.O.I.	S	Cu	Pd
41.25	10.42	13.4	24.18	8.51	8.06	2.61	1.03	2	0.37	1.297	-0.03	0.27	4249	0.596

Thin Section Petrography			
Silicates			
Mineral	Modal %	Grainsize	Description
Plagioclase	33	1-5mm	Forms strong ophitic texture with Cpx, subhedral to euhedral
Olivine	32	1-7mm	Skeletal textured, high relief, very dark in PPL
Biotite	1	<1mm	Weakly rims magnetite grains, foxy-brown coloured in PPL
Magnetite	4	1mm	Grains are generally stubby to skeletal textured and disseminated
Clinopyroxene	22	1-2mm	Generally altered to actinolite, especially when near albite alteration
Apatite	1	<1mm	Disseminated, euhedral with medium relief
Albite	4	<1mm	Weak patches of cloudy grey-brown completely overprint plagioclase and Cpx
Actinolite	1	1-2mm	Pseudomorph after Cpx that is interstitial to albitized plagioclase
Sulfides			

Mineral	Modal %	Dominant Grainsize	Description
Chalcopyrite	2	<1mm	Interstitial to albitized plagioclase grains and near weak actinolite alteration
Bornite	Tr	<1mm	Associated with Ccp mineralization as exsolution lamellae
Pentlandite	Tr	<1mm	Associated with bornite, and Ccp
Galena	Tr	<1	Associated with bornite, and Ccp

Sample name	Drill-hole	Depth	Lithology
G-10-16-140m-2	G-10-16	140-142m	Skeletal troctolite

Hand Sample	Thin section
-------------	--------------

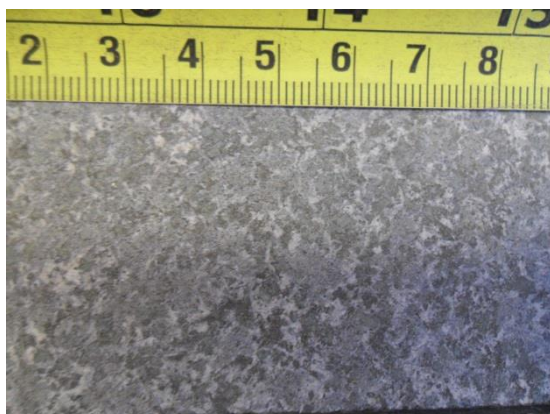


Geochemistry of Sample														
SiO ₂	Al ₂ O ₃	FeO	Fe ₂ O ₃	CaO	MgO	Na ₂ O	K ₂ O	TiO ₂	MnO	P ₂ O ₅	L.O.I.	S	Cu	Pd
-	-	-	-	-	-	-	-	-	-	-	-	0.10	714	0.08

Thin Section Petrography			
Silicates			
Mineral	Modal %	Grainsize	Description
Plagioclase	37	1-2mm	Forms strong ophitic texture with Cpx, subhedral to euhedral
Biotite	1	<1mm	Weakly rims magnetite grains and is also associated with actinolite alteration of Cpx, foxy-brown coloured in PPL
Magnetite	5	1mm	Grains are generally stubby and disseminated, but occurs in aggregate clusters
Clinopyroxene	18	1-2mm	Generally altered to actinolite, especially when near albite alteration
Apatite	1	<1mm	Disseminated, euhedral with medium relief. More concentrated in regions of strong albite alteration
Albite	16	<1-2mm	Weak patches of cloudy grey-brown completely overprint plagioclase and Cpx, but also weakly mantles plagioclase laths
Actinolite	6	1-2mm	Pseudomorphic after Cpx that is interstitial to albitized plagioclase, but also occurs interstitial to relatively fresh plagioclase
Sulfides			
Mineral	Modal %	Dominant Grainsize	Description
Chalcopyrite	<1	<1mm	Interstitial to albitized plagioclase grains and near weak actinolite alteration

Sample name	Drill-hole	Depth	Lithology
IM-40	G-10-16	86-88m	Homogeneous gabbro

Hand Sample	Thin section
-------------	--------------



Geochemistry of Sample														
SiO ₂	Al ₂ O ₃	FeO	Fe ₂ O ₃	CaO	MgO	Na ₂ O	K ₂ O	TiO ₂	MnO	P ₂ O ₅	L.O.I.	S	Cu	Pd
46.33	13.89	11.9	17.86	7.7	4.19	3.63	2.01	2.08	0.27	1.047	0.52	0.04	244	0.023

Thin Section Petrography			
Silicates			
Mineral	Modal %	Grainsize	Description
Plagioclase	18	1-2m	Plag laths are generally thin and needle-like, form an ophitic texture with Cpx
Albite	26	1-3mm	Albite pods are patchy and quite common. Form a pervasive network throughout the section
Biotite	Tr	<1mm	Weak mantling of magnetite crystals
Actinolite	16	1mm	Pseudomorphic alteration of Cpx that is interstitial to albitized plagioclase
Magnetite	13	<1mm	Disseminated stubby crystals, subhedral to anhedral
Clinopyroxene	25	1-2mm	Medium relief, interstitial to plagioclase. Forms ophitic texture
Apatite	2	<1mm	Finely disseminated throughout the sample
Epidote	Tr	<1mm	Associated with actinolite alteration
Sulfides			
Mineral	Modal %	Dominant Grainsize	Description
Chalcopyrite	<1	<1mm	Weakly disseminated, associated strongly with actinolite alteration near albite alteration

Sample name	Drill-hole	Depth	Lithology
IM-41	G-10-16	146-148m	Skeletal troctolite to heterogeneous gabbro

Hand Sample	Thin section
-------------	--------------



Geochemistry of Sample														
SiO ₂	Al ₂ O ₃	FeO	Fe ₂ O ₃	CaO	MgO	Na ₂ O	K ₂ O	TiO ₂	MnO	P ₂ O ₅	L.O.I.	S	Cu	Pd
43.94	12.91	12.2	20.91	7.38	5.24	3.25	1.85	2.37	0.29	0.908	0.35	0.06	1196	0.118

Thin Section Petrography			
Silicates			
Mineral	Modal %	Grainsize	Description
Plagioclase	24	1-3mm	Euhedral to subhedral, medium relief and forms ophitic texture with Cpx. Laths have a high aspect ratio
Albite	10	1-3mm	Albite pods are patchy and irregular, generally encloses smaller actinolite pods
Biotite	Tr	<1mm	Strong rimming of magnetite grains
Actinolite	6	1mm	Forms small pods that enclose wormy chalcopyrite blebs
Magnetite	12	<1mm	Stubby to equant crystals that are strongly associated with olivine
Olivine	24	1-2mm	Stubby, irregular crystals. High relief, dark brown to grey in PPL
Clinopyroxene	22	1-2mm	Medium relief, interstitial to plagioclase. Forms ophitic texture with plagioclase
Apatite	1	<1mm	Finely disseminated throughout the sample, but more abundant in albite altered zones
Epidote	Tr	<1mm	Associated with actinolite alteration
Sulfides			

Mineral	Modal %	Dominant Grainsize	Description
Chalcopyrite	1	<1mm	Weakly disseminated, associated strongly with actinolite alteration near albite alteration
Bornite	<1	<1mm	Associated with Ccp mineralization as exsolution lamellae

Sample name	Drill-hole	Depth	Lithology
IM-UM-2	G-10-04	15m	Plag lineated gabbro

Thin section



Geochemistry of Sample														
SiO ₂	Al ₂ O ₃	FeO	Fe ₂ O ₃	CaO	MgO	Na ₂ O	K ₂ O	TiO ₂	MnO	P ₂ O ₅	L.O.I.	S	Cu	Pd
44.9	13.75	12.45	18.4	7.87	4.5	3.11	1.6	2.1	0.27	0.83	0.66	0.03	251	0.02

Thin Section Petrography			
Silicates			
Mineral	Modal %	Grainsize	Description
Plagioclase	35	1-5mm	Euhedral laths exhibiting weak alignment in NS and EW orientations
Albite	4	1-3mm	Very weakly replaces plag rims
Biotite	8	1mm	Rims equant magnetite grains. Mainly brown
Actinolite	15	1-2mm	Alters clinopyroxene, commonly associated with biotite and chlorite
Magnetite	6	<1mm	Forms equant, stubby subhedral grains. Weakly disseminated
Chlorite	1	<1mm	Occurs only near actinolite and biotite alteration zones
Clinopyroxene	29	2-5mm	Interstitial to plagioclase, anhedral. Commonly altered to actinolite
Apatite	3	1-2mm	Euhedral, stubby to elongated grains. Common near albite alteration
Epidote	tr	<1mm	Uncommon, but occurs near actinolite/chlorite alteration
Sulfides			
Mineral	Modal %	Dominant Grainsize	Description
Chalcopyrite	tr	<1mm	Very trace disseminations within actinolite blebs

Sample name	Drill-hole	Depth	Lithology
IM-UM-3	G-10-04	30.3m	Plag lineated gabbro

Hand Sample	Thin section
-------------	--------------



Plagioclase laths weakly aligned perpendicular to the core length, plagioclase grains on average $\sim <1.5$ cm, interstitial clinopyroxene and no olivine. Magnetite is subhedral forming rounded clusters of ~ 0.5 cm.

Geochemistry of Sample														
SiO ₂	Al ₂ O ₃	FeO	Fe ₂ O ₃	CaO	MgO	Na ₂ O	K ₂ O	TiO ₂	MnO	P ₂ O ₅	L.O.I.	S	Cu	Pd
46.4	14.35	11.95	17.45	8.05	4.09	3.6	1.56	2.07	0.25	0.84	0.31	0.04	284	0.029

Thin Section Petrography			
Silicates			
Mineral	Modal %	Grainsize	Description
Plagioclase	34	3-10mm	Euhedral laths exhibiting weak to moderate alignment in NS and EW orientations
Albite	9	1-3mm	Replaces rims of plagioclase. Frosty white alteration rim
Biotite	2	1mm	Rims equant magnetite grains. Appears greenish brown
Actinolite	16	1-2mm	Alters clinopyroxene, commonly associated with biotite and chlorite
Magnetite	8	1-2mm	Forms equant, stubby subhedral grains. Disseminated
Chlorite	1	1-2mm	Occurs only near actinolite and biotite alteration zones
Clinopyroxene	27	2-4mm	Interstitial to plagioclase, anhedral. Commonly altered to actinolite
Apatite	3	1-2mm	Euhedral, stubby to elongated grains. Common near albite alteration
Epidote	tr	<1mm	Uncommon, but occurs near actinolite/chlorite alteration
Sulfides			

Mineral	Modal %	Dominant Grainsize	Description
Chalcopyrite	tr	<1mm	Very trace disseminations within actinolite blebs
Pyrrhotite	tr	<1mm	Very trace disseminations within actinolite blebs
Pyrite	tr	<1mm	Very trace disseminations within actinolite blebs

Sample name	Drill-hole	Depth	Lithology
IM-UM-4	G-10-04	45m	Plag lineated gabbro

Thin section

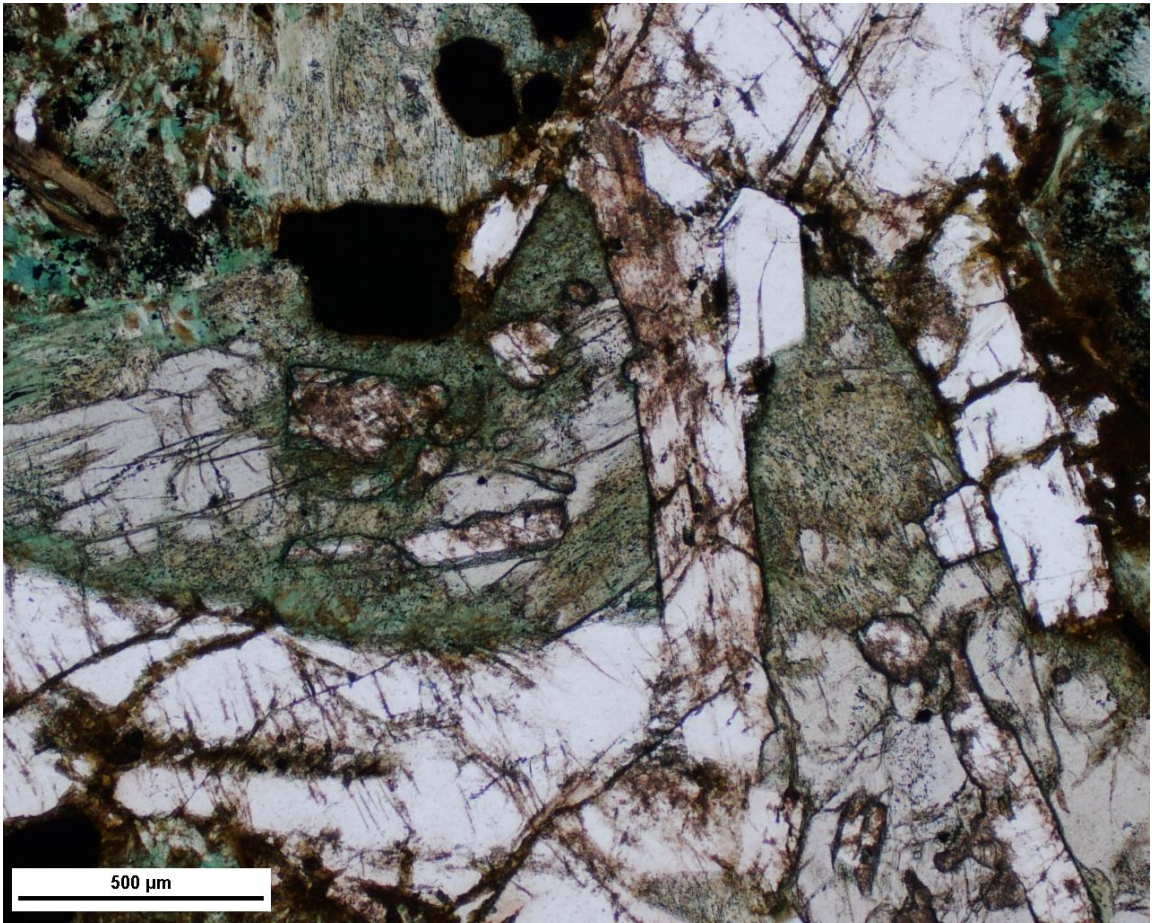


Geochemistry of Sample														
SiO ₂	Al ₂ O ₃	FeO	Fe ₂ O ₃	CaO	MgO	Na ₂ O	K ₂ O	TiO ₂	MnO	P ₂ O ₅	L.O.I.	S	Cu	Pd
44.8	14.35	13.45	18.2	7.06	4.22	3.16	2.47	2.09	0.26	0.95	0.72	0.04	252	0.016

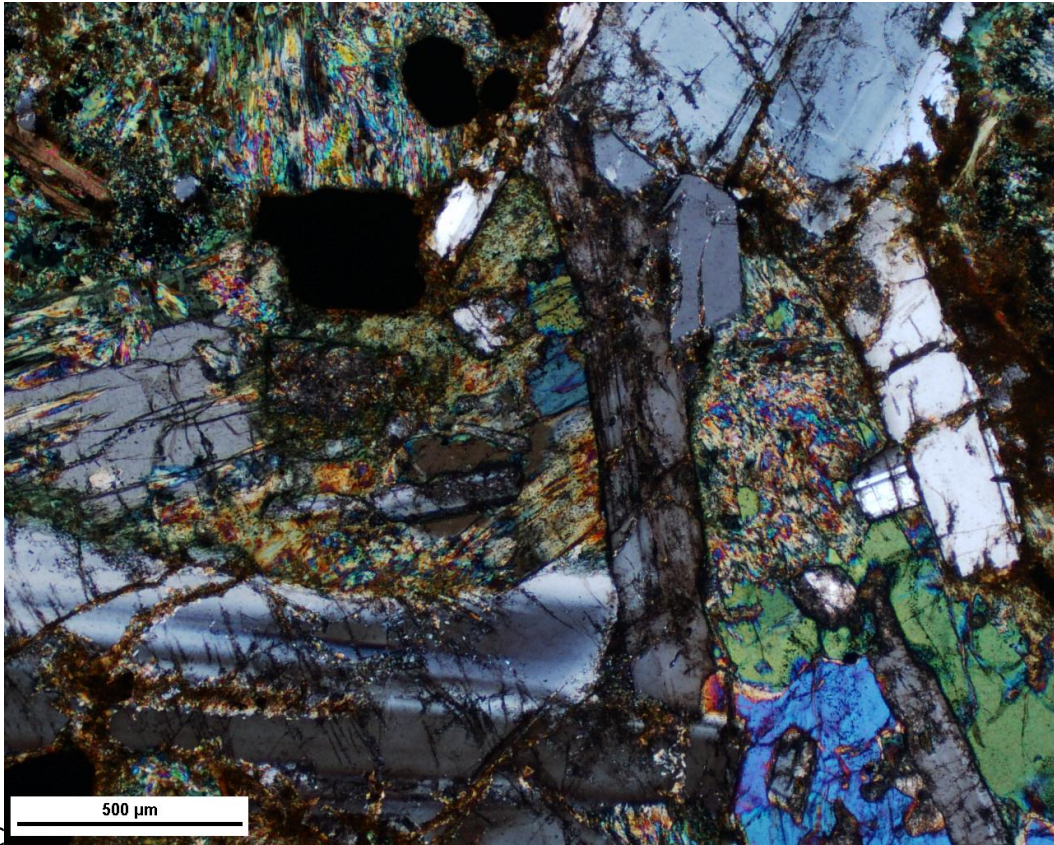
Thin Section Petrography			
Silicates			
Mineral	Modal %	Grainsize	Description
Plagioclase	35	1-5mm	Euhedral laths exhibiting mainly NS alignment, with minor E-W alignment
Albite	4	1-3mm	Replaces plag rims, observed to also entirely replaces plag
Biotite	13	1-8mm	Rims equant magnetite grains and pervasively alters clinopyroxene. Brown, dirty text
Actinolite	15	1-2mm	Alters clinopyroxene, commonly associated with biotite and chlorite
Magnetite	6	<1mm	Forms equant, stubby subhedral grains. Weakly disseminated
Chlorite	3	<1mm	Occurs primarily in association with biotite
Clinopyroxene	16	2-5mm	Interstitial to plagioclase, anhedral. Commonly altered to actinolite
Apatite	3	1-2mm	Euhedral, stubby to elongated grains. Common near albite alteration
Epidote	2	1-3mm	Alters CPX, associated with actinolite/chlorite
Sulfides			
Mineral	Modal %	Dominant Grainsize	Description
Chalcopyrite	tr	<1mm	Very trace disseminations within actinolite blebs

Photomicrographs

C



Chlorite, biotite and epidote alteration of CPX. Plagioclase is altered brown at its fractures.



Same image as above but in XPL.

Sample name	Drill-hole	Depth	Lithology
IM-UM-5	G-10-04	50m	Plag lineated gabbro

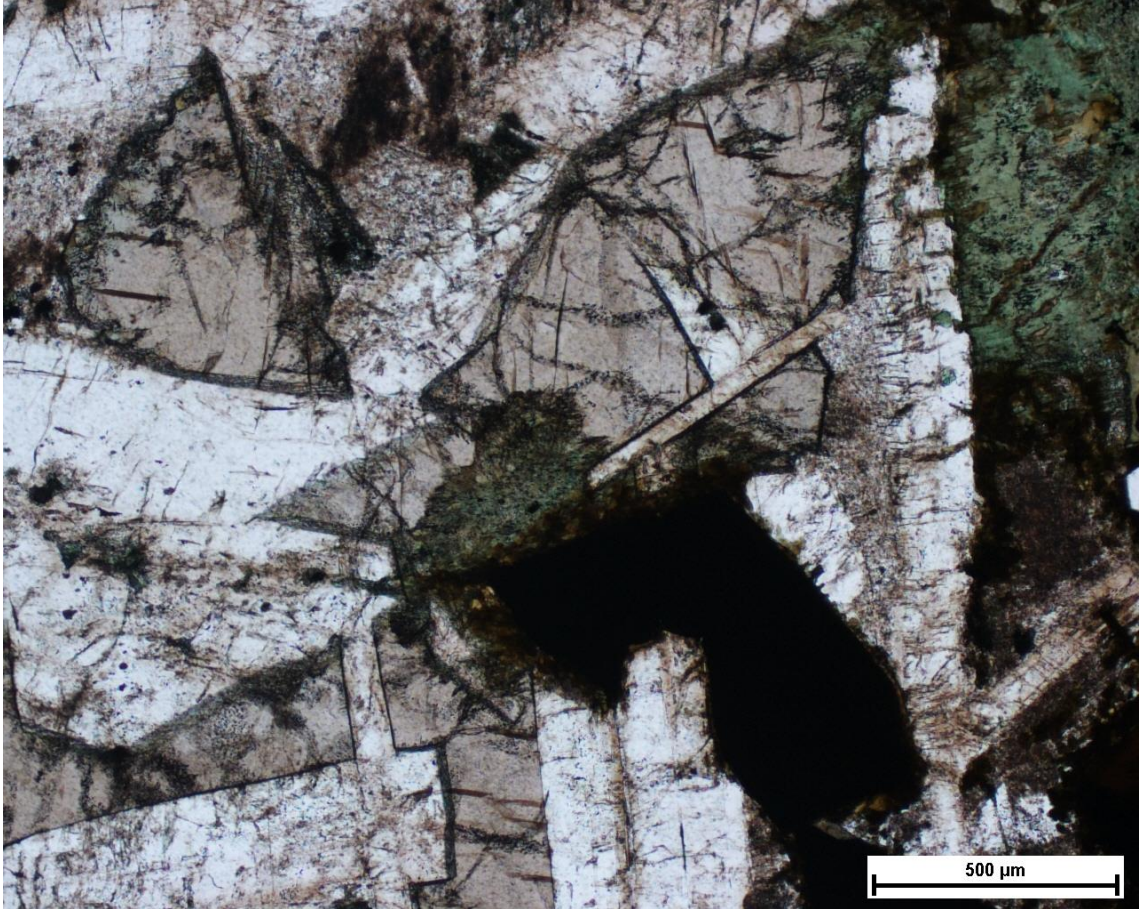
Thin section



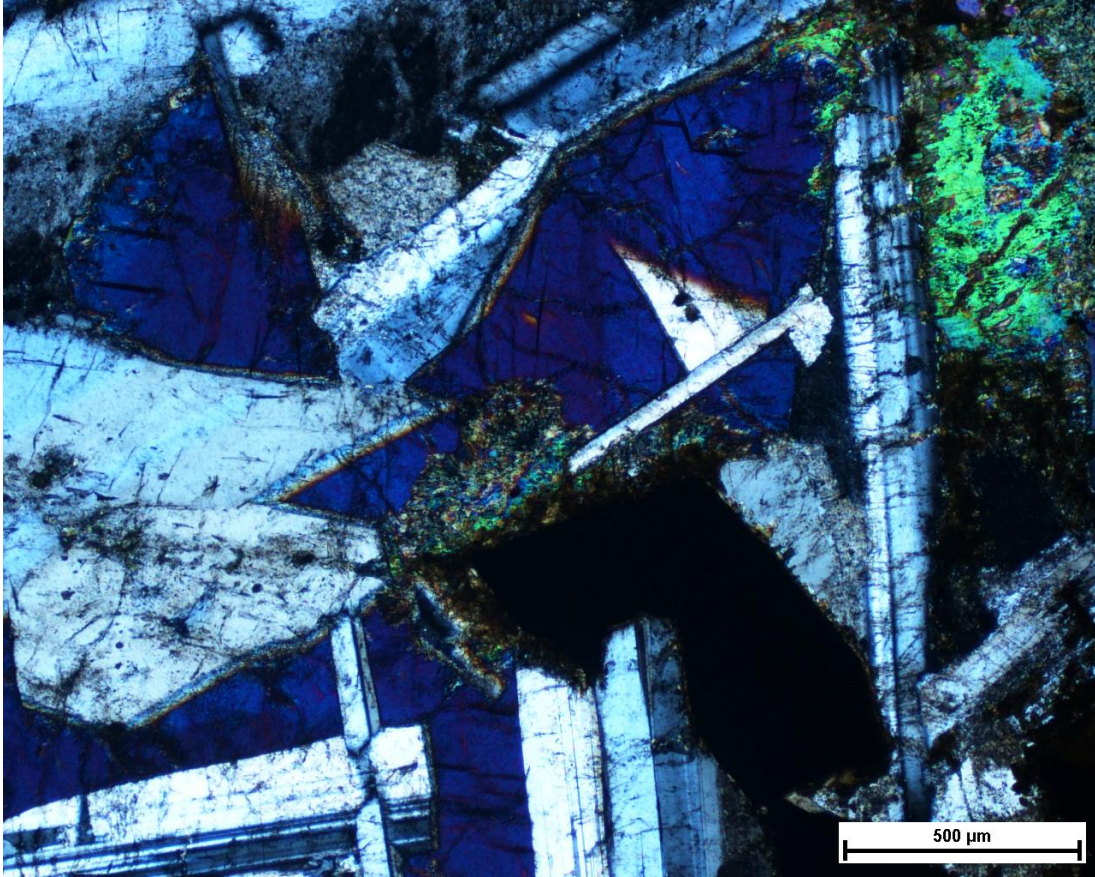
Geochemistry of Sample														
SiO ₂	Al ₂ O ₃	FeO	Fe ₂ O ₃	CaO	MgO	Na ₂ O	K ₂ O	TiO ₂	MnO	P ₂ O ₅	L.O.I.	S	Cu	Pd
48	14.3	12.1	18.05	7.67	4.07	3.94	1.81	2.08	0.26	1	0.51	0.05	271	0.027

Thin Section Petrography			
Silicates			
Mineral	Modal %	Grainsize	Description
Plagioclase	29	1-5mm	Euhedral laths exhibiting mainly NS alignment, with minor E-W alignment
Albite	8	1-4mm	Replaces plag rims, less commonly replaces entire plag grains
Biotite	4	1-2mm	Typically rims equant magnetite grains
Actinolite	15	1-2mm	Alters interstitial CPX grains
Magnetite	4	1mm	Forms equant, stubby subhedral grains. Weakly disseminated
Chlorite	2	<1mm	Associated with biotite
Clinopyroxene	27	2-6mm	Interstitial to plagioclase, anhedral
Apatite	3	<1mm	Euhedral stubby grains
Sulfides			
Mineral	Modal %	Dominant Grainsize	Description
Chalcopyrite	tr	<1mm	Very trace disseminations within actinolite blebs

Photomicrographs



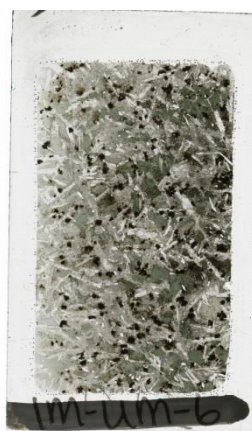
Typical ophitic texture, with plag (white long mineral) with interstitial CPX (light grey-brown) in PPL



Same picture as above but in XPL. The opaque mineral is a magnetite grain.

Sample name	Drill-hole	Depth	Lithology
IM-UM-6	G-10-04	60.38m	Plag lineated gabbro

Thin section



Geochemistry of Sample

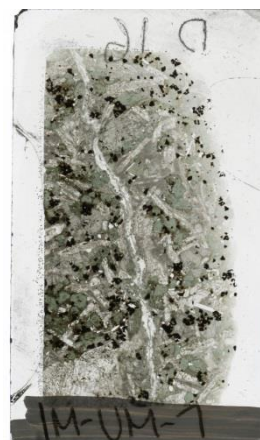
SiO ₂	Al ₂ O ₃	FeO	Fe ₂ O ₃	CaO	MgO	Na ₂ O	K ₂ O	TiO ₂	MnO	P ₂ O ₅	L.O.I.	S	Cu	Pd
47.8	13.8	12.25	17.8	7.83	3.92	3.77	1.91	2.08	0.28	1.06	0.59	0.05	274	0.02

Thin Section Petrography

Silicates			
Mineral	Modal %	Grainsize	Description
Plagioclase	24	1-2mm	Euhedral laths exhibiting to distinct alignment
Albite	8	1-2mm	Replaces plag rims, less commonly replaces entire plag grains
Biotite	2	1-2mm	Spatially associated with actinolite, also commonly rims magnetite grains
Actinolite	14	1-2mm	Alters interstitial CPX grains
Magnetite	6	1mm	Forms equant, stubby subhedral grains. Weakly disseminated
Chlorite	2	<1mm	Associated with biotite and actinolite
Clinopyroxene	28	2-6mm	Interstitial to plagioclase, anhedral. Strongly altered to actinolite
Apatite	3	<1mm	Euhedral stubby grains, common where albite alteration is present
Sulfides			
Mineral	Modal %	Dominant Grainsize	Description
Chalcopyrite	tr	<1mm	Very trace, only a few specks present

Sample name	Drill-hole	Depth	Lithology
IM-UM-7	G-10-16	0m	Plagioclase lineated gabbro

Hand Sample	Thin section
-------------	--------------



Geochemistry of Sample														
SiO ₂	Al ₂ O ₃	FeO	Fe ₂ O ₃	CaO	MgO	Na ₂ O	K ₂ O	TiO ₂	MnO	P ₂ O ₅	L.O.I.	S	Cu	Pd
43	12.9	13.6	21.2	7.1	5.6	3.18	1.92	2.39	0.31	0.85	0.49	0.02	210	0.048

Thin Section Petrography			
Silicates			
Mineral	Modal %	Grainsize	Description
Plagioclase	45	1-3mm	Subhedral, the majority of plag laths exhibit weak to moderate albite alteration
Albite	11	1-3mm	Alters plagioclase rims and cores. Patchy, irregular dirty-brown to grey coloured in PPL
Biotite	5	<1mm	Strong rimming of magnetite grains, but also occurs near actinolite altered Cpx grains. Foxy-brown coloured in PPL
Actinolite	13	1-2mm	Pseudomorphic alteration of Cpx grains
Magnetite	7	<1mm	Stubby to equant crystals, disseminated. Some crystals are skeletal textured
Clinopyroxene	18	1-2mm	Medium relief, interstitial to plagioclase. Forms ophitic texture with plagioclase. Strongly altered to actinolite
Apatite	1	<1mm	Weakly disseminated
Epidote	Tr	<1mm	Associated with actinolite alteration
Chlorite	Tr	<1mm	Associated with actinolite alteration
Sulfides			
Mineral	Modal %	Dominant Grainsize	Description
Chalcopyrite	Tr	<1mm	Very weakly disseminated, associated strongly with actinolite altered Cpx grains

Sample name	Drill-hole	Depth	Lithology
IM-UM-8	G-10-16	15m	Plagioclase lineated gabbro

Thin section



Geochemistry of Sample														
SiO ₂	Al ₂ O ₃	FeO	Fe ₂ O ₃	CaO	MgO	Na ₂ O	K ₂ O	TiO ₂	MnO	P ₂ O ₅	L.O.I.	S	Cu	Pd
46.3	14.6	11.55	17.2	8.01	4.04	3.8	1.57	1.96	0.25	1	0.57	0.03	212	0.018

Thin Section Petrography			
Silicates			
Mineral	Modal %	Grainsize	Description
Plagioclase	45	1-4mm	Euhedral to subhedral, low relief and forms ophitic texture with Cpx
Albite	9	1-3mm	Alters plagioclase rims and even cores. Patchy, irregular dirty-brown to grey coloured in PPL
Biotite	3	<1mm	Strong rimming of magnetite grains, but also occurs near actinolite altered Cpx grains
Actinolite	25	1-2mm	Pseudomorphic alteration of Cpx grains
Magnetite	6	<1mm	Stubby to equant crystals, disseminated
Clinopyroxene	12	1-2mm	Medium relief, interstitial to plagioclase. Forms ophitic texture with plagioclase. Strongly altered to actinolite
Apatite	1	<1mm	Weakly disseminated
Epidote	Tr	<1mm	Associated with actinolite alteration
Chlorite	Tr	<1mm	Associated with actinolite alteration
Sulfides			
Mineral	Modal %	Dominant Grainsize	Description
Chalcopyrite	Tr	<1mm	Very weakly disseminated, associated strongly with actinolite altered Cpx grains

Photomicrographs			
Sample name	Drill-hole	Depth	Lithology
IM-UM-9	G-10-16	30.36m	Plagioclase lineated gabbro

Thin section



Geochemistry of Sample														
SiO ₂	Al ₂ O ₃	FeO	Fe ₂ O ₃	CaO	MgO	Na ₂ O	K ₂ O	TiO ₂	MnO	P ₂ O ₅	L.O.I.	S	Cu	Pd
45.9	13.9	11.55	18.45	7.74	4.38	3.43	1.64	2.15	0.28	0.85	0.3	0.03	274	0.024

Thin Section Petrography			
Silicates			
Mineral	Modal %	Grainsize	Description
Plagioclase	47	1-3mm	Euhedral to subhedral, low to medium relief and forms ophitic texture with Cpx
Albite	8	1-3mm	Alters plagioclase rims and even cores. Patchy, irregular dirty-brown to grey coloured in PPL
Biotite	4	<1mm	Strong rimming of magnetite grains, but also occurs near actinolite altered Cpx grains
Actinolite	13	1-2mm	Pseudomorphic alteration of Cpx grains
Magnetite	7	<1mm	Stubby to equant crystals, disseminated
Clinopyroxene	20	1-2mm	Medium relief, interstitial to plagioclase. Forms ophitic texture with plagioclase. Strongly altered to actinolite
Apatite	1	<1mm	Weakly disseminated
Epidote	Tr	<1mm	Associated with actinolite alteration
Chlorite	Tr	<1mm	Associated with actinolite alteration
Sulfides			
Mineral	Modal %	Dominant Grainsize	Description

Chalcopyrite	Tr	<1mm	Very weakly disseminated, associated strongly with actinolite altered Cpx grains
--------------	----	------	--

Sample name	Drill-hole	Depth	Lithology
IM-UM-10	G-10-16	45m	Plagioclase lineated gabbro

Thin section



Geochemistry of Sample															
SiO ₂	Al ₂ O ₃	FeO	Fe ₂ O ₃	CaO	MgO	Na ₂ O	K ₂ O	TiO ₂	MnO	P ₂ O ₅	L.O.I.	S	Cu	Pd	
47.7	14.8	12.35	17.85	8.07	4.04	3.79	1.67	2.12	0.27	0.87	0.35	0.03	231	0.016	

Thin Section Petrography			
Silicates			
Mineral	Modal %	Grainsize	Description
Plagioclase	45	1-3mm	Euhedral to subhedral, low to medium relief and forms ophitic texture with Cpx. Some grains are stubby and have low aspect ratios, while others are slender and have high aspect ratios
Albite	3	1-3mm	Alters plagioclase rims and even cores. Patchy, irregular dirty-brown to grey coloured in PPL
Biotite	5	<1mm	Strong rimming of magnetite grains, but also occurs near actinolite altered Cpx grains
Actinolite	18	1-2mm	Pseudomorphic alteration of Cpx grains
Magnetite	6	<1mm	Stubby to equant crystals, disseminated
Clinopyroxene	22	1-2mm	Medium relief, interstitial to plagioclase. Forms ophitic texture with plagioclase. Strongly altered to actinolite
Apatite	1	<1mm	Weakly disseminated
Epidote	Tr	<1mm	Associated with actinolite alteration
Chlorite	Tr	<1mm	Associated with actinolite alteration
Sulfides			

Mineral	Modal %	Dominant Grainsize	Description
Chalcopyrite	Tr	<1mm	Trace, weakly disseminated, associated strongly with actinolite altered Cpx grains

Sample name	Drill-hole	Depth	Lithology
IM-UM-10	G-10-16	45m	Plagioclase aligned gabbro

Thin section



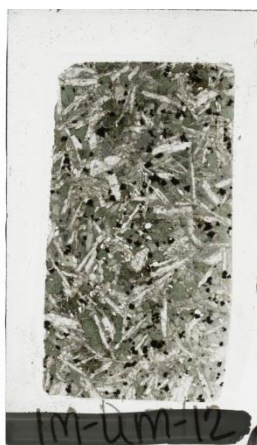
Geochemistry of Sample														
SiO ₂	Al ₂ O ₃	FeO	Fe ₂ O ₃	CaO	MgO	Na ₂ O	K ₂ O	TiO ₂	MnO	P ₂ O ₅	L.O.I.	S	Cu	Pd
47.7	14.8	12.35	17.85	8.07	4.04	3.79	1.67	2.12	0.27	0.87	0.35	0.03	231	0.016

Thin Section Petrography			
Silicates			
Mineral	Modal %	Grainsize	Description
Plagioclase	36	1-3mm	Euhedral to subhedral, low to medium relief and forms ophitic texture with Cpx. Some grains are stubby and have low aspect ratios, while others are slender and have high aspect ratios
Albite	2	1-3mm	Alters plagioclase rims and even cores. Patchy, irregular dirty-brown to grey coloured in PPL
Biotite	4	<1mm	Strong rimming of magnetite grains, but also occurs near actinolite altered Cpx grains
Actinolite	33	1-2mm	Pseudomorphic alteration of Cpx grains
Magnetite	6	<1mm	Stubby to equant crystals, disseminated
Clinopyroxene	18	1-2mm	Medium relief, interstitial to plagioclase. Forms ophitic texture with plagioclase. Strongly altered to actinolite
Apatite	1	<1mm	Weakly disseminated
Epidote	Tr	<1mm	Associated with actinolite alteration
Chlorite	Tr	<1mm	Associated with actinolite alteration

Sulfides			
Mineral	Modal %	Dominant Grainsize	Description
Chalcopyrite	Tr	<1mm	Very trace, weakly disseminated, associated strongly with actinolite altered Cpx grains

Sample name	Drill-hole	Depth	Lithology
IM-UM-12	G-10-16	60m	Plagioclase aligned gabbro

Thin section



Geochemistry of Sample															
SiO ₂	Al ₂ O ₃	FeO	Fe ₂ O ₃	CaO	MgO	Na ₂ O	K ₂ O	TiO ₂	MnO	P ₂ O ₅	L.O.I.	S	Cu	Pd	
46.6	14	11.9	16.85	8.18	4.07	3.6	1.56	2.01	0.26	0.85	0.44	0.03	252	0.011	

Thin Section Petrography			
Silicates			
Mineral	Modal %	Grainsize	Description
Plagioclase	37	1-3mm	Euhedral to subhedral, low to medium relief and forms ophitic texture with Cpx. Some grains are stubby and have low aspect ratios, while others are slender and have high aspect ratios
Albite	5	1-3mm	Alters plagioclase rims and even cores. Patchy, irregular dirty-brown to grey coloured in PPL
Biotite	3	<1mm	Strong rimming of magnetite grains, but also occurs near actinolite altered Cpx grains
Actinolite	23	1-2mm	Pseudomorphic alteration of Cpx grains
Magnetite	6	<1mm	Stubby to equant crystals, disseminated
Clinopyroxene	25	1-2mm	Medium relief, interstitial to plagioclase. Forms ophitic texture with plagioclase. Strongly altered to actinolite
Apatite	1	<1mm	Weakly disseminated
Sulfides			

Mineral	Modal %	Dominant Grainsize	Description
Chalcopyrite	Tr	<1mm	Very trace, weakly disseminated, associated strongly with actinolite altered Cpx grains

Curriculum Vitae

Name: Imran Meghji

Post-secondary Education and Degrees: Western University
London, Ontario, Canada
2006-2011 BSc

Western University
London, Ontario, Canada
2011-2016 MSc.

Honours and Awards: J.P. Bickell Foundation Mining Scholarship
2011

Targeted Geosciences Initiative Research Affiliate Program
Scholarship
2011

Related Work Experience Geologist
Stillwater Canada Inc.
2011-2012

Production Geologist
Kirkland Lake Gold Ltd.
2014-Present